UNIVERSITÀ DEGLI STUDI DI NAPOLI
FEDERICO II

DOCTORATE SCHOOL OF INDUSTRIAL ENGINEERING

DOCTORATE PROGRAM IN
AEROSPACE, NAVAL AND TOTAL QUALITY MANAGMENT
ENGINEERING

XXII CYCLE

PhD THESIS
Volume I

HYDRODYNAMICS OF PLANING HULLS

A POWER PREDICTION METHOD FOR WARPED V-BOTTOM HULL FORMS

Tutors
Chiar.mo Prof. Ing. Francesco Saverio MARULO
Prof. Ing. Carlo Francesco Mario BERTORELLO

Candidate
Ing. Luciano OLIVIERO

UNIVERSITÀ DEGLI STUDI DI NAPOLI
FEDERICO II

SCUOLA DI DOTTORATO IN
INGEGNERIA INDUSTRIALE

Dottorato di Ricerca in
Ingegneria Aerospaziale, Navale e della Qualità
XXII CICLO

TESI di DOTTORATO

HYDRODYNAMICS OF PLANING HULLS

A POWER PREDICTION METHOD FOR WARPED V-BOTTOM HULL FORMS

Relatori
Chiar.mo Prof. Ing. Francesco Saverio MARULO
Prof. Ing. Carlo Francesco Mario BERTORELLO

Dottorando
Ing. Luciano OLIVIERO

"Success is not final, failure is not fatal:
it is the courage to continue that counts."

Winston CHURCHILL

"Rem tene, verba sequentur."

CATONE

"Per ogni ambito di fenomeni
esiste un insieme di teorie possibili…
ed il fisico si limiterà ad indicarne una:
la più semplice o la più elegante."

Giuliano TORALDO di FRANCIA

Dedicated to
Elio COPPOLINO[1]
My Father-in-Law

Without whose help I never would
have had the chance to be a better man,
learning what I have.

[1] Naples (Italy): 03 June 1941 - 07 November 2009

CONTENTS

VOLUME I

APPENDIXES
VOLUME II -NO. 1

VOLUME II -NO. 2

CHAPTER 1

INTRODUCTION TO

PLANING CRAFT

1.1 Table of Contents

1.2 Introduction

Planing craft are the most common boats used all around the world for small commercial, military and pleasure craft. Hulls available for planing craft are many, differing for geometry, shape and dimensional ratios.

Despite of that, there is a lack of experimental data on these hulls and there are no effective and user-friendly tools, available for Power and Resistance Assessment in the Preliminary Design Phase, except in the case of very simple hull geometry.

The goal of this PhD Thesis work is to try out a new effective and robust tool useful to the small-boat Naval Architect, to attack the Resistance Assessment Problem for a planing craft in calm water during the Preliminary Design Phase.

1.3 Planing Craft

In each condition, static or dynamic, the weight of a craft is balanced by the pressure acting on the wetted surface.

This pressure is composed by two components: hydrostatic, related to the buoyancy, and hydrodynamic, related to the speed of the craft.

It is possible to classify the vessels according to the kind of pressure field acting during their steady motion:

- *displacement vessels* - if hydrostatic pressure is much higher than hydrodynamic ones,
- *semi-displacement vessels* - if hydrostatic and hydrodynamic pressure have the same order of magnitude,
- *planing vessels* - if hydrostatic pressure is much lower than hydrodynamic ones.

Per each family of craft, or per each kind of pressure field, there is a hull form that is the best one for achieving the lower value of Resistance.

This classification is useful to understand physical phenomena and choose the right hull form, but it is not practical in usual design.

To avoid this, Naval Architects are use to classify vessels in these three families (displacement, semi-displacement and planing) by the value of a characteristic number, related to the craft and its steady cruising speed: the Froude number Fn.

Reminding that $Fn = \frac{V}{\sqrt{gL}}$, where V is the craft speed, L is the waterline length[(2)] and g is the acceleration of gravity, we have: [Faltinsen 2005]

- displacement vessels $Fn \leq 0.4$,
- semi-displacement vessels $0.4 \leq Fn \leq 1.0 - 1.2$,
- planing vessels $Fn > 1.0 - 1.2$.

This classification is not quite manageable: the waterline length L is not a constant and known quantity for semi-displacement and planing craft.

It is possible to solve this problem adopting, as geometric dimension in Froude number formula, another (sometime constant) characteristic's dimension of the craft.

The most used are:

---

(2) Overall submerged length of the craft. In Literature this length is indicated as L_{WL}.

- the wetted beam b,

$$C_V = Fn_b = \frac{V}{\sqrt{gb}} \quad \text{beam Froude number}$$

- the "volume" length $\nabla^{\frac{1}{3}}$,

$$Fn_\nabla = \frac{V}{\sqrt{g\sqrt[3]{\frac{W}{\gamma}}}} \quad \text{volume Froude number}^{(3)}$$

where W is the weight of craft, γ is the unit weight of water and g is the gravity acceleration.

From an experimental point of view, a craft is deeply in planing condition if $Fn_b > 3$ [Savitsky 1951] or $Fn_\nabla > 5$ [Fédiaevski 1974], but it is acceptable the value $Fn_b \geq 1.5$ [Savitsky & Brown 1976] or $Fn_\nabla \geq 3$ [Fédiaevski 1974] as lower limit for planing.

It is easy to show the power of this way of work: by the knowledge of two data (speed and characteristic dimension), via the calculation of just one number (the Froude ones), it is possible to classify the craft[4].

Keeping in mind the goal of this work, we focus our attention on the flow field around a planing craft and the optimum hull shape related to.

A marine craft, moving through the water surface, generates a transverse wave system having a velocity C equal to the craft speed V: this cause a loss of propulsive energy of the craft. Despite of this phenomenon cannot be avoided, it is possible to reduce this loss of energy. In order to achieve this goal, it is useful to introduce the "wave-making" resistance of a hull: a "virtual force" defined as the load pertinent to the energy spent by the craft for generating this wave system. This force and the speed of the craft V have reversed direction.

As a first order approximation, the characteristics of this transverse wave can be likened to sine waves [Savitsky 2003]:

---

(3) Sottorf [Sottorf 1937] suggested to use the volume Froude number Fn_∇ instead of the beam Froude number Fn_b as matter of fact that the wetted beam b could not always be constant and equal to the distance between the hull chines. In Literature the beam Froude number Fn_b is the most, but not the only, used. In his paper Sottorf named Fn_∇ as "Froude number referred to a length corresponding to the load".

(4) According to the writer, Froude numbers have an high uncertain degree on the motion field achieved. On the matter, see "third observation", paragraph G.9, Appendix G.

$$\frac{C}{\sqrt{\lambda}} \cong 1.34 \text{ (5)}$$

where the λ is the length of the wave, in feet, and C is the celerity, in kn, or in term of Froude number:

$$Fn_\lambda = 0.4 .$$

If L_{WL} is the load water line length and n the number of (transverse bow) wave on the side of the craft, we have:

$$n = \frac{L_{WL}}{\lambda} = \frac{L_{WL}}{\frac{2\pi C^2}{g}} = \frac{1}{2\pi}\frac{1}{\left(\frac{C}{\sqrt{gL_{WL}}}\right)^2} = \frac{1}{2\pi}\frac{1}{\left(\frac{V}{\sqrt{gL_{WL}}}\right)^2} = \frac{1}{2\pi}\frac{1}{Fn^2} \cong \frac{0.16}{Fn^2}$$

so for:

$Fn < 0.4 \rightarrow n > 1$ (craft supported by more than one wave)

$Fn = 0.4 \rightarrow n = 1$ (craft supported by only one wave)

$Fn > 0.4 \rightarrow n < 1$ (craft supported by less than one wave)

For $Fn < 0.28$, very low speed, the craft is supported by more than two waves.

---

(5) For a sine wave in deep water the speed (celerity) is given by [Miranda 2001]:

$$C^2 = \frac{g}{2\pi}\lambda$$

with C, λ and g expressed in the same system unit.
In International System units, the relative speed (or Speed/Length Ratio SLR) of a sine wave in deep water is:

$$\frac{C}{\sqrt{\lambda}} \cong 1.25\left(\frac{m^{\frac{1}{2}}}{s}\right)$$

or, in term of Froude number:

$$Fn_\lambda = \frac{C}{\sqrt{g\lambda}} = \frac{1}{\sqrt{2\pi}} \cong 0.4$$

In our case, with C in knots, λ in feet and g in meter per squared seconds, we have:

$$g = 9.81\frac{m}{s^2} \qquad \lambda(ft) \qquad C(kn)$$

$$C\left(\frac{m}{s}\right)\cdot\frac{3600}{1852} = C(kn) \rightarrow C\left(\frac{m}{s}\right) = \frac{1}{1.944}C(kn)$$

$$\lambda(m)\cdot 3.281 = \lambda(ft) \rightarrow \lambda(m) = \frac{1}{3.281}\lambda(ft)$$

$$\left[C(kn)\frac{1}{1.944}\right]^2 = \frac{9.81\frac{m}{s^2}}{2\pi}\frac{\lambda(ft)}{3.281} \rightarrow \frac{C^2}{\lambda} \approx 1.798\frac{m\ ft}{s^2\ kn^2} \qquad \frac{C(kn)}{\sqrt{\lambda(ft)}} \cong 1.34\frac{m^{\frac{1}{2}}\ ft^{\frac{1}{2}}}{s\ kn}$$

$$\frac{C}{\sqrt{\lambda}} \cong 1.34$$

If the hull has a convex shape (waterlines, buttock lines, stern and bilges) the residual drag component of the hull reaches its minimum value due to the lack of flow separation [Savitsky 2003].

Each sharp edge introduced is cause of flow separation, with an overall increase of the hull resistance due to the main growth of the form drag component[(6)].

Accordingly to this phenomenon the best hull shape is the "full convex" one, known as *displacement* hull form.

For $Fn < 0.4$, low speed, the craft is supported by one or more waves.

The convex hull has a small sinkage with a slight increase of the trim due to suction pressure increasing [Savitsky 2003]; these phenomena have a magnitude related to the speed and drive to an increase of hull resistance.

In this speed range, each sharp edge introduced on the hull drives to an increment of the hull resistance due to the flow separation effects.

The best hull shape remains the "displacement" one.

At $0.4 \le Fn < 0.6$ craft is supported by less than one wave: craft is advancing up the oncoming flank of its own bow wave[(7)].

At the turn of $Fn = 0.4$, the convex hull begins to squat[(8)] and trim down by the stern climbing up the back of its own bow wave. Increasing the speed, the flow along the convex geometry of the hull bottom develops large suction pressures that further increase the squat and trim of the vessel, and the hull resistance has a steeply increase: a barrier to further increases in speed [Savitsky 2003].

To avoid the suction pressure problem and overcame the "speed barrier" of the "full convex" hull it is useful generate [Savitsky 2003]:

- a flow separation from the stern by introducing a sharp wide transom in the hull form,
- a positive dynamic pressures, to lift the stern, raise the hull slightly, and reduce the trim, by introducing straight buttock lines in the aft body of the hull.

---

(6) Wetted surface reduction due to the sharp edges (e.g.: transom stern, spray-rails, etc.) drives to a reduction of the viscous component of the hull resistance but, in this speed range, this reduction is not able to balance the growth of the form drag component: at very low speed a viscous resistance variation has a small effect on the hull resistance overall.

(7) See Appendix D:" An Hypothesis on pre-planing motion phase of a craft".

(8) The squat of the craft is not related to an increment of the draft [Russo Krauss 1994]; as matter of the fact, for $Fn > 0.4$, the wavelength of the bow wave is higher than the length of craft and the wake of bow wave is made by its trough: the craft starts climbing up the back of its bow wave moving onto a "groove" (local water level, close to the craft, is lower than far calm water level). This drives to a "drop" of the craft Center of Gravity (CG) versus the calm water level without any increment of its draft.

In this speed range, convex hull with transom stern reaches its maximum values of squat and trim[9], further the transverse flow from the bottom clings to the round bilges due to the "negative pressures"[10] in this area; despite of these phenomena, the effects on hull resistance are small [Savitsky 2003].

The best hull shape is the convex one, with transom stern and straight buttock lines in the aft body, known as *semi-displacement* hull form.

At $0.6 < Fn \leq 1.0$ craft is supported by less than one wave.

The semi-displacement hull rises to its original static draft and the trim angle decreases with increasing speed. The spray formation on the hull sides, due to the round bilges, rises rapidly with increasing speed till the upper limit of the speed range. Increasing the speed, the trim is reduced and the total wetted surface becomes larger than the static wetted area (due to the spray effects): the hull resistance has a quickly increase becoming a barrier to further increases in speed.

Although properly designed spray rails can attenuate the bow spray there is insufficient dynamic lift for the craft to plane [Savitsky 2003].

For $0.4 < Fn < 1.0 - 1.2$ the best hull shape is the semi-displacement hull form.

For $Fn > 1.0 - 1.2$, high speed, to avoid the spray formation problem and overcame the "speed barrier" of the semi-displacement hull, it is useful generate [Savitsky 2003]:

- a flow separation from the craft sides by introducing sharp edge chines,
- a steeply reduction of the bottom suction pressure avoiding any other convex surface of the hull,
- a clear flow separation from the stern by introducing a sharp trailing edge between transom stern and straight bottom.

This new hull shape, known as *Hard-Chine planing* (or *planing*) hull form, is widely used for high speed craft.

---

[9] The depth of the "groove" depends on the high of the bow wave, that is related to the draft and the kinetic energy of the craft. Increasing the craft speed, from the starting value of $Fn = 0.4$, the lift effects can be neglected: squat and trim increase their values. The effects of lift can be neglected till the hull has not been reached its maximum value of squat and trim. With a further increasing of the speed the lift is not anymore negligible and starts to reduce the draft of the craft with a CG elevation; this drive to a reduction of the high of the bow wave with a further CG elevation; hence CG starts rising up due to draft reduction and high bow wave reduction: a "leverage" effect of the lift.

[10] In Fluid Mechanics pressure can be defined as the amount of energy per unit of volume of a fluid: it is always not negative according to the assumption that, in Classic Mechanics where the speed of each phenomenon is much lower than the light celerity, volume and energy are not negative quantity.
Many authors are use to adopt the atmospheric pressure as the "zero" benchmark, and values of pressure lower than the atmospheric one are called "negative".

All these shape modifications, introduced onto displacement hull to get semi-displacement and planing hull form, were developed by analysis of tests results on planing surfaces, the most of which were conducted in the first half of the last century.

The shape characteristics suggested for an Hard-Chine planing craft are [Russo Krauss 1994] [Savitsky 2003]:

- no convex surfaces,
- sharp edge chines at the bottom and sides intersection,
- wide transom with a sharp trailing edge,
- straight horizontal buttock lines at the aft end,
- water entry lines fine with narrow angle at the bow,
- Vee-bottom transverse sections with the deadrise increasing towards the bow[(11)].

[(11)] The deadrise is required to reduce the wave impact loads in a seaway and to provide lateral wetted surface required for course-keeping stability and manoeuvring. [Savitsky 2003]

1.4 Historical Review

1.4.1 Planing Hull Craft

At the turn of the 1900's first experimental works on High Speed Craft, planing boats and foil-supported ones, were developing thanks to the adoption of the Internal-Combustion Engines (ICE). These engines, already available in automotive field, were firstly adopted on small boats: their power/weight ratio higher than the steam engines and the lightness of small boats drove to a growth of the speed.

The goal of these experimental works was to develop the optimum design of an High Speed Craft and there were three key-ways to achieve this goal:

- growth of slenderness of the hull, with reduction of the Wave Resistance,
- reduction of wetted surface, with reduction of the Friction Resistance,
- growth of power engine;

moreover, there were two different approaches to the reduction of wetted surface:

- via redans (used with planing boats, flying boats and seaplanes)
- via foils (used with foil-supported boats).

The speed of foil-supported boats was higher than any other else planing boats (related to the same value of power), and this forced the interest of most researchers towards the boats foil-supported.

First studies on High Speed Craft, in Italy, were made by Gaetano Arturo CROCCO and Ottavio RICALDONI in the first years of 1900's. The goal of their experimental studies was related to the performance of a dirigible during the phases of landing and taking off from water surfaces. Their efforts were focused on the hull of the gondola[(12)], and the model of boat developed for their studies, known as "barchino idroscivolante"[(13)], was foil-supported and, furthermore, propelled by two large airscrews installed on the afterbody of the boat [Courtesy of Italian Air Force].

Few years later Enrico FORLANINI, for the first time in Italy and all over the world, developed and patented an hydrofoils support system for motorboats, propelled by marine propeller.

---

(12) A gondola is the shuttle on the bottom of a dirigible.
(13) It can be translated as "gliding small boat".

Despite of its good performance, Forlanini's "idroplano"[14], as he called his motorboat, was not a commercial success neither in Europe nor in United State of America[15].

The business failure was due to:

- the lack of strength of that wooden boats (foils and structural elements) related to the high level of acceleration, speed end kinetic energy achieved,
- seakeeping in rough water and high speed manoeuvrability problems.

In despite of these "growth" of technologies, there is no evidence of systematic studies on these topics.

In the first years of 1910's, planing surfaces began a new worldwide aeronautical field of study, due to increasing interest in seaborne landing and take-off of airplanes.

The first researches in this field were focused on the stress analysis of a seaplane, but at the middle of 1920's researchers turned their efforts onto modeling the loads on planing hull shapes: that was the starting point of planing surface studies[16].

Later, in the 1950ies, the reduction of interest on seaplanes and flying boats, forced the focus of the research towards planing craft [Rosén 2004].

1.4.2 Planing Surface Applications

At the end of eighteenth century, English explorers recorded, for the first time all over the world, an application of planing surface at Hawaiian Islands.

Captain James Cook witnessed the first board surfers and recorded it in his journal: that was the Hawaiian National Pastime. [Edge 2001]

Surfboards will be the only planing surface application[17] till the end of nineteenth century.

At the beginning of twentieth century, few years later Mr. Wright had made his first flight, planing surfaces began a new aeronautical field of study, as above mentioned,

---

[14] It can be translated as "hydro-plane".

[15] Enrico FORLANINI sold the commercial exploitation of his patent for the North America to Alexander G. BELL [Bruce 1974], but neither Forlanini nor Bell were able to do business with this new craft.
The first business application of Forlanini's idea has been developed in the first years of 1950ies. Carlo RODRIQUEZ and Frederik LOBAU built, in RODRIQUEZ Shipyard in Messina -Italy- and for the first time in the world, a boat foil-supported for commercial application: the "Freccia del Sole", a fast ferry. [Courtesy of Rodriquez Cantieri Navali].

[16] Sottorf [Sottorf 1937] quoted as the early research on planing surfaces a work made by Baker and Millar in 1912, "*who, did not continue any further work of fundamental investigation. In order to create a sufficiently wide basis, tests on planing surfaces have been conducted by the author since 1928*...". Baker's work seems to be not anymore available.

[17] See Appendix A: "Surf Hydromechanics"

while, in the same years, first experimental works on High Speed Craft, planing boats and foil-supported craft, were developing.

Planing surface studies, on seaplane and flying boats, were the key for a quickly development of planing boats versus foil-supported ones. [Bertorello & Oliviero 2007]

The understanding of the planing surface physics passes through the knowledge of fluid dynamics models and fluid dynamics history too.

The development of the history and models of fluid dynamics are not a goal of this work, but, at the same time, it is important to highlight the milestone progresses in this field on the right timeline.

1.4.3 Math tools

In the seventeenth century researchers, as Galileo and Descartes, started to use math to describe physical models; they were use to deduce physical model properties by a few fundamental principles on that field. [Kline 1972]

But were those fundamental principles correct?

For Galileo, and also for Newton later, the answer should come from the analysis of data from experimental tests. This was the "new approach" to research in all field of physics: the scientific method.

In the first years of eighteenth century the study on scalar functions related to vector fields was moving his first steps [Kline 1972], meanwhile scientists started to share two fundamental approaches in the research [Giusti Doran 1975]:

- Math describes every physical law, whatever hypothesis or constrains have been fixed;
- Similarity in math equations drive to analogy in the behavior of physical models.

These scalar functions, related to vector fields, were introduced as new tool for research on gravity, but few years later Daniel Bernoulli applied these function in his studies on fluids. In his *Hydrodynamica* (1738) he introduced a scalar function, related to a force field, and called it "potential function".

The first attempt to use a potential function related to the velocity field of a fluid flow were made by Euler in *Pricipia motus fluidorum* (1752); that potential function will be called later "velocity potential" by Helmholtz [Helmholtz 1858]. Euler, in his paper, wrote the equation $\frac{\partial^2 S}{\partial x^2}+\frac{\partial^2 S}{\partial y^2}+\frac{\partial^2 S}{\partial z^2}=0$ were S is the velocity potential of a fluid

flow, but he did not recognized neither the importance of this equation nor the usefulness in other physical fields. [Kline 1972]

The first who developed a Theory of potential functions was Laplace in *Mècanique cèleste* (1799-1825). He showed clearly the physical meaning of potential function related to a vector field:

in each point of the field, the derivative of the potential function to a direction is equal to the vector component in that direction.

In his *Mècanique cèleste*, Laplace introduced a new math operator $\nabla^2 = \frac{\partial^2}{\partial x^2} + \frac{\partial^2}{\partial y^2} + \frac{\partial^2}{\partial z^2}$, known as Laplace's operator, with an important property: if f is a scalar function, $\nabla^2 f$ is a scalar function not depending on coordinate system; the equation $\nabla^2 f = 0$ is a second-order linear partial differential equation, known as Laplace's equation or potential equation. [Boyer 1968]

In fluid dynamics, the Laplace's equation of velocity potential is obtained from the balance equation of mass, known as continuity equation, for a perfect fluid flow[18]:

$$\frac{\partial \rho}{\partial t} + \frac{\partial (\rho u)}{\partial x} + \frac{\partial (\rho v)}{\partial y} + \frac{\partial (\rho w)}{\partial w} = 0$$

where:

x, y, z	coordinate of a point P of the fluid flow field
t	time
$\rho = \rho(x, y, z, t)$	density of fluid
$\left.\begin{array}{l} u = u(x, y, z) \\ v = v(x, y, z) \\ w = w(x, y, z) \end{array}\right\}$	component along the three axis, respectively, of fluid flow velocity $\overline{V}$

It easy to show[19], in the hypothesis of incompressible fluid, that the continuity equation drives to Laplace's equation:

$$\nabla^2 \varphi = 0$$

with φ ,velocity potential, related to velocity field by the relationships:

---

[18] See Appendix B: "Continuity Equation and Laplace's Equation for a Perfect Fluid Flow"
[19] See Appendix B

$$u = \frac{\partial \varphi}{\partial x} \qquad v = \frac{\partial \varphi}{\partial y} \qquad w = \frac{\partial \varphi}{\partial z}.$$

In his treatise, Laplace showed further the usefulness of the potential equation in the physical research. [Boyer 1968]

Later, in the middle of nineteenth century, William Thomson (Lord Kelvin) showed the math similarity among the laws of heat flow, fluid flow, elasticity of solids and some properties of electric and magnetic patterns. [Giusti Doran 1975]

Few years later, in 1858, Helmholtz published a fundamental work on hydrodynamics using, from the physics point of view, the analogy between electromagnetic field and hydrodynamics, and working, from math point of view, with three new tools related to: [Peruzzi 1999]

- Riemann's works (Abelian function theory),
- Green's works (Green's theorems),
- Lapalce's works (Potential function theory).

These two works, above cited, were a milestone in Physics: a steeply improvement of knowledge was possible by exchanging properties, in analogy, among different physical fields, and by using the new available math tools.

These first steps have been fundamental for following development of hydrodynamics and fluid dynamics above all.

The solutions of Laplace's equation were available only for a few simple cases per each field of physics; e.g. in hydrodynamics, the velocity potential function related to a frictionless fluid flow around a cylinder.

Each available solution, in each physics field, represents a different type of fluid flow and, due to linearity of Laplace's equation, each linear combination of solutions is a solution itself.

The assumptions of incompressible and perfect fluid, in Laplace's equation, simplify the equation that otherwise cannot generally be solved; the resulting solutions represent reasonable approximations to many actual flows except for high speed gases (due to the compressible effect). [Abbott & Doenhoff 1959]

However, a generically solution requires satisfying not only the differential equation but also specific boundary conditions. This latter requirement often makes the general solution of Laplace's equation difficult. [Granger 1985]

In the second half of nineteenth century the most of researchers' efforts, in hydrodynamics, were directed to the development of math tools to solve Laplace's

equation: since nineteenth century the research on potential functions (or on the methods to solve Laplace's equation) has been the goal of the "theoretical" researchers.

Many methods to solve Laplace's equation have been developed [Luchini & Quadrio 2003] [Granger 1985]:

Separation of variables	Analytic solutions
Green's function	
Conformal transformation[20]	Based on Reimann's mapping theorem (complex analysis of one variable)
Direct Method	The first-order partial differential equation $\vec{V} = \vec{\nabla}\varphi$ is directly integrate; e.g.: Morino Method.
Indirect Methods	Based on superposition principle applied to elementary solution of Laplace's equation; e.g.: Hess & Smith Method (known as Panel Method)
Numerical Solutions	Developed in the second half of twentieth century for computer machines, are based on same statement that drives to a "translation" of the differential equation into an algebraic equations system with high number of unknown; e.g.: Finite Element Method, Computational Fluid Dynamics, Boundary Element Method, etc.

Except for Conformal transformation, the explanation of these methods is not the goal of this thesis.

Nowadays, the most of solutions and methods, available for Laplace's equation, are associated to 2-dimensional fields: growing up the complexity of fluid flow problem, the number of available solutions drops down.

The 3-dimensional fluid flow around a planing surface is an highly complex problem due to the critical issue in the boundary conditions at the hull and free surfaces: the wetted area of hull and the free surfaces, where boundary conditions should be satisfied, are not constant but depend on the potential solution [Garme & Rosén 2003].

[20] See Appendix C: " The Conformal Transformations"

Despite of the many solutions and methods available in hydrodynamics, for the 3-dimensional fluid flow around a planing surface, no analytical – close form solution has been developed yet [Bertorello & Oliviero 2007].

1.4.4 Physical models

In the hydrodynamic model of a fluid flow, the goal is to calculate the velocity field by means of the physical phenomena could be described.

There are two different approaches to this problem: the theoretical and semi-empirical ones.

In the first approach, the development of physical models has always been strictly linked to the development of math tools and vice versa [KLINE 1972].

In the theoretical approach there are two possible ways to calculate the velocity field related to a model: the analytical and the numerical ones.

In the most of cases, the real hydrodynamic models are so too complex as math models pertinent to and there is no function available to describe the velocity field.

The approach to this problem is to downsize the complexity of the real model by the assumption of simplified hypothesis: per each hypothesis added a physical model is available.

The simplest model, with the largest number of simplified hypothesis, is the incompressible perfect fluid flow[21].

In the semi-empirical approach, the second one, the development of physical models has been related to the level of technology available for the tests: from the first experiments of Galileo and Torricelli [Maffioli 1998] to Savitsky's experiments on prismatic hull forms [Savitsky 1964].

In this second approach the test results are elaborated, using regression formulas, to up date simplified theoretical model by introduction of empirical coefficient in formulas or empirical formulas in math model.

Further, there are other two ways to attack the problem of resistance assessment of a planing hull:

- Statistical models (e.g.: Egorov's method [Voitkounski 1985] and Radojcic's method [Radojcic 1985]),
- Systematic Series (e.g.: TMB Series 62 [Clement & Blount 1963]),

each one related to a family of hull forms.

These two ways (or methods) are not physical models, because they are not able to calculate the velocity field, but only some tips related to.

[21] See Appendix B

In order to achieve the goal of this thesis work, our attention will be focused on planing surface physical models.

1.4.4.1 Theoretical approaches

The most of theoretical planing surface models available were developed in aeronautical field mainly by German researchers, at the turn of the 1930's: their works have had a profound influence on several subsequent research efforts.

The first fundamental work was developed by von Karman "to determine the maximum pressure acting on the seaplane floats during landing" in order to make a stress analysis of the seaplane floats [von Karman 1929].

In this work, von Karman used the added mass concept, developed by Munk [Munk 1922], and the conservation of momentum to derive an Impact Formula related to a wedge impacting on a still water[22].

Later, Wagner engaged himself to determine the pressure distribution on the seaplane floats (or on flying boat hull) during the planing phases: landing and take off.

He knew that the seaplane behaviour in landing phase were quite different than take off one: in the landing phase there was mainly an impact phenomenon while in the take off phase there was mainly a planing one; further, he firstly pointed out the importance of pressure distribution calculation for the hydrodynamic resistance assessment.

In his first work on the matter [Wagner 1931] he proposed an impact wedge model, that looks like von Karman's one, using the expanding-plate analogy to calculate the local water surface elevation.

His second work [Wagner 1932] was the first attempt to develop a theoretical planing surface model: the non linear planing flat plate model with analytical solution; further, he improved his impact wedge model above cited. Some years later[23], this paper will be recognized as a milestone for theoretical developments in hydrodynamics [Pierson & Leshnover 1950].

In his third work [Wagner 1933] he proposed, for the take off of a seaplane/flying boat, to split the float/hull in two different parts: the area afterward the spay jets (the area behind the stagnation line), for which the planing flat plate model can be used, and the forward part for which impact wedge is the model related to.

---

[22] Horizontal surface of water.

[23] "*…in many cases Wagner was content to indicate merely the final results of a line of reasoning on a particular problem, without presenting, in any degree of detail, the intermediate mathematical steps which are necessary. Mainly because of this difficulty, much of his work, has not received the attention it deserves*." [Pierson & Leshnover 1948]

Many years later, Tulin applied, for the first time, the slender body theory, introduced by Munk [Munk 1924], to the problem of a planing surface [Tulin 1957].

In the slender body theory the hypothesis of body slenderness and the smallness of surge perturbation speed, allow us to consider the flow field around each transverse section identical. This drives to a 2-dimensional model of a surface impacting on a horizontal surface of water.

Tulin's work will be a fundamental and starting model for many numerical methods.

In the same years USSR[(24)] researchers, as Kotchine and Sédov, developed a planing surface model based on the Wave Theory: the linear planing flat plate model with analytical solution [Fédiaevski et al. 1974].

First attempts to solve the problem of a planing surfaces were developed assuming the velocity field as sum of two components: one (known) related to the asymptotic fluid flow and one (unknown) related to the planing surface and known as perturbation velocity field.

This approach will be assumed as the starting point for all theoretical models developed.

[(24)] Union of Soviet Socialist Republics. This union of States does not exist anymore since 26 December 1991.

1.4.4.1.1 Analytical model

1.4.4.1.1.1 Impacting wedge

The two impact wedge models developed, by von Karman and Wagner, allow us to calculate the load per unit of length acting on a cylindrical body with a wedge shape.

These models are 2-dimensional from a physical point of view but not from a mathematical ones: no hypothesis have been made on the geometry of the body (or on the flow field component) linked to the axial direction of length (or of motion).

As a result the 3-dimensional perturbation flow field around the hull can be approximated by the sum of a series of 2-dimensional sections each one resembling an impacting wedge falling through the water surface [Akers 1999].

The modeling of the problem has been developed through the years [Mayo 1945] in order to get an analytical solution by which to describe the real phenomena.

The spreading of computer machines, in the second half of the twentieth century, has been driven to modeling the problem in order to get numerical solutions, that are closer than the analytical ones to the real phenomena.

All of them, in their zero gravity ideal flow formulation, assumed the hypothesis of small perturbation in the surge direction of the craft. This assumption allows the 3-dimensional problem to reduce to a 2-dimensional one: the flow field in a transverse plane (cross-flow plane) [Savander et al. 2002].

1.4.4.1.1.2 Planing flat plate.

A few years later, Wagner published an analytical solution of a 2-dimensional potential fluid flow based upon both Helmholtz-Kirchhoff method(25) and conformal transformations in terms of Schwarz-Christoffel differential equation(26) [Wagner 1932].

This analytical solution of a 2-dimensional potential fluid flow around a body of arbitrary shape was based on a theorem in conformal representation stated by Riemann more than a century before, known as the fundamental theorem of conformal representation.

This theorem (in simple form) states that it is possible to transform the region bounded by a simple curve on a plane into the region bounded by a circle on another plane, so

(25) "*Kirchhoff proposed the idea of a 'wake' bounded by free streamlines as a model for the flow behind a finite bluff body. He used the mathematical methods of Helmholtz to find the irrotational solution for a flat plate set normal to an oncoming stream. The pressure in the wake was assumed to be constant and equal to the upstream pressure. Under this conditions the wake extends infinitely far downstream of the body. It is interesting to note that Kirchhoff's work appeared many years before Prandtl discovered boundary layers and the reason for the wake structure behind a body*." [Brennen 1995]

(26) See Appendix C

that the potential field of the first region is readily obtained in terms of the potential field of the second region and vice versa [Theodorsen & Garrick 1933].

Schwarz and Christoffel focused, separately, their efforts on some particular applications of Riemann's theorem[27] [Kline 1972], and their results were used by Wagner in his work above citied.

A number of transformations have been found by means of which it is possible to transform a circle into a contour resembling an airfoil shape. These theoretical airfoils possess no particular qualities which make them superior to the types of more empirical origin. However, the attempts which have been made to solve the general case of an arbitrary airfoil shape by direct processes have resulted in intricate and practically unmanageable solutions [Theodorsen & Garrick 1933].

The modeling of the planing surface problem, by conformal mapping, has been developed through the years by other researchers as Pierson [Pierson & Lashnover 1948], Tchaplyguine and Sédov [Fédiaevski et al. 1974] [Payne 1988].

Further, an attempt to extend the method developed to the impacting wedge were made by Korvin-Kroukivsky [Korvin-Kroukovsky & Chabrow 1948] and Pierson [Pierson 1948, 1950].

[27] See Appendix C

1.4.4.1.2 Numerical models

A different approach in 3-dimensional research efforts was obtained with panel methods.

All solutions of Laplace's equation are scalar potential functions; among these, elementary solutions include point source, doublets and vortices.

Panel methods take advantage of the fact that polynomial sums of these elementary solutions also satisfy Laplace's equation.

In panel methods the vessel surface is replaced by a set of panels, and to each panel is assigned one or more of those elementary solutions. Furthermore, per each panel is assigned a control location or "collocation point" for which the solid boundary condition must be met.

A panel method solver must find a combination of source strengths, doublet strengths or vortex circulations such that the boundary conditions are met at surface, at the object body and at the far field. Once all of the panel strengths are known the velocities and the pressures can be calculated for each panel [Akers 1999].

Panel methods do not reduce the complexity of 3-dimensional problem of a planing surface. The critical issue pertinent to the boundary conditions is approximately solved by iterative or time-stepping solutions.

A typical problem of panel methods, related to the boundary conditions, is that the geometry of the problem is a function of the solution to the problem: the panels location and their resulting normal vectors are a function of the fluid velocity potential, which is a function of geometry. Again iterative or time-stepping methods must be employed [Akers 1999].

Panel methods are extremely computationally intensive and require special skill to panelize the surfaces appropriately [Barry et al. 2002].

Other ways to attack the problem have been developed through the years in different approaches, all based on potential theory.

Some of them are: non-linear boundary element solution, explicit finite element analysis, strip methods for steady planing in calm water, slender planing surface, time-domain strip application, and computational fluid dynamics, here reported for a general overview. [Rosén 2004]

1.4.4.2 Semi-empirical approaches

Several empirical researches were developing in parallel with the theoretical ones, cited above. Sottorf, Shoemaker, Korvin-Kroukovksy, Clement, and Savitsky are among the large number of researchers that tested planing surface models.

Experiments have been performed on craft in full-scale as well as model scale.

Several experiments have also addressed the 2-dimensional problem of a prismatic body impacting on a water surface, by the so called drop tests [Rosén 2004].

Korvin-Kroukovksy [Korvin-Kroukovksy et al 1949] and Savitsky [Savitsky 1964] developed regression formulas based on prismatic hull form model tests to estimate the hydrodynamic and hydrostatic forces. [Savander et al. 2002]

Besides the methods above cited, other methods to predict the speed-power relationships for planing hulls were developed. Among these: Hadler's method [Hadler 1966], Blount's method [Blount & Fox 1976].

The most popular was developed by Savitsky [Savitsky 1964] and refined later by Savitsky and Brown [Savitsky & Brown 1976] and by Savitsky and Koebel [Savitsky & Koebel 1993].

In Savitsky's long form method [Savitsky & Koebel 1993], the designers iterate through a series of steps to predict the running trim and the required thrust for their planing hulls.

The first major advantage of Savitsky's method is that it is simple to perform.[Akers 1999]

This method only accounts for a few parameters of the design, generally maximum chine beam, a single characteristic value for the deadrise angle, ship weight and longitudinal position of the centre of gravity. [Barry et al. 2002]

The second major advantage to Savitsky's method is that it is accurate for many common prismatic hull forms.

There are a number of disadvantages to Savitsky's method. Wave resistance component and viscous resistance due to the wetted surface of hull sides are neglected. Spray resistance is not directly estimated and spray effects are not correctly taken in account at all.

Deadrise angle variation either longitudinal or transversal can not be considered by Savitsky's method.

Further, the method is quasi-static and does not directly predict transient behaviour.

Finally, the method lumps all forces into a series of empirical relationships so point or panel hydrodynamic loads cannot be predicted using the method [Akers 1999].

Hadler [Hadler 1966] developed a practical method for power performance prediction of planing craft bringing together research on marine propellers with that on planing [Rosén 2004].

This method presents the same disadvantages of Savitsky's method.

Since '70s semiempirical methods based on statistical studies have been developed. These works were based on the hypothesis that dimensionless resistance of the bare hull (normalized versus the weight of the hull) could be expressed as a series expansion associated to a few dimensionless variables: the main dimensionless resistance value as well as the derivative coefficient values were computed by regression analysis of towing tests results available. Egorov, Bunkov and Sadovnikov, USSR researchers, used BK series test results for their regression analysis on planing hull form [Voitkounski 1985]; meanwhile Radojcic used test results related to Series TMB 62, Series 62-DUT and Series NSRDC 65 [Radojcic 1985].

1.5 Symbols

b	Beam of hull	[m]
C	Celerity of the wave: speed of a transverse wave system	$[m/s]$, or [kn]
CG	Center of Gravity	
C_V	Froude number related to the beam b	$C_V = \frac{V}{\sqrt{gb}}$
Fn	Froude number	$Fn = V/\sqrt{gL}$
Fn_b	Froude number related to the beam b	$Fn \equiv C_V$
Fn_∇	Volume Froude number	$Fn_\nabla = \frac{V}{\sqrt{g\sqrt[3]{\frac{W}{\gamma}}}}$
Fn_λ	Froude number related to the wavelength λ	$Fn_\lambda = \frac{C}{\sqrt{g\lambda}}$
g	Gravitational acceleration	$9.81 m/s^2$
ICE	Internal-Combustion Engines	
L	Overall submerged length	[m]
L_{WL}	Load water line length	[m]
n	Number of (transverse bow) wave on the craft side	$n = \frac{L_{WL}}{\lambda}$
S	Velocity potential of a fluid flow (Euler's symbol)	
SLR	Speed/Length Ratio	$V/\sqrt{L}$
t	Time	
$u = u(x, y, z)$ $v = v(x, y, z)$ $w = w(x, y, z)$	Component along the three axis, respectively, of $\overline{V}$	$[m/s]$
V	Speed craft	$[m/s]$
$\overline{V}$	Fluid flow velocity	$[m/s]$
W	Hull weight	[N]
x, y, z	Coordinate of a point P of the fluid flow field	
φ	Velocity potential	
γ	Unit weight of water	$[N/m^3]$
λ	Wave length	[ft]

ρ	Density of fluid	$\rho = \rho(x, y, z, t)$
∇	Volume displaced by the craft	$[m^3]$
∇^2	Laplace's operator	$\nabla^2 = \frac{\partial^2}{\partial x^2} + \frac{\partial^2}{\partial y^2} + \frac{\partial^2}{\partial z^2}$

1.6 References

Abbott, H.I. & Doenhoff, A.E. 1959. *THEORY OF WING SECTIONS*. New York (USA): Dover Publications ISBN 0-486-60586-8

Akers, R.H. 1999. Dynamic Analysis of Planing Hulls in Vertical Plane. *New England SNAME Meeting 1999.* Jersey City (USA): SNAME

Barry, C.R., Gosh D., Akers R., Ulak A. 2002. Implementation, Application and Validation of the Zarnick Strip Theory Analysis Technique for Planing Boats. *Proceeding of first High Performance Yacht Design Conference (HPYD1),* Auckland, Australia.

Bertorello, C. & Oliviero, L. 2007. Planing hull hydrodynamics. A critical review of the state of the art in theoretical resistance assessment. *Proceeding 12th Conference of International Maritime Association of the Mediterranean (IMAM 2007)*, Vol. 1, pages 13-19. Varna, Bulgaria. ISBN-13 987-0-415-45521-3

Brennen, C.E. 1995. *CAVITATION AND BUBBLE DYNAMICS*. New York (USA): Oxford University Press. ISBN 0-19-509409-3

Bruce, R.V. 1990. *BELL: ALEXANDER GRAHAM BELL AND THE CONQUEST OF SOLITUDE*. New York (USA): Oxford University Press. ISBN 0801496918

Boyer, C.B. 1968. *A HISTORY OF MATHEMATICS*. Hoboken, NJ (USA): John Wiley & Sons – [Italian version : STORIA DELLA MATEMATICA. 1980. Segrate (MI): Arnoldo Mondadori Editore (Italy) ISBN 88-04-33431-2]

Clement, E.P. & Blount, D.L. 1963. Resistance Tests of a Systematic Series of Planing Hull Forms. *Transactions SNAME,* pages 491-579. Jersey City (USA): SNAME

Edge, R. 2001. Surf Physics. *The Physics Teacher* Vol. 39 (ISSN: 0031-921X) - USA

Faltinsen, O.M., 2005. *HYDRODYNAMICS OF HIGH-SPEED MARINE VEHICLES*. New York, NY (USA): Cambridge University Press. ISBN-13 978-0-521-84568-7

Fédiaevski, C., Voïtkounski, I., Faddéev, Y. 1974. *MECANIQUE DES FLUIDES.* Moscou: Ed. MIR. pp. 542-543 (French version)

Giusti Doran, B. 1975. *Origins and Consolidation of Field Theory in Nineteenth-Century Britain: From the Mechanical to the Electromagnetic View of Nature*. From Historical Studies in Physical Sciences, Vol. VI, ed. by R. McCormmach. Princeton, NJ (USA): Princeton University Press – [Italian version:

Dalla concezione meccanica alla concezione elettromagnetica della natura. 1981. Bologna (Italy): il Mulino.]

Garme, K. & Rosén, A. 2003. Time-Domain Simulations and Full-Scale Trials on Planing Craft in Waves. *International Shipbuilding Progress* Vol.50 No.3. Delft (the Netherlands): Delft University Press.

Granger, R.A. 1985. *Fluid Mechanics*. New York (USA): CBS College Publishing.

Hadler, J.B. 1966. The prediction of power performance on planing craft. *SNAME Transactions,* Vol. 74. pp563-610 Jersey City (USA): SNAME

Helmholtz, H. 1858. Über Integrale der hydrodynamischen Gleichungen, welche der Wirbelbewegungen entsprechen. *Crelle's Journal* (*Journal für die reine und angewandte Mathematik*), No 58, pp. 25-55.

Journée, J.M.J. & Massie, W.W. 2001. *Offshore Hydromechanics*. Delft (the Netherlands): Delft University of Technology (TU Delft Library web site: www.library.tudelft.nl)

Karman, T. von, 1929. The Impact on Seaplane Floats During Landing. *Report NACA TN 321* Washington, D.C. (USA). (web site: http://ntrs.nasa.gov/search.jsp)

Kline, M. 1972. *Mathematical Thought from ancient to modern times.*. New York (USA): Oxford University Press – [Italian version : STORIA DEL PENSIERO MATEMATICO. 2002. Vol. 1 e Vol. 2 Giulio Enaudi Editore Torino (Italy). Vol.1 ISBN 88-06-15417-6. Vol.2 ISBN 88-06-15418-4]

Korvin-Kroukovsky B.V. & Chabrow, F.R. 1948. The Discontinuous Fluid Flow Past an Immersed Wedge. *Report SIT-DL-48-9-334 Davidson Laboratory* Stevens Institute of Technology. Hoboken, New Jersey (USA)

Luchini, P. & Quadrio, M. 2003. *Aerodinamica*. Milano (Italy): Politecnico di Milano (Dipartimento di Ingegneria Aerospaziale web site: www.aero.polimi.it/~quadrio -Italian language.)

Maffoli, C.S. 1998. GLI ALBORI DELLA FISICA MODERNA E L'IDRAULICA NEL TARDO RINASCIMENTO. *Atti del XVIII Congresso Nazionale di Storia della Fisica e dell'Astronomia*. Milano (Italy), pages 109-128. (Italian language).

Mayo, W.L. 1945. Analysis and Modification of Theory for Impact of Seaplane on Water. *Report NACA TN 1008* Washington, D.C. (USA). (web site: http://ntrs.nasa.gov/search.jsp)

Miranda, S. 2001 *Appunti di Architettura Navale*. Napoli: Dipartimento di Ingegneria Navale, Università degli Studi di Napoli "FEDERICO II" (Italian language - web site: http://wpage.unina.it/miranda/)

Munk, M. 1922. Notes on the Aerodynamic Force – I. Rectilinear Motion. *Report NACA TN 104* Washington, D.C. (USA). (web site: http://ntrs.nasa.gov/search.jsp)

Munk, M. 1924. Notes on the Pressure Distribution Over the Hull of Elongated Airship with Circular Cross Section. *Report NACA TN 192* Washington, D.C. (USA). (web site: http://ntrs.nasa.gov/search.jsp)

Payne P.R. 1988. *Design of High-Speed Boats: Planing*. Annapolis(USA): Fishergate Publishing Company Inc. ISBN 0942720067.

Peruzzi, G. 1999. Vortici, Campi e Lanterne Magiche. *Atti del XIX Congresso Nazionale di Storia della Fisica e dell'Astronomia*. Milano (Italy), pages 46-62. (Italian language).

Pierson, J.D. 1948. On the Pressure Distribution for a Wedge Penetrating a Fluid Surface. *Report SIT-DL-48-6-366 Davidson Laboratory* Stevens Institute of Technology. Hoboken, New Jersey (USA)

Pierson, J.D. 1950. The Penetration of a Fluid Surface by a Wedge. *Report SIT-DL-50-381 Davidson Laboratory* Stevens Institute of Technology. Hoboken, New Jersey (USA)

Pierson, J.D. & Leshnover S. 1948. An Analysis of the Fluid Flow in the Spray Root and Wake Regions of Flat Planing Surfaces. *Report SIT-DL-48-335 Davidson Laboratory* Stevens Institute of Technology. Hoboken, New Jersey (USA)

Pierson, J.D. & Leshnover S. 1950. A Study of the Flow, Pressures, and Loads Pertaining to Prismatic Vee-Planing Surfaces. *Report SIT-DL-50-382 Davidson Laboratory* Stevens Institute of Technology. Hoboken, New Jersey (USA)

Radojcic, D. 1985. An Approximate Method For Calculation of Resistance and Trim of the Planing Hulls. *Ship Science Report No.23* University of Southampton (UK)

Russo Krauss, G. 1994. *NAVI A SOSTENTAMENTO IDRODINAMICO*. Parte Prima. Napoli: Dipartimento di Ingegneria Navale, Università degli Studi di Napoli "FEDERICO II" (Italian language).

Savander, B.R., Scorpio, S.M., Taylor, R.K. 2002. Steady Hydrodynamic Analysis of Planing Surfaces. *Journal of Ship Research* Vol.46 No. 4. Jersey City (USA): SNAME

Savitsky, D. 1951. Wetted Length and Center of Pressure of Vee-Step Planing Surfaces. *Report SIT-DL-51-378 Davidson Laboratory* Stevens Institute of Technology. Hoboken, New Jersey (USA)

Savitsky, D. 1964. Hydrodynamic Design of Planing Hull. *Marine Technology*, Vol.1, No.1, Jersey City (USA): SNAME

Savitsky, D. 2003. ON THE SUBJECT OF HIGH-SPEED MONOHULLS. *Proceedings of Symposium SNAME Greek Section*. October 2, 2003. Athens, Greece. (web site: http://www.sname.org/newsletter/Savitskyreport.pdf)

Savitsky, D. & Brown, P.W. 1976. Procedures for Hydrodynamic Evaluation of Planing Hulls in Smooth and Rough Water. *Marine Technology*, Vol.13, No.4, pp381-400, Jersey City (USA): SNAME

Savitsky, D., Koebel, J.G. 1993. Seakeeping Considerations in Design and Operation of Hard Chine Planing Hulls, *Technical Research Bulletin* R-42, pp124 Jersey City (USA): SNAME

Savitsky, D., DeLorme M.F., Datla R. 2006. Inclusion of "Whisker Spray" Drag in Performance Prediction Method for High-Speed Planing Hulls. *Report SIT-DL-06-9-2845 Davidson Laboratory* Stevens Institute of Technology. Hoboken, New Jersey (USA)

Sottorf, W. 1937. Analyse experimenteller Untersuchungon über den Gleitvorgang an der Wasseroberfläche. *Jahrbuch der deutschen Luftfahrtforschung,* pp 320-339. [English version: Analysis of Experimental Investigations of the Planing Process on the Surface of the Water. *Report NACA TM 1061*, 1944. Washington, D.C. (USA). (web site: http://ntrs.nasa.gov/search.jsp)]

Theodorsen, T. & Garrick I.E. 1933. General Potential Theory of Arbitrary Wing Sections. *Report NACA TR 452* Washington, D.C. (USA). (web site: http://ntrs.nasa.gov/search.jsp)

Tulin, M.P. 1957. The Theory of slender Surface Planing at High Speeds. *Schiffstechnik*, Vol. 4, pp. 125-133.

Voitkounski, Y.I. 1985. *Ship Theory Handbook:. Vol.3. Manoeuvrability of conventional Ships. Hydrodynamics of Gliders Hydrofoils and Hovercrafts.* Leningrad (Russia): Sudostroenie. pp. 277-283 (Russian language)

Wagner, H. 1931. Landing of Seaplanes. *Report NACA TM 622* Washington, D.C. (USA). (web site: http://ntrs.nasa.gov/search.jsp)

Wagner, H. 1932. Über Stoss und Gleitvorgänge an der Oberfläche von Flüssigkeiten. *Z.A.M.M.* No.4 Vol.12. [English version: Phenomena associated with Impacts and Sliding on liquid surfaces. *Report NACA TR N-23507*, 1936. Washington, D.C. (USA). (web site: http://ntrs.nasa.gov/search.jsp)]

Wagner, H. 1933. Über das Gleiten von Wasserfahrzeugen. *Jahrbuch der Schiffbautechnik*, Vol.34, pp. 205-227 [English version: Planing of Watercraft. *Report NACA TM 1139*, 1948. Washington, D.C. (USA). (web site: http://ntrs.nasa.gov/search.jsp)]

CHAPTER 2

FUNDAMENTAL MODELS

2.1 Table of Contents

2.2 Figure Index

2.3 Introduction

Hydrodynamics of planing surfaces is focused on surface loads estimation in order to get information useful to performance analysis, stress analysis, engine and propeller design choice, and other design problems.

These loads are pertinent to the hydromechanics stress tensor[28]: they are computed by integration of stress tensor on the wetted surface of the craft [Miranda 2001].

"*The force acting on each element of the bottom may be decomposed into the tangential and normal components. The normal component is determined by the pressure of the liquid at the element, while the tangential component depends on the viscosity of the liquid and is determined by the motion of the liquid in the boundary layer.*" [Sedov 1939]

In a first approximation, in the hypothesis of inviscid fluid flow, the stress tensor involves into a diagonal matrix and the only information required is the pressure.

In the hypothesis of inviscid fluid, the Bernoulli's equation can be applied and pressure will be related to the velocity of flow field.

In a first rude approximation there are two ways to take into account viscosity effects: a theoretical way and an empirical one.

In the theoretical way, it is possible to take into account viscosity effects via Newton's model: shear stress contributes will be related to the velocity flow field.

[28] An hydromechanics stress tensor is, from a math point of view, a matrix with pressure value as principal diagonal elements and shear stresses as others.

Meanwhile in empirical way, base on Froude's assumption[29], it is possible to take in account viscosity effect via statistical conservative relationships[30].

[29] Viscous component of surface load acting on a hull, is equivalent to that of rectangular flat plate of equal wetted area and mean wetted length, moving at the same speed. [Miranda 2001]

[30] Some examples of friction coefficient formulas are:

Laminar flow, $Rn \le 5.3 \cdot 10^5 \rightarrow C_f = 1.328 \cdot Rn^{-0.5}$

(Blasius)

Transient flow, $5.0 \cdot 10^5 < Rn < 1.0 \cdot 10^7 \rightarrow C_f = 0.074 \cdot Rn^{-0.2} - \frac{1700}{Rn}$ (Prandtl)

Turbulent flow, $1.0 \cdot 10^7 < Rn \rightarrow C_f^{-0.5} = 4.13 \cdot \log_{10}\left(C_f Rn\right)$ (Schoenherr or ATTC '47)

2D turbulent flow, $2.0 \cdot 10^6 \le Rn \le 3.0 \cdot 10^8 \rightarrow C_f = \frac{0.075}{\left(\log_{10} Rn - 2\right)^2}$ (ITTC '57)

2.4 The fluid flow field related to a planing craft

The flat bottom of a planing hull is configured to develop, at high speed, a lift able to balance the craft weight.

As a consequence the wetted bottom surface, when planning, is smaller than the static wetted one [Savitsky 2003].

Most of water encountered by the planing surface passes beneath it and leaves the body in the form of a trailing wake. In the meantime, in the forward area of planing surface, two layers of water spray up and out along both sides of the surface. [Pierson & Leshnover 1950]

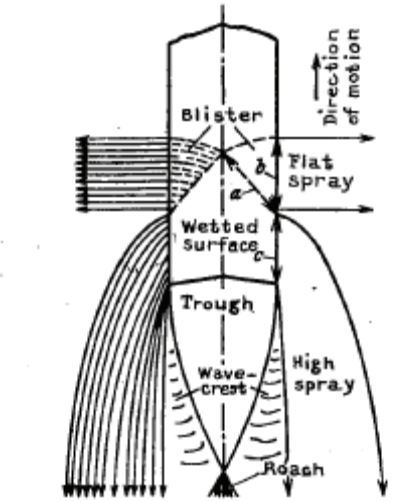

Figure 2.4-1 Top view of planing V-bottom surfaces [Sottorf 1932]

Planing surfaces and spray layers have the same degree of symmetry related to the free-stream velocity: if the planing surface has a longitudinal plane of symmetry Π and free-stream velocity is parallel to this plane, spray sheets will be symmetrically too, about the same Π-plane of symmetry.

If the free-stream flow results divided into two flows then there exists a separation line on the planing surface; this has been confirmed by countless observations: the separation line is on both sides of planing surface and has been called *stagnation line*. [Pierson & Leshnover 1950]

Each point of the stagnation line is the end point of a streamline[31]; streamlines related to stagnation line draw altogether a surface which divides free-stream flow into two parts: the upper part will be deflected in the spray sheets and the lower one will be deflected in the flow beneath planing surface.

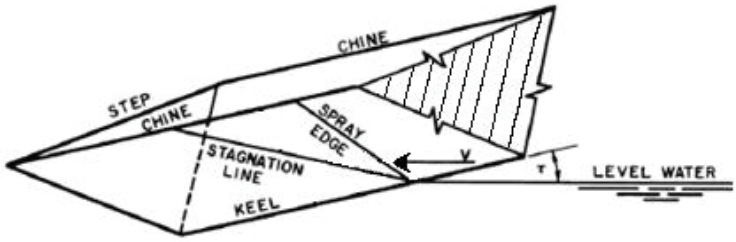

Figure 2.4-2 V-bottom Planing surface
[Savitsky et al. 2006]

As matter of fact the wetted bottom surface of a planing hull, regarding the flow velocity, is divided into two regions by the stagnation line as shown in Figure 2.4-2 and Figure 2.4-3:

- the pressure area, in the aft part,
- the whisker spray area, in the forward one.

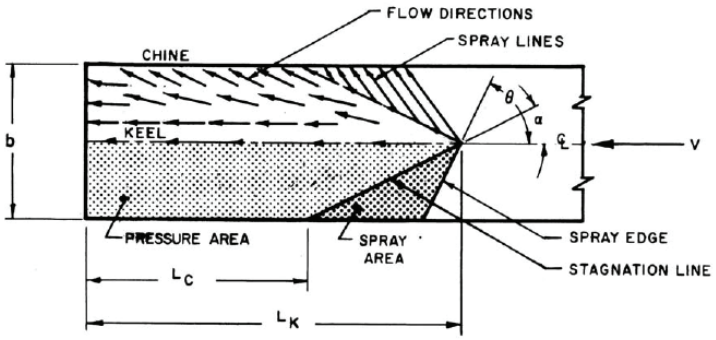

Figure 2.4-3 View of bottom on plane parallel to keel
[Savitsky et al 2006]

2.4.1 The velocity field.

The flow velocity vector, on either sides of the stagnation line, generally has components perpendicular and parallel to the line: parallel component is nearly constant (neglecting viscosity), meanwhile normal component goes to zero coming near the stagnation line and reverses its direction at turn of the line.

[31] *Streamline* is a line that, at all of its points, is tangent to the velocity vector of a fluid particle: a velocity field pattern. *Pathline* is the locus of the spatial positions traversed by a fluid particle as it moves in the flow field. For a steady flow, the streamlines and pathlines are identical. [Zucrow & Hoffman 1976]

Hence stagnation line is defined as all points on planing surface where the fluid velocity reaches its minimum value. [Pierson & Leshnover 1950]

In the pressure area the fluid velocity direction is mainly afterward directed.

In the whisker spray area, at low trim angle, the fluid flow direction is such that the space angle between the oncoming free-stream velocity and the stagnation line is equal to the space angle between the direction of the spray velocity and the stagnation line. [Savitsky et al 2006]

This phenomena is close to a "reflection[32]" about the stagnation line of the incident free-stream velocity.

In point of fact classical examples of reflection involves:

- angles of incidence and reflection in the same plane,
- angles of incidence equal to reflection one (no loss of energy of the system);

meanwhile, in this hydrodynamic case these angles are in different planes, and the conservation of the total energy drives to neglect viscosity. [Pierson & Leshnover 1950]

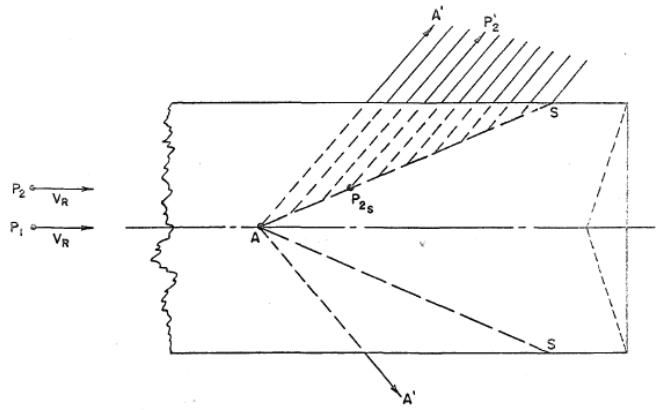

Figure 2.4-4 Flow path near planing prism[33]
[Pierson & Leshnover 1950]

As a consequence, any fluid particle located on stagnation line will have its motion directed along the line [Pierson & Leshnover 1950]; further the flow velocity along the

---

[32] The reason for this "reflection" phenomena follows from consideration on Bernoulli's equation. As matter of the fact, at the instant the particle of fluid flow reaches the spray root near the stagnation line, the perpendicular component of the velocity goes to zero, and immediately reverses its direction into the spray along the inclined side of the planing surface. As the motion of the particle continues along the spray away from the spray root region, the perpendicular component of the particle velocity recovers the magnitude it had during the approach to the body in the free stream, because the pressure drops to zero where the flow in the spray becomes uniform. [Pierson & Leshnover 1950]

[33] LEGEND:

P_1, P_2	particles of water,
P_{2s}	particle of water P_2 on stagnation line,
P'_2	particle of water P_2 on whisker spray area,
AS	stagnation line.

spray-root line[34] is primarily along the direction of the stagnation line. [Savitsky et al 2006].

The validity of the reflection principle is supported by the available experimental data only at smaller trim angles[35] [Pierson & Leshnover 1950].

The flow in the spray portion of the fluid near a planing prism plays a very important part in the overall picture of the flow surrounding the body. [Pierson & Leshnover 1950]

At this time, the viscous drag in this area has not been defined so it is not included in any analytical method for computing the total resistance of the hull [Savitsky et al 2006].

2.4.2 The Pressure distribution.

Pressure distribution on wetted surface of a planing craft has an uneven shape, as shown in Figure 2.4-5. The high complexity of the phenomena does not allow a direct computing of the pressure distribution.

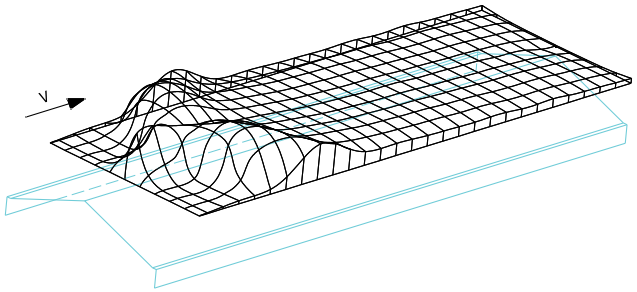

Figure 2.4-5 Pressure distribution on a V-bottom planing surface[36]

---

[34] All points on planing surface defined as intersection of planing surface with all straight line, normal to the still-water level and tangent to the spray surface. [Pierson & Leshnover 1950]
Spray root and stagnation lines are sometimes referred to each other since the longitudinal distance between these two lines is quite small, especially at trim angles representative of planing hull operation [Savitsky et al 2006].

[35] As matter of the fact, in the range of higher trim angles (between 8° and 12°), and by taking into consideration the inaccuracy of measurement at this value of trim angles, the spray edge results[Pierson & Leshnover 1950]:

- less distinct because of a tendency for the spray sheet to break up into foam near the edge,
- originated not at the exact intersection of keel and level water surface but at some point in a curl of water slightly forward of this intersection,
- somewhat curved instead of remaining straight as for the lower trim angles.

[36] Data source NACA Report 3477 [Kapryan & Boyd 1955]:
Model: 301-A ($\beta = 20°$, $\lambda = 3$, $\tau = 9°$)
Test Case: run 8

In order to go deep into the phenomena, researchers have studied longitudinal and transversal trends separately, starting from the simplest model available: the planing flat plate.

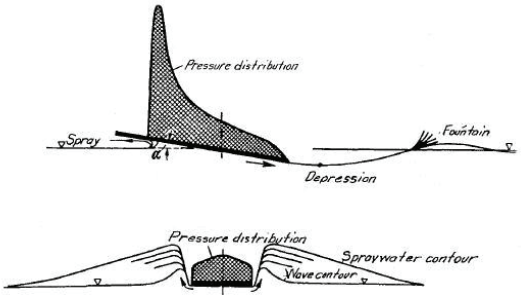

Figure 2.4-6 Planing surface during planing process [Sottorf 1937]

Summarized results of these investigations are reported below.

2.4.2.1 Longitudinal pressure distribution

Longitudinal pressure distribution on planing flat plate is shown in Figure 2.4-6. It is characterized by a max value position (stagnation point) close to the leading edge of the wetted surface. Pressure drops down quickly just moving from the stagnation point, and its value will be equal to the atmospheric pressure on both edges (leading and trailing) of the planing flat plate wetted surface.

Longitudinal pressure distribution on planing flat plate with very low length-beam ratio is qualitatively and quantitatively similar in each longitudinal section, except near the lateral edges due to 3-D fluid flow effects.

From a comparison of the experimental data with the two-dimensional flat plate theory (Wagner's theory [Wagner 1932]) results for the longitudinal pressure distribution, the shape of the experimental curves is found to be similar to the shape of the theoretical curves, but the curves are not quantitatively similar for the same experimental and theoretical trim. The experimental and theoretical pressure distributions along the center line are usually found to be quantitatively similar for the same experimental and theoretical normal-load coefficient. [Smiley 1951]

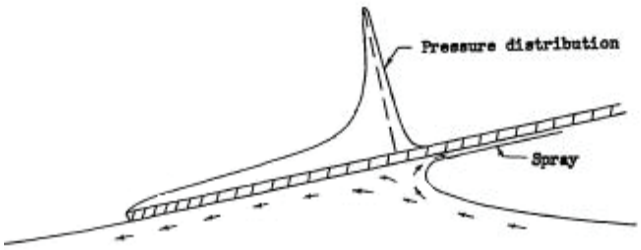

Figure 2.4-7 Semi-infinite flat plate pressure distribution
[Smiley 1951]

For a rectangular flat plate of finite length-beam ratio, experimental observations indicate that longitudinal pressure distribution on center line model is larger than the corresponding pressure along all other longitudinal sections: all pressure distributions are similar in shape but their magnitude decrease toward the edges of the plate. [Smiley 1951]

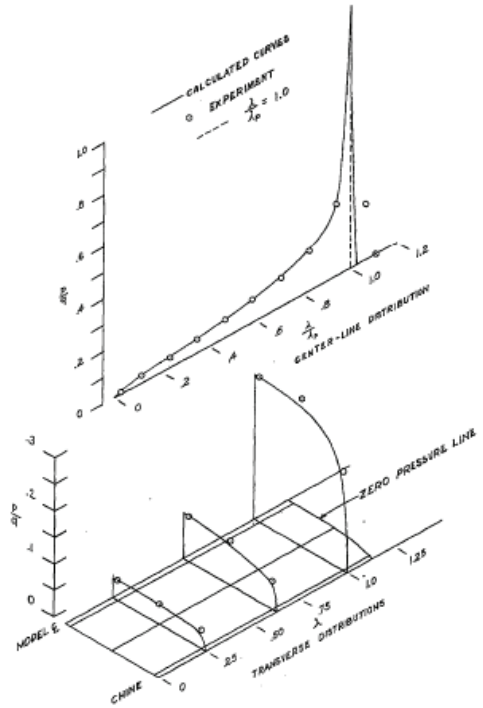

Figure 2.4-8 Center line and transverse pressure distributions of a finite flat plate[37]
[Kapryan & Boyd 1955]

Experimental results substantiate the use of the normal-load coefficient as the key parameter in predicting flat-plate center-line pressures. [Kapryan & Boyd 1955]

---

[37] LEGEND:
- p measured pressure without static displacement contribute,
- q theoretical dynamic pressure,
- λ ratio of distance forward of trailing edge of model with respect to beam,
- λp value of λ related to the stagnation point.

For all planing flat plates, the max value of pressure depends on the speed flow and its longitudinal position (measured by the distance between the trailing edge and the stagnation point) is related to the trim angle: higher speed higher pressure and lower trim higher distance.

A secondary trim effect is connected to the rate of pressure around the stagnation point: lower trim higher rate.

At the same time, longitudinal position of the Center of Pressure is associated to the trim angle: lower trim higher distance (from the trailing edge).

All these results are immediately shown by Wagner's model of pressure distribution for a flat planing plate:

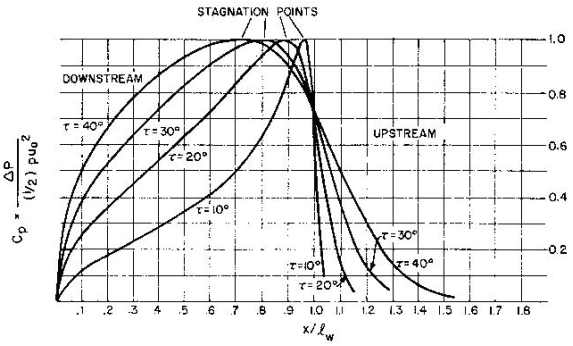

Figure 2.4-9 Wagner's pressure distribution for a flat planing plate [Payne 1988]

For V-bottom planing surface, the longitudinal pressure distribution has qualitatively similar shape related to the flat plate one: higher magnitude distribution on the center line model and lower ones toward the chines [Kapryan & Boyd 1955]. It exists a strong similarity in the region of wetted surface where the chines are immersed below the water surface, whereas a weak similarity is achieved in region with chines not immersed. Thereby, the agreement on similarity is seen to be best where the chine-immersed fraction of the total wetted area is large. Where the fraction is small the agreement is not so good. [Smiley 1951]

For all V-bottom planing surface, by the transom, the longitudinal flow separates and the hydromechanic pressure adjusts to atmospheric value as by the chines [Rosèn 2004].

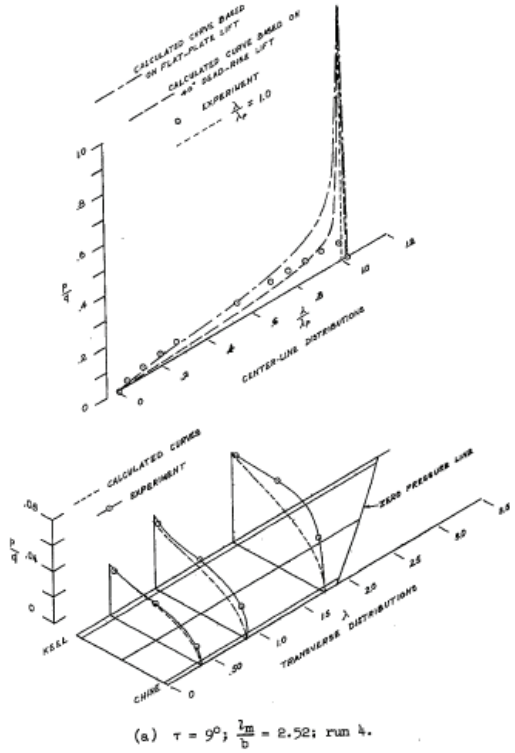

Figure 2.4-10 Center line and transverse pressure distributions of a V-bottom planing surface with 40° dead rise angle[38]
[Kapryan & Boyd 1955]

For a V-bottom planing surface, the magnitude of longitudinal pressure distribution in center line model is lower than flat plate one[39], due to the dead rise angle effect: higher dead rise angle lower pressure magnitude. [Kapryan & Boyd 1955]

[38] LEGEND:
- p measured pressure without static displacement contribute,
- q theoretical dynamic pressure, lm mean wetted length,
- b beam,
- λ ratio of distance forward of trailing edge of model with respect to beam,
- λp value of λ related to the stagnation point,
- τ trim angle.

[39] This statement has been elaborated via regression analysis of test data pertinent to rectangular flat plate of finite length-beam ratio and V-bottom surface, with the same beam and length, and hence the same length-beam ratio.

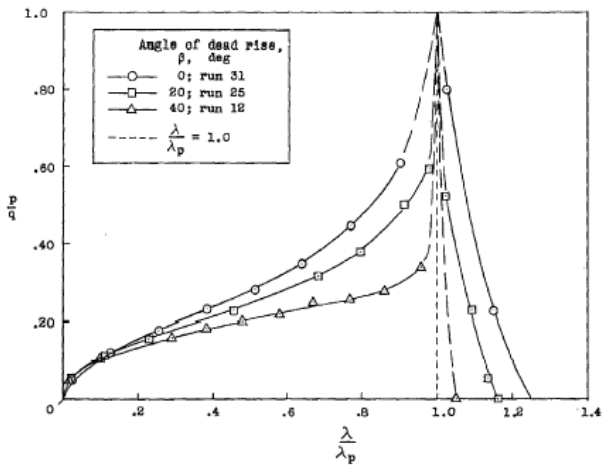

Figure 2.4-11 Center line pressure distribution for V-bottom planing surfaces with different values of dead rise angle(40)
[Kapryan & Boyd 1955]

Furthermore, for a given condition of load, speed, and trim, an increase in angle of dead rise increased the wetted length and hydrodynamic resistance and moved the Center of Pressure location forward. [Chambliss & Boyd 1953]

The growth of hydrodynamic resistance of V-bottom surfaces is due to the much greater spray formation at the sides. This explains the attempt to keep the spray at minimum by special design of the edges of the planing bottom. [Sottorf 1932]

When the V-bottom surfaces are modified with the addition of horizontal chine flare, the primary effect on the pressure distribution is the increase of pressure near the chines.

(40) LEGEND:
- p measured pressure without static displacement contribute,
- q theoretical dynamic pressure,
- lm mean wetted length,
- b beam,
- λ ratio of distance forward of model trailing edge with respect to beam,
- λp value of λ related to the stagnation point,
- β dead rise angle.

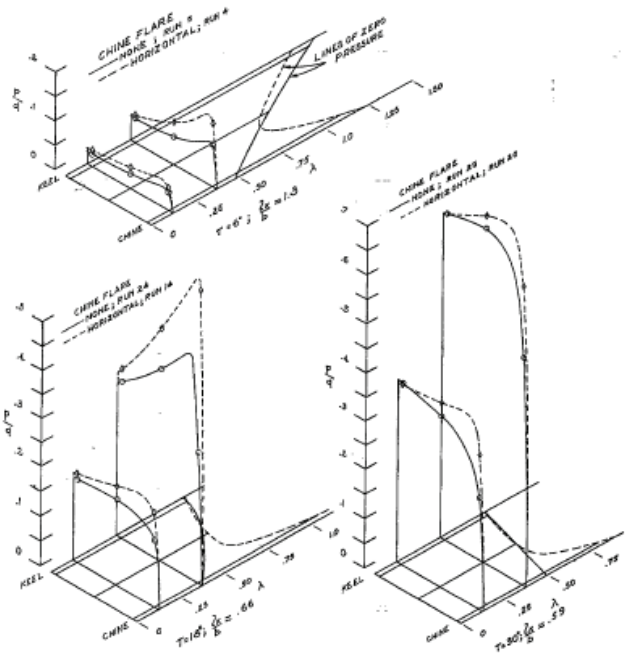

Figure 2.4-12 Effect of horizontal chine flare
[Kapryan & Boyd 1955]

Further, with reference to longitudinal pressure distribution along the chine buttocks, the extension of the positive pressures region is further forward of the stagnation point than the case for the unflared surface.

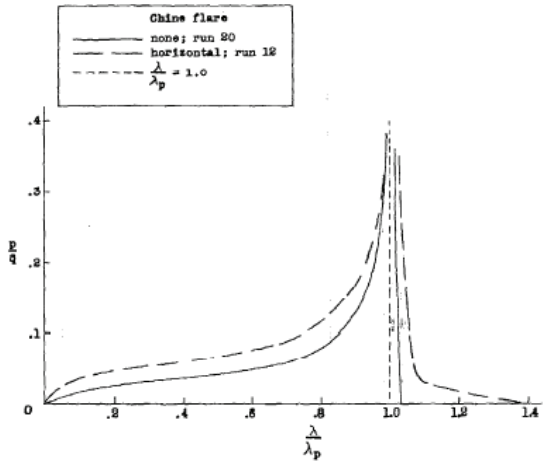

Figure 2.4-13 Longitudinal pressure distribution along the chines buttock for V-bottom planing surfaces with different chine form.
[Kapryan & Boyd 1955]

This is largely due to the lower effective deadrise angle that results when chine flare is introduced, and it is also believed to be due, to some extent, to the downward deflection imparted to the water just forward of the stagnation line (when the flow over the surface is primarily lateral) as it travels from keel to chines. [Kapryan & Boyd 1955]

2.4.2.2 Transversal pressure distribution

Transverse pressure distribution does not make sense for infinite planing flat plate. As matter of fact, for an infinite flat plate, longitudinal pressure distribution is the same in each longitudinal section meanwhile in each transverse one pressure is constant.

Transverse pressure distribution on planing flat plate with a finite length-beam ratio is shown in the lower side of Figure 2.4-6. It is characterized by a max value position in the middle (symmetry point) and the pressure drops down quickly to atmospheric ones just close to both lateral edges.

For V-bottom planing surfaces, transverse pressure distribution has a shape quite different to the flat plate one. This is due to the static component of the pressure, which increases linearly with the distance below the water surface, according to Stevin's law:

$$p_{stat} = \rho g z$$

with:

ρ fluid density,

g gravitational acceleration,

z vertical distance below the water surface.

A static pressure distribution is equal to the pressure subjected to a craft at zero speed as shown in figure below:

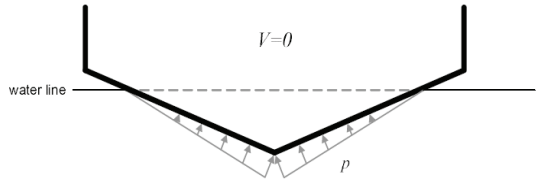

Figure 2.4-14 Static transverse pressure distribution [Rosèn 2004]

The pressure distribution at low Froude number (displacement craft) has a similar character, with small additional contributions from dynamic effects. [Rosèn 2004]

For a planing craft, with V-bottom hull form, there are three different kind of transverse pressure distributions. With reference Figure 2.4-15, these transverse pressure distributions are related to:

- Transverse section with dry chines ($b < x \leq a$);
- Transverse section with chines wetted by spray (chines above still water line: $c < x < b$);
- Transverse section with wetted chines (chines under still water line: $d < x < c$);

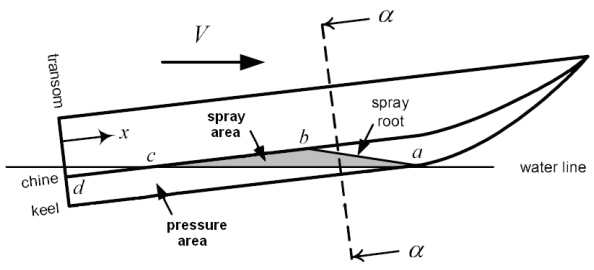

Figure 2.4-15 Profile view of a planing craft at constant speed V
[Rosèn 2004]

As shown in Figure 2.4-16, in the transverse sections with dry chines ($b < x \leq a$) the water surface is deformed and piles-up close to the hull. In addition there is a peak in the pressure distribution on the chine side of the section, and this peak is related to the formation of the jet [Rosèn 2004].

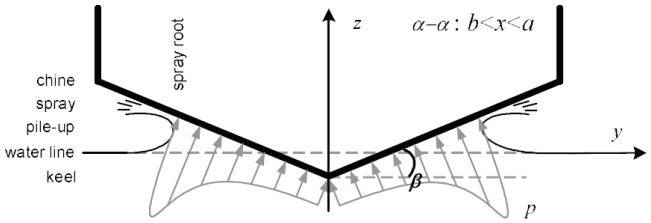

Figure 2.4-16 Dry chines characteristics
[Rosèn 2004]

In the transverse sections with chines wetted by spray ($c < x < b$) the sideways flow separates at the sharp chine meanwhile the pressure drops down to the atmospheric value, as shown in Figure 2.4-17.

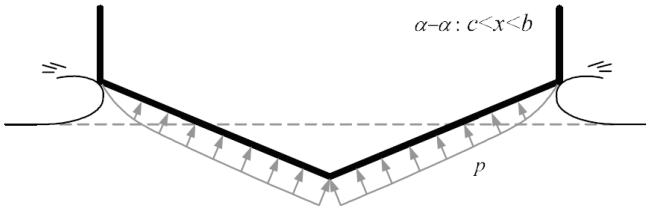

Figure 2.4-17 Spray wetted chines characteristics
[Rosèn 2004]

In the aftermost region, with wetted chines below the still water line ($d < x < c$), the sideways flow separates at the sharp chine, the pressure drops down to the atmospheric value and the water line deforms into a hollow:

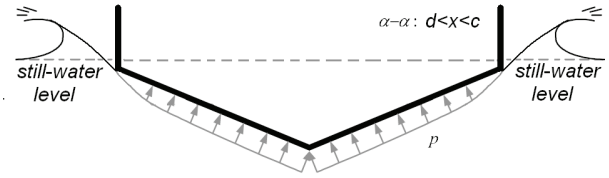

Figure 2.4-18 Characteristics of a wetted chines below still water line

The analysis of test data on all planing surfaces has had highlighted that the hydrodynamic pressure is related to the hull deadrise: higher deadrise lower pressure[41]. This statement is true also in the dry chines region ($b < x \leq a$) as shown in Figure 2.4-19, where a peak in the transverse pressure distribution occurs: lower deadrise higher peak pressure.

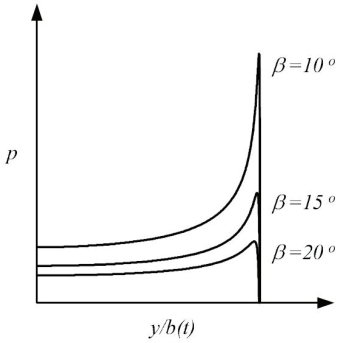

Figure 2.4-19 Transverse pressure distribution on dry chines region of a V-bottom planing hull for different deadrise angle at the same speed[42]
[Rosèn 2004]

2.5 Models

A real hull generally has a complex geometry: deadrise variation, multi-chines section, spray rails, transom stern, steps, orifices and notches, etc., and all these without taking in account the appendages.

This complexity is a problem in order to evaluate the influence of each single geometrical parameter as well as their mutual influences on the hydrodynamics of the planing hull.

The approach to this problem is to downsize the complexity of the real model by the assumption of simplified hypothesis: per each hypothesis added a geometrical model is available.

The simplest model, with the largest number of simplified hypothesis, is the flat plate.

The first simplified hull model is the monohedral hull. This has been developed, from the real one, applying the hypothesis:

---

[41] See Appendix E "Hydrodynamic Pressure Distribution Trends on a V-Bottom Planing Surface"

[42] LEGEND:
b(t) momentary wetted beam at the time t
p pressure
y transversal dimension
β deadrise angle

- deadrise angle constant,
- single chine section,
- transom stern,
- sharp edge chines at the intersection of the bottom and sides.

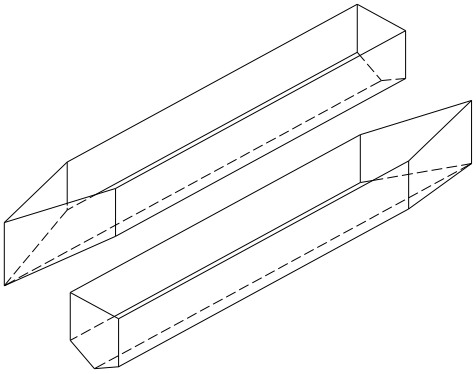

Figure 2.5-1 Monohedral hull
[Korvin-Kroukovsky et al 1948]

A second simplified geometrical hull model is the V-bottom surface.

This has been developed, from the monohedral hull, in the hypothesis:

- no transom,
- no bow,
- no sides.

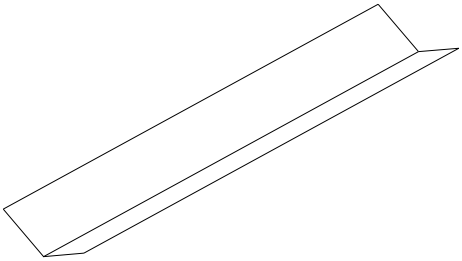

Figure 2.5-2 V-bottom surface

The Third and simplest geometrical hull model of a is the flat plate, developed from the V-bottom surface in the hypothesis of deadrise angle null.

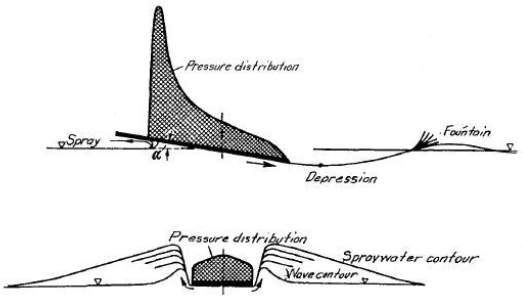

Figure 2.5-3 Planing surface during planing process (top: side section - bottom: front section) [Sottorf 1937]

In a timeline approach, the flat plate has been the first geometrical model developed.

Researches on planing surfaces have been developed into two ways [Korvin-Kroukovsky et al 1949]:

- Theoretical, related to the investigation of the fundamental nature of the hydrodynamic planing process
- Empirical, related to the collection and organization of design data for the establishment of rational design methods and for comparison with theoretical results.

2.5.1 Flat plate model

The simplest surface available to investigate the fundamental nature of the hydrodynamic planing process is the flat plate.

2.5.1.1 Flat planing plate: the empirical model

First experiment on planing surfaces were conducted by Baker, Sottorf, Sambraus and Shoemaker on flat planing plates [Korvin-Kroukovsky et al 1949].

In one of his first work on the matter, Sottorf exposed the reasons, hereinafter reported, that lead to this choice: the rectangular flat plate was the simplest model available with the lowest value of resistance.[Sottorf 1932]

When planing all forces produced by the pressure work on the wetted side of the plate, where the fluid "touches" the body, meanwhile the dry under side of the plate as well as the upper side are under the atmospheric pressure. These forces have a tangential and a normal component to the plate. [Sottorf 1932]

"*In the case of frictionless fluid the tangential or friction forces are null. From* Figure 2.5-4 *it is seen that the resultant of the normal force N*[43] *for trim angle a gives:*

$$R = L\tan\alpha \qquad \textbf{(2–1)}$$

as minimum resistance.

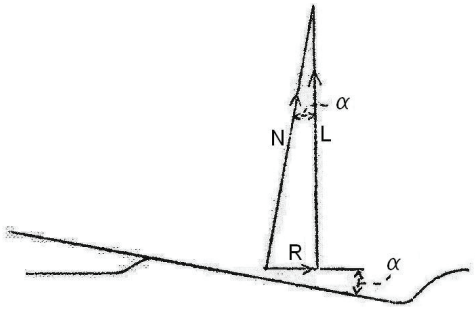

Figure 2.5-4 Forces on the flat plate in a frictionless fluid. [Sottorf 1932]

From Figure 2.5-5 it is seen that, assuming the addition of the friction force D_F*, the resistance becomes:*

$$R = L\tan\alpha + \frac{D_F}{\cos\alpha} \qquad \textbf{(2–2)}$$

as, in accordance with the conditions of the tests, the lift L[44] *is assumed to be constant.*

[43] For a frictionless fluid the normal force N is the resultant of the pressure distribution acting on the wetted surface of the plate.

[44] The hydrodynamic lift L is the vertical component of the hydrodynamic load F. It is important to remind that F is unknown.

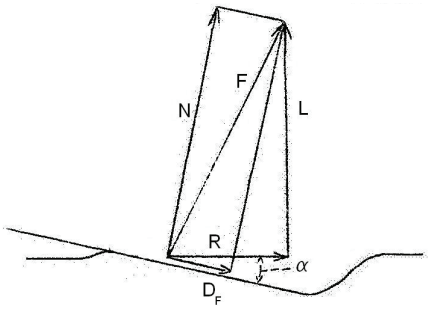

Figure 2.5-5 Forces on the flat plate in a viscous fluid.
[Sottorf 1932]

If one consider the cross section of a V-bottom plate with plane inclined surfaces and assume for simplicity that the trim angle is small and may be neglected, the normal force on one side, according to the Figure 2.5-6, *is:*

$$N = \frac{L}{\sin\frac{\beta}{2}} \qquad \textbf{(2–3)}$$

For the flat plate $\sin\left(\frac{\beta}{2}\right) = 1$, *hence* $N = L$.

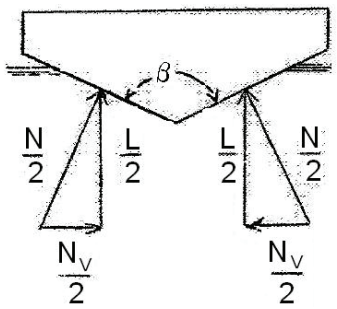

Figure 2.5-6 Forces on the flat plate with deadrise at small angles of trim
[Sottorf 1932]

With increasing deadrise, N and lost component N_V both increase, as well as the wetted surface, if the constant lift L is maintained, as a result of which the total resistance of the V-bottom, and also the curved bottom, exceeds that of flat plate." [Sottorf 1932]

The equation (2–2) is known as Sottorf's formula.

Further, Sottorf's formula can be easily obtained, in the hypothesis of steady planing motion, by the equilibrium equation along the vertical axes:

$$L = W \qquad \textbf{(2–4)}$$

and the geometrical relationship between the viscous force D_F and the vertical and horizontal component of the hydrodynamic force F [Russo Krauss 1994]:

$$D_F = R\cos\alpha - L\sin\alpha \qquad \textbf{(2–5)}$$

hence:

$$R = W\tan\alpha + \frac{D_F}{\cos\alpha} \qquad \textbf{(2–6)}$$

In this formula the unknown resistance R is sum of two term:

- the first related to the weight W and the trim α,
- the second related to the friction force D_F and the trim α.

The problem of the assessment of the resistance R is related to the assessment of the friction force D_F and the trim α[45].

In order to compare results pertinent to different models as well as models with different kinematic conditions, some nondimensional coefficients, or characteristic numbers, have been introduced, e.g.: λ as wetted length l_w to beam b, and C_V[46] (the coefficient speed) which is the Froude number related to the beam b.

First dimensional reasoning highlighted that any hydrodynamic force F, acting on a body-surface planing, can be defined as [Korvin-Kroukovsky et al 1949]:

$$F = k\left(\frac{1}{2}\rho V^2\right)L^2 \qquad \textbf{(2–7)}$$

where the term in parenthesis is the dynamic pressure and:

ρ is the density of the fluid, in mass units,

V is the velocity,

L is any characteristic linear dimension of the body-surface,

k is a nondimensional quantity.

For a planing surface supporting a load W, it is convenient to take the beam b as the characteristic length:

$$W = C_L\left(\frac{1}{2}\rho V^2\right)b^2 \qquad \textbf{(2–8)}$$

In the hypothesis of low viscosity fluid and neglecting the surface tension of water, the nondimensional coefficient C_L, known as lift coefficient, is a function of the trim

---

[45] The symbol α for the trim is used by Sottorf [Sottorf 1932]. Hereinafter for the trim angle will be used the symbol τ.

[46] The Froude number related to the beam can be indicated as C_V or F_{nb}: $F_{nb} = C_V = \frac{V}{\sqrt{gb}}$.

angle τ, the ratio λ of the mean wetted length l_w to beam b, and the Froude number C_V [Korvin-Kroukovsky et al 1949]:

$$C_L = C_L(\tau, \lambda, C_V) \qquad \textbf{(2–9)}$$

The goal of these first tests was to establish an empirical equation which would express the relation (2–9).

In their first attempt to understand the hydrodynamic behavior of a planing flat plate, researchers used their knowledge on the fluid dynamic of the airfoils. For little value of the trim angle τ, the lift of an airfoil is proportional to the trim angle:

$$\frac{C_L}{\tau} = f(\lambda, C_V) \qquad \textbf{(2–10)}$$

Further simplification was related to the of gravity effect: in the high Froude number range the gravity force effects can be neglected related to dynamic force ones, thereby:

$$\frac{C_L}{\tau} = f(\lambda) \qquad \textbf{(2–11)}$$

Researchers adopted for the (2–11) the expression:

$$\frac{C_L}{\tau} = A\lambda^{\alpha} \qquad \textbf{(2–12)}$$

where the coefficient A and the exponent α were given by the analysis of tests results.

For each set of tests different values of A and α have been found, with $0 < \alpha < 1$; these discrepancies arose from the above hypothesis on trim and Froude number effects.

In order to improve this model researchers formulated new hypothesis on the matter.

In connection with the trim angle τ, "*the hypothesis of C_L directly proportional to τ, is true for high value of aspect ratio AR*[(47)]*, where the flow is basically in longitudinal, chordwise direction. For a lamina of small span and infinite length $(\lambda = \infty)$, the flow is in transverse direction and C_L is proportional to τ^2.*" [Korvin-Kroukovsky et al 1949]

In general, the flow around a hydrofoil of small span have a longitudinal as well as transversal component, and in first approximation, we can write:

$$C_L = A\tau + B\tau^2 \qquad \textbf{(2–13)}$$

---

(47) The Aspect Ratio AR is the ratio of the squared beam to the wetted surface, or as well as the beam to the wetted length: $AR = \frac{b^2}{S_W} = \frac{b}{l_W}$. Further: $AR = 1/\lambda$.

The most tests developed with flat plate were characterized by models with finite length and positive Aspect Ratio value, hence the second term of the (2–13) was little and lower than the first: it was considered as a small correction to the first. Accordingly, an approximated expression of the (2–13) has been developed:

$$\frac{C_L}{\tau^{1.1}} = f\left(\lambda, C_V\right) \qquad \textbf{(2–14)}$$

With reference to Froude number effects, researchers[48] made the hypothesis that the (2–14) could be expressed as a sum of two terms:

$$\frac{C_L}{\tau^{1.1}} = f_1(\lambda) + f_2\left(\lambda, C_V\right) \qquad \textbf{(2–15)}$$

where $f_1(\lambda)$ was given by $f_1(\lambda) = A\lambda^{\alpha}$, and refers to the high speed planing condition, meanwhile the second term was related to the added force at low speed due to the hydrostatic pressure[49]:

$$f_2\left(\lambda, C_V\right) = B\frac{\lambda^2}{C_V^2} \qquad \textbf{(2–16)}$$

hence:

$$\frac{C_L}{\tau^{1.1}} = A\lambda^{\alpha} + B\frac{\lambda^2}{C_V^2} \qquad \textbf{(2–17)}$$

An early version of this formula has been proposed by Korvin-Kroukovsky [Korvin-Kroukovsky et al 1949]:

$$\frac{C_L}{\tau^{1.1}} = 0.0120\lambda^{1/2} + 0.0095\frac{\lambda^2}{C_V^2} \qquad \textbf{(2–18)}$$

Next step was the estimation of the Center of Pressure[50] position.

From a study of Sottorf's and Shoemaker's data, an empirical formula[51] was developed [Korvin-Kroukovsky et al 1949]:

---

[48] This hypothesis was first stated by Sedov [Sedov 1939] with the early hypothesis of hydrodynamic lift directly proportional to the trim angle τ.

[49] The added force to the hydrodynamic lift L_h, due to the hydrostatic pressure acting on a flat plate of length l, beam b, trim τ, and draft $h = l\sin\tau$, can be expressed as $L_h = \frac{1}{2}\rho g\left(l^2 b\sin\tau\right)$: the water weight "displaced" by the plate. The correction term to the coefficient lift can be obtained by dividing through by $\frac{1}{2}\rho V^2 b^2$; reminding the expressions of C_V and λ, we get: $C_{L_h} = \left(\lambda^2/C_V^2\right)\sin\tau$. In first rude approximation $\sin\tau \cong \tau^{1.1}$, we get: $C_{L_h}/\tau^{1.1} \cong \lambda^2/C_V^2$ [Korvin-Kroukovsky et al 1949].

[50] "*The Center of Pressure is defined as the point of intersection of the hydrodynamic force vector with the keel of a planing surface*" [Korvin-Kroukovsky et al 1949].

$$\frac{p}{l} = K\lambda^n \qquad \textbf{(2–19)}$$

where:

- p is the distance from the rear edge of a planing surface to the intersection point of the hydrodynamic force vector with the keel[52],
- l is the wetted length[53],
- K is a coefficient related to the trim τ : $K = 0.84/\tau^m$,
- n is a constant equal to -0.05,
- m is a constant equal to 0.125 .

The equations (2–8), $W = C_L\left(\frac{1}{2}\rho V^2\right)b^2$ (2–8) $\frac{C_L}{\tau^{1.1}} = 0.0120\lambda^{1/2} + 0.0095\frac{\lambda^2}{C_V^2}$, (2–19), define the empirical model of a planing flat plate.

With these equations we are able to evaluate the trim angle τ and the wetted length l_w of a planing flat plate, whereas the input data, pertinent to the plate, are: the weight W, the Center of Gravity position L_{CG}, the speed V and the beam b.

Computational Procedure

1° step: from the equation

$$W = C_L\left(\frac{1}{2}\rho V^2\right)b^2 \qquad (2–8)$$

we get the lift coefficient C_L:

$$C_L = \frac{W}{\left(\frac{1}{2}\rho V^2\right)b^2};$$

2° step: per each attempt value of trim angle τ, we calculate the ratio $C_L/\tau^{1.1}$;

3° step: from the equation

$$\frac{C_L}{\tau^{1.1}} = 0.0120\lambda^{1/2} + 0.0095\frac{\lambda^2}{C_V^2}$$

---

[51] Formula here reported was developed for a V-bottom planing surface [Korvin-Kroukovsky et al 1949]; coefficient values here reported has been calculated for deadrise angle null.

[52] The symbol *p* for the Center Pressure position is used by Korvin-Kroukovsky [Korvin-Kroukovsky et al 1949]. Nowadays for the Center Pressure position is used the symbol L_{CP}.

[53] The symbol *l* for the wetted length is used by Korvin-Kroukovsky [Korvin-Kroukovsky et al 1949]. Nowadays for the wetted length is used the symbol l_w, as well as L_W.

and by the evaluation of C_V, we get the ratio λ, as well as the wetted length l_w;

4° step: from the equation

$$\frac{p}{l} = K\lambda^n \qquad (2\text{–}19)$$

we get the center pressure position p (L_{CP});

5° step: if $p = L_{CG}$, or $(L_{CP} = L_{CG})$, we stop the procedure and τ and l_w are the values we were looking for, else we define a new attempt value for τ, go back to the second step and repeat the procedure again.

2.5.1.2 Flat planing plate: the theoretical model

The simplest surface planing model is the flat plate with infinite span planing on the surface of a perfect and incompressible fluid in the hypothesis of gravity effects negligible.

In the hypotheses of flat plate with infinite span $(b = \infty)$, the fluid flow field has the same characteristics (in terms of pressure distribution, as well as velocity field) in each longitudinal section[(54)]; thereby the fluid flow field evaluation under the planing plate, a 3-dimensional problem, is downsized to a 2-dimensional one: the evaluation of the fluid flow field in a longitudinal plane.

The hypothesis of perfect and incompressible fluid drive to a simplified form of the field equations: the 2-dimensional Laplace's equation[(55)].

The Laplace's equation, related to a 2-dimensional problem, can be solved in the complex plane.

This way of calculus, admitted only for 2-dimensional problems, allow us:

- reduce the number of variables connected to the problem (from two real to one complex) simplifying the math model;
- fit solutions available to the problem via geometrical transformations (mapping).

The hypothesis of gravity effects negligible is related to two assumptions:

- the sheet of spray, in the fore part of the planing plate, continues to infinity, where the streamlines[(56)] tend to become straight and parallel to the plate [Pierson & Leshnover 1948];

---

(54) A longitudinal section is obtained by the intersection of the flat plate with the longitudinal plane: the plane defined by the velocity vector of the fluid flow and the local vertical.

(55) See Appendix B "Continuity Equation and Laplace's Equation for a Perfect Fluid Flow".

- the plate is planing on still-water: no wave phenomena will be taken in account.

An important study on potential fluid flow properties of a planing surface has been developed by Wagner. He published an analytical solution of a 2-dimensional potential fluid flow based upon both Helmholtz-Kirchhoff method and conformal transformations in terms of Schwarz-Christoffel differential equation(57) [Wagner 1932].

The exposition of this brief work(58) of Wagner is not the goal of this Thesis, further a good exposition of Wagner's work on the matter has been already presented by Pierson [Pierson & Leshnover 1948].

Hereinafter a brief summary is proposed.

With reference to the following figures,

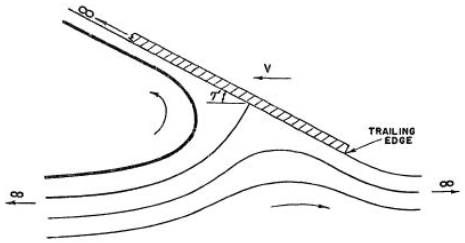

Figure 2.5-7 Flat plate planing at constant velocity V and at a fixed positive trim τ.
[Pierson & Leshnover 1948]

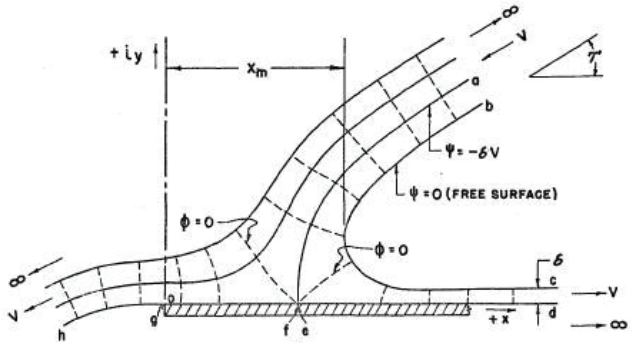

Figure 2.5-8 Flat plate planing, at constant velocity V and at a fixed positive trim τ, in the complex plane.
[Pierson & Leshnover 1948]

we get:

Free surface coordinates (bc curve):

---

(56) See footnote 31, Chapter 2.

(57) See Appendix C "The Conformal Transformations"

(58) Wagner's work is not user-friendly as matter of fact "*in many case Wagner was content to indicate merely the final results of a line of reasoning on a particular problem without presenting, in any degree of detail, the intermediate mathematical steps which are necessary*".[Pierson & Leshnover 1948]

$$\frac{x\pi}{\delta} = \frac{1}{1-\cos\tau}\left[(1+\xi)\cos\tau - (1-\cos\tau)\ln\left(\frac{\xi-1}{2}\right) + \pi\sin\tau\right]$$
$$\frac{y\pi}{\delta} = \frac{1}{1-\cos\tau}\left[\pi(1-\cos\tau) + \sqrt{\xi^2-1}\sin\tau + \sin\tau\ln\left(\xi+\sqrt{\xi^2-1}\right)\right] \quad \textbf{(2–20)}$$

with $\xi \in [1, +\infty[$

Free trailing surface coordinates (hg curve):

$$\frac{x\pi}{\delta} = \frac{1}{1-\cos\tau}\left[(1+\xi)\cos\tau - (1-\cos\tau)\ln\left(\frac{1-\xi}{2}\right)\right]$$
$$\frac{y\pi}{\delta} = \frac{1}{1-\cos\tau}\left[\sin\tau\ln\left(\sqrt{\xi^2-1}-\xi\right) - \sqrt{\xi^2-1}\sin\tau\right] \quad \textbf{(2–21)}$$

with $\xi \in]-\infty, -1]$

Flat plate surface coordinates (gd curve):

$$\frac{x\pi}{\delta} = \frac{1}{1-\cos\tau}\left[(1+\xi)\cos\tau - (1-\cos\tau)\ln\left(\frac{1-\xi}{2}\right) - \sqrt{1-\xi^2}\sin\tau\right]$$
$$\frac{y\pi}{\delta} = 0 \quad \textbf{(2–22)}$$

with $\xi \in [-1, +1]$

Spray root point coordinate

$$\frac{x_m \pi}{\delta} = \left[\frac{1+\cos\tau}{1-\cos\tau} - \ln\left(\frac{1-\cos\tau}{2\cos\tau} \right) + \frac{\pi \sin\tau}{1-\cos\tau} \right] \quad \textbf{(2–23)}$$

Speed on plate

$$u = V \left(\frac{\xi - \cos\tau}{1 - \xi\cos\tau + \sin\tau\sqrt{1-\xi^2}} \right) \quad \textbf{(2–24)}$$

with $\xi \in [-1, +1]$

Pressure coefficient

$$\frac{p}{\frac{1}{2}\rho V^2} = 1 - \left(\frac{\xi - \cos\tau}{1 - \xi\cos\tau + \sin\tau\sqrt{1-\xi^2}} \right)^2 \quad \textbf{(2–25)}$$

with $\xi \in [-1, +1]$

where

- p is the pressure at any point of the flow field,
- u is the component of the fluid velocity, at any point in the flow field, positive in the direction of the +x-axis,
- V is the magnitude of the field velocity,
- δ is the spray thickness at an infinite distance from the curved part of the free fluid surface,
- ρ is the mass density of incompressible fluid,
- τ is the trim angle: the angle between the fixed plane boundary and the direction of fluid velocity at an infinite distance upstream from the boundary,
- ξ is the real part of a complex number related to the conformal mapping procedure.

By the equations (2–22), (2–23), (2–25) it is possible to draw the pressure distribution on the flat plate per each value of trim τ.

Computational Procedure

1° step: let fix a value of trim τ;

2° step: let fix a set of *n* values of ξ in the range $[-1,+1]$: $\xi_0 = -1 < \ldots < \xi_n = +1$;

3° step: per each value of ξ and from the equations (2–22) and (2–23) we get $\frac{x\pi}{\delta}$, $\frac{x_m\pi}{\delta}$ and $\frac{x}{x_m}$;

4° step: per each value of ξ and from the equation (2–25) we get $\frac{p}{\frac{1}{2}\rho V^2}$

Now, per each value of trim τ, we have two functions: $\frac{x}{x_m} = f(\xi)$ and $\frac{p}{\frac{1}{2}\rho V^2} = g(\xi)$, with $\xi \in [-1,+1]$, by which is possible to draw the pressure distribution on the flat plate: $\frac{p}{\frac{1}{2}\rho V^2} = h\left(\frac{x}{x_m}\right)$.

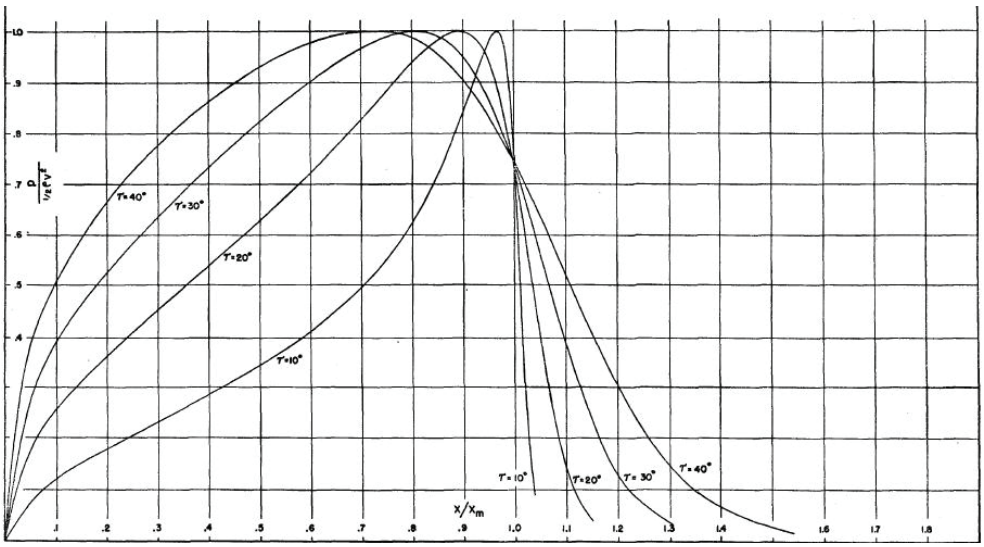

Figure 2.5-9 Variation with trim angle of pressure distribution over flat planing surface [Pierson & Leshnover 1948]

2.5.2 V-bottom surface model

This model of planing surface was easy to study as well as the flat plate: the additional difficulties related to a further parameter (the deadrise β) was balanced by the best performance in term of maneuvering as well as the lowest acceleration and stresses during the landing impact.

2.5.2.1 V-bottom surface: the empirical model

The equation (2–8), equilibrium condition between weight and hydrodynamic lift, has been developed for each kind of planing surface. For a V-bottom surface, the beam b is the distance between the chines[59] (lateral edges) and the coefficient lift C_L is a function further of the deadrise angle β:

$$C_L = C_L(\tau, \beta, \lambda, C_V) \qquad \textbf{(2–26)}$$

In order to establish an empirical equation which would express the relation (2–26) many tests were performed.

Most of them were conducted by Sottorf, Sambraus and Shoemaker, and reported in their early works, previously cited. Further tests have been developed by Korvin-Kroukovsky [Korvin-Kroukovsky et al 1949].

Despite of these, there were a lack of data: data available on V-bottom planing surfaces were much smaller than flat planing plate data. In order to overcome this lack of data, the flat plate was considered as a V-bottom with deadrise angle null, and the related test results were adopted as V-bottom ones.

Thereby, the evaluation of the empirical relationship between the five variables present in the (2–26) have been developed taking in account both the results available on flat planing plate by the equation $\frac{C_L}{\tau^{1.1}} = 0.0120\lambda^{1/2} + 0.0095\frac{\lambda^2}{C_V^2}$ (2–18) and the influence of the deadrise angle on the lift coefficient.

According to this way of work the relation (2–26) has been split into two formulas:

- the first, in which the lift coefficient, indicated with C_{L0}, is related to a flat plate with identical value of τ, λ, and C_V of the V-bottom surface: $C_{L0} = f(\tau, \lambda, C_V)$;
- the last, in which the lift coefficient of the V-bottom surface, indicated with $C_{L\beta}$[60], is related to the deadrise angle β, taking in account the lift coefficient value C_{L0} of the flat plate related to: $C_{L\beta} = f(C_{L0}, \beta)$.

From the $\frac{C_L}{\tau^{1.1}} = 0.0120\lambda^{1/2} + 0.0095\frac{\lambda^2}{C_V^2}$ (2–18) equation, the first formula is:

$$C_{L0} = \tau^{1.1}\left(0.0120\lambda^{1/2} + 0.0095\frac{\lambda^2}{C_V^2}\right) \qquad \textbf{(2–27)}$$

[59] Some authors are use to write B_C (*beam between the chines*) instead of b, to indicate the beam of a V-bottom surface as well as of a hull.

[60] Some Authors used to write C_{Lb} instead of $C_{L\beta}$.

meanwhile the second one, developed by the regression analysis of tests data available[61], is:

$$C_{L\beta} = C_{L0} - 0.0065\beta C_{L0}^{0.6} \qquad \textbf{(2–28)}$$

The Center of Pressure position of a V-bottom surface can be calculated by the equation [Korvin-Kroukovsky et al 1949]:

$$\frac{p}{l} = K\lambda^n \qquad \textbf{(2–19)}$$

where:

- p is the distance from the rear edge of a planing surface to the point of intersection of the hydrodynamic force vector with the keel[62],
- l is the wetted length[63],
- K is a coefficient related to the trim τ : $K = (0.84 + 0.015\beta)/\tau^m$,
- n is equal to: $-(0.05 + 0.01\beta)$,
- m is equal to: $0.125 + 0.042\beta$.

The equations (2–8), (2–19), (2–27), (2–28) define the empirical model of a V-bottom planing surface.

With these equations we are able to evaluate the trim angle τ and the wetted length l_w of a V-bottom planing surface, whereas the input data, related to the surface, are: the weight W, the Center of Gravity position L_{CG}, the speed V, the deadrise β and the beam b.

Computational Procedure

1° step: from the equation

$$W = C_L\left(\frac{1}{2}\rho V^2\right)b^2 \qquad \textbf{(2–8)}$$

we get the lift coefficient $C_{L\beta}$:

$$C_{L\beta} = \frac{W}{\left(\frac{1}{2}\rho V^2\right)b^2};$$

[61] For any further detail see Appendix E "Hydrodynamic Pressure Distribution Trends on a V-Bottom Planing Surface"

[62] See footnote 52.

[63] See footnote 53.

2° step: from the equation

$$C_{L\beta} = C_{L0} - 0.0065\beta C_{L0}^{0.6} \qquad \textbf{(2–28)}$$

we get the lift coefficient of the equivalent flat plate C_{L0};

3° step: per each attempt value of trim angle τ, we calculate the ratio $C_{L0}/\tau^{1.1}$;

4° step: from the equation

$$\frac{C_L}{\tau^{1.1}} = 0.0120\lambda^{1/2} + 0.0095\frac{\lambda^2}{C_V^2} \qquad \textbf{(2–18)}$$

and by the evaluation of C_V, we get the ratio λ, as well as the wetted length l_w;

5° step: from the relations

$$\frac{p}{l} = K\lambda^n \qquad \textbf{(2–19)}$$

$$K = \left(0.84 + 0.015\beta\right)/\tau^m$$

$$n = -\left(0.05 + 0.01\beta\right)$$

$$m = 0.125 + 0.042\beta$$

we get the center pressure position p (L_{CP});

6° step: if $p = L_{CG}$, or $\left(L_{CP} = L_{CG}\right)$, we stop the procedure and τ and l_w are the values we were looking for, else we define a new attempt value for τ and go back to the third step and repeat the procedure again.

It is important to highlight that the procedure to evaluate trim and wetted length for a flat plate can be obtained by the V-bottom one in the hypothesis of deadrise angle null.

2.5.2.2 V-bottom surface: the theoretical model

There have been developed different approaches to predict the fluid flow field under a V-bottom planing surface:

1. Added-Mass Planing Theory[64]
2. Conformal Mapping (Potential Theory)
3. Panel Method in Slender Body Hypothesis (Strip Theory)[65]

[64] The exposition of this Theory is not the goal of Thesis; for any further detail see Chapter 1, Paragraph 3, Sub-Paragraph 4.

[65] See above Footnote 64.

Conformal Mapping application to a V-bottom planing surface has been introduced by Wagner [Wagner 1932]. In his work Wagner adapted the conformal mapping theory applied to the planing flat plate (Schwarz-Christoffel differential equation under Helmholtz-Kirchhoff hypothesis) to the impacting wedge on a calm-water surface[66]. The exposition of this Wagner's work[67] is not a goal of this Thesis, further a good exposition of that work on the matter has been already presented by Pierson [Pierson 1948].

Further developments of this model have been formulated by Korvin-Kroukovsky [Korvin-Kroukovsky & Chabrow 1948] and Pierson [Pierson 1950].

Pierson's work is related to a V-bottom planing surface with not immersed chines and it is useful to describe the pressure distribution on the transversal sections associated to the area where the stagnation line works. Korvin-Kroukovsky's work is related to a V-bottom planing surface with immersed chines and is useful to describe the pressure distribution on the transversal sections associated to the abaft transversal sections [Kapryan & Boyd 1955].

The exposition of these works are not a goal of this Thesis. Hereinafter a brief summary is proposed.

2.5.2.2.1 V-bottom surface planing without immersed chines.

With reference to the following figures,

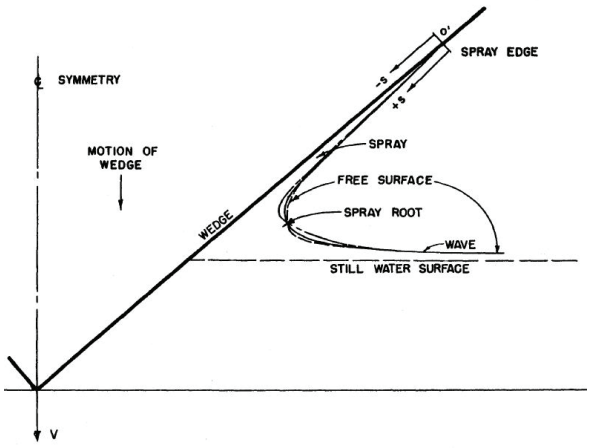

Figure 2.5-10 General shape of the free surface of a fluid due to penetration by a wedge [Pierson 1950]

(66) See Charter 1, Paragraph 3, Sub-Paragraph 4 of this Thesis.

(67) See Footnote 58.

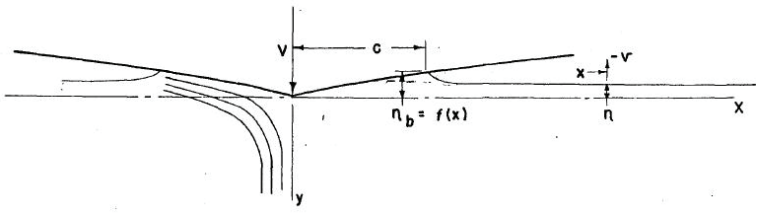

Figure 2.5-11 Expansion rate of the wetted width on a wedge [Pierson 1948]

we get:

Pressure coefficient

$$\frac{p}{\frac{1}{2}\rho V^2} = \left(\frac{\pi}{\tan\beta \cdot \sqrt{1-\frac{x^2}{c^2}}} - \frac{1}{\frac{c^2}{x^2}-1} + 1 \right) \quad \textbf{(2–29)}$$

with $0 \le x < c$ and $0 \le c < b/2$

Pressure coefficient on keel

$$\frac{p}{\frac{1}{2}\rho V^2} = \left(\frac{\pi}{2\tan\beta} \right)^2 \left[1 + 2\left(\frac{2\tan\beta}{\pi} \right)^2 \right] \quad \textbf{(2–30)}$$

Spray root point coordinate

$$\left(\frac{x_{SR}}{c} \right)^2 \cong \left(1 - \frac{\tan^2\beta}{2\pi^2} \right)^2 \quad \textbf{(2–31)}$$

with $0 \le c < b/2$.

Stagnation point coordinate

$$\frac{x_{SP}}{c} = \sqrt{1 - \left(\frac{2\tan\beta}{\pi} \right)^2} \quad \textbf{(2–32)}$$

with $0 \le c < b/2$.

Max Pressure coefficient

$$\frac{p_{\max}}{\frac{1}{2}\rho V^2} = \left(\frac{\pi}{2\tan\beta} \right)^2 + 2 \quad \textbf{(2–33)}$$

where

- b is the width of the wedge (beam),
- c is the wetted half-width,
- p is the pressure on the wedge,
- U is the magnitude of the fluid flow field velocity,
- $V = U\tan\tau$ is the penetration velocity of wedge,
- β is the deadrise angle,
- ρ is the mass density of incompressible fluid,
- τ is the trim of the V-bottom surface.

In order to develop a computational procedure, it is important to highlight that the ratio x/c is the geometrical input parameter for the pressure coefficient formula. This drives to a similarity in term of solutions: in two wedge sections with different value of c, for the same value of the ratio x/c, we get the same value of pressure coefficient. Thereby, in term of nondimensional coordinate x/c, we have to evaluate just one solution.

Computational Procedure

1° step: let fix a value for the trim τ, we have:

$$V = U \tan \tau \, ;$$

2° step: let fix a set of *n* values of x/c in the range $[0,1[$:

$$\left.\frac{x}{c}\right|_0 = 0 < \ldots < \left.\frac{x}{c}\right|_n = (1-\varepsilon), \text{ with } \varepsilon << 1$$

3° step: per each value $\left.\frac{x}{c}\right|_i$ with $i = 0,1,\ldots,n$ and from the equation (2–29) we get $\frac{p}{\frac{1}{2}\rho V^2}$

and the function $\frac{p}{\frac{1}{2}\rho V^2} = f\left(\frac{x}{c}\right)$ is known.

4° step: from the equations (2–30), (2–31), (2–32), (2–33), we get: the pressure coefficient on keel $\frac{p_{keel}}{\frac{1}{2}\rho V^2}$, the spray root point coordinate x_{SR}/c, the stagnation point coordinate x_{SP}/c, the max pressure coefficient $\frac{p_{\max}}{\frac{1}{2}\rho V^2}$.

2.5.2.2.2 V-bottom surface planing with immersed chines.

With reference to the following figures,

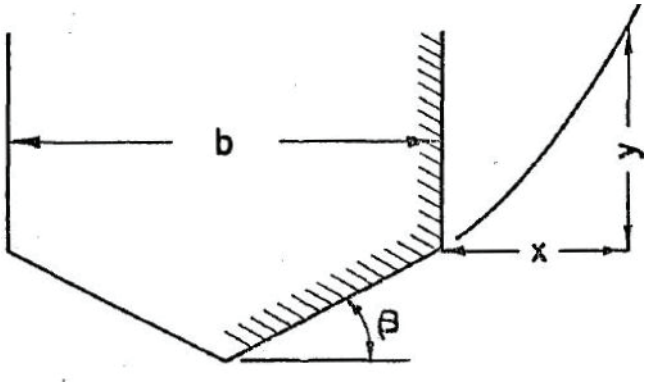

Figure 2.5-12 Shape of free streamline for immersed V-bottom surface [Korvin-Kroukovsky & Chabrow 1948]

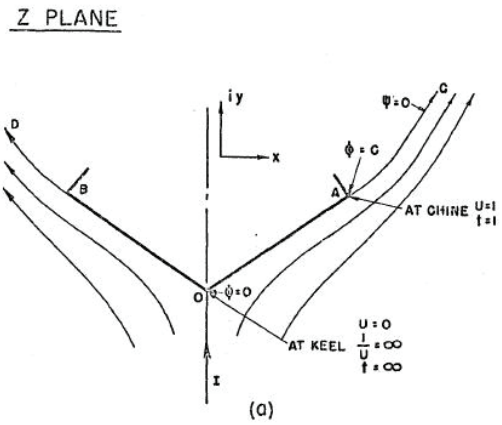

Figure 2.5-13 Immersed V-bottom surface in complex plane [Korvin-Kroukovsky & Chabrow 1948]

we get:

Pressure coefficient

$$\frac{p}{\frac{1}{2}\rho V^2} = 1 - \left(\frac{\cos\gamma}{1+\sin\gamma}\right)^{2n} \qquad \textbf{(2–34)}$$

with $n = 1 - 2\frac{\beta}{\pi}$ and $0 \le \gamma < \pi/2$

V-bottom surface coordinates (AO curve):

$$x = \frac{b}{2}\frac{\int_{\gamma}^{\frac{\pi}{2}} (1+\sin\gamma)^n (\cos\gamma)^{1-n} \sin\gamma \, d\gamma}{\int_{0}^{\frac{\pi}{2}} (1+\sin\gamma)^n (\cos\gamma)^{1-n} \sin\gamma \, d\gamma} \qquad \textbf{(2–35)}$$

with $n = 1 - 2\frac{\beta}{\pi}$ and $0 \le \gamma < \pi/2$.

where

- b is the width of the wedge (beam),
- c is the wetted half-width,
- p is the pressure on the wedge,
- U is the magnitude of the fluid flow field velocity,
- $V = U\tan\tau$ is the penetration velocity of wedge,
- β is the deadrise angle,
- γ is the real number related to the conformal mapping procedure.
- ρ is the mass density of incompressible fluid,
- τ is the trim of the V-bottom surface.

Computational Procedure

1° step: let fix a value for the trim τ:

$$V = U\tan\tau;$$

2° step: let fix a set of n values of γ in the range $\left[0, \frac{\pi}{2}\right[$:

$$\gamma_0 = 0 < \ldots < \gamma_n = \left(\frac{\pi}{2} - \varepsilon\right), \text{ with } \varepsilon << 1$$

3° step: per each value of γ and from the equation (2–35) we get x;

4° step: per each value of γ and from the equation (2–34) we get $\frac{p}{\frac{1}{2}\rho V^2}$.

Now we have, per each value of trim τ, two functions: $x = f(\gamma)$ and $\frac{p}{\frac{1}{2}\rho V^2} = g(\gamma)$, with $\lambda \in \left[0, \frac{\pi}{2}\right[$, by which is possible to draw the pressure coefficient distribution on each side of the wedge: $\frac{p}{\frac{1}{2}\rho V^2} = h(x)$.

Potential methods for V-bottom surface, here exposed, are not quite manageable, and give us just an idea of how fluid works. With these methods it is not possible to evaluate the equilibrium set of a V-bottom planing surface: these are not useful tools in a design procedure.

In order to overcome this problem Smiley [Smiley 1951] proposed a method for computing the pressure distribution on a V-bottom planing surface using potential methods [Kapryan & Boyd 1955]; this method is based on the idea that the longitudinal pressure distribution on the keel is equal to the equivalent flat plate[(68)] one meanwhile the transverse pressure distributions are computed by Pierson and Korvin-Kroukosvky potential methods with the constrain that the pressure value on the keel related to this transverse distribution is equal to the pressure value on that transversal section due to the longitudinal one.

In this method the instantaneous velocities, the trim, the deadrise angle and the wetted length are known [Smiley 1951], thereby further this method is not useful.

2.5.3 Monohedral hull model: an empirical way

This is the closest model to a hull surface available to investigate the hydrodynamic planing process of a planing boat.

No theoretical model has been developed yet: all model available are based on basin test results.

Despite of the large number of tests developed, there were a lack of data: data available on monohedral hull model were much smaller than data pertinent to the planing surfaces (V-bottom planing surfaces as well as flat planing plate).

(68) Flat plate with the same trim τ and the same wetted length l_w of the V-bottom planing surface.

In order to overcome this lack of data, the planing surface formulas were adopted in these models: some of them have been modified in order to take in account the effects of the transom and the sides[69].

A first attempt to develop a procedure for predicting the planing performance of a monohedral hull was made by Murray [Murray 1950], based on Sottorf's work [Sottorf 1932] and Korvin-Kroukovsky's work [Korvin-Kroukovsky et al 1949] on planing surfaces. In that model, except for the trust, all forces pass through the Center of Gravity, the trust is parallel to the keel and the equilibrium equation of the pitching moment is an identity always satisfied. That model were improved by other authors until Savitsky's model [Savitsky 1964] has been introduced. Later, other methods[70] have been proposed, but the most popular is till now the Savitsky's method[71].

All these methods have been developed "forcing" airfoil results, flat planing plate results, as well as V-bottom planing surface ones, into the monohedral planing hull model. These results have been "weighted", in the hull model, by empirical coefficients related to the planing test results on monohedral hull, V-bottom planing surfaces as well as flat planing plate.

2.5.3.1 The Murray's model

The exposition of Murray's method is not a goal of this Thesis. Hereinafter a brief summary is proposed.

Per each value of speed V and per each defined value of trim τ, we get the longitudinal Center of Pressure position L_{CP} and the bare hull resistance R_H; so, per each value of speed V, we can draw two diagram on the same abscissa τ, as shown in the next figure:

---

[69] The effects of transom and sides are: the buoyancy force, not much negligible at low value of Froude number, and the friction force on these surfaces.

[70] For any further detail see Chapter 1, Paragraph 3, Sub-Paragraph 4.2 .

[71] Hereinafter we will use the words "model" as well as "method" with the same meaning: the amount of formulas and diagrams, arranged in a procedure and useful to predict the hydrodynamic field under the planing hull.

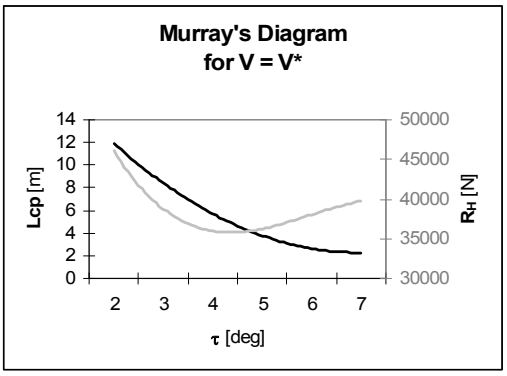

Figure 2.5-14 Example of Murray's diagram for the speed V*

In order to get the resistance value R_H related to the speed V* we start from the equilibrium condition: $L_{CP} = L_{CG}$, where L_{CG} is known. By the diagram, we get the equilibrium value of τ*, at speed V*, as shown in Figure 2.5-15;

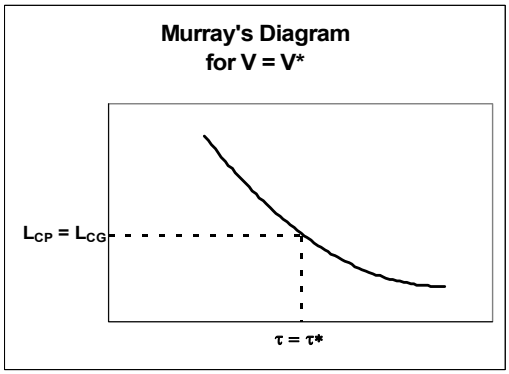

Figure 2.5-15 Murray's diagram: determination of the equilibrium trim angle τ*

by the knowledge of τ* we get the value of resistance R_H related to, as shown in Figure 2.5-16.

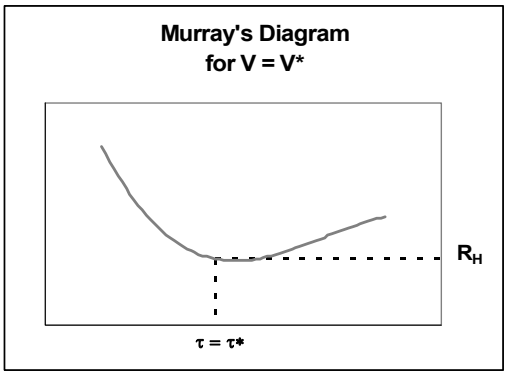

Figure 2.5-16 Murray's diagram: determination of the resistance R_H

Computational Procedure

1° step: Let V the speed of the craft, from the equation

$$W = C_L\left(\frac{1}{2}\rho V^2\right)b^2 \qquad \textbf{(2–8)}$$

we get the lift coefficient $C_{L\beta}$:

$$C_{L\beta} = \frac{W}{\left(\frac{1}{2}\rho V^2\right)b^2};$$

2° step: from the equation

$$C_{L\beta} = C_{L0} - 0.0065\beta C_{L0}^{0.6} \qquad \textbf{(2–28)}$$

we get the lift coefficient of the equivalent flat plate C_{L0};

3° step: per each attempt value of trim angle τ, we calculate the ratio $C_{L0}/\tau^{1.1}$;

4° step: from the equation

$$\frac{C_L}{\tau^{1.1}} = 0.0120\lambda^{1/2} + 0.0095\frac{\lambda^2}{C_V^2} \qquad \textbf{(2–18)}$$

and by the evaluation of C_V, we get the ratio λ, as well as the wetted length L_w;

5° step: from the relations

$$\frac{p}{l} = K\lambda^n \qquad \textbf{(2–19)}$$

$$K = \left(0.84 + 0.015\beta\right)/\tau^m$$

$$n = -\left(0.05 + 0.01\beta\right)$$

$$m = 0.125 + 0.042\beta$$

we get the center pressure position p (L_{CP}) and l is the wetted length L_W;

6° step: by the knowledge of L_W, we get the Reynolds number:

$$R_N = \frac{VL_W}{\nu}$$

7° step: by the knowledge of R_N, we get the friction coefficient C_f via Schoenherr's formula:

$$C_f^{-0.5} = 4.13 \cdot \log_{10}\left(C_f Rn\right)$$

8° step: by the knowledge of L_W, we get the wetted surface S_W:

$$S_W = \frac{L_W b}{\cos\beta}$$

9° step: by the knowledge of C_f, we get the friction load D_F:

$$D_F = \frac{1}{2}\rho V^2 S_W \left(C_f + \Delta C_f\right)$$

where ΔC_f is the increment of the friction coefficient due to the rough of the surface[72].

10° step: by the Sottorf's formula, we get the bare hull resistance of R_H:

$$R_H = W \tan\tau + \frac{D_F}{\cos\tau}$$

11° step: by the knowledge of L_{CP} and R_H per each value of τ, let draw the Murray's diagram related to the speed V.

12° step: by the equilibrium condition $L_{CP} = L_{CG}$ we get the equilibrium trim angle τ^* and the bare hull resistance R_H, related to.

13° step: repeat this procedure per each value of design speed (e.g.: V_{CRUISE} and V_{MAX}).

[72] In literature: $\Delta C_f = 0.0004$.

2.5.3.2 The Savitsky's model

At present, the two fundamental Savitsky's methods are:

- the Short Form Method (SF),
- the Long Form Method (LF).

In the SF method, per each value of trim τ, all forces pass through Center of Gravity and the equilibrium equation of the pitching moment is an identity always satisfied, as shown below:

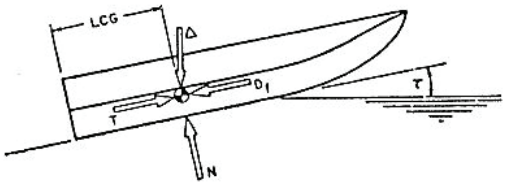

Figure 2.5-17 Equilibrium planing condition in the Savitsky's Short Form Method[73] [Savitsky 1964]

In the LF method the gravity is the only force that passes through Center of Gravity for each trim τ, meanwhile there is one and only one value of the trim angle $\tau*$ corresponding to, all forces pass through the Center of Gravity and the equilibrium equation of the pitching moment is satisfied, as shown in the beneath figure:

[73] LEGEND:
- Δ weight of boat [N]
- D_f viscous drag component (assumed as acting parallel to keel line, midway between keel and chine lines) [N]
- N pressure resultant force acting normal to bottom [N]
- T propeller thrust [N]
- CG Center of Gravity of the craft
- LCG longitudinal distance of CG from the transom (measure along the keel) [m]
- τ trim angle of keel [deg]

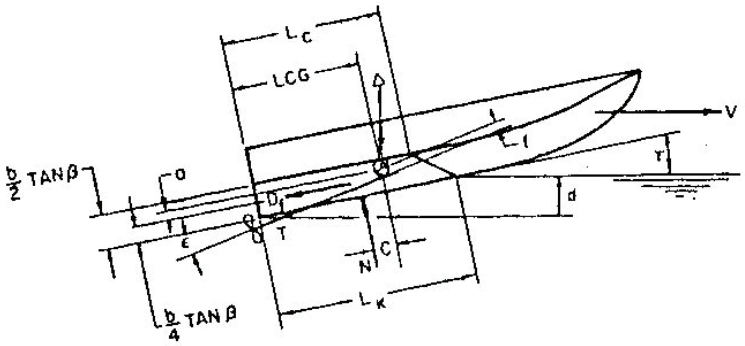

Figure 2.5-18 Equilibrium planing condition in the Savitsky's Long Form Method(74) **[Savitsky 1964]**

The equilibrium equations are:

vertical

$$\Delta = N\cos\tau + T\sin(\tau+\varepsilon) - D_f\sin\tau \qquad \textbf{(2–36)}$$

horizontal

$$T\cos(\tau+\varepsilon) = D_f\cos\tau + N\sin\tau \qquad \textbf{(2–37)}$$

pitching moment

$$N\cdot c + D_f\cdot a - T\cdot f = 0 \qquad \textbf{(2–38)}$$

By the vertical equilibrium equation we get the load N, meanwhile from the horizontal one we get the thrust T:

$$N = \frac{\Delta - T\sin(\tau+\varepsilon) + D_f\sin\tau}{\cos\tau} \qquad \textbf{(2–39)}$$

---

(74) LEGEND:

- Δ weight of boat [N]
- D_f viscous drag component (assumed as acting parallel to keel line, midway between keel and chine lines) [N]
- N pressure resultant force acting normal to bottom [N]
- T propeller thrust [N]
- CG Center of Gravity of the craft
- LCG longitudinal distance of CG from the transom (measure along the keel) [m]
- c distance between N and CG (measured normal to N) [m]
- a distance between D_f and CG (measured normal to D_f) [m]
- f distance between T and CG (measured normal to T) [m]
- L_C wetted chine length [m]
- L_K wetted keel length [m]
- ε thrust line inclination relative to keel line [deg]
- d draft of keel at transom [m]
- V planing speed [m/s]
- τ trim angle of keel [deg]
- β deadrise angle [deg]
- b beam [m]

$$T = \frac{\Delta \sin \tau + D_f}{\cos \varepsilon} \qquad \textbf{(2–40)}$$

These results and the knowledge of distances versus the Center of Gravity, allow us to compute the equilibrium trim angle τ* by the pitching moment equilibrium equation.

Results obtained by these two methods are quiet lower than those measured in towing tests. This is due to approximations[75] related to viscous phenomena, as well as the use of same empirical coefficients[76].

Murray's method and SF method have the same procedure in order to compute the bare hull resistance: the main differences are pertinent to the lift coefficient as well as to the Center of Pressure position formulas.

With reference to the coefficient lift C_L, Savitsky improved the precision of the Korvin-Kroukovsky formula

$$\frac{C_L}{\tau^{1.1}} = 0.0120\lambda^{1/2} + 0.0095\frac{\lambda^2}{C_V^2}$$

taking in account the "splash-up" phenomena[77]: during the planing the water rises above the still-water level in the fore part of the planing surface, and this rise is greatest for a flat planing plate [Payne 1994].

The formula, proposed by Savitsky [Savitsky & Neidinger 1954], was:

$$\frac{C_L}{\tau^{1.1}} = 0.0120\lambda^{1/2} + 0.0055\frac{\lambda^{5/2}}{C_V^2} \qquad \textbf{(2–41)}$$

and since than, no other corrections, based on new test results, have been proposed.

With reference to the longitudinal position of the Center of Pressure, Savitsky improved the precision of the Korvin-Kroukovsky formula

$$\frac{p}{l} = K\lambda^n \qquad \textbf{(2–19)}$$

"forcing" on the airfoil result[78] a correction[79] related to the planing surfaces:

---

[75] See Appendix F "The Savitsky's method approximations"

[76] These coefficients are computed by a regression analysis of test results on elementary planing surfaces as flat plate or V-bottom surfaces. The hydrodynamic behaviour of these surfaces is close but not equal to the monohedral one, due to the effects of transom and sides. These differences rise up for the non monohedral hull forms.

[77] In order to evaluate a more correct expression for the added force L_h, a new expression has been proposed: $L_h = \frac{1}{2}\rho g b^3 (\lambda - 0.30)^2 \tan\tau$. Assuming that $(\lambda - 0.30)^2 \cong D\lambda^n$ and $\tan\tau \cong \tau^{1.1}$, a new correction term to the coefficient lift has been obtained: $C_{L_h}/\tau^{1.1} \cong D\lambda^n/C_V^2$, and by the analysis of planing data available, the value of D and n has been evaluated: $C_{L_h}/\tau^{1.1} \cong 0.0055\lambda^{5/2}/C_V^2$ [Savitsky & Neidinger 1954].

$$C_P = 0.75 - \frac{1}{5.21\frac{C_V^2}{\lambda^2} + 2.39} \qquad \textbf{(2–42)}$$

where

$$C_P = \frac{l_p}{\lambda b} \qquad \textbf{(2–43)}$$

"*is the ratio of the longitudinal distance from the transom to the Center of Pressure divided by the mean wetted length.*" [Savitsky 1964]

Savitsky SF: Computational Procedure

1° step: Let V the speed of the craft, from the equation

$$W = C_L\left(\frac{1}{2}\rho V^2\right)b^2 \qquad \textbf{(2–8)}$$

we get the lift coefficient $C_{L\beta}$:

$$C_{L\beta} = \frac{W}{\left(\frac{1}{2}\rho V^2\right)b^2};$$

2° step: from the equation

$$C_{L\beta} = C_{L0} - 0.0065\beta C_{L0}^{0.6} \qquad \textbf{(2–28)}$$

we get the lift coefficient of the equivalent flat plate C_{L0};

3° step: per each attempt value of trim angle τ, we calculate the ratio $C_{L0}/\tau^{1.1}$;

4° step: from the equation

$$\frac{C_L}{\tau^{1.1}} = 0.0120\lambda^{1/2} + 0.0055\frac{\lambda^{5/2}}{C_V^2} \qquad \textbf{(2–41)}$$

---

(78) "*The aerodynamic center of most commonly used wing sections is found to be approximately the quarter-chord point at speeds where the velocity of sound is not reached in the field of flow.*" [Abbott & von Doenhoff 1959]
On an airfoil the distances are measured along the chord starting from the leading edge, and the center of a pressure distribution is at 25% of the chord length from the leading edge or, in equivalent way, at 75% of the chord length from the trailing edge.
For a planing surface the leading edge is unknown so all distances are measured from the trailing edge, and the mean wetted length l_w is adopted as the "chord length".

(79) In this formula it is clearly highlighted that the Center of Pressure of a hull is beyond the theoretical position for an airfoil, and this gap is related to the geometrical and kinematical characteristics of the planing hull.

and by the evaluation of C_V, we get the ratio λ, as well as the wetted length L_w;

5° step: from the relations

$$C_P = 0.75 - \frac{1}{5.21\frac{C_V^2}{\lambda^2} + 2.39} \qquad \textbf{(2–42)}$$

we get the center pressure position C_P (L_{CP});

6° step: by the knowledge of L_W, we get the Reynolds number:

$$R_N = \frac{VL_W}{\nu}$$

7° step: by the knowledge of R_N, we get the friction coefficient C_f via Schoenherr's formula:

$$C_f^{-0.5} = 4.13 \cdot \log_{10}\left(C_f Rn\right)$$

8° step: by the knowledge of L_W, we get the wetted surface S_W:

$$S_W = \frac{L_W b}{\cos\beta}$$

9° step: by the knowledge of C_f, we get the friction load D_F:

$$D_F = \frac{1}{2}\rho V^2 S_W\left(C_f + \Delta C_f\right)$$

10° step: by the Sottorf's formula, we get the bare hull resistance of R_H:

$$R_H = W\tan\tau + \frac{D_F}{\cos\tau}$$

11° step: by the knowledge of L_{CP} and R_H per each value of τ, let draw the diagram related to the speed V.

12° step: by the equilibrium condition $L_{CP} = L_{CG}$ we get the equilibrium trim angle τ* and the bare hull resistance R_H, related to.

13° step: repeat this procedure per each value of design speed (e.g.: V_{CRUISE} and V_{MAX}).

Savitsky LF: Computational Procedure

1° step: Let V the speed of the craft, from the equation

$$W = C_L\left(\frac{1}{2}\rho V^2\right)b^2 \qquad \textbf{(2–8)}$$

we get the lift coefficient $C_{L\beta}$:

$$C_{L\beta} = \frac{W}{\left(\frac{1}{2}\rho V^2\right)b^2};$$

2° step: from the equation

$$C_{L\beta} = C_{L0} - 0.0065\beta C_{L0}^{0.6} \qquad \textbf{(2–28)}$$

we get the lift coefficient of the equivalent flat plate C_{L0};

3° step: per each attempt value of trim angle τ, we calculate the ratio $C_{L0}/\tau^{1.1}$;

4° step: from the equation

$$\frac{C_L}{\tau^{1.1}} = 0.0120\lambda^{1/2} + 0.0055\frac{\lambda^{5/2}}{C_V^2} \qquad \textbf{(2–41)}$$

and by the evaluation of C_V, we get the ratio λ, as well as the wetted length L_w;

5° step: from the relations

$$C_P = 0.75 - \frac{1}{5.21\frac{C_V^2}{\lambda^2} + 2.39} \qquad \textbf{(2–42)}$$

we get the center pressure position C_P (L_{CP});

6° step: by the knowledge of L_W, we get the Reynolds number:

$$R_N = \frac{VL_W}{\nu}$$

7° step: by the knowledge of R_N, we get the friction coefficient C_f via Schoenherr's formula:

$$C_f^{-0.5} = 4.13 \cdot \log_{10}\left(C_f Rn\right)$$

8° step: by the knowledge of L_W, we get the wetted surface S_W:

$$S_W = \frac{L_W b}{\cos\beta}$$

9° step: by the knowledge of C_f, we get the friction load D_F:

$$D_F = \frac{1}{2}\rho V^2 S_W\left(C_f + \Delta C_f\right)$$

10° step: by the Sottorf's formula, we get the bare hull resistance of R_H:

$$R_H = W \tan\tau + \frac{D_F}{\cos\tau}$$

11° step: by the knowledge of L_{CP} and L_{CG} we get:

$$c = L_{CG} - L_{CP}$$

12° step: by the knowledge of b, β and V_{CG}, in first approximation, we get:

$$a = V_{CG} - \frac{b}{4}\tan\beta$$

13° step: by the knowledge of *f*, it is possible to compute the pitching moment around the Center of Gravity CG:

$$M = N \cdot c + D_f \cdot a - T \cdot f$$

14° step: if $M = 0$ we stop the procedure with τ and R_H as the equilibrium values we were looking for, else we define a new attempt value for τ and go back to the third step and repeat the procedure again.

2.6 Symbols

a	Distance of CG from the line of D_F	[m]
A, B, C, D, n	Empirical coefficients	
AR	Aspect Ratio	$AR = \frac{b^2}{S_W} = \frac{b}{l_W} = \frac{1}{\lambda}$
b	Hull beam	[m]
B_C	Beam between the chines	[m]
c	Distance of CG from the line of N	[m]
C_f	Friction coefficient	
CG	Center of Gravity	
C_L	Lift coefficient	
C_{Lb}, $C_{L\beta}$	Lift coefficient of a V-bottom surface	$C_{Lb} \equiv C_{L\beta} = \frac{W}{\frac{1}{2}\rho V^2 S_W}$
C_{L_h}	Coefficient lift related to the added force L_h	
C_{L0}	Lift coefficient of a flat plate equivalent to a V-bottom surface	
C_V	Froude number related to the beam b	$C_V = \frac{V}{\sqrt{gb}}$
d, h	Draft	[m]
D_F	Friction force	[N]
f	Distance of CG from the line of T	[m]
F	Hydrodynamic force acting on the wetted planing surface	[N]
F_{nb}	Froude number related to the beam b	$F_{nb} \equiv C_V$
g	Gravitational acceleration	$9.81 m/s^2$
k	Nondimensional coefficient	
K	Coefficient related to the trim	
L	Hydrodynamic Lift	[N]
L_c	Wetted length on chines	[m]
L_{CG}	Center of Gravity position measured from the transom	[m]
L_{CP}	Center Pressure position measured from the transom	[m]

L_h	Added force to the hydrodynamic lift due to the hydrostatic pressure	[N]
L_k	Wetted length on keel	[m]
LF	Long Form	
lw, L_W	Mean wetted length	[m]
M	Pitching moment around the CG of the hull	[Nm]
N	Normal component of the resultant of the pressure distribution acting on the wetted surface of the plate	[N]
Nv	Horizontal component of N	[N]
R	Hull resistance	[N]
R_H	Bare hull resistance	[N]
Rn	Reynolds number	
SF	Short Form	
S_W	Wetted surface of a planing surface	$\left[m^2\right]$
T	Thrust force	[N]
V	Speed craft	$\left[m/s\right]$
V_{CRUISE}	Hull Cruising speed	$\left[m/s\right]$
V_{MAX}	Hull Max speed	$\left[m/s\right]$
W, Δ	Hull weight	[N]
z	Vertical distance below the water surface.	[m]
α	Stagnation line angle	[deg]
β	Deadrise angle	[deg]
θ	Spray edge angle	[deg]
ε	Propeller inclination	[deg]
λ	Mean wetted length-beam ratio	$\lambda = \frac{lw}{b}$
ν	Kinematic viscous coefficient	
Π	Plane of symmetry	
ρ	Fluid density	$\left[\frac{kg}{m^3}\right]$
τ	Trim angle	[deg]

2.7 References

Abbott, H. I. & Doenhoff, A. E. 1959. *THEORY OF WING SECTIONS*. New York (USA): Dover Publications ISBN 0-486-60586-8

Chambliss, D.B. & Boyd, G.M. Jr. 1953. The Planing Characteristics of Two V-Shaped Prismatic Surfaces Having Angles of Dead Rise of 20° and 40°. *Report NACA TN 2876.* Washington, D.C. (USA). (web site: http://ntrs.nasa.gov/search.jsp)

Kapryan, W.J. & Boyd, G.M. Jr. 1955. Hydrodynamic Pressure Distributions Obtained During a Planing Investigation of Five Related Prismatic Surfaces. *Report NACA TN 3477.* Washington, D.C. (USA). (web site: http://ntrs.nasa.gov/search.jsp)

Korvin-Kroukovsky B.V. & Chabrow, F.R. 1948. The Discontinuous Fluid Flow Past an Immersed Wedge. *Report SIT-DL-48-9-334 Davidson Laboratory* Stevens Institute of Technology. Hoboken, New Jersey (USA)

Korvin-Kroukovsky B.V., Savitsky D., Lehman W.F. 1948. Wave Contours in the Wake of a 20° Deadrise Planing Surface. *Report SIT-DL-48-337 Davidson Laboratory* Stevens Institute of Technology. Hoboken, New Jersey (USA)

Korvin-Kroukovsky B.V., Savitsky D., Lehman W.F. 1949. Wetted Area and Center of Pressure of Planing Surfaces. *Report SIT-DL-49-9-360 Davidson Laboratory* Stevens Institute of Technology. Hoboken, New Jersey (USA)

Miranda, S. 2001 *Appunti di Architettura Navale*. Napoli: Dipartimento di Ingegneria Navale, Università degli Studi di Napoli "FEDERICO II" (Italian language - web site: http://wpage.unina.it/miranda/)

Murray, A.B. 1950. The hydrodynamic of Planing Hulls. *New England SNAME Meeting 1950.* Jersey City (USA): SNAME

Payne P.R. 1988. *Design of High-Speed Boats: Planing*. Annapolis(USA): Fishergate Publishing Company Inc. ISBN 0942720067.

Payne P.R. 1994. The water rise in front of a model planing hull. *Experiments in Fluids,* Vol.17, Issue 1-2, pp. 96-104. Berlin (Germany): Springer-Verlag. ISSN 0723-4864.

Pierson, J.D. 1948. On the Pressure Distribution for a Wedge Penetrating a Fluid Surface. *Report SIT-DL-48-6-366 Davidson Laboratory* Stevens Institute of Technology. Hoboken, New Jersey (USA)

Pierson, J.D. 1950. The Penetration of a Fluid Surface by a Wedge. *Report SIT-DL-50-381 Davidson Laboratory* Stevens Institute of Technology. Hoboken, New Jersey (USA)

Pierson, J.D. & Leshnover S. 1948. An Analysis of the Fluid Flow in the Spary Root and Wake Regions of Flat Planing Surfaces. *Report SIT-DL-48-335 Davidson Laboratory* Stevens Institute of Technology. Hoboken, New Jersey (USA)

Pierson, J.D. & Leshnover S. 1950. A Study of the Flow, Pressures, and Loads Pertaining to Prismatic Vee-Planing Surfaces. *Report SIT-DL-50-382 Davidson Laboratory* Stevens Institute of Technology. Hoboken, New Jersey (USA)

Rosén, A. 2004. *Loads and Responses for Planing Craft in Waves*. PhD Thesis. Naval Systems Division, Aeronautical and Vehicle Engineering Dept., Royal Institute of Technology KTH (Kungliga Tekniska Högskolan), Stockholm, Sweden. ISBN 91-7283-936-8

Russo Krauss, G. 1994. *NAVI A SOSTENTAMENTO IDRODINAMICO*. Parte Prima. Napoli: Dipartimento di Ingegneria Navale, Università degli Studi di Napoli "FEDERICO II" Italy. (Italian language).

Savitsky, D. 1964. Hydrodynamic Design of Planing Hull. *Marine Technology*, Vol.1, No.1, Jersey City (USA): SNAME

Savitsky, D. & Neidinger, J.W. 1954. Wetted Area and Center of Pressure of Planing Surfaces at Very Low Speed Coefficients. *Report SIT-DL-54-493 Davidson Laboratory* Stevens Institute of Technology. Hoboken, New Jersey (USA)

Savitsky, D. 2003. ON THE SUBJECT OF HIGH-SPEED MONOHULLS. *Proceedings of Symposium SNAME Greek Section*. October 2, 2003. Athens, Greece.

Savitsky, D., DeLorme M.F., Datla R. 2006. Inclusion of "Whisker Spray" Drag in Performance Prediction Method for High-Speed Planing Hulls. *Report SIT-DL-06-9-2845 Davidson Laboratory* Stevens Institute of Technology. Hoboken, New Jersey (USA)

Sedov, L.I. 1939. Scale Effect and Optimum Relations for Sea Surface Planing. *Report n.409 Central Aero-Hydrodynamical Institute.* Moskva. [English version: Scale Effect and Optimum Relations for Sea Surface Planing. *Report NACA TM 1097*, 1947. Washington, D.C. (USA). (web site: http://ntrs.nasa.gov/search.jsp)]

Smiley, R.F. 1951. A Semiempirical Procedure for Computing the Water-Pressure Distribution on Flat and V-Bottom Prismatic Surfaces During Impact or Planing. *Report NACA TN 2583.* Washington, D.C. (USA). (web site: http://ntrs.nasa.gov/search.jsp)

Sottorf, W. 1932. Versuche mit Gleitflächen. *Werft-Reederei-Hafen,* pp 285-290 October 1932; pp 43-47 February 1933; pp 61-66 March 1933. [English version: Experiments with Planing Surfaces. *Report NACA TM 739*, 1934. Washington, D.C. (USA). (web site: http://ntrs.nasa.gov/search.jsp)]

Sottorf, W. 1937. Analyse experimenteller Untersuchungon über den Gleitvorgang an der Wasseroberfläche. *Jahrbuch der deutschen Luftfahrtforschung,* pp 320-339. [English version: Analysis of Experimental Investigations of the Planing Process on the Surface of the Water. *Report NACA TM 1061*, 1944. Washington, D.C. (USA). (web site: http://ntrs.nasa.gov/search.jsp)]

Wagner, H. 1932. Über Stoss und Gleitvorgänge an der Oberfläche von Flüssigkeiten. *Z.A.M.M*. No.4 Vol.12. [English version: Phenomena associated with Impacts and Sliding on liquid surfaces. *Report NACA TR N-23507*, 1936. Washington, D.C. (USA). (web site: http://ntrs.nasa.gov/search.jsp)]

Zucrow, M.J. & Hoffman, J.D. 1976. *Gas Dynamics*. Vol I. Hoboken (NJ): John Wiley & Sons (USA) ISBN: 978-0-471-98440-5

CHAPTER 3

THE ANALYTICAL SEMI-EMPIRICAL METHOD

In recently years the demand for better seakeeping performances of planing hulls has led to prefer non-monohedral hull forms and, despite the hypothesis of monohedral hull form is not satisfied, Savitsky's methods are still widely used. The results are consequently affected by errors due to wrong assessment of both hydrodynamic lift and Center of Pressure position. [Bertorello & Oliviero 2007 - ①]

The application of Savitsky's method to more realistic hull forms, with deadrise angle varying along to the hull length, is considered in this chapter.

3.1 Table of Contents

3.2 Introduction

Despite the method is based on a simplified geometry, Savitsky's method has proven effective and has been widely used until nowadays.

The hypothesis of constant deadrise has proven not too much restrictive as long as deep V hulls with strictly monohedral afterbody were used.

Recently years the demand for better seakeeping performances of planing hulls combined with the availability of higher power/weight ratios of main engines and with lower structural weight has led to prefer non-monohedral hull forms.

Although this geometry is noticeably different from the V plate on which has been developed, the Savitsky method is still widely used, sometimes referring to a conventional deadrise value[80] [Bertorello & Oliviero 2007 - ①].

This type of simplified assumption can be effective for hydrodynamic lift assessment, provided an appropriate conventional deadrise value has been chosen, but does not result in the true value of the Center of Pressure longitudinal position that is strictly connected to the deadrise values along the ship length.

The conventional value, typically, gives a position of the Center of Pressure much more forward than it really is.

The consequent longitudinal trim is higher than that one observed in the reality. The total resistance evaluation is not correct and approximate in excess. [Bertorello & Oliviero 2007 - ①]

[80] A common value used is the deadrise angle at the L_{CG} [Savitsky et al 2006]

3.3 The Savitsky's method: an attempt of extension

The goal to achieve is the extension of the Savitsky's method to non-monohedral hull form.

Hereinafter the superposition principle is applied to the pressure distribution of the fluid flow field related to the non-monohedral planing hull.

The hull is divided into a number of transversal elements (strips) characterized by a constant value deadrise and beam between the chines: the pressure distribution will be the sum of the contributes due to each element.

In despite Savitsky's method is not able to compute the pressure distribution, we are able to evaluate a few parameters related to, as the ratio L_{CP}/L_{ws} .

The superposition principle will be applied to this ratio: the L_{CP}/L_{ws} value pertinent to the hull will be the weighted sum of the ratio value related to each element.

Each ratio value will be computed via Savitsky's method meanwhile the weight will be calculated by Wagner's analytical solutions [Wagner 1932] of Laplace's equation related to that element.

In this way Savitsky's method is deeply integrated with Wagner's solutions and the result is an Analytical Semi-Empirical Method (ASEM). [Bertorello & Oliviero 2007 - ②]

Each strip of the non-monohedral hull is related to a Finite Prismatic Hull and a Planing Flat Plate.

Finite Prismatic Hull (FPH) is a monohedral hull with the same value of: weight W, lengths (L_{OA}, L_{PP}) and CG position of the non-monohedral hull and with the same deadrise angle of the strip related to.

The L_{CP}/L_{ws} value of each element is evaluated via Savitsky's method applied to the FPH related to.

At the same time, the normalized pressure distribution of a Planing Flat Plate, with the same speed and trim of the FPH related to, will be evaluated.

Hereinafter a *normalized pressure distribution* is a 2D dimensionless pressure distribution on a flat plate, where the dimensionless abscissa is the longitudinal

position[81] versus the wetted length, and the dimensionless ordinate is the ratio of the coefficient pressure[82] versus its maximum value along the plate.

By the knowledge of Wagner's solution it is possible to draw the normalized pressure distribution on the Planing Flat Plate.

At the same time, the longitudinal strip position along the hull can be done dimensionless via the ratio versus the wetted length of the FPH related to.

Thereby, the value of the normalized pressure evaluated in the dimensionless abscissa equal to the dimensionless longitudinal strip position, is the "weight" related to that strip.

The ratio L_{CP}/L_{ws} computed is that of a monohedral hull equivalent to the non-monohedral one in term of pressure distribution.

From this data it is possible to evaluate all other information required in a resistance assessment design process by an inverse Savitsky's method application.

[81] Measured from the trailing edge along the plate.

[82] The coefficient pressure is the ratio of the pressure versus the theoretical dynamic component $\left(\frac{1}{2}\right)\rho V^2$.

3.4 ASEM Method: physical model and base hypothesis

3.4.1 Physical model

The physical model of a non-monohedral planing hull is not much different qualitatively from the typical one of a planing V plate: the streamlines below the bottom are mainly in aft direction developed and present a transversal component toward the after part of the hull[83].

It is common practice to divide the flow field around the hull into two components: the longitudinal one aligned with the motion direction and the transversal one, with vertical component in opposite direction to the gravity force.

Further, the velocity field can be assumed as sum of two components: one (known) associated to the asymptotic fluid flow[84] and one (unknown) pertinent to the planing surface and known as perturbation velocity field.

The hypothesis of body slenderness and the smallness of surge perturbation speed allow us to consider the flow field around the hull as sum of transverse fields[85] [Munk 1924].

With these assumptions the longitudinal flow field can be considered as relative to a plane plate with angle of incidence different from zero, meanwhile the transverse flow field is considered as relative to the field around a wedge with zero lift angle[86].

3.4.2 Base hypothesis

Despite in ASEM Savitsky's method is deeply integrated with Wagner's solution, the base hypothesis of the ASEM are not simply the sum of both base hypothesis.

---

[83] In the hypothesis of planing surface with a diametrical plane (longitudinal plane of symmetry) and of rectilinear motion with velocity vector on this plane of symmetry, the fluid flow field under the planing surface is composed by two parts -one per each side of the hull- symmetrically versus the diametrical plane of the hull. Hereinafter, whereas clearly not explained in a different manner, the fluid flow field described is related to a generically one side of the hull.

[84] In equivalent manner, the known component of the speed is the speed of the craft.

[85] In this case, the fluid flow field is the sum of the transversal component related to each transversal section, and no mutual interaction, due to the deadrise variation, is taken in account.

[86] The ways to attack this problem have been described in the Chapter 1, Paragraph 3, Sub-Paragraph 4, as well as in Chapter 2, Paragraph 3, Sub-Paragraph 2.2.

ASEM base hypothesis are composed by three groups of hypothesis and each one works in a different manner.

The first group, which is related to the Savitsky's method, take in account some restrictions of the Towing Test results:

- $\beta \leq 30\,\text{deg}$
- $2\,\text{deg} \leq \tau \leq 15\,\text{deg}$
- $\lambda \leq 4.0$
- $0.60 \leq C_V \leq 13.00$
- Single chine with sharp edge chines at the intersection of the bottom and sides,
- Transom stern - wide transom with a sharp trailing edge,
- No convex surfaces,
- Calm water,
- Uniform straight motion,
- Friction effects out the pressure area negligible - Spray sheet and wake effects neglected,

which define limitations on:

- hull geometry (max deadrise angle),
- hull shape (max mean wetted length, single chine, transom stern, no convex surface),
- planing conditions (min-max trim, min-max Froude number, calm water, uniform straight motion, partial friction effects).

The second group, which is related to the Wagner's method, take in account some limitations of the Potential Theory:

- Incompressible Perfect fluid - frictionless fluid,
- Gravitational effects negligible - high Froude number.

This second group define the applicability of Wagner's solutions: friction, turbulence and wave effects are not taken in account.

These effects are not negligible in the boundary layer, in the spray sheet and in the wake. But reminding the goal to achieve -the evaluation of each strip "weight" in term of Center Pressure position-, as well as the limitation of Potential Theory, we are able to neglect gravitational and viscous effects at all. Hence spray sheet and wake are not taken in account, as well as the viscous effects in the boundary layer.

The third group is strictly related to the ASEM:

- Smallness of surge perturbation speed,
- Superposition Principle applicable.

These hypothesis define the applicability of ASEM: the contribution to the center pressure position of each strip does not depend by the contribution of the other ones. This allow us to consider the contribution of each strip separately: every pressure perturbation due to the longitudinal deadrise rate has not been take in account.

3.5 ASEM Procedure[87]

Here and after, Savitsky's Long Form method will be used.

1° step

The hull, between perpendicular, is divided into N transversal elements.

With reference to a standard system of coordinates with x axis aligned along the keel and oriented toward the bow, the generic i-th element is defined by the transverse plans Π_i, with abscissa x_i, and Π_{i+1}, with abscissa x_{i+1}.

The generic i-th element will be characterized by an average abscissa

$$x_i^* = \frac{x_i + x_{i+1}}{2} \qquad \textbf{(3–1)}$$

and by a constant deadrise angle

$$\beta_i = \beta\left(x_i^*\right) \qquad \textbf{(3–2)}$$

2° step

Let introduce the Finite Prismatic Hull related to the i-th element of non-monohedral hull, $(FPH)_i$,as the monohedral hull with the same value of weight W, lengths (L_{OA}, L_{PP}) and CG position of the non-monohedral hull and with the same deadrise angle β_i of the strip related to.

$\forall i = 1,2,...,N$, Savitsky's method is applied to $(FPH)_i$.

It is defined *n* as the minimum value of *i* index which satisfies: $L_{ws,n+1} > x_{n+1}^*$.

All sections with index $m > n$ are ignored as they do not contribute to hydrodynamic lift.

3° step

$\forall i = 1,2,...,n$ the following quantities are known:

[87] Presented at the High-Performance Marine Vehicles Conference 2006 and published on the Australian Journal of Mechanical Engineering. Here reported in Reference as [Bertorello & Oliviero 2007 - ①]

$$\left.\begin{matrix}\beta_i \\ x_i^*\end{matrix}\right\} \rightarrow \text{ from hull geometric characteristics,}$$

$$\left.\begin{matrix}\tau_i \\ L_{ws,i} \\ L_{CP,i}\end{matrix}\right\} \rightarrow \text{ by Savitsky's method applied to } (FPH)_i.$$

4° step

$\forall i = 1,2,...,n$ we consider a planing plate with incidence angle τ_i.

Applying the conformal mapping based on Schwarz-Christoffel differential equations, we can determine the function:

$$C_{p,i} = C_{p,i}\left(\frac{x}{L_{ws,i}}\right) \qquad \textbf{(3–3)}$$

As matter of the fact, we have:

$$C_{p,i} = \frac{p}{\frac{1}{2}\rho V^2} = 1 - \left(\frac{\xi - \cos\tau_i}{1 - \xi\cos\tau_i + \sin\tau_i\sqrt{1-\xi^2}}\right)^2 \qquad \textbf{(3–4)}$$

$$\frac{x}{L_{ws,i}} \cong \frac{x}{x_m}\bigg|_i = \frac{x\pi}{\delta}\bigg|_i \frac{\delta}{x_m\pi}\bigg|_i \qquad \textbf{(3–5)}$$

where

$$\frac{x\pi}{\delta}\bigg|_i = \frac{1}{1-\cos\tau_i}\left[(1+\xi)\cos\tau_i - (1-\cos\tau_i)\ln\left(\frac{1-\xi}{2}\right) + \right. \\ \left. - \sqrt{1-\xi^2}\sin\tau_i - \sin\tau_i \arccos\xi + \pi\sin\tau_i\right] \qquad \textbf{(3–6)}$$

$$\frac{x_m\pi}{\delta}\bigg|_i = \left[\frac{1+\cos\tau_i}{1-\cos\tau_i} - \ln\left(\frac{1-\cos\tau_i}{2\cos\tau_i}\right) + \frac{\pi\sin\tau_i}{1-\cos\tau_i}\right] \qquad \textbf{(3–7)}$$

with $\xi \in [-1,1]$.

In the above formulas δ is a motion field characteristic dimension and ξ is an arbitrary variable in conformal mapping.

Despite the analytical form of the (3–3) is unknown, we are able to evaluate its values: for each value of ξ there is one point on the flat plate, with dimensionless abscissa $\frac{x}{L_{ws,i}}$, and with the value of $C_{p,i}$ related to.

5° step

$\forall i = 1,2,...,n$, the functions $C_{p,i} = C_{p,i}\left(\frac{x}{L_{ws,i}}\right)$ and their maximum values $C_{p,i}^{\max}$, have been calculated.

Their normalized values evaluated in x_i^* can be determined and the function:

$$C_{p,i}^{norm} = \frac{C_{p,i}\left(\frac{x_i^*}{L_{ws,i}}\right)}{C_{p,i}^{\max}} \qquad \textbf{(3–8)}$$

can be evaluated.

The value of this function in the way of i-th element represents the "weight" of the contribute of this element to the hydrodynamic lift for a hull with constant deadrise β_i.

6° step

The value $\frac{L_{CP}}{L_{ws}}$ of the examined hull has been obtained as averaged weight of the determined values $C_{p,i}^{norm}$, $\forall i = 1,2,...,n$ as shown in the following formula:

$$\frac{L_{CP}}{L_{ws}} = \frac{\sum_{i=1}^{n} \frac{L_{CP}}{L_{ws}}\Big|_i C_{p,i}^{norm}}{\sum_{i=1}^{n} C_{p,i}^{norm}} \qquad \textbf{(3–9)}$$

7° step

When determined $\frac{L_{CP}}{L_{ws}}$ through B_C (projected beam at chine that is considered constant), the factor λ and the wetted length L_{ws} can be calculated according to Savitsky's method:

$$\frac{L_{CP}}{L_{ws}} = 0.75 - \frac{1}{5.21\left(\frac{Cv}{\lambda}\right)^2 + 2.39} \qquad \textbf{(3–10)}$$

and

$$L_{ws} = \lambda B_C \qquad \textbf{(3–11)}$$

it follows:

$$L_{CP} = \frac{L_{CP}}{L_{ws}} \lambda B_c \qquad \textbf{(3–12)}$$

and

$$\frac{C_{LO}}{\tau^{1.1}} = 0.012\lambda^{0.5} + 0.0055\frac{\lambda^{2.5}}{C_v^2} \qquad \textbf{(3–13)}$$

8° step

Savitsky's procedure is applied again. A first tentative value for the longitudinal trim angle τ is fixed and C_{LO} is obtained by $\frac{C_{LO}}{\tau^{1.1}}$.

When C_{LO} and $C_{L\beta}$ are known, the deadrise angle β of the equivalent hull can be determined and, by the Sottorf formula, the bare hull total resistance R_H can be evaluated. In fact when β and τ are known it is possible to evaluate $\Delta\lambda$, and then λ_F, Rn, S_{WL}, D_F and R_H.

The equilibrium condition on which Savitsky's procedure is based can be verified. If the values of the determined forces do not verify the equilibrium a new value for τ is fixed and the process is continued to convergence.

9° step

The first tentative value for τ can be obtained using the position:

$$C_{L0} = 1.1 \cdot C_{L\beta} \qquad \textbf{(3–14)}$$

and then by $\frac{C_{LO}}{\tau^{1.1}}$.

3.6 Limitations

A first limitation is associated to the deadrise angle.

It is not possible to take in account the contribution of strips with deadrise angle greater than 30 degree. It drives to an approximation on the resistance value and the error pertinent to depends by the extension of the pressure area which transversal sections have a deadrise angle greater than 30 deg.

A second limitation is associated to the longitudinal deadrise angle rate.

A small and constant value of the longitudinal deadrise angle rate allows us to neglect the longitudinal pressure perturbation related to. The approximations linked to this rate are on the contribution as well as on the "weight" of each strip. Further it is not possible to evaluate the error related to, due to the lack of data available. By the way, the surge perturbation speed is strictly related to the longitudinal deadrise angle rate: higher rate higher surge perturbation speed so the first hypothesis on the applicability of ASEM is not satisfied.

Another limitation is associated to the hull shape: steps, redan, notches, appendages, spray rails or transversal deadrise angle variation can not be taken in account.

At the end a last consideration: the most of models used in towing tests were made by ply-wood.

In all resistance assessment methods the fluid flow field under a planing hull is evaluated in steady condition considering the hull as a rigid body: no hydro-elastic[88] behavior contribution of the hull is taken in account.

At the same time the empirical coefficients of these methods -evaluated via regression analysis of towing test results- take in account the hydro-elastic contribution of the models.

Thereby:

- resistance assessment methods take in account, in an implicit way, the hydro-elastic contribution of the model via empirical coefficients,
- resistance assessment methods do not take in account the hydro-elastic contribution of the real hull,

[88] If the hull is an elastic body, during the planing its shape, keel curvature as well as local deadrise angle, will change. It drives to a fluid flow field variation under the hull, which will drive to a further variation of the hull shape. If these changes are time dependent, inertial effects have to be taken in account.

- models and real hulls have a different dimensions, inertial and mass distribution as well as different structures and materials, that drives to a different hydro-elastic behavior.

It is not possible to evaluate the error related to due to the lack of data available.

3.7 Symbols

b	Hull Beam	[m]
B_C	Beam between the chines	[m]
CG	Center of Gravity	
C_L	Lift coefficient	
$C_{L\beta}$	Lift coefficient of a V-bottom surface	$C_{L\beta} = \frac{W}{\frac{1}{2}\rho V^2 S_W}$
C_{L0}	Lift coefficient of a flat plate equivalent to a V-bottom surface	
C_P	Pressure Coefficient	$C_P = C_P(x) = \frac{p}{\frac{1}{2}\rho V^2}$
$C_P^{\max}$	Max value of a pressure coefficient distribution	
C_P^{norm}	Normalized pressure coefficient	$C_P^{norm} = \frac{C_P\left(\frac{x^*}{L_{ws}}\right)}{C_P^{\max}}$
C_V	Froude number related to the beam b	$C_V = \frac{V}{\sqrt{gb}}$
D_F	Friction force	[N]
FPH	Finite Prismatic Hull	
i	Index	
L_{CG}	Center of Gravity position measured from the transom	[m]
L_{CP}	Center Pressure position measured from the transom	[m]
LF	Long Form	
L_{PP}	Length between perpendicular	[m]
L_{OA}	Length Over All	[m]
L_{ws}	Mean wetted length	[m]
$L_{ws,i}$	Mean wetted length of the FPH related to i-th element	[m]
R	Hull resistance	[N]
p	Measured pressure	[MPa]
m	Index	
n	Index	
N	Number of elements	
R_H	Bare hull resistance	[N]
Rn	Reynolds number	
SF	Short Form	

S_W	Wetted surface of a planing surface	$\left[m^2\right]$
V	Craft Speed	$\left[m/s\right]$
W	Craft Weight	[N]
x	Axis aligned along the keel and oriented toward the bow	
x_i	Abscissa of i-th transversal section of the hull	[m]
x_i^*	Average abscissa of i-th element	[m]
x_m	Spray root point abscissa of a flat plate planing	[m]
β	Deadrise angle	[deg]
δ	Motion field characteristic dimension	[m]
$\Delta\lambda$	Mean wetted length-beam ratio variation due to the spray sheet	$\Delta\lambda = \Delta\lambda(\beta, \tau)$
λ	Mean wetted length-beam ratio	$\lambda = \frac{lw}{b}$
λ_F	Corrected Mean wetted length-beam ratio	$\lambda_F = \lambda + \Delta\lambda$
π	Pi	3.1415….
Π	Plane of symmetry	
ρ	Fluid density	$\left[kg/m^3\right]$
τ	Trim angle	[deg]
ξ	Arbitrary variable in conformal mapping	

3.8 References

Bertorello, C. & Oliviero, L. 2007. ①. Hydrodynamic Resistance Assessment of Non-Monohedral Planing Hull Forms based on Savitsky's Method. *Australian Journal of Mechanical Engineering,* Vol. 4 No.2, pp 209-224. Engineers Media, CROWS NEST, Australia. (ACN001311511).

Bertorello, C. & Oliviero, L. 2007. ②. Planing hull hydrodynamics. A critical review of the state of the art in theoretical resistance assessment. *Proceeding 12th Conference of International Maritime Association of the Mediterranean (IMAM 2007)*, Vol. 1, pages 13-19. Varna, Bulgaria. ISBN-13 987-0-415-45521-3

Munk, M. 1924. Notes on the Pressure Distribution Over the Hull of Elongated Airship with Circular Cross Section. *Report NACA TN 192* Washington, D.C. (USA). (web site: http://ntrs.nasa.gov/search.jsp)

Savitsky, D. 1964. Hydrodynamic Design of Planing Hull. *Marine Technology*, Vol.1, No.1, Jersey City (USA): SNAME

Savitsky, D., DeLorme M.F., Datla R. 2006. Inclusion of "Whisker Spray" Drag in Performance Prediction Method for High-Speed Planing Hulls. *Report SIT-DL-06-9-2845 Davidson Laboratory* Stevens Institute of Technology. Hoboken, New Jersey (USA)

Wagner, H. 1932. Über Stoss und Gleitvorgänge an der Oberfläche von Flüssigkeiten. *Z.A.M.M.* No.4 Vol.12. [English version: Phenomena associated with Impacts and Sliding on liquid surfaces. *Report NACA TR N-23507*, 1936. Washington, D.C. (USA). (web site: http://ntrs.nasa.gov/search.jsp)]

CHAPTER 4

ASEM: APPLICATIONS AND COMPARISONS

Analytical Semi-Empirical Method has been developed in order to predict Resistance and Power performance versus hull speed related to a warped bare monohull.

In this chapter, ASEM will be applied to a few hull forms, which towing tank test results are available, in order to check reliability and efficiency.

Further, Savitsky‘s method will be applied too, in order to get an overall comparison.

4.1 Table of Contents

4.2 Figure Index

4.3 Table Index

4.4 Introduction

In early ‘70s, Savitsky [Savitsky et al 1972] proposed a hull form for fast monohull, with:

- wide transom,
- warped planing surface (longitudinal and transversal deadrise angle variations),
- double chine,
- fine bow lines.

Despite good results obtained with two different hull prototypes [Blount & Hankley 1976], this way was not started due to the level of building technologies available [Grigoropoulos 2004].

Since early 90’s, with the new available technologies, this hull form has been adopted more and more often. Further this new hull form has been developed in various versions: with or without spray rails and/or steps.

Despite of this large use of warped hulls, there is a lack of data on deep planing condition about them, and the few data available are not related to a systematic series.

Further, no semi-empirical method have been developed or adapted to this hull form yet.

4.5 Comparison with a Systematic Series results

A first attempt to check reliability and efficiency of ASEM has been developed keeping in account test results, pertinent to systematic series of planing hull as well as Towing Tests.

Hereinafter ASEM and Savitsky's results, without physical meaning, have not been taken in account (i.e.: results related to a mean wetted length higher than hull length overall), meanwhile results with physical meaning coupled with data out of range (i.e.: results associated to a mean wetted length/beam ratio higher than four times) have been reported with dash line in diagrams or in red color in tables of results.

4.5.1 Introduction

In order to get the best resistance performance, many systematic series of fast monohull have been developed and tested [Grigoropoulos 2004]:

- KTH/NSMB Series of round-bilge and hard-chines hull, developed in SSPA Towing Tank [Nordstrom 1951, Lindgren et al 1969]
- Series 62 single chine [Clement & Blount 1963]
- Series 63 [Beys 1963]
- Series 64 [Yeh 1965, Clement 1964]
- Series 65 [Holling & Hubble 1974]
- NPL Series of round-bilge hulls [Bailey 1976]
- NRC Series of Naval Ships [Schmitke et al 1979, Murdey & Simoes Re 1985]
- Deep-V single chine base on Series 62 [Keuning & Gerritsma 1982]
- HSVA C' Series [Kracht and Grim 1960]
- NSMB Series of round-bilge, semi-displacement hullforms [Oossanen & Pieffers 1984]
- YP Series [Compton 1986]
- VTT Series [Lahtiharju et al 1991]
- NTUA Series [Grigoropoulos & Loukalis 1999]

whereas, for the most of them, “fast” means *not displacement vessels* instead of *planing vessels:* the most of them are semi-displacement hullforms tested up to planing speed.

Other series of planing hulls, BK as well as MBK series, have been developed and tested [Voitkounski 1985]. These are not systematic series. Meanwhile BK tests data are not available anymore [Radojcic 1985], same test results, in form of diagrams, are quite available in literature.

At the same time, in order to estimate the resistance in the preliminary design phase, many semi-empirical methods have been developed [Grigoropoulos 2004]:

- Savitsky’s method for prismatic hull [Savitsky 1964, Savitsky & Brown 1976]
- Van Oortmerssen method [Van Oortmerssen 1971]
- Egorov method [Voitkounski 1985]
- Mercier & Savitsky method [Mercier & Savitsky 1973]
- Tang method [Ping-Zhong et al 1980]
- Holtrop method [Holtrop 1984]
- Radojcic method [Radojcic 1985]
- Compton method [Compton 1986]

Despite of all these are based on model test results, only a few of them are based on systematic experimental data.

4.5.2 Systematic Series 62

4.5.2.1 Description of models and tests [Clement & Blount 1963]

Series 62 is composed by five hull models with different length-beam ratio value:

Table 4.5-1 Series 62: geometrical characteristics

Model	L_{OA} [ft]	L_P / B_{PX}	
4665	4.0	2.00	
4666	6.0	3.06	
4667-1	8.0	4.09	Parent Model
4668	8.0	5.50	
4669	8.0	7.00	

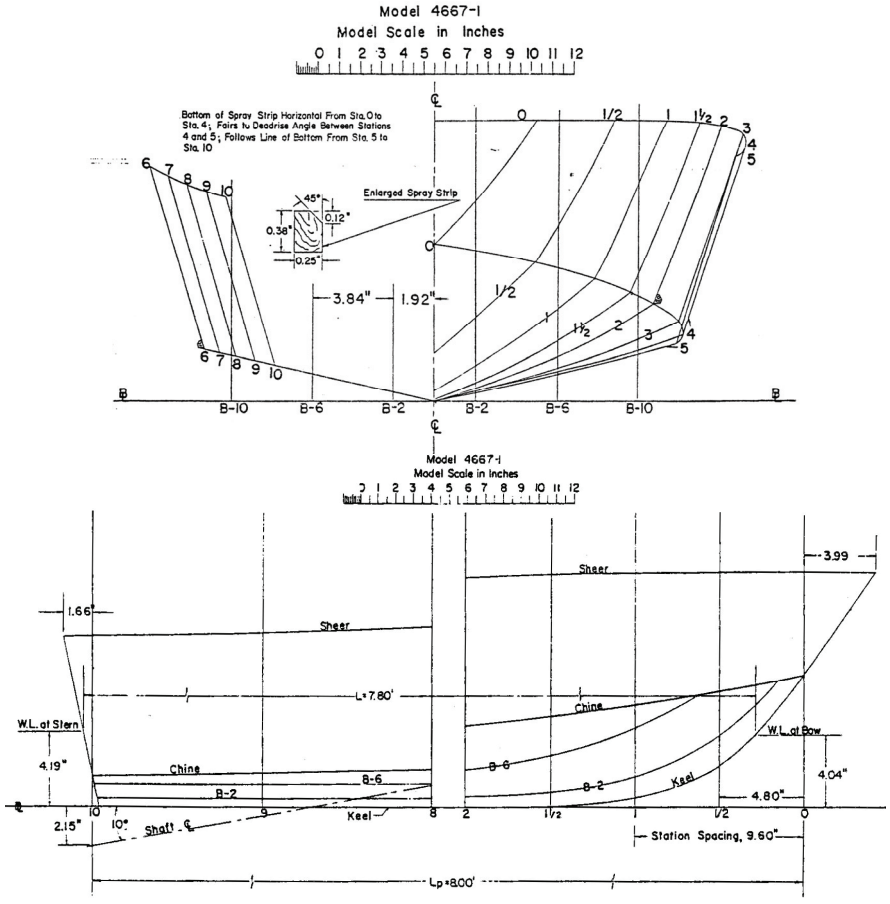

Figure 4.5-1 Body plan and end profile of parent model 4667-1

The four additional models of the series were derived from the parent by maintaining the same shape of body plan but adjusting the station spacing and the size of the body plan to give the different length-beam ratio desired.

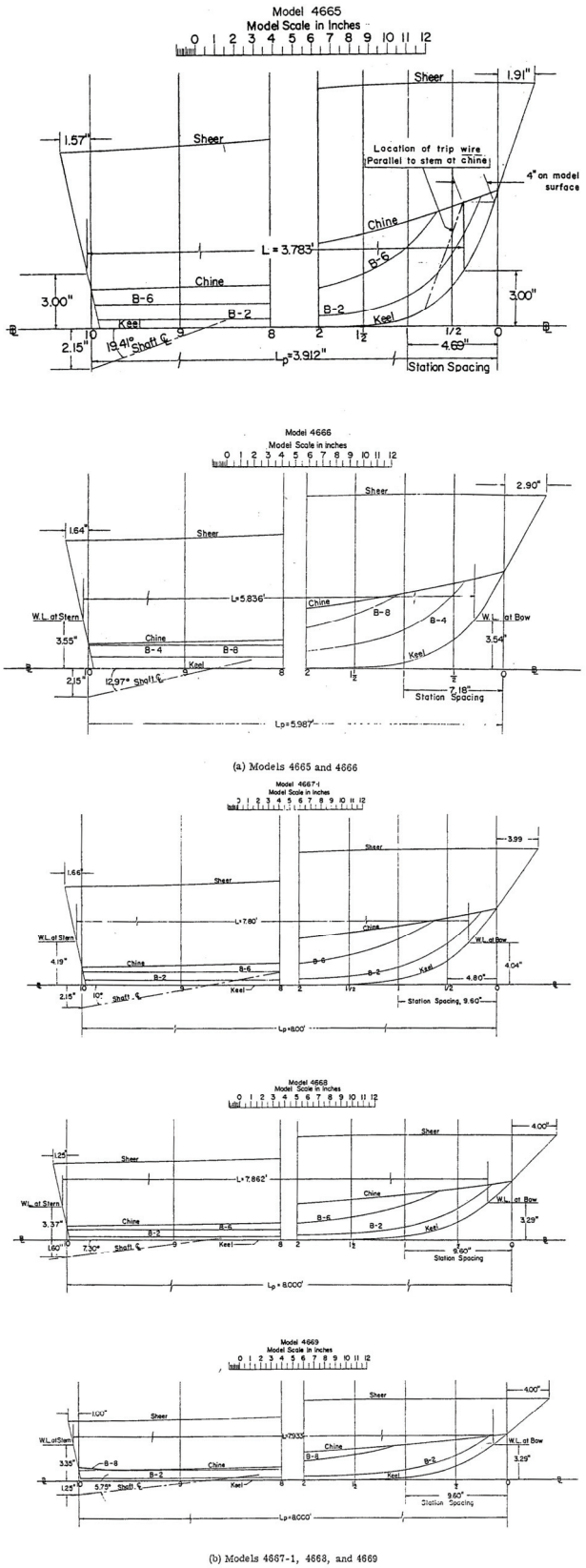

Figure 4.5-2 Bow and stern endings of five model of series

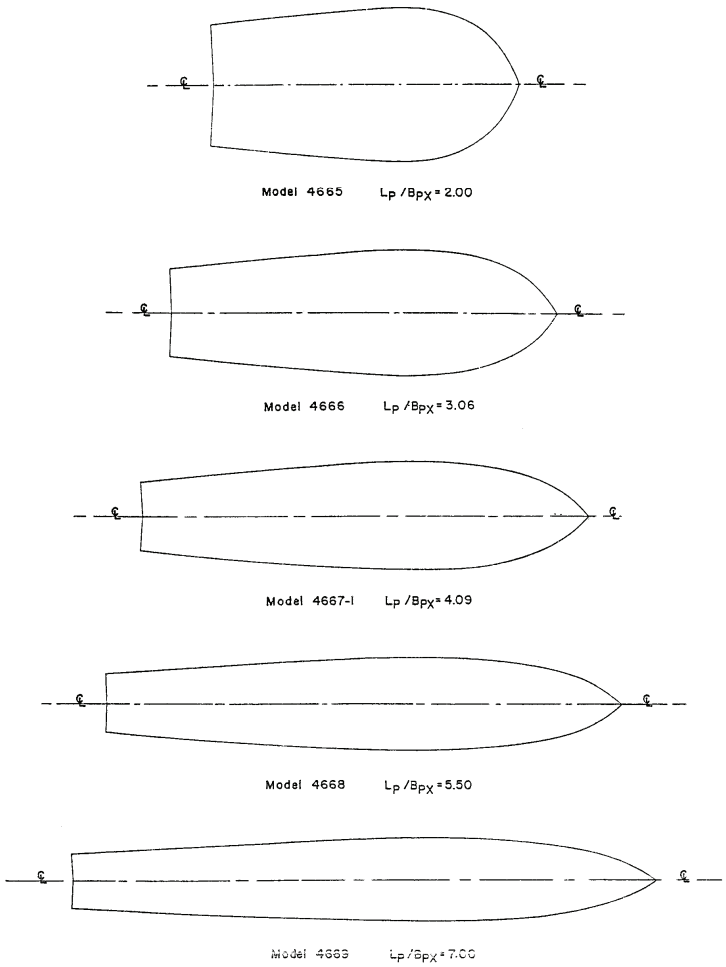

Figure 4.5-3 Chine lines in plan view of five model of series

All models have the same following characteristics:

- deadrise angle value of 12.5 deg, at transom,
- deadrise angle constant in the afterward part of the hull,
- stern narrow, with transom width equal to 65% of max chine width,
- bow sections convex.

The parent model was made of fiberglass and plastic meanwhile the remaining models were of wood.

Models have been tested for resistance at a number of loads and longitudinal Center of Gravity locations, at David Taylor Model Basin.

In term of Fn_{∇}, the speed range was about 0.2 up to 6.0, and not all tests have been developed up to planing condition; the L_{CG} locations were 0, 4, 8 and 12 percent L_P aft of the centroid of the projected planing bottom area.

Per each model seventeen test cases has been developed, in order to investigate semi-displacement condition performance as well as planing condition ones.

4.5.2.2 Results Comparison

Detailed comparison analysis of results is available in Appendix G of this Thesis. Hereinafter a briefly synthesis has been reported.

In order to get a comparison among data related to planing condition, tests developed only up to semi-displacement condition (in term of volumetric Froude number $Fn_{\nabla} \leq 3$) have not been taken in account.

Data comparison has been developed with reference to Resistance and Power trends related to hull speed.

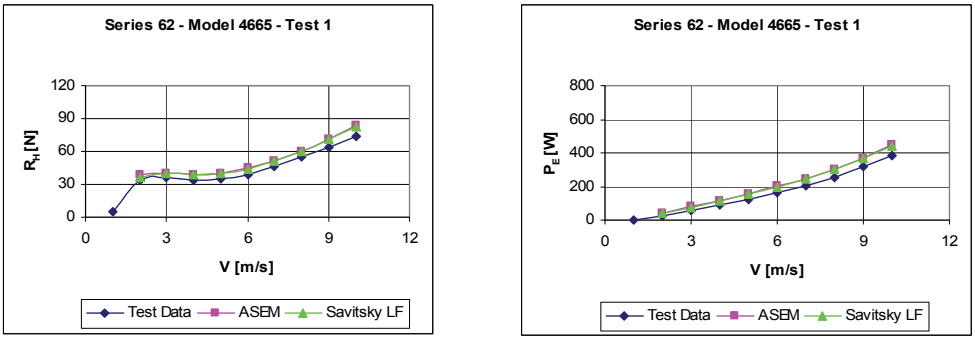

[a] **[b]**

Figure 4.5-4 Data Comparison: Model 4665 - Test 1

Analysis of data comparison have been developed computing dimensionless variation of both resistance and power versus hull speed.

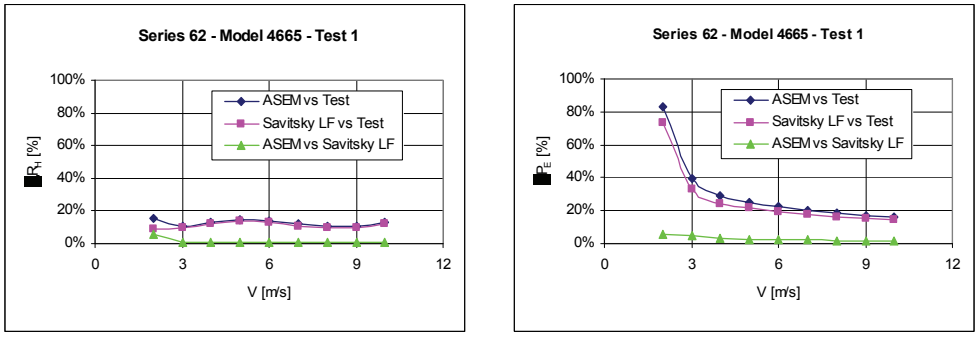

[a] **[b]**

Figure 4.5-5 Dimensionless data comparison analysis: Model 4665 - Test 1

A first remark is related to the Resistance: in the most of cases, the max dimensionless variation has a value less than 20%, within the overall range of hull speed. The few test cases with dimensionless variations higher than 20% are related to the longitudinal position of the Center of Gravity: higher the forward longitudinal position of the Center of Gravity (versus the Center of Buoyancy as well as the centroid of A_P), higher the error on results related to.

A second remark is related to the Power: the absolute value of the dimensionless variation has a decreasing trend at all, and with a steeply downsizing at low hull speed.

As matter of fact Power grows up with the hull speed meanwhile difference between predicted value (with ASEM as well as Savitsky's LF method) and computed ones, by test results, is quite constant with the hull speed. Thereby Power dimensionless variation decreases with the hull speed: lower hull speed higher Power dimensionless variation magnitude.

The last remark is related to the Resistance prediction methods. There is a common trends of ASEM results versus Savitsky's LF ones: higher hull speed closer results. This is due to the geometry of the models tested: the afterward part of the hull has a constant deadrise angle and, in planing condition, it is the only part interested by the pressure distribution.

Thereby, in planing condition, models of Series 62 work as monohedral hull form does.

Accordingly to the above remarks, ASEM results, as well as Savitsky's results, are in good agreement with tests results.

4.5.3 BK Series

4.5.3.1 Description of models and Test Results

Series BK was composed by nine hull models with the same dimensions and different hull shape [Voitkounski 1985].

Model BK-1 has a single chine per side: a sharp edge chine at each intersection of the bottom and side; this single chine is developed throughout the length of the hull itself.

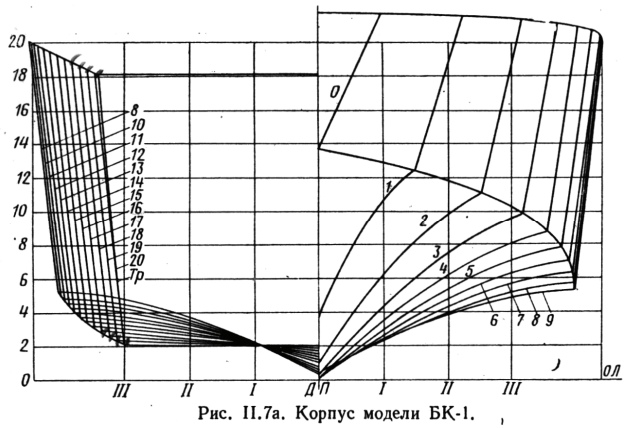

Рис. II.7а. Корпус модели БК-1.

Figure 4.5-6 Transversal sections of Model BK-1

Model BK-2 has the same shape of model BK-1: the distinctive feature of the model BK-2 is the rounding to the keel.

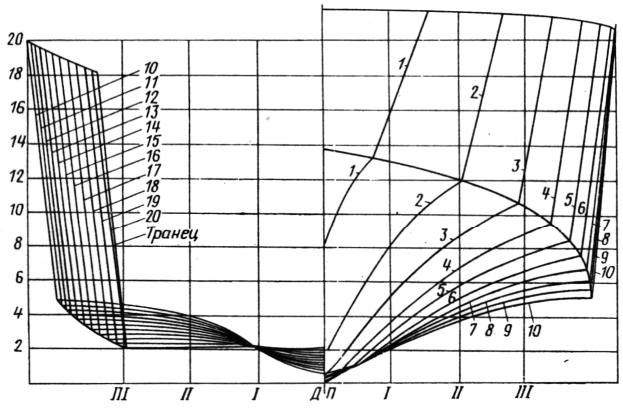

Рис. II.7б. Корпус модели БК-2.

Figure 4.5-7 Transversal sections of Model BK-2

In the model BK-3 the hull shape between the transom and the 5th section is the same of BK-1, meanwhile sections foreword the 5th section (bow direction) are "rounded" on the template.

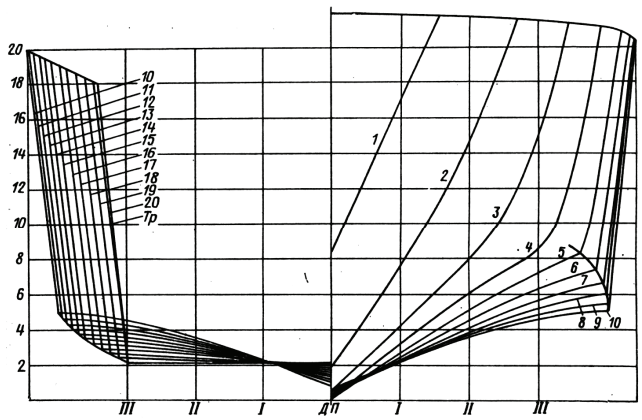

Рис. II.7в. Корпус модели БК-3.

Figure 4.5-8 Transversal sections of Model BK-3

Model BK-4 is derived from the model BK-1 by the introduction of a step in the central trunk of the hull: transverse height of the step remained unchanged.

Model BK-5 is a mixed hull: there are two single chine (one per each side), present from the transom to the 5th section, then softening towards the bow. This model has been developed in order to operate in semi-displacement field.

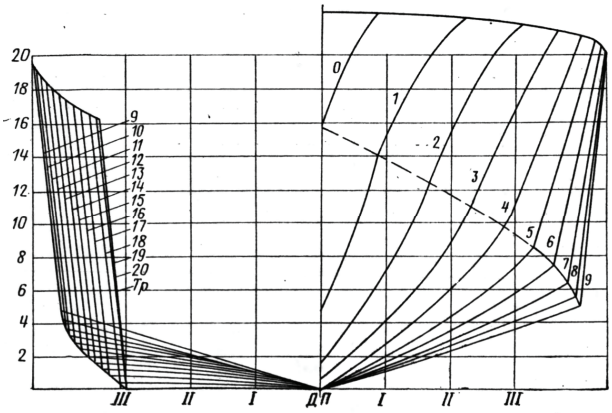

Рис. II.7г. Корпус модели БК-5.

Figure 4.5-9 Transversal sections of Model BK-5

Model BK-6 has a step in the central part of the hull and an high value of deadrise angle along the hull.

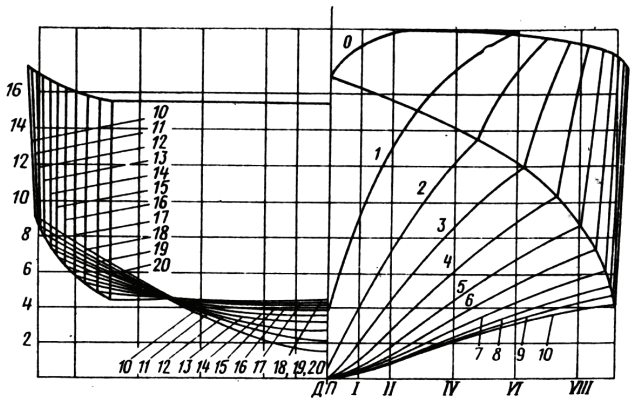

Рис. II.7д. Корпус модели БК-6.

Figure 4.5-10 Transversal sections of Model BK-6

Model BK-7 has monohedral shape in the aft part of the hull, meanwhile model BK-8 has edges like “Cissoid”.

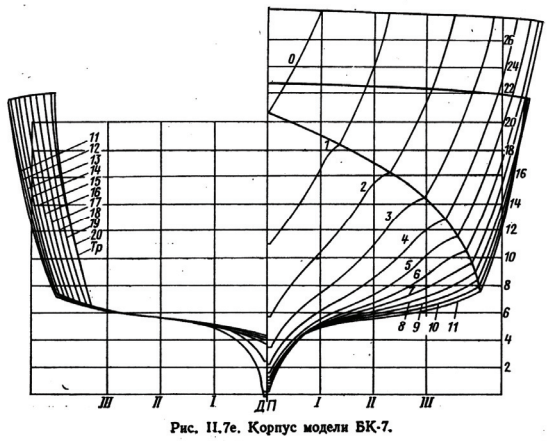

Рис. II.7е. Корпус модели БК-7.

Figure 4.5-11 Transversal sections of Model BK-7

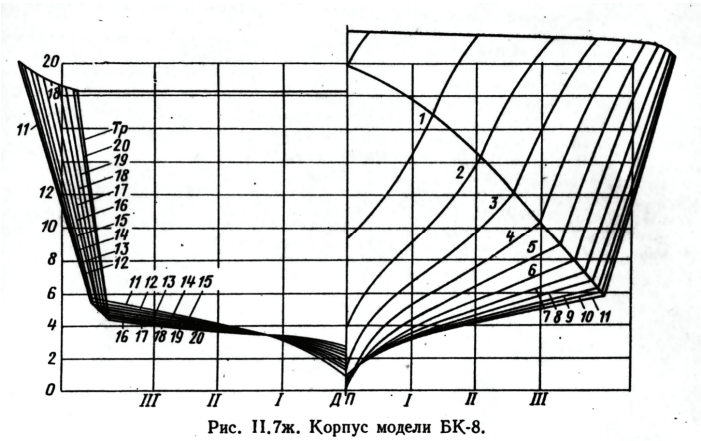

Рис. II.7ж. Корпус модели БК-8.

Figure 4.5-12 Transversal sections of Model BK-8

Model BK-9 is characterized by a line break that is located above the knee

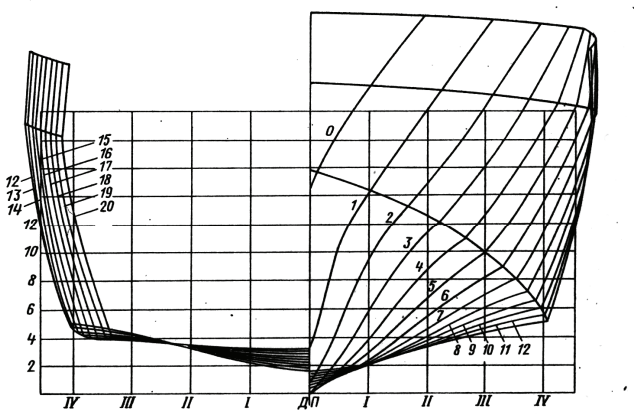

Рис. II.7з. Корпус модели БК-9.

Figure 4.5-13 Transversal sections of Model BK-9

Despite Series BK is out of date, and related test results are not anymore available in the original form, same results are released in literature [Radojcic 1985]. These results are pertinent to Model BK-1, which is:

- Vee-bottom transverse sections with the deadrise increasing towards the bow (not monohedral),
- sharp edge chines at the intersection of the bottom and sides,
- wide transom with a sharp trailing edge,
- straight horizontal buttock lines at the aft end,
- water entry lines fine with narrow angle at the bow,

In term of F_∇, the speed range was about 1.0 up to 4.5; λ was about 4.00 up to 7.00. The CG locations $\bar{x}_g$, as percent of L_P forward the transom stern, was about 0.35 up to 0.45; and in term of C_Δ, the range was about 0.427 up to 0.854.

With reference to Model BK-1, 12 cases of study have been defined and analyzed.

4.5.3.2 Results Comparison

Detailed comparison analysis of results is available in Appendix H of this Thesis. Hereinafter a briefly synthesis has been reported.

Data comparison has been developed with reference to Resistance and Power trends related to hull speed. In order to get the best comparison available, Egorov's method [Voitkounski 1985] have been applied too.

The most of data available in literature are reported in dimensionless form, and all results computed have been replaced with their relative dimensionless sizes: the

volumetric Froude number Fr_V [89] instead of hull speed, the ratio $\varepsilon = \frac{R_H}{\Delta}$ instead of the bare hull resistance R_H and the ratio $\mu = \frac{P_E}{\Delta \cdot V}$ for the effective power P_E.

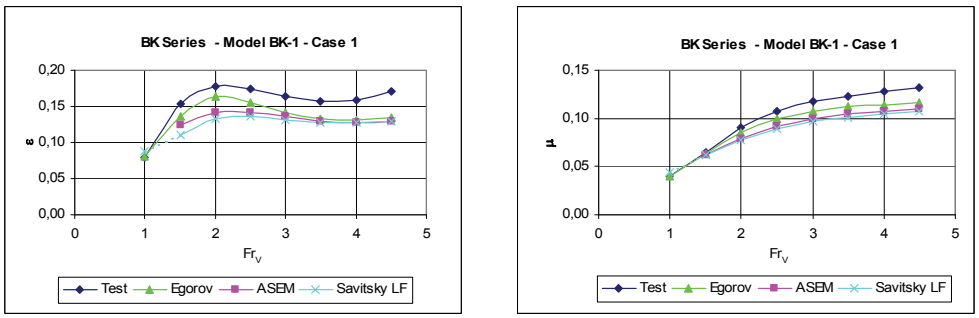

[a] **[b]**

Figure 4.5-14 Data Comparison: Model BK-1 - Case 1

Analysis of data comparison have been developed computing dimensionless variation of both resistance and power versus hull speed, with $\Delta\varepsilon = \Delta R_H$ and $\Delta\mu = \Delta P_E$.

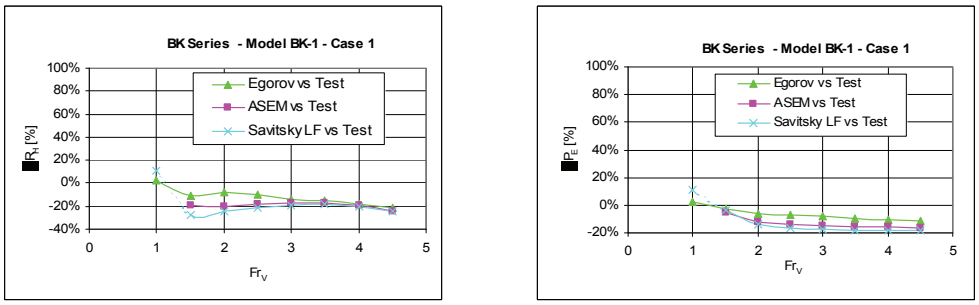

[a] **[b]**

Figure 4.5-15 Data Comparison Analysis: Model BK-1 - Case 1

Egorov's method presents the best results, and this is due to its nature: a regression method which coefficients have been computed by statistical analysis of results related to BK as well as MBK Series.

ASEM dimensionless result trends present low variations as function of volumetric Froude Number Fn_∇. In first approximation model results, in term of resistance as well as power, can be computed by ASEM's ones multiplied by 1.25, whereas ASEM's results shall be not out of range.

ASEM results are a little bit closer to test results than Savitsky's ones, but at the same time, the computational effort required by ASEM is the highest among prediction methods used.

Thereby, in term of results goodness versus computational efforts, Savitsky's method is more efficient then ASEM one.

---

[89] Here is reported the Russian symbol for the volumetric Froude number: Fr_V.

4.5.4 YP Series

4.5.4.1 Description of models and Test Results

Series YP was composed by six transom-stern hull models with the same length (5 ft) and different hull shape [Compton 1986].

Model YP81-1 is the parent model has been developed applying to the Yard Patrol Craft YP676 the form features of three hull series: Series NPL, Series 63 and Series 64.

Models have been developed and tested in order to evaluate the influence of some hull form parameters on planing hull performances:

- the length to beam ratio L_{PP}/B_{REF},
- the displacement to length ratio ∇,
- the longitudinal distance from amidships to Center of Gravity related to the hull length x_g [(90)]

Models YP81-1 to YP81-3 are soft-chine shapes with different length to beam ratio. Models YP81-4 to YP81-6 have been developed respectively as the hard-chine counterparts of soft-chine models.

In order to get a comparison among data associated to planing condition of hard-chine hull form, models of series YP81 with soft-chines have not been take in account.

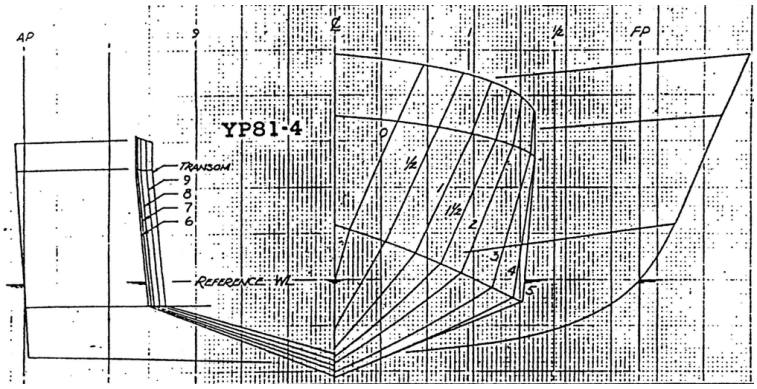

Figure 4.5-16 Body plans & end profiles: Model YP81-4

[(90)] In his paper, Compton used the symbol L_{CG} as longitudinal distance from amidships to Center of Gravity, positive in stern direction. In order to avoid confusion -in this thesis work L_{CG} indicates the distance between the Center of Gravity and the transom stern of the hull- Compton's symbol L_{CG} here has been replaced with X_g, and thereby: $x_g = X_g / L_{PP}$.

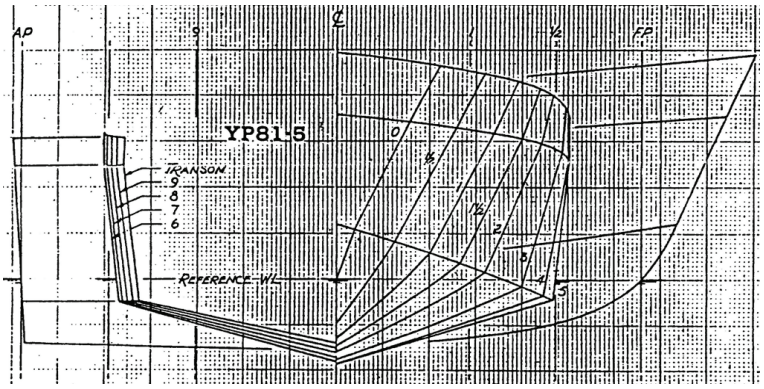

Figure 4.5-17 Body plans & end profiles: Model YP81-5

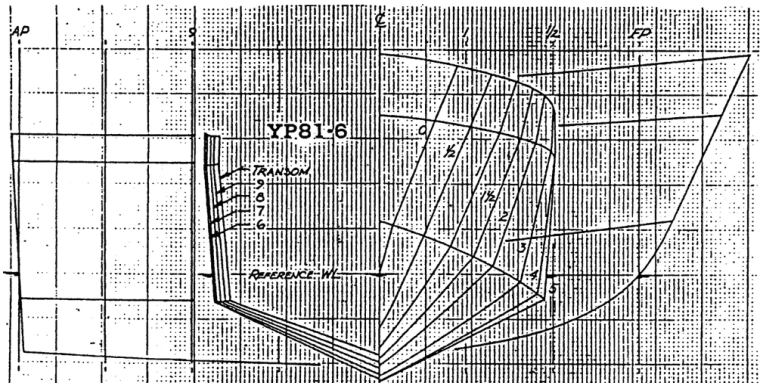

Figure 4.5-18 Body plans & end profiles: Model YP81-6

Table 4.5-2 Hull characteristics at reference waterline

	YP81-4	YP81-5	YP81-6
L_{PP}/B_{REF}	4.49	3.86	5.17
B_{REF}/T	3.90	5.25	3.03
∇	158.3	164.7	154.8
S	6.818	7.345	6.513
C_B	0.437	0.452	0.437
C_P	0.721	0.720	0.719
C_{WP}	0.802	0.804	0.809
LCB/L_{PP}	-0.086	-0.086	-0.084
KM_T/B_{REF}	0.684	0.817	0.598
BM_L/L_{PP}	1.986	2.246	1.798
$i_e[\text{deg}]$	17.7	21.5	17.3
$\beta_{10}[\text{deg}]$	16.4	12.4	21.0

Per each model and per each value of x_g, a set of five curves have been developed: each curve represents the residual resistance coefficient[91] versus Froude number based on waterline length at rest Fn [92] for a fixed value of the displacement to length ratio ∇.

In detail:

- the speed range, in term of Fn, was about 0.1 up to 0.65;
- the ∇ values were 110, 120, 130, 140, 150 $[LTSW/ft^3]$;
- the x_g values were 0.0244, 0.0778 and 0.1312.

4.5.4.2 Results Comparison

Detailed comparison analysis of results is available in Appendix I of this Thesis. Hereinafter a briefly synthesis has been reported.

Data comparison has been developed with reference to Resistance and Power trends related to hull speed. Power data pertinent to the models of Series YP have been derived by hull speed and resistance measurements.

[91] In order to evaluate the residual resistance ITTC 1957 formula has been adopted as friction line.

[92] Compton considered the Froude number based on the waterline length at rest. According to remarks on Froude numbers in paragraph G.9 of Appendix G of this Thesis work, this Froude number (related to the waterline length at rest) is a "mechanical" Froude number. As matter of the fact the geometric term (waterline length at rest) is in connection with a mechanical hull parameter: the weight W. Thereby this Froude number is linear with the hull speed, but his trend is associated to the weight value adopted in towing test.

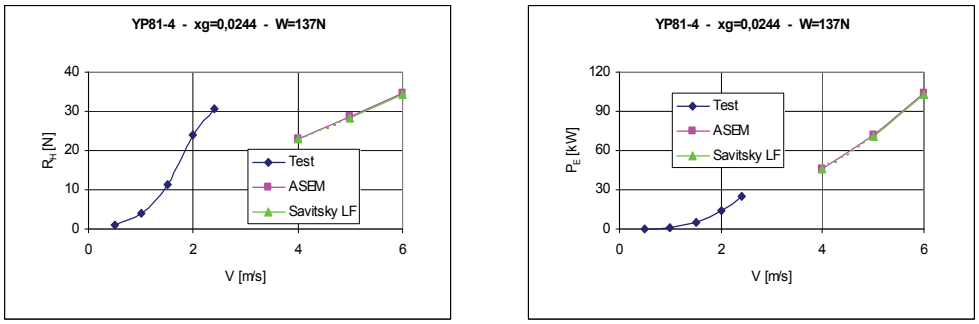

[a] **[b]**

Figure 4.5-19 Data Comparison: Model YP81-4 - xg=0.0244 - W=137N

A first look shows us a common trend of ASEM and Savitsky's results, which are quite different versus test results.

In all cases analyzed, at low speed, no comparison among test results and computed results is achievable.

Models of Series YP81 are semi-displacement hull form, and have been tested in semi-displacement condition, thereby Savitsky's method as well as ASEM are not applicable to hull forms optimized for work only up to semi-displacement field.

4.6 Comparison with experimental test results

The differences in the bare hull resistance values for monohedral hull forms obtained by Savitsky's method and by experimental tests had been already investigated at Naples University DIN[(93)] towing tank. Bare hull resistance of strictly monohedral (80% of the length) hull forms with different deadrise angles had been experimentally assessed. [Bertorello & Oliviero 2007]

Experimental tests have been developed at DIN due to the increasing interest, in term of resistance and seakeeping, for non monohedral hull form applied to pleasure boats. [Bertorello & Oliviero 2009]

A first set of experimental tests were already available at the beginning of this work thesis and a first attempt to check reliability and efficiency of ASEM was developed. Encouraging results gave a boost to us to carry on with the research[(94)].

Few years later a second set of experimental tests have been developed at DIN in order to improve performances of a motor yacht with non monohedral hull form. The second check on reliability and efficiency of ASEM has given results not much encouraging[(95)].

Both results are below reported.

---

(93) Department of Naval Architecture and Marine Engineering (DIN - Dipartimento di Ingegneria Navale) of the University of Naples "Federico II".

(94) These results were exposed in the 5th International Conference on High Performance Marine Vehicles (HYPER 06) and have been published on the *Australian Journal of Mechanical Engineering,* here reported in References.

(95) These results were exposed in the 13th Congress of International Maritime Association of Mediterranean (IMAM 2009) here reported in References.

4.6.1 Naples Towing Tank Lab

The Naples Towing Tank is located within the building of DIN, in Naples, Italy [Begovic et al 2007].

4.6.1.1 Towing Tank characteristics

The Towing Tank, equipped with a towing carriage, has the following dimensions:

Table 4.6-1 Towing tank dimensions

Description	Value	Unit
Length	137.2	[m]
Beam	9.0	[m]
Water depth	4.2	[m]
Freeboard	0.5	[m]

meanwhile, the towing carriage has the following characteristics:

Table 4.6-2 Towing carriage characteristics

Description	Value	Unit
Weight	18	[t]
Maximum forward speed	10.0	[m/s]
Maximum backward speed	4.0	[m/s]
Maximum forward acceleration	1.0	[m/s^2]
Maximum backward acceleration	0.5	[m/s^2]
Maximum deceleration	3.0	[m/s^2]

Further, the Towing Tank is equipped with a wave maker, which allow to conduct the model tests in rough sea. The wave maker is able to generate the regular waves in the range: 1.0 m to 12.0 m length. With reference to the wave of 9.0 m length, the steepness ratio (height/length H/λ) could be varied in the range: 1/100 up to 1/15.

In order to generate an irregular sea, wave maker is able to superimpose hundreds sinusoidal waves of different wavelengths. All the standard sea spectrum (ITTC, ISSC, Pierson Moskowitz, JONSWAP, Ochi, Neumann) can be generated as well as user defined spectrum.

4.6.1.2 Model fitting out and instruments positioning

The setting model phase is developed in two different parts: a fitting out phase and a weight-ballast phase.

The first one consists of instrument positioning (dynameters, strings, potentiometers, accelerometers, inertia platforms, etc) and preparing the rig connection (if it is used) to the hull.

The second one starts with the hull weighing, fitted out with all internal fittings (such as instrumentation, batteries, propulsion motor, etc), in order to define the dry ballast weight useful to get the requirements in term of displacement and immersion. After the model is placed in water: the dry ballast will be fitted in order to get the required trim. Even more, the rig weight, supported by the model, is considered in ballasting and trimming of model.

At the end of this second phase, the longitudinal position of the Center of Gravity of the model will be get by oscillation period measurements.

4.6.2 Model, tests and experimental results

In order to get a numerical benchmark for the ASEM results, Savitsky Long Form method has been applied.

Three set of Savitsky's bare hull resistance R_H values have been obtained by application of the method to three different value of the deadrise angle:

- $\beta_{Transom}$ - the deadrise angle measured at transom;
- $\beta_{L_{PP}/4}$ - the deadrise angle measured at 1/4 L_{PP} from the stern;
- $\beta_{L_{CG}}$ - the deadrise angle measured at Center of Gravity position.

4.6.2.1 First set of Experiments

This non-monohedral hull model refers to a 30.48 m L_{OA} high speed motor-yacht.

4.6.2.1.1 Description of model

A 1/12 scale model has been wood made. The main dimensions of the model are hereinafter summarized

Table 4.6-3 Model Main Dimensions

Dimensions	Value	Unit
L_{PP}	2.229	[m]
B_C	0.614	[m]
T	0.104	[m]
W	578.8	[N]
L_{CG}	1.120	[m]
λ_{SHIP}	12.0	[-]

4.6.2.1.2 Test Condition and Results

The investigated Froude numbers were:

Table 4.6-4 First set: Froude numbers

Fn	0.46 up to 1.23
C_V	0.91 up to 2.42
F_∇	1.14 up to 3.04

The model was tested with and without stimulating devices.

Among several test performed, results related to test without any stimulating device are here reported.

Table 4.6-5 Test Conditions

Test	Total Weight	Water Temp.
	[N]	[°C]
1	578.8	10.8
2	657.3	11.0

and diagrams of Test 1 and Test 2 are:

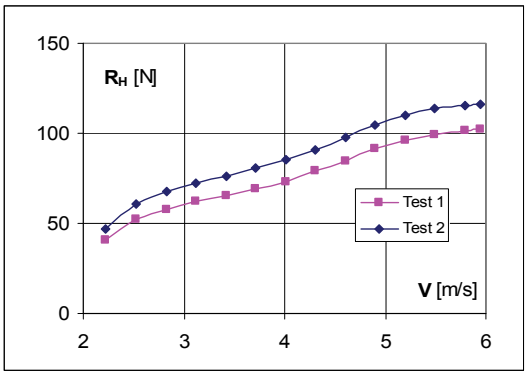

Figure 4.6-1 Resistance Results: first set

4.6.2.1.3 Computational Results

Savitsky Long Form method has been applied with three different value of the deadrise angle:

Table 4.6-6 Fundamental deadrise angle value

$L_{Transom}$	0.000	[m]	$\beta_{Transom}$	8.4	[deg]
$L_{PP/4}$	0.555	[m]	$\beta_{Lpp/4}$	8.6	[deg]
L_{CG}	1.120	[m]	β_{LCG}	9.9	[deg]

with results:

Table 4.6-7 Savitsky LF results: Test 1

	$\beta_{Transom}$	$\beta_{LPP/4}$	$\beta_{L_{CG}}$
V	**R_H**		
[m/s]	[N]		
5,0	77	77	78
6,0	92	92	93
7,0	106	106	107
8,0	122	122	123
9,0	140	140	141
10,0	160	160	161

Table 4.6-8 Savitsky LF results: Test 2

	$\beta_{Transom}$	$\beta_{LPP/4}$	$\beta_{L_{CG}}$
V	**R_H**		
[m/s]	[N]		
5,0	83	83	85
6,0	98	99	100
7,0	113	113	114
8,0	128	128	129
9,0	145	145	146
10,0	165	165	166

In both Tests, the differences among Savitsky's results are negligible due to marginal variation of the deadrise angle in the after part of the hull.

Values obtained by the ASEM method application are reported:

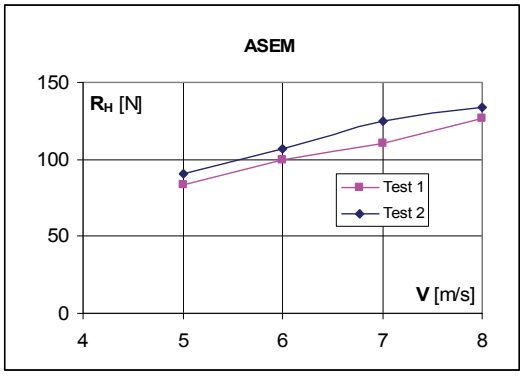

Figure 4.6-2 ASEM Resistance Results: first set

4.6.2.1.4 Comparison

In order to achieve a comparison among results available, experimental as well as computed, Savitsky's results related to deadrise angle measured at Center of Gravity position have been taken in account.

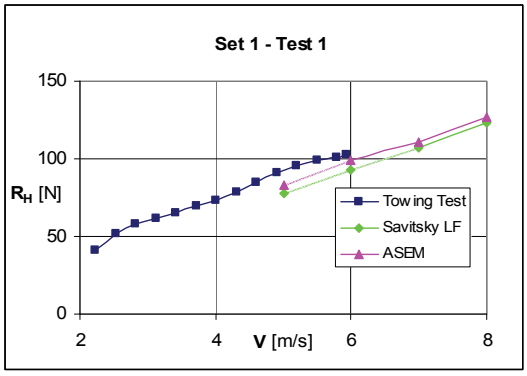

Figure 4.6-3 Results Comparison: first test of first set

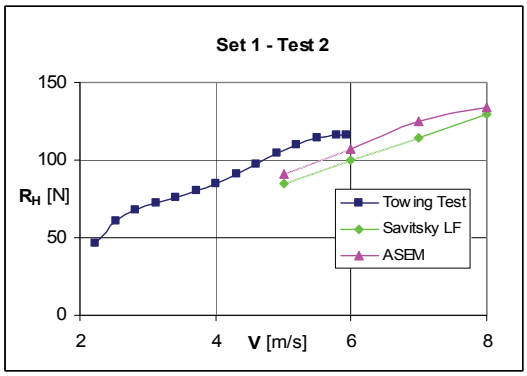

Figure 4.6-4 Results Comparison: second test of first set

Comparison has been performed in the speed range (5.0 m/s ÷ 6.0 m/s). Off this range comparison has no sense; as point of fact, for speed lower than 5.0 m/s computed results have no physical meaning (wetted length higher than length over all), meanwhile 6.0 m/s is the highest tested speed.

ASEM results have a better and closer fit to the experimental values than those obtained by Savitsky's long form method. At the same time, uncertain related to ASEM results is higher than Savitsky's ones as well as ASEM computational efforts and costs are higher than Savitsky's.

4.6.2.2 Second set of Experiments

The investigated hull form has been developed in order to improve performances of a motor yacht with non monohedral hull form.

4.6.2.2.1 Description of model

A 1/10 scale model (13.65 m L_{OA}) has been built in GRP. The main model dimensions are hereinafter summarized:

Table 4.6-9 Model Main Dimensions

Dimension	Value	Unit
L_{PP}	1.090	[m]
B_C	0.360	[m]
T	0.072	[m]
W	138.3	[N]
L_{CG}	0.278	[m]
λ_{SHIP}	10.0	[-]

4.6.2.2.2 Test Condition and Results

The investigated Froude numbers were:

Table 4.6-10 Second set: Froude numbers

Fn	0.29 up to 1.62
C_V	0.52 up to 2.94
F_∇	0.64 up to 3.60

The model was tested with bare hull and without any stimulating device.

Test condition data were:

Table 4.6-11 Test Conditions

Test	Total Weight	Water Temp.
	[N]	[°C]
3	141.5	21.2
4	141.1	
5	138.9	16.6

and diagrams of Test results are:

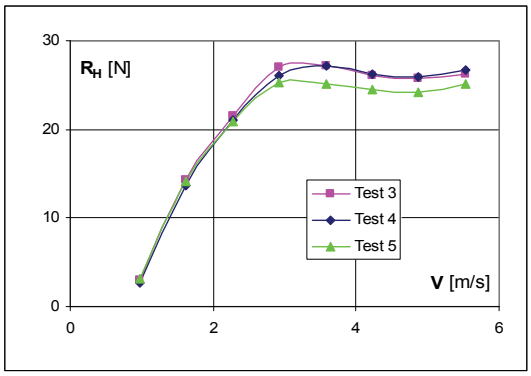

Figure 4.6-5 Resistance Results: second set

Differences among test results are negligible due to marginal variation of the weight.

4.6.2.2.3 Computational Results

Savitsky Long Form method has been applied with three different deadrise angle value:

Table 4.6-12 Fundamental deadrise angle value

$L_{Transom}$	0.000	[m]	$\beta_{Transom}$	10.4	[deg]
$L_{PP/4}$	0.270	[m]	$\beta_{Lpp/4}$	13.4	[deg]
L_{CG}	0.278	[m]	β_{LCG}	13.4	[deg]

In first approximation it has been adopted $L_{PP/4} = L_{CG}$, with results:

Table 4.6-13 Savitsky LF results

	Test 3		Test 4		Test 5	
	$\beta_{Transom}$	$\beta_{LPP/4}$	$\beta_{Transom}$	$\beta_{LPP/4}$	$\beta_{Transom}$	$\beta_{LPP/4}$
V	**R_H**					
[m/s]	[N]					
4,0	28	29	27	29	27	28
5,0	23	26	23	25	23	25
6,0	23	24	23	24	22	24
7,0	24	25	24	25	23	24
8,0	26	27	26	27	26	27
9,0	29	30	29	30	29	30
10,0	33	34	33	34	32	33

Differences among Savitsky's results, related to the same deadrise angle value, are negligible due to marginal weight variation. At the same time, despite the deadrise angle variation is not negligible, differences due to the deadrise angle variation are quite negligible, according to the low "weight" of the deadrise parameter on the bare hull resistance overall.

Values obtained by the ASEM method application are hereinafter reported:

Table 4.6-14 ASEM results

	Test 3	Test 4	Test 5
V	**R_H**		
[m/s]	[N]		
4,0	29	29	28
5,0	25	25	25
6,0	24	24	23
7,0	24	24	24
8,0	26	26	26
9,0	29	29	29
10,0	33	33	33

Differences among ASEM results are negligible due to marginal variation of the weight.

4.6.2.2.4 Comparison

Among experimental as well as computed results, differences are negligible, due to marginal weight variation. Thereby comparison will be developed on results related to Test 3, and $\beta_{L_{PP}/4}$ will be the deadrise value adopted for the Savitsky's method.

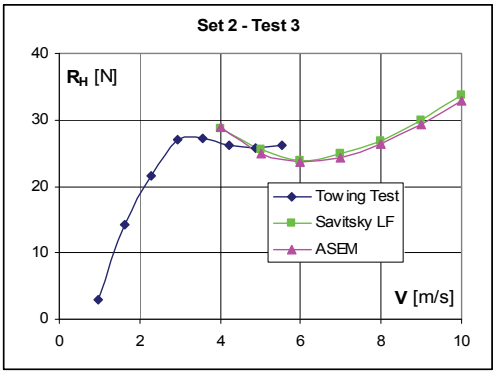

Figure 4.6-6 Results Comparison: Test 3 of second set

Comparison among results has been performed within the speed range (4.0 m/s ÷ 5.5 m/s) [Bertorello & Oliviero 2009]. Off this range comparison has no sense; as matter of fact, for speed lower than 4.0 m/s computed results are not available due to the equilibrium set over to 12 deg, meanwhile for 5.5 m/s is the highest tested speed.

In this short speed range, test results and computed results present different trends with quite different values.

4.6.3 Final Considerations

In term of comparison between computed and experimental data, the speed range available is too short: the lack of experimental data in planing field don't allow us to perform a complete and useful comparison.

The lack of test results in high-speed planing condition is due to limitations of DIN Towing Tank: geometrical dimensions of the tank as well as kinematic characteristics of the carriage. As matter of fact, taking in account the towing carriage speed , acceleration, deceleration and rates related to, the max speed of 10 m/s is achievable not much more than few seconds. At the same time, models with length lower than one meter are not useful and effective for tests[(96)].

[(96)] In the resistance test for a high-speed planing craft, in order to satisfy the relation of Froude's law of similarity, it is necessary to use a very small model. If the model is short in length (lower than 1.5m) scale effects on running attitudes appears and causes different resistance: lower the length higher the effect. On the other hand, if a larger model is used, a towing carriage should run very fast. Then a very long tank with a very fast towing carriage is needed. Furthermore, the wall and bottom effects may appear in resistance [Katayama et al. 2002].

Further, for both models tested, there is an high uncertain degree on the motion field achieved[97]: the Froude number Fn, related to the max hull speed, shows us a planing condition achieved whereas C_V and F_∇ values indicate that the motion has been developed up to the semi-displacement field.

According to these remarks, tests results achieved are useful as benchmark for checking reliability and efficiency of prediction methods focused on semi-displacement field, but are not useful for planing prediction methods.

[97] On the matter, see Remarks on Appendix G of this work thesis.

4.7 Conclusion

ASEM has been applied to hulls of Systematic Series, as Series 62, Series BK and Series YP81, in order to evaluate its reliability and efficiency. Savitsky Long Form method has been applied to as benchmark.

Further, error propagation analysis has been applied to both prediction methods, with the objective of evaluating their sensitivity[98].

ASEM procedure is longer than Savitsky's one; this drives to a sensitivity of ASEM higher than Savitsky's: ASEM relative errors on results will never be lower than Savitsky's.

Hulls of Series 62 are monohedral in planing condition[99] and, in this case only, Savitsky's method presents the best results with the lowest relative errors.

Hulls of Series YP81 are no-monohedral: they have been developed for semi-displacement field. ASEM as well as Savitsky's method do not work well: in all cases analyzed, at low speed, no comparison among test results and computed results is achievable.

Model BK-1 of Series BK presents longitudinal variation of the deadrise angle. Results are not anymore available in the original form, but same data are released in literature yet. ASEM results are a little bit closer to test results than Savitsky's ones but with the highest relative errors.

Several tests on non monohedral hull form have been developed at DIN Towing Tank. Two set of experimental data related to two different hull form have been analyzed and compared with ASEM as well as Savitsky's results. Despite Savitsky and ASEM are applicable to planing field as well as semi-displacement one, in the most of cases predicted results were available[100] starting from speed pertinent to the upper side of semi-displacement field meanwhile experimental data were available up to the beginning of planing field.

---

[98] See Appendix J "Error Propagation Analysis".

[99] Hulls of Series 62 are monohedral, starting from the transom stern, for the most of the length between perpendicular. In planing condition hull wetted area is monohedral at all.

[100] Savitsky as well as ASEM results without physical meaning have been neglected. The most of neglected data are related to low values of hull speed: $Fn \leq 0.6 \div 0.8$.

Further, for both models analyzed, the motion field achieved is not uniquely defined: planing condition could be not achieved.

According to these remarks, tests results analyzed are not useful for checking reliability and efficiency of planing prediction methods.

Finally, in the lower side of planing motion field, ASEM and Savitsky's results are quite close. Reminding that ASEM results present sensitivity higher than Savitsky's ones, follows that Savitsky's method is more reliable, effective and easy to apply than ASEM.

In high-speed planing condition no comparison have been achieved due to the lack of data on the influence of hull warping on the pressure field under the hull and on the bare hull resistance at all.

ASEM has been developed in order to take in account the longitudinal deadrise variation effects on the resistance value. Further, it is possible to take in account the effects related to the longitudinal variation of beam between chines and curvature of the keel.

In the same way it is possible to take in account transversal variation of hull geometrical size and, finally it is possible to take in account both longitudinal and transversal variations.

Each improvement of ASEM, above suggested, is related to the availability of a further amount of experimental data on the matter for the benchmark. Despite nowadays non monohedral planing crafts are one of the most common boats, systematic experimental data are not available yet.

4.8 Symbols

A_P	Projected planing bottom area, excluding area of external spray strips	[m^2]
B_C	Beam between chines	[m]
$B_{C,ms}$	Beam between chines in mean section	[m]
BM_L	Longitudinal metacentric radius	[m]
B_{PX}	Maximum breadth over chines, excluding external spray strips	[m]
B_{REF}	Beam at waterline	[m]
B_{WL}	Water line beam	[m]
CG	Center of Gravity	
C_B	Block coefficient	
C_P	Prismatic coefficient	
C_V	Froude number related to the beam	$C_V = \frac{V}{\sqrt{gB_c}}$
C_{WP}	Waterplane coefficient	
C_Δ	Weight coefficient	$C_\Delta = \frac{W}{\frac{1}{2}\gamma B_C^3}$
Fn	Froude number	$Fn = \frac{V}{\sqrt{gL_{WL}}}$
Fr_V	Volumetric Froude number - Russian Symbol	$Fr_V = \frac{V}{\sqrt{g\sqrt[3]{\frac{W}{\gamma}}}}$
Fn_∇	Volumetric Froude number	$Fn_\nabla = \frac{V}{\sqrt[2]{g\sqrt[3]{\nabla}}}$
GRP	Glass Reinforced Plastic	
H	Height of wave	[m]
i_e	Half angle of entrance	[deg]
ISSC	International Ship and Offshore Structures Congress	
ITTC	International Towing Tank Conference	
KM_T	Height of transverse metacenter above keel	[m]
LCB	Longitudinal distance from amidships to center of buoyancy	[m]
LF	Long Form	
LTSW	Long Tons Salt Water	
L_{CG}	Center op gravity distance from the stern	[m]
L_{OA}	Length Over All	[m]

L_P	Projected chine length	[m]
L_{PP}	Length between perpendiculars	[m]
L_{WL}	Water line length	[m]
P_E	Effective power	[W]
R_H	Bare hull resistance	[N]
T	Immersion	[m]
V	Hull speed	[m/s]
V_{MOD}	Model speed	[m/s]
V_{SHIP}	Boat speed	[kn]
x_g	Longitudinal distance from amidships to Center of Gravity related to the hull length	$x_g = X_g / L_{PP}$
X_g	Longitudinal distance from amidships to Center of Gravity, positive in stern direction	[m]
$\bar{x}_g$	Dimensionless CG location as percent of L_P forward the transom stern	[%]
W	Weight of hull	[N]
α_0	Angle of attack	[deg]
β	Deadrise angle	[deg]
$\beta_{L_{CG}}$	Deadrise angle measured at Center of Gravity position	[deg]
$\beta_{L_{PP}/4}$	Deadrise angle measured at $L_{PP}/4$ from the stern	[deg]
$\beta_{Transom}$	Deadrise angle measured at transom	[deg]
β_{10}	Deadrise angle at transom	[deg]
Δ	Weight of the water displaced by the hull	[N]
ΔP_E	Dimensionless variation of the effective power	$\Delta P_E = \frac{P_{E,\mathrm{Predicted}} - P_{E,Tested}}{P_{E,Tested}}$
ΔR_H	Dimensionless variation of the resistance	$\Delta R_H = \frac{R_{H,\mathrm{Predicted}} - R_{H,Tested}}{R_{H,Tested}}$
$\Delta\varepsilon$	Dimensionless variation of the resistance	$\Delta\varepsilon = \Delta R_H$
$\Delta\mu$	Dimensionless variation of the resistance	$\Delta\mu = \Delta P_E$
ε	Dimensionless resistance - Russian symbol	$\varepsilon = \frac{R_H}{\Delta}$
γ	Unit weight of water	$\left[N/m^3\right]$
λ	Length between perpendicular to beam between chines of mean section ratio	$\lambda = \frac{L_{PP}}{B_{C,ms}}$
λ	Wavelength	[m]
λ_{SHIP}	Scale factor	
μ	Dimensionless power	$\mu = \frac{P_E}{\Delta \cdot V}$

∇	Displacement of the hull	$\nabla = \frac{W}{\gamma}$; [m]
	Centerline	
	Displacement-length ratio	$\left[LTWS/ft^3\right]$
s	Wetted Surface Area - displaced volume ratio	$s = WSA/\nabla^{2/3}$

4.9 References

Bailey, D. 1976. The NPL High Speed Round Bilge Displacement Hull Series: Resistance, Propulsion, Maneuvering and Seakeeping Data. *National Maritime Institute Monograph* Vol.4, Royal Institute of Naval Architects(UK).

Begovic E., Boccadamo G, Bove A, Caldarella S. 2007. Prismatic Hull Tests in Regular Waves in DIN TOWING TANK. In: *CENTRE OF COMPETENCE FOR TRANSPORT SYSTEMS OF THE CAMPANIA REGION. An Experience of Innovation and Training*. Vol. 1, pp. 273-292. ISBN: 978-88-548-1269-7. ROMA (ITALY): ARACNE Editrice S.r.l.

Bertorello, C. & Oliviero, L. 2007. Hydrodynamic Resistance Assessment of Non-Monohedral Planing Hull Forms based on Savitsky's Method. *Australian Journal of Mechanical Engineering,* Vol. 4 No.2, pp 209-224. Engineers Media, CROWS NEST, Australia. (ACN001311511).

Bertorello, C. & Oliviero, L. 2009. Hydrodynamic Resistance Assessment of Non-Monohedral Planing Hull. In: *Proceeding 13th Conference of International Maritime Association of the Mediterranean* (IMAM '09). İstanbul, Turkey.

Beys, P.M. 1963. Series 63 Round Bottom Boats, *Report SIT-DL-63-949 Davidson Laboratory* Stevens Institute of Technology. Hoboken, New Jersey (USA).

Blount, D.L. & Hankley, D.W. 1976. Full-Scale Trials and Analysis of High-Performance Planing Craft Data, *Transactions SNAME*, Vol. 84, pp. 251-277. Jersey City (USA): SNAME

Clement E.P. 1964. Graphs for predicting the resistance of round bottom boats. *International Shipbuilding Progress* Vol.11 nr.114. Amsterdam (The Netherlands): IOS Press

Clement, E.P. & Blount, D.L. 1963. Resistance Tests of a Systematic Series of Planing Hull Forms. *Transactions SNAME,* Vol. 71, pages 491-579. Jersey City (USA): SNAME

Compton R.H. 1986. Resistance of systematic series of semi-planing transom stern hulls. *Marine Technology*, Vol.23, No.4, Jersey City (USA): SNAME

Grigoropoulos, G.J 2004. Advanced Monohulls. *Working Paper on Small Ship Design*. NATO NAVAL GROUP 6.

Grigoropoulos, G.J. & Loukakis, T.A. 1999. Resistance of double-chine, large, high-speed craft. *Bulletin de L' Association Technique Maritime et Aeronautique* ATMA, Vol. 99, Paris.

Holling, H.D. & Hubble, E.N. 1974. Model resistance data of Series 65 hull forms applicable to hydrofoils and planing craft, DTNSRDC, Report 4121.

Holtrop J. 1984. A Statistical Re-Analysis of Resistance and Propulsion Data. *International Shipbuilding Progress* Vol.31 nr.363. Amsterdam (The Netherlands): IOS Press

Katayama T., Hayashita S., Suzuki K. and Ikeda Y. 2002. Development of Resistance Test for High-Speed Planing Craft Using Very Small Model - Scale Effects on Drag Force. In: *Proceeding of Asia Pacifc workshop on Marine Hydrodynamics* (AP Hydro2002) ,pp.7-14.

Keuning, J.A. & Gerritsma, J. 1982. Resistance Tests of a Series of Planing Hull Forms with 25 Degrees Deadrise Angle, *International Shipbuilding Progress*, Vol. 29, No. 337, September 1982, pp. 222-249. Amsterdam (The Netherlands): IOS Press

Kracht, A. & Grim, O. 1960. Widerstand, Propulsion, Bewegung und Be-anspruchung schneller Verdrangunsfahrzeuge in glattem Wasser und in regel-maessigem Seegang, IFS-Bericht No. 167.

Lahtiharju, E.; Karppinen, T.; Hellevaara, M.; Aitta, T. 1991. Resistance and seakeeping characteristics of fast transom stern hulls with systematically varied form. New York Section SNAME Annual Meeting. Jersey City (USA): SNAME

Lindegren H., & Williams A. 1969. Systematic tests with small fast displacement vessels, including a study of the influence of spray strips. Publication nr. 65 SSPA. Goteborg

Mercier J.A. & Savitsky D. 1973. Resistance of transom-stern craft in the pre-planing regime. *Report SIT-DL-73-1667 Davidson Laboratory* Stevens Institute of Technology. Hoboken, New Jersey (USA).

Murdey, D.C. & Simoes Re, A.J. 1985. The NRC hull form series - an update, MARIN Symp.

Nordstrom H.F. 1951. Some tests with model of small vessels. Publication nr. 19 SSPA . Goteborg

Oossanen van P. 1980. Resistance Prediction of small high-speed displacement vessels state of art. *International Shipbuilding Progress* Vol.27 nr.313. Amsterdam (The Netherlands): IOS Press

Oossanen, van P. & Pieffers, J.B.M. 1985. NSMB-Systematic series of high-speed displacement ship hull forms, MARIN Workshop on developments in Hull Form Design, Wageningen.

Ping-Zhong J., Ba-Jing S., Zhang-Kai T. 1980. A parametric study on high-speed round bilge displacement hulls. High Speed Surface Craft Vol. 19 nr.12.

Radojcic, D. 1985. An Approximate Method For Calculation of Resistance and Trim of the Planing Hulls. *Ship Science Report No.23* University of Southampton (UK)

Savitsky, D. 1964. Hydrodynamic Design of Planing Hull. *Marine Technology*, Vol.1, No.1, Jersey City (USA): SNAME

Savitsky, D. & Brown, P.W. 1976. Procedures for Hydrodynamic Evaluation of Planing Hulls in Smooth and Rough Water. *Marine Technology*, Vol.13, No.4, pp381-400, Jersey City (USA): SNAME

Savitsky, D., Roper, J., Benen, L. 1972. Hydrodynamic Development of a High Speed Planing Hull for Rough Water, 9th O.N.R. Symposium, Paris.

Schmitke, R.T., Glen, I.F., Murdey, D.C. 1979. Development of a frigate hull form for superior seakeeping, Eastern Canadian Section SNAME. Jersey City (USA): SNAME

Voitkounski, Y.I. 1985. *Ship Theory Handbook:. Vol.3. Manoeuvrability of conventional Ships. Hydrodynamics of Gliders Hydrofoils and Hovercrafts*. Leningrad (Russia): Sudostroenie. pp. 277-283 (Russian language)

Yeh, H.Y.H. 1965. Series 64 resistance experiments on high-speed displacement forms, *Marine Technology*, Vol.2, No.3. Jersey City (USA): SNAME

ACKNOWLEDGEMENTS

According to me, ACKNOWLEDGEMENTS is the hardest paragraph to write.

During the development of all my work, I received data, information, tips as well as support (when things went wrong), and the most of these helps were due to the generosity of people around me.

Thanks to professor Franceso Saverio MARULO and Mr Carlo BERTORELLO, PhD tutors: this Thesis could not be developed without their help.

Thanks to professor Antonio MOCCIA, Doctorate School of Industrial Engineering director, for his patience with me.

Thanks to professor Michael R. DAVIS for his interest and for his helpful advices at the beginning of this research.

Thanks to all professors and researchers of DIN for their help.

Thanks to Mrs Lucia Itria LAI, for her aid in English.

The last words, my last thanks, are for my wife Laura: she believes in me and this is my strength.

Luciano OLIVIERO
viale CASTELLUCCIO 26F
80059 Torre del Greco (NA) - ITALY

+39 081 882 68 23
+39 347 186 76 21 (mobile)

luciano.oliviero@tin.it
luciano.oliviero@gmail.com

UNIVERSITÀ DEGLI STUDI DI NAPOLI
FEDERICO II

DOCTORATE SCHOOL OF INDUSTRIAL ENGINEERING

DOCTORATE PROGRAM IN
AEROSPACE, NAVAL AND TOTAL QUALITY MANAGMENT
ENGINEERING

XXII CYCLE

PhD THESIS

APPENDICES
Volume II - No. 1

HYDRODYNAMICS OF PLANING HULLS

A POWER PREDICTION METHOD FOR WARPED V-BOTTOM HULL FORMS

Tutors
Chiar.mo Prof. Ing. Francesco Saverio MARULO
Prof. Ing. Carlo Francesco Mario BERTORELLO

Candidate
Ing. Luciano OLIVIERO

UNIVERSITÀ DEGLI STUDI DI NAPOLI
FEDERICO II

SCUOLA DI DOTTORATO IN
INGEGNERIA INDUSTRIALE

Dottorato di Ricerca in
Ingegneria Aerospaziale, Navale e della Qualità
XXII CICLO

TESI di DOTTORATO

APPENDICI
Volume II - Tomo 1

HYDRODYNAMICS OF PLANING HULLS

A POWER PREDICTION METHOD FOR WARPED V-BOTTOM HULL FORMS

Relatori
Chiar.mo Prof. Ing. Francesco Saverio MARULO
Prof. Ing. Carlo Francesco Mario BERTORELLO

Dottorando
Ing. Luciano OLIVIERO

CONTENTS

VOLUME I

APPENDIXES
VOLUME II -NO. 1

VOLUME II -NO. 2

APPENDIX A

SURF

HYDROMECHANICS

A surfboard is a waterproof plank used to plan on surface sea waves.

"Surf" is the planing run on a surface sea wave of a surfboard propelled by gravity force, and a "surfer" is the driver of a surfboard.

Following notes[101] are written only for planing surface moved by gravity force.

[101] This work has been presented in September 2008 at 6th International Conference on High Performance Marine Vehicles (HIPER '08), in Naples, Italy. It has been reported in References as Bertorello & Oliviero 2008.

5.1 Table of Contents

5.2 Figure Index

5.3 Introduction

The first application of planing surface was recorded by English explorers in Hawaiian Islands, at the end of eighteenth century.

Captain James Cook witnessed the first board surfers and recorded it in his journal: the Hawaiian National Pastime. [Edge 2001]

Surfboards will be the only planing surface application till the end of nineteenth century.

The goal of this work is to highlight the relationships between the kinematic and dynamic surfboard behavior and geometrical and environmental parameters related to.

Hydrodynamic behavior has been investigated too, in order to analyze the dynamics of some fundamental performances.

In order to achieve these goals, planing surface models have been applied to the surfboard.

5.4 Planing Conditions

Let define the planing conditions for a surfboard riding on a wave, and advancing with the same propagation direction of the front wave.

5.4.1 Kinematic Planing Conditions

The Froude number related to the beam *b* of a surfboard is

$$F_{nb} = \frac{V}{\sqrt{g\,b}} \qquad \textbf{(A. 1)}$$

and the speed wave formula in shallow water[(102)] is

$$V_c = \sqrt{g\,h} \qquad \textbf{(A. 2)}$$

Starting to surf, surfer and wave have the same speed.

If the surfboard is propelled, along the front wave propagation, much slower (or much faster) than the wave, it cannot exchange energy with the wave. If the surfboard is moving slightly slower than the wave, it can be caught and pushed along and gets further accelerated by wave: the surfboard gains energy and the wave loses the same amount of energy. [CHEN 1984]

This, and the above formulas, drive to:

$$F_{nb}^2 = \frac{h}{b} \qquad \textbf{(A. 3)}$$

A vessel or a surfboard planing condition, cannot be defined by a unique Froude number value. Some authors suggest a range of value for each kind of Froude number; in our case, the planing condition related to the beam *b* is $F_{nb} \geq 1.5$ [Savitsky & Brown 1976], and substituting in (A. 3):

$$h \geq 2.25\,b \qquad \textbf{(A. 4)}$$

That is the first "kinematic" condition for planing, in which the beam of the surfboard *b* is linked to the deep of water *h*, both in the same unit length.

---

(102) Shallow water range: $h/\lambda < 0.04$, where *h* is the depth of water and λ is the length-wave.[Miranda 2001]

Some authors [Fédiaevski et al. 1974] suggest to use the Froude number related to the total weight:

$$F_{n\nabla} = \frac{V}{\sqrt{g\sqrt[3]{\frac{W}{\gamma}}}} \qquad \textbf{(A. 5)}$$

and the planing condition is reached if $F_{n\nabla} \geq 3$.

Reminding the formula in (A. 2), we have:

$$h \geq 9 \cdot \sqrt[3]{\frac{W}{\gamma}} \qquad \textbf{(A. 6)}$$

This is the second "kinematic" condition for planing, in which the total weight (sum of the surfer weight and the surfboard one) is linked to the deep of water h.

5.4.2 Mechanical Planing Condition

These kinematic conditions are necessary but not sufficient for planing, as a matter of fact planing is completely developed if the weight W is balanced only by the force F'[(103)]:

$$W = F'$$

With reference to Figure 5.4-1

$$F' = L\cos\alpha + D\sin\alpha$$

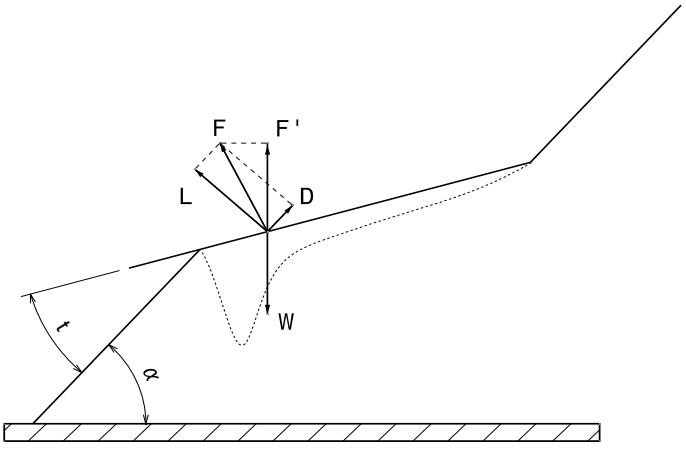

Figure 5.4-1 Pressure distribution and loads on a planing flat plate

[(103)] Planing is fully developed if the Archimedean force (hydrostatic force) is negligible versus the hydrodynamic one.

Reminding, for flat plate planing:

$$\frac{D}{L} = \frac{C_D}{C_L} = \tan\tau$$

we have

$$F' = L\left(\cos\alpha + \tan\tau \sin\alpha\right)$$

hence

$$W = L\frac{\cos(\alpha - \tau)}{\cos\tau}$$

or

$$W = \frac{1}{2}\rho V^2 S_w C_L(\tau, AR)\frac{\cos(\alpha - \tau)}{\cos\tau} \qquad \textbf{(A. 7)}$$

For planing flat plate, a non linear lift coefficient formula is [Wadlin & Christopher 1958]:

$$C_L(\tau, AR) = \frac{0.5\pi\, AR}{1 + AR}\tau\,\cos^2\tau + \frac{4}{3}\left(1 - \frac{AR}{10}\right)\sin^2\tau\cos^3\tau \qquad \textbf{(A. 8)}$$

with $AR \in [0.125, 10]$.

In the range $AR \in [0.125, 10]$, $\dfrac{C_L}{\cos\tau}$ has a maximum value of $\left.\dfrac{C_L}{\cos\tau}\right|_{\max} = 0.899 < 0.9$.

Further:

$$S_w \le S\,,$$

$$\cos(\alpha - \tau) \le 1\,,$$

and

$$\left.\frac{C_L}{\cos\tau}\right|_{\max} S_w \cos(\alpha - \tau) < 0.9\,S\,,$$

so:

$$W = \frac{1}{2}\rho V^2 S_w C_L(\tau, AR) < 0.45\,\rho V^2 S$$

and reminding that:

$$V^2 = g\,h \text{ and } \gamma^* = \rho g$$

we have:

$$W < 0.45\,\gamma^{*}\,h\,S \qquad \textbf{(A. 9)}$$

The equation (A. 9) must be satisfied for each value of h from equation (A. 4); for $h = h_{\min} = 2.25b$:

$$W < 1.01\,\gamma^{*} b S \qquad \textbf{(A. 10)}$$

and for sea water ($\gamma^{*} = 1025\frac{kgf}{m^3} = 10055\frac{N}{m^3}$)

$$\begin{array}{lll} a) & W < 1038\ \ b^2\,l & [kgf] \\ b) & W < 10181\,b^2 l & [N] \end{array} \qquad \textbf{(A. 11)}$$

That is a "mechanical" condition for planing, with the surfboard dimensions, in meter [m], related to the total weight.

Formulas (A. 4), (A. 6) and (A. 10) are the conditions to be satisfied for planing with a surfboard.

5.5 Incipient wave breaking

Surfer has to catch the wave before its breaking.

An important geometrical parameter related to the wave performance, in shallow water, is the wave steepness, H/λ which describe the incipient wave breaking[(104)].

As a wave approaches a beach, its shape may change increasing the steepness wave value. It has been noted, from math models and experiments, that as the depth decreases, the wave length reduces. So the height of the wave increases, and the speed of the wave decreases, and the period remain constant . The wave crest at the surface gradually assumes a higher speed than the wave trough in front of it, and when the slope between them becomes increasingly steeper, the crest, becoming instable, spills over forming a breaker [de Mestre 2003].

Waves break as they reach a limiting value of steepness, which is a function of the relative depth h/H and the sea bed slope $\tan\alpha_w$. [Smith 2002]

The term "breaker depth index" is used to describe nondimensional breaker height:

$$\gamma_b = \frac{H_b}{h_b} \qquad \textbf{(A. 12)}$$

in which the subscript "b" stands for "breaking wave".

Early studies on breaker indices were conducted using solitary waves (regular waves field), and the theoretically value determined was $\gamma_b = 0.78$.

For low steepness waves, we have $0.78 < \gamma_b < 1.56$, with [Smith 2002]:

$$\gamma_b = 0.78 \text{ if } \alpha_w = 0\,\text{deg}$$

$$\gamma_b = 1.56 \text{ if } \alpha_w = 90\,\text{deg}.$$

Some authors suggest to use value of the break depth index in the range 1.1 to 1.3 [de Mestre 2003].

The lowest value of the breaker depth index ($\gamma_b = 0.78$) is commonly used in engineering practice as a first estimate of the breaker index [Smith 2002]. Reminding the (A. 4), we have:

(104) H is the height of the wave and λ is the wave length, in the same unit of length.

$$\begin{cases} H_{\max} = 1.75\, b \\ h_{\min} = 2.25\, b \end{cases} \qquad \textbf{(A. 13)}$$

with

$$H_{\max} \le 0.78\, h_{\min} \qquad \textbf{(A. 14)}$$

that is a “no breaking wave” condition.

5.6 Hydrodynamic model

Let consider the movement of a rigid body Γ on an inclined plane Π, which is moving at V_C speed, as shown in Figure 5.6-1:

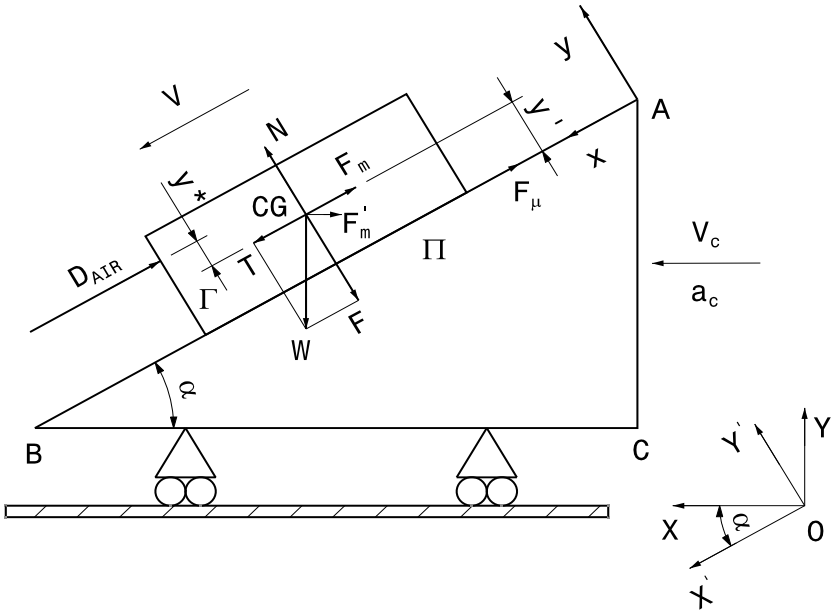

Figure 5.6-1 Rigid body Γ on an inclined plane Π

From the equilibrium equation of force and moments in $\{O, X', Y'\}$:

$$\begin{cases} N - F - F_m' \sin\alpha = 0 \\ T - D_{AIR} - F_m - F_m' \cos\alpha - F_\mu = 0 \\ F_\mu y' - D_{AIR} y^* = 0 \end{cases} \qquad \textbf{(A. 15)}$$

reminding that

$$F_m = \frac{W}{g} a_x$$

$$F_m' = \frac{W}{g} a_c$$

$$F_\mu = \mu\left(F + F_m' \sin\alpha\right)$$

$$D_{AIR} = \frac{1}{2} \rho_{AIR} V^2 A$$

$$F = W\cos\alpha$$

$$T = W\sin\alpha$$

we have:

$$a_x = g\left[\left(\frac{\tan\alpha - \mu}{\sqrt{1+\tan^2\alpha}}\right) - \frac{a_c}{g}\left(\frac{1+\mu\tan\alpha}{\sqrt{1+\tan^2\alpha}}\right) - \frac{1}{2}\left(\frac{\rho_{AIR}V^2A}{W}\right)\right] \quad \textbf{(A. 16)}$$

Let consider the inclined plane Π as a fluid body (side of a wave); at the equilibrium, the rigid body Γ will be inclined of an angle τ (angle of attack) versus the inclined plane Π.

In first approximation, let assume the hypothesis:

- all forces pass through CG, which involve that the moment equilibrium is satisfied.
- the hydrostatic force is negligible: the volume of the surfboard displaced is null $\nabla_\Gamma \cong 0$.

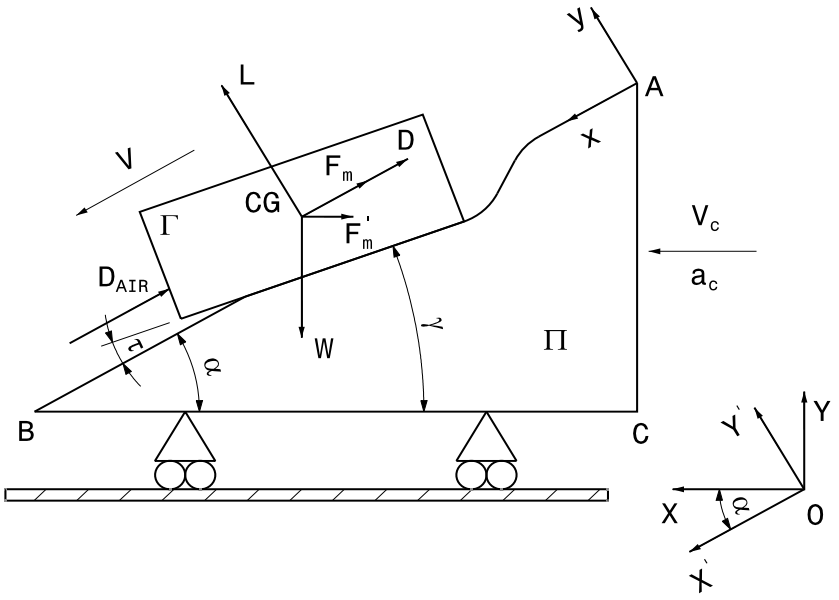

Figure 5.6-2 Rigid body on a side wave

At the equilibrium in $\{O, X', Y'\}$

$$\begin{cases} W\cos\alpha - F_m - D - F_m'\cos\alpha - D_{AIR} = 0 \\ L - F_m'\sin\alpha - W\cos\alpha = 0 \end{cases} \quad \textbf{(A. 17)}$$

Reminding that

$$L = \frac{1}{2}\rho V^2 S_w C_L(\tau, AR) \qquad D = \frac{1}{2}\rho V^2 S_w C_D(\tau, AR)$$

and for flat plate planing

$$\frac{C_D}{C_L} = \frac{D}{L} = \tan\tau$$

we have:

$$a_x = g\left[\left(\frac{\tan\alpha - \tan\tau}{\sqrt{1+\tan^2\alpha}}\right) - \frac{a_c}{g}\left(\frac{1+\tan\tau\tan\alpha}{\sqrt{1+\tan^2\alpha}}\right) - \frac{1}{2}\left(\frac{\rho_{AIR}V^2A}{W}\right)\right] \qquad \textbf{(A. 18)}$$

Note that equations (A. 16) and (A. 18) look like the same, whereas μ is known and τ is unknown.

Further, in both formulas, a_x is sum of three terms:

- the first is pertinent to the movement of the rigid body Γ versus the wave Π;
- the second is associated to the movement of the wave Π;
- the third is due to the aerodynamics.

The term related to aerodynamic drag is negligible versus the others; as a matter of fact in (A. 17) we have

$$D = \frac{1}{2}\rho V^2 S_w C_D(\tau, AR) \qquad D_{AIR} = \frac{1}{2}\rho_{AIR}V^2A$$

$$o\left(\frac{\rho_{AIR}}{\rho}\right) \approx 10^{-3} \text{ and } o\left(\frac{A}{S_w C_D}\right) \approx 1,$$

$$D_{AIR} << D$$

so:

$$a_x \cong g\left[\left(\frac{\tan\alpha - \tan\tau}{\sqrt{1+\tan^2\alpha}}\right) - \frac{a_c}{g}\left(\frac{1+\tan\tau\tan\alpha}{\sqrt{1+\tan^2\alpha}}\right)\right] \qquad \textbf{(A. 19)}$$

It is important to remark that a surfer "fills" his weight force direction (local vertical[105]) and the surfboard trim, so the surfer is able to fill the pitch angle γ of the surfboard versus the horizontal plane[106]. By Figure 5.6-2, it is easy to show that $\gamma = \alpha - \tau$, with $\gamma > 0$ for surfboard nose down.

Let determine the expression of a_c.

[105] Local vertical is the local gravity force direction.

[106] Horizontal plane is a plane perpendicular to the local vertical.

Reminding that $V_c = \sqrt{gh}$:

$$a_c = \frac{dV_c}{dt} = g \tan \alpha_w \qquad \textbf{(A. 20)}$$

with α_w slope of the sea bed.

We note that for deep water constant $\alpha_w = 0$ and $a_c = 0$; while for deep water decreasing moving closer to the shoreline $\alpha_w < 0$ and $a_c < 0$.

The time length of planing is related to the difference between the surfer and the wave speed: less difference longer time.

In the "start up" phase (rising up phase before planing) surfer has to both rise up the side wave and avoid to be overtaken by the wave: $a_x \neq 0$.

In the "surf" phase (planing phase), surfer tries to maximize the time of planing [or the speed (kinetic energy)], driving the surfboard with a speed close to the wave speed: $a_x \cong 0$ [or with a speed greater than the wave speed: $a_x >> 0$].

The time length of "start up" should not be greater than half period T_w of the wave: for time grater than $\frac{T_w}{2}$ the wave will overtaken the surfer.

5.6.1 The "Start up" phase

At time $t = 0$ let $\alpha = 0$, from (A. 19):

$$a_x\big|_{t=0} = -g \tan \tau - a_c$$

or

$$a_x\big|_{t=0} = -g \tan \tau + g \tan|\alpha_w| \qquad \textbf{(A. 21)}$$

If the surfboard is initially horizontal ($\gamma = 0$ and $\tau = 0$ for $t = 0$)

$$a_x = g \tan|\alpha_w| > 0 \qquad \textbf{(A. 22)}$$

If the surfer speed at time $t = \frac{T_w}{2}$ is not close to the speed wave, surfboard bobs up and down as the wave goes by. To avoid this case it is possible to rise up the initial value of speed V and/or to rise up the acceleration a_x .

From the (A. 21), to get an higher initial value of a_x , surfer has to turn the surfboard to an angle $\tau < 0$: surfer waits the wave with the surfboard nose down.

At time $t = t^* > 0$, rising up the side wave, $\alpha > 0$, $\tau \geq 0$ (with $\tau < 0$ surfboard cannot plan), and for $a_x \geq 0$ it must be $\tau < (|\alpha_w| + \alpha)$, or $\gamma > -|\alpha_w|$, with $\alpha + |\alpha_w| < \frac{\pi}{2}$: surfer can get $a_x = 0$ driving the surfboard nose up with a pitch angle equal to $|\alpha_w|$, while nose up value lower than $|\alpha_w|$ drives to $a_x > 0$, further nose down angle value drives to $a_x >> 0$.

5.6.2 The "Surfing" phase

In the "surfing" phase, surfer will drive the surfboard trimming the pitch angle γ to get $a_x \approx 0$ (max time of planing) or $a_x >> 0$ (max kinetic energy).

For constant deep water, $\alpha_w = 0$ and $a_c = 0$:

$$\begin{aligned} a_x = 0 \quad &\Leftrightarrow \quad \tau = \alpha \quad \gamma = 0 \\ a_x >> 0 \quad &\Leftrightarrow \quad \tau < \alpha \quad \gamma > 0 \end{aligned}$$

($\gamma > 0 \quad \rightarrow$ surfboard nose down).

For decreasing deep water, $\alpha_w < 0$ and $a_c < 0$:

$$\begin{aligned} a_x = 0 \;\Leftrightarrow\; \tau = |\alpha_w| + \alpha \;\; ; \; \gamma = -|\alpha_w| \\ a_z >> 0 \Leftrightarrow\; \tau < |\alpha_w| + \alpha \;\; ; \; \gamma > -|\alpha_w| \end{aligned} \qquad \textbf{(A. 23)}$$

surfer will drive the surfboard with a pitch angle related to the value of a_x.

5.6.3 Surfer's max speed

Let determine the max surfer speed in the hypothesis of steady motion wave and horizontal sea bed ($\alpha_w = 0 \deg$).

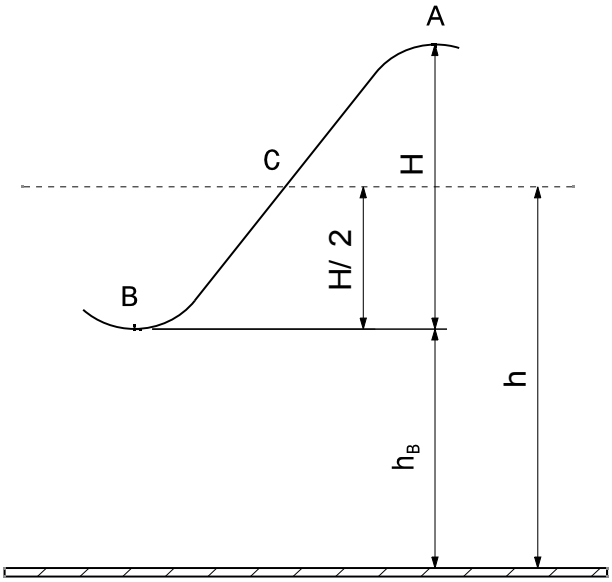

Figure 5.6-3 Wave geometry: lateral view

From the Bernoulli's equation (conservation of energy equation):

$$\frac{1}{2}mV_A^2 + mg(H + h_B) = \frac{1}{2}mV_B^{'2} + mgh_B \qquad \textbf{(A. 24)}$$

we have:

$$V_B^{'} = V_B\sqrt{1+\frac{3H}{h_B}} \qquad \textbf{(A. 25)}$$

with

$$V_A = \sqrt{g(h_B + H)} \qquad \text{and} \qquad V_B = \sqrt{gh_B}$$

wave speed in A and B respectively, and $V_B^{'}$ the surfer speed in B.

From the (A. 14) we can write $H_{\max} = 0.78h$ ($\alpha_w = 0\deg$) where h is the average depth of the wave; as shown in Figure 5.6-3, $h = h_B + \frac{H}{2}$, so:

$$H_{\max} = 1.28\, h_B$$

$$V_{B.\max}^{'} = 2.2\, V_B$$

$$V_A = 1.5\, V_B$$

$$V_C = 1.28\, V_B$$

and

$$V_{B,\max}^{'} = 1.72\, V_C \qquad \textbf{(A. 26)}$$

the speed of surfer is not greater than 1.72 times the speed of wave V_C for $\alpha_w = 0\deg$.

If we take $H_{\max} = 1.56h$ ($\alpha_w = 90\,\text{deg}$), it will be:

$$H_{\max} = 7.09\,h_B$$

$$V_B^{'} = 4.7\,V_B$$

$$V_A = 2.8\,V_B$$

$$V_C = 2.1\,V_B$$

$$V_B^{'} = 2.25\,V_C \qquad \textbf{(A. 27)}$$

the speed of surfer is not greater than 2.25 times the speed of wave V_C for $\alpha_w = 90\,\text{deg}$. So the maximum theoretical value of surface speed, related to the wave speed V_C, is in the range [1.72 ; 2.25].

Reminding that:

- surfer starts to coast down the advancing front of the wave, from the top A to the bottom B, before the incipient wave breaking,
- Bernoulli's equation does not take in account the loss of energy due to viscous effects,

the surfer speed will be less than the maximum theoretical value of $V_B^{'}$.

5.7 “Hanging ten” performance

An interesting surfing exercise is termed “hanging ten”: it involves having one’s 10 toes over the front end of the surfboard.

This is a trick that is not so common nowadays because for most people it requires a very heavy board, which is not readily available anymore. [Edge 2001]

5.7.1 OLO Surfboard

Let analyze this performance case related to an “OLO” surfboard[107].

DATUM

$l = 18\,ft \cong 5.5\,m \qquad \lambda \cong 12.5$

$W_S \cong 55\,kgf \qquad W_M \cong 80\,kgf$

At the equilibrium, with a constant speed[108], we have:

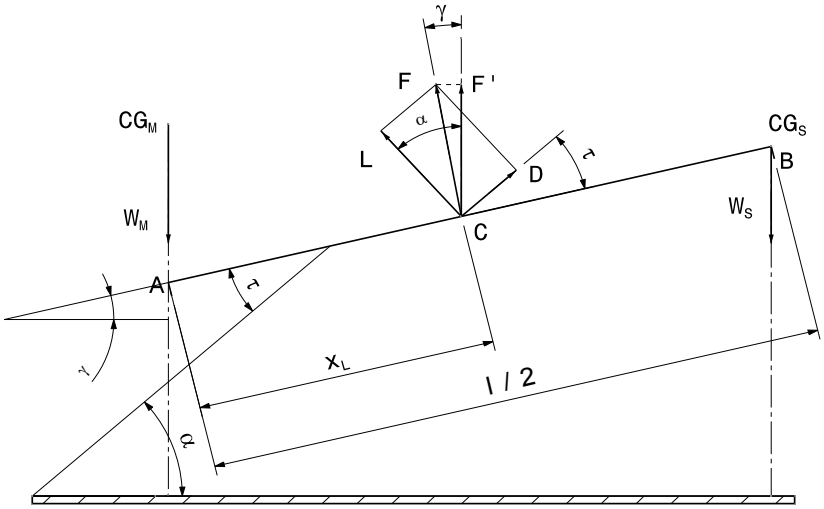

Figure 5.7-1 Hanging ten: loads and geometry

$$\begin{cases} F' = W_s + W_M \\ F' x_L = W_S \dfrac{l}{2} \end{cases} \qquad \textbf{(A. 28)}$$

[107] The *OLO* surfboards were reserved for Hawaiian royalty; it was the biggest surfboard. Cut from native Hawaiian trees, trimmed to shape, polished with coral and finished with nut oil, an *OLO* board sometimes measured 24 feet [about 7.3 m] long and weighed up to 200 pounds [about 91 kg].

[108] In this exercise the surfer is not able to balance the inertial loads, so at the equilibrium $a_x = 0\,m/s^2$ and $\gamma = 0\,\text{deg}$.

Reminding that

$$F' = L\cos\alpha + D\sin\alpha \qquad \textbf{(A. 29)}$$

we have

$$\begin{cases} L\dfrac{\cos(\alpha-\tau)}{\cos\tau} = W_S + W_M \\ x_L\dfrac{L}{\cos\tau} = W_S\dfrac{l}{2}\cos(\alpha-\tau) \end{cases} \qquad \textbf{(A. 30)}$$

and

$$x_L = \frac{W_S}{W_S+W_M}\frac{l}{2}\cos^2(\alpha-\tau)$$

During the *hanging ten* exercise surfer has foot closer themselves and closer to the front end of the surfboard. This drives to a set with surfer in bolt upright and surfboard in (or closer to) horizontal plane: $\gamma = \alpha - \tau \cong 0$.

Hence:

$$x_L = \frac{W_S}{W_S+W_M}\frac{l}{2} \qquad \%x_L = \frac{W_S}{2(W_S+W_M)} \qquad \textbf{(A. 31)}$$

$$\%L_{CP} = 1 - \%x_L \qquad L_{CP} = \%L_{CP}\, l \qquad \textbf{(A. 32)}$$

and

$$F = 135kg \qquad \%x_L = \frac{55kg}{270kg} = 0.2037$$

$$\%L_{CP} = 0.7963 \quad L_{CP} \cong 4.4m$$

For each speed of a flat plate, the equilibrium set is known if τ and l_w (or $AR = \frac{b}{l_w}$) are known.

From Wagner's model of planing flat plane [Wagner 1932], we know that $\forall\tau\ \exists!\frac{L_{CP}}{l_w}$, so for each fixed value of AR exists, for the equilibrium, only one value of τ obtained by Wagner's model:

$$\forall\, AR\ \exists!\tau: \qquad \frac{L_{CP}}{b}AR\Big|_{Surfboard} = \frac{L_{CP}}{l_w}\Big|_{Wagner} \qquad \textbf{(A. 33)}$$

The couple of value (τ, AR) that satisfy the planing condition $(F_{nb} \geq 1.5)$ will describe an "hanging ten" equilibrium set:

$$F_{nb} = \sqrt{\frac{2(W_M + W_S) AR \cos\tau}{\gamma^* b^3 \cdot C_L(\tau, AR)}} \geq 1.5 \qquad \textbf{(A. 34)}$$

where C_L is known by (A. 8).

The first step is to find out the range value of AR, within we define the trial values of AR.

We know that $L_{CP} < l_w \leq l$, so it follows $\frac{b}{l} \leq AR < \frac{b}{L_{CP}}$.

Let $AR_{\min} = \frac{b}{l}$ and $AR_{\max} = \frac{b}{L_{CP}}$, we have:

$$\left.\frac{L_{CP}}{l_w}\right|_{\min} = \frac{L_{CP}}{b} AR_{\min} = 1 - \left[\frac{W_S}{2(W_M + W_S)}\right]$$

$$\left.\frac{L_{CP}}{l_w}\right|_{\max} = \frac{L_{CP}}{b} AR_{\max} = 1$$

so

$$1 - \left[\frac{W_S}{2(W_M + W_S)}\right] \leq \frac{L_{CP}}{l_w} < 1$$

Values of $\frac{L_{CP}}{l_w}$ off range do not make sense, as matter of fact:

- $\frac{L_{CP}}{l_w} < 1 - \frac{W_S}{2(W_M + W_S)}$ means $l_w > l$,
- $\frac{L_{CP}}{l_w} > 1$ means that the center of pressure is out of wetted area.

In our case:

$$AR_{\min} = 0.080 \qquad \text{and} \qquad AR_{\max} = 0.100\,.$$

Let fix other two arbitrary values of AR within the range $[AR_{\min}, AR_{\max}]$, we have:

$$AR = AR_{\min} = 0.080 \rightarrow \%L_{CP} = 0.7963 \rightarrow \tau = 15.5\,\text{deg} \rightarrow C_L = 0.1138 \rightarrow$$

$$\rightarrow F_{nb} = 1.5 \qquad V = 3.0\frac{m}{s}$$

$$AR = 0.087 \quad \rightarrow \quad \%L_{CP} = 0.8635 \rightarrow \tau = 19.5\,\text{deg} \rightarrow C_L = 0.1613 \rightarrow$$
$$\rightarrow F_{nb} = 1.3 \quad V = 2.6\frac{m}{s}$$

$$AR = 0.094 \quad \rightarrow \quad \%L_{CP} = 0.9328 \rightarrow \tau = 23.0\,\text{deg} \rightarrow C_L = 0.2031 \rightarrow$$
$$\rightarrow F_{nb} = 1.2 \quad V = 2.4\frac{m}{s}$$

$$AR = AR_{\max} = 0.100 \rightarrow \%L_{CP} = 1.000 \rightarrow \tau = 26.0\,\text{deg} \rightarrow C_L = 0.2367 \rightarrow$$
$$\rightarrow F_{nb} = 1.1 \quad V = 2.3\frac{m}{s}$$

there is only one "hanging ten" equilibrium set for a planing surfboard "OLO":

$$\tau \cong 15.5\,\text{deg} \qquad \text{and} \qquad AR \cong 0.080\,.$$

5.7.2 Commercial surfboard

Let repeat this procedure for a commercial surfboard:

DATUM

$l = 2.40\,m \quad b = 0.61\,m$

$W_S = 5\,kgf \quad W_M = 80\,kgf$

$$AR_{\min} = 0.250 \qquad AR_{\max} = 0.258 \qquad L_{CP} = 2.37\,m$$

$$AR = AR_{\min} = 0.250 \rightarrow \%L_{CP} = 0.9706 \rightarrow \tau = 24.5\,\text{deg} \rightarrow C_L = 0.2797 \rightarrow$$
$$\rightarrow F_{nb} = 0.77 \quad V = 1.9\frac{m}{s}$$

$$AR = AR_{\max} = 0.258 \rightarrow \%L_{CP} = 1.000 \rightarrow \tau = 26.0\,\text{deg} \rightarrow C_L = 0.2992 \rightarrow$$
$$\rightarrow F_{nb} = 0.75 \quad V = 1.8\frac{m}{s}$$

no "hanging ten" exercises can be performed with this commercial surfboard.

5.8 Cross running

The minimum speed that a surfer can reach is the wave speed.

In each point of the side wave the surfer's speed component along the wave direction (propagation) is equal to the wave speed on that point.

In fact if the surfer's speed component were less than the speed wave the surfer would bob up and down as the wave goes by, while if the surfer's speed component were higher than the speed wave the surfer should fly!

In each point on the side wave the surfer's velocity can be higher, in modulus, than the wave velocity. As matter of fact, from Bernoulli's equation, we have:

$$\frac{1}{2}mV_A^2 + mg\left(h_B + H\right) = \frac{1}{2}mV'^2 + mgh^* \qquad \textbf{(A. 35)}$$

with:

$$V_A^2 = g\left(h_B + H\right) \text{ and } V^* = gh^*$$

so:

$$V' = V^*\sqrt{\frac{3\left(h_B + H\right)}{h^*} - 2}\text{, with } h_B \le h^* \le h_B + H\,.$$

The surfer's velocity and the wave direction, in the horizontal plane[(109)], define an angle θ (yaw angle), as shown in Figure 5.8-1:

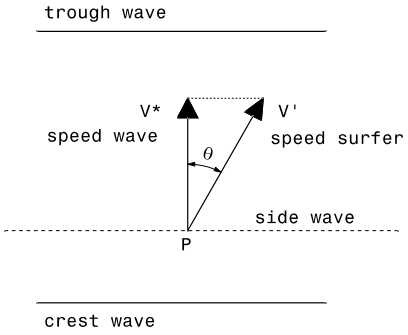

Figure 5.8-1 Wave sketch: top view

and reminding that $V^* = V'\cos\theta$, we have:

[(109)] The horizontal plane is a general plane normal to the local gravity force direction.

$$\theta = \arccos \frac{1}{\sqrt{\frac{3(h_B + H)}{h^*} - 2}} \qquad \textbf{(A. 36)}$$

with $h^* = h_B$ in B and $h^* = h_B + H$ in A, as shown in Figure 5.8-2.

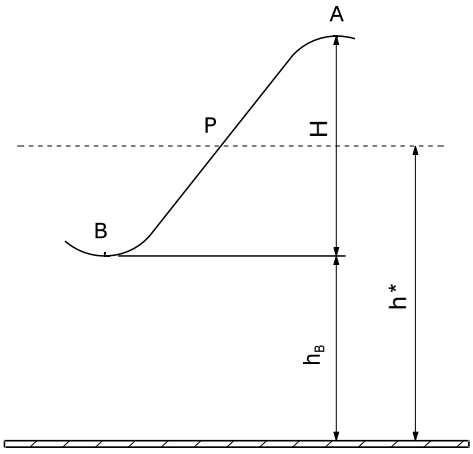

Figure 5.8-2 Wave sketch: lateral view

This yaw angle θ is not constant and its value is related to the surfer's position on the side wave:

- in A (crest) $h^* = h_B + H \quad \theta_A = 0\,\text{deg}$
- in B (through) $h^* = h_B \quad \theta_B = \arccos \frac{1}{\sqrt{3\frac{H}{h_B} + 1}}$ and in "no braking wave" condition for $\alpha_w = 0°$ ($H \le 0.78 \cdot h$) we have $\theta_B \le 63°$ (lower limit value), while for $\alpha_w = 90°$ ($H \le 1.56 \cdot h$) we have $\theta_B \le 78°$ (upper limit value).

5.9 Example of application

Surfboard and surfer datum:

$l = 2.40\,m \quad b = 0.61\,m \qquad W_S = 5\,kgf \qquad W_M = 85\,kgf$

In first approximation we have:

1° "kinematic" planing condition

$h \geq 2.25b = 2.25 \cdot 0.61\,m = 1.37\,m \qquad\qquad h \geq 1.37\,m$

2° "kinematic" planing condition

$$h \geq 9 \cdot \sqrt[3]{\frac{W}{\gamma}} = 9 \cdot \sqrt[3]{\frac{90\,kg}{1025\,\frac{kg}{m^3}}} = 4.00\,m \qquad\qquad h \geq 4.00\,m$$

"mechanical" planing condition

$$W < 1038\,b^2 l = 1038\,\frac{kgf}{m^3} \cdot (0.61\,m)^2 \cdot 2.40\,m = 927\,kgf \qquad\qquad W < 927\,kgf$$

(surfer must have a weight less than 927 kgf !)

"no breaking wave" conditions:

$H_{\max} < 0.78h$ for $\alpha_w = 0°$

$H_{\max} < 1.56h$ for $\alpha_w = 90°$

Let $h = 10\,m$, we have

$H_{\max} < 7.8\,m$ (lower limit value)

$H_{\max} < 15.6\,m$ (upper limit value)

1. $H = 2.0\,m \qquad h_B = h - \frac{H}{2} = 9.0\,m \qquad \vartheta_B \cong 39°$
2. $H = 4.0\,m \qquad h_B = 8.0\,m \qquad \vartheta_B \cong 51°$
3. $H = 6.0\,m \qquad h_B = 7.0\,m \qquad \vartheta_B \cong 58°$
4. $H = H_{\max} = 7.8\,m \qquad h_B = 6.1\,m \qquad \vartheta_B \cong 63°$
5. $H = H_{\max} = 10\,m \qquad h_B = 5.0\,m \qquad \vartheta_B = 68°$
6. $H = H_{\max} = 12\,m \qquad h_B = 4.0\,m \qquad \vartheta_B = 72°$

7. $H = H_{\max} = 14\,m \qquad h_B = 3.0\,m \qquad \vartheta_B = 75°$

8. $H = H_{\max} = 15.6\,m \quad h_B = 2.2\,m \qquad \vartheta_B = 78°$

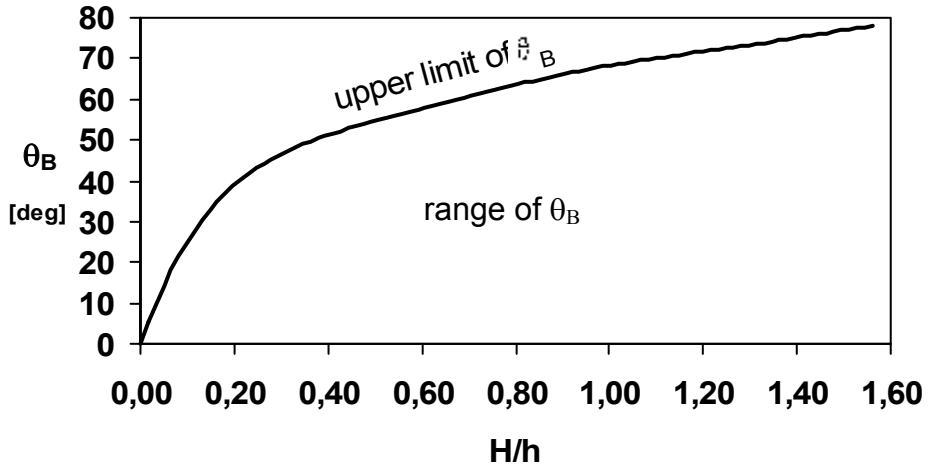

Figure 5.9-1 Yaw angle diagram

$$V_C = \sqrt{gh} \cong 10\frac{m}{s}$$

$$F_{nb} = \frac{V_C}{\sqrt{gb}} = \sqrt{\frac{h}{b}} = \sqrt{\frac{10\,m}{0.61\,m}} \cong 4 \qquad \Rightarrow \qquad F_{nb} > 1.5$$

$$F_{n\nabla} = \frac{V_C}{\sqrt{g\sqrt[3]{\frac{W}{\gamma}}}} = \sqrt{\frac{h}{\sqrt[3]{\frac{W}{\gamma}}}} = \sqrt{\frac{10\,m}{\sqrt[3]{\frac{90\,kg}{1025\frac{kg}{m^3}}}}} = 4.7 \qquad \Rightarrow \qquad F_{n\nabla} > 3$$

$$V'_{B.\max} = 1.72 V_C = 17.2\frac{m}{s} \quad (\alpha_W = 0\deg)$$

$$V'_{B.\max} = 2.25 V_C = 22.5\frac{m}{s} \quad (\alpha_W = 90\deg)$$

Further:

$$\frac{C_L(\tau, AR)}{AR} = \frac{W}{\frac{1}{2}\rho V^2 b^2} = \frac{90kgf\,9.81\frac{N}{kgf}}{\frac{1}{2}1025\frac{kg}{m^3}\left(10\frac{m}{s}\right)^2 (0.61m)^2} = 0.0463$$

$$C_L(\tau, AR) = 0.0463\,AR$$

For $AR = AR_{\min} = 0.254$

$$C_L(\tau, AR) = 0.0463 \cdot 0.254 \cong 0.0118 \quad \rightarrow \quad \tau \cong 1.5\,\text{deg}$$

$$S_{w,\max} = \frac{b^2}{AR_{\min}} = \frac{(0.61m)^2}{0.254} \cong 1.46m^2 \quad \rightarrow \quad l_w = 2.4m = l$$

but $l = l_w$ if and only if $\tau = 0\,\text{deg}$, so this case $AR = AR_{\min}$ (with $l = l_w$ and $\tau > 0\,\text{deg}$) has no physical meaning.

For $AR = AR_{\max} = 10$

$$C_L(\tau, AR) = 0.0463 \cdot 10 = 0.463 \quad \rightarrow \quad \tau \cong 21.5\,\text{deg}$$

$$S_{w,\min} = \frac{b^2}{AR_{\max}} = \frac{(0.61m)^2}{10} = 0.037m^2 \quad \rightarrow \quad l_w = 0.061m$$

So for $h = 10m$:

$F_{nb} = 4$

$F_{n\nabla} = 4.7$

$V_C = 10\frac{m}{s} \qquad 17.2\frac{m}{s} \le V'_{B,\max} \le 22.5\frac{m}{s}$

$V'_B < 17.2\frac{m}{s} \quad \alpha_w = 0\,\text{deg}; \qquad V'_B < 22.5\frac{m}{s} \quad \alpha_w = 90\,\text{deg}$

$1.5° < \tau \le 21.5°$

$63° \le \vartheta_{B\max} \le 78°$

and the planing will start to be over for $1.37m < h < 4.00m$ and will be off for $h < 1.37m$.

5.10 Conclusion

Surfboards are planing surfaces subjected only to the gravity force.

The kinematic behavior of a surfboard is related to geometrical and environmental parameters.

Some formulas considering the kinematic and dynamic conditions and the "no breaking wave" condition, in order to get the surfboard in planning, are proposed.

Hydrodynamic behavior has been investigated too, and some tips are proposed in order to improve the overall performances as well as to understand some fundamental performances: the fastest run, the “hanging ten” exercise and the cross running.

Finally an example in order to get useful information for greater surf performance is presented.

5.11 Symbols

BASIC

A	Wave crest	
A	Projected area of Γ on a plane normal to Π	[m^2]
a_c	Wave (or Π) acceleration	$\left[m/s^2\right]$
a_x	Surfer (or Γ) acceleration component	$\left[m/s^2\right]$
AR	Aspect Ratio	$AR = b^2/S_W$
b	Surfboard beam	[m]
B	Wave trough	
CG	Center of Gravity	
CP	Center of Pressure	
C_D	Hydrodynamic drag coefficient	$C_D = C_D(\tau, AR)$
C_L	Hydrodynamic lift coefficient	$C_L = C_L(\tau, AR)$
D	Hydrodynamic drag	[N]
D_{AIR}	Aerodynamic drag	[N]
F	Weight component perpendicular to Π	[N]
$F_m, F_m^{'}$	Inertial forces	[N]
F_{nb}	Froude number related to the beam b	$F_{nb} = \frac{V}{\sqrt{gb}}$
F_μ	Friction force	[N]
g	Gravity acceleration:	$g \cong 9.81 m/s^2$
h	Depth of water	[m]
H	Wave height	[m]
h^*	Height of a point P on the side wave	[m]
h_B	Crest wave height	[m]
l	Surfboard length	[m]
L	Hydrodynamic lift	[N]
L_{CP}	Center of Pressure location (measured from aft end of surfboard)	[m]
l_w	Wetted length	[m]; $l_w = S_W/b$
$\frac{L_{CP}}{l_w}$	Nondimensional location of the center of pressure linked to the wetted length of the surfboard	
$\%L_{CP}$	Nondimensional location of the center of pressure related to the length of the surfboard	$\%L_{CP} = L_{CP}/l$
m	Mass	[kg]
N	Reaction force of the inclined plane Π	[N]
S	Surfboard Projected area on Π	[m^2]; $S = lb$
S_W	Surfboard wetted surface	[m^2]

t	Time	[s]
T	Towing force: weight component on Π	[N]
T_w	Wave period	[s]
V	Surfboard speed component, along x-axis	$[m/s]$
V'	Surfer speed in a point P of the side wave	$[m/s]$
V^*	Wave speed in a point P of its side	$[m/s]$
V_A	Wave speed in A (crest)	$[m/s]$
V_B	Wave speed in B (trough)	$[m/s]$
V_B'	Surfer speed of in B	$[m/s]$
V_C	Wave speed	$[m/s]$
V_X	Component of V along X-axis	$[m/s]$
W	Total weight	[N]
x_{CP}	Distance of CP versus the surfboard front end	[m]
x_L	Distance of CP versus the front edge of the surfboard wetted surface	[m]
$\%x_L$	Nondimensional distance of CP versus the surfboard front end	$\%x_L = x_L/l$
y'	Moment arm of F_μ versus CG in $\{A,x,y\}$	[m]
$y*$	Moment arm of D_{AIR} versus CG in $\{A,x,y\}$	[m]
α	Side wave slope (or slope of inclined plane Π)	[°,deg]
α_W	Sea bed slope	[°,deg]
γ	Surfboard pitch angle (or pitch angle of the rigid body Γ)	[°,deg]
$\gamma*$	Unit weight of water	$[N/m^3]; \gamma* = \rho g$
γ_b	Breaker depth index	
Γ	Rigid body	
θ	Yaw angle of surfer speed vs wave direction	[°,deg]
λ	Wave length	[m]
μ	Friction coefficient	
Π	Inclined plane	
ρ	Mass density of water	$[kg/m^3]$
ρ_{AIR}	Mass density of air	$[kg/m^3]$
τ	Angle of attack of the surfboard versus the wave side	[°,deg]
$\{A,x,y\}$	Cartesian coordinate system, fixed on Π, with x-axis on Π and top-bottom oriented	
$\{O,X,Y\}$	Cartesian coordinate system, Earth fixed, with X-axis horizontal and oriented to the water's edge	
$\{O,X',Y'\}$	Cartesian coordinate system, Earth fixed, obtained by a counterclockwise rotation of magnitude α versus $\{O,X,Y\}$	

SUBSCRIPT

b	breaking wave	

M	surfer	
max	maximum value	
min	minimum value	
S	surfboard	

5.12 References

Bertorello, C. & Oliviero, L. 2008. Surf Hydromechanics. *Proceeding 6th International Conference on High Performance Marine Vehicles (HIPER '08)*. Italy. Comitato Organizzatore HIPER 08, Naples, Italy. Vol. 1, pp. 281-290. ISBN/ISSN: 88-901174-9-4.

Chen, F. F. 1984. *INTRODUCTION TO PLASMA PHYSICS AND CONTROLLED FUSION.*. Berlin: Springer. pp. 245-247 (ISBN 03046413329)

de Mestre, N. 2003. *THE MATHEMATICS AND PHYSICS OF BODY SURFING*. 5th International Congress on Industrial and Applied Mathematics (ICAM 2003), Minisymposium 2116 ICM161U-08, Paper 7286, Sydney, Australia, 7-11 July 2003

Edge, R. 2001. Surf Physics. *The Physics Teacher* Vol. 39, pp. 272-277 (ISSN: 0031-921X)

Fédiaevski, C., Voïtkounski, I., Faddéev, Y. 1974. *MECANIQUE DES FLUIDES.* Moscou: Ed. MIR. pp. 542-543 (French version)

Miranda, S. 2001 *Appunti di Architettura Navale*. Napoli: Dipartimento di Ingegneria Navale, Università degli Studi di Napoli "FEDERICO II" (Italian language - web site: http://wpage.unina.it/miranda/)

Savitsky, D. & Brown, P.W. 1976. Procedures for Hydrodynamic Evaluation of Planing Hulls in Smooth and Rough Water. *Marine Technology* Vol. 13, No 4, pp. 381-400

Smith, J.M. 2002. *SURF ZONE HYDRODYNAMICS.* In *Coastal Engineering Manual EM 1110-2-1100 (Part II)*. Vicksburg (Mississippi): US Army Corps of Engineers (USA). Part 2, Chapter 4, pp 1-5. [web site: http://www.usace.army.mil/publications/eng-manuals/em1110-2-1100/PartII/PartII.htm]

Wadlin, K.L. & Christopher, K.W. 1958. A Method for Calculation of Hydrodynamic Lift for Submerged and Planing Rectangular Lifting Surfaces. *Report NACA TN 4168*. Washington, D.C. (USA). (web site: http://ntrs.nasa.gov/search.jsp)]

Wagner, H. 1932. Über Stoss und Gleitvorgänge an der Oberfläche von Flüssigkeiten. *Z.A.M.M.* No.4 Vol.12. [English version: Phenomena associated with Impacts and Sliding on liquid surfaces. *Report NACA TR N-23507*, 1936. Washington, D.C. (USA). (web site: http://ntrs.nasa.gov/search.jsp)]

APPENDIX B

CONTINUITY EQUATION AND LAPLACE'S EQUATION FOR A PERFECT FLUID FLOW

6.1 Table of Contents

6.2 Figure Index

6.3 The continuity equation

In fluid dynamics one of the fundamental conditions that must be satisfied is that no fluid can be created or destroyed within the flow field considered.

This condition means that the amount of fluid entering any small element of volume must equal the amount of fluid leaving the element. The *equation of continuity* express this condition. [Abbott & Doenhoff 1959]

A fluid continuous, homogeneous and frictionless is known as *perfect fluid*.

The assumption of frictionless, or zero viscosity or zero shearing stresses, simplifies the motion equations, and among these the continuity equation, that otherwise cannot generally be solved.

The direct effects of viscosity are negligible except in the layer of fluid adjacent to the surface, and viscosity has little effect on the general flow pattern unless the local effects are such as to make the flow separate from the surface. [Abbott & Doenhoff 1959]

Let introduce a differential control volume, with a block shape, in a Cartesian coordinate system as shown in Figure 6.3-1:

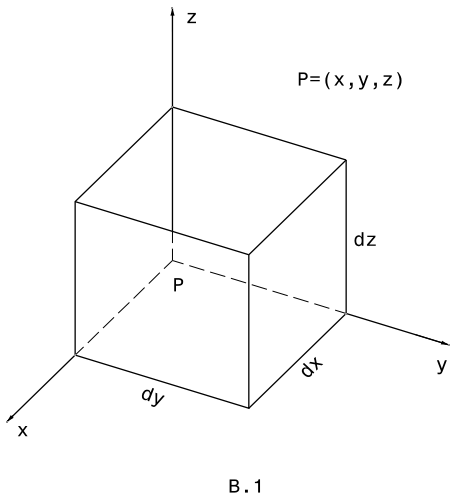

Figure 6.3-1 Differential control block

let:

dx, dy, dz	Edge dimensions of the control volume along the three axis, respectively
x, y, z	Coordinate of the point P, a vertex of the control volume, and origin of the Cartesian coordinate system

t	Time
$\rho = \rho(x, y, z, t)$	Density of fluid in the control volume
m	Mass of fluid in the control volume
$\left.\begin{array}{l} u = u(x, y, z) \\ v = v(x, y, z) \\ w = w(x, y, z) \end{array}\right\}$	Component along the three axis, respectively, of the fluid flow velocity $\overline{V}$

The mass of fluid in the differential control volume is:

$$m = \int_{\delta V} \rho(\xi, \eta, \zeta, t) \mathrm{d}\xi \, \mathrm{d}\eta \, \mathrm{d}\zeta \qquad \textbf{(B. 1)}$$

with $\delta V = dx\,dy\,dz$.

For the differential control volume, it may be assumed (to a first-order approximation) that the fluid properties are constant over each of its six faces. [Zucrow & Hoffman 1976]

This assumption drives to:

$$m = \int_{\delta V} \rho(\xi, \eta, \zeta, t) d\xi \, d\eta \, d\zeta = \rho(x, y, z, t) \int_{\delta V} d\xi \, d\eta \, d\zeta = \rho(x, y, z, t) dx \, dy \, dz$$

$$m = \rho \, dx \, dy \, dz \qquad \textbf{(B. 2)}$$

where ρ is constant only within the differential control volume, but not in each point of flow field.

The increase of mass per unit of time in the differential control volume is:

$$\frac{\partial m}{\partial t} = -\frac{\partial}{\partial t}(\rho \, dx \, dy \, dz) = -\frac{\partial \rho}{\partial t} dx \, dy \, dz \qquad \textbf{(B. 3)}$$

The minus sign comes from the fact that if the flow through out the faces of differential control volume increase, then there will be a net loss of mass within it, and vice versa.[Journée & Massie 2001]

Let point out the flow mass along x-axis.

The flow mass through in the plane $dydz$ in x station during the time dt is:

$$m_x^{in} = \rho(u \, dt) dy \, dz$$

$$m_x^{in} = \rho u \, dy \, dz \, dt \qquad \textbf{(B. 4)}$$

The flow mass through out the plane $dy\,dz$ in station $x + dx$ during the time dt is:

$$m_{x+dx}^{out} = \left\{ \rho(u\,dt) + \frac{\partial}{\partial x}[\rho(u\,dt)]dx \right\} dy\,dz$$

$$m_{x+dx}^{out} = \left[\rho u + \frac{\partial(\rho u)}{\partial x} dx \right] dy\,dz\,dt \qquad \textbf{(B. 5)}$$

The net mass flow through the x-axis will be:

$$\left(\frac{\partial m}{\partial t}\right)_x = \frac{m_{x+dx}^{out} - m_x^{in}}{dt} = \left[\rho u + \frac{\partial(\rho u)}{\partial x} dx \right] dy\,dz - \rho u\,dy\,dz$$

$$\left(\frac{\partial m}{\partial t}\right)_x = \frac{\partial(\rho u)}{\partial x} dx\,dy\,dz \qquad \textbf{(B. 6)}$$

Similarly, along y and z directions:

$$\left(\frac{\partial m}{\partial t}\right)_y = \frac{\partial(\rho v)}{\partial y} dx\,dy\,dz \qquad \textbf{(B. 7)}$$

$$\left(\frac{\partial m}{\partial t}\right)_z = \frac{\partial(\rho w)}{\partial z} dx\,dy\,dz \qquad \textbf{(B. 8)}$$

Reminding that "*the amount of fluid entering any small element of volume must be equal the amount of fluid leaving the element*", we have:

$$\frac{\partial m}{\partial t} = \left(\frac{\partial m}{\partial t}\right)_x + \left(\frac{\partial m}{\partial t}\right)_y + \left(\frac{\partial m}{\partial t}\right)_z$$

$$-\frac{\partial \rho}{\partial t} dx\,dy\,dz = \frac{\partial(\rho u)}{\partial x} dx\,dy\,dz + \frac{\partial(\rho v)}{\partial y} dx\,dy\,dz + \frac{\partial(\rho w)}{\partial z} dx\,dy\,dz$$

$$\frac{\partial \rho}{\partial t} + \frac{\partial}{\partial x}(\rho u) + \frac{\partial}{\partial y}(\rho v) + \frac{\partial}{\partial z}(\rho w) = 0 \qquad \textbf{(B. 9)}$$

or in vector notation:

$$\frac{\partial \rho}{\partial t} + \overline{\nabla} \cdot (\rho \overline{V}) = 0 \qquad \textbf{(B. 10)}$$

where:

$$\overline{\nabla} \equiv \left(\frac{\partial}{\partial x}, \frac{\partial}{\partial y}, \frac{\partial}{\partial z} \right) \text{ and } \rho \overline{V} \equiv (\rho u, \rho v, \rho w).$$

The equation (B.9), or (B.10), is the *continuity equation* for a perfect fluid.

For incompressible fluids, the density ρ is constant:

$$\rho(x,y,z,t) = \rho_0 = const.$$

and continuity equation will show a simplified form:

$$\frac{\partial u}{\partial x} + \frac{\partial v}{\partial y} + \frac{\partial w}{\partial z} = 0 \qquad \textbf{(B. 11)}$$

or

$$\overline{\nabla} \cdot \overline{V} = 0 \qquad \textbf{(B. 12)}$$

This means that for an incompressible perfect fluid flow the streamlines (velocity field patterns) have a ring shape unless they start and terminate at boundaries. [Helmholtz 1858]

6.4 From continuity to Laplace equation

The frictionless, or zero shearing stresses, perfect fluid property drives to the property of irrotational velocity field.

DEM.

Let consider the differential control volume face on xy plane:

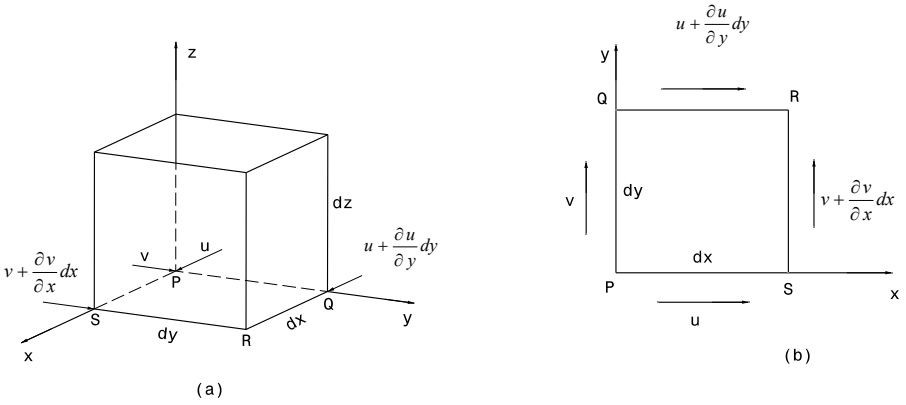

Figure 6.4-1 Differential block
(a) 3D view - (b) top view

At the equilibrium, the stresses in the field are related to the deformations and rotations of the volume of fluid.

With reference Figure 6.4-2, let:

$\left|\overline{SS'}\right| = \frac{\partial v}{\partial x} dx\, dt$ shift component of S versus P, along y-axis

$\left|\overline{PS}\right| = dx$ distance of S versus P

$\left|\overline{QQ'}\right| = \frac{\partial u}{\partial y} dy\, dt$ shift component of Q versus P, along x-axis

$\left|\overline{PQ}\right| = dy$ distance of Q versus P

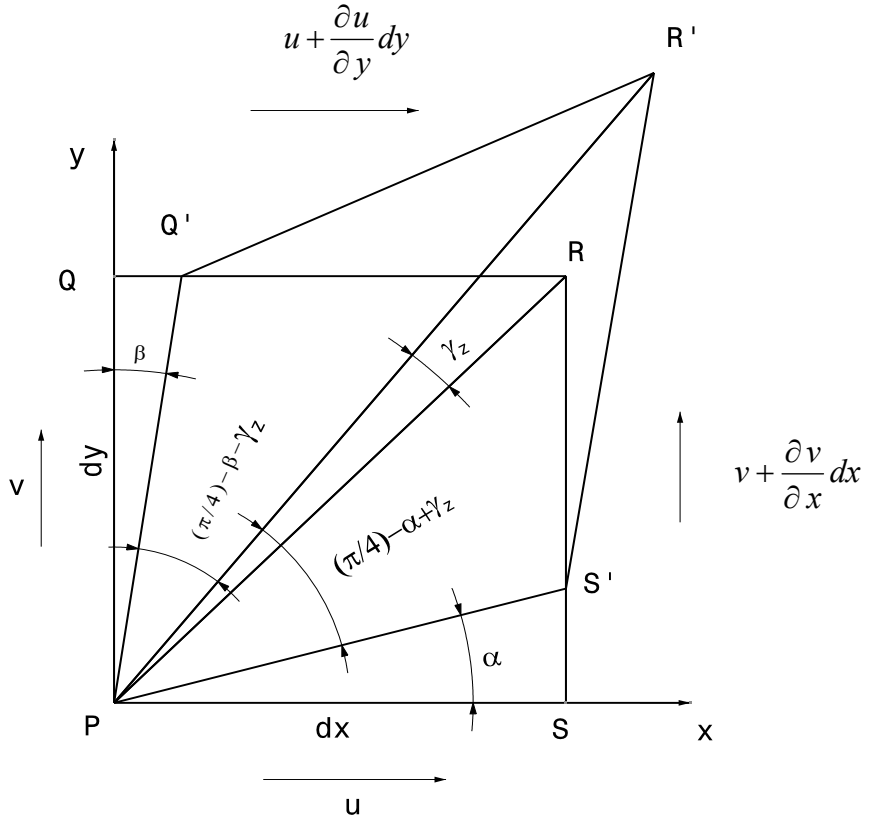

Figure 6.4-2 Deformed control block
Top view

we have

$$\alpha \approx \frac{\left|\overline{SS'}\right|}{\left|\overline{PS}\right|} \qquad \beta \approx \frac{\left|\overline{QQ'}\right|}{\left|\overline{PQ}\right|} \qquad \gamma_z : R'\hat{P}Q' = R'\hat{P}S'$$

that drives to

$$\alpha = \frac{\partial v}{\partial x}dt \qquad \beta = \frac{\partial u}{\partial y}dt \qquad \gamma_z = \frac{1}{2}(\alpha - \beta)$$

Reminding that:

$$\dot{\xi} = \frac{d}{dt}\xi \qquad \text{with } \xi = \alpha, \beta, \gamma_Z$$

it follows

$$\dot{\alpha} = \frac{\partial v}{\partial x} \qquad \dot{\beta} = \frac{\partial u}{\partial y}$$

and

$$\dot{\gamma}_z = \frac{1}{2}\left(\frac{\partial v}{\partial x} - \frac{\partial u}{\partial y}\right) \qquad \textbf{(B. 13)}$$

In the similar way, for the other planes we found:

$$\dot{\gamma}_x = \frac{1}{2}\left(\frac{\partial w}{\partial y} - \frac{\partial v}{\partial z}\right) \qquad \textbf{(B. 14)}$$

$$\dot{\gamma}_y = \frac{1}{2}\left(\frac{\partial u}{\partial z} - \frac{\partial w}{\partial x}\right) \qquad \textbf{(B. 15)}$$

and in vector notation:

$$\left(\dot{\gamma}_x, \dot{\gamma}_y, \dot{\gamma}_z\right) = \frac{1}{2}\begin{vmatrix} \frac{\partial}{\partial x} & \frac{\partial}{\partial y} & \frac{\partial}{\partial z} \\ u & v & w \end{vmatrix} = \frac{1}{2}\left(\overline{\nabla} \wedge \overline{V}\right)$$

In zero shearing stresses fluid flow there are no rotations, and this means:

$$\dot{\gamma}_x = 0 \qquad \dot{\gamma}_y = 0 \qquad \dot{\gamma}_z = 0$$

or

$$\overline{\nabla} \wedge \overline{V} = 0 \qquad \textbf{(B. 16)}$$

The assessment "*a perfect fluid flow is related to an irrotational velocity field*" has been demonstrated.

We remind, in vector calculus, that:

$$\overline{\nabla} \wedge \overline{\nabla} f = 0$$

with $f = f(x, y, z)$ a general scalar function; so we can rewrite $\overline{V}$ in (B.16) as a gradient of a scalar function:

$$\overline{V} = \overline{\nabla}\varphi \qquad \textbf{(B. 17)}$$

or

$$u = \frac{\partial \varphi}{\partial x},\ v = \frac{\partial \varphi}{\partial y},\ w = \frac{\partial \varphi}{\partial z} \qquad \textbf{(B. 18)}$$

with $\varphi = \varphi(x, y, z)$.

Applying the velocities in equation (B.17), or (B.18), to the continuity equation for incompressible fluid (B.11), or (B.12) respectively, we have:

$$\frac{\partial^2 \varphi}{\partial x^2} + \frac{\partial^2 \varphi}{\partial y^2} + \frac{\partial^2 \varphi}{\partial z^2} = 0 \qquad \textbf{(B. 19)}$$

or

$$\nabla^2 \varphi = 0 \qquad \textbf{(B. 20)}$$

both known as *Laplace's equation* or *potential equation*.

6.5 Conclusion

It has been demonstrated that, in fluid dynamics, Laplace's equation is the continuity equation pertinent to an incompressible perfect fluid or the balance equation of mass related to a continuous, homogeneous, frictionless and incompressible fluid.

All solutions of Laplace's equation are scalar functions termed *harmonic functions* and if Laplace's equation is related to a fluid flow field, these functions are further called *velocity potentials*.

It is important to highlight the powerful of potential theory: use of the velocity potential transforms the continuity equation, a first-order partial differential equation in three unknowns (velocity component u,v,w), into Laplace's equation: a second-order linear partial differential equation with only one unknown (velocity potential φ). [Granger 1985]

6.6 Symbols

$f = f(x,y,z)$	General scalar function	
m	Mass of fluid in the control volume	[kg]
m_x^{in}	Flow mass through in the plane $dydz$ in x station during the time dt	
m_{x+dx}^{out}	Flow mass through out the plane $dy\,dz$ in station $x+dx$ during the time dt	
$\left(\frac{\partial m}{\partial t}\right)_x$	Net mass flow through the x-axis of the control volume	
$\left(\frac{\partial m}{\partial t}\right)_y$	Net mass flow through the y-axis of the control volume	
$\left(\frac{\partial m}{\partial t}\right)_z$	Net mass flow through the z-axis of the control volume	
$\left(\frac{\partial m}{\partial t}\right)$	Net mass flow through the control volume	
P, Q, R, S	Points, vertex of a face of a control volume	
Q', R', S'	Points, vertex of a face of a deformed control volume	
$\overline{V}$	Fluid flow velocity vector	
t	Time	[s]
$\{P,x,y,z\}$	Cartesian coordinate system, Earth fixed, with origin P	
(x,y,z)	Coordinate of the point P	
(dx,dy,dz)	Control volume edge dimensions along the three axis, respectively	
$\left.\begin{array}{l} u = u(x,y,z) \\ v = v(x,y,z) \\ w = w(x,y,z) \end{array}\right\}$	Component along the three axis, respectively, of the fluid flow velocity $\overline{V}$	$[m/s]$
α, β, γ_z	Angles related to the deformation of the control volume	[deg]
$\dot{\alpha}, \dot{\beta}, \dot{\gamma}_z$	Angular speed	$[\mathrm{deg}/s]$

δV	Control volume value	$\delta V = dx\,dy\,dz$
φ	Potential function or Laplace's function	$\varphi = \varphi(x, y, z)$
$(\dot{\gamma}_x, \dot{\gamma}_y, \dot{\gamma}_z)$	Component of the curl of $\overline{V}$: $(\overline{\nabla} \wedge \overline{V})$	
$\rho = \rho(x, y, z, t)$	Fluid Density in the control volume	$[kg/m^3]$
ρ_0	Value of the fluid density in the control volume	$[kg/m^3]$
(ξ, η, ζ)	Integration variables	
$\overline{\nabla}$	Differential operator	$\overline{\nabla} \equiv \left(\frac{\partial}{\partial x}, \frac{\partial}{\partial y}, \frac{\partial}{\partial z}\right)$

6.7 References

Abbott, H. I. & Doenhoff, A. E. 1959. *THEORY OF WING SECTIONS*. New York: Dover Publications (USA)

Granger, R.A. 1985. *Fluid Mechanics*. New York: CBS College Publishing (USA)

Helmholtz, H.,1858. Über Integrale der hydrodynamischen Gleichungen, welche der Wirbelbewegungen entsprechen. *Crelle's Journal* (*Journal für die reine und angewandte Mathematik*), No 58, page 25-55.

Journée, J.M.J. & Massie, W.W. 2001 *Offshore Hydromechanics*. Delft: Delft University of Technology (TU Delft Library web site: www.library.tudelft.nl)

Zucrow, M.J. & Hoffman, J.D. 1976. *Gas Dynamics*. Vol I. Hoboken (NJ): John Wiley & Sons (USA) ISBN: 978-0-471-98440-5

APPENDIX C

THE CONFORMAL TRANSFORMATIONS

A Conformal Transformation consists in mapping a region of one plane to another one in such a way that the detailed shape of infinitesimal elements of area is not changed. This restriction does not mean that the shape of finite areas cannot be considerably altered [Abbott & Doenhoff 1959].

Conformal Transformations are a powerful tool: the potential field of a complex-shape domain can be obtained in term of elementary potential field of a simple-shape domain.

7.1 Table of Contents

7.2 Figure Index

7.3 Table Index

7.4 Introduction

The Laplace's equation, related to a 2-dimensional problem, can be solved in the complex plane. This way of calculus, admitted only for 2-dimensional problems, allow us:

- reduce the number of variable of the problem (from two real to one complex) simplifying the math model;
- fit solutions available to the problem via geometrical transformations (mapping).

The geometric properties of analytic functions, and the conformal mapping related to, were examined for the first time by Riemann in his thesis work on Theory of complex variables [Kline 1972] [Boyer 1968].

Riemann stated:

If D is any simply connected domain in the plane Z (other than the entire plane itself), then there exists a one-to-one conformal mapping $W = F(Z)$ that maps D onto the unit disk $|W| < 1$ [Mathews & Howell.2006].

In despite of Riemann did not demonstrated his Theorem, many applications have been developed. Among these: Mobius transformation and Schwarz-Christoffel ones.

Mobius transformation $W = \frac{i(1+Z)}{1-Z}$ is a one-to-one conformal mapping of the unit disk $|Z| < 1$ onto the upper half-plane $\mathrm{Im}(W) > 0$, and the inverse is $Z = \frac{W-i}{W+i}$.

Accordingly, Riemann's Mapping Theorem can be stated:

If D is any simply connected domain in the plane W-plane, then there exists a one-to-one conformal mapping $W = F(Z)$ that maps the upper half-plane $\mathrm{Im}(Z) > 0$ onto D. [Mathews & Howell.2006]

This assumption drives to the Schwarz-Christoffel transformation, that maps the upper half plane $\mathrm{Im}(Z) > 0$ onto a polygon G. This kind of conformal mapping will be very useful for PDEs[(110)] solution setting [Kline 1972].

Riemann Mapping Theory was developed in the complex plane (2-dimensional theory) and in the most of case fails in higher dimensions.

[(110)] PED stands for Partial Differential Equation, and Laplace's equation is one of them.

7.5 The Analytic Functions

Let $Z = x + iy$ a complex variable defined in the Z-plane (with $\{x, y\}$ Cartesian coordinate system), $W = u + iv$ a complex variable defined in the W-plane (with $\{u, v\}$ curvilinear orthogonal coordinate system), and $W = F(Z)$ a function that transforms one-to-one the points of Z-plane onto the points of W-plane:

$$W = u(x, y) + iv(x, y) = F(Z) = F(x + iy)$$

The function $F(Z)$ is analytical if its derivative $F'(Z) = \frac{dW}{dZ}$ has only one value per each point of the Z-plane.

Theorem:

A complex function $F(Z)$ is analytical if and only if its components $u(x, y)$ and $v(x, y)$ are continuous in Z-plane and further they satisfy the Cauchy-Riemann condition:

$$\frac{\partial u}{\partial x} = \frac{\partial v}{\partial y} \qquad \frac{\partial v}{\partial x} = -\frac{\partial u}{\partial y} \qquad \textbf{(C. 1)}$$

The curvilinear coordinate system $\{u, v\}$ is orthogonal if and only if :

$$\nabla u \cdot \nabla v = \left(\frac{\partial u}{\partial x}\frac{\partial v}{\partial x} + \frac{\partial u}{\partial y}\frac{\partial v}{\partial y} \right) = 0 \qquad \textbf{(C. 2)}$$

or in unit vector:

$$\bar{a}_u \cdot \bar{a}_v = 0$$

with $\bar{a}_u = \frac{\nabla u}{|\nabla u|}$ and $\bar{a}_v = \frac{\nabla v}{|\nabla v|}$.

If $F(Z)$ is an analytical function the condition (C.2) is satisfied as matter of fact that Cauchy-Riemann condition (C.1) is satisfied: any analytical function generates an orthogonal curvilinear coordinate system in the image plane.

7.5.1 Geometrical Properties

Let:

- $W = F(Z)$ an analytical function: a one-to-one mapping of the Z-plane onto the W-plane,
- P a point of Z and Q a point of W, related to P by the transformation function $W = F(Z)$,
- dZ_1 an infinitesimal segment with origin in P and dW_1 an infinitesimal segment with origin in Q, related to dZ_1 by the transformation function $W = F(Z)$,
- $F'(Z) = \dfrac{dW}{dZ}$ the derivative of the analytical function $W = F(Z)$.

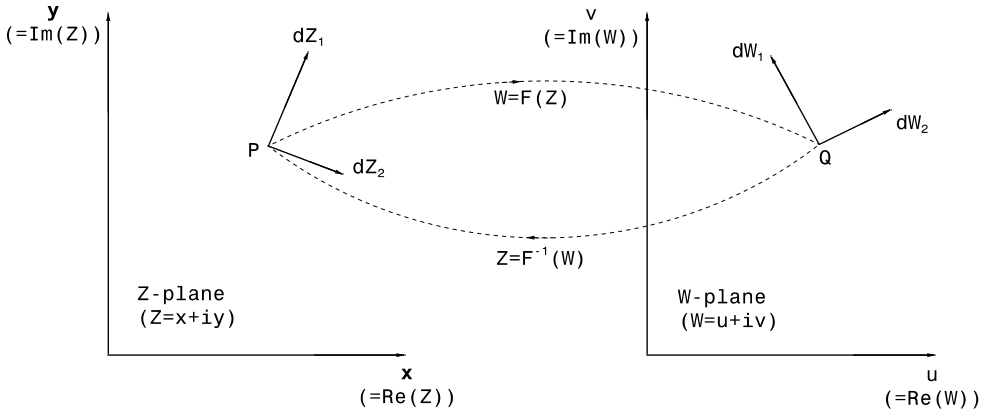

Figure 7.5-1 Complex planes

Reminding that:

$$dW = d(F(Z)) = F'(Z)dZ$$

we have

$$dW_1 = F'(Z)_P dZ_1 \text{ or } dW_1 = \left.\frac{dW}{dZ}\right|_P dZ_1 \qquad \textbf{(C. 3)}$$

where $F'(Z)\big|_P = \left.\dfrac{dW}{dZ}\right|_P$ is the value of $F'(Z)$ in P.

In order to achieve our goal, the length of segments will be expressed in exponential form:

$$dZ_1 = dL_1 \exp(i\Phi_1) \qquad dW_1 = dl_1 \exp(i\vartheta_1) \qquad \textbf{(C. 4)}$$

or

$$|dZ_1| = dL_1 \qquad |dW_1| = dl_1 \qquad \textbf{(C. 5)}$$

$$\arg(dZ_1) = \Phi_1 \qquad \arg(dW_1) = \vartheta_1 \qquad \textbf{(C. 6)}$$

Further, the derivative $\frac{dW}{dZ}$ can be expressed, in each point of Z-plane where is not null, as a complex number:

$$\frac{dW}{dZ} = H\exp(ib) \qquad \textbf{(C. 7)}$$

with H and b real number whose value are related to the chosen point P in Z-plane.

Hence:

$$dl_1 \exp(i\vartheta_1) = H\exp(ib)\cdot dL_1 \exp(i\Phi_1) \qquad \textbf{(C. 8)}$$

with

$$dl_1 = H\,dL_1 \text{ or } |dW_1| = \left|F'(Z)\right|_P |dZ_1| \qquad \textbf{(C. 9)}$$

$$\vartheta_1 = b + \Phi_1 \text{ or } \arg(W_1) = \arg\left(F'(Z)\right|_P) + \arg(Z_1) \qquad \textbf{(C. 10)}$$

Let:

- dZ_2 an infinitesimal segment with origin in P and different from dZ_1,
- dW_2 an infinitesimal segment with origin in Q, related to dZ_2 by the transformation function $W = F(Z)$.

If $W = F(Z)$ is an analytical function its derivative, in each point of Z-plane, has only one value that does not depend on the direction along which it has been determined, and hence:

$$|dW_2| = H|dZ_2| \text{ and } \arg(dW_2) = b + \arg(dZ_2) \qquad \textbf{(C. 11)}$$

So, we have:

$$\frac{|dW_1|}{|dW_2|} = \frac{|dZ_1|}{|dZ_2|} \qquad \textbf{(C. 12)}$$

and

$$\arg(dW_2) - \arg(dW_1) = \arg(Z_2) - \arg(Z_1) \qquad \textbf{(C. 13)}$$

the ratio between lengths and the angle between the segments are the same: shapes and angles are preserved.

A transform mapping that preserves oriented angles between curves and their shapes is called conformal mapping.

Conformal mapping preserves both angles and shape of infinitesimal small figure around each point P of a domain in Z-plane, but that is not true for whole domain at all: the value of derivative changes in each point of Z-plane and so the shape of a finite area is not preserved.

7.6 Laplace's equation Invariance

Let:

- dl_u and dl_v two infinitesimal segment in the W-plane,
- $\{u,v\}$ an orthogonal curvilinear coordinate system in W-plane.

We can write:

$$dl_u = h_u\, du \qquad dl_v = h_v dv \tag{C. 14}$$

so:

$$h_u = \frac{dl_u}{du} \qquad h_v = \frac{dl_v}{dv} \tag{C. 15}$$

where h_u and h_v are scalar known as scale factors.

Reminding that:

$$\frac{du}{dl_u} = \nabla u \cdot \overline{a_u} = |\nabla u| \text{ and } \frac{dv}{dl_v} = \nabla v \cdot \overline{a_v} = |\nabla v| \tag{C. 16}$$

we have:

$$h_u = \frac{1}{|\nabla u|} \qquad h_v = \frac{1}{|\nabla v|} \tag{C. 17}$$

Let $W = F(Z)$ a conformal mapping of the Z-plane onto W-plane:

$$W = u(x,y) + iv(x,y) = F(x+iy) = F(Z)$$

we have:

$$h_u = \frac{1}{|\nabla u|} = \frac{1}{\sqrt{\nabla u \cdot \nabla u}} = \frac{1}{\sqrt{\left(\frac{\partial u}{\partial x}\right)^2 + \left(\frac{\partial u}{\partial y}\right)^2}} \tag{C. 18}$$

$$h_v = \frac{1}{|\nabla v|} = \frac{1}{\sqrt{\nabla v \cdot \nabla v}} = \frac{1}{\sqrt{\left(\frac{\partial v}{\partial x}\right)^2 + \left(\frac{\partial v}{\partial y}\right)^2}} \tag{C. 19}$$

and, from Cauchy-Riemann condition, it follows:

$$h_u = h_v = h \tag{C. 20}$$

Let write Laplace's equation in $\{u,v\}$ coordinate system:

$$\nabla^2\Phi = \nabla\cdot\nabla\Phi = \frac{1}{h_u h_v}\left[\frac{\partial}{\partial u}\left(\frac{h_v}{h_u}\frac{\partial\Phi}{\partial u}\right)+\frac{\partial}{\partial v}\left(\frac{h_u}{h_v}\frac{\partial\Phi}{\partial v}\right)\right]=0 \qquad \textbf{(C. 21)}$$

or

$$\nabla^2\Phi = \frac{1}{h^2}\left[\frac{\partial^2\Phi}{\partial u^2}+\frac{\partial^2\Phi}{\partial v^2}\right]=0 \qquad \textbf{(C. 22)}$$

hence:

$$\nabla^2\Phi = \frac{\partial^2\Phi}{\partial u^2}+\frac{\partial^2\Phi}{\partial v^2}=0 \qquad \textbf{(C. 23)}$$

that has the same form of the ones in Z-plane:

$$\nabla^2\Phi = \frac{\partial^2\Phi}{\partial x^2}+\frac{\partial^2\Phi}{\partial y^2}=0 \qquad \textbf{(C. 24)}$$

a conformal mapping preserves the form of Laplace's equation, further each harmonic function $\Phi=\Phi(x,y)$ in Z-plane, transformed via conformal map onto W-plane is harmonic: $\Phi=\Phi(u,v)$.

DEM.

$$\nabla\Phi\big|_W = \left(\frac{\partial\Phi}{\partial u},\frac{\partial\Phi}{\partial v}\right) \qquad \nabla\Phi\big|_Z = \left(\frac{\partial\Phi}{\partial x},\frac{\partial\Phi}{\partial y}\right)$$

$$\frac{\partial\Phi}{\partial u}=\frac{\partial\Phi}{\partial x}\frac{\partial x}{\partial u}=h_u\frac{\partial\Phi}{\partial x} \qquad \frac{\partial\Phi}{\partial v}=\frac{\partial\Phi}{\partial y}\frac{\partial y}{\partial v}=h_v\frac{\partial\Phi}{\partial y}$$

$$\frac{\partial\Phi}{\partial x}=\frac{1}{h_u}\frac{\partial\Phi}{\partial u} \qquad \frac{\partial\Phi}{\partial y}=\frac{1}{h_y}\frac{\partial\Phi}{\partial v}$$

$$\nabla\Phi\big|_W = (h_u,h_v)\cdot\nabla\Phi\big|_Z \qquad \nabla\Phi\big|_Z = \left(\frac{1}{h_u},\frac{1}{h_v}\right)\cdot\nabla\Phi\big|_W$$

$$\frac{\partial^2\Phi}{\partial x^2}=\frac{\partial}{\partial x}\left(\frac{\partial\Phi}{\partial x}\right)=\frac{\partial}{\partial u}\left(\frac{\partial\Phi}{\partial x}\right)\frac{\partial u}{\partial x}=\frac{\partial}{\partial x}\left(\frac{1}{h_u}\frac{\partial\Phi}{\partial u}\right)\frac{1}{h_u}=\frac{1}{h_u^2}\frac{\partial^2\Phi}{\partial u^2}$$

$$\frac{\partial^2\Phi}{\partial y^2}=\frac{\partial}{\partial y}\left(\frac{\partial\Phi}{\partial y}\right)=\frac{\partial}{\partial v}\left(\frac{\partial\Phi}{\partial y}\right)\frac{\partial v}{\partial y}=\frac{\partial}{\partial v}\left(\frac{1}{h_v}\frac{\partial\Phi}{\partial v}\right)\frac{1}{h_v}=\frac{1}{h_v^2}\frac{\partial^2\Phi}{\partial v^2}$$

$$\nabla^2\Phi\big|_Z = \left(\frac{\partial^2\Phi}{\partial x^2}+\frac{\partial^2\Phi}{\partial y^2}\right)=\left(\frac{1}{h_u^2}\frac{\partial^2\Phi}{\partial u^2}+\frac{1}{h_v^2}\frac{\partial^2\Phi}{\partial v^2}\right)$$

but in a conformal mapping:

$$h_u = h_v = h$$

and:

$$\nabla^2\Phi\big|_Z = \left(\frac{\partial^2\Phi}{\partial x^2}+\frac{\partial^2\Phi}{\partial y^2}\right)=\frac{1}{h^2}\left(\frac{\partial^2\Phi}{\partial u^2}+\frac{\partial^2\Phi}{\partial v^2}\right)=\frac{1}{h^2}\nabla^2\Phi\big|_W$$

Hence, if:

$$\nabla^2\Phi\big|_Z = \frac{\partial^2\Phi(x,y)}{\partial x^2}+\frac{\partial^2\Phi(x,y)}{\partial y^2}=0$$

than:

$$\nabla^2\Phi\big|_W = \frac{\partial^2\Phi(u,v)}{\partial u^2}+\frac{\partial^2\Phi(u,v)}{\partial v^2}=0$$

and formally:

$$\nabla^2\Phi\big|_Z = \nabla^2\Phi\big|_W = \nabla^2\Phi = 0$$

The assessment "*a conformal mapping preserves the form of the Laplace's equation*" has been demonstrated.

7.7 The Schwarz-Christoffel Transformation

Schwarz-Christoffel transformation is a one-to-one conformal mapping from the upper half-plane $\mathrm{Im}(Z) > 0$ onto a domain G in the W-plane where the boundary consists of straight line segments.

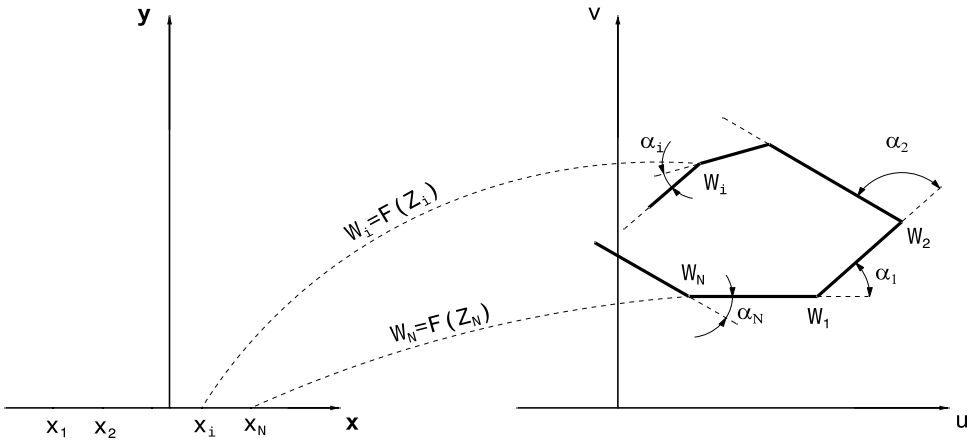

Figure 7.7-1 Schwarz-Christoffel transformation planes

Let G be a polygon in the W-plane with vertices $W_1, W_2, \ldots, W_N$ and exterior angles $\alpha_1, \alpha_2, \ldots, \alpha_N$ where $-\pi < \alpha_i < \pi$ for $i = 1,2,\ldots,N$.

There exists a one-to-one conformal mapping $W = F(Z)$ from the upper half-plane $\mathrm{Im}(Z) > 0$ onto G that satisfies the boundary conditions:

$$W_i = F(x_i) \text{ for } i = 1,2,\ldots,N \text{ and } W_{N+1} = F(x_{N+1} = \infty),$$

where $x_1 < x_2 < \ldots < x_N < x_{N+1} = \infty$ are points of the real axis in Z-plane.

The derivative $F'(Z)$ is:

$$F'(Z) = A(Z - x_1)^{-k_1}(Z - x_2)^{-k_2}\ldots(Z - x_N)^{-k_N} = A\prod_1^N (Z - x_i)^{-k_i} \qquad \textbf{(C. 25)}$$

where $k_i = \dfrac{\alpha_i}{\pi}$.

The equation (C.25) is known as Schwarz-Christoffel differential equation.

The function $W = F(Z)$ will be expressed as an indefinite integral:

$$W = F(Z) = B + A\int (Z - x_1)^{-k_1} (Z - x_2)^{-k_2} ... (Z - x_N)^{-k_N} dZ \qquad \textbf{(C. 26)}$$

The term A is a complex number by which polygon can be rotated and scaled in the W-plane, while the term B is a complex number by which polygon can be shifted in the W-plane. [Mathews & Howell.2006]

Reminding that:

$$\arg(W) = \arg(Z) + \arg(F'(Z)) \qquad \textbf{(C. 27)}$$

and $\arg(Z) = 0$ if all points P considered are on x-axis of the Z-plane, we have:

$$\arg(W) = \arg(F'(Z)) \qquad \textbf{(C. 28)}$$

or

$$\arg(W) = \arg(A) - \sum_{i=1}^{N} k_i \arg(Z - x_i) \qquad \textbf{(C. 29)}$$

At the same time, we have:

$$x < x_i \qquad \arg(x - x_i) = \pi$$

$$x > x_i \qquad \arg(x - x_i) = 0$$

Hence, moving along x-axis on Z-plane, when $x > x_i$ the angle $\arg(W)$ abruptly changes its value of a quantity equal to $k_i\pi$ and in the W-plane it starts a new side of the polygon.

The polygon will be closed if and only if the sum of all exterior angles is equal to 2π :

$$\sum_{i=1}^{N} \alpha_i = 2\pi \text{ or } \sum_{i=1}^{N} k_i = 2 \qquad \textbf{(C. 30)}$$

It is important to highlight that Schwarz-Christoffel transformation is a conformal mapping and it is expressed by an analytical function, but only its derivative leads up to a closed-form problem. [Luchini & Quadrio 2003]

As a matter of fact the equation (C.26) gives a representation of the analytical function $W = F(Z)$ in terms of an indefinite integral, that do not represent elementary functions, unless the image is an infinite region. [Mathews & Howell.2006]

7.8 Numerical Example

7.8.1 Conformal mapping example

The transformation $W = \tan Z$ is a one-to-one conformal mapping of the vertical strip $|x| < \frac{\pi}{4}$ onto the disk $|W| < 1$.

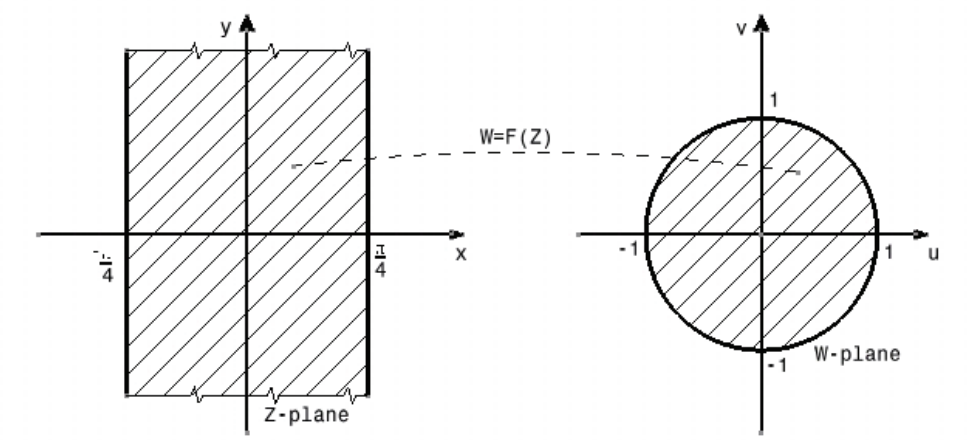

Figure 7.8-1 Conformal mapping of the vertical strip $|x| < \frac{\pi}{4}$ onto the disk $|W| < 1$.

The complex trigonometric identities:

$$\cos Z = \frac{\exp(iZ) + \exp(-iZ)}{2} \quad \sin Z = \frac{\exp(iZ) - \exp(-iZ)}{2i} \quad \textbf{(C. 31)}$$

allows us to write:

$$W = \tan Z = \frac{\sin Z}{\cos Z} = \frac{1}{i}\frac{\exp(iZ) - \exp(-iZ)}{\exp(iZ) + \exp(-iZ)} = \frac{-i\exp(i2Z) + i}{\exp(i2Z) + 1} \qquad \textbf{(C. 32)}$$

Let $\Omega = \exp(i2Z)$ with $\Omega = X + iY$, then the transformation can be considered composed by a bilinear transformation $W = \frac{-i\Omega + i}{\Omega + 1}$ and an exponential transformation $\Omega = \exp(i2Z)$.

The exponential one maps the vertical strip $|x| < \frac{\pi}{4}$ one-to-one onto the right half-plane $\mathrm{Re}(Z) > 0$, and the bilinear one maps the right half-plane one-to-one onto the disk $|W| < 1$.

1° Step: $\Omega = \exp(i2Z)$

$$Z = x + iy \qquad \xrightarrow{\Omega=\exp(i2Z)} \qquad \Omega = X + iY$$

and reminding that:

$$\exp(ix) = \cos x + i \sin x$$
$$\exp(-ix) = \cos x - i \sin x$$

we have:

Id	x	y	Z	Ω	X	Y
[1]	$-\frac{\pi}{4}$	0	$-\frac{\pi}{4}$	$\exp\left(-i\frac{\pi}{2}\right) = -i$	0	-1
[2]	$\frac{\pi}{4}$	0	$\frac{\pi}{4}$	$\exp\left(i\frac{\pi}{2}\right) = i$	0	1
[3]	0	$\frac{1}{2}$	$\frac{i}{2}$	$\exp(-1) = \frac{1}{e}$	$\frac{1}{e}$	0
[4]	0	$-\frac{1}{2}$	$-\frac{i}{2}$	$\exp(1) = e$	e	0
[5]	$-\frac{\pi}{8}$	$\frac{1}{4}$	$-\frac{\pi}{8}+\frac{i}{4}$	$\exp\left(-\frac{1}{2}-i\frac{\pi}{4}\right) = \exp\left(-\frac{1}{2}\right)\frac{\sqrt{2}}{2}(1-i)$	$(2e)^{-\frac{1}{2}}$	$-(2e)^{-\frac{1}{2}}$
[6]	$\frac{\pi}{8}$	$\frac{1}{4}$	$\frac{\pi}{8}+\frac{i}{4}$	$\exp\left(-\frac{1}{2}+i\frac{\pi}{4}\right) = \exp\left(-\frac{1}{2}\right)\frac{\sqrt{2}}{2}(1+i)$	$(2e)^{-\frac{1}{2}}$	$(2e)^{-\frac{1}{2}}$
[7]	$\frac{\pi}{8}$	$-\frac{1}{4}$	$\frac{\pi}{8}-\frac{i}{4}$	$\exp\left(+\frac{1}{2}+i\frac{\pi}{4}\right) = \exp\left(\frac{1}{2}\right)\frac{\sqrt{2}}{2}(1+i)$	$\left(\frac{e}{2}\right)^{\frac{1}{2}}$	$\left(\frac{e}{2}\right)^{\frac{1}{2}}$
[8]	$-\frac{\pi}{8}$	$-\frac{1}{4}$	$-\frac{\pi}{8}-\frac{i}{4}$	$\exp\left(+\frac{1}{2}-i\frac{\pi}{4}\right) = \exp\left(\frac{1}{2}\right)\frac{\sqrt{2}}{2}(1-i)$	$\left(\frac{e}{2}\right)^{\frac{1}{2}}$	$-\left(\frac{e}{2}\right)^{\frac{1}{2}}$

Table 7.8-1 Conformal mapping data: exponential transformation.

or in graphic form:

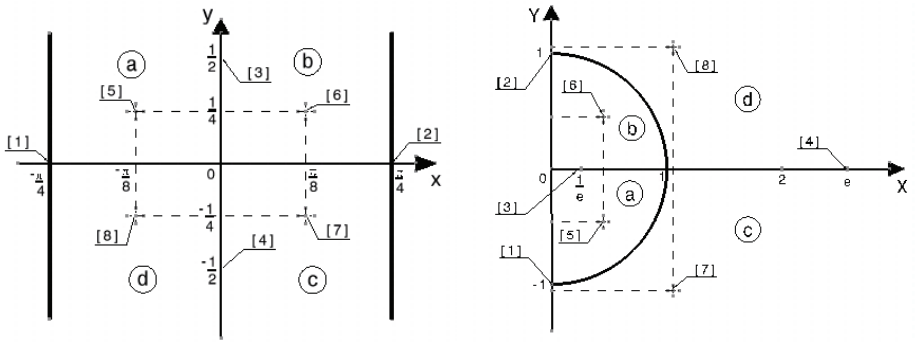

Figure 7.8-2 Conformal mapping: exponential transformation.

2° Step: $W = \dfrac{-i\Omega + i}{\Omega + 1}$

$$\Omega = X + iY \quad \xrightarrow{W=\frac{-i\Omega+i}{\Omega+1}} \quad W = u + iv$$

Id	X	Y	Ω	W	u	v
[1]	0	-1	$-i$	-1	-1	0
[2]	0	1	i	1	1	0
[3]	$\frac{1}{e}$	0	$\frac{i}{e}$	$i\left(\frac{1-\frac{1}{e}}{1+\frac{1}{e}}\right)$	0	$\frac{e-1}{e+1}$
[4]	e	0	e	$i\left(\frac{1-e}{1+e}\right)$	0	$\frac{1-e}{e+1}$
[5]	$(2e)^{-\frac{1}{2}}$	$-(2e)^{-\frac{1}{2}}$	$(2e)^{-\frac{1}{2}}(1-i)$	$\frac{-e-(2e)^{\frac{1}{2}}+ie}{e+(2e)^{\frac{1}{2}}+1}$	$\frac{-(2e)^{\frac{1}{2}}}{e+(2e)^{\frac{1}{2}}+1}$	$\frac{e-1}{e+(2e)^{\frac{1}{2}}+1}$
[6]	$(2e)^{-\frac{1}{2}}$	$(2e)^{-\frac{1}{2}}$	$(2e)^{-\frac{1}{2}}(1+i)$	$\frac{(2e)^{\frac{1}{2}}+i(e-1)}{e+(2e)^{\frac{1}{2}}+1}$	$\frac{(2e)^{\frac{1}{2}}}{e+(2e)^{\frac{1}{2}}+1}$	$\frac{e-1}{e+(2e)^{\frac{1}{2}}+1}$
[7]	$\left(\frac{e}{2}\right)^{\frac{1}{2}}$	$\left(\frac{e}{2}\right)^{\frac{1}{2}}$	$\left(\frac{e}{2}\right)^{\frac{1}{2}}(1+i)$	$\frac{(2e)^{\frac{1}{2}}+i(1-e)}{e+(2e)^{\frac{1}{2}}+1}$	$\frac{(2e)^{\frac{1}{2}}}{e+(2e)^{\frac{1}{2}}+1}$	$\frac{1-e}{e+(2e)^{\frac{1}{2}}+1}$
[8]	$(2e)^{\frac{1}{2}}$	$-(2e)^{\frac{1}{2}}$	$(2e)^{\frac{1}{2}}(1-i)$	$\frac{-(2e)^{\frac{1}{2}}+i(1-e)}{e+(2e)^{\frac{1}{2}}+1}$	$-\frac{(2e)^{\frac{1}{2}}}{e+(2e)^{\frac{1}{2}}+1}$	$\frac{1-e}{e+(2e)^{\frac{1}{2}}+1}$

Table 7.8-2 Conformal mapping data: bilinear transformation.

or in graphic form:

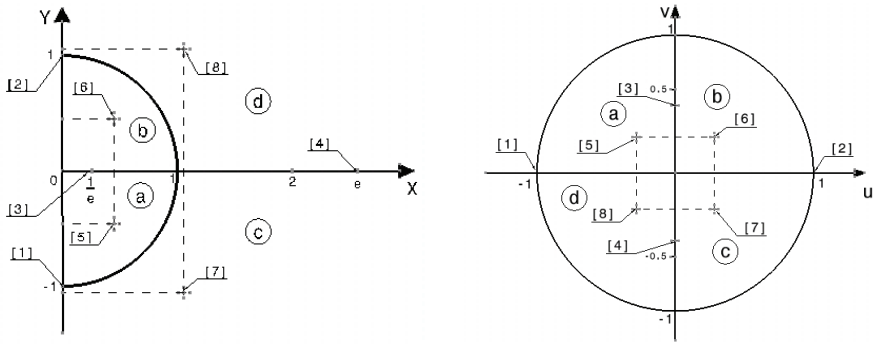

Figure 7.8-3 Conformal mapping: bilinear transformation.

In short: $W = \tan Z$

$$Z = x + iy \qquad \xrightarrow{W=\tan(Z)} \qquad W = u + iv$$

Id	x	y	Z	W	u	v
[1]	$-\frac{\pi}{4}$	0	$-\frac{\pi}{4}$	-1	-1	0
[2]	$\frac{\pi}{4}$	0	$\frac{\pi}{4}$	1	1	0
[3]	0	$\frac{1}{2}$	$\frac{i}{2}$	$i\left(\frac{1-\frac{1}{e}}{1+\frac{1}{e}}\right)$	0	$\frac{e-1}{e+1}$
[4]	0	$-\frac{1}{2}$	$-\frac{i}{2}$	$i\left(\frac{1-e}{1+e}\right)$	0	$\frac{1-e}{e+1}$
[5]	$-\frac{\pi}{8}$	$\frac{1}{4}$	$-\frac{\pi}{8}+\frac{i}{4}$	$\frac{-e-(2e)^{\frac{1}{2}}+ie}{e+(2e)^{\frac{1}{2}}+1}$	$\frac{-(2e)^{\frac{1}{2}}}{e+(2e)^{\frac{1}{2}}+1}$	$\frac{e-1}{e+(2e)^{\frac{1}{2}}+1}$
[6]	$\frac{\pi}{8}$	$\frac{1}{4}$	$\frac{\pi}{8}+\frac{i}{4}$	$\frac{(2e)^{\frac{1}{2}}+i(e-1)}{e+(2e)^{\frac{1}{2}}+1}$	$\frac{(2e)^{\frac{1}{2}}}{e+(2e)^{\frac{1}{2}}+1}$	$\frac{e-1}{e+(2e)^{\frac{1}{2}}+1}$
[7]	$\frac{\pi}{8}$	$-\frac{1}{4}$	$\frac{\pi}{8}-\frac{i}{4}$	$\frac{(2e)^{\frac{1}{2}}+i(1-e)}{e+(2e)^{\frac{1}{2}}+1}$	$\frac{(2e)^{\frac{1}{2}}}{e+(2e)^{\frac{1}{2}}+1}$	$\frac{1-e}{e+(2e)^{\frac{1}{2}}+1}$
[8]	$-\frac{\pi}{8}$	$-\frac{1}{4}$	$-\frac{\pi}{8}-\frac{i}{4}$	$\frac{-(2e)^{\frac{1}{2}}+i(1-e)}{e+(2e)^{\frac{1}{2}}+1}$	$-\frac{(2e)^{\frac{1}{2}}}{e+(2e)^{\frac{1}{2}}+1}$	$\frac{1-e}{e+(2e)^{\frac{1}{2}}+1}$

Table 7.8-3 Conformal mapping data: trigonometric transformation of the vertical strip $|x| < \frac{\pi}{4}$ onto the disk $|W| < 1$.

or in graphic form:

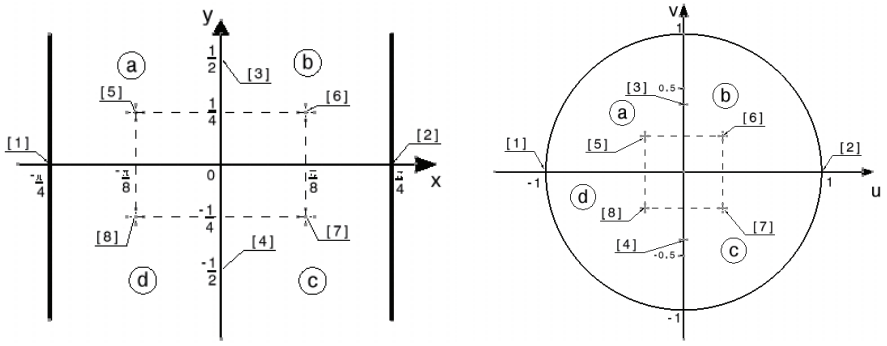

Figure 7.8-4 Conformal mapping: trigonometric transformation of the vertical strip $|x| < \frac{\pi}{4}$ onto the disk $|W| < 1$..

7.8.2 Schwarz-Christoffel conformal mapping example

Let determine a one-to-one conformal mapping $w = f(z)$ of the upper half-plane $y \geq 0$ onto the polygonal region defined by $u \geq 0, -1 \leq v \leq +1$.

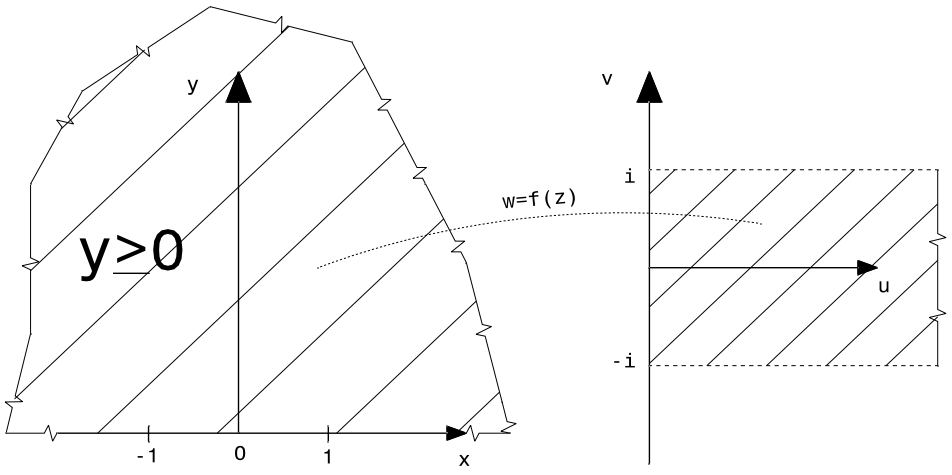

Figure 7.8-5 Schwarz-Christoffel conformal mapping

The polygonal region is a semi-infinite strip with vertices $w_1 = -i, w_2 = +i$ with interior angles related to $\alpha_1 = \alpha_2 = \frac{\pi}{2}$.

Adopting $x_1 = -1, x_2 = +1$, we have:

$$f'(z) = A(z+1)^{-\frac{1}{2}}(z-1)^{-\frac{1}{2}} \qquad \textbf{(C. 33)}$$

and

$$f'(z) = \frac{A}{(z^2-1)^{\frac{1}{2}}} = \frac{A}{\left[-(1-z^2)\right]^{\frac{1}{2}}} = \frac{A}{\left[(i)^2(1-z^2)\right]^{\frac{1}{2}}} = \frac{A}{i(1-z^2)^{\frac{1}{2}}}$$

it follows

$$f'(z) = \frac{-iA}{(1-z^2)^{\frac{1}{2}}} \qquad \textbf{(C. 34)}$$

Reminding that:

$$\frac{d}{dz}\sin^{-1} z = \frac{1}{\left(1-z^2\right)^{\frac{1}{2}}} \qquad \textbf{(C. 35)}$$

we have:

$$f'(z) = -iA\frac{d}{dz}\sin^{-1} z \qquad \textbf{(C. 36)}$$

and

$$f(z) = -iA\sin^{-1} z + B \qquad \textbf{(C. 37)}$$

where A and B are complex constants and $\sin^{-1} z$ is a branch of inverse Sine[111]: the single-valued function is obtained by using the principal square root and principal value of the logarithm. [Zill & Shanahan 2006]

Constants A and B can be computed by conditions:

$$x_1 \xrightarrow{w=f(z)} w_1 \text{ and } x_2 \xrightarrow{w=f(z)} w_2 .$$

or $f(-1) = -i$ and $f(+1) = +i$,that drive to the system of equations:

$$\begin{aligned} -iA\sin^{-1}(-1) + B &= -i \\ -iA\sin^{-1}(1) + B &= i \end{aligned} \qquad \textbf{(C. 38)}$$

or

$$\begin{aligned} iA\frac{\pi}{2} + B &= -i \\ -iA\frac{\pi}{2} + B &= i \end{aligned} \qquad \textbf{(C. 39)}$$

by which

$$\begin{aligned} A &= -\frac{2}{\pi} \\ B &= 0 \end{aligned} \qquad \textbf{(C. 40)}$$

Therefore:

$$w = f(z) = \frac{2i}{\pi}\sin^{-1} z \qquad \textbf{(C. 41)}$$

---

[111] The inverse sine expression, in complex plane, is $\sin^{-1} z = -i\ln\left[iz + \left(1-z^2\right)^{\frac{1}{2}}\right]$.

It is multiple-value function, as matter of fact it is defined in terms of the complex logarithm $\ln z$. The inverse sine can be made single-valued by specifying a single value of the square root to use for the expression $\left(1-z^2\right)^{\frac{1}{2}}$ and a single value of the complex logarithm $\ln z$ [Zill & Shanahan 2006].

7.9 Symbols

A	Complex number	
a_u	Unit vector u-axis	
a_v	Unit vector v-axis	
b	Real number	
B	Complex number	
D	Simply connected domain in Z-plane	
dl_i, dL_i	Infinitesimal segments	
e	Napier's constant	e = 2.7182 …
$F(Z)$	Complex function	W=F(Z)
$F'(Z)$	Derivative of F(Z)	$F'(Z)=\frac{dW}{dZ}$
G	Polygon onto W-plane	
H	Real number	
h_u, h_v, h	Scalar factor	
i	Imaginary unit	$i=\sqrt{-1}$
k_i	Real number	$k_i=\frac{\alpha_i}{\pi}$
Z	Complex variable on Z-plane	$Z=x+iy$
Z-plane	Plane Z	
W	Complex variable on W-plane	$W=u+iv$
W_i	Vertices of polygon G	
W-plane	Plane W	
x	Real part of Z	$x=\mathrm{Re}(Z)$
X	Real part of Ω	$X=\mathrm{Re}(\Omega)$
x_i	Points of x-axis	
y	Imaginary part of Z	$y=\mathrm{Im}(Z)$
Y	Imaginary part of Ω	$Y=\mathrm{Im}(\Omega)$
u	Real part of W	$u=\mathrm{Re}(W)$
v	Imaginary part of W	$v=\mathrm{Im}(W)$
$\mathrm{Re}(Z)>0$	Real axis on Z-plane	x-axis
$\mathrm{Im}(Z)>0$	Imaginary axis on Z-plane	y-axis
$\mathrm{Re}(W)>0$	Real axis on W-plane	u-axis
$\mathrm{Im}(W)>0$	Imaginary axis on W-plane	v-axis
∇	Nabla or Differential operator	$\nabla\equiv\left(\frac{\partial}{\partial x},\frac{\partial}{\partial y},\frac{\partial}{\partial z}\right)$
∇^2	Laplace's operator	$\nabla^2\equiv\left(\frac{\partial^2}{\partial x^2}+\frac{\partial^2}{\partial y^2}+\frac{\partial^2}{\partial z^2}\right)$

α_i	Exterior angles of the polygon G	
Φ	Potential function	$\Phi = \Phi(x, y)$ or $\Phi = \Phi(u, v)$
θ_i, Φ_i	Angles between curves	
Ω	Complex variable on Ω-plane	$\Omega = X + iY$
$\{x, y\}$	Cartesian coordinate system on Z-plane	
$\{u, v\}$	Curvilinear orthogonal coordinate system on W-plane	

7.10 References

Abbott, H. I. & Doenhoff, A. E. 1959. *THEORY OF WING SECTIONS*. New York: Dover Publications (USA) ISBN 0-486-60586-8

Boyer, C. B. 1968. *A HISTORY OF MATHEMATICS*. Hoboken (NJ): John Wiley & Sons (USA) – [Italian version : STORIA DELLA MATEMATICA. 1980. Segrate (MI): Arnoldo Mondadori Editore (Italy) ISBN 88-04-33431-2]

Kline, M. 1972. *Mathematical Thought from ancient to modern times.*. New York (USA): Oxford University Press – [Italian version : STORIA DEL PENSIERO MATEMATICO. 2002. Vol. 1 e Vol. 2 Giulio Enaudi Editore Torino (Italy). Vol.1 ISBN 88-06-15417-6. Vol.2 ISBN 88-06-15418-4]

Luchini, P. & Quadrio, M. 2003. *Aerodinamica*. Milano (Italy): Politecnico di Milano (Dipartimento di Ingegneria Aerospaziale web site: www.aero.polimi.it/~quadrio)

Mathews, J.H. & Howell, R.W. 2006. *Complex Analysis for Mathematics and Engineering*. Fifth Edition. Sundbury, MA (USA): Jones & Bartlett Publisher Inc. ISBN: 0-7637-3748-8. [http://math.fullerton.edu/mathews/complex.html]

Zill, D.G. & Shanahan, P. 2006. *A First Course in Complex Analysis with Applications*. Second Edition. Sundbury, MA (USA): Jones & Bartlett Publisher Inc. ISBN: 0-7637-4658-4.

APPENDIX D

AN HYPOTHESIS ON THE PRE-PLANING PHASE OF A CRAFT

8.1 Table of Contents

8.2 Figure Index

8.3 Table Index

8.4 Introduction

Let consider a craft moving in smooth water: all waves are craft generated.

Earlier $Fn = 0.4$ the craft is supported by two waves: the bow ("fore") and the stern ("aft") ones.

Rising up to $Fn = 0.4$ aft wave outplaces the stern: the craft goes down gliding on the front flank of the aft wave and turning around the bow one[(112)].

Beyond $Fn = 0.4$ the craft is supported by less than one wave, the wavelength of the bow wave is higher than the load water line length of the craft $L_{WL.}$

This bow wave draws a "groove" whose throat level is lower than the calm water one [Russo Krauss 1994].

At turn of $Fn = 0.4$ the craft, advancing up the oncoming flank of its own bow wave, starts to move onto this wave groove getting the squat and trim effect [Savitsky 2003].

This drop down of craft and its center of gravity (CG) is achieved without increases of draft [Russo Krauss 1994].

As matter of fact the draft is related to the buoyancy that, with lift negligible, balances the overall weight of the craft: a weight of craft constant involves a draft constant too.

The longitudinal slope and the depth (throat level) of the wave groove (or equivalent the squat and the trim of the craft) depend on the high of the bow wave, that is related to kinetic energy of the craft [Miranda2001] and draft.

Increasing craft speed, lift and kinetic energy rise up, but till lift will be negligible versus buoyancy, the main effect will be related to the growth of kinetic energy: higher kinetic energy higher slope and depth of groove and lower level of CG.

Until lift is negligible versus buoyancy, increasing the craft speed the sink speed of CG decreases.

As point of fact with a further increasing of speed the tiny lift starts to reduce just a little bit the draft of the craft, which drives to a very little reduction of the bow wave height. This little height wave reduction is overcome by the growth of height wave due to the growth of kinetic energy: higher speed lower growth height wave and lower sink speed of CG.

[(112)] In Literature this is known as "squat and trim" effect in pre-planing phase of craft motion.

Just beyond $Fn = 0.4$ hydrodynamic lift is negligible versus buoyancy: lift and its effects will be negligible till the hull has not been reached its maximum squat and trim value.

With a further increment of speed, the lift is not anymore negligible and starts to reduce the draft of the craft and the bow wave height.

In this phase, CG starts rising up due to draft and height bow wave reduction: a "leverage" effect of the lift.

In the hypothesis of uniformly accelerated craft motion in the horizontal plane, the leverage effect of the lift drives to a quickly elevation of CG: the uplift speed rate is higher than the sink speed one.

Statement

A uniformly accelerated craft motion in the horizontal plane involves a non-uniform motion of CG along the normal to the horizontal plane, with the uplift speed higher than the sink one.

Most of Model Basin Tests have been conducted running the model at a series of predetermined speeds and loads.

There is a lack of experimental data on the topic: CG vertical acceleration induced by CG horizontal one.

Accordingly to this, the statement cannot be demonstrated.

In first approximation, using the data available, it is possible demonstrate the first part of the statement:

A uniformly accelerated craft motion in the horizontal plane involves a non-uniform motion of CG along the normal to the horizontal plane.

DEM.

In order to achieve this goal two kind of data will be used:

- V bottom planing surfaces data [Shoemaker 1934]
- Semi-displacement hull data[(113)]

First approximation hypothesis:

- rigid body model,
- draft variation equal to CG displacement.

Let indicate with:

[(113)] University of Naples Model Basin Test Report

- D, draft,
- V, speed,
- a, acceleration.

Let indicate with the footnote:

- CG, each quantity pertinent to the craft Center of Gravity,
- i, each quantity related to the time $t = t_i$ with $t_i < t_{i+1}$.

Further, let consider each kinetic quantity at initial time $t_0 = 0$ null, and D_0 the draft of the craft in static condition.

We write:

$$a_i = \frac{V_{i+1} - V_i}{t_{i+1} - t_i} \qquad i \in N_0 \qquad \textbf{(D. 1)}$$

$$V_{CGi} = \frac{D_{i+1} - D_i}{t_{i+1} - t_i} \qquad i \in N_0 \qquad \textbf{(D. 2)}$$

$$a_{CGi} = \frac{V_{CGi+1} - V_{CGi}}{t_{i+1} - t_i} \qquad i \in N_0 \qquad \textbf{(D. 3)}$$

hence:

$$a_{CGi} = a_i \left[a_{i+1} \frac{D_{i+2} - D_{i+1}}{(V_{i+2} - V_{i+1})(V_{i+1} - V_i)} - a_i \frac{D_{i+1} - D_i}{(V_{i+1} - V_i)^2} \right] \quad \forall i \in N_0 \qquad \textbf{(D. 4)}$$

With the Hypothesis of uniformly accelerated craft motion, we have:

$$a_i = k = \cos t \qquad \textbf{(D. 5)}$$

$$a_{CGi} = k^2 \left[\frac{D_{i+2} - D_{i+1}}{(V_{i+2} - V_{i+1})(V_{i+1} - V_i)} - \frac{D_{i+1} - D_i}{(V_{i+1} - V_i)^2} \right] \qquad \textbf{(D. 6)}$$

or

$$a_{CGi} = \frac{k^2}{V_{i+1} - V_i} \left[\frac{D_{i+2} - D_{i+1}}{(V_{i+2} - V_{i+1})} - \frac{1}{k^2} \sum_{j=0}^{i-1} \left[a_{CGj} (V_{j+1} - V_j) \right] - \frac{D_1 - D_0}{V_1} \right] \qquad \textbf{(D. 7)}$$

$$\forall i \in N_0$$

With the Hypothesis of uniformly accelerated motion of CG along the local vertical, we have:

$$a_{CGi} = h = \cos t \qquad \textbf{(D. 8)}$$

$$h = \frac{k^2}{V_{i+1} - V_i}\left[\frac{D_{i+2} - D_{i+1}}{\left(V_{i+2} - V_{i+1}\right)} - \frac{h}{k^2}\sum_{j=0}^{i-1}\left(V_{j+1} - V_j\right) - \frac{D_1 - D_0}{V_1}\right]$$

$$h = \frac{k^2}{V_{i+1} - V_i}\left[\frac{D_{i+2} - D_{i+1}}{\left(V_{i+2} - V_{i+1}\right)} - \frac{h}{k^2}V_i - \frac{D_1 - D_0}{V_1}\right]$$

$$\frac{h}{k^2} = \frac{1}{V_{i+1}}\left[\frac{D_{i+2} - D_{i+1}}{V_{i+2} - V_{i+1}} - \frac{D_1 - D_0}{V_1}\right] \qquad \textbf{(D. 9)}$$

hence $h = const \quad \forall i \in N_0$ if and only if

$$\Omega = \frac{1}{V_{i+1}}\left[\frac{D_{i+2} - D_{i+1}}{V_{i+2} - V_{i+1}} - \frac{D_1 - D_0}{V_1}\right] = const \qquad \textbf{(D. 10)}$$

where Ω is unknown.

According to the mathematical Principle of Induction [Giordano 1991]:

$$\frac{1}{V_i}\left[\frac{D_{i+1} - D_i}{V_{i+1} - V_i} - \frac{D_1 - D_0}{V_1}\right] = \frac{1}{V_{i+1}}\left[\frac{D_{i+2} - D_{i+1}}{V_{i+2} - V_{i+1}} - \frac{D_1 - D_0}{V_1}\right]$$

and

$$\frac{V_{i+1}}{V_{i+1} - V_i}\frac{D_{i+1} - D_i}{V_{i+1} - V_i} - \frac{V_i}{V_{i+1} - V_i}\frac{D_{i+2} - D_{i+1}}{V_{i+2} - V_{i+1}} = \frac{D_1 - D_0}{V_1} \qquad \forall i \in N_0 \qquad \textbf{(D. 11)}$$

Further, according to the Principle of Induction, if there is just one value of *i* that does not satisfy relationship (D.11) the hypothesis $h = const$ is not satisfied, thereby we have a uniformly accelerated craft motion in the horizontal plane and a non-uniform CG motion along the local vertical: the statement is demonstrated.

If the craft has a uniform motion

$$a_i = k = 0$$
$$V_i = V_1 \qquad \forall i \in N_0$$

than the relationship (D.6) will drive to an undetermined form $\frac{0}{0}$.

In this case the knowledge of the motion equation $D = D(t)$ drives to:

$$a_{CGi} = \lim_{t \to t_i} \frac{d^2 D}{dt^2}$$

where a_{CGi} is, now, the instant acceleration value at $t = t_i$ ([114]).

In order to achieve the goal of this Demonstration, let examine two set of data, above cited.

[114] In the relationship (D.6) a_{CGi} is the mean value of a_{CG} in the time range (t_i, t_{i+1}).

8.5 Validation Analysis

Set 1

Source data: Report NACA TN 509 – 1934 [Shoemaker 1934]

These data are related to planing surfaces and the value of D_0 is not available: the relationship (D.11) is not useful. In order to verify the truth of statement the relationship (D.6) will be used instead of (D.11).

Model data

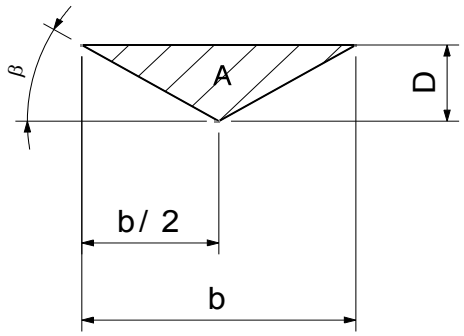

Figure 8.5-1 Transversal Section of model with V-bottom

$$b_{\max} = 16\,inch \qquad \beta = 10°, 20°, 30°$$

$$D = \frac{b}{2}\tan\beta \qquad A = \frac{b^2}{4}\tan\beta \qquad v = \frac{W}{\gamma}$$

$$D_{\max} = \frac{b_{\max}}{2}\tan\beta = 8in\cdot\tan\beta \qquad A_T = \frac{b_{\max}^2}{4}\tan\beta = 64in^2\cdot\tan\beta$$

Per each given configuration of planing surface in NACA report, we calculate, from (D.6):

$$\frac{h}{k^2} = f(i) = \frac{D_{i+2} - D_{i+1}}{(V_{i+2} - V_{i+1})(V_{i+1} - V_i)} - \frac{D_{i+1} - D_i}{(V_{i+1} - V_i)^2}$$

If there is a value of *i* for that

$$f(i) \neq f(i+1) \qquad \textbf{(D. 12)}$$

the statement has been demonstrated.

Table 8.5-1 Model 28 - β = 10 deg, τ = 2 deg

Model 28	β	10	[deg]				b	16	[in.]			A_T	11,3	[in^2]	
	γ	63,5	[lb/ft^3]									D_T	1,4	[in.]	
τ [deg]		2													
		V [fps]	D [in.]	$D_{i+1}-D_i$ / $V_{i+1}-V_i$	f(i)		V [fps]	D [in.]	$D_{i+1}-D_i$ / $V_{i+1}-V_i$	f(i)		V [fps]	D [in.]	$D_{i+1}-D_i$ / $V_{i+1}-V_i$	f(i)
W [lb]	5	20,9	1,0	-1,00	0,23	10	20,8	1,3	-1,00	-0,24	20	20,7	1,7	-0,50	1,88
		21,0	0,9	-0,02	-0,01		21,0	1,1	0,00	-0,52		21,1	1,5	-0,09	-0,15
		25,3	0,8	0,00			21,1	1,1	-0,05			25,7	1,1	0,67	
		26,6	0,8	-0,03			25,3	0,9	-0,10			26,3	1,5	-0,04	
		36,2	0,5				26,3	0,8	0,03			35,3	1,1		
τ [deg]		2													
		V [fps]	D [in.]	$D_{i+1}-D_i$ / $V_{i+1}-V_i$	f(i)		V [fps]	D [in.]	$D_{i+1}-D_i$ / $V_{i+1}-V_i$	f(i)					
W [lb]	40	21,1	2,2	0,00	-0,01	60	35,6	1,5	0,00	-0,05					
		22,4	2,2	-0,08	0,29		36,6	1,5	0,00	0,24					
		26,1	1,9	-0,09			37,5	1,5	-0,05						
		36,3	1,0	1,00			45,4	1,1	0,17						
		36,5	1,2				46,0	1,2							

Table 8.5-2 Model 28 - β = 10 deg, τ = 4 deg

Model 28	β	10	[deg]				b	16	[in.]			A_T	11,3	[in^2]	
	γ	63,5	[lb/ft^3]									D_T	1,4	[in.]	
τ [deg]		4													
		V [fps]	D [in.]	$D_{i+1}-D_i$ / $V_{i+1}-V_i$	f(i)		V [fps]	D [in.]	$D_{i+1}-D_i$ / $V_{i+1}-V_i$	f(i)		V [fps]	D [in.]	$D_{i+1}-D_i$ / $V_{i+1}-V_i$	f(i)
W [lb]	5	14,0	0,6	0,07	-0,03	10	14,1	0,9	-0,08	-0,22	20	13,9	1,6	-0,20	-0,14
		15,5	0,7	0,04	-0,11		15,4	0,8	0,14	0,03		15,4	1,3	0,05	0,02
		17,8	0,8	0,00			17,6	1,1	-0,15			17,6	1,4	-0,17	
		18,8	0,8	-0,25			18,9	0,9	-0,09			18,8	1,2	-0,12	
		20,0	0,5				20,0	0,8				21,3	0,9		
τ [deg]		4													
		V [fps]	D [in.]	$D_{i+1}-D_i$ / $V_{i+1}-V_i$	f(i)		V [fps]	D [in.]	$D_{i+1}-D_i$ / $V_{i+1}-V_i$	f(i)		V [fps]	D [in.]	$D_{i+1}-D_i$ / $V_{i+1}-V_i$	f(i)
W [lb]	40	17,8	2,4	-0,56	-2,25	60	18,2	2,9	-0,07	-0,15	80	19,3	3,5	0,00	0,70
		19,6	1,4	4,00	-9,44		19,7	2,8	0,00	-0,10		20,0	3,5	-0,40	-0,32
		19,7	1,8	-0,06			19,9	2,8	-0,23			21,0	3,1	0,09	
		21,5	1,7	-1,00			21,2	2,5	-0,25			22,1	3,2	-0,23	
		21,6	1,6				21,6	2,4				26,9	2,1		

Table 8.5-3 Model 28 - β = 10 deg, τ = 6 deg

Model 28	β	10	[deg]				b	16	[in.]			A_T	11,3	[in^2]	
	γ	63,5	[lb/ft^3]									D_T	1,4	[in.]	
τ [deg]		6													
		V	D	$D_{i+1}-D_i$ / $V_{i+1}-V_i$	f(i)		V	D	$D_{i+1}-D_i$ / $V_{i+1}-V_i$	f(i)		V	D	$D_{i+1}-D_i$ / $V_{i+1}-V_i$	f(i)
		[fps]	[in.]				[fps]	[in.]				[fps]	[in.]		
W [lb]	5	13,2	0,5	0,00	-0,02	10	12,2	0,9	-0,22	-2,28	20	12,1	1,7	-0,21	0,25
		15,2	0,5	0,04	-0,04		13,1	0,7	0,05	0,99		14,0	1,3	-0,50	-0,19
		17,7	0,6	0,00			15,2	0,8	-2,00			14,4	1,1	-0,03	
		20,4	0,6	-0,11			15,3	0,6	0,08			18,0	1	-0,11	
		22,3	0,4				17,8	0,8				19,9	0,8		
τ [deg]		6													
		V	D	$D_{i+1}-D_i$ / $V_{i+1}-V_i$	f(i)		V	D	$D_{i+1}-D_i$ / $V_{i+1}-V_i$	f(i)		V	D	$D_{i+1}-D_i$ / $V_{i+1}-V_i$	f(i)
		[fps]	[in.]				[fps]	[in.]				[fps]	[in.]		
W [lb]	40	12,1	2,9	-0,11	0,06	60	13,2	3,9	-0,30	-0,03	80	16,1	4,1	-0,21	0,30
		14,0	2,7	-0,50	0,97		16,2	3	-0,28	1,15		18,9	3,5	-1,00	-0,07
		14,4	2,5	-0,39			18,7	2,3	-0,37			19,4	3	-0,16	
		16,2	1,8	0,00			19,5	2	2,50			21,3	2,7	-0,19	
		17,8	1,8				19,7	2,5				27,5	1,5		

Table 8.5-4 Model 28 - β = 10 deg, τ = 8 deg

Model 28	β	10	[deg]			b	16	[in.]			A_T	11,3	[in^2]	
	γ	63,5	[lb/ft^3]								D_T	1,4	[in.]	
τ [deg]		8												
		V [fps]	D [in.]	$D_{i+1}-D_i$ / $V_{i+1}-V_i$	f(i)		V [fps]	D [in.]	$D_{i+1}-D_i$ / $V_{i+1}-V_i$	f(i)		V [fps]	D [in.]	$D_{i+1}-D_i$ / $V_{i+1}-V_i$	f(i)
W [lb]	5	13,0	0,6	-2,00	-10,48	10	12,2	0,9	-0,22	-2,28	20	12,1	1,7	-0,21	0,25
		13,1	0,4	0,05	0,52		13,1	0,7	0,05	0,99		14,0	1,3	-0,50	-0,19
		15,2	0,5	-1,00			15,2	0,8	-2,00			14,4	1,1	-0,03	
		15,4	0,3	0,08			15,3	0,6	0,08			18,0	1	-0,11	
		17,8	0,5				17,8	0,8				19,9	0,8		
τ [deg]		8													
		V [fps]	D [in.]	$D_{i+1}-D_i$ / $V_{i+1}-V_i$	f(i)		V [fps]	D [in.]	$D_{i+1}-D_i$ / $V_{i+1}-V_i$	f(i)		V [fps]	D [in.]	$D_{i+1}-D_i$ / $V_{i+1}-V_i$	f(i)
W [lb]	40	12,1	2,9	-0,11	0,06	60	13,2	3,9	-0,30	-0,03	80	16,1	4,1	-0,21	0,30
		14,0	2,7	-0,50	0,97		16,2	3	-0,28	1,15		18,9	3,5	-1,00	-0,07
		14,4	2,5	-0,39			18,7	2,3	-0,37			19,4	3	-0,16	
		16,2	1,8	0,00			19,5	2	2,50			21,3	2,7	-0,19	
		17,8	1,8				19,7	2,5				27,5	1,5		

Table 8.5-5 Model 28 - β = 20 deg, τ = 4 deg

Model 28	β	20	[deg]				b	16	[in.]			A_T	23,3	[in^2]	
	γ	63,5	[lb/ft^3]									D_T	2,9	[in.]	
τ [deg]		4													
		V [fps]	D [in.]	$D_{i+1}-D_i$ / $V_{i+1}-V_i$	f(i)		V [fps]	D [in.]	$D_{i+1}-D_i$ / $V_{i+1}-V_i$	f(i)		V [fps]	D [in.]	$D_{i+1}-D_i$ / $V_{i+1}-V_i$	f(i)
W [lb]	5	14,5	1,3	-0,03	0,00	10	14,5	1,7	-0,05	0,00	20	14,6	2,5	-0,01	0,01
		29,7	0,8	-0,02			30,0	1	-0,03			30,2	2,4	-0,22	
		35,7	0,7	0,00			36,0	0,8	0,02			35,6	1,2	-0,01	
		45,1	0,7				44,5	1				45,0	1,1		
τ [deg]		4													
		V [fps]	D [in.]	$D_{i+1}-D_i$ / $V_{i+1}-V_i$	f(i)		V [fps]	D [in.]	$D_{i+1}-D_i$ / $V_{i+1}-V_i$	f(i)		V [fps]	D [in.]	$D_{i+1}-D_i$ / $V_{i+1}-V_i$	f(i)
W [lb]	40	30,1	2,0	-0,07	n/a	60	30,3	2,3	-0,05	n/a	80	30,4	2,7	-0,08	n/a
		37,2	1,5	-0,01			35,9	2,0	-0,03			35,3	2,3		
		45,6	1,4				45,1	1,7							

Table 8.5-6 Model 28 - β = 20 deg, τ = 6 deg

Model 28	β	20	[deg]			b	16	[in.]		A_T	23,3	[in^2]	
	γ	63,5	[lb/ft^3]							D_T	2,9	[in.]	
τ [deg]		6											

		V [fps]	D [in.]	$D_{i+1}-D_i$ / $V_{i+1}-V_i$	f(i)		V [fps]	D [in.]	$D_{i+1}-D_i$ / $V_{i+1}-V_i$	f(i)		V [fps]	D [in.]	$D_{i+1}-D_i$ / $V_{i+1}-V_i$	f(i)
W [lb]	5	17,2	1,0	0,10	0,10	10	12,3	1,2	0,04	-0,05	20	12,3	2,6	-0,20	0,05
		19,2	1,2	-0,20	-0,01		17,1	1,4	0,00	0,11		14,3	2,2	-0,15	-0,02
		21,2	0,8	0,00			19,3	1,4	-0,24			17,0	1,8	-0,05	
		23,9	0,8	-0,02			21,0	1	0,00			19,1	1,7	-0,11	
		29,5	0,7				24,1	1				21,0	1,5		

τ [deg]		6													
		V [fps]	D [in.]	$D_{i+1}-D_i$ / $V_{i+1}-V_i$	f(i)		V [fps]	D [in.]	$D_{i+1}-D_i$ / $V_{i+1}-V_i$	f(i)		V [fps]	D [in.]	$D_{i+1}-D_i$ / $V_{i+1}-V_i$	f(i)
W [lb]	40	14,4	3,6	-0,26	0,02	60	21,0	2,9	-0,14	0,02	80	24,5	2,9	-0,11	0,00
		17,1	2,9	-0,22	0,04		24,5	2,4	-0,11	0,01		29,1	2,4	-0,04	
		19,4	2,4	-0,16			29,0	1,9	-0,03			34,8	2,2	-0,05	
		21,3	2,1	-0,06			35,0	1,7	-0,01			43,0	1,8		
		24,4	1,9				44,9	1,6							

Table 8.5-7 Model 28 - β = 20 deg, τ = 8 deg

Model 28	β	20	[deg]				b	16	[in.]			A_T	23,3	[in^2]	
	γ	63,5	[lb/ft^3]									D_T	2,9	[in.]	
τ [deg]		8													
		V [fps]	D [in.]	$D_{i+1}-D_i$ / $V_{i+1}-V_i$	f(i)		V [fps]	D [in.]	$D_{i+1}-D_i$ / $V_{i+1}-V_i$	f(i)		V [fps]	D [in.]	$D_{i+1}-D_i$ / $V_{i+1}-V_i$	f(i)
W [lb]	5	12,7	1,3	-0,14	-0,06	10	12,7	1,7	-0,10	-0,07	20	12,6	2,4	-0,18	-0,04
		14,8	1,0	0,08	0,00		14,8	1,5	0,04	-0,03		14,8	2,0	0,00	-0,01
		17,4	1,2	-0,05			17,2	1,6	-0,10			17,1	2,0	-0,10	
		19,3	1,1	-0,05			19,3	1,4	-0,17			19,2	1,8	-0,11	
		21,2	1,0				21,1	1,1				21,0	1,6		
τ [deg]		8													
		V [fps]	D [in.]	$D_{i+1}-D_i$ / $V_{i+1}-V_i$	f(i)		V [fps]	D [in.]	$D_{i+1}-D_i$ / $V_{i+1}-V_i$	f(i)		V [fps]	D [in.]	$D_{i+1}-D_i$ / $V_{i+1}-V_i$	f(i)
W [lb]	40	12,6	4,1	-0,45	-0,09	60	17,3	3,7	-0,26	0,08	80	19,1	4,2	-0,37	0,02
		14,8	3,1	-0,08	0,09		19,2	3,2	-0,28	0,03		21,0	3,5	-0,18	0,02
		17,2	2,9	-0,27			21,0	2,7	-0,12			25,5	2,7	-0,14	0,00
		19,4	2,3	-0,06			25,2	2,2	-0,06			29,9	2,1	-0,03	
		21,2	2,2				30,5	1,9				36,2	1,9	-0,04	
												43,8	1,6		

Table 8.5-8 Model 28 - β = 20 deg, τ = 10 deg

Model 28	β	20	[deg]				b	16	[in.]			A_T	23,3	[in^2]	
	γ	63,5	[lb/ft^3]									D_T	2,9	[in.]	
τ [deg]		10													
		V [fps]	D [in.]	$D_{i+1}-D_i$ / $V_{i+1}-V_i$	f(i)		V [fps]	D [in.]	$D_{i+1}-D_i$ / $V_{i+1}-V_i$	f(i)		V [fps]	D [in.]	$D_{i+1}-D_i$ / $V_{i+1}-V_i$	f(i)
W [lb]	5	13,2	0,9	-0,05	0,00	10	13,1	1,2	-0,05	-0,19	20	13,1	1,9	-0,10	-0,13
		15,2	0,8	0,00	-0,01		15,1	1,1	0,12	0,09		15,1	1,7	0,00	0,08
		17,9	0,8	0,00			17,7	1,4	-0,26			17,7	1,7	-0,25	
		19,5	0,8	-0,02			19,6	0,9	-0,02			19,3	1,3	-0,04	
		24,2	0,7				24,2	0,8				24,3	1,1		
τ [deg]		10													
		V [fps]	D [in.]	$D_{i+1}-D_i$ / $V_{i+1}-V_i$	f(i)		V [fps]	D [in.]	$D_{i+1}-D_i$ / $V_{i+1}-V_i$	f(i)		V [fps]	D [in.]	$D_{i+1}-D_i$ / $V_{i+1}-V_i$	f(i)
W [lb]	40	12,9	3,6	-0,36	-0,01	60	14,9	3,9	-0,36	-0,01	80	17,4	4,2	-0,25	0,10
		15,1	2,8	-0,14	0,01		17,7	2,9	-0,11	0,04		19,4	3,7	-0,27	0,01
		18,0	2,4	-0,15			19,6	2,7	-0,14			24,5	2,3	-0,08	
		19,3	2,2	-0,13			24,6	2	-0,06			34,6	1,5	-0,02	
		24,5	1,5				34,5	1,4				40,3	1,4		

Table 8.5-9 Model 28 - β = 30 deg, τ = 4 deg

Model 28	β	30	[deg]			b	16	[in.]		A_T	37,0	[in^2]	
	γ	63,5	[lb/ft^3]							D_T	4,6	[in.]	

τ [deg]		4													
		V [fps]	D [in.]	$D_{i+1}-D_i$ / $V_{i+1}-V_i$	f(i)		V [fps]	D [in.]	$D_{i+1}-D_i$ / $V_{i+1}-V_i$	f(i)		V [fps]	D [in.]	$D_{i+1}-D_i$ / $V_{i+1}-V_i$	f(i)
W [lb]	5	11,3	2,2	-0,05	0,02	10	11,3	2,8	-0,05	0,01	20	20,2	3,1	-0,11	0,06
		13,2	2,1	-0,04	0,00		13,2	2,7	-0,07	0,02		24,6	2,6	-0,01	-0,01
		15,8	2,0	0,00			16,1	2,5	-0,06			39,8	2,4	0,26	
		18,2	2,0	0,00			17,8	2,4	0,00			35,9	1,4	0,04	
		20,0	2,0				20,0	2,4				45,2	1,8		

τ [deg]		4			
		V [fps]	D [in.]	$D_{i+1}-D_i$ / $V_{i+1}-V_i$	f(i)
W [lb]	40	29,8	3,1	2,82	n/a
		35,8	20,0	-3,61	
		40,7	2,3		

Table 8.5-10 Model 28 - β = 30 deg, τ = 6 deg

Model 28	β	30	[deg]				b	16	[in.]			A_T	37,0	[in^2]	
	γ	63,5	[lb/ft^3]									D_T	4,6	[in.]	
τ [deg]		6													
		V [fps]	D [in.]	$D_{i+1}-D_i$ / $V_{i+1}-V_i$	f(i)		V [fps]	D [in.]	$D_{i+1}-D_i$ / $V_{i+1}-V_i$	f(i)		V [fps]	D [in.]	$D_{i+1}-D_i$ / $V_{i+1}-V_i$	f(i)
W [lb]	5	10,8	2,3	-0,13	0,07	10	11,1	3,1	-0,17	-0,03	20	11,3	4,0	-0,17	0,14
		13,2	2,0	-0,08	-0,03		12,9	2,8	-0,07	0,02		13,1	3,7	-0,18	-0,13
		15,6	1,8	0,08			15,7	2,6	-0,12			15,9	3,2	0,08	
		18,1	2,0	0,00			18,2	2,3	-0,06			18,4	3,4	-0,28	
		20,0	2,0				20,0	2,2				20,2	2,9		
τ [deg]		6													
		V [fps]	D [in.]	$D_{i+1}-D_i$ / $V_{i+1}-V_i$	f(i)		V [fps]	D [in.]	$D_{i+1}-D_i$ / $V_{i+1}-V_i$	f(i)		V [fps]	D [in.]	$D_{i+1}-D_i$ / $V_{i+1}-V_i$	f(i)
W [lb]	40	13,4	4,9	-0,16	-0,08	60	19,8	4,6	-0,15	0,01	80	25,2	4,4	-0,12	n/a
		15,9	4,5	-0,09	0,02		25,1	3,8	-0,13	0,00		29,4	3,9		
		18,2	4,3	-0,29			29,0	3,3	-0,06						
		19,6	3,9	-0,25			35,5	2,9	-0,06						
		20,4	3,7				40,8	2,5							

Table 8.5-11 Model 28 - β = 30 deg, τ = 8 deg

Model 28	β	30	[deg]				b	16	[in.]			A_T	37,0	[in^2]	
	γ	63,5	[lb/ft^3]									D_T	4,6	[in.]	
τ [deg]		8													
		V [fps]	D [in.]	$D_{i+1}-D_i$ / $V_{i+1}-V_i$	f(i)		V [fps]	D [in.]	$D_{i+1}-D_i$ / $V_{i+1}-V_i$	f(i)		V [fps]	D [in.]	$D_{i+1}-D_i$ / $V_{i+1}-V_i$	f(i)
W [lb]	5	12,1	2,0	-0,14	-0,01	10	12,0	2,8	-0,17	0,08	20	11,9	3,8	-0,21	0,12
		14,3	1,7	-0,04	0,00		14,3	2,4	-0,04	-0,15		14,3	3,3	-0,17	-0,12
		17,1	1,6	-0,06			16,9	2,3	0,15			16,7	2,9	0,12	
		18,8	1,5	-0,06			18,2	2,5	-0,23			18,4	3,1	-0,18	
		20,5	1,4				20,4	2				21,2	2,6		
τ [deg]		8													
		V [fps]	D [in.]	$D_{i+1}-D_i$ / $V_{i+1}-V_i$	f(i)		V [fps]	D [in.]	$D_{i+1}-D_i$ / $V_{i+1}-V_i$	f(i)		V [fps]	D [in.]	$D_{i+1}-D_i$ / $V_{i+1}-V_i$	f(i)
W [lb]	40	11,8	5,4	-0,23	0,03	60	12,0	6,5	-0,78	-0,24	80	13,8	7,0	-0,28	0,00
		14,4	4,8	-0,23	-0,03		13,8	5,1	0,14	0,02		17,4	6,0	-0,25	0,03
		17,0	4,2	-0,14			16,7	5,5	-0,30			21,0	5,1	-0,24	
		18,4	4,0	-0,23			18,7	4,9	-0,25			26,4	3,8	-0,15	
		21,0	3,4				21,1	4,3				30,4	3,2		

Table 8.5-12 Model 28 - β = 30 deg, τ = 10 deg

Model 28	β	30	[deg]				b	16	[in.]			A_T	37,0	[in^2]	
	γ	63,5	[lb/ft^3]									D_T	4,6	[in.]	
τ [deg]		10													
		V	D	$D_{i+1}-D_i$ / $V_{i+1}-V_i$	f(i)		V	D	$D_{i+1}-D_i$ / $V_{i+1}-V_i$	f(i)		V	D	$D_{i+1}-D_i$ / $V_{i+1}-V_i$	f(i)
		[fps]	[in.]				[fps]	[in.]				[fps]	[in.]		
W [lb]	5	10,9	2,0	-0,15	0,07	10	11,1	2,8	-0,21	-0,01	20	11,1	3,9	-0,31	0,09
		13,6	1,6	-0,07	-0,07		13,5	2,3	-0,08	0,03		14,0	3,0	-0,19	-0,14
		16,3	1,4	0,12			16,0	2,1	-0,11			16,1	2,6	0,08	
		18,0	1,6	-0,08			17,9	1,9	-0,04			18,5	2,8	-0,21	
		20,6	1,4				20,5	1,8				20,4	2,4		
τ [deg]		10													
		V	D	$D_{i+1}-D_i$ / $V_{i+1}-V_i$	f(i)		V	D	$D_{i+1}-D_i$ / $V_{i+1}-V_i$	f(i)		V	D	$D_{i+1}-D_i$ / $V_{i+1}-V_i$	f(i)
		[fps]	[in.]				[fps]	[in.]				[fps]	[in.]		
W [lb]	40	11,3	5,6	-0,37	0,09	60	12,3	6,6	-0,40	-0,17	80	12,3	7,8	-0,37	0,01
		14,0	4,6	-0,35	-0,01		13,3	6,2	-0,25	0,47		15,0	6,8	-0,43	0,11
		16,3	3,8	-0,10			13,7	6,1	-0,42			16,4	6,2	-0,41	
		18,3	3,6	-0,13			16,1	5,1	-0,23			18,1	5,5	-0,26	
		20,6	3,3				18,3	4,6				20,4	4,9		

Table 8.5-13 Model 28 - β = 30 deg, τ = 12 deg

Model 28	β	30	[deg]				b	16	[in.]			A_T	37,0	[in^2]	
	γ	63,5	[lb/ft^3]									D_T	4,6	[in.]	
τ [deg]		12													
		V [fps]	D [in.]	$D_{i+1}-D_i$ / $V_{i+1}-V_i$	f(i)		V [fps]	D [in.]	$D_{i+1}-D_i$ / $V_{i+1}-V_i$	f(i)		V [fps]	D [in.]	$D_{i+1}-D_i$ / $V_{i+1}-V_i$	f(i)
W [lb]	5	30,8	0,7	-0,03	n/a	10	30,9	0,8	0,00	n/a	20	31,1	1,3	-0,05	n/a
		37,0	0,5				37,3	0,8				37,0	1,0		
τ [deg]		12													
		V [fps]	D [in.]	$D_{i+1}-D_i$ / $V_{i+1}-V_i$	f(i)		V [fps]	D [in.]	$D_{i+1}-D_i$ / $V_{i+1}-V_i$	f(i)					
W [lb]	40	31,3	1,9	-0,05	n/a	60	30,7	2,3	-0,05	n/a					
		37,2	1,6				36,4	2,0							

Set 2

Source data: Report UNINA Model Basin – 1993

Model data

Base Model: C931

$L_{BP} = 26.749\,m$

$L_{WL} = 28.345\,m$

$B = 7.368\,m$

Table 8.5-14 Test cases Unina Model C931

Hull	W	D	Spray	Flaps			
	[t]	[m]	Rails	0°	2,5°	5°	7,5°
Serie 1	103,77	1,250	-	-	-	-	-
Serie 2	108,18	1,350	-	-	-	-	-
Serie 3	103,77	1,250	X	X	-	-	-
Serie 4	103,77	1,250	X	-	X	-	-
Serie 5	103,77	1,250	X	-	-	X	-
Serie 6	103,77	1,250	X	-	-	-	X
Serie 7	108,18	1,350	X	X	-	-	-
Serie 8	108,18	1,350	X	-	X	-	-
Serie 9	108,18	1,350	X	-	-	X	-
Serie 10	108,18	1,350	X	-	-	-	X

Table 8.5-15 Unina C931: Test cases Serie 1 & Serie 2

serie 1	D_0	1,25	[m]				serie 2	D_0	1,35	[m]			
		V	ΔD	D	$D_{i+1}-D_i$ / $V_{i+1}-V_i$	f(i)			V	ΔD	D	$D_{i+1}-D_i$ / $V_{i+1}-V_i$	f(i)
		[kn]	[m]	[m]					[kn]	[m]	[m]		
W [t]	103,77	15	0,192	1,44	-0,02	0,01	W [t]	118,18	15	0,216	1,47	-0,02	-0,02
		17	0,161	1,41	-0,02	-0,04			17	0,172	1,42	-0,02	-0,03
		19	0,116	1,37	-0,03	-0,07			19	0,127	1,38	-0,02	-0,02
		21	0,063	1,31	-0,02	-0,05			21	0,082	1,33	-0,02	-0,02
		23	0,014	1,26	-0,02	0,02			23	0,038	1,29	-0,02	-0,01
		25	-0,026	1,22	-0,02	0,01			25	-0,007	1,24	-0,02	-0,01
		27	-0,061	1,19	-0,02	0,02			27	-0,053	1,20	-0,02	0,04
		29	-0,102	1,15	-0,02	0,05			29	-0,101	1,15	-0,03	0,06
		31	-0,148	1,10	-0,03	0,02			31	-0,151	1,10	-0,03	0,04
		33	-0,200	1,05	-0,03	0,02			33	-0,211	1,04	-0,04	-0,02
		35	-0,263	0,99	-0,03	-0,04			35	-0,283	0,97	-0,04	-0,02
		37	-0,332	0,92	-0,04				37	-0,365	0,89	-0,04	
		39	-0,408	0,84	-0,04				39	-0,449	0,80	-0,04	
		40	-0,446	0,80					40	-0,492	0,76		
$(D_1-D_0)/V_1$	0,01						$(D_1-D_0)/V_1$	0,01					

Table 8.5-16 Unina C931: Test cases Serie 3 & Serie 4

serie 3	D_0	1,25	[m]					serie 4	D_0	1,25	[m]				
W [t]		V	ΔD	D	$D_{i+1}-D_i$ / $V_{i+1}-V_i$	f(i)		W [t]		V	ΔD	D	$D_{i+1}-D_i$ / $V_{i+1}-V_i$	f(i)	
		[kn]	[m]	[m]						[kn]	[m]	[m]			
	103,77	15	0,166	1,42	-0,01	0,02			103,77	15	0,162	1,41	-0,01	0,02	
		17	0,143	1,39	-0,02	-0,04				17	0,140	1,39	-0,02	-0,05	
		19	0,101	1,35	-0,03	-0,06				19	0,096	1,35	-0,03	-0,06	
		21	0,049	1,30	-0,02	-0,05				21	0,042	1,29	-0,02	-0,07	
		23	0,000	1,25	-0,02	-0,06				23	-0,006	1,24	-0,02	-0,03	
		25	-0,041	1,21	-0,02	-0,02				25	-0,046	1,20	-0,02	-0,02	
		27	-0,077	1,17	-0,01	-0,01				27	-0,077	1,17	-0,01	0,00	
		29	-0,106	1,14	-0,01	0,00				29	-0,106	1,14	-0,01	-0,02	
		31	-0,134	1,12	-0,01	0,01				31	-0,134	1,12	-0,02	0,01	
		33	-0,163	1,09	-0,02	-0,05				33	-0,164	1,09	-0,02	-0,03	
		35	-0,194	1,06	-0,02	0,06				35	-0,194	1,06	-0,02	-0,04	
		37	-0,228	1,02	-0,02					37	-0,227	1,02	-0,02		
		39	-0,258	0,99	-0,02					39	-0,258	0,99	-0,01		
		40	-0,277	0,97						40	-0,272	0,98			
$(D_1-D_0)/V_1$	0,01							$(D_1-D_0)/V_1$	0,01						

Table 8.5-17 Unina C931: Test cases Serie 5 & Serie 6

serie 5	D_0	1,25	[m]					serie 6	D_0	1,25	[m]				
		V	ΔD	D	$D_{i+1}-D_i$ / $V_{i+1}-V_i$	f(i)				V	ΔD	D	$D_{i+1}-D_i$ / $V_{i+1}-V_i$	f(i)	
		[kn]	[m]	[m]						[kn]	[m]	[m]			
W [t]	103,77	15	0,134	1,38	-0,01	0,01		W [t]	103,77	15	0,134	1,38	-0,01	0,02	
		17	0,115	1,37	-0,02	0,00				17	0,115	1,37	-0,02	0,00	
		19	0,080	1,33	-0,02	-0,06				19	0,080	1,33	-0,02	-0,07	
		21	0,037	1,29	-0,02	-0,08				21	0,035	1,29	-0,03	-0,08	
		23	-0,012	1,24	-0,02	-0,04				23	-0,016	1,23	-0,02	-0,06	
		25	-0,054	1,20	-0,02	-0,03				25	-0,058	1,19	-0,02	-0,03	
		27	-0,084	1,17	-0,01	-0,01				27	-0,089	1,16	-0,01	-0,04	
		29	-0,110	1,14	-0,01	0,00				29	-0,112	1,14	-0,01	-0,01	
		31	-0,134	1,12	-0,01	-0,04				31	-0,132	1,12	-0,01	-0,01	
		33	-0,158	1,09	-0,01	-0,03				33	-0,148	1,10	-0,01	-0,02	
		35	-0,184	1,07	-0,01	-0,03				35	-0,164	1,09	-0,01	0,01	
		37	-0,206	1,04	-0,01					37	-0,180	1,07	-0,01		
		39	-0,226	1,02	-0,01					39	-0,194	1,06	-0,01		
		40	-0,235	1,02						40	-0,202	1,05			
$(D_1-D_0)/V_1$	0,01							$(D_1-D_0)/V_1$	0,01						

Table 8.5-18 Unina C931: Test cases Serie 7 & Serie 8

serie 7	D_0	1,350	[m]					serie 8	D_0	1,350	[m]				
		V	ΔD	D	$D_{i+1}-D_i$ / $V_{i+1}-V_i$	f(i)				V	ΔD	D	$D_{i+1}-D_i$ / $V_{i+1}-V_i$	f(i)	
		[kn]	[m]	[m]						[kn]	[m]	[m]			
W [t]	118,18	15	0,182	1,53	-0,02	0,01		W [t]	118,18	15	0,164	1,51	-0,02	0,02	
		17	0,150	1,50	-0,02	-0,02				17	0,133	1,48	-0,02	0,00	
		19	0,113	1,46	-0,02	-0,03				19	0,100	1,45	-0,02	-0,02	
		21	0,068	1,42	-0,02	-0,04				21	0,058	1,41	-0,02	-0,04	
		23	0,022	1,37	-0,02	-0,01				23	0,012	1,36	-0,02	-0,06	
		25	-0,022	1,33	-0,02	0,02				25	-0,035	1,32	-0,02	-0,04	
		27	-0,062	1,29	-0,02	0,02				27	-0,078	1,27	-0,02	0,00	
		29	-0,103	1,25	-0,02	0,05				29	-0,114	1,24	-0,02	0,03	
		31	-0,151	1,20	-0,03	0,01				31	-0,146	1,20	-0,02	0,00	
		33	-0,206	1,14	-0,03	0,02				33	-0,180	1,17	-0,02	0,00	
		35	-0,271	1,08	-0,04	-0,05				35	-0,220	1,13	-0,02	0,01	
		37	-0,341	1,01	-0,04					37	-0,262	1,09	-0,02		
		39	-0,418	0,93	-0,04					39	-0,306	1,04	-0,02		
		40	-0,456	0,89						40	-0,330	1,02			
$(D_1-D_0)/V_1$	0,01							$(D_1-D_0)/V_1$	0,01						

Table 8.5-19 Unina C931: Test cases Serie 9 & Serie 10

serie 9	D_0	1,350	[m]				serie 10	D_0	1,350	[m]			
		V	ΔD	D	$D_{i+1}-D_i$ / $V_{i+1}-V_i$	f(i)			V	ΔD	D	$D_{i+1}-D_i$ / $V_{i+1}-V_i$	f(i)
		[kn]	[m]	[m]					[kn]	[m]	[m]		
W [t]	118,18	15	0,158	1,51	-0,02	0,01	W [t]	118,18	15	0,151	1,50	-0,02	0,00
		17	0,126	1,48	-0,02	-0,03			17	0,116	1,47	-0,02	-0,01
		19	0,088	1,44	-0,02	-0,04			19	0,077	1,43	-0,02	-0,04
		21	0,041	1,39	-0,02	-0,05			21	0,034	1,38	-0,02	-0,05
		23	-0,005	1,35	-0,02	-0,05			23	-0,011	1,34	-0,02	-0,04
		25	-0,048	1,30	-0,02	-0,04			25	-0,053	1,30	-0,02	-0,07
		27	-0,086	1,26	-0,02	-0,01			27	-0,089	1,26	-0,02	-0,03
		29	-0,118	1,23	-0,01	-0,03			29	-0,122	1,23	-0,01	-0,02
		31	-0,146	1,20	-0,01	-0,01			31	-0,146	1,20	-0,01	0,02
		33	-0,175	1,18	-0,01	0,02			33	-0,167	1,18	-0,01	0,03
		35	-0,202	1,15	-0,01	-0,02			35	-0,187	1,16	-0,01	-0,02
		37	-0,230	1,12	-0,02				37	-0,211	1,14	-0,01	
		39	-0,262	1,09	-0,02				39	-0,240	1,11	-0,01	
		40	-0,278	1,07					40	-0,254	1,10		
$(D_1-D_0)/V_1$	0,01						$(D_1-D_0)/V_1$	0,01					

8.6 Concluding Remarks

The analysis of data underlines that a uniformly accelerated CG motion in the horizontal plane involves in a not-uniform CG motion along the normal to the horizontal plane.

The simplified form statement has been demonstrated.

Thereby the vertical component of CG acceleration in the pre-planing phase is composed by two parts:

- one related to the wave system generated by the craft motion,
- one related to the environmental wave system.

The first depends on design parameters and craft speed; the knowledge of the relationships related to, help naval architect to trim the design parameters in order to achieve the CG acceleration required.

The second depends also on environmental wave parameters.

Two fundamental works on CG accelerations have been developed by Fridsma (Fridsma 1969, 1971), related to the craft motion in regular and in irregular waves.

In both works, there is no evidence of studies on CG acceleration related to the wave system generated by the craft motion.

The phenomena, above described, is very important in the pre-planing phase of a craft's motion:

- an high level of CG vertical acceleration leads up to a quickly achievement of planing condition (required, e.g., on navy small boats),
- a low level of CG vertical acceleration leads up to a high level of comfort (required, e.g., on pleasure small boats).

Researches on this topic will be useful to achieve the vertical CG acceleration required, improving craft performance (or comfort).

8.7 Symbols

a	Craft acceleration	$\left[m/s^2\right]$
A	Transverse section area of the craft	$\left[m^2\right]$
a_{CG}	Center of Gravity acceleration	$\left[m/s^2\right]$
A_T	Craft transom stern area	$\left[m^2\right]$
b	Craft beam	$\left[m\right]$
CG	Center of Gravity (of the craft)	
D	Draft of the craft	$\left[m\right]$
D_0	Draft in static condition	$\left[m\right]$
$f(i)$	Numerical value at $t = t_i$	$f(i) = \frac{D_{i+2} - D_{i+1}}{(V_{i+2} - V_{i+1})(V_{i+1} - V_i}$
Fn	Froude number	$Fn = V/\sqrt{gL}$
h, k, Ω	Constants	
i, j	Index	
L_{BP}	Length Between Perpendicular	$\left[m\right]$
L_{WL}	Load Water Line Length of the Craft	$\left[m\right]$
N_0	Integer number set with zero	
t	Time	$\left[s\right]$
v	Volume displaced	$\left[m^3\right]$
V	Craft speed	$\left[m/s\right]$
V_{CG}	Center of Gravity Speed	$\left[m/s\right]$
W	Craft weight	[t]
β	Deadrise angle	[deg]
γ	Unit weight of water	$\gamma = 1.025\left[10^3 kg/m^3\right]$
ΔD	Draft increment	$\left[m\right]$

8.8 References

Fridsma, G. 1969. A Systematic Study of the Rough-Water Performance of Planing Boats. *Report SIT-DL-69-9-1275 Davidson Laboratory* Stevens Institute of Technology. Hoboken, New Jersey (USA)

Fridsma, G. 1971. A Systematic Study of the Rough-Water Performance of Planing Boats (Irregular Waves – Part II). *Report SIT-DL-71-1495 Davidson Laboratory* Stevens Institute of Technology. Hoboken, New Jersey (USA)

Giordano, G. 1991. *CORSO DI ALGEBRA – Appunti delle Lezioni*. E.DI.SU. NAPOLI 1. Napoli, Italy. (Italian language)

Miranda, S. 2001 *Appunti di Architettura Navale*. Napoli: Dipartimento di Ingegneria Navale, Università degli Studi di Napoli "FEDERICO II" (Italian language - web site: http://wpage.unina.it/miranda/)

Russo Krauss, G. 1994. *NAVI A SOSTENTAMENTO IDRODINAMICO*. Parte Prima. Napoli: Dipartimento di Ingegneria Navale, Università degli Studi di Napoli "FEDERICO II" Italy. (Italian language).

Savitsky, D. 2003. ON THE SUBJECT OF HIGH-SPEED MONOHULLS. *Proceedings of Symposium SNAME Greek Section*. October 2, 2003. Athens, Greece. (web site: http://www.sname.org/newsletter/Savitskyreport.pdf)

Shoemaker, J. M. 1934. TANK TESTS OF FLAT AND V-BOTTOM PLANING SURFACES. *Report NACA TN 509* Washington, D.C. (USA) (web site: http://ntrs.nasa.gov/search.jsp)

APPENDIX E

HYDRODYNAMIC PRESSURE DISTRIBUTION TRENDS ON A V-BOTTOM PLANING SURFACE

Test results on prismatic planing surfaces have been reexamined.

During this work some new tips came out. The goal of this Appendix is to highlight these new results.

9.1 Table of Contents

9.2 Figure Index

9.3 Tables Index

9.4 Introduction

In order to confirm some statements on planing surfaces[115] reported in this Thesis, two set of data have been analyzed:

- hydrodynamic pressure distribution,
- geometrical data relate to the fluid flow field, e.g.: wetted length, center of pressure location, stagnation line location, and spray edge location.

Sources data adopted are tests results on prismatic planing surfaces, available on some NACA Reports[116].

Further, in source data there are a few random typing errors that drive to a "spike" or a "drift" in the trend of some quantities; despite of this results are not deeply affected by these errors and no correction of data has been made.

The beginning goal of this Appendix work was to examine the characteristics of a hydrodynamic pressure distribution related to a fluid flow field developed under a prismatic planing surface, but during this work a few new tips came out: these new results and their analysis will be the final goal and will be hereinafter reported.

Results and conclusions of NACA Reports are not here.

---

[115] See Chapter 2 "Fundamental Models", Paragraph 2.2 "The fluid flow field related to a planing craft".

[116] The complete list is reported in Paragraph 9.14 "References".

9.5 Tests Data Analysis

9.5.1 Introduction to models and tests

All tests had developed on the same prismatic surfaces, whose characteristics are here reported:

Table 9.5-1 Model test: geometrical characteristics

	Models				
	301	301-A	302	302-A	303
L_{OA}	36 inches				
b	4 inches				
β	20°		40°		0°
Horizontal chine flared	no	yes	no	yes	-

In order to get accurate pressure measurements "*each model had a total of 100 orifices, 1/32 of an inch in diameter. The orifices were arranged along three major buttocks, one of which was 0.1 inch outboard of the model center line, another was 0.1 inboard of the chine, while the third was located midway between model center line and chine. A few auxiliary orifices were placed buttock midway between the major buttocks.*" [Kapryan & Boyd 1955]

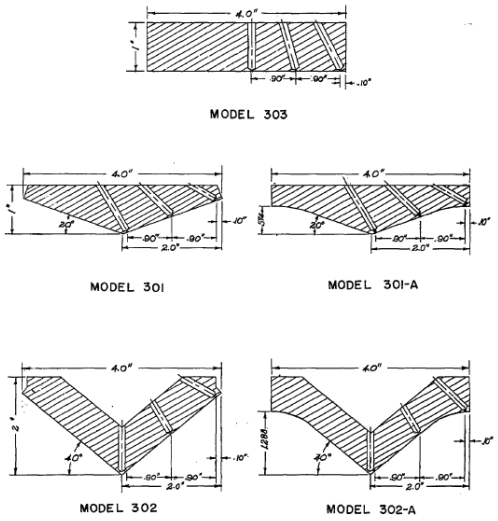

Figure 9.5-1 Cross sections of models [Kapryan & Boyd 1955]

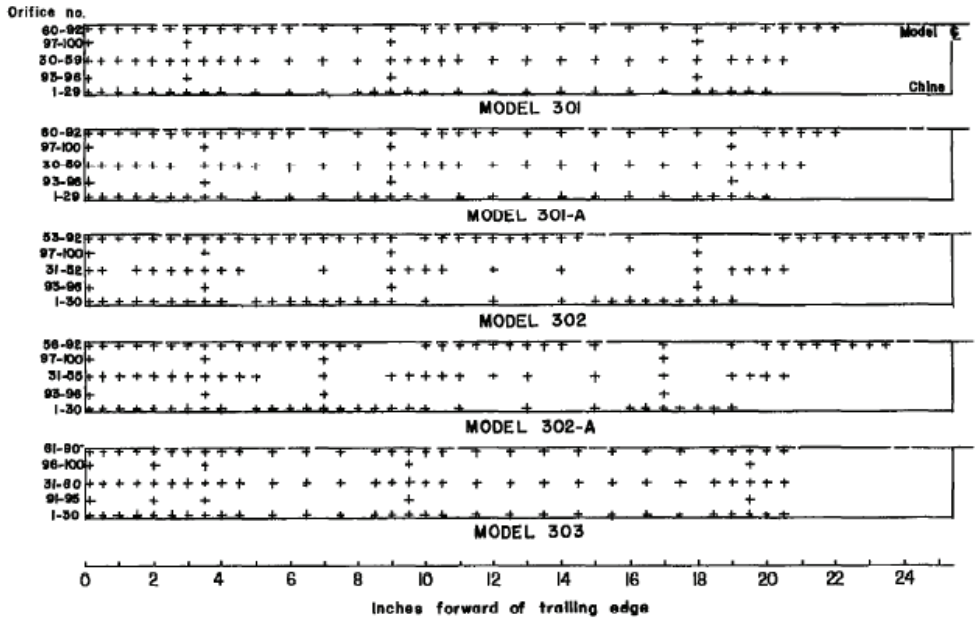

Figure 9.5-2 Location of orifices in models
[Kapryan & Boyd 1955]

The pressures are presented in form of ratio p/q, where p is the measured dynamic pressure at orifice (does not include static displacement) and q is the dynamic pressure based on the towing carriage speed.

All test data are ordered in table form, in which each row is a run test.

Each run test is identified by the value of a set of quantities: trim angle τ, beam loading C_Δ, Froude number C_V, mean wetted length ratio λ_m, Center pressure location ratio λ_p, Lift coefficient C_{Lb}. The first three quantities (trim, beam loading and Froude number) are the independent variable of the set; meanwhile the others are dependent variable.

The bulk of pressure data available are pertinent to a Froude number equal to 12.2, with trim angle ranging from 4° to 30° and beam load ranging from 2.77 to 40.14. The same amount of pressure data related to other values of Froude number had not been made available. Despite the luck of pressure data available, results and conclusions here obtained have been confirmed by the analysis of other test results, taking in account strictly the data associated to the variable above cited. For these others data we have: Froude number values in excess of 7.0, trim angles starting from 2° and beam load ranging from 0.83 to 87.33 [Kapryan & Weinstein 1952].These high value

of C_V , τ and C_Δ are due to the goal of that NACA research: "*... to extend the range of experimental data on planing surfaces to cover the high trim and loading conditions of importance in the design of high-speed water-based aircraft.*" [Kapryan & Boyd 1955]

In line with above written, these are pure planing surface models.

9.5.2 Pressure distribution analysis

The analysis of pressure distribution, in transverse and in longitudinal way, has confirmed the statements[(117)] summarized below:

- longitudinal pressure distribution is characterized by a max value position close to the leading edge of the wetted surface;
- except close to the stagnation line, longitudinal pressure distribution on center line model (keel) is larger than the corresponding pressure along all other longitudinal sections (middle and chine): all pressure distributions are similar in shape but their magnitude decrease toward the edges;
- along the stagnation line, there is a peak in pressure distribution moving from the keel to the chine side;

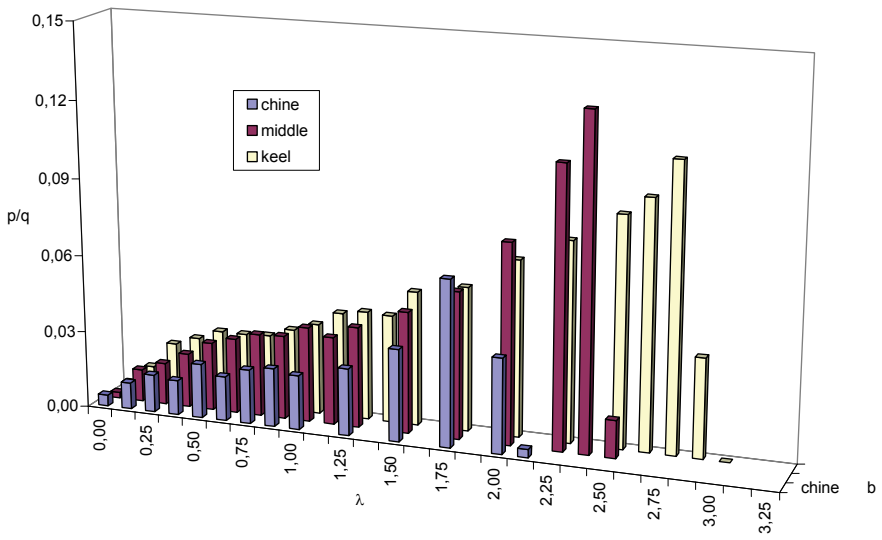

(model 301, run7, τ = 6°, β = 20°, C_{Lb}= 0.1144 [Kapryan & Boyd 1955])

Figure 9.5-3 Pressure distribution on prismatic planing surface

(117) See Charter 2, Paragraph 2.2

- the hydrodynamic pressure is related to the hull deadrise, as matter of fact higher deadrise drives to lower pressure, higher wetted length and higher distance of the center of pressure versus transom;

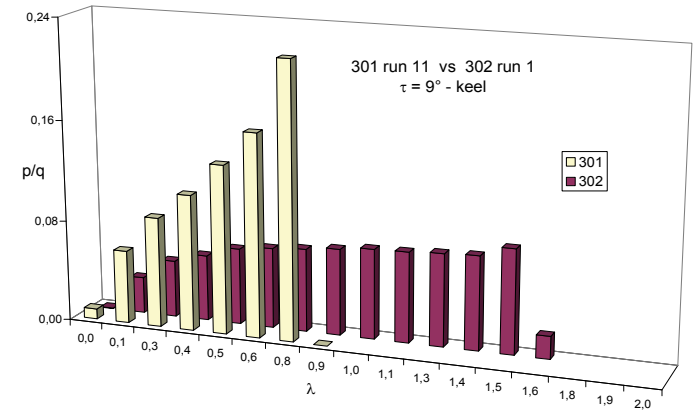

a] keel buttock

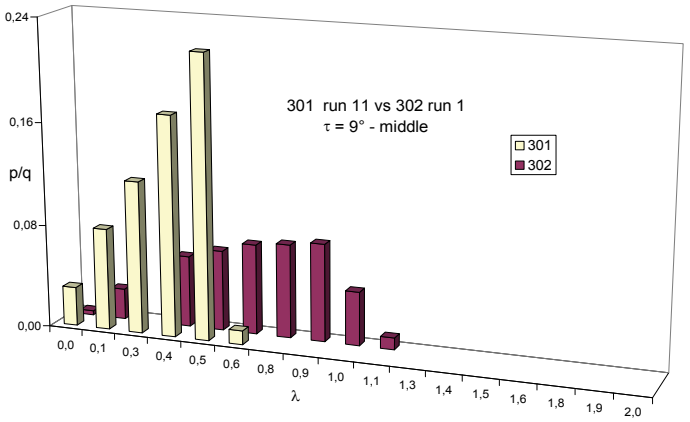

b] middle buttock

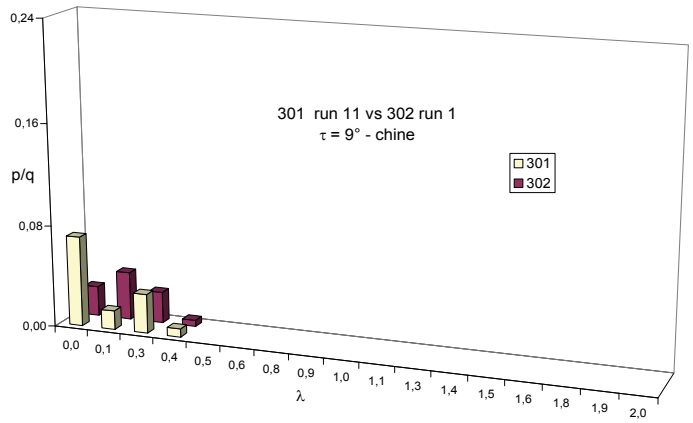

c] chine buttock

(model 301, run 11, β = 20°, C_{Lb}= 0.0686 vs model 302, run 1, β = 40°, C_{Lb}= 0.0564 [Kapryan & Boyd 1955])

Figure 9.5-4 Pressure distribution on two prismatic planing surfaces with a trim angle τ = 9°

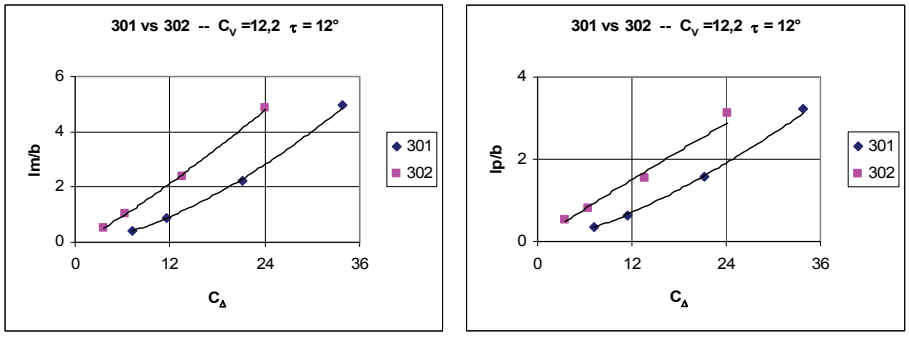

[a] **[b]**

(Data: [Kapryan & Boyd 1955])

Figure 9.5-5 Deadrise effect on mean wetted length and on longitudinal center pressure location for V-bottom planing surfaces with C_V = 12.2 and τ = 12°

- with the addition of horizontal chine flared the pressure distribution increases near the chines and there is an extension of the positive pressures region farther forward of the stagnation point close to the chines;
- the other effects due to the horizontal chine flared can be summarized as due to a reduction of the deadrise angle by which the pressure distribution is related to. In line with this, the concept of "effective" deadrise angle[(118)] has been introduced, but there is no evidence that this is the right choice value.

[(118)] Angle between horizontal plane and tangent plane to keel and chine.

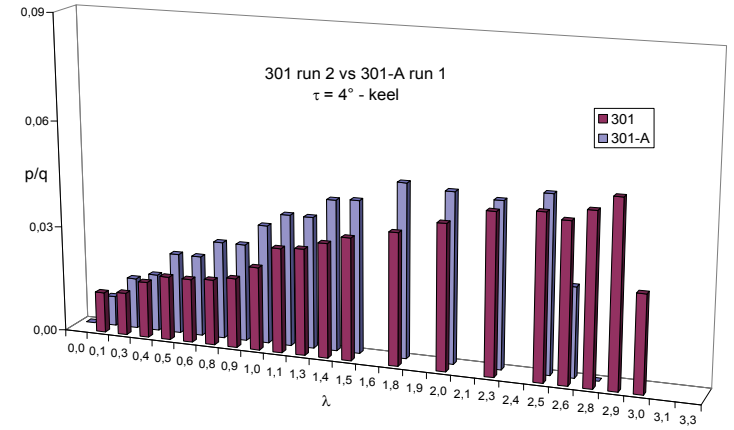

a] keel buttock

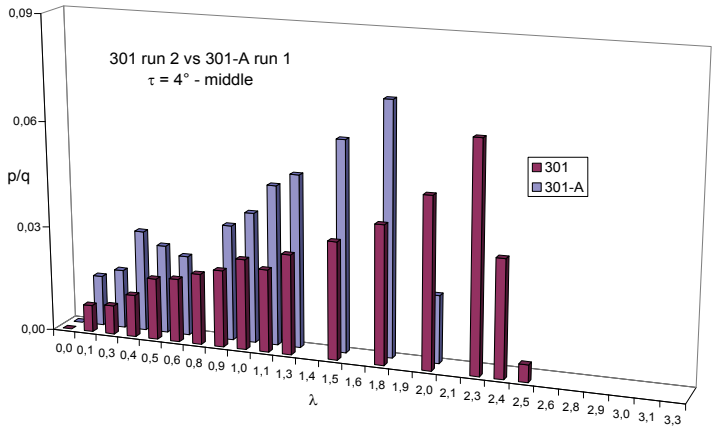

b] middle buttock

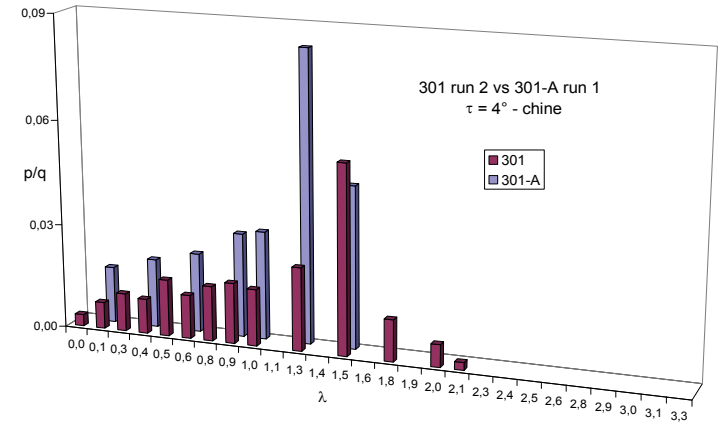

c] chine buttock

(model 301, run 2, C_{Lb}= 0.0662 – vs – model 301-A, run 1, C_{Lb}= 0.0740

[Kapryan & Boyd 1955])

Figure 9.5-6 Pressure distribution on two prismatic planing surfaces with deadrise angle β = 20° and trim angle τ = 4°

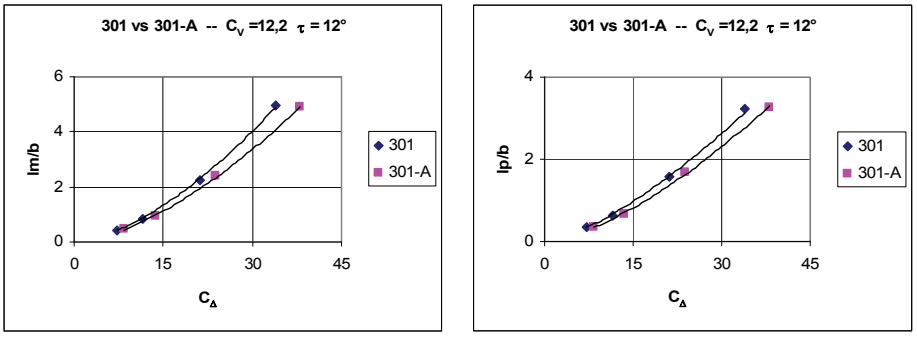

[a] **[b]**

(Data source: [Kapryan & Boyd 1955])

Figure 9.5-7 Horizontal chine flared effect on V-bottom planing surfaces with C_V = 12.2, β = 20° and τ = 12°

9.5.3 Geometrical data analysis

There have been available two set of data: the first linked to the Froude number $C_V = 12.2$, and the second related to a few values of the beam loading C_Δ.

For all data wetted length, center of pressure location and spray edge location has been analyzed. Accordingly the lack of pressure data, stagnation line location analysis has been developed only for the first set of data (with $C_V = 12.2$).

The trends associated to deadrise angle variation and horizontal chine flare introduction are confirmed further for the stagnation line and the spray edge positions[(119)], and this analysis has been developed per each buttock line: keel, middle and chine[(120)].

[(119)] These positions are measured from the transom.

[(120)] Here are reported only the diagrams related to trim angle τ = 12°.

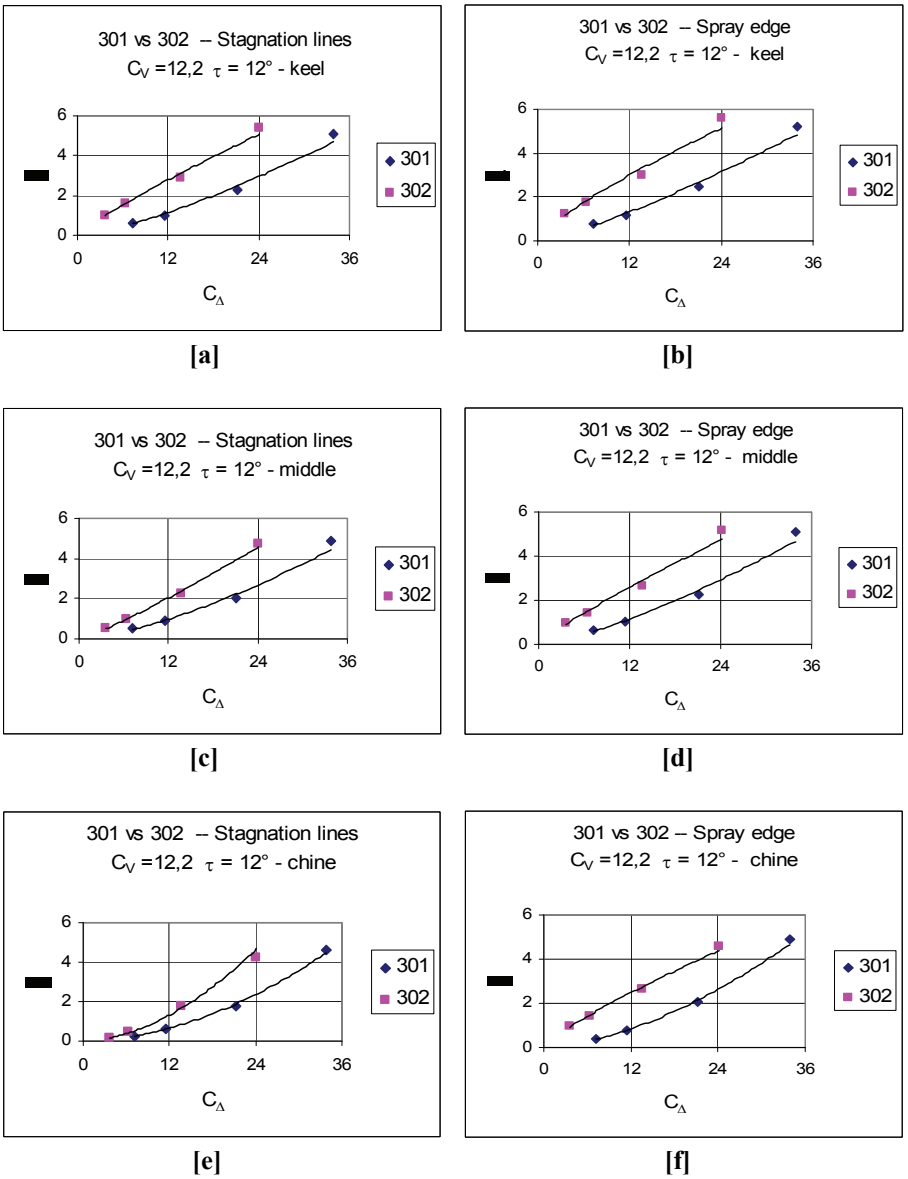

(Data source: [Kapryan & Boyd 1955])

Figure 9.5-8 Deadrise effect on Stagnation and spray edge line trends for V-bottom planing surfaces with C_V = 12.2 and τ =12°

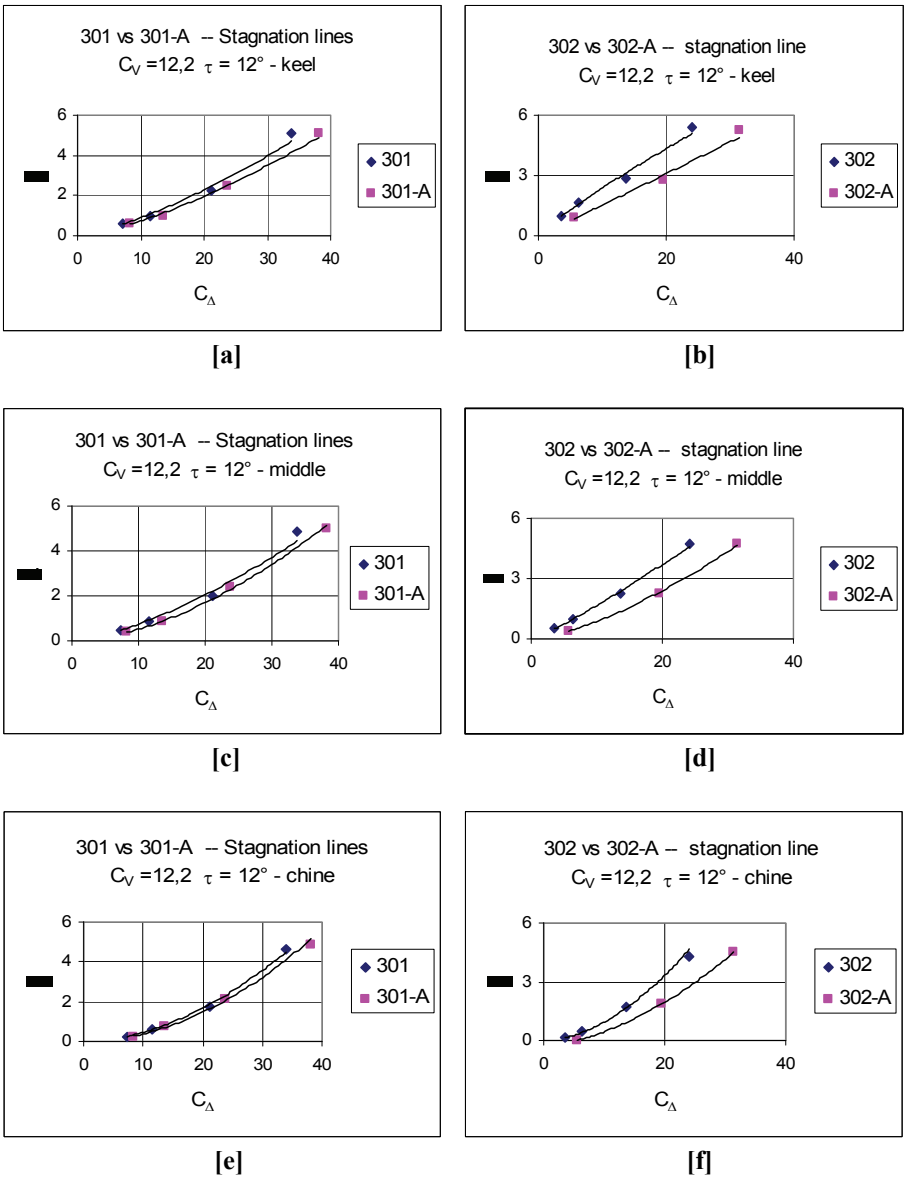

(Data source: [Kapryan & Boyd 1955])

Figure 9.5-9 Horizontal chine flared effect on stagnation line trends

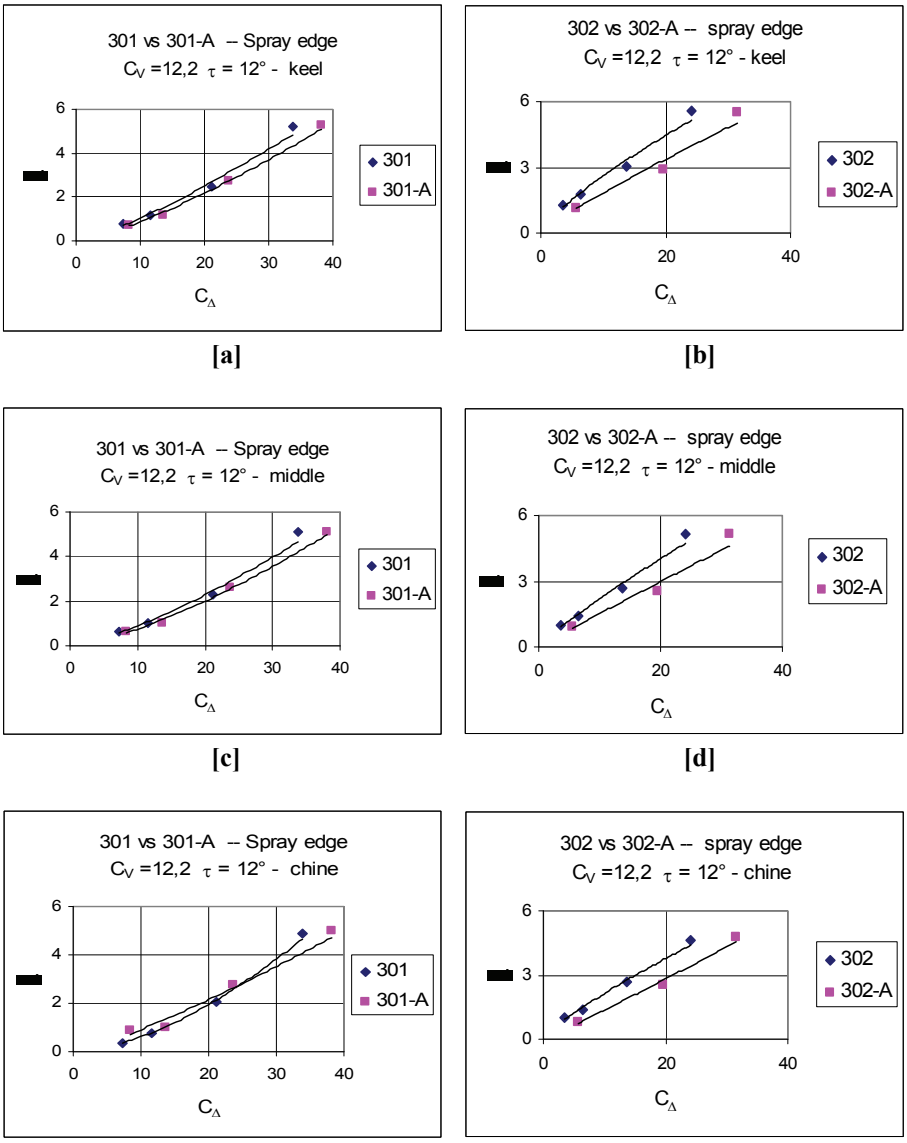

(Data source: [Kapryan & Boyd 1955])

Figure 9.5-10 Horizontal chine flare effect on spray line trends

These diagrams highlight an effect of the horizontal chine flare: the lines (Stagnation and Spray edges) move back. Further, this effect drops down for lower value of beam loading C_Δ and lift coefficient C_{Lb}, becoming negligible: the shape of the chine does not work at low value of vertical loads.

This is according to Sottorf's remark [Sottorf 1937]: he suggested that the wetted beam b could not always be constant and equal to the distance between the chines of the hull. In his opinion this is due to the influence of

planing conditions on wetted beam value, but he did not give any proof of this statement[121].

Further, the stagnation line ratio[122] λ^*_{SL} and the spray edge ratio[123] λ^*_{SE} trends have been investigated.

Per each buttock line, both ratios present the same trend[124]:

$$\lambda^*\big|_{keel} \to 1^+ \qquad \textbf{(E. 1)}$$

$$\lambda^*\big|_{chine} \to 1^- \qquad \textbf{(E. 2)}$$

as a consequence of one or both cases:

- increasing the beam loading C_Δ, as shown in Figure 9.5-11 ([a] – [d]), with $C_V = const$,
- decreasing the Froude number C_V, as shown in Figure 9.5-11 ([e] – [h]), with $C_\Delta = const$.

In depth, ratios as function of C_Δ present a rate related to the Froude number C_V: lower Froude number higher rate.

At the same time, ratios as function of C_V present a rate related to the beam loading C_Δ: higher beam loading higher rate.

---

[121] According to his remarks, Sottorf suggested to use the volume Froude number Fn_∇ instead of the beam Froude number Fn_b. Further note: Chapter 1, paragraph 1.2, page 3, of this Thesis.

[122] Ratio of the stagnation line position, on keel or on chine buttock, versus the stagnation line position on middle; e.g.: $\lambda^*_{SL}\big|_{keel} = \dfrac{\lambda_{SL}\big|_{keel}}{\lambda_{SL}\big|_{middle}} = \dfrac{l_{SL}\big|_{keel}}{l_{SL}\big|_{middle}}$.

[123] Ratio of the spray edge position, on keel or on chine buttock, versus the spray edge position on middle; e.g.: $\lambda^*_{SE}\big|_{keel} = \dfrac{\lambda_{SE}\big|_{keel}}{\lambda_{SE}\big|_{middle}} = \dfrac{l_{SE}\big|_{keel}}{l_{SE}\big|_{middle}}$.

[124] On the buttock "middle" both ratios are equal to one: λ*=1; thereby this case is not taken in account as a case of study.

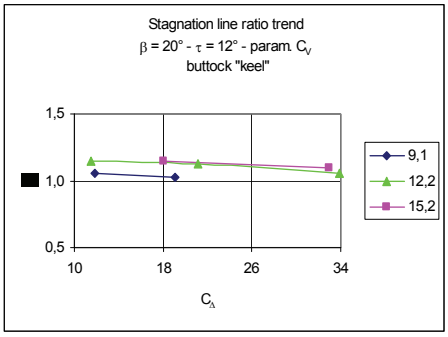

[a]

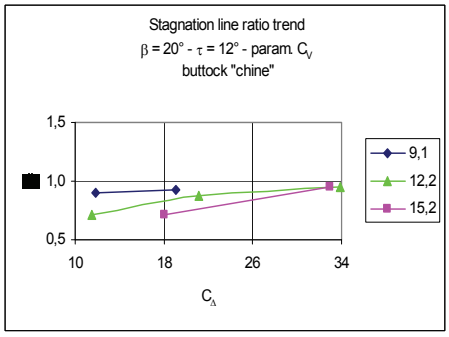

[b]

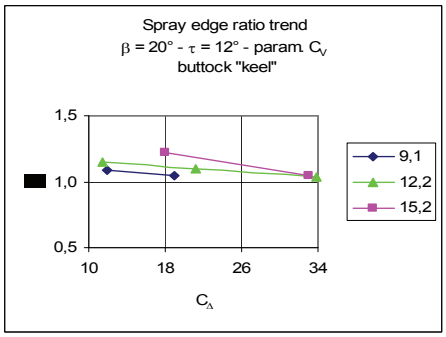

[c]

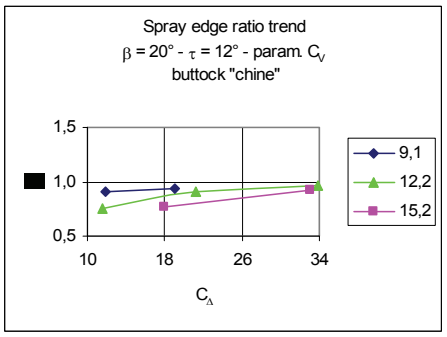

[d]

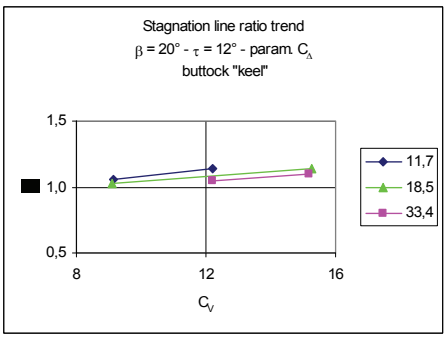

[e]

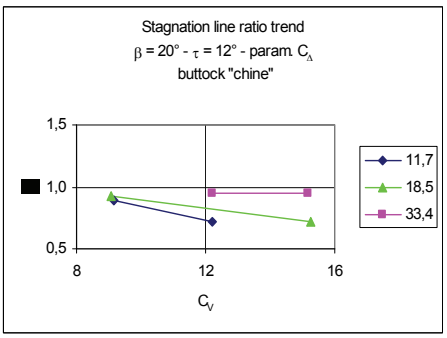

[f]

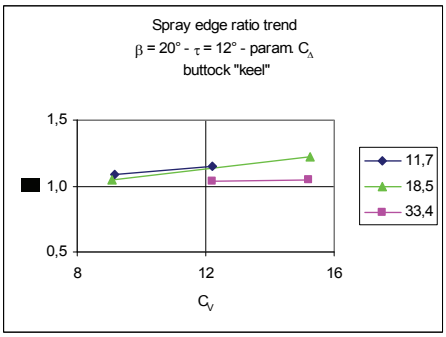

[g]

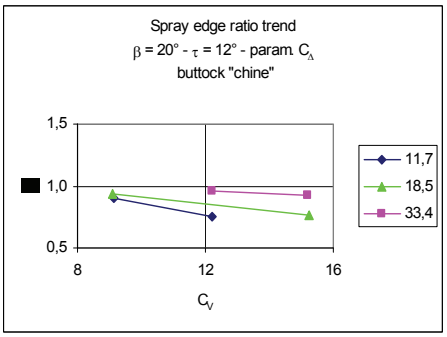

[h]

(Data source: [Kapryan & Boyd 1955])

Figure 9.5-11 Stagnation line ratio and Spray edge ratio trends related to Froude number and beam loading - Model 301

In order to take in account these observations, the ratios have been investigated related to the lift coefficient C_{Lb}.

Results highlight a clear trend:

$$\lambda^*\big|_{keel} \to 1^+ \qquad \textbf{(E. 3)}$$

$$\lambda^*\big|_{chine} \to 1^- \qquad \textbf{(E. 4)}$$

increasing C_{Lb} value.

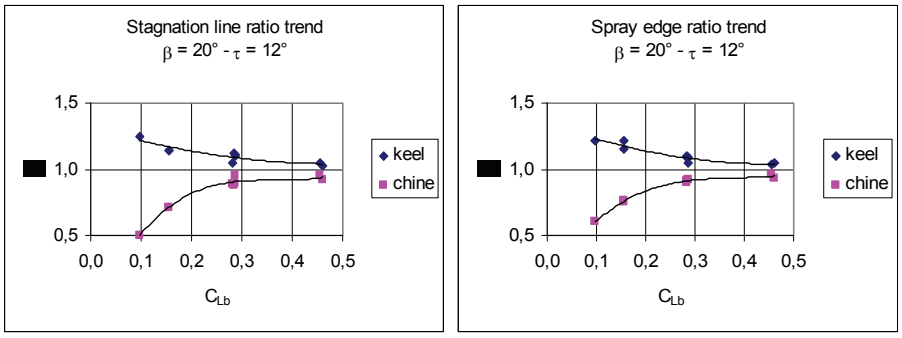

[a] **[b]**

(Data source: [Kapryan & Boyd 1955])

Figure 9.5-12 Stagnation line and Spray edge trends related to the lift coefficient - Model 301

Moreover every sets of C_Δ and C_V values that drive to the same value of C_{Lb}, give close-set results in terms of ratios λ^*. The differences are related to the errors on data and are not greater than a few percentage units.

Physical meaning of these trends are pointed out in a movement of Stagnation and Spray edge lines related to the growing up of Lift coefficient:

1. the lines rotate becoming closer perpendicular to the fluid flow direction;
2. the lines translate forward in the opposite direction of the fluid flow.

Further, the ratio of the pressure center location to the mean wetted length l_p/l_m appears to be almost constant, whereas, as function of C_{Lb}, decreases to a lower limit value, increasing the lift coefficient.

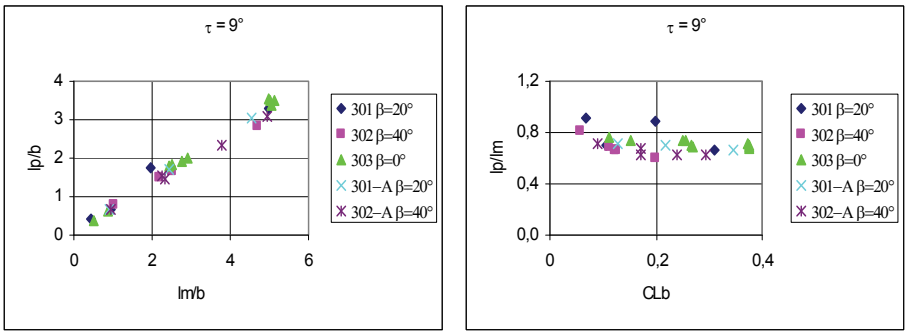

[a] **[b]**

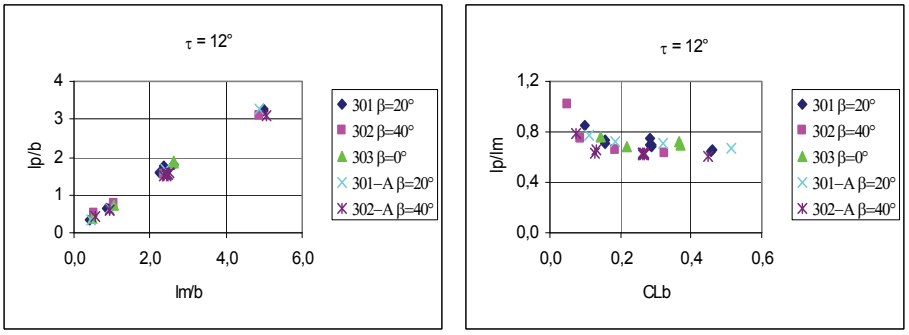

[c] **[d]**

(Data source: [Kapryan & Boyd 1955])

Figure 9.5-13 Center of pressure location to the mean wetted length ratio

All these phenomena are common to all V-bottom hull, with or without horizontal chine flared, and give us the evidence that, raising up the lift coefficient, the fluid flow field comes close to the planing flat plate ones and, thereby, the effect of deadrise angle as well as the effect of the chine shape (e.g.: with or without horizontal chine flared) decrease.

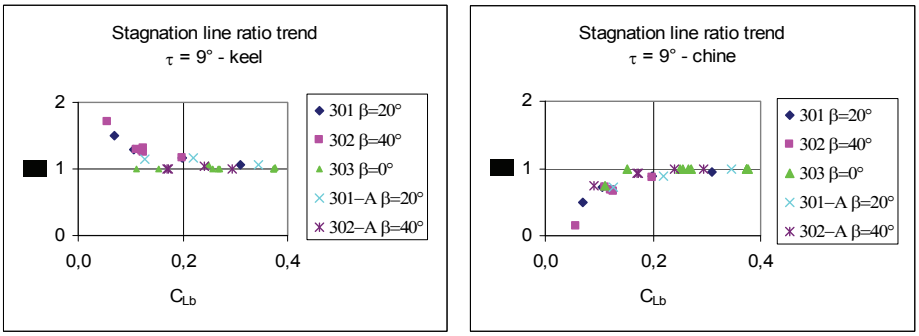

[a] **[b]**

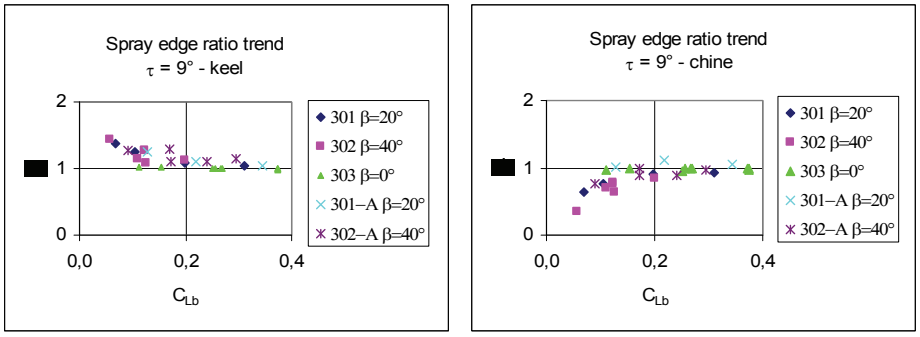

[c] **[d]**

(Data source: [Kapryan & Boyd 1955])

Figure 9.5-14 Stagnation lines and Spray edge lines trends with τ = 9°

According to this observation, the relationship[125]:

$$C_{Lb} = C_{L0} - 0.0065\,\beta\,C_{L0}^{0.6} \qquad \textbf{(E. 5)}$$

cannot be applied for every value of C_{Lb}[126], as a matter of fact the deadrise angle has the same influence for each value of C_{Lb} and this denies the above remark.

The formula (E. 5) is an empirical relation based on *"... test data of Shoemaker and those obtained from two series of ETT (Experimental Towing Test) tests..."* [Korvin-Kroukovsky et al. 1949].

The most data of this set are related to values of C_{Lb} not much greater than 0.15 and the most data of this sub-set are close to the diagram of (E. 5); meanwhile data related to values of C_{Lb} greater than 0.20 are not many and, further, are more scattered than the above set.

[125] A fundamental formula in many resistance prediction methods for a planing hull in still water (e.g. Savitsky's method).

[126] Some authors are use to write $C_{L\beta}$ instead of C_{Lb}.

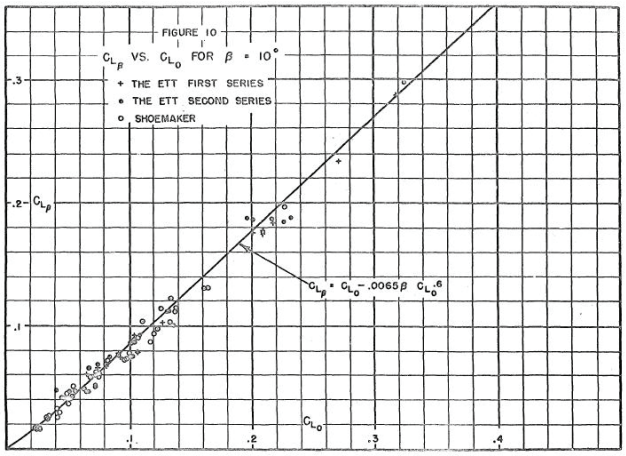

[a]: C_{Lb} vs C_{L0} for β = 10 °

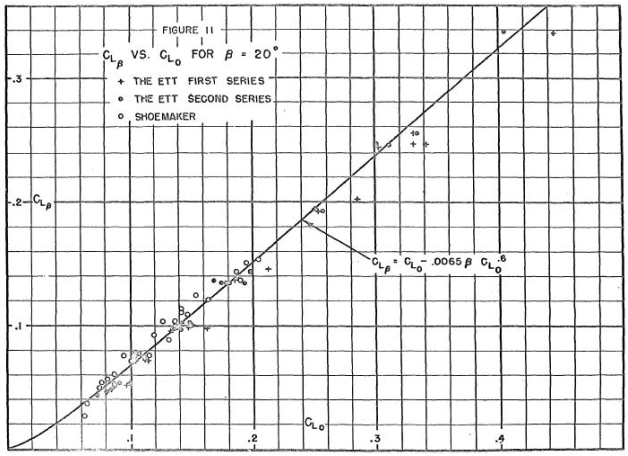

[b]: C_{Lb} vs C_{L0} for β = 20 °

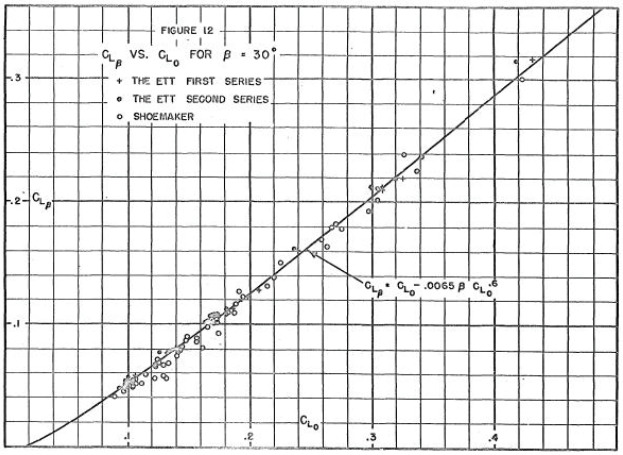

[c]: C_{Lb} vs C_{L0} for β = 30 °

(Data source: [Korvin-Kroukovsky et al. 1949])

Figure 9.5-15 Lift Coefficient of a V-bottom surface C_{Lb} versus Lift Coefficient of a flat plate C_{L0} for three value of deadrise angle β

This drives to a limitation of the formula (E. 5) within the range $0 \le C_{Lb} \le 0.20$: for values $C_{Lb} > 0.20$ results are not quite close to empirical value.

When the fluid flow field under a V-bottom planing hull looks like the planing flat plate one the deadrise angle has an influence just on the viscous component of Drag Resistance via wetted length: higher deadrise angle higher wetted length[(127)] and higher Resistance (viscous component)[(128)].

In general, for a given condition of load, speed and trim, higher deadrise angle higher wetted length, higher Resistance and center of pressure location more forward [Chambliss & Boyd 1953].

According to the above observations let $C^*_{Lb,SL}$ the lower limit value of lift coefficient C_{Lb} for which the deadrise angle effects are negligible in term of Stagnation Line position, and let $C^*_{Lb,SE}$ the equivalent to $C^*_{Lb,SL}$ in term of Spray Edge position. Further, let define C^*_{Lb} as the lower limit value of lift coefficient for which the deadrise angle effects are negligible: $C^*_{Lb} = \max\left\{C^*_{Lb,SL}, C^*_{Lb,SE}\right\}$.

---

(127) Dem.

Let $\overline{dF}$ the elementary force acting on the planing surface due to the dynamic pressure p_{dyn}: $dF = p_{dyn} dS \hat{n}$, with dS the small area where the dynamic pressure is acting on and $\hat{n}$ the normal unit vector to the surface.

In the dynamic equilibrium condition the vertical component of $\overline{dF}$ integrated on whole wetted surface S_W have to balance the weight (or the vertical load): $W = F_z$ with $F_z = \left(\int_{Sw} p_{dyn} \overline{dS} \right) \cdot \hat{z}$ where $\hat{z}$ is the local vertical unit vector.

It follows: $F_z = \left(\frac{1}{2}\rho V^2\right) S_W \left(\hat{n} \cdot \hat{z}\right)$ with $Sw = l_m \cdot l_{Tm}$ and $\hat{n} \cdot \hat{z} = \cos\beta$; l_m is the mean wetted length, l_{Tm} is the mean transverse wetted perimeter and β is the deadrise angle, of the surface. Further, let $S_{W,norm} = l_{Tm} l_m \cos\beta$ the wetted surface projected on the horizontal plane we have: $W = \left(\frac{1}{2}\rho V^2\right) S_{W,norm}$. If we assume for l_{Tm} its max value (the transverse perimeter between the chines), in steady planing condition $S_{W,norm} = const$ so that $l_m \cos\beta = const$ and the statement is demonstrated.

(128) According to Sottorf's remarks, this is not true at all, if, per each wetted hull section, the transverse wetted perimeter (l_{TW}) projected over the beam (known as wetted beam b_W) is less than the beam b: $b_W = l_{TW} \cos\beta < b$. In this case an increment of deadrise angle β drives to an increment of the wetted surfaces S_W but there is no evidence that this increment of the wetted surface is related only to an increment of wetted length l_m.

If $C_{Lb} > C^*_{Lb}$ the deadrise angle does not affect anymore the overall value of the resistance: it just affects the viscous component via the geometrical influence on the wetted length.

In this case the deadrise angle value can be chosen with relation to the hull seakeeping instead of the resistance performance; in the presence of a high deadrise angle, for a good seakeeping behavior, it will be possible to reduce the wetted length, as well as the Resistance, assuming a step on the hull.

The step will be placed on the abaft part of the hull, behind the center of gravity[129], where both values and rate of pressure are low.

A way to get the value of C^*_{Lb} is by comparison the curves $\lambda^* = \lambda^*(C_{Lb}, \beta)$ related to two different value of deadrise β (β_1 and β_2, with $\beta_1 < \beta_2$): for $C_{Lb} \geq C^*_{Lb}$ the curves overlap and the value of λ^* does not depend by the deadrise angle β anymore (with $\beta_1 \leq \beta \leq \beta_2$): $\lambda^* = \lambda^*(C_{Lb})$.

This value of C^*_{Lb} depends by the trim τ, the buttock line and the deadrise angle range (β_1, β_2).

If each range is very little $(\beta_1 \cong \beta_2)$ it is possible to build a function that per each value of β gives the value of C^*_{Lb} related to. In the plane (β, C^*_{Lb}) with a Cartesian Coordinate System this function describes a curve that divides the plane in two fields: inner (which include the origin) and outer. If the design values of β and C_{Lb} define a point in the inner plane than β influences the overall resistance, else, in the outer field, β influences just the viscous component of resistance.

The lack of data, in term of deadrise angle available (β = 0°, 20°, 40°) drive to a step diagram with two different value of C^*_{Lb} in β = 20°: these kind of diagrams are not quite manageable and are, further, too approximate.

[129] In first approximation the step can be placed at a distance of 0.2 beam behind the center of gravity [Mori 1940].

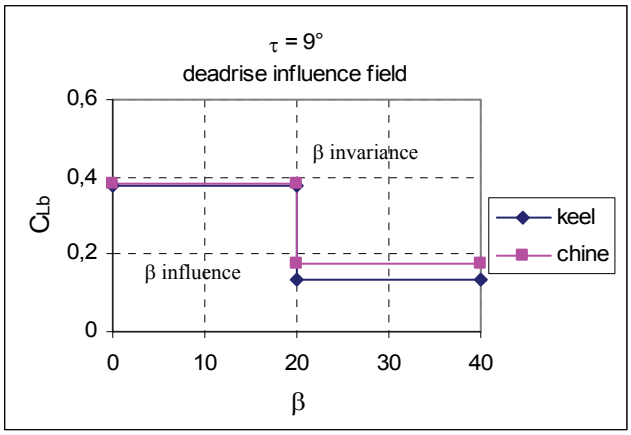

(Data source: [Kapryan & Boyd 1955])

Figure 9.5-16 Deadrise angle influence field for τ = 9°

9.6 Conclusion

Dynamic pressure distribution on planing surface is related to:

- geometrics (shape and trim of the surface)
- kinematics (speed of the surface)
- dynamics (weight or vertical load)

This distribution can be described by the knowledge of Stagnation Line and Spray Edge position as well as the peak pressure values (pressure on Stagnation Line).

On a flat planing plate Stagnation Line and Spray Edge are quite straight, just curved close to the border lines.

On a V-bottom planing surface Stagnation Line and Spray Edge seem to be obtained applying a set of transformations to the flat planing plate ones: one translation and two rotations.

Translation is related to the deadrise angle β: higher deadrise angle higher wetted length and more forward locations of pressure center, Stagnation Line and Spray Edge.

The first rotation is developed around the keel with a magnitude equal to β: it is strictly connected to the geometrical transformation of a flat plate into a V-bottom surface.

The second rotation is developed around an axis, normal to both keel and local vertical, and passing through the point K, intersection of the keel with the free water surface. The magnitude of this rotation is pertinent to the trim τ, the lift coefficient C_{Lb} and the deadrise angle β.

The analysis of the data has been highlighted that, per each value of trim τ, an increment of the lift coefficient C_{Lb} drives to a decrease of the second rotation magnitude. Further, per each value of τ, there is a lift coefficient value C_{Lb}^{*} over which the second rotation is null: in each side of the V-bottom surface the pressure distribution looks like the flat planing plate ones.

In this case the resistance pressure component reaches its minimum value, that is not related to the deadrise angle β of the V-bottom surface: the deadrise angle β influences only the resistance viscous component via the wetted length; further, the relationship (E. 5) does not work well: the influence of the deadrise angle β is the same for each value of C_{Lb}, and this denies the above remarks.

9.7 Pressure Distribution Diagrams

9.7.1 Model 303 - $\beta = 0°$

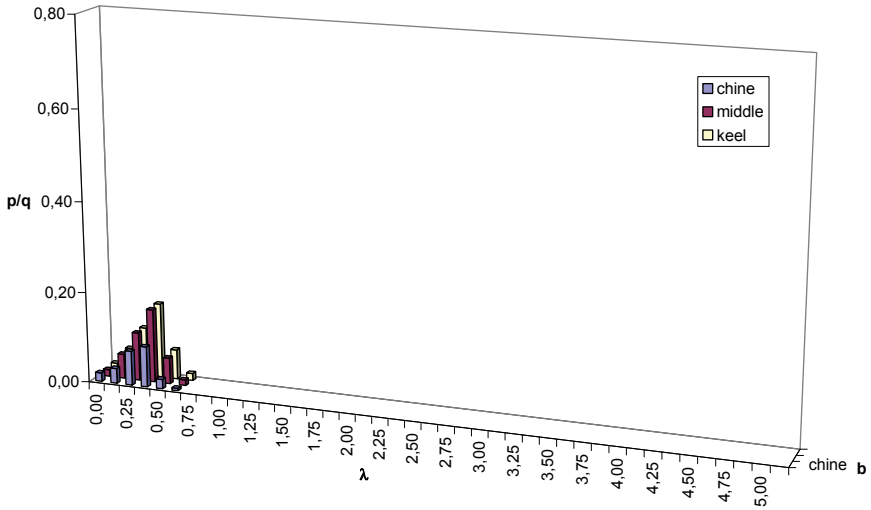

[a] : τ = 4 ° - run 1 - C_Δ = 3.28 - C_V = 12.20 - C_{Lb} = 0.0440

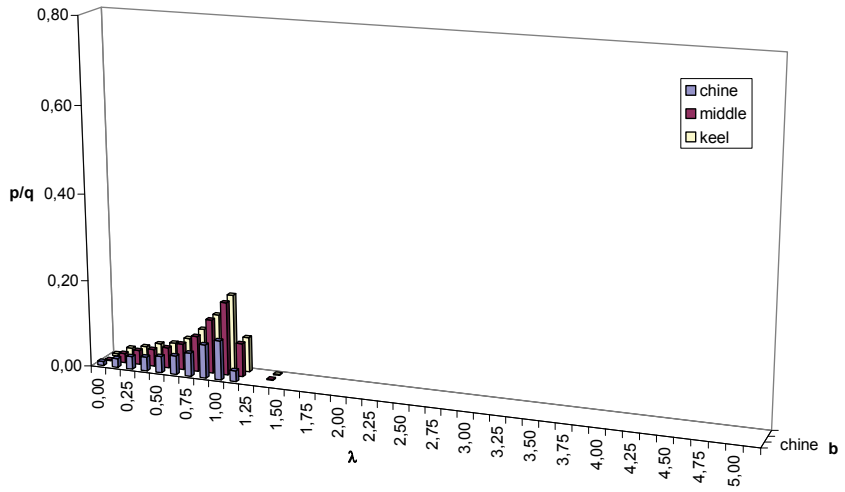

[b] : τ = 4 ° - run 2 - C_Δ = 4.77 - C_V = 12.20 - C_{Lb} = 0.0640

Figure 9.7-1 Pressure distribution on rectangular flat planing plate - Model 303 (continue)

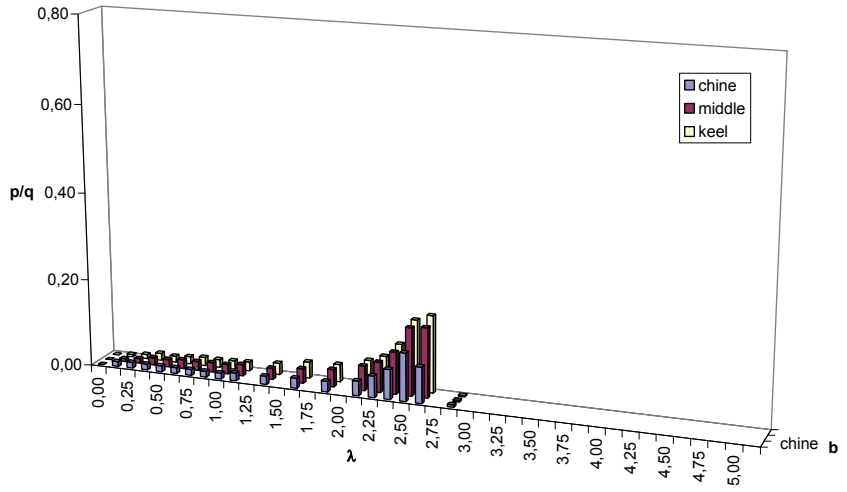

[c] : τ = 4 ° - run 3 - C_Δ = 7.46 - C_V = 12.23 - C_{Lb} = 0.0998

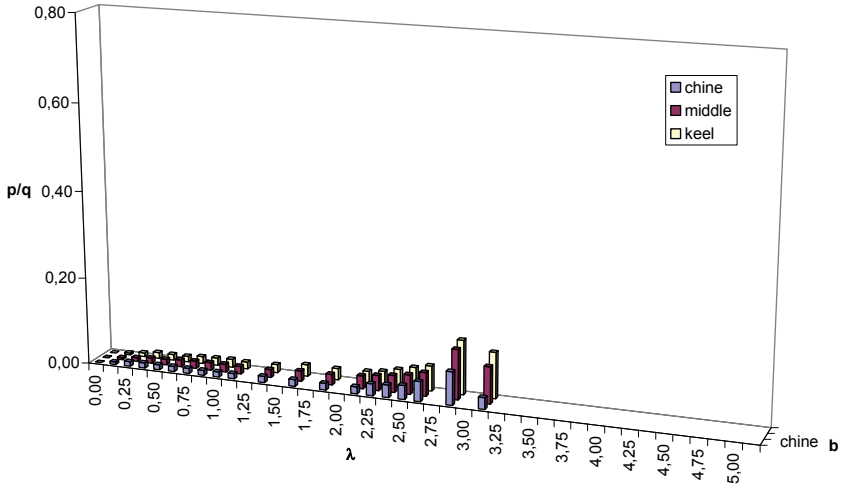

[d] : τ = 4 ° - run 4 - C_Δ = 7.33 - C_V = 12.20 - C_{Lb} = 0.0984

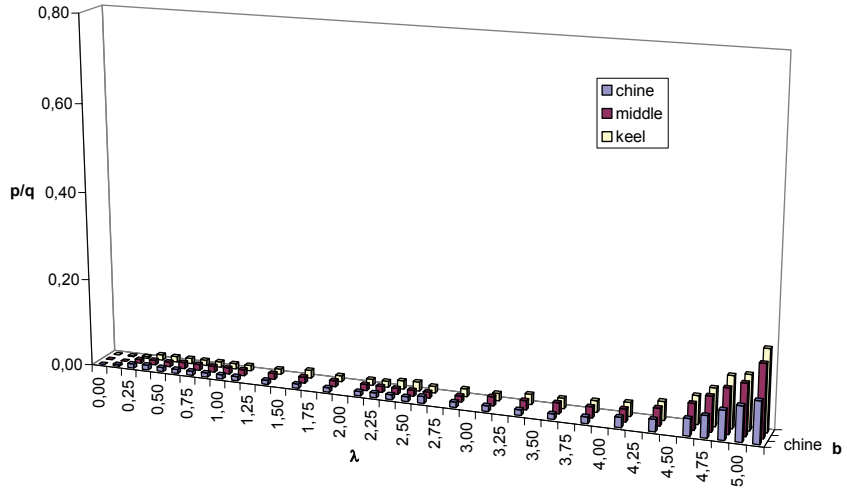

[e] : τ = 4 ° - run 5 - C_Δ = 10.01 - C_V = 12.26 - C_{Lb} = 0.1332

Figure 9.7-1 Pressure distribution on rectangular flat planing plate - Model 303 (continue)

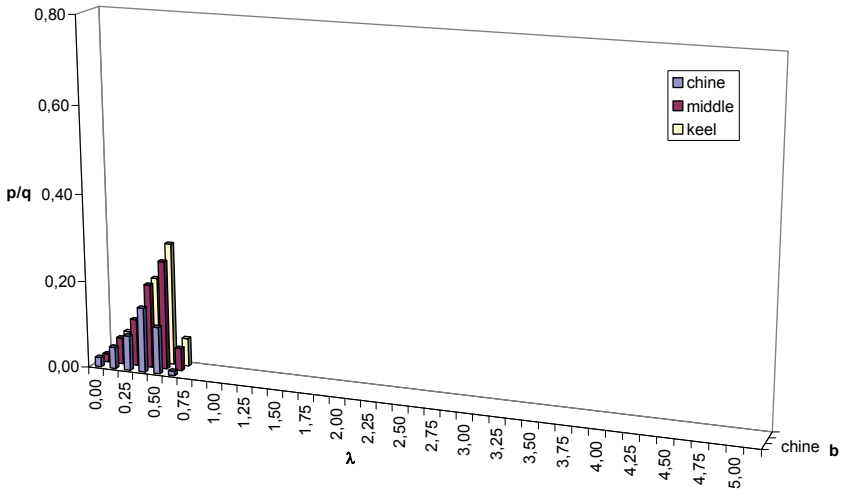

[f] : τ = 6 ° - run 6 - C_Δ = 5.45 - C_V = 12.20 - C_{Lb} = 0.0732

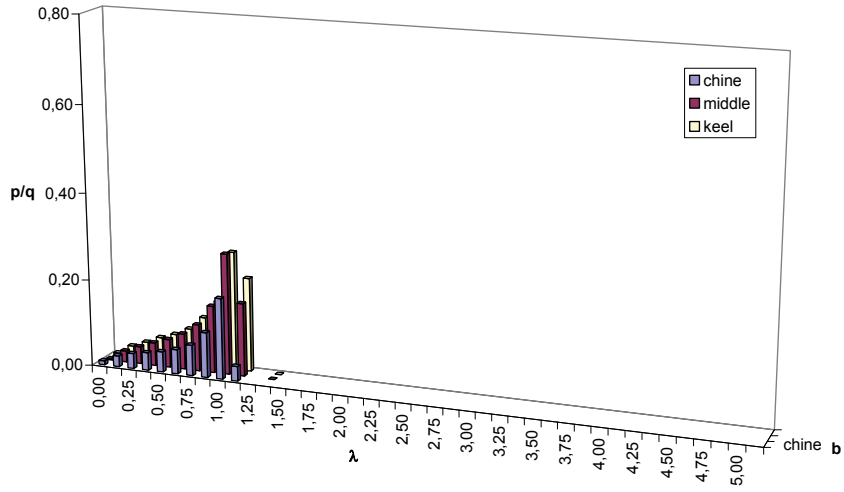

[g] : τ = 6 ° - run 7 - C_Δ = 7.75 - C_V = 12.17 - C_{Lb} = 0.1046

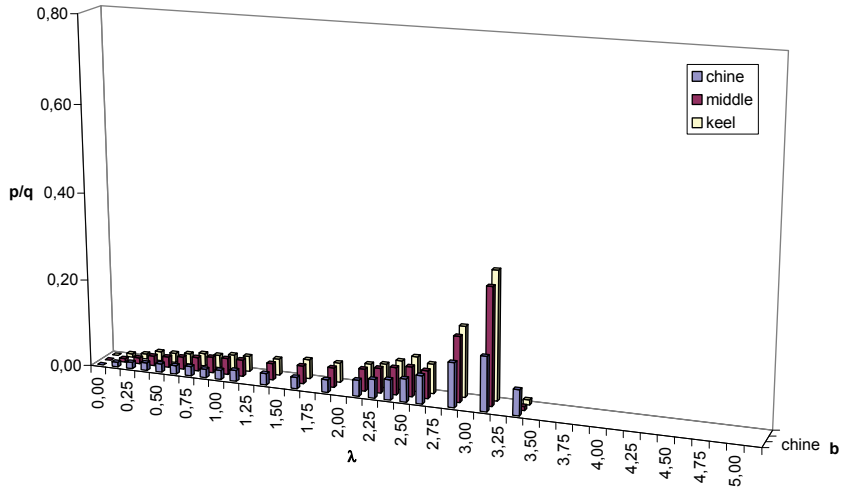

[h] : τ = 6 ° - run 8 - C_Δ = 7.05 - C_V = 9.12 - C_{Lb} = 0.1690

Figure 9.7-1 Pressure distribution on rectangular flat planing plate - Model 303 (continue)

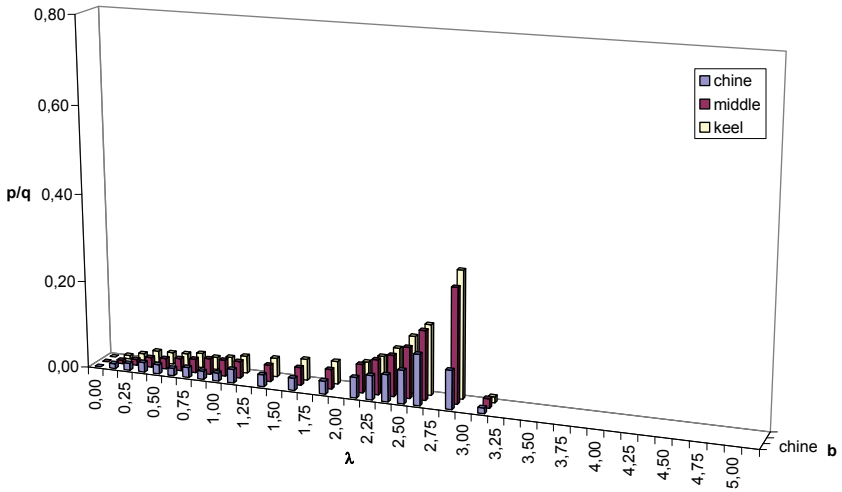

[i] : τ = 6 ° - run 9 - C_Δ = 8.56 - C_V = 10.13 - C_{Lb} = 0.1668

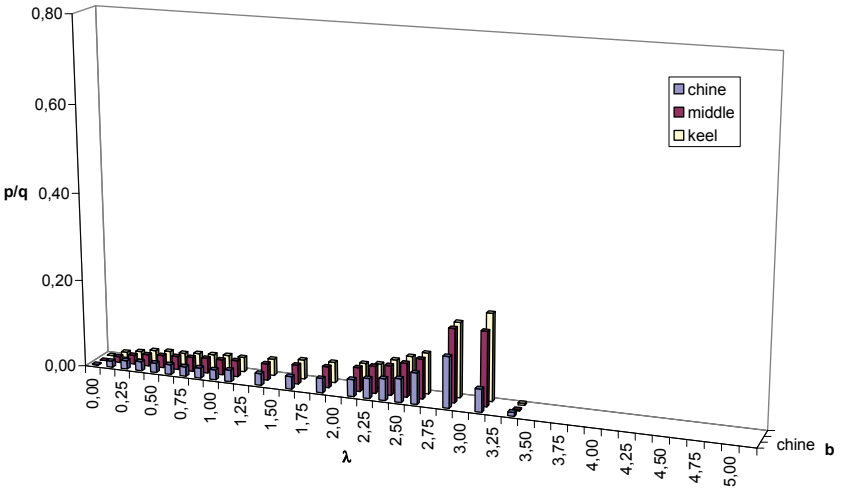

[j] : τ = 6 ° - run 10 - C_Δ = 12.48 - C_V = 12.20 - C_{Lb} = 0.1676

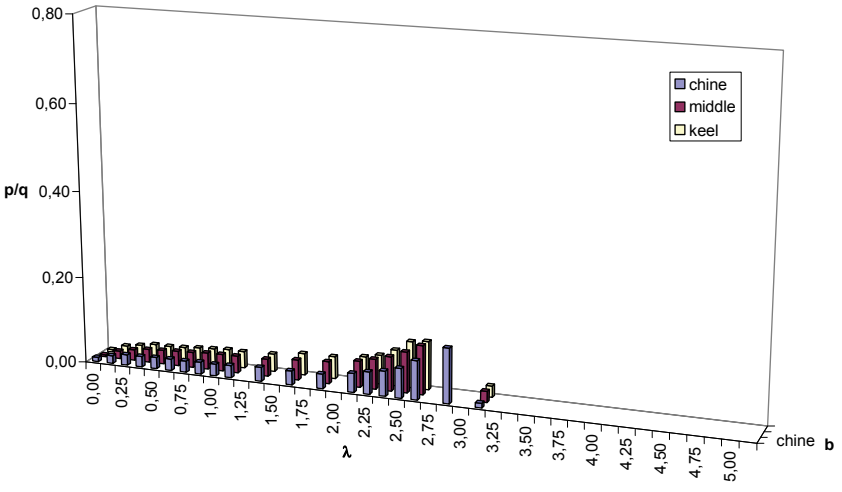

[k] : τ = 6 ° - run 11 - C_Δ = 19.38 - C_V = 15.28 - C_{Lb} = 0.1660

Figure 9.7-1 Pressure distribution on rectangular flat planing plate - Model 303 (continue)

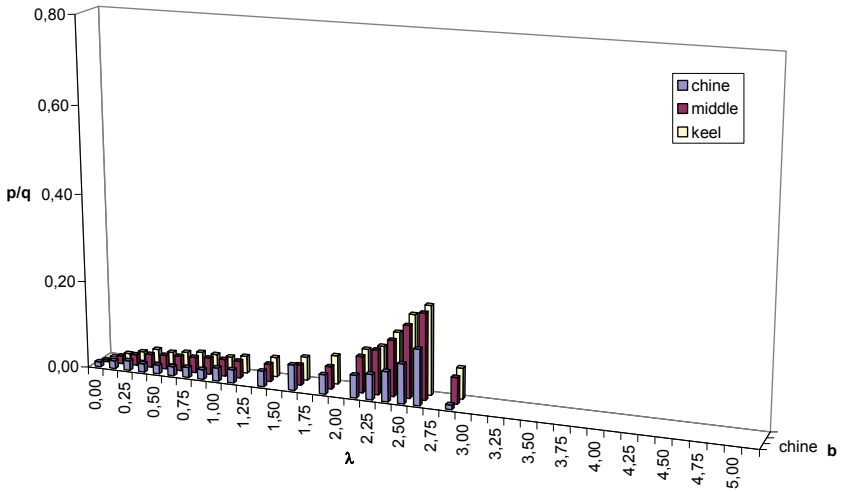

[l] : τ = 6 ° - run 12 - C_Δ = 12.99 - C_V = 12.23 - C_{Lb} = 0.1736

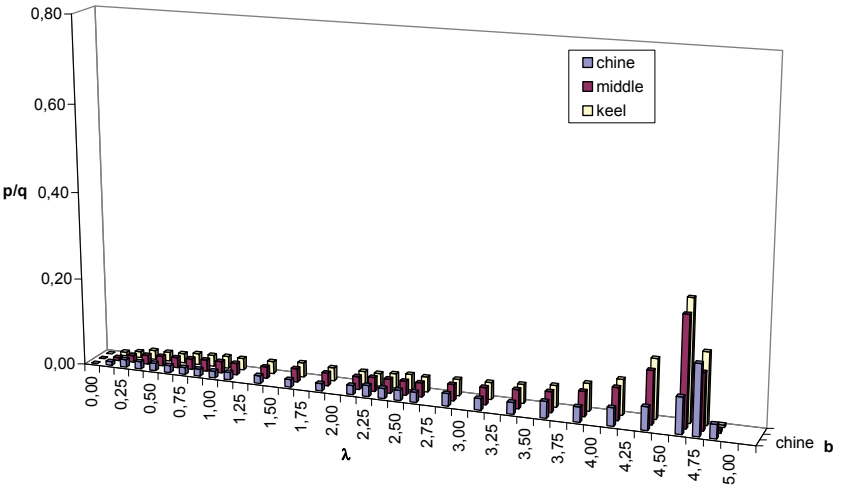

[m] : τ = 6 ° - run 13 - C_Δ = 15.63 - C_V = 12.20 - C_{Lb} = 0.2110

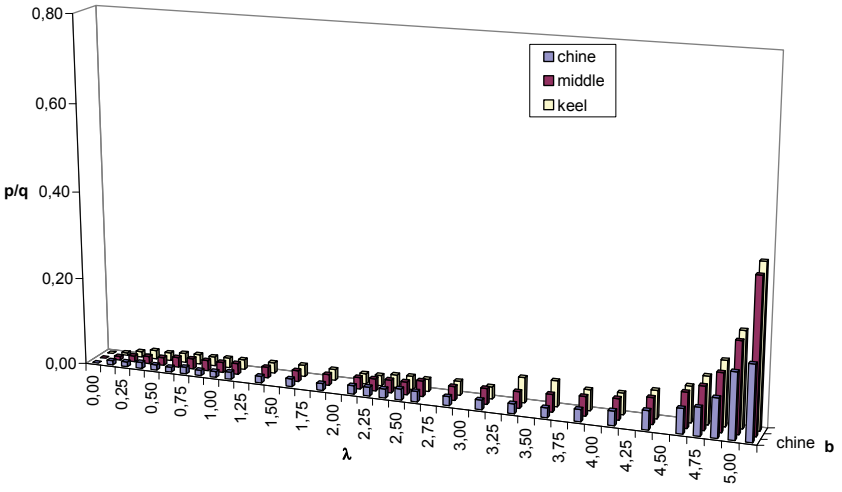

[n] : τ = 6 ° - run 14 - C_Δ = 16.29 - C_V = 12.20 - C_{Lb} = 0.2188

Figure 9.7-1 Pressure distribution on rectangular flat planing plate - Model 303 (continue)

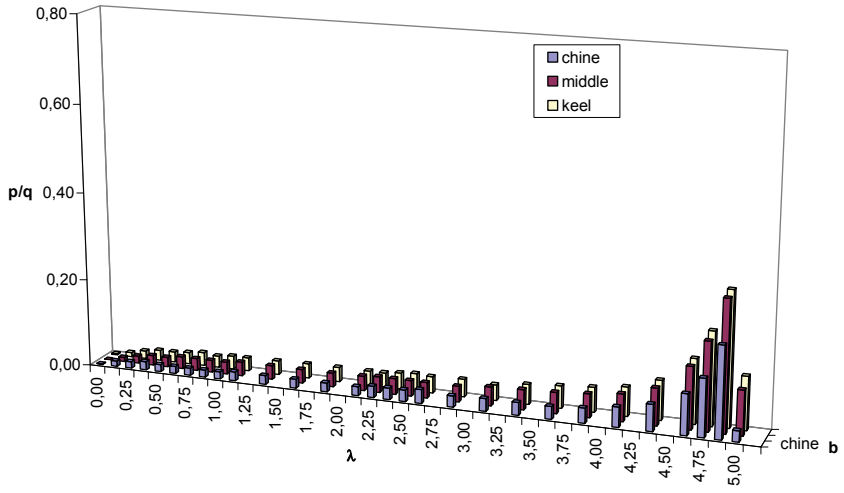

[o] : τ = 6 ° - run 15 - C_Δ = 16.29 - C_V = 12.26 - C_{Lb} = 0.2168

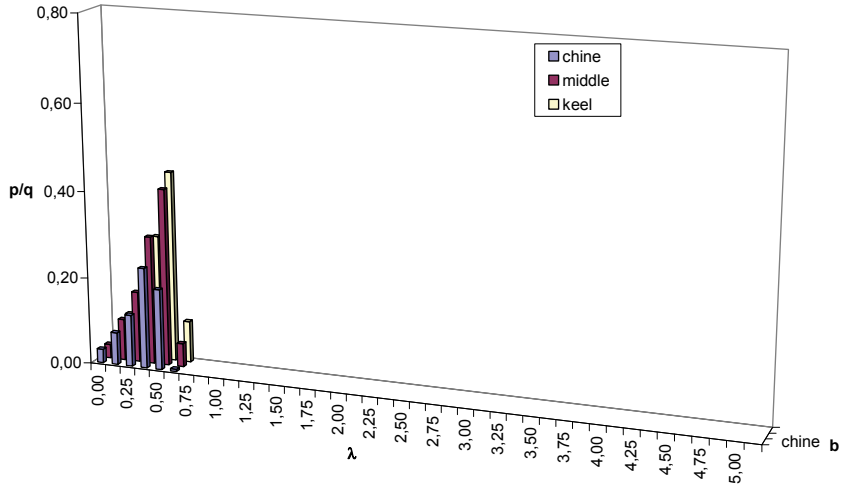

[p] : τ = 9 ° - run 16 - C_Δ = 8.31 - C_V = 12.23 - C_{Lb} = 0.1112

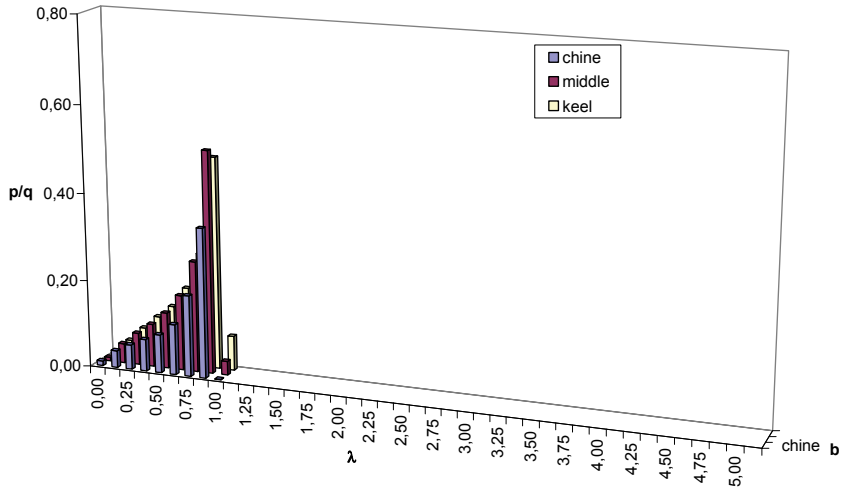

[q] : τ = 9 ° - run 17 - C_Δ = 11.42 - C_V = 12.20 - C_{Lb} = 0.1534

Figure 9.7-1 Pressure distribution on rectangular flat planing plate - Model 303 (continue)

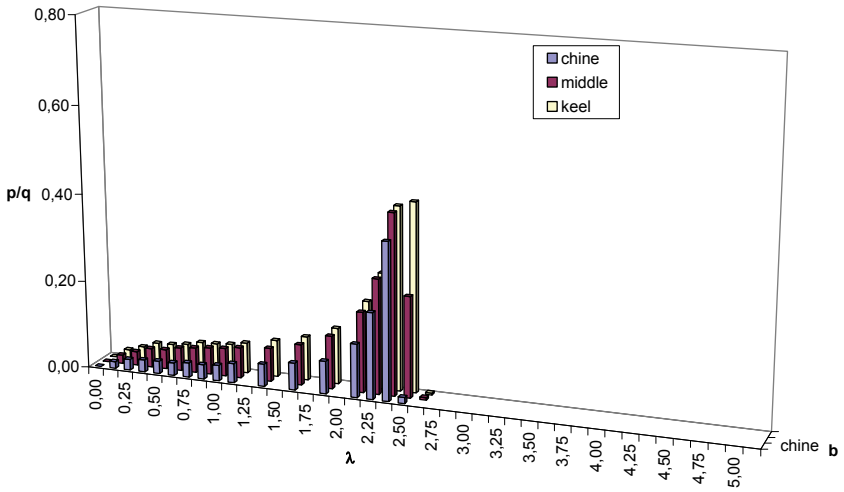

[r] : τ = 9 ° - run 18 - C_Δ = 18.62 - C_V = 12.20 - C_{Lb} = 0.2502

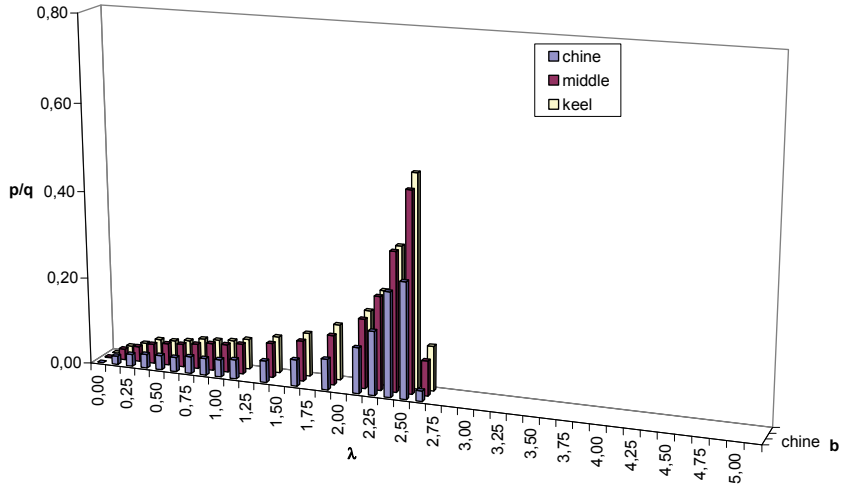

[s] : τ = 9 ° - run 19 - C_Δ = 19.04 - C_V = 12.20 - C_{Lb} = 0.2558

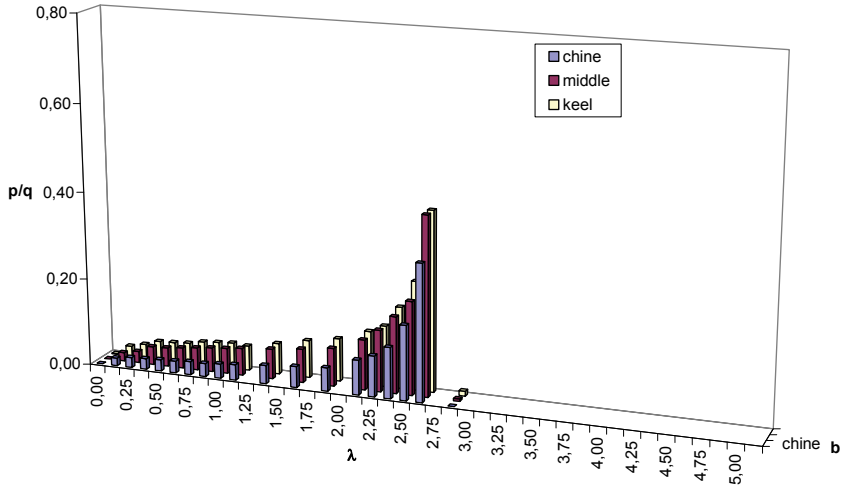

[t] : τ = 9 ° - run 20 - C_Δ = 19.94 - C_V = 12.23 - C_{Lb} = 0.2666

Figure 9.7-1 Pressure distribution on rectangular flat planing plate - Model 303 (continue)

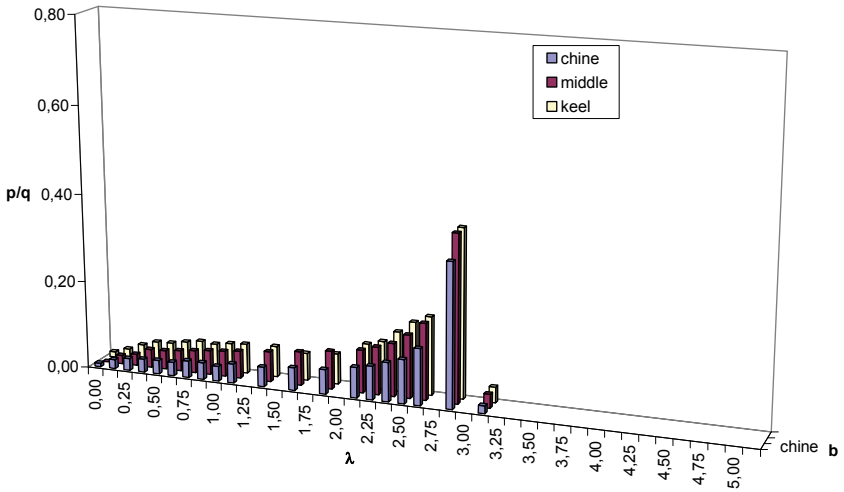

[u] : τ = 9 ° - run 21 - C_Δ = 20.32 - C_V = 12.26 - C_{Lb} = 0.2704

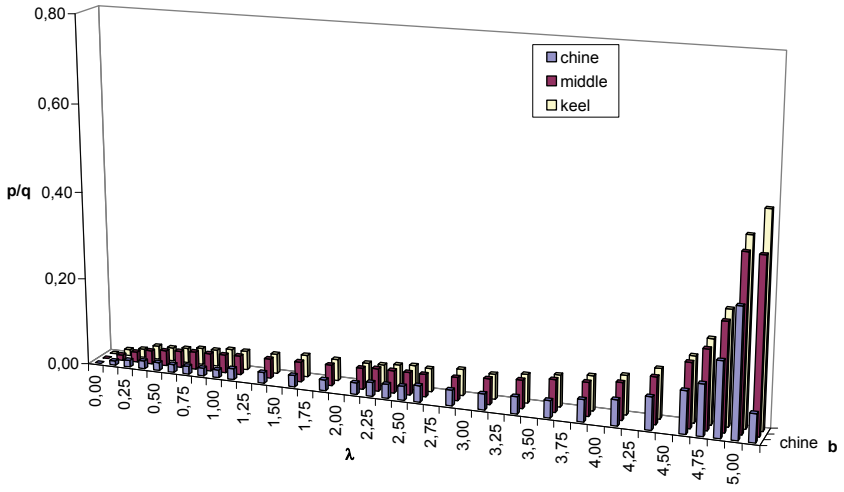

[v] : τ = 9 ° - run 22 - C_Δ = 27.90 - C_V = 12.17 - C_{Lb} = 0.3768

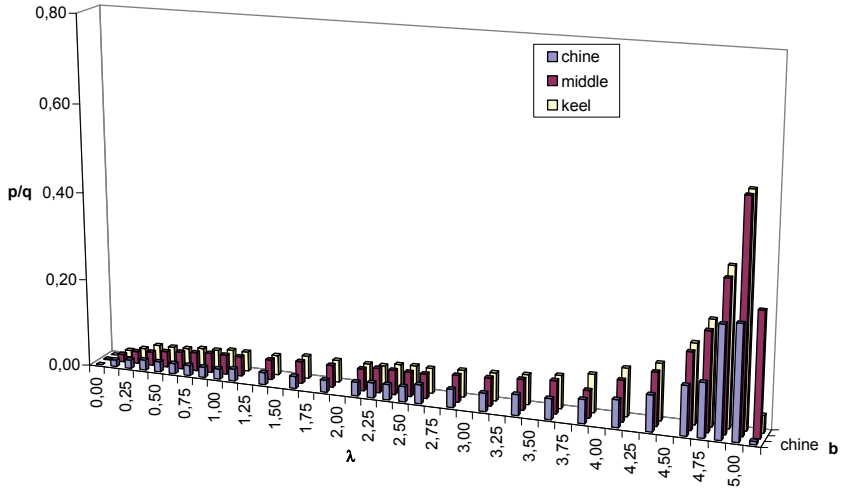

[w] : τ = 9 ° - run 23 - C_Δ = 27.90 - C_V = 12.20 - C_{Lb} = 0.3748

Figure 9.7-1 Pressure distribution on rectangular flat planing plate - Model 303 (continue)

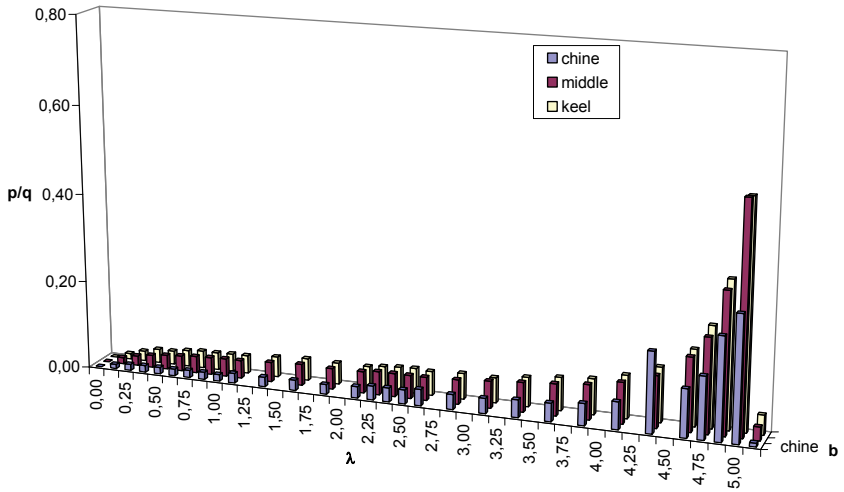

[x] : τ = 9 ° - run 24 - C_Δ = 27.90 - C_V = 12.20 - C_{Lb} = 0.3748

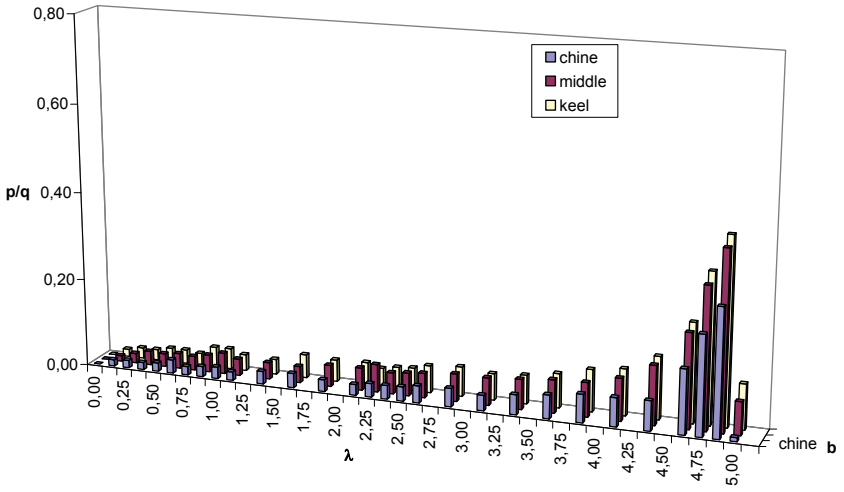

[y] : τ = 9 ° - run 25 - C_Δ = 27.90 - C_V = 12.23 - C_{Lb} = 0.3730

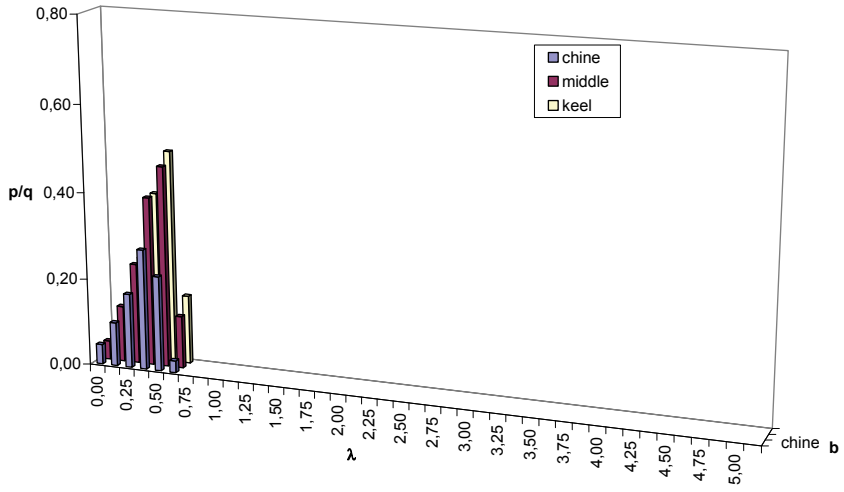

[z] : τ = 12 ° - run 26 - C_Δ = 10.65 - C_V = 12.20 - C_{Lb} = 0.1432

Figure 9.7-1 Pressure distribution on rectangular flat planing plate - Model 303 (continue)

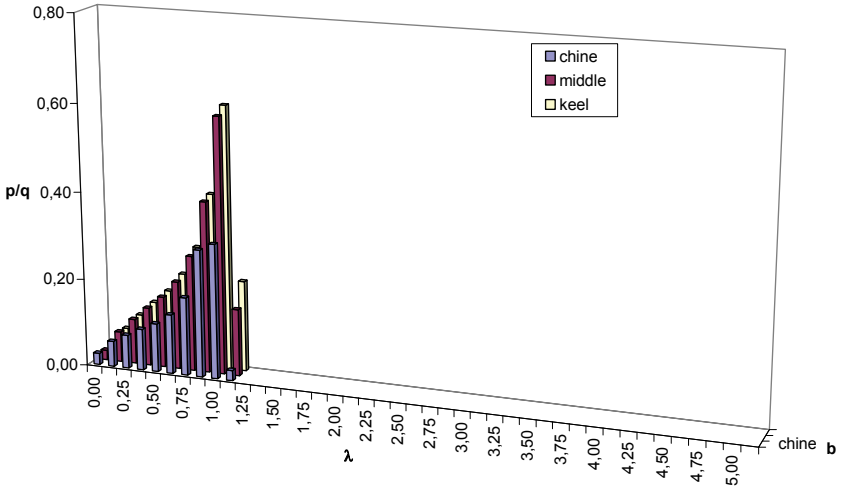

[aa] : τ = 12 ° - run 27 - C_Δ = 16.17 - C_V = 12.17 - C_{Lb} = 0.2198

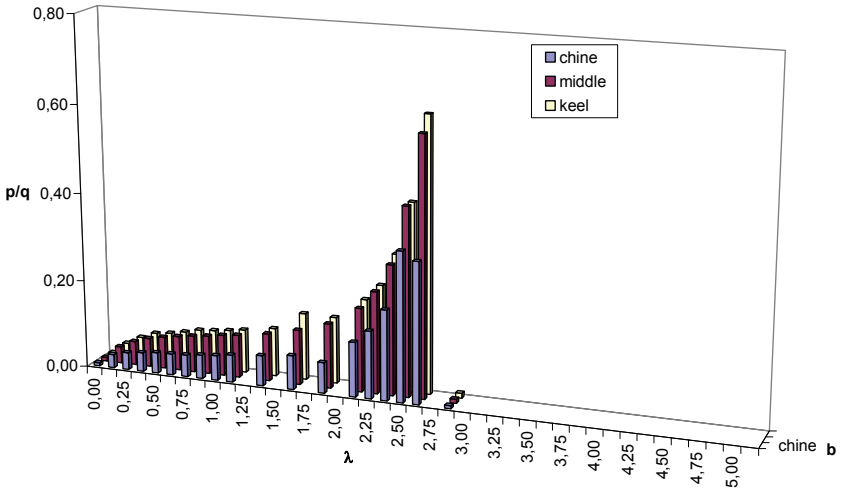

[ab] : τ = 12 ° - run 28 - C_Δ = 27.48 - C_V = 12.20 - C_{Lb} = 0.3692

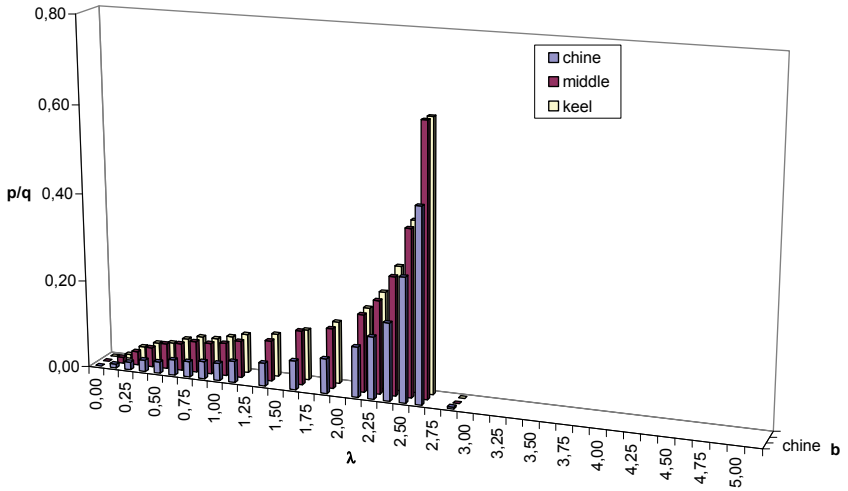

[ac] : τ = 12 ° - run 29 - C_Δ = 8.52 - C_V = 6.83 - C_{Lb} = 0.3652

Figure 9.7-1 Pressure distribution on rectangular flat planing plate - Model 303 (continue)

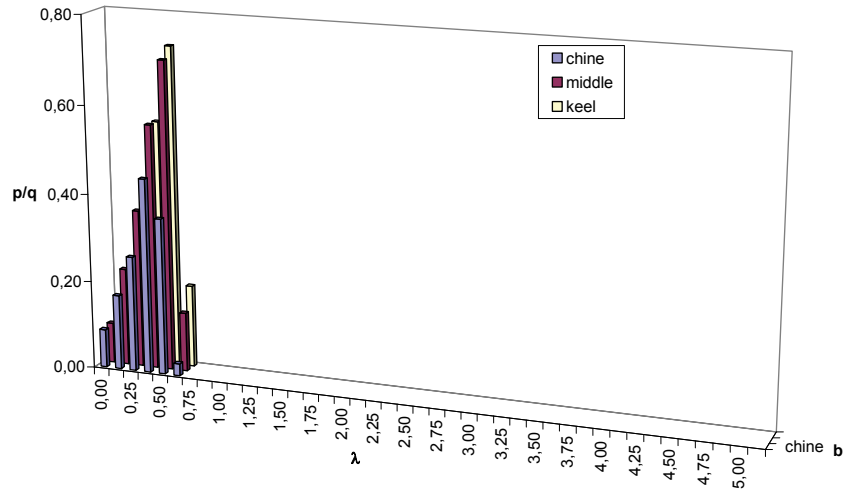

[ad] : τ = 18 ° - run 30 - C_Δ = 15.34 - C_V = 12.20 - C_{Lb} = 0.2062

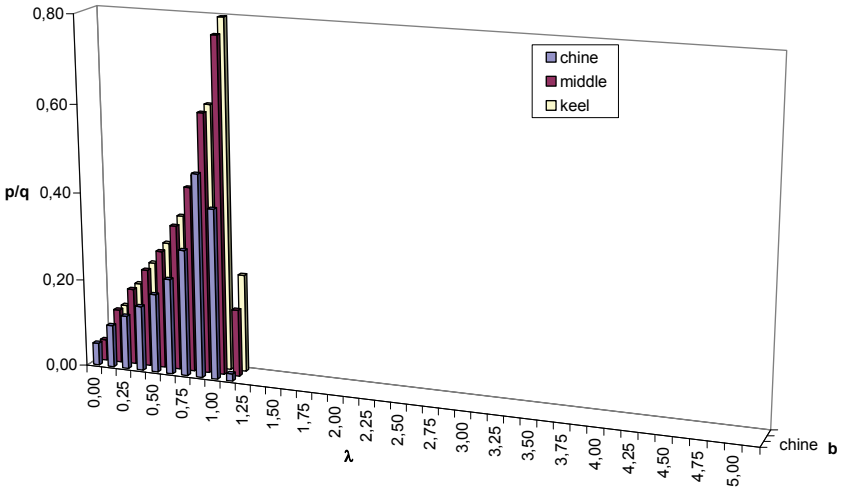

[ae] : τ = 18 ° - run 31 - C_Δ = 24.28 - C_V = 12.23 - C_{Lb} = 0.3246

(Data source: [Kapryan & Boyd 1955])

Figure 9.7-1 Pressure distribution on rectangular flat planing plate - Model 303

9.7.2 Model 301 - $\beta = 20°$

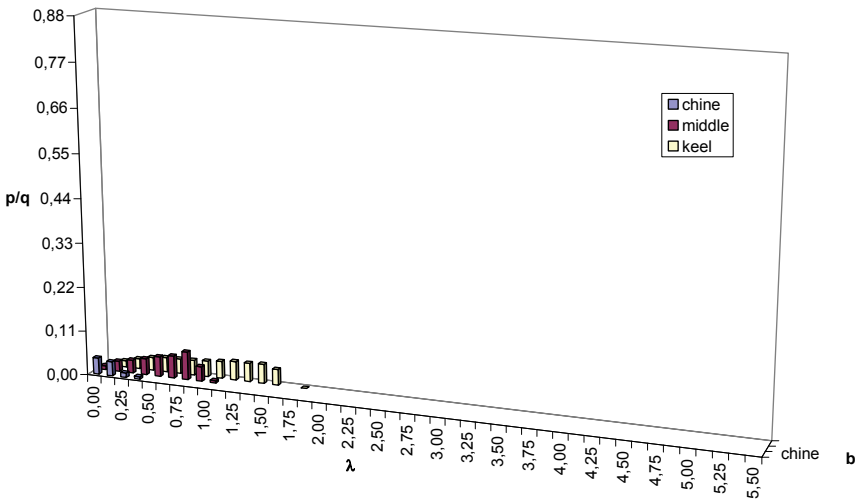

[a] : τ = 4 ° - run 1 - C_Δ = 2.77 - C_V = 12.14 - C_{Lb} = 0.0376

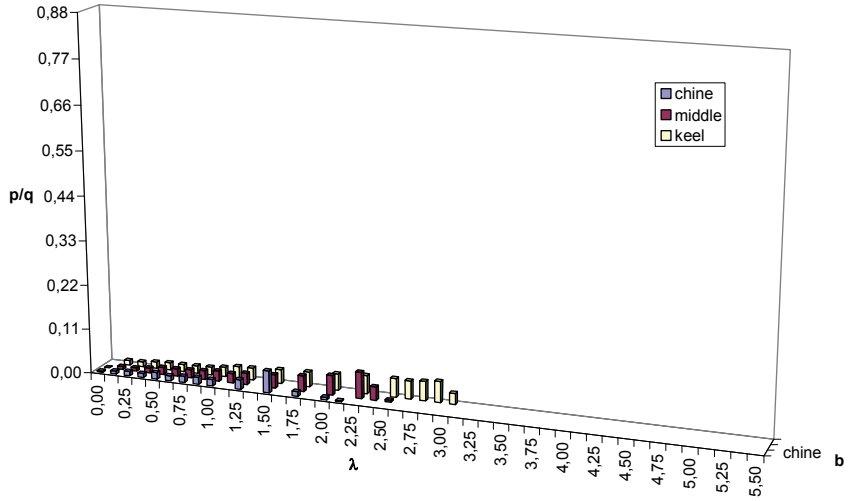

[b] : τ = 4 ° - run 2 - C_Δ = 4.90 - C_V = 12.17 - C_{Lb} = 0.0662

Figure 9.7-2 Pressure distribution on V-bottom planing surfaces - Model 301 (continue)

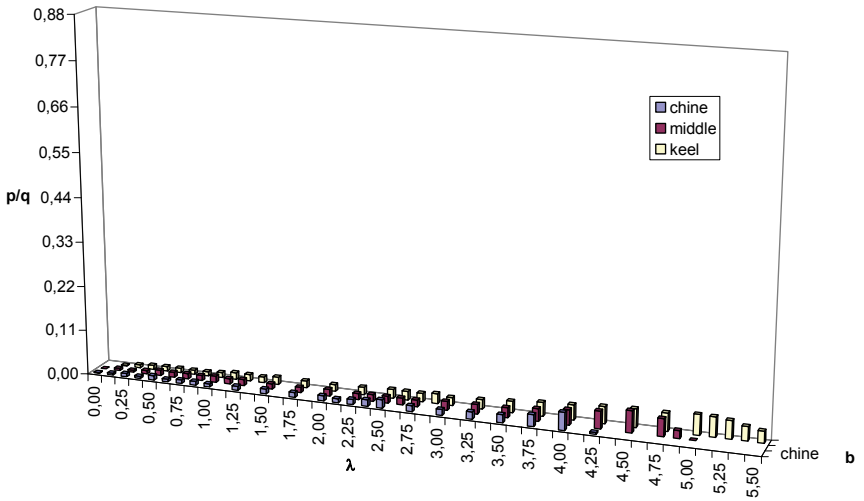

[c] : τ = 4 ° - run 3 - C_Δ = 7.35 - C_V = 12.11 - C_{Lb} = 0.1002

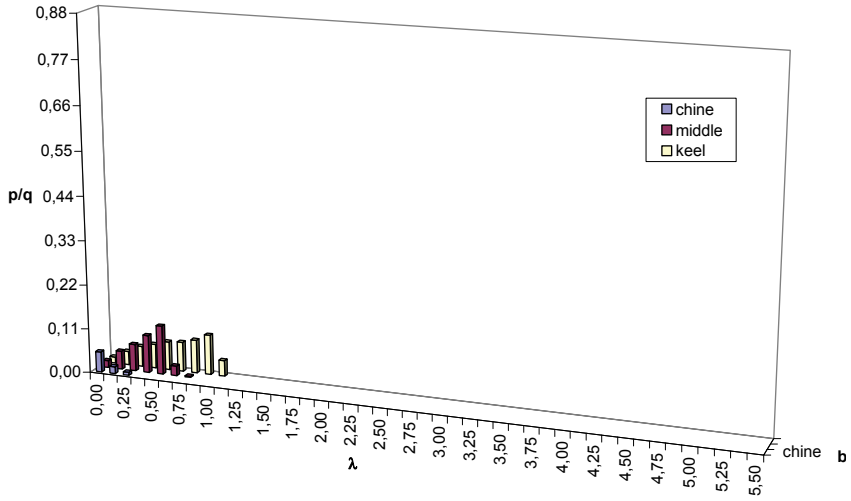

[d] : τ = 6 ° - run 4 - C_Δ = 2.98 - C_V = 12.20 - C_{Lb} = 0.04

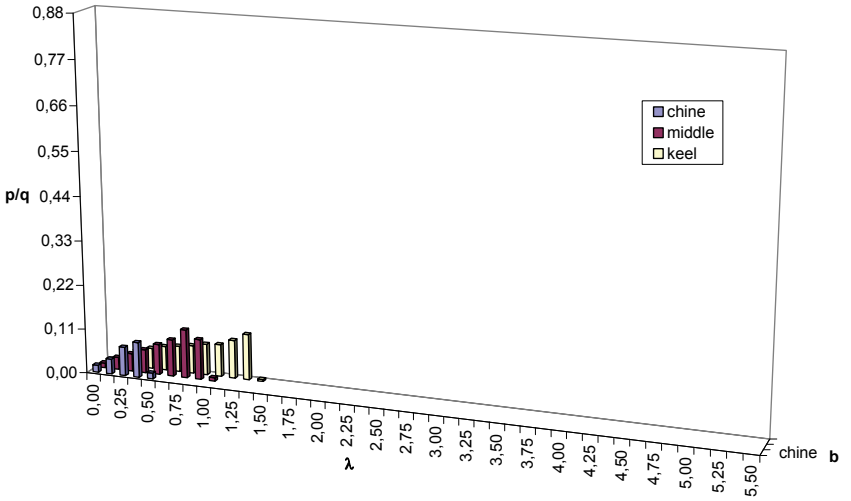

[e] : τ = 6 ° - run 5 - C_Δ = 4.69 - C_V = 12.20 - C_{Lb} = 0.063

Figure 9.7-2 Pressure distribution on V-bottom planing surfaces - Model 301 (continue)

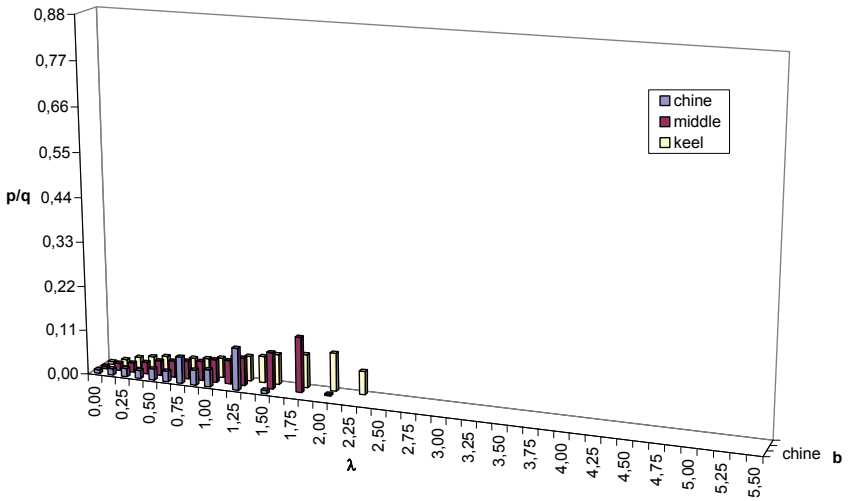

[f] : τ = 6 ° - run 6 - C_Δ = 7.24 - C_V = 12.23 - C_{Lb} = 0.0968

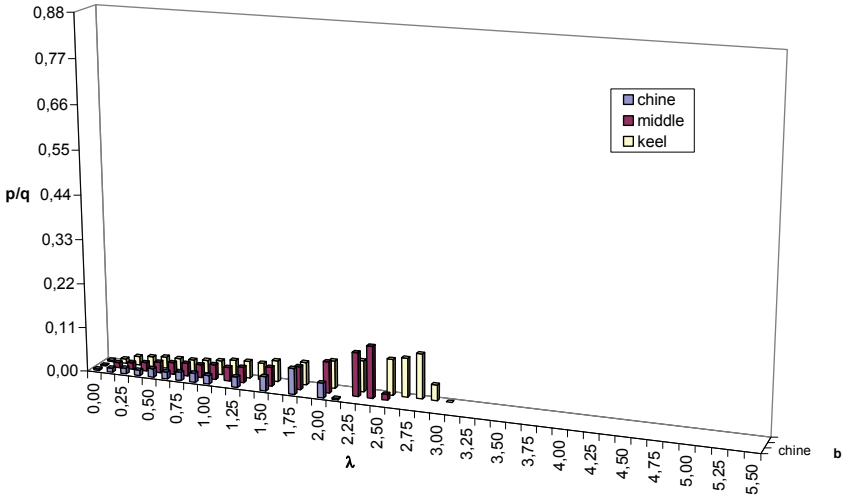

[g] : τ = 6 ° - run 7 - C_Δ = 8.52 - C_V = 12.20 - C_{Lb} = 0.1144

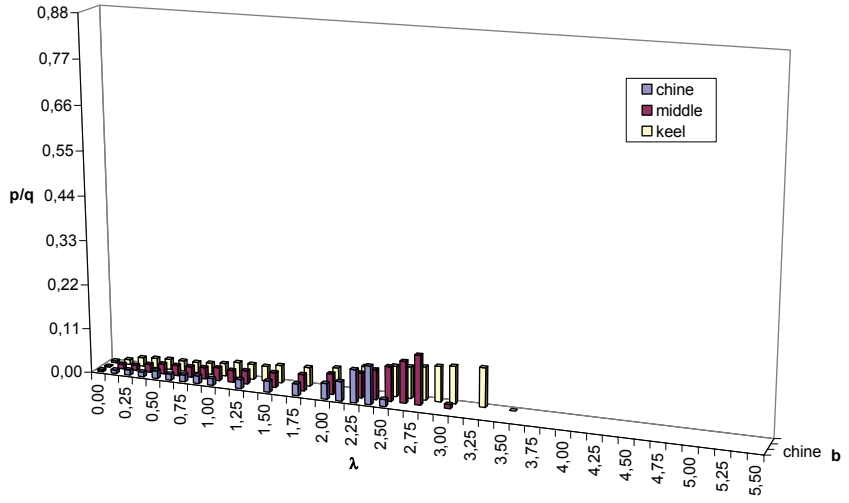

[h] : τ = 6 ° - run 8 - C_Δ = 9.37 - C_V = 12.23 - C_{Lb} = 0.1252

Figure 9.7-2 Pressure distribution on V-bottom planing surfaces - Model 301 (continue)

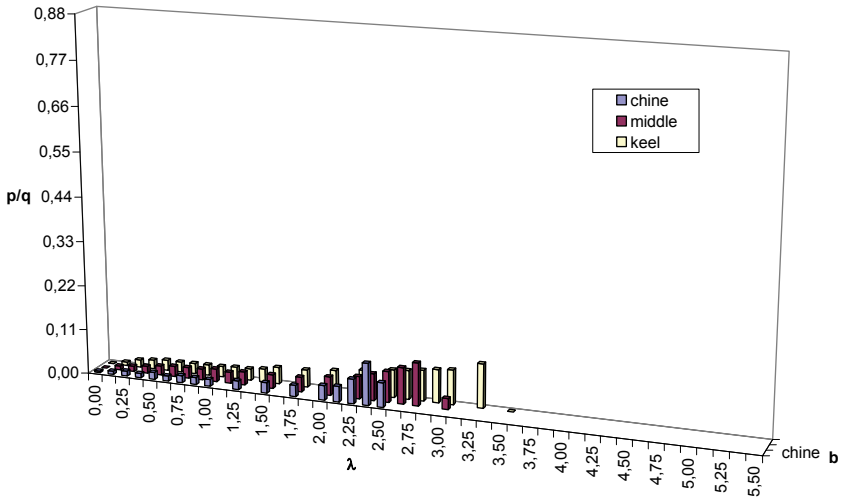

[i] : τ = 6 ° - run 9 - C_Δ = 9.58 - C_V = 12.20 - C_{Lb} = 0.1288

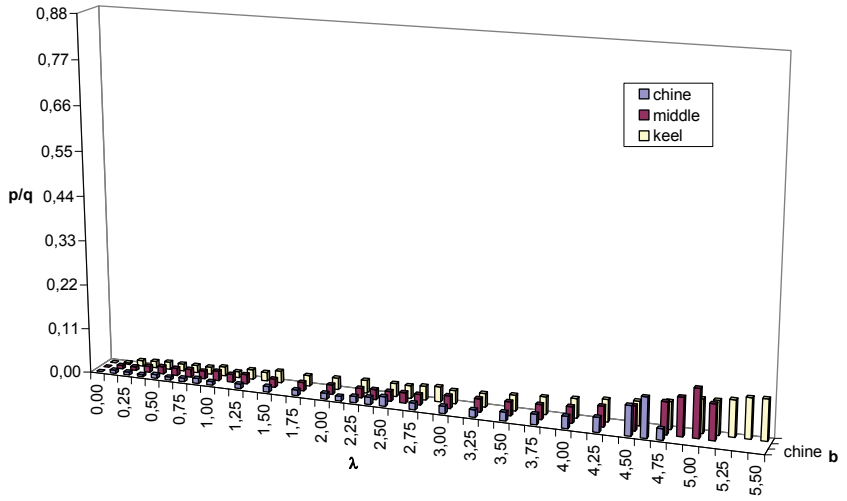

[j] : τ = 6 ° - run 10 - C_Δ = 13.42 - C_V = 12.20 - C_{Lb} = 0.1804

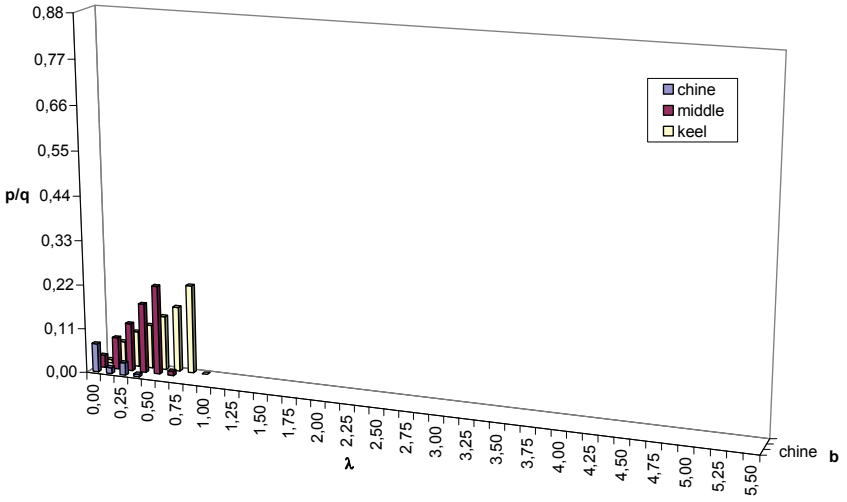

[k] : τ = 9 ° - run 11 - C_Δ = 5.11 - C_V = 12.20 - C_{Lb} = 0.0686

Figure 9.7-2 Pressure distribution on V-bottom planing surfaces - Model 301 (continue)

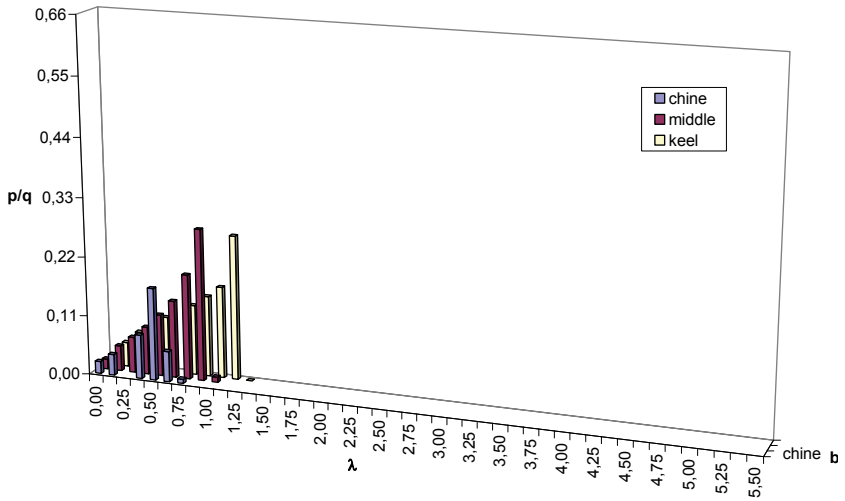

[l] : τ = 9 ° - run 12 - C_Δ = 7.88 - C_V = 12.20 - C_{Lb} = 0.1058

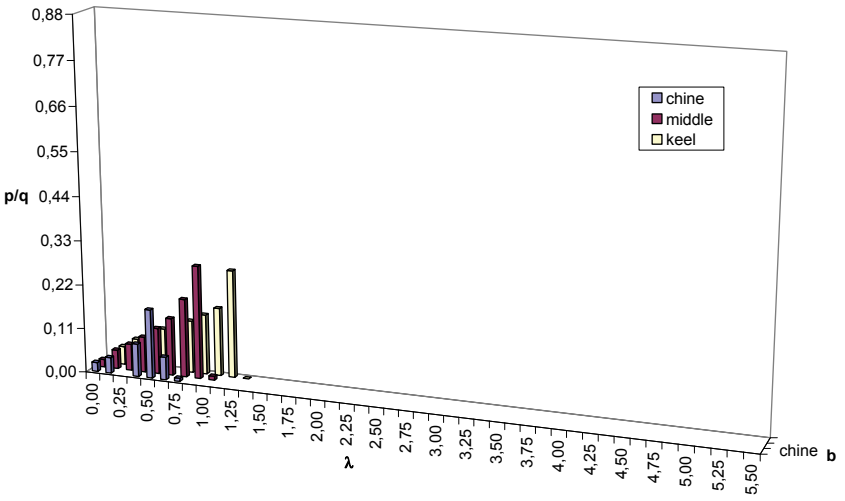

[m] : τ = 9 ° - run 13 - C_Δ = 14.78 - C_V = 12.23 - C_{Lb} = 0.1976

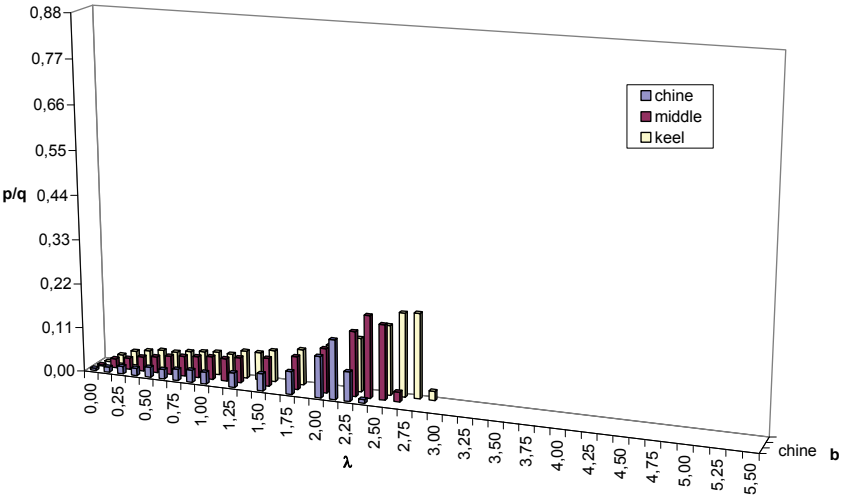

[n] : τ = 9 ° - run 14 - C_Δ = 23.13 - C_V = 12.20 - C_{Lb} = 0.3108

Figure 9.7-2 Pressure distribution on V-bottom planing surfaces - Model 301 (continue)

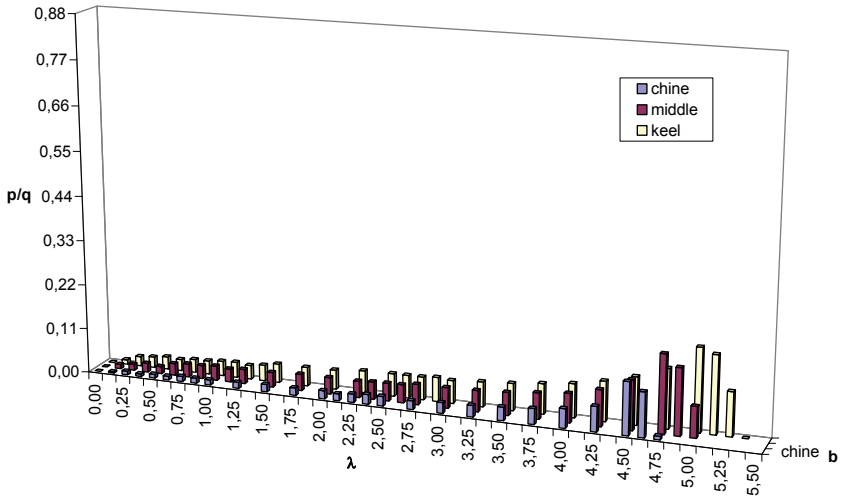

[o] : τ = 12 ° - run 15 - C_Δ = 7.24 - C_V = 12.17 - C_{Lb} = 0.0978

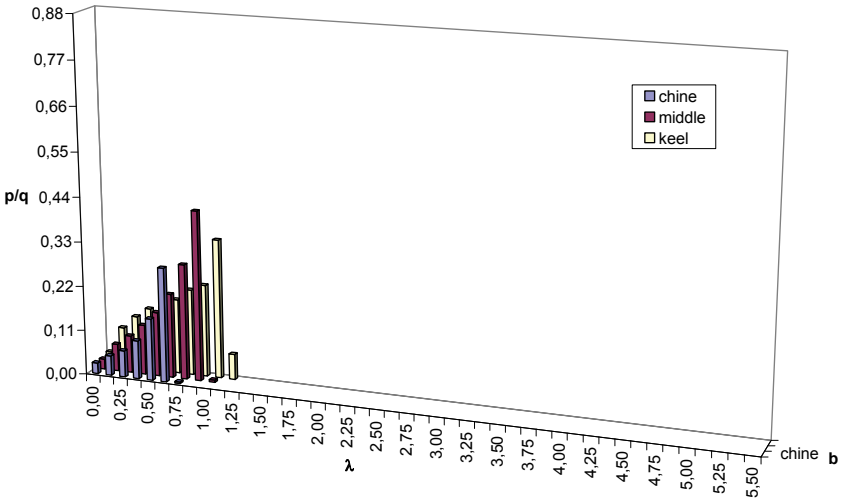

[p] : τ = 12 ° - run 16 - C_Δ = 11.50 - C_V = 12.20 - C_{Lb} = 0.1546

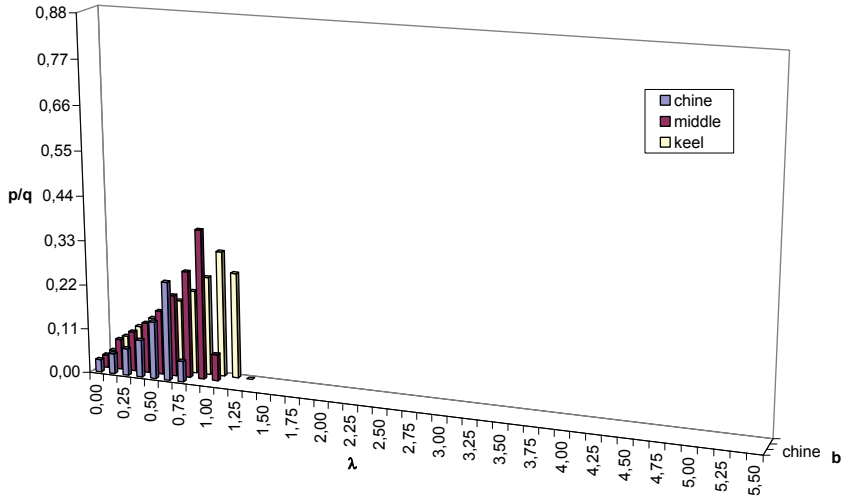

[q] : τ = 12 ° - run 17 - C_Δ = 18.02 - C_V = 15.25 - C_{Lb} = 0.1550

Figure 9.7-2 Pressure distribution on V-bottom planing surfaces - Model 301 (continue)

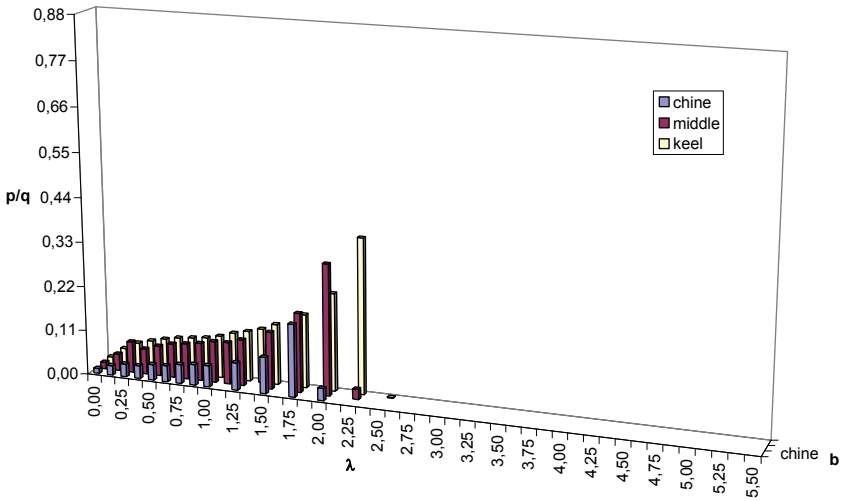

[r] : τ = 12 ° - run 18 - C_Δ = 21.17 - C_V = 12.20 - C_{Lb} = 0.2844

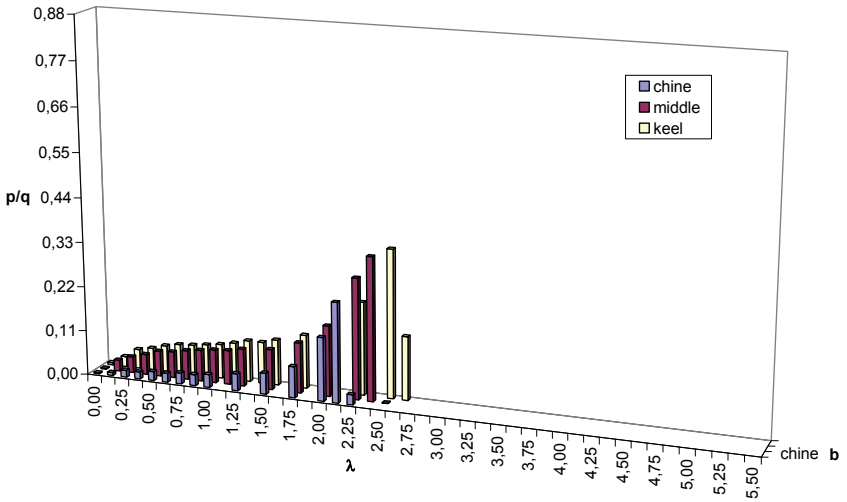

[s] : τ = 12 ° - run 19 - C_Δ = 11.84 - C_V = 9.15 - C_{Lb} = 0.2828

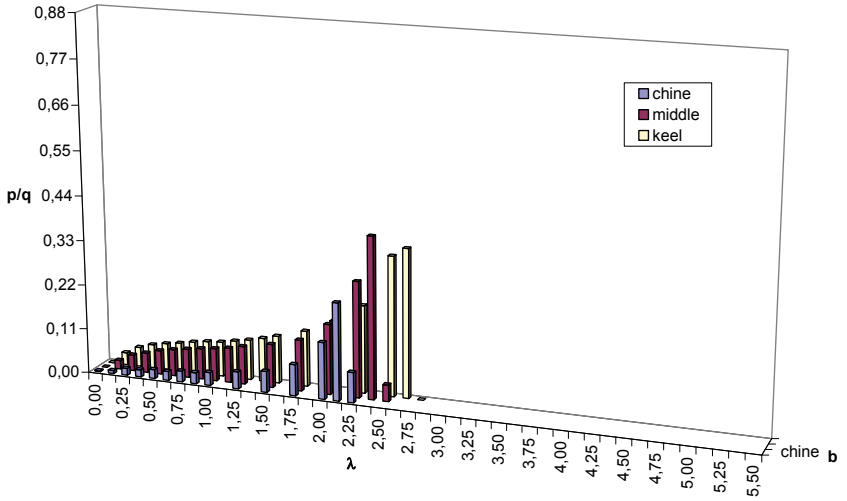

[t] : τ = 12 ° - run 20 - C_Δ = 8.52 - C_V = 7.72 - C_{Lb} = 0.2860

Figure 9.7-2 Pressure distribution on V-bottom planing surfaces - Model 301 (continue)

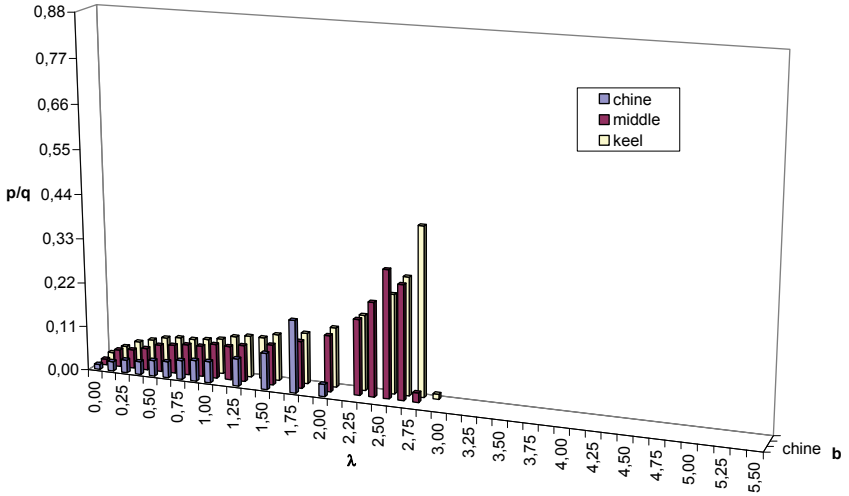

[u] : τ = 12 ° - run 21 - C_Δ = 33.01 - C_V = 15.19 - C_{Lb} = 0.2862

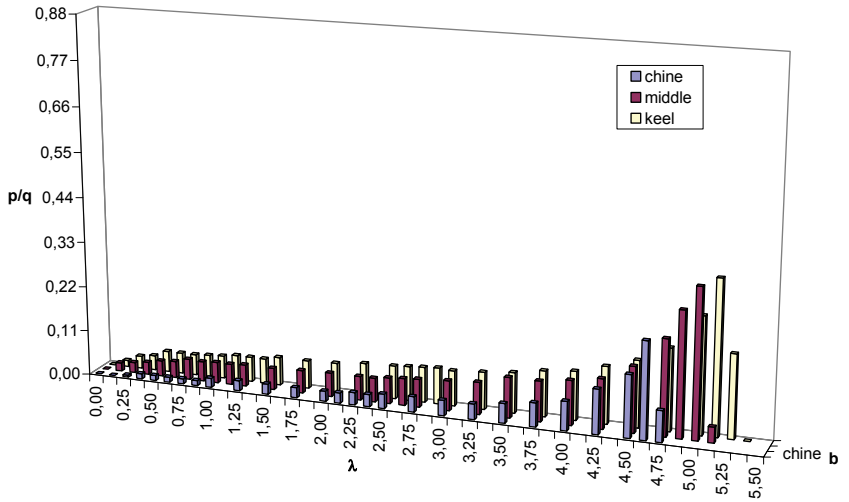

[v] : τ = 12 ° - run 22 - C_Δ = 19.04 - C_V = 9.09 - C_{Lb} = 0.4608

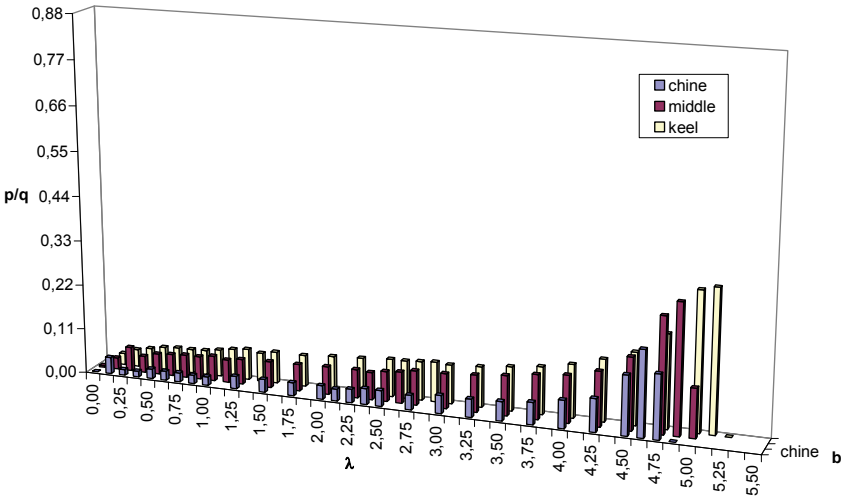

[w] : τ = 12 ° - run 23 - C_Δ = 33.87 - C_V = 12.20 - C_{Lb} = 0.4552

Figure 9.7-2 Pressure distribution on V-bottom planing surfaces - Model 301 (continue)

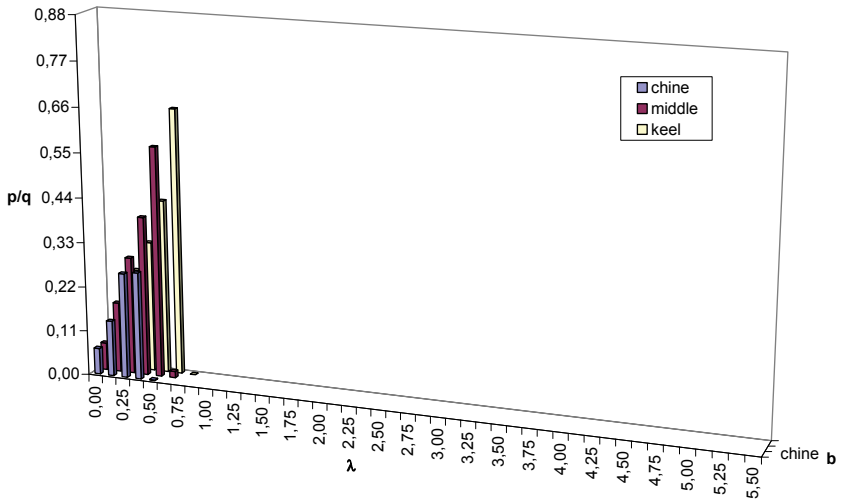

[x] : τ = 18 ° - run 24 - C_Δ = 11.50 - C_V = 12.17 - C_{Lb} = 0.1552

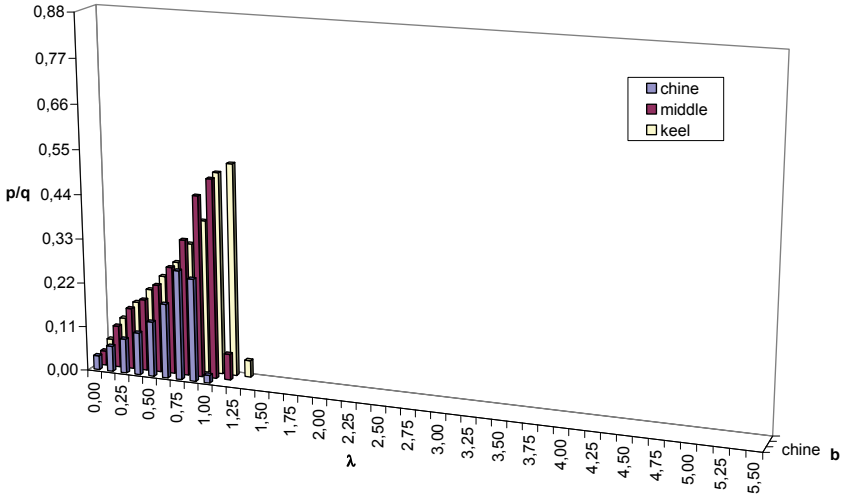

[y] : τ = 18 ° - run 25 - C_Δ = 18.62 - C_V = 12.26 - C_{Lb} = 0.2478

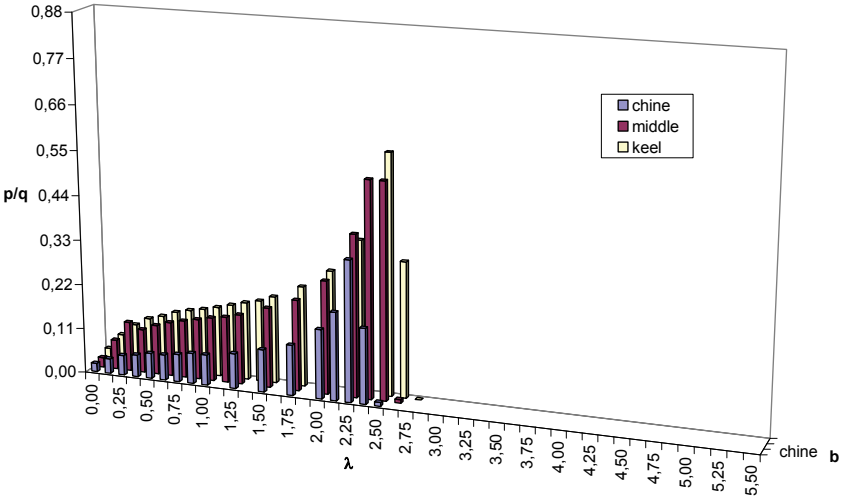

[z] : τ = 18 ° - run 26 - C_Δ = 34.93 - C_V = 12.20 - C_{Lb} = 0.4694

Figure 9.7-2 Pressure distribution on V-bottom planing surfaces - Model 301 (continue)

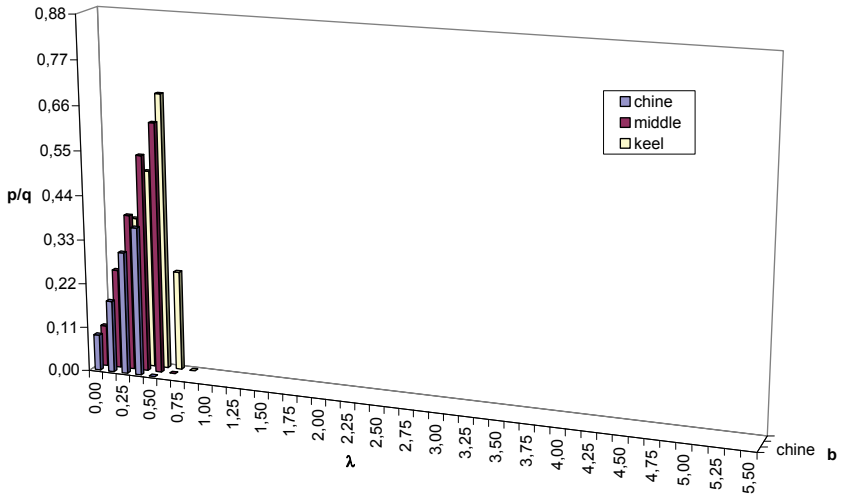

[aa] : τ = 24 ° - run 27 - C_Δ = 14.37 - C_V = 12.20 - C_{Lb} = 0.1918

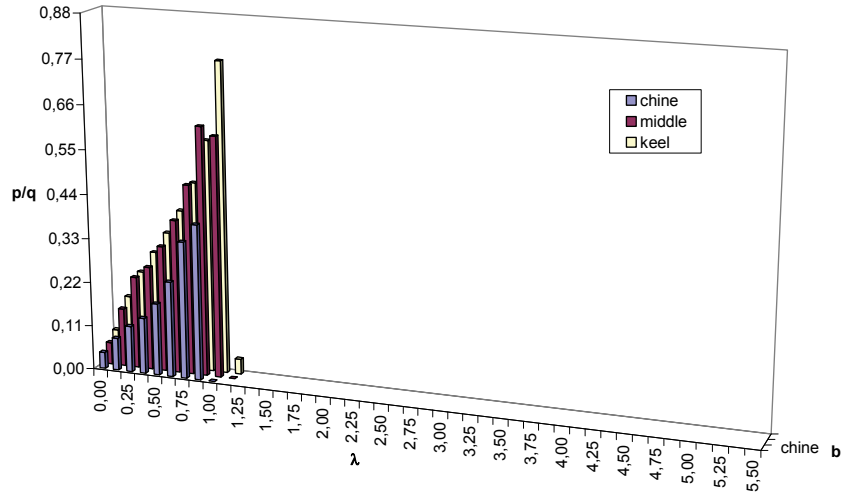

[ab] : τ = 24 ° - run 28 - C_Δ = 24.07 - C_V = 12.20 - C_{Lb} = 0.3234

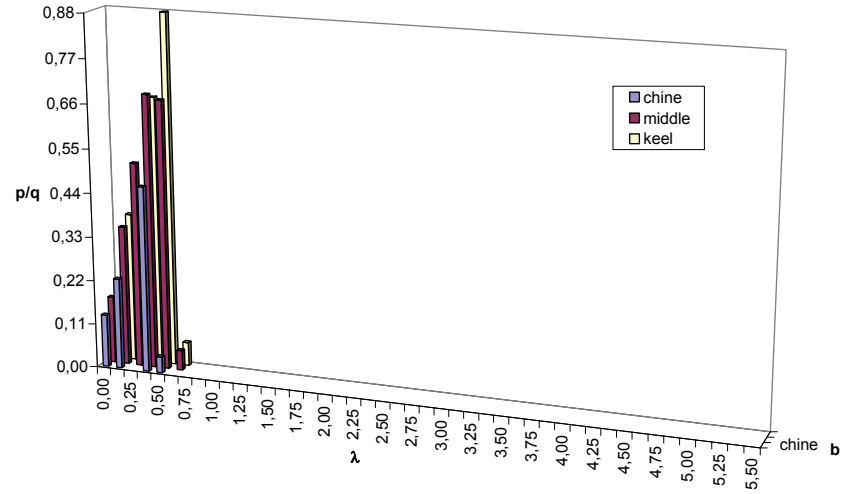

[ac] : τ = 30 ° - run 29 - C_Δ = 16.40 - C_V = 12.17 - C_{Lb} = 0.2214

Figure 9.7-2 Pressure distribution on V-bottom planing surfaces - Model 301 (continue)

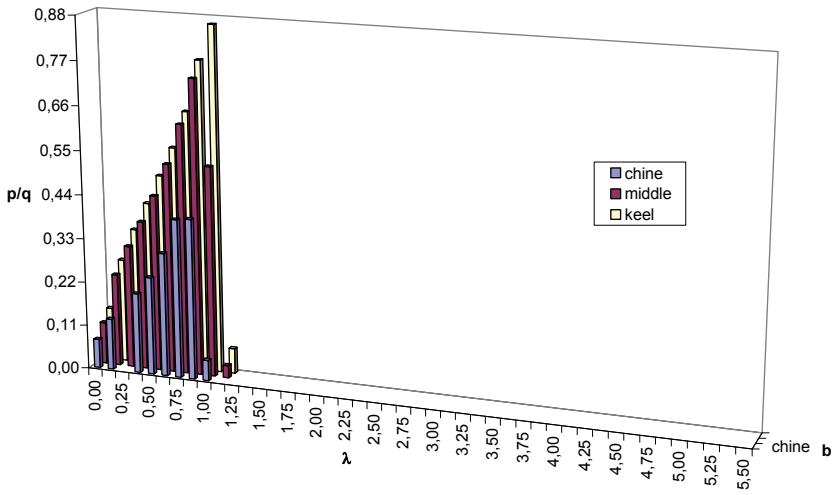

[ad] : τ = 30 ° - run 30 - C_Δ = 28.33 - C_V = 12.20 - C_{Lb} = 0.3806

(Data source: [Kapryan & Boyd 1955])

Figure 9.7-2 Pressure distribution on V-bottom planing surfaces - Model 301

9.7.3 Model 301-A - $\beta = 20°$ with Horizontal Chine Flared

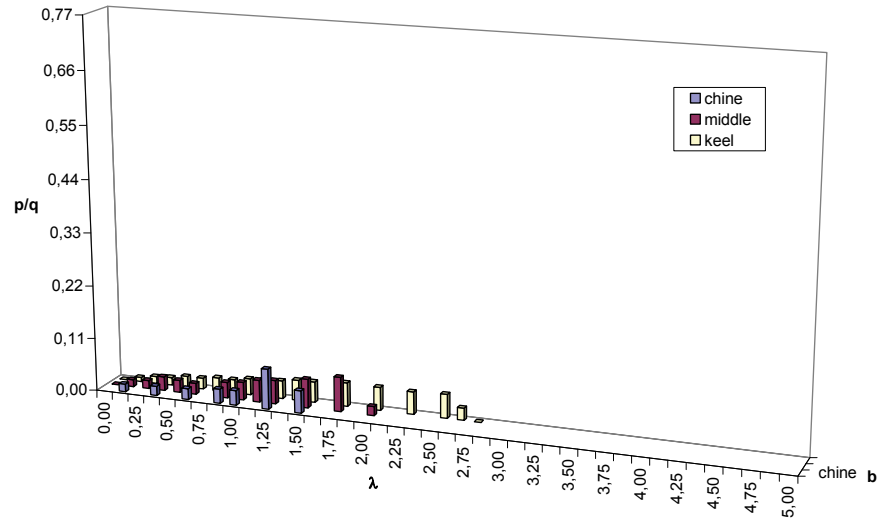

[a] : τ = 4 ° - run 1 - C_Δ = 5.45 - C_V = 12.14 - C_{Lb} = 0.0740

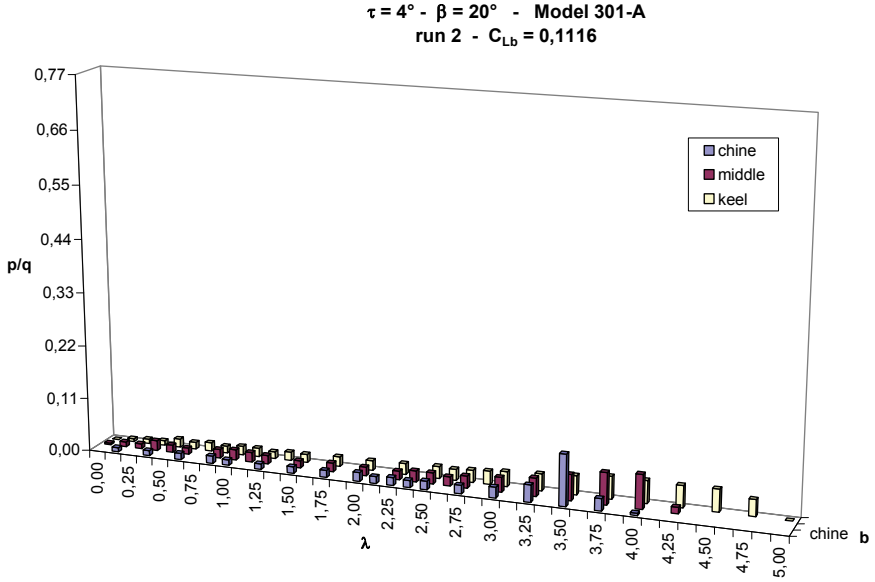

[b] : τ = 4 ° - run 2 - C_Δ = 8.39 - C_V = 12.26 - C_{Lb} = 0.1116

Figure 9.7-3 Pressure distribution on V-bottom planing surfaces - Model 301-A (continue)

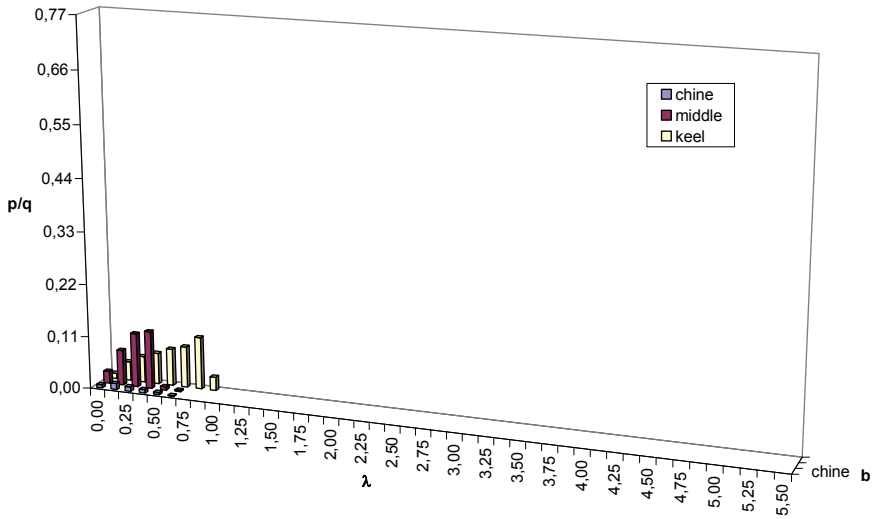

[c] : τ = 6 ° - run 3 - C_Δ = 3.11 - C_V = 12.20 - C_{Lb} = 0.0418

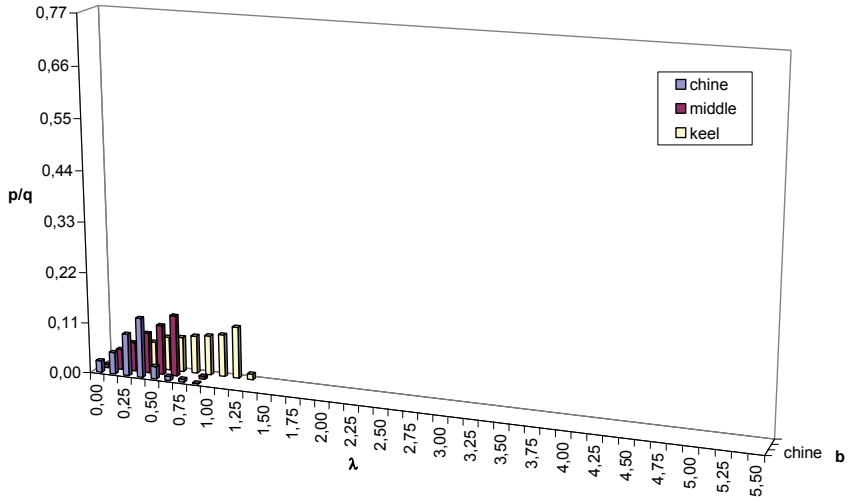

[d] : τ = 6 ° - run 4 - C_Δ = 5.28 - C_V = 12.23 - C_{Lb} = 0.0706

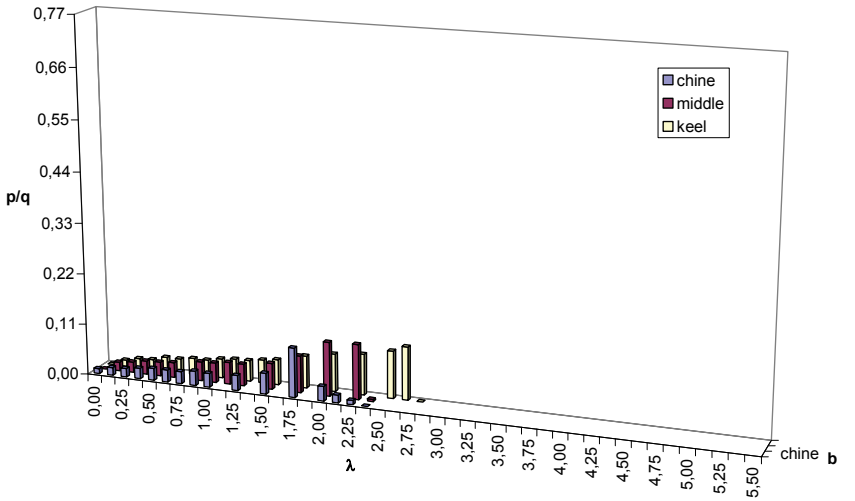

[e] : τ = 6 ° - run 5 - C_Δ = 9.50 - C_V = 12.11 - C_{Lb} = 0.1296

Figure 9.7-3 Pressure distribution on V-bottom planing surfaces - Model 301-A (continue)

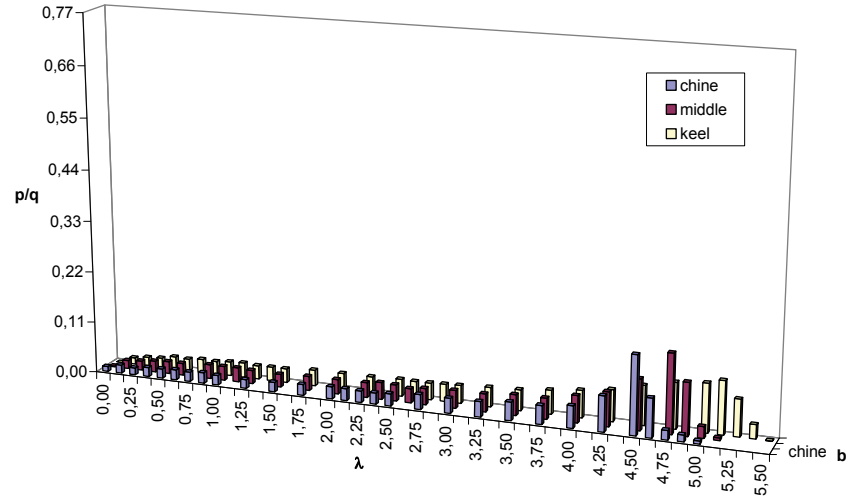

[f] : τ = 6 ° - run 6 - C_Δ = 14.61 - C_V = 12.20 - C_{Lb} = 0.1964

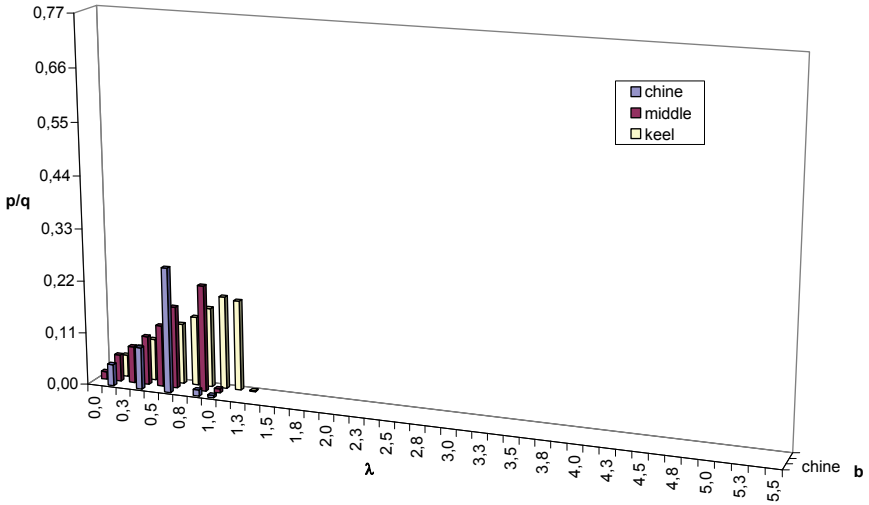

[g] : τ = 9 ° - run 7 - C_Δ = 9.54 - C_V = 12.23 - C_{Lb} = 0.1276

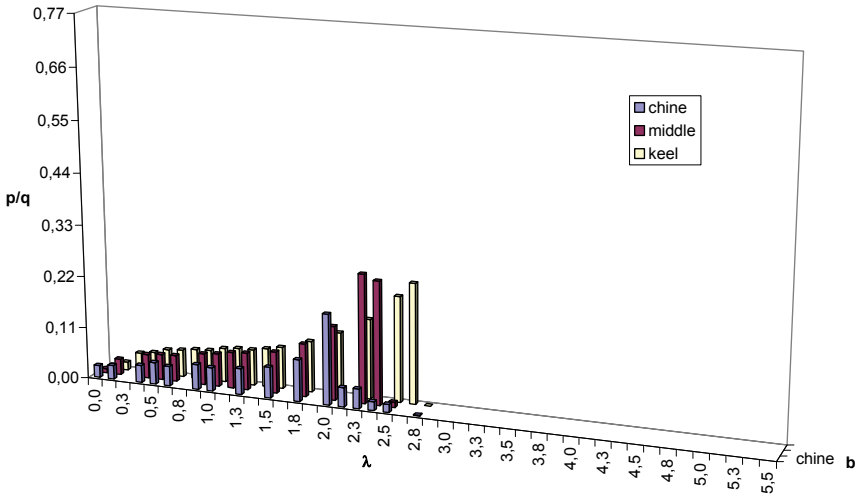

[h] : τ = 9 ° - run 8 - C_Δ = 16.36 - C_V = 12.23 - C_{Lb} = 0.2188

Figure 9.7-3 Pressure distribution on V-bottom planing surfaces - Model 301-A (continue)

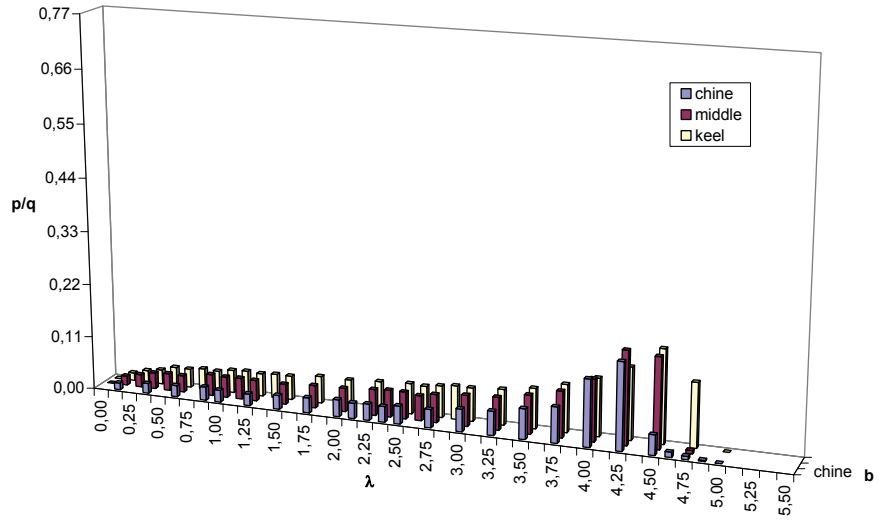

[i] : τ = 9 ° - run 9 - C_Δ = 25.65 - C_V = 12.20 - C_{Lb} = 0.3446

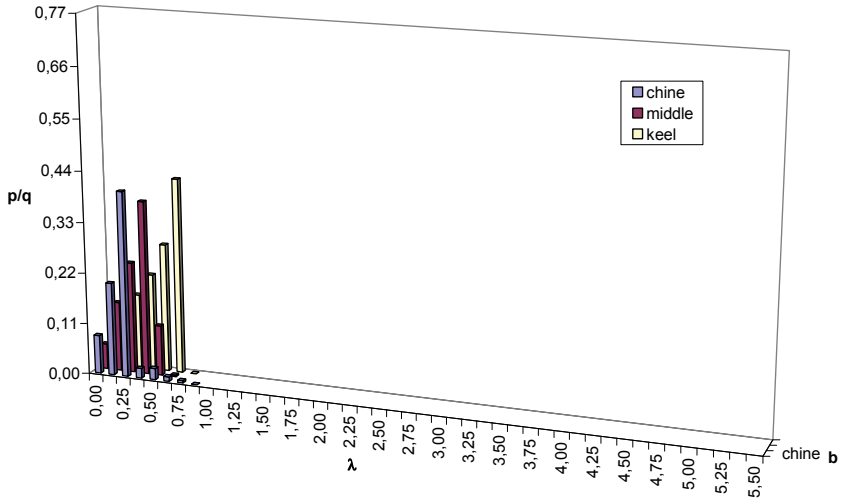

[j] : τ = 12 ° - run 10 - C_Δ = 8.31 - C_V = 12.23 - C_{Lb} = 0.1112

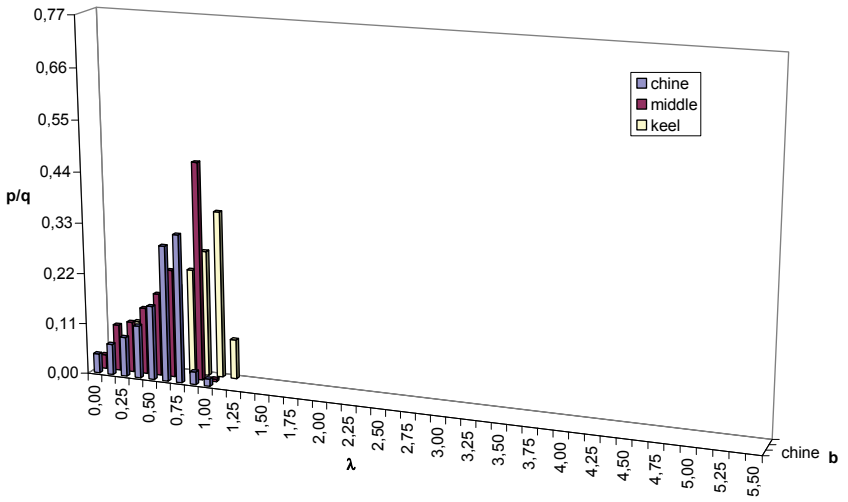

[k] : τ = 12 ° - run 11 - C_Δ = 13.63 - C_V = 12.20 - C_{Lb} = 0.1832

Figure 9.7-3 Pressure distribution on V-bottom planing surfaces - Model 301-A (continue)

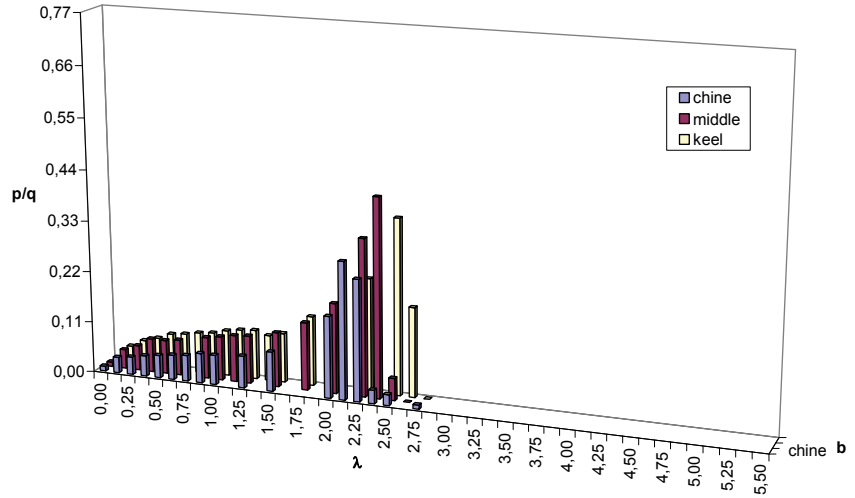

[l] : τ = 12 ° - run 12 - C_Δ = 23.73 - C_V = 12.17 - C_{Lb} = 0.3204

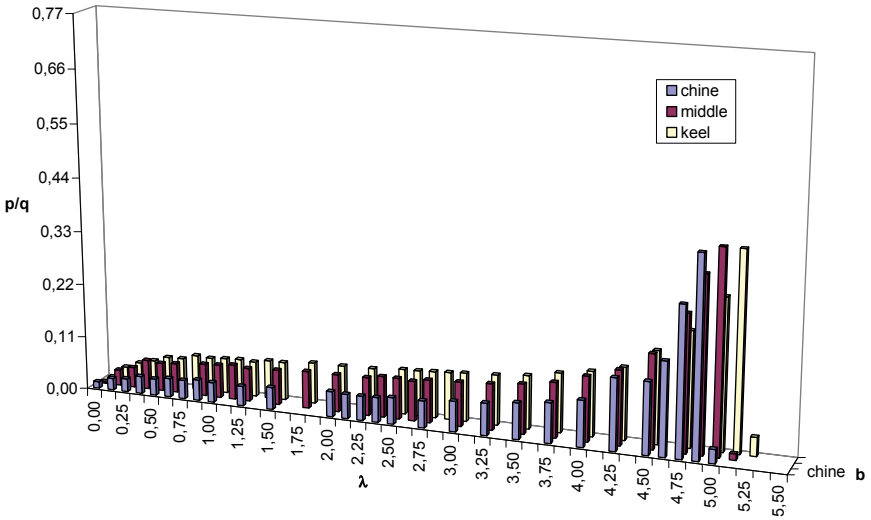

[m] : τ = 12 ° - run 13 - C_Δ = 38.13 - C_V = 12.20 - C_{Lb} = 0.5124

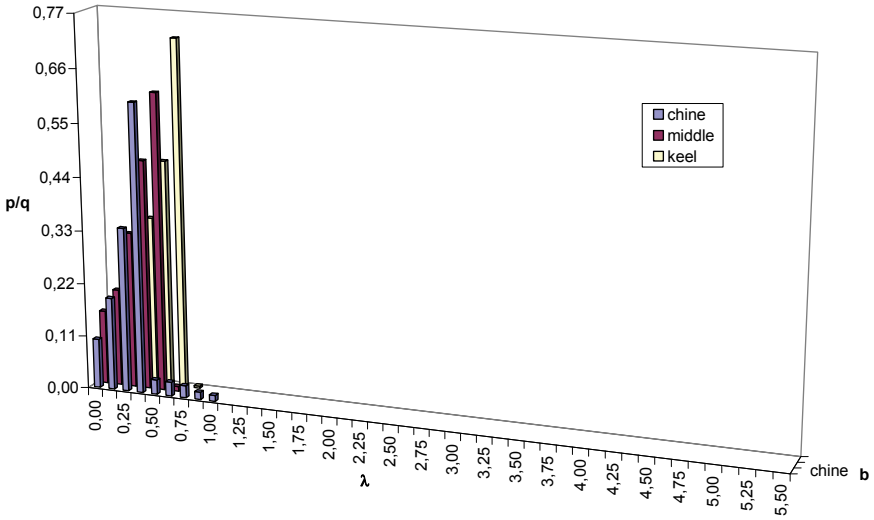

[o] : τ = 18 ° - run 14 - C_Δ = 13.12 - C_V = 12.17 - C_{Lb} = 0.1772

Figure 9.7-3 Pressure distribution on V-bottom planing surfaces - Model 301-A (continue)

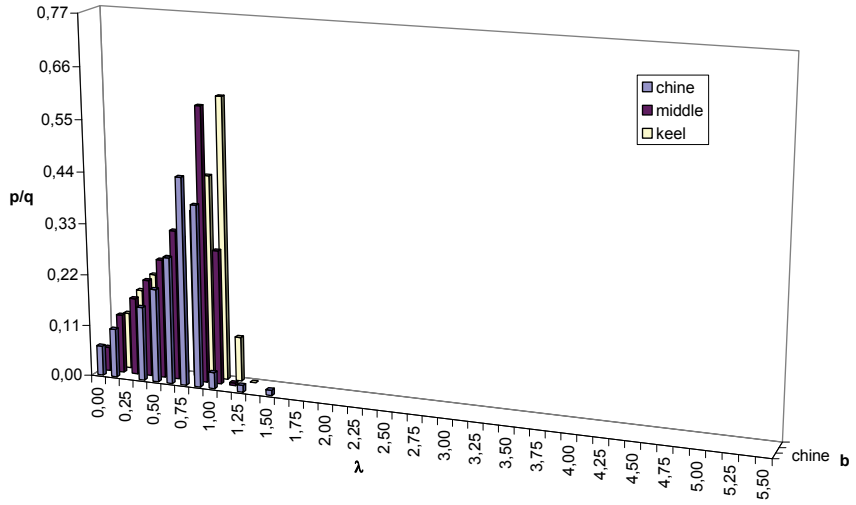

[p] : τ = 18 ° - run 15 - C_Δ = 20.96 - C_V = 12.20 - C_{Lb} = 0.2816

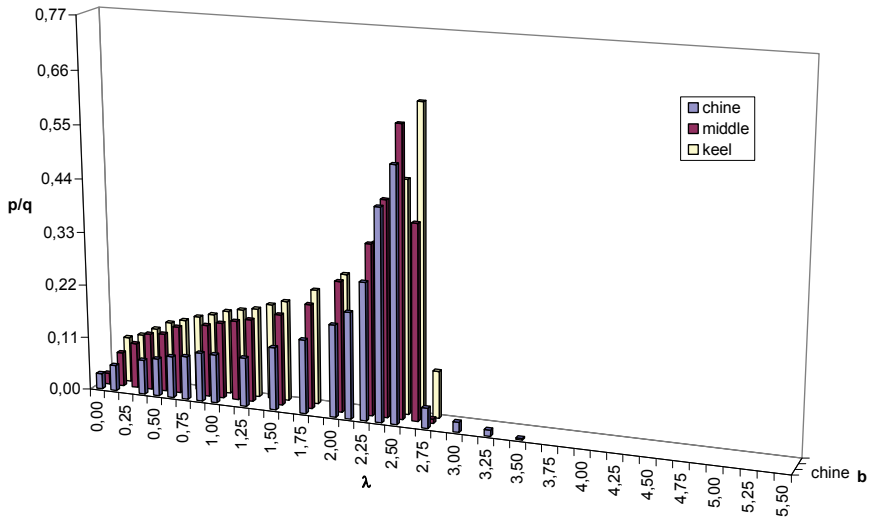

[q] : τ = 18 ° - run 16 - C_Δ = 40.13 - C_V = 12.20 - C_{Lb} = 0.5392

(Data source: [Kapryan & Boyd 1955])

Figure 9.7-3 Pressure distribution on V-bottom planing surfaces - Model 301-A

9.7.4 Model 302 - $\beta = 40°$

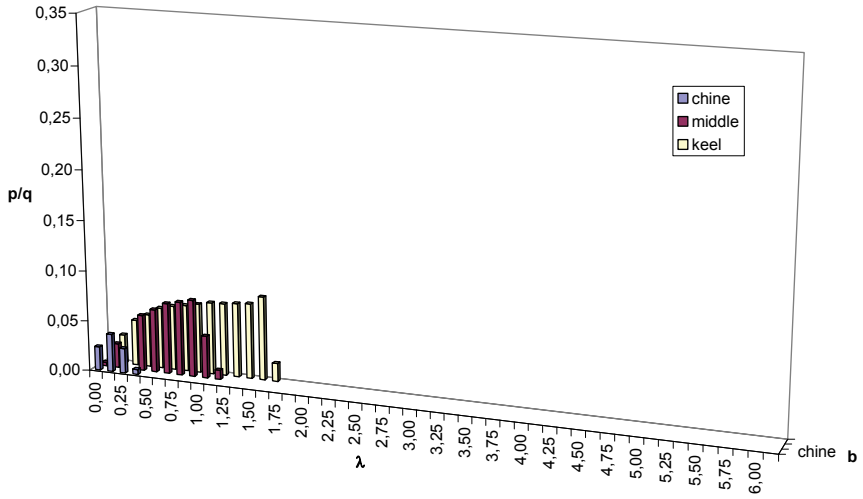

[a] : τ = 9 ° - run 1 - C_Δ = 4.26 - C_V = 12.29 - C_{Lb} = 0.0564

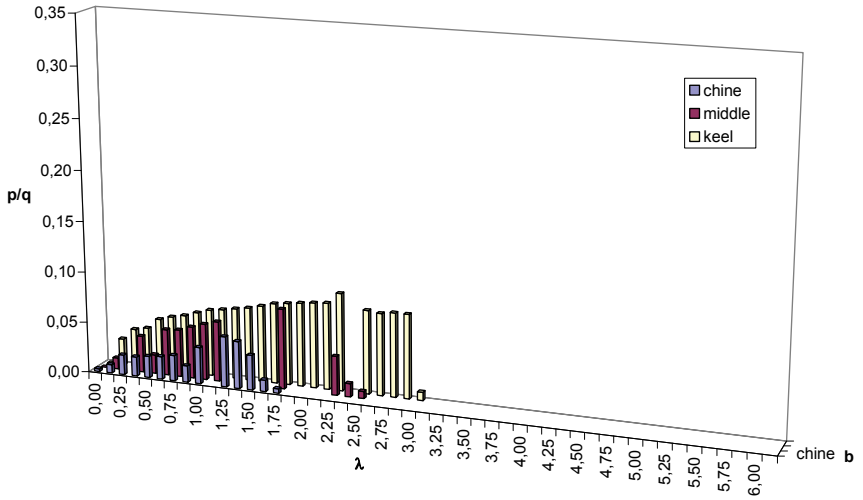

[b] : τ = 9 ° - run 2 - C_Δ = 8.31 - C_V = 12.26 - C_{Lb} = 0.1106

Figure 9.7-4 Pressure distribution on V-bottom planing surfaces - Model 302 (continue)

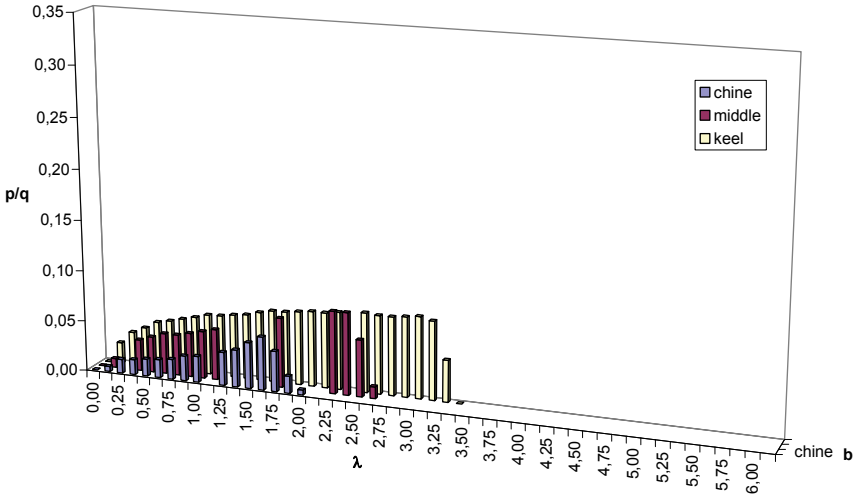

[c] : τ = 9 ° - run 3 - C_Δ = 9.16 - C_V = 12.26 - C_{Lb} = 0.1218

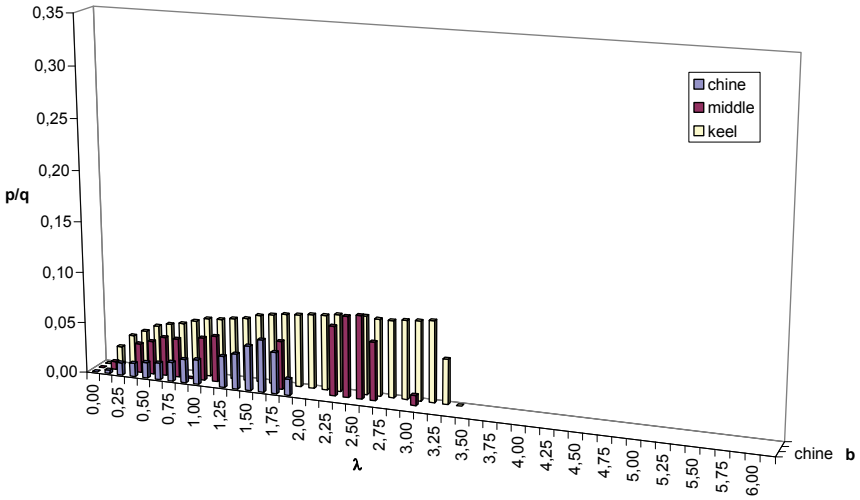

[d] : τ = 9 ° - run 4 - C_Δ = 9.37 - C_V = 12.23 - C_{Lb} = 0.1252

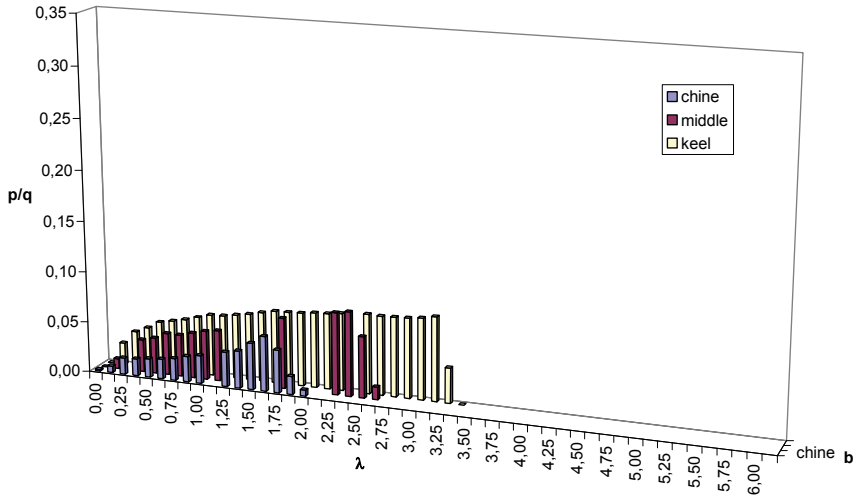

[e] : τ = 9 ° - run 5 - C_Δ = 9.37 - C_V = 12.32 - C_{Lb} = 0.1234

Figure 9.7-4 Pressure distribution on V-bottom planing surfaces - Model 302 (continue)

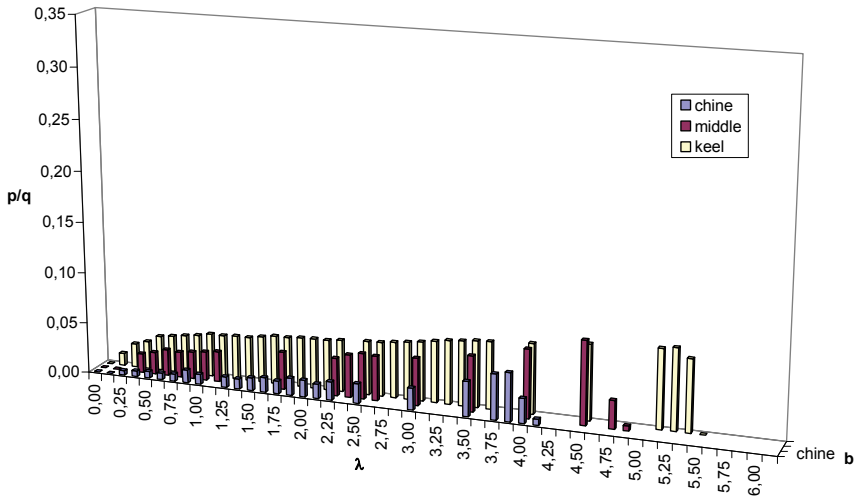

[e] : τ = 9 ° - run 6 - C_Δ = 14.91 - C_V = 12.23 - C_{Lb} = 0.1994

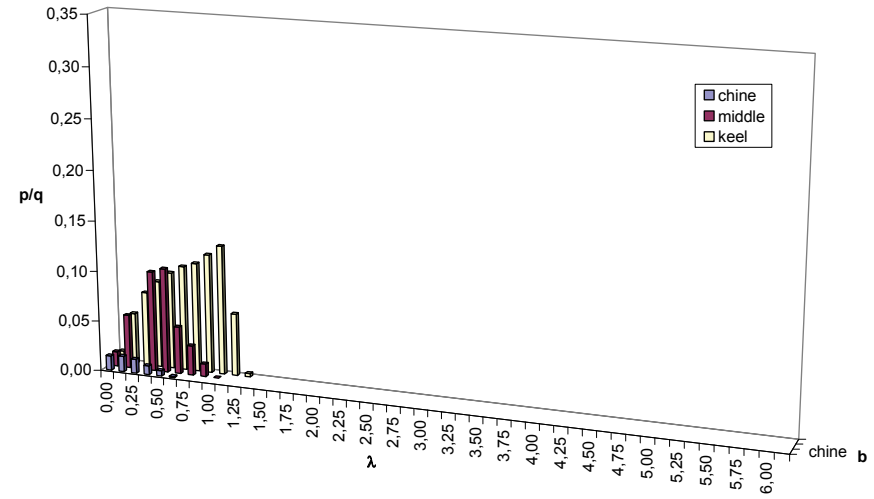

[f] : τ = 12 ° - run 7 - C_Δ = 3.58 - C_V = 12.20 - C_{Lb} = 0.0482

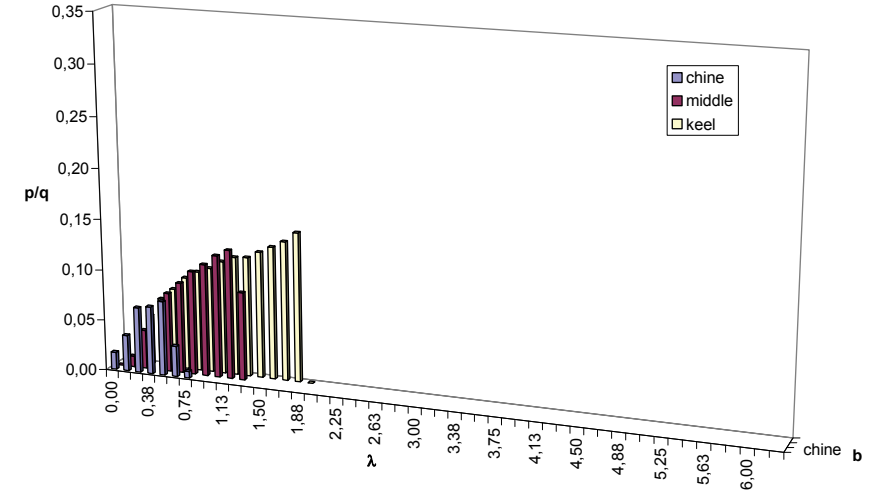

[g] : τ = 12 ° - run 8 - C_Δ = 6.39 - C_V = 12.20 - C_{Lb} = 0.0858

Figure 9.7-4 Pressure distribution on V-bottom planing surfaces - Model 302 (continue)

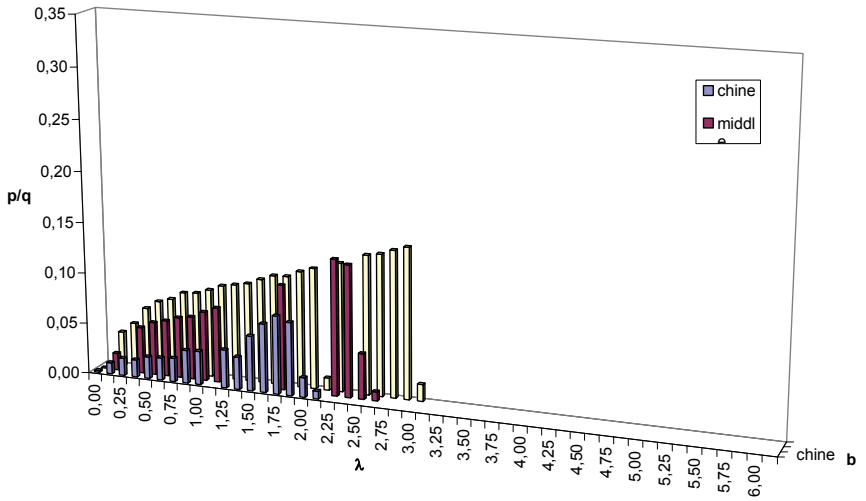

[h] : τ = 12 ° - run 9 - C_Δ = 13.63 - C_V = 12.20 - C_{Lb} = 0.1832

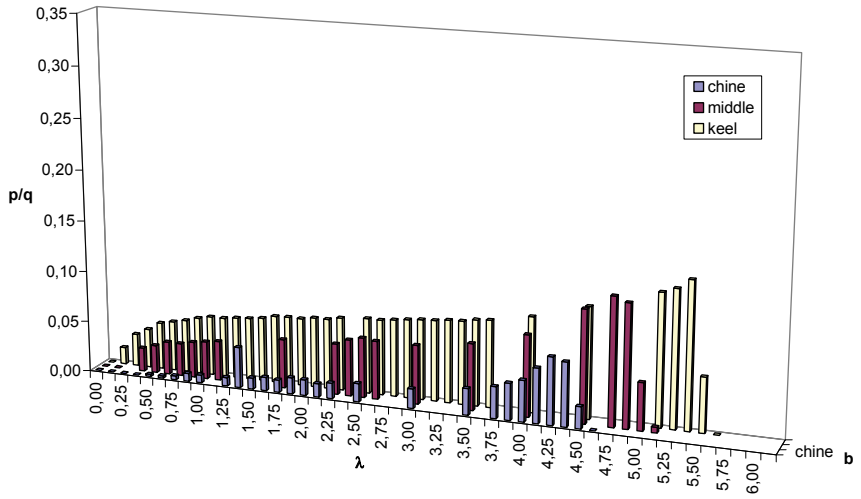

[i] : τ = 12 ° - run 10 - C_Δ = 24.15 - C_V = 12.23 - C_{Lb} = 0.3230

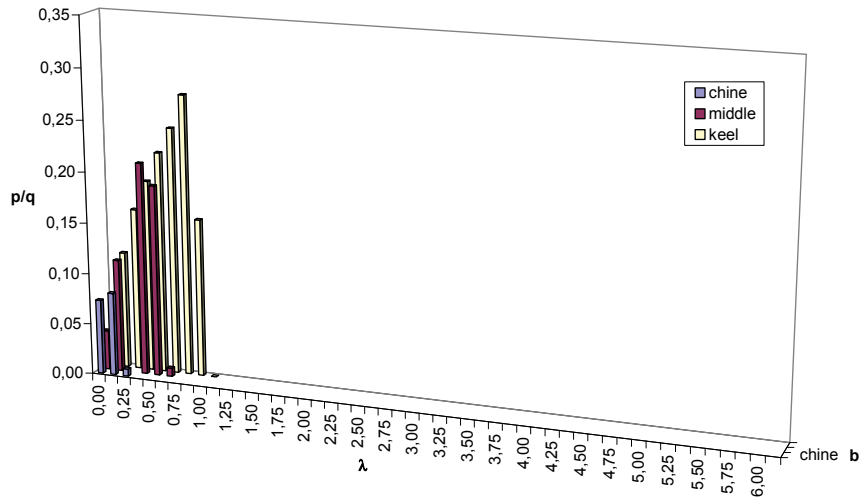

[j] : τ = 18 ° - run 11 - C_Δ = 6.30 - C_V = 12.20 - C_{Lb} = 0.0846

Figure 9.7-4 Pressure distribution on V-bottom planing surfaces - Model 302 (continue)

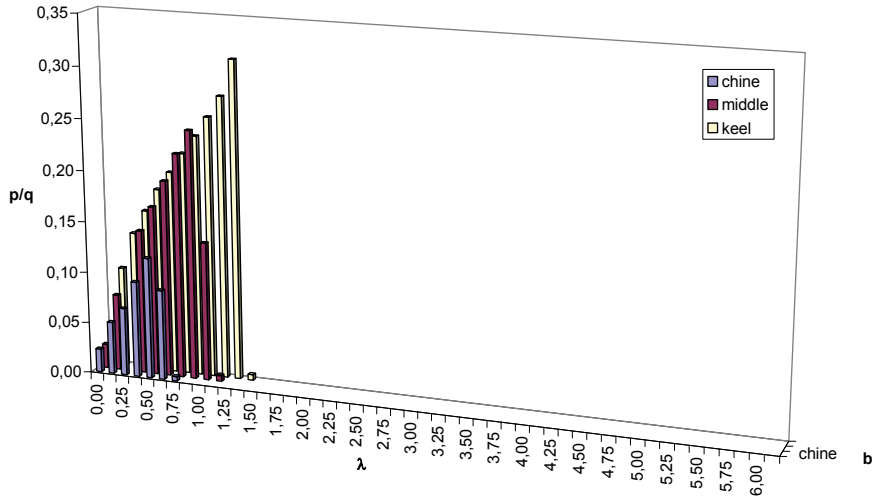

[k] : τ = 18 ° - run 12 - C_Δ = 11.16 - C_V = 12.20 - C_{Lb} = 0.1500

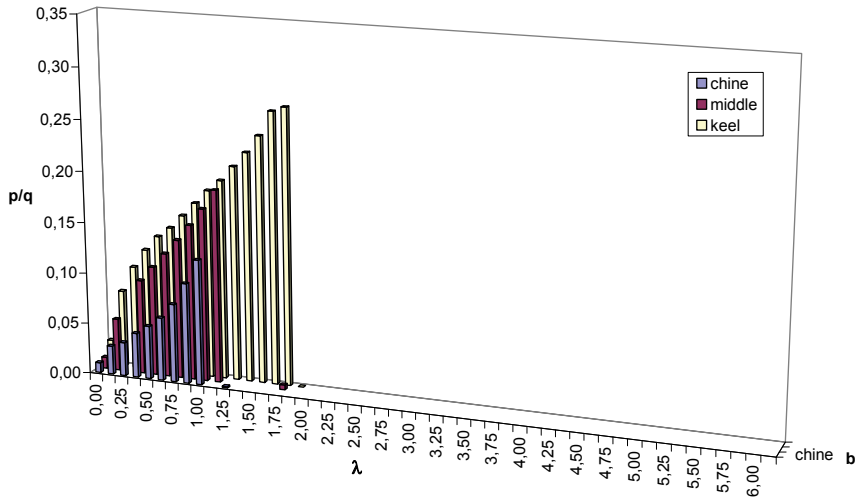

[l] : τ = 18 ° - run 13 - C_Δ = 15.42 - C_V = 12.99 - C_{Lb} = 0.1828

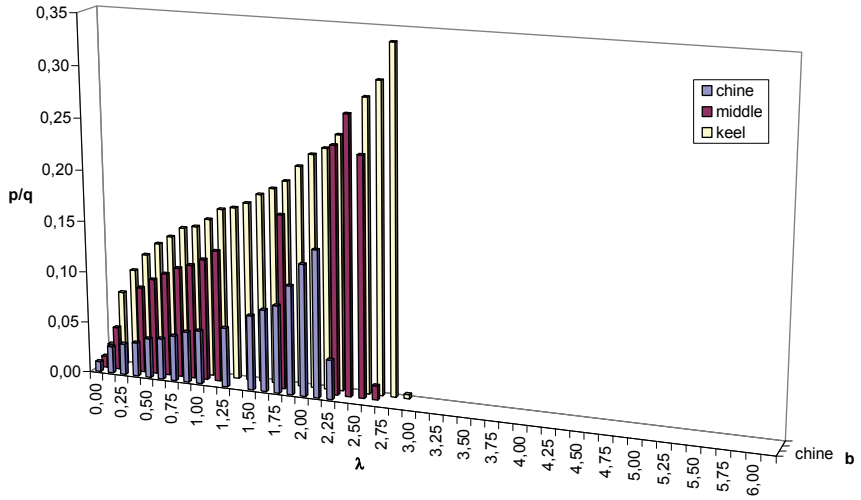

[m] : τ = 18 ° - run 14 - C_Δ = 23.94 - C_V = 12.00 - C_{Lb} = 0.3216

(Data source: [Kapryan & Boyd 1955])

Figure 9.7-4 Pressure distribution on V-bottom planing surfaces - Model 302

9.7.5 Model 302-A - $\beta = 40°$ with Horizontal Chine Flared

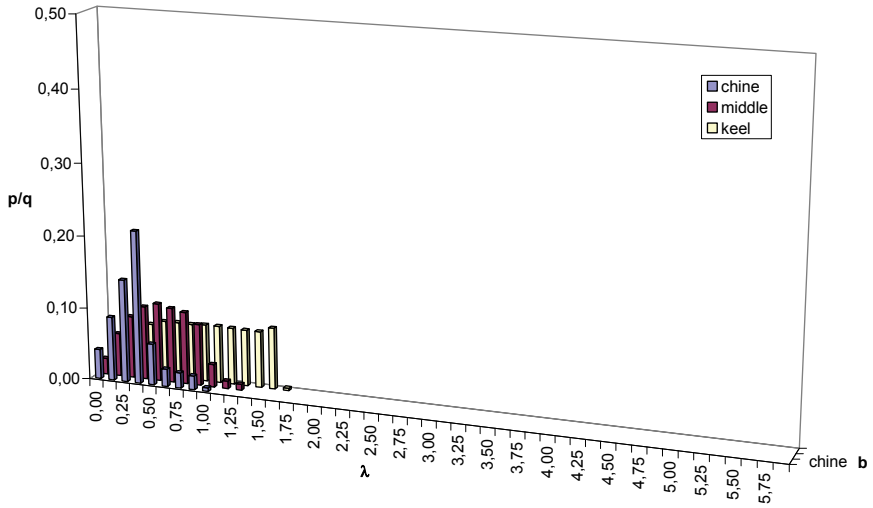

[a] : τ = 9 ° - run 1 - C_Δ = 6.71 - C_V = 12.00 - C_{Lb} = 0.0902

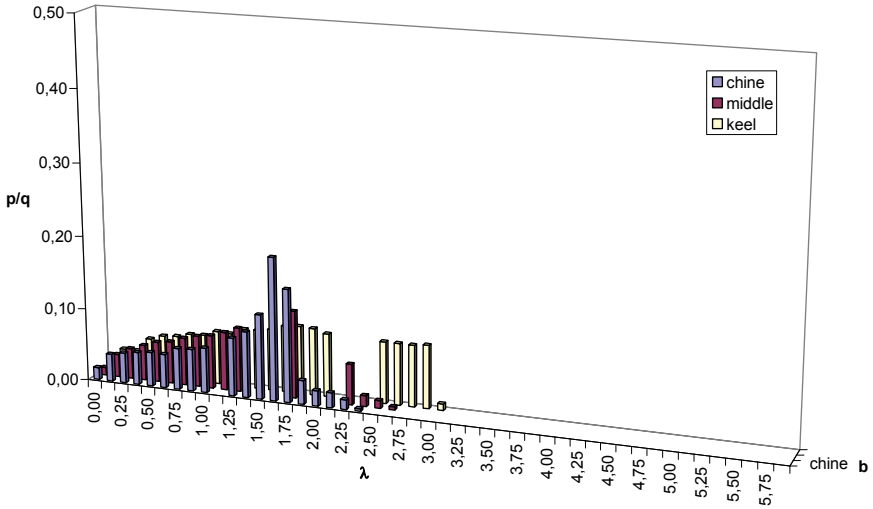

[b] : τ = 9 ° - run 2 - C_Δ = 12.78 - C_V = 12.17 - C_{Lb} = 0.1726

Figure 9.7-5 Pressure distribution on V-bottom planing surfaces - Model 302-A (continue)

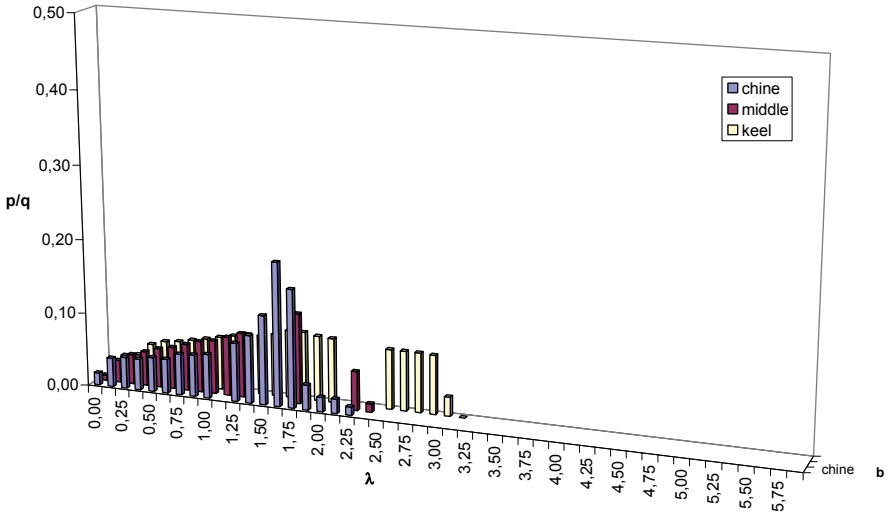

[c] : τ = 9 ° - run 3 - C_Δ = 12.78 - C_V = 12.23 - C_{Lb} = 0.1708

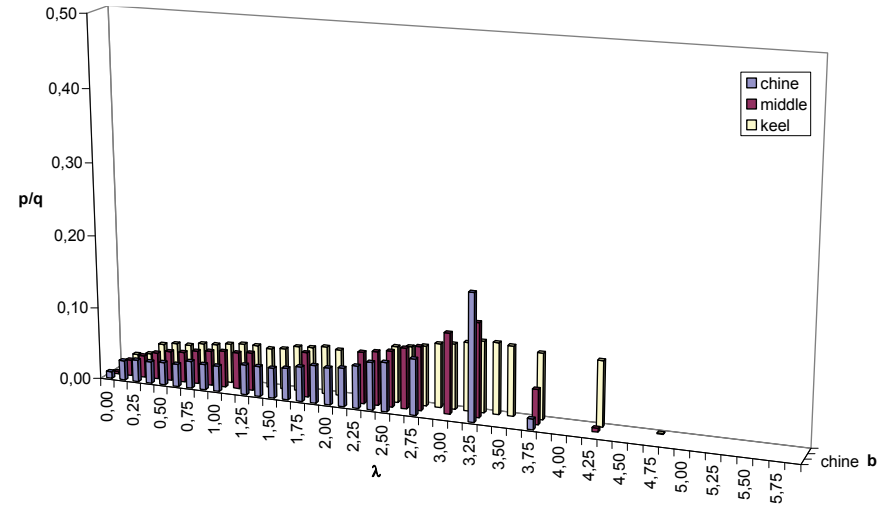

[d] : τ = 9 ° - run 4 - C_Δ = 17.89 - C_V = 12.20 - C_{Lb} = 0.2404

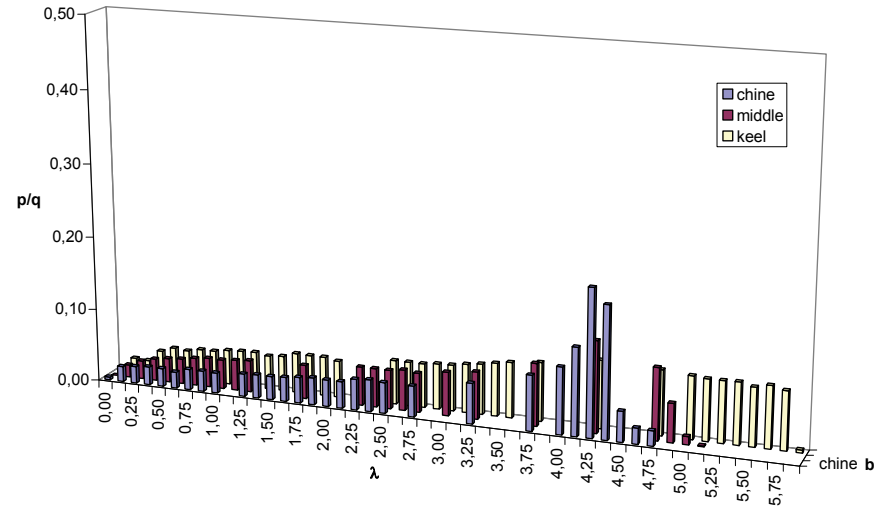

[e] : τ = 9 ° - run 5 - C_Δ = 21.94 - C_V = 12.20 - C_{Lb} = 0.2948

Figure 9.7-5 Pressure distribution on V-bottom planing surfaces - Model 302-A (continue)

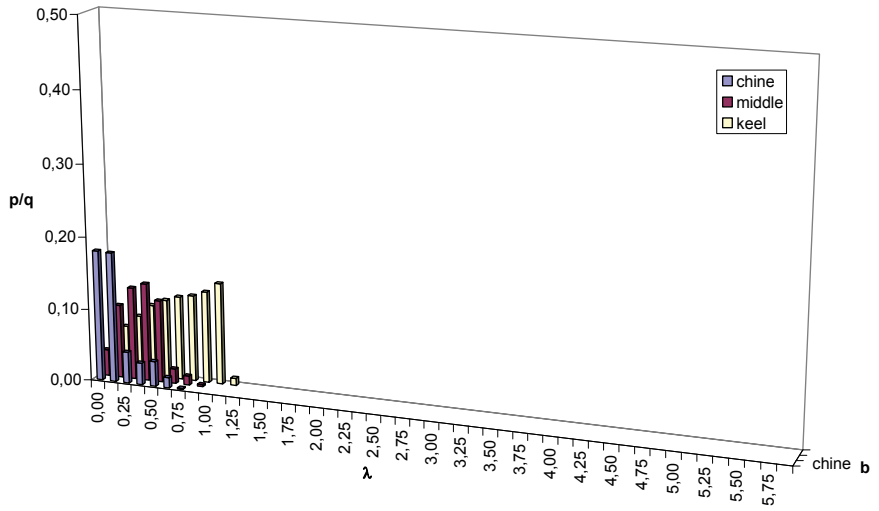

[f] : τ = 12 ° - run 6 - C_Δ = 5.64 - C_V = 12.23 - C_{Lb} = 0.0754

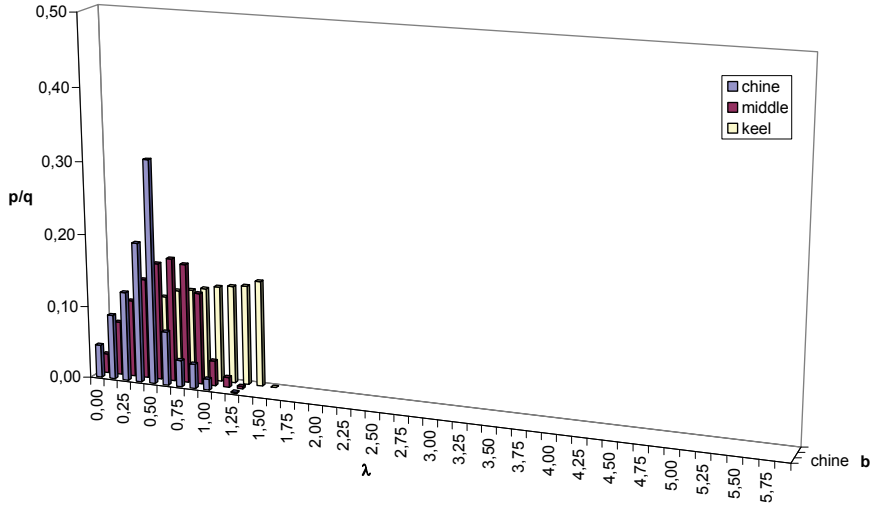

[g] : τ = 12 ° - run 7 - C_Δ = 9.69 - C_V = 12.08 - C_{Lb} = 0.1328

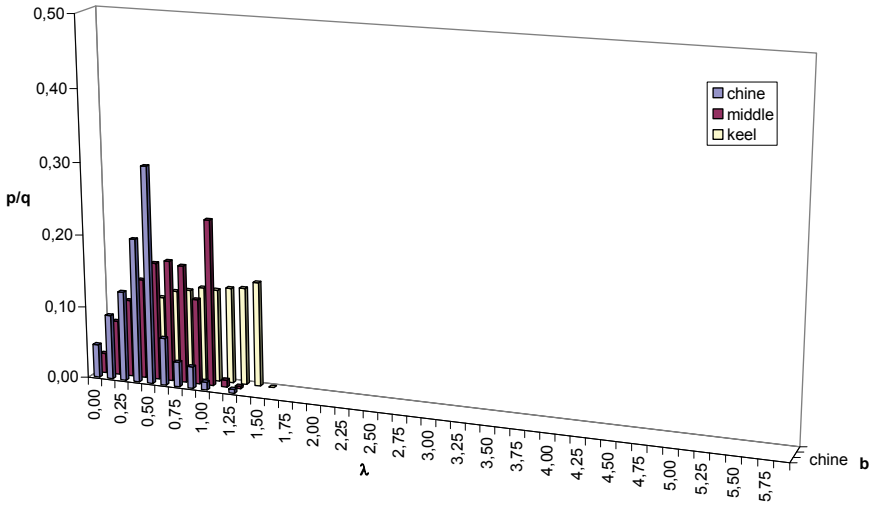

[h] : τ = 12 ° - run 8 - C_Δ = 9.69 - C_V = 12.26 - C_{Lb} = 0.1290

Figure 9.7-5 Pressure distribution on V-bottom planing surfaces - Model 302-A (continue)

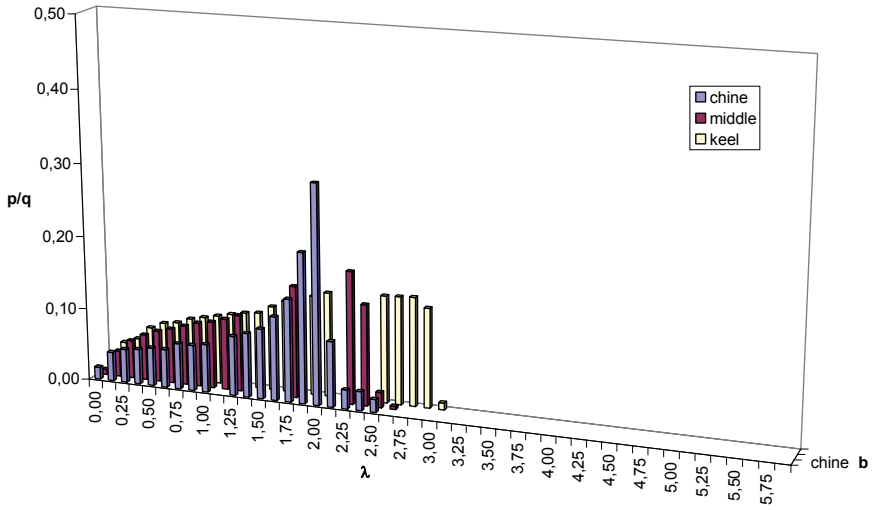

[i] : τ = 12 ° - run 9 - C_Δ = 19.60 - C_V = 12.14 - C_{Lb} = 0.2660

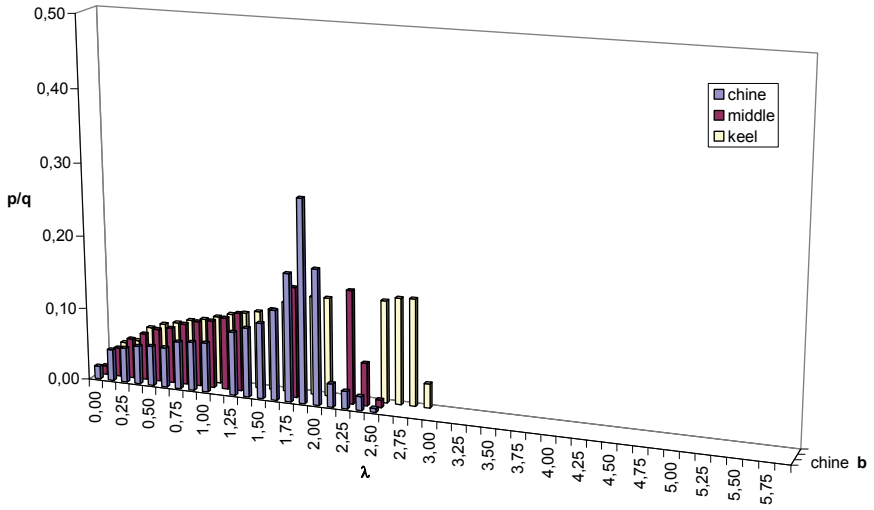

[j] : τ = 12 ° - run 10 - C_Δ = 19.60 - C_V = 12.20 - C_{Lb} = 0.2634

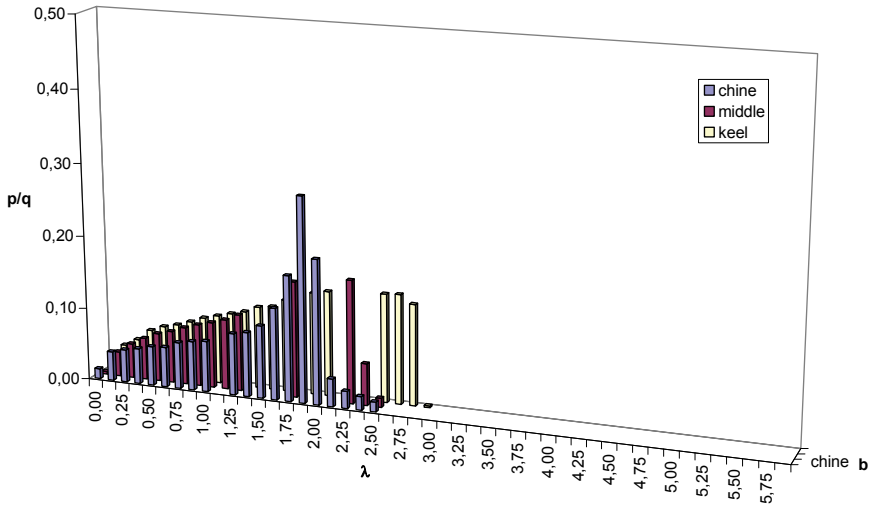

[k] : τ = 12 ° - run 11 - C_Δ = 8.61 - C_V = 8.11 - C_{Lb} = 0.2618

Figure 9.7-5 Pressure distribution on V-bottom planing surfaces - Model 302-A (continue)

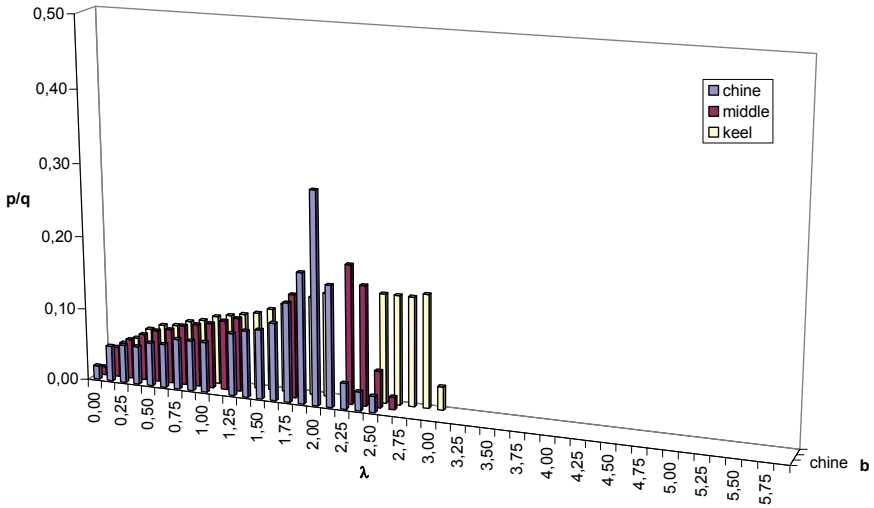

[l] : τ = 12 ° - run 12 - C_Δ = 11.08 - C_V = 9.09 - C_{Lb} = 0.2680

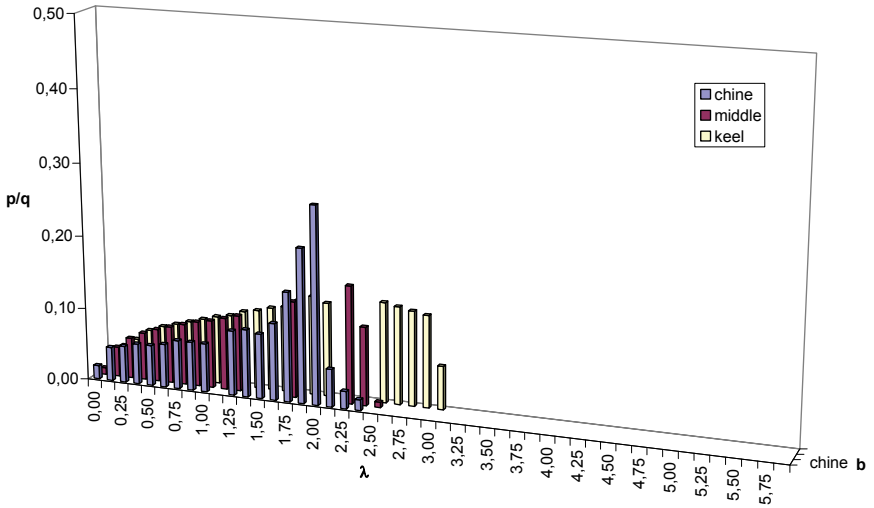

[m] : τ = 12 ° - run 13 - C_Δ = 11.08 - C_V = 9.12 - C_{Lb} = 0.2664

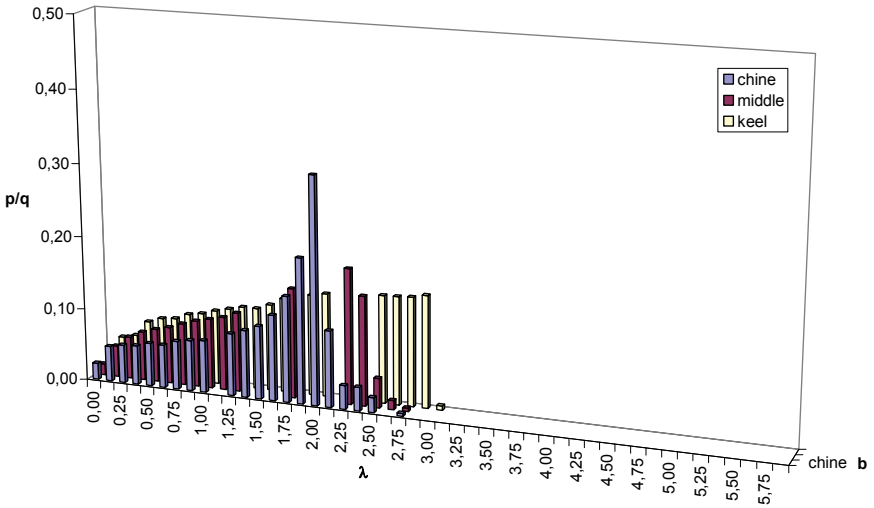

[n] : τ = 12 ° - run 14 - C_Δ = 30.67 - C_V = 15.25 - C_{Lb} = 0.2638

Figure 9.7-5 Pressure distribution on V-bottom planing surfaces - Model 302-A (continue)

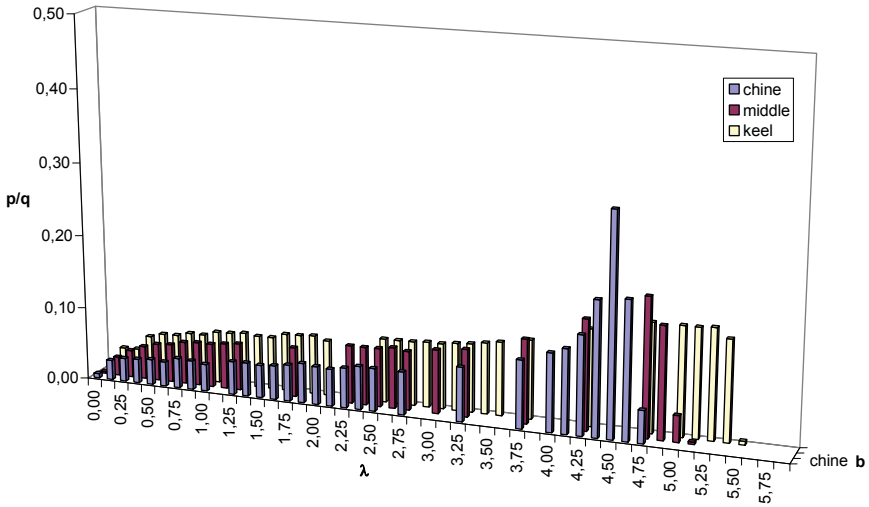

[o] : τ = 12 ° - run 15 - C_Δ = 31.44 - C_V = 12.20 - C_{Lb} = 0.4494

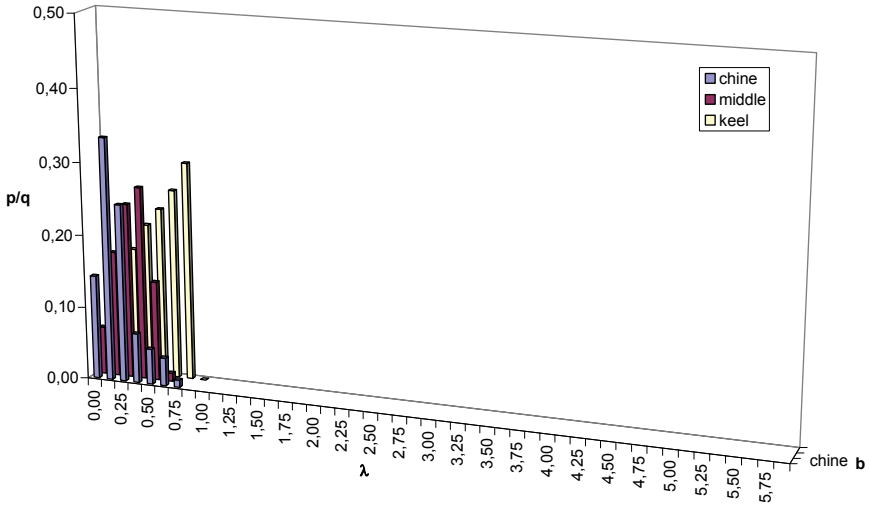

[p] : τ = 18 ° - run 16 - C_Δ = 9.27 - C_V = 12.29 - C_{Lb} = 0.1228

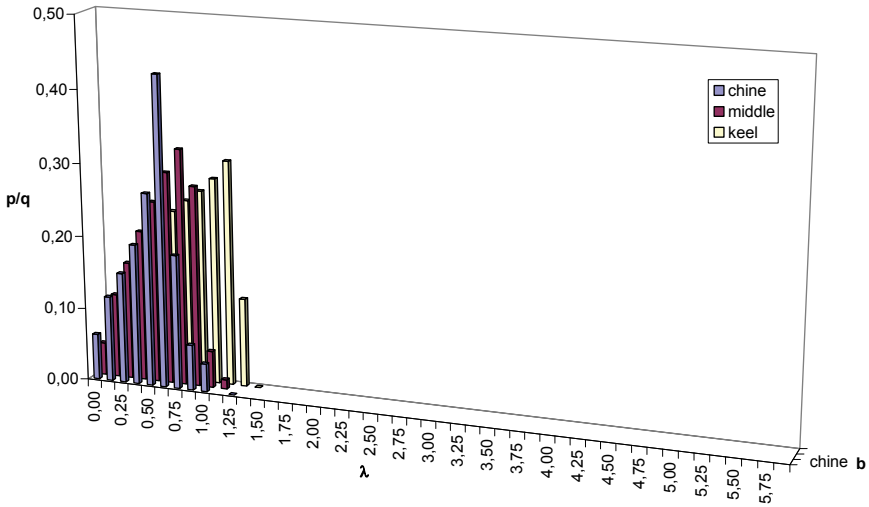

[q] : τ = 18 ° - run 17 - C_Δ = 16.29 - C_V = 12.26 - C_{Lb} = 0.2168

Figure 9.7-5 Pressure distribution on V-bottom planing surfaces - Model 302-A (continue)

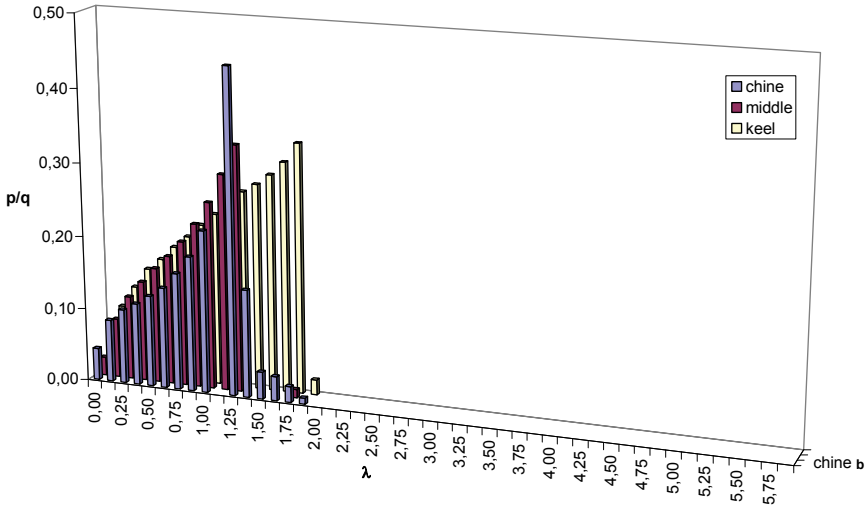

[r] : τ = 18 ° - run 18 - C_Δ = 23.86 - C_V = 12.20 - C_{Lb} = 0.3206

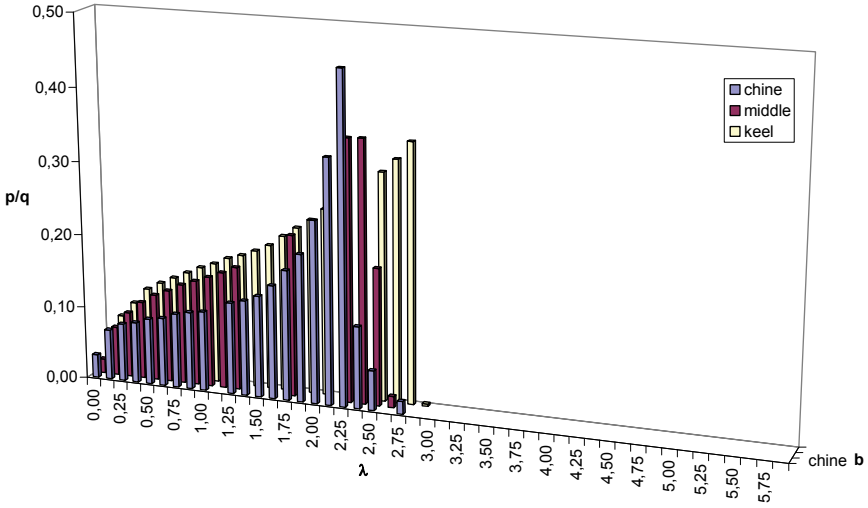

[s] : τ = 18 ° - run 19 - C_Δ = 34.81 - C_V = 12.26 - C_{Lb} = 0.4632

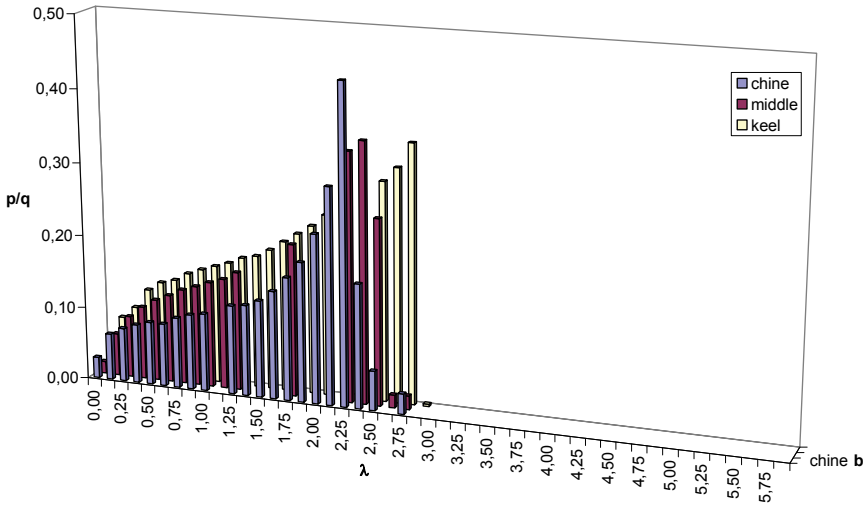

[t] : τ = 18 ° - run 20 - C_Δ = 34.83 - C_V = 12.23 - C_{Lb} = 0.4658

Figure 9.7-5 Pressure distribution on V-bottom planing surfaces - Model 302-A (continue)

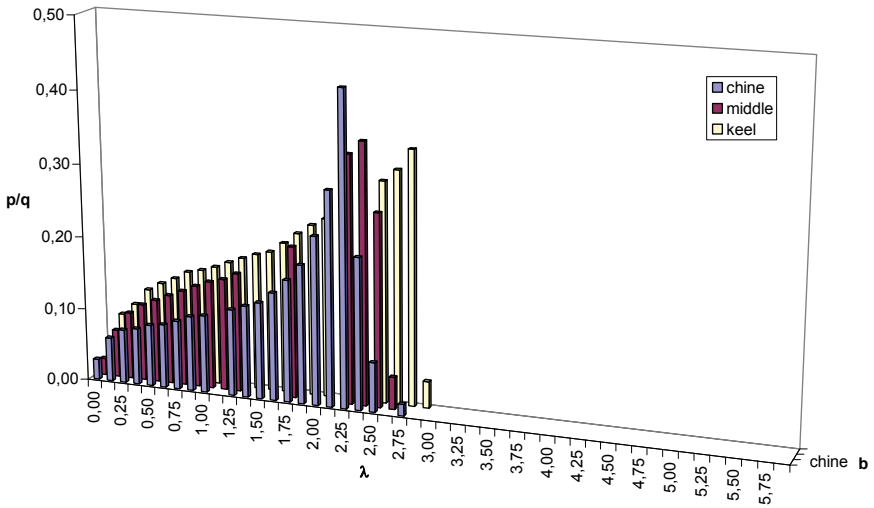

[u] : τ = 18 ° - run 21 - C_Δ = 34.83 - C_V = 12.23 - C_{Lb} = 0.4658

(Data source: [Kapryan & Boyd 1955])

Figure 9.7-5 Pressure distribution on V-bottom planing surfaces - Model 302-A

9.8 Diagrams: Deadrise Effects

9.8.1 Mean Wetted Length Ratio $\frac{l_m}{b}$ vs C_Δ with $C_V = 12.2$

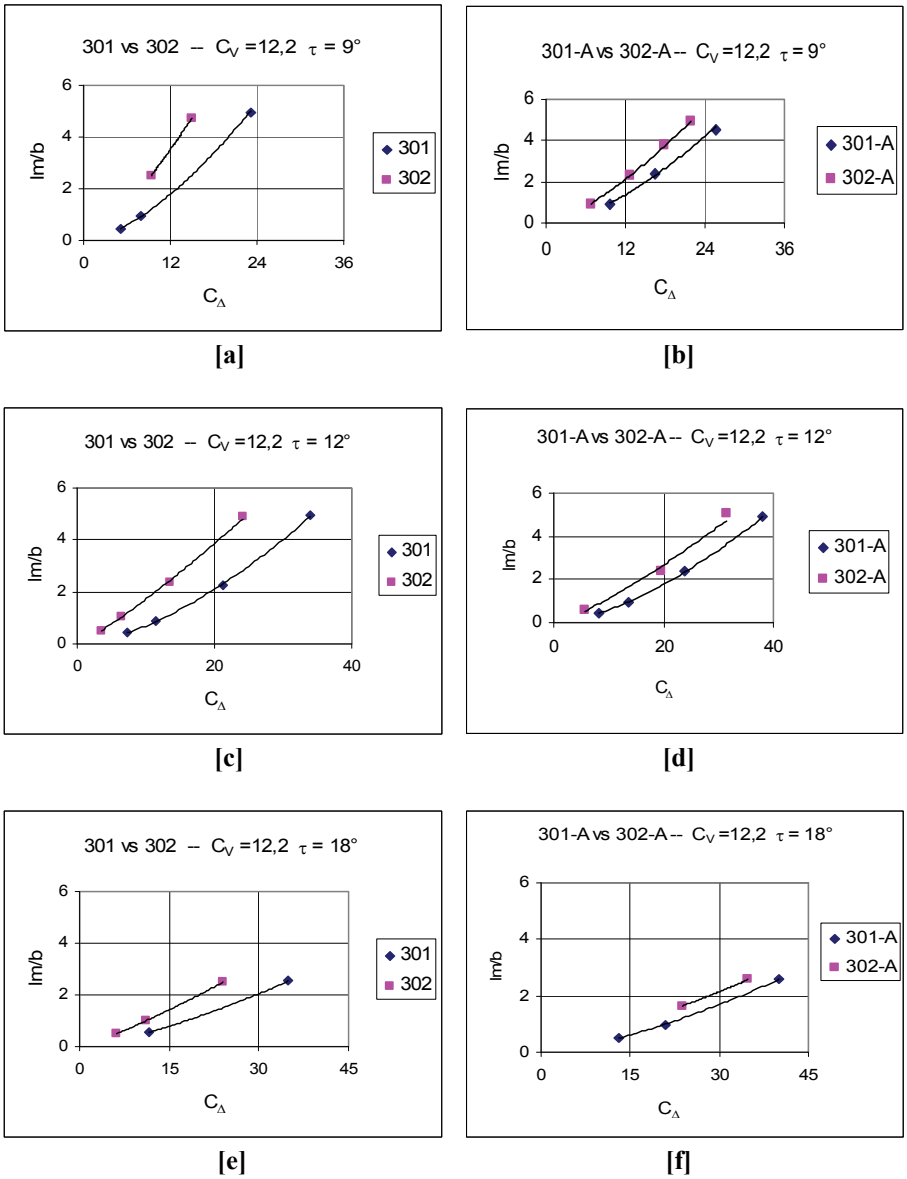

(Data source: [Kapryan & Boyd 1955])

Figure 9.8-1 Deadrise effects on mean wetted length for V-bottom planing surfaces with $C_V = 12.2$

9.8.2 Mean Wetted Length Ratio $\frac{l_m}{b}$ vs C_V, without Horizontal Chine Flared

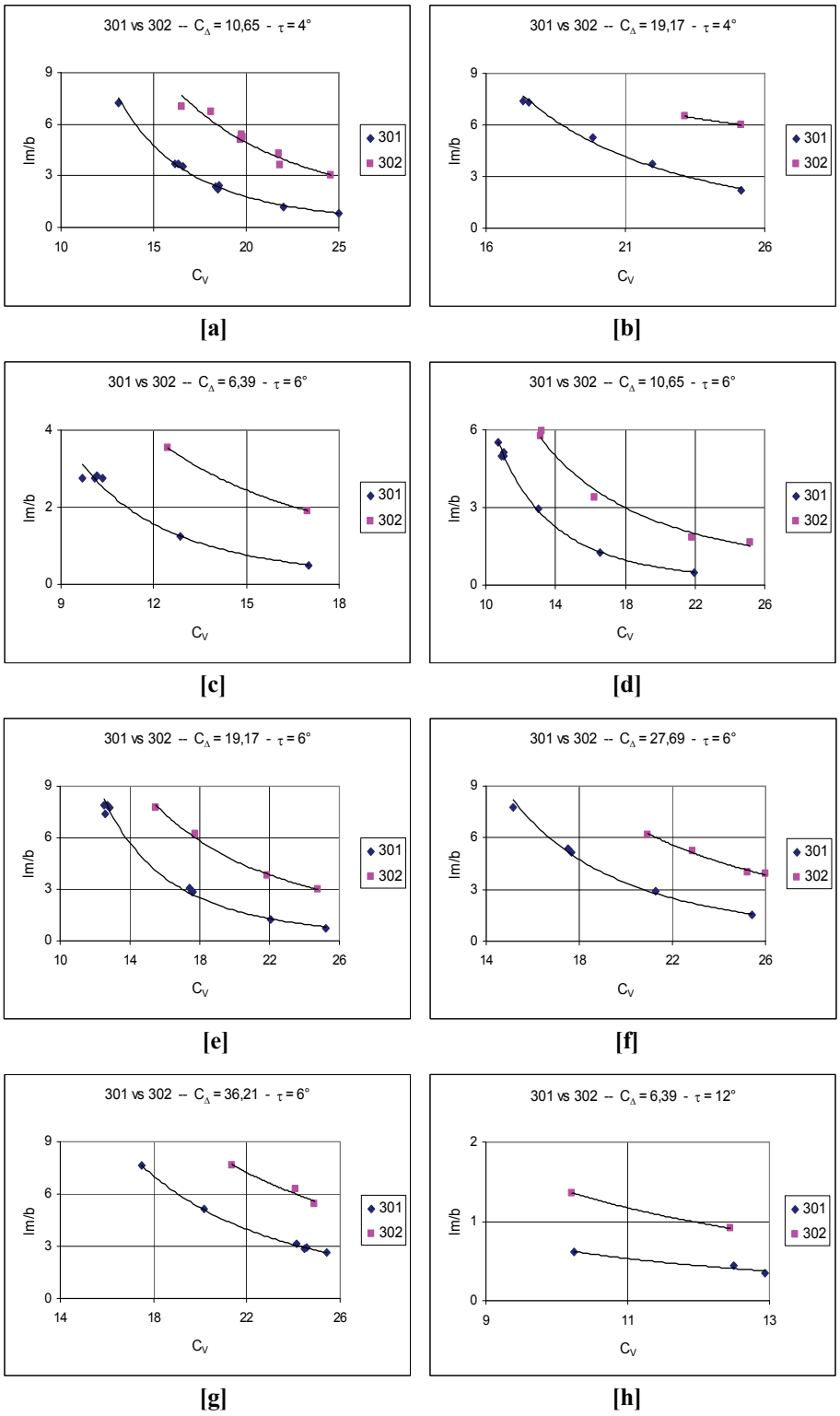

Figure 9.8-2 Deadrise angle effect on mean wetted length of V-bottom planing surfaces without horizontal chine flared (continue)

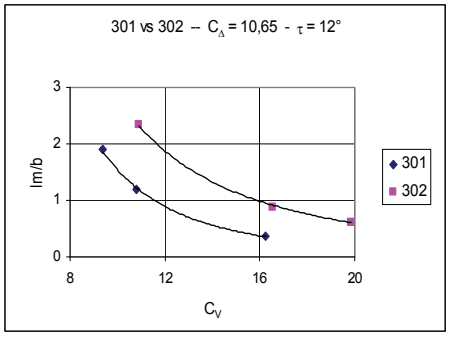

[i]

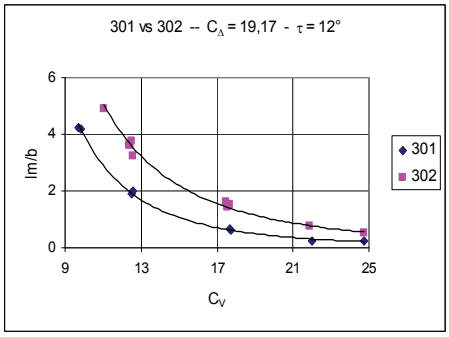

[j]

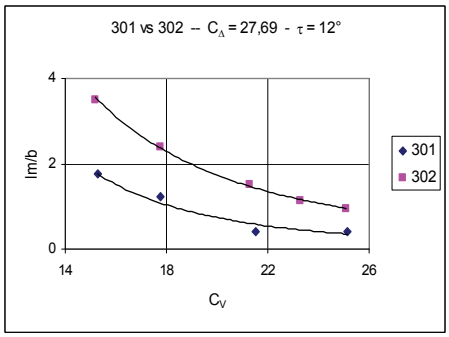

[k]

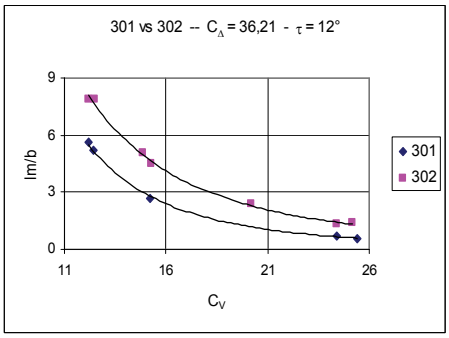

[l]

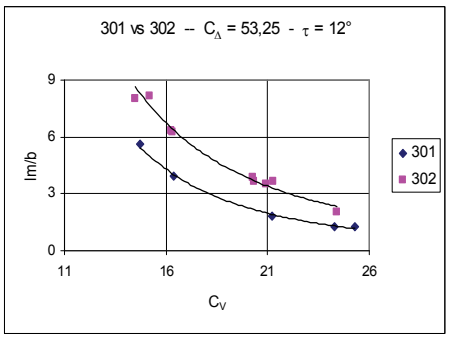

[m]

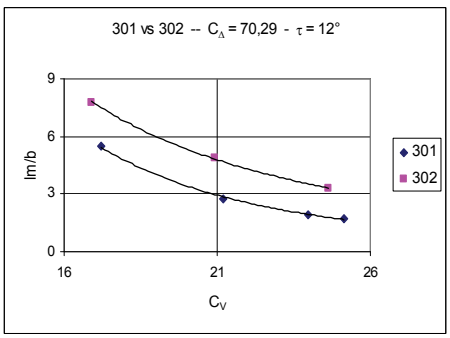

[n]

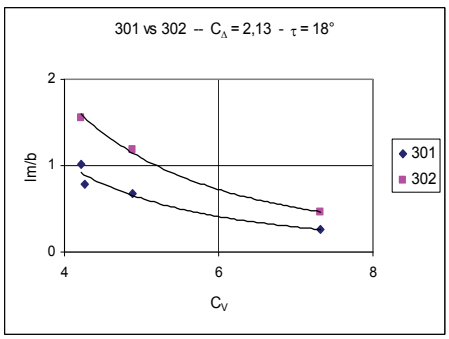

[o]

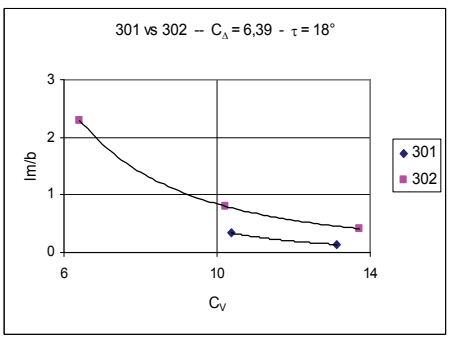

[p]

Figure 9.8-2 Deadrise angle effect on mean wetted length of V-bottom planing surfaces without horizontal chine flared (continue)

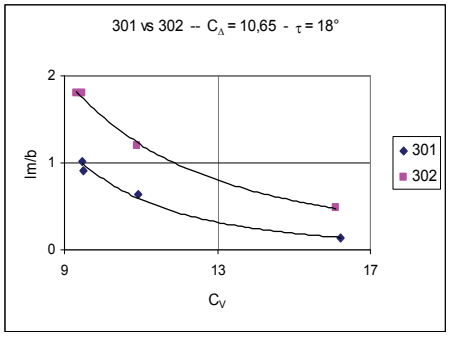

[q]

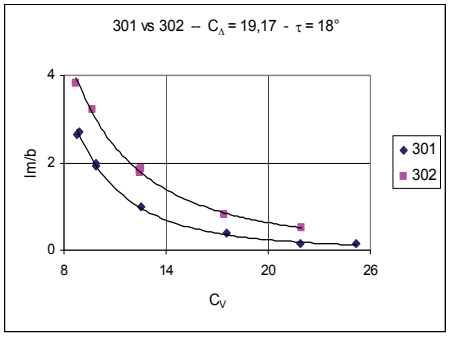

[r]

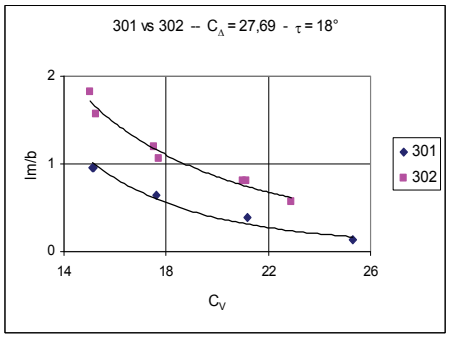

[s]

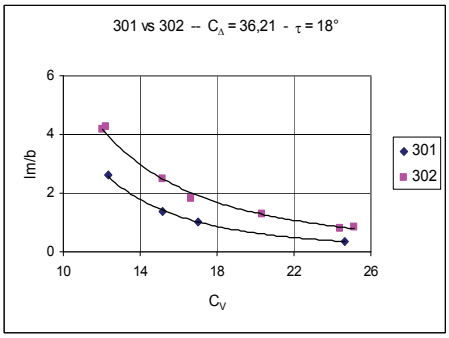

[t]

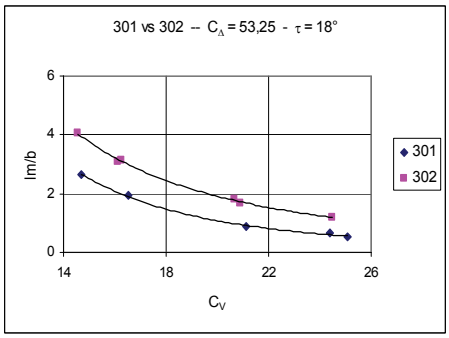

[u]

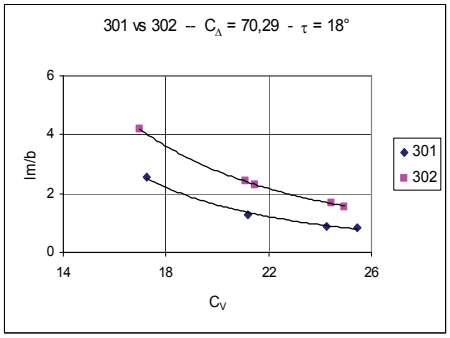

[v]

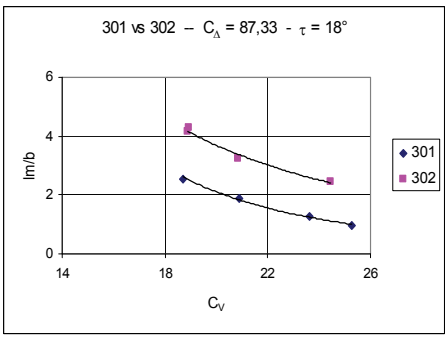

[w]

(Data source: [Chambliss & Boyd 1953])

Figure 9.8-2 Deadrise angle effect on mean wetted length of V-bottom planing surfaces without horizontal chine flared

9.8.3 Mean Wetted Length Ratio $\frac{l_m}{b}$ vs C_V, with Horizontal Chine Flared

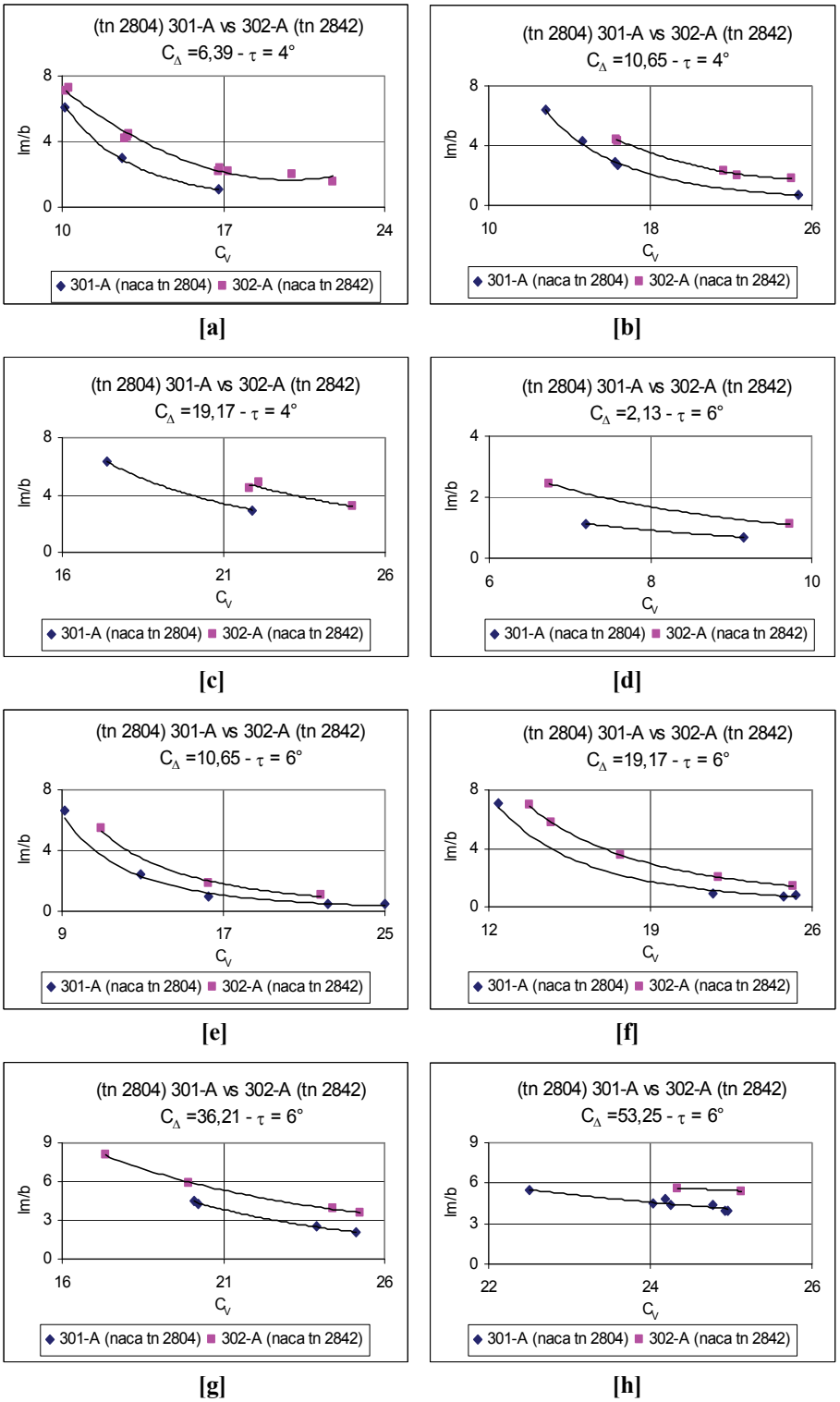

Figure 9.8-3 Deadrise angle effect on mean wetted length of V-bottom planing surfaces with horizontal chine flared (continue)

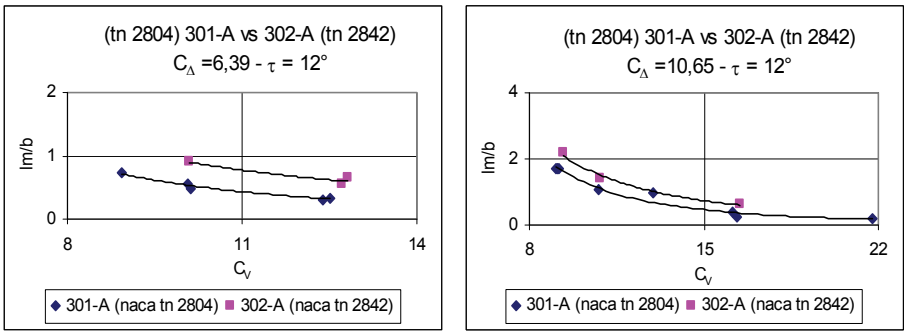

[i]

[j]

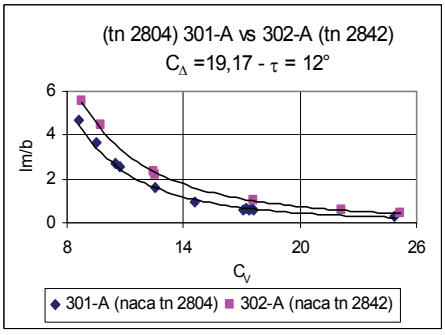

[k]

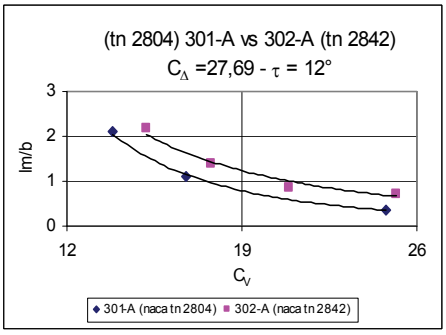

[l]

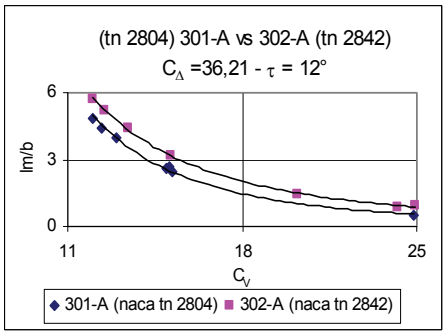

[m]

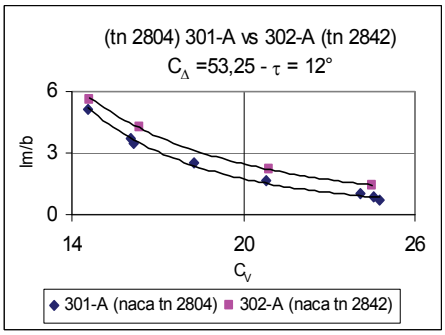

[n]

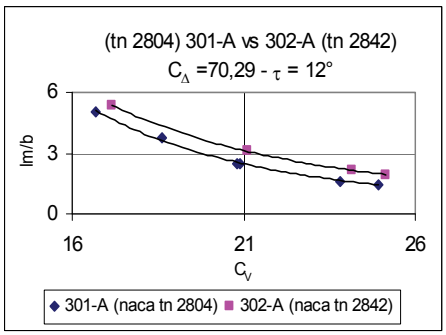

[o]

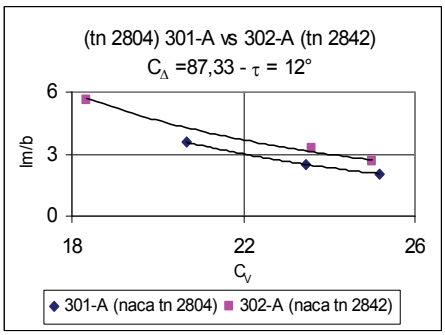

[p]

Figure 9.8-3 Deadrise angle effect on mean wetted length of V-bottom planing surfaces with horizontal chine flared (continue)

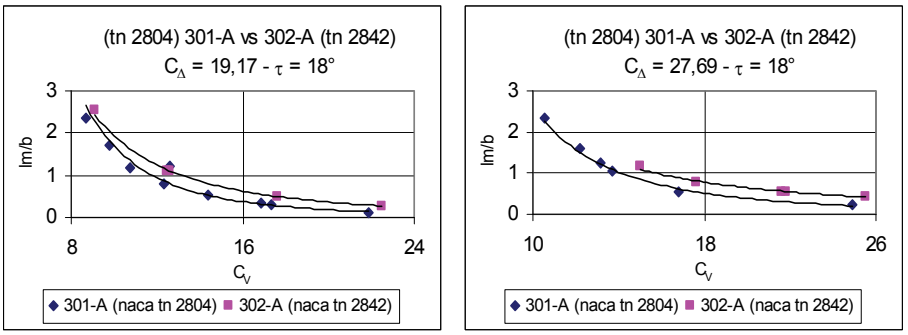

[q]

[r]

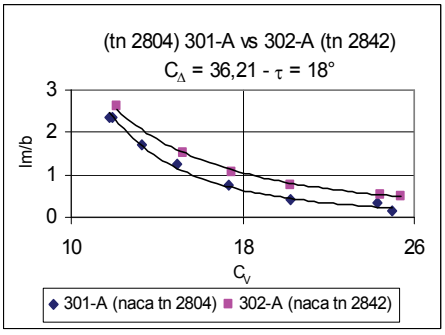

[s]

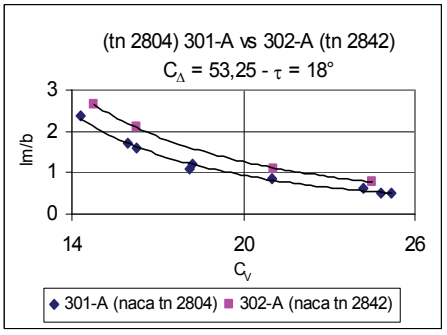

[t]

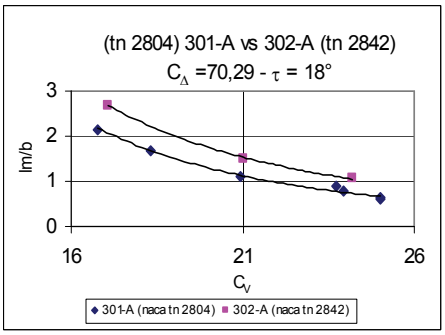

[u]

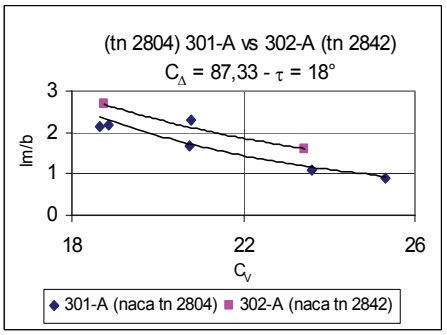

[v]

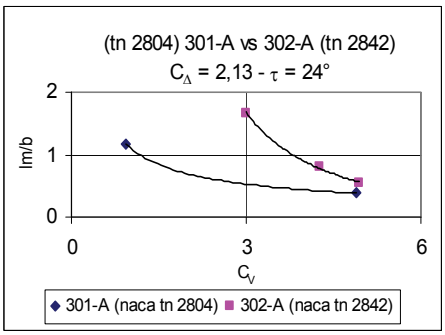

[w]

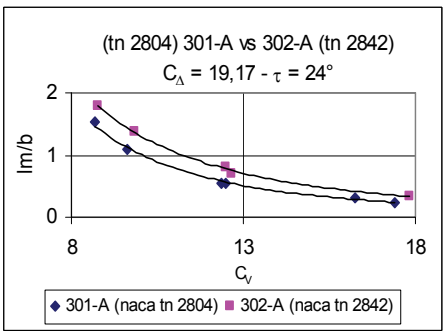

[x]

Figure 9.8-3 Deadrise angle effect on mean wetted length of V-bottom planing surfaces with horizontal chine flared (continue)

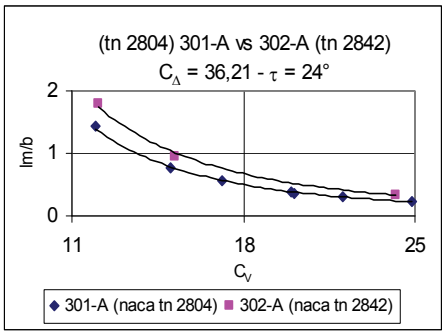

[y]

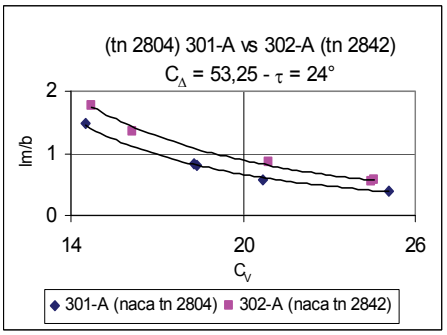

[z]

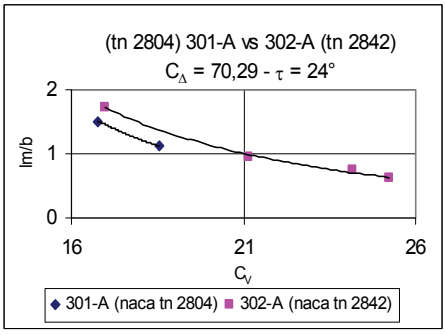

[aa]

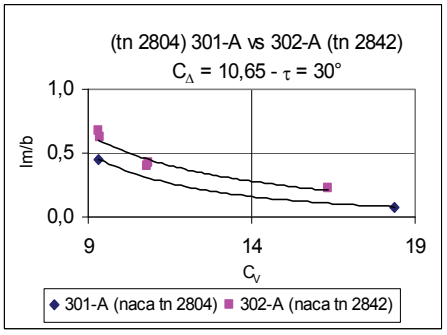

[ab]

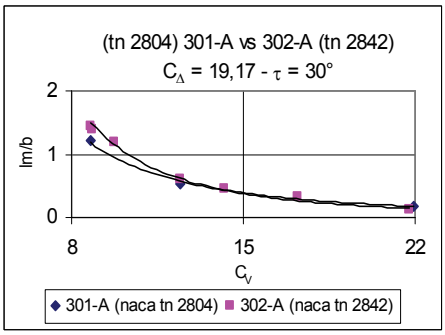

[ac]

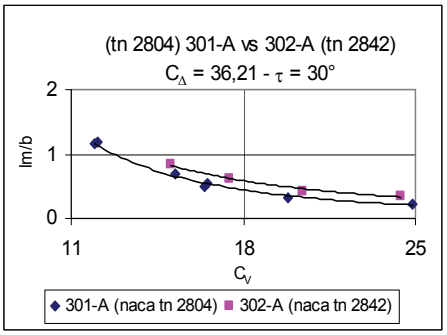

[ad]

(Data sources: [Kapryan & Weinstein 1952] and [Blanchard 1952])

Figure 9.8-3 Deadrise angle effect on mean wetted length of V-bottom planing surfaces with horizontal chine flared

9.8.4 Mean Wetted Length Ratio $\frac{l_m}{b}$ vs C_{Lb}

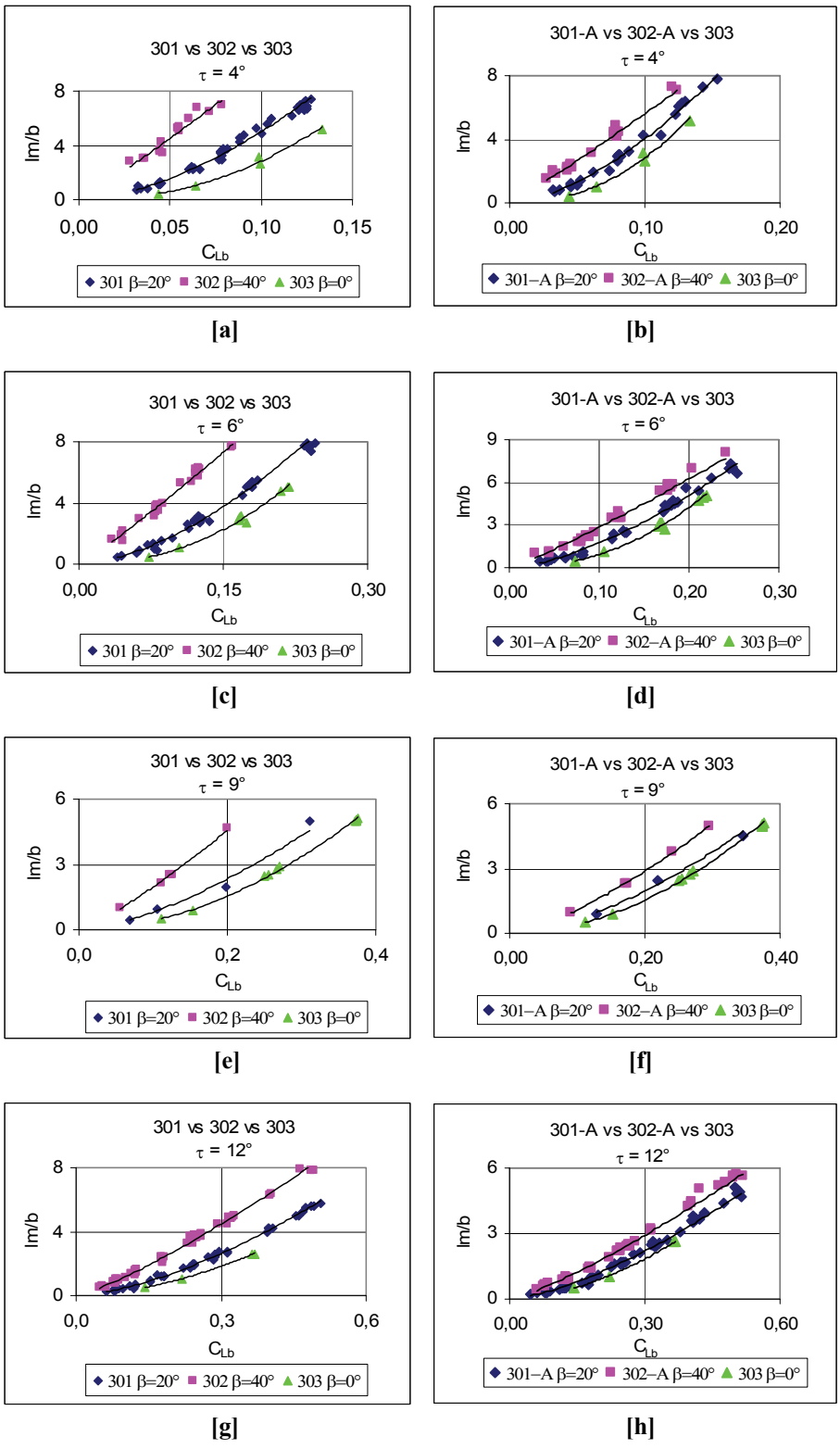

Figure 9.8-4 Deadrise angle effect on mean wetted length of planing surfaces (continue)

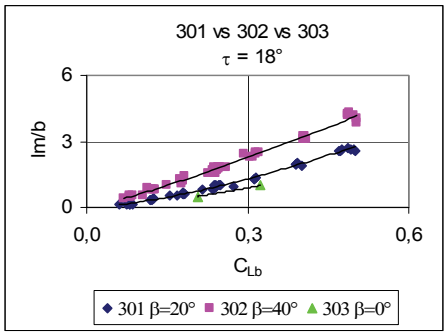

[i]

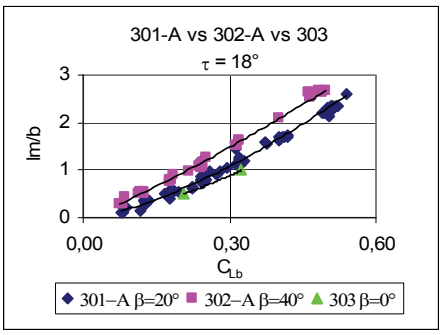

[j]

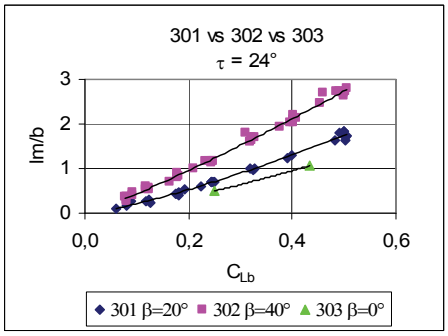

[k]

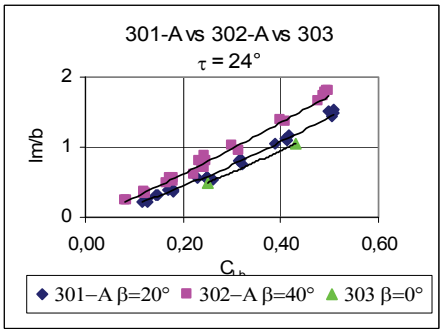

[l]

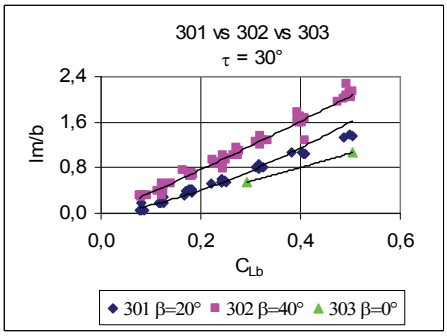

[m]

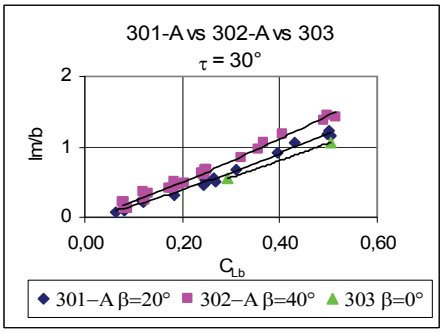

[n]

(Data sources: [Blanchard 1952], [Kapryan & Weinstein 1952], [Kapryan & Boyd 1955])

Figure 9.8-4 Deadrise angle effect on mean wetted length of planing surfaces

9.8.5 Center of Pressure: Longitudinal Position Ratio $\frac{l_p}{b}$ vs C_Δ with $C_V = 12.2$

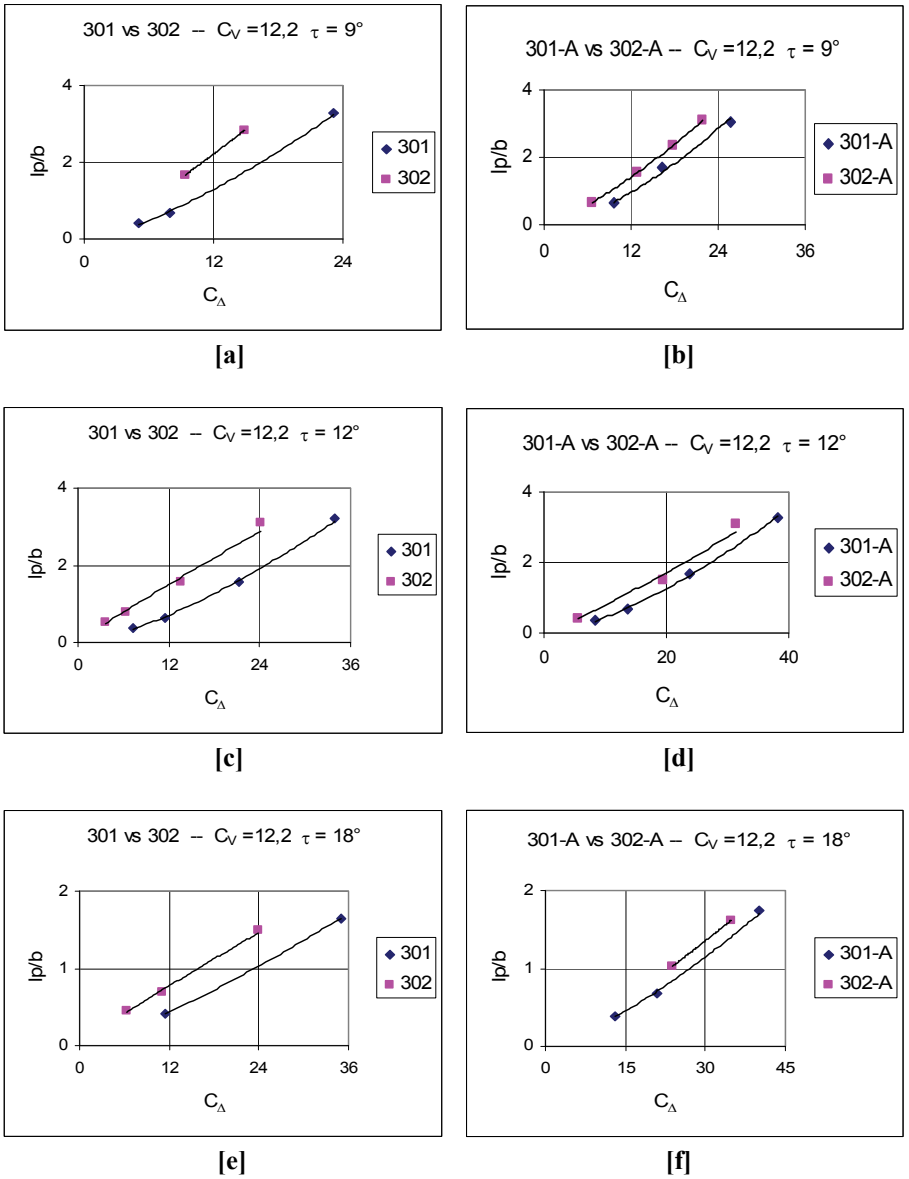

(Data source: [Kapryan & Boyd 1955])

Figure 9.8-5 Deadrise angle effects on longitudinal center pressure location for V-bottom planing surface with $C_V = 12.2$

9.8.6 Center of Pressure: Longitudinal Position Ratio $\frac{l_p}{b}$ vs C_V, without Horizontal Chine Flared

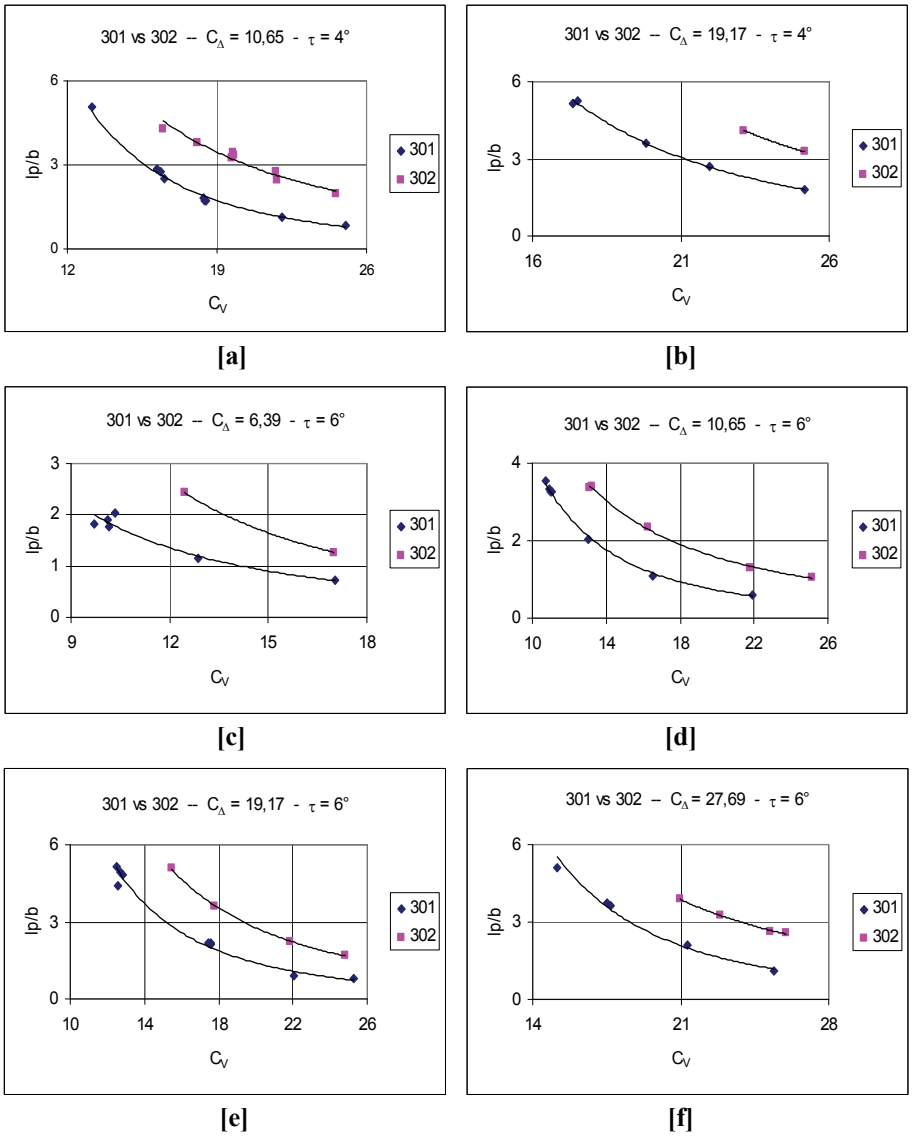

Figure 9.8-6 Deadrise angle effect on longitudinal center pressure position for V-bottom planing surfaces without horizontal chine flared (continue)

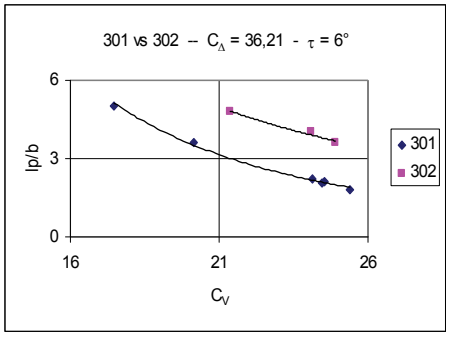

[g]

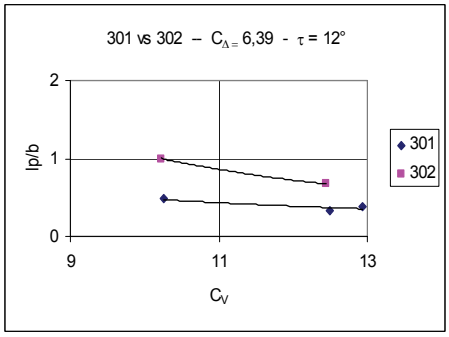

[h]

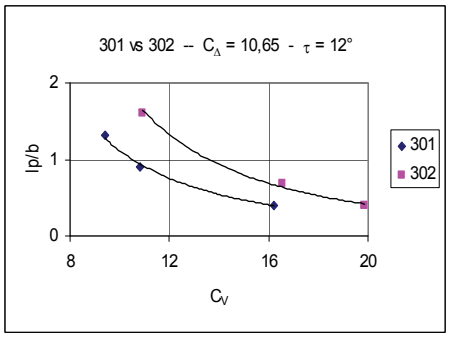

[i]

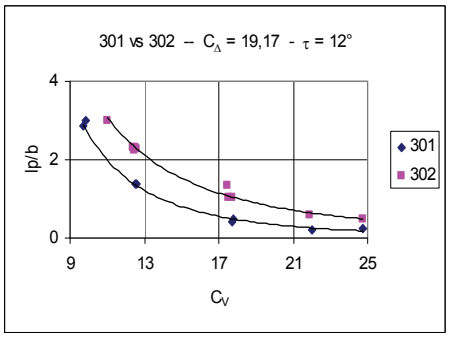

[j]

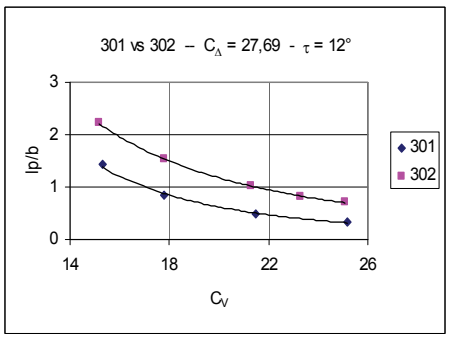

[k]

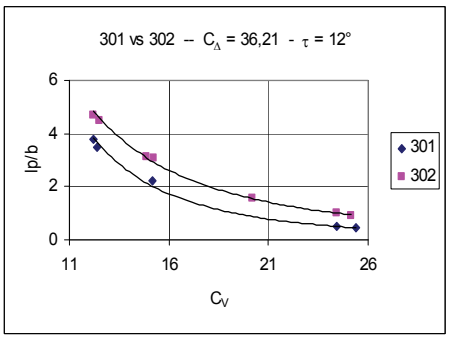

[l]

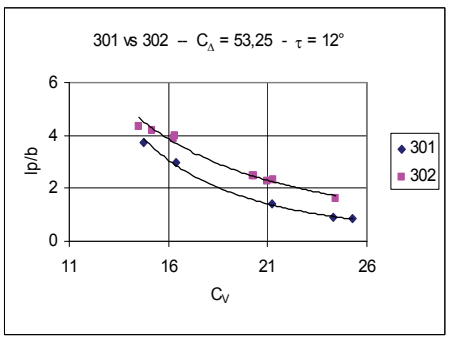

[m]

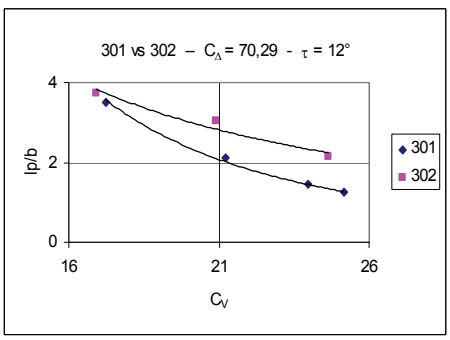

[n]

Figure 9.8-6 Deadrise angle effect on longitudinal center pressure position for V-bottom planing surfaces without horizontal chine flared (continue)

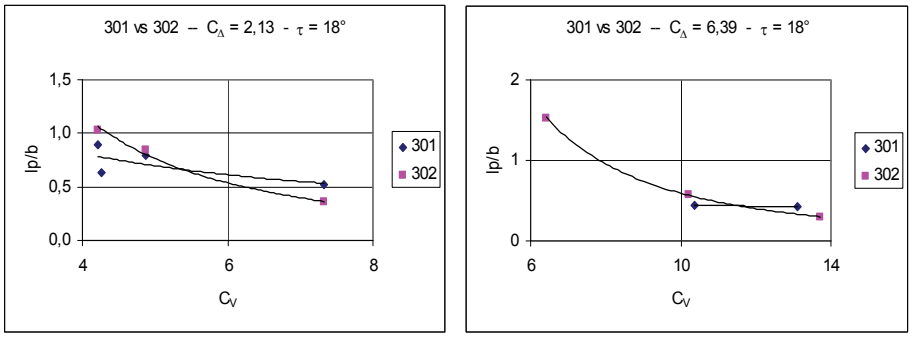

[o]

[p]

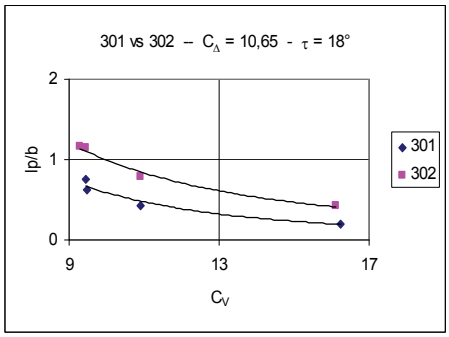

[q]

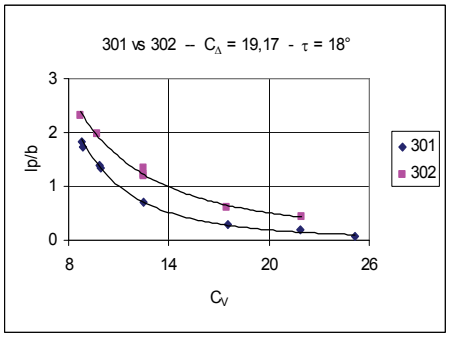

[r]

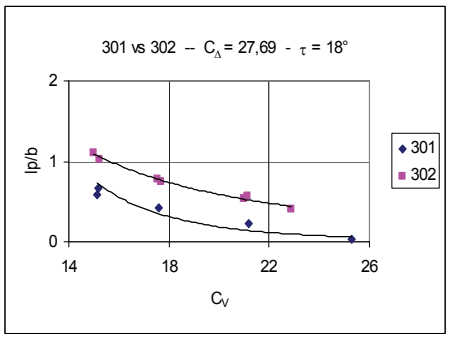

[s]

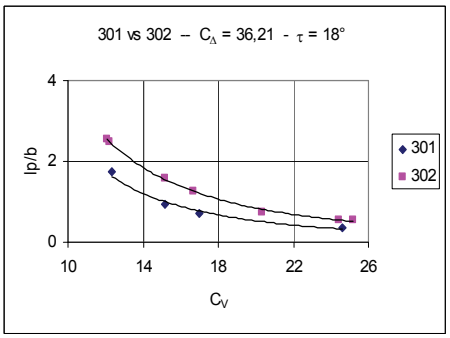

[t]

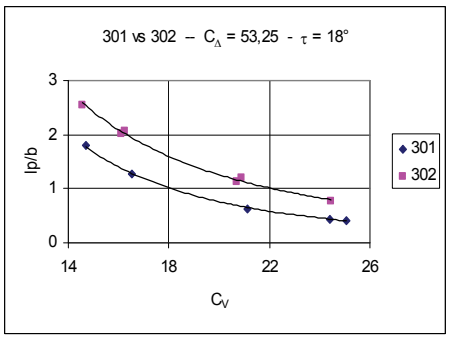

[u]

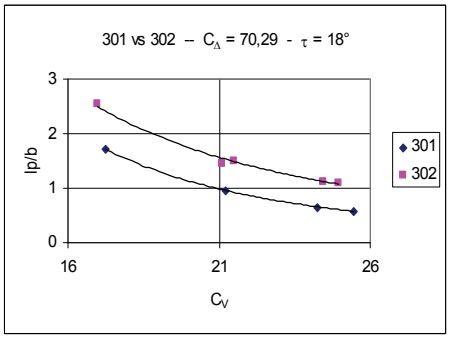

[v]

Figure 9.8-6 Deadrise angle effect on longitudinal center pressure position for V-bottom planing surfaces without horizontal chine flared (continue)

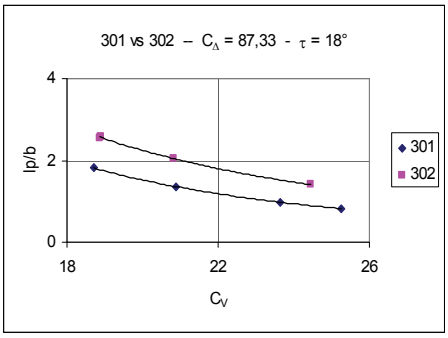

[w]

(Data source: [Chambliss & Boyd 1953])

Figure 9.8-6 Deadrise angle effect on longitudinal center pressure position for V-bottom planing surfaces without horizontal chine flared

9.8.7 Center of Pressure: Longitudinal Position Ratio $\frac{l_p}{b}$ vs C_V, with Horizontal Chine Flared

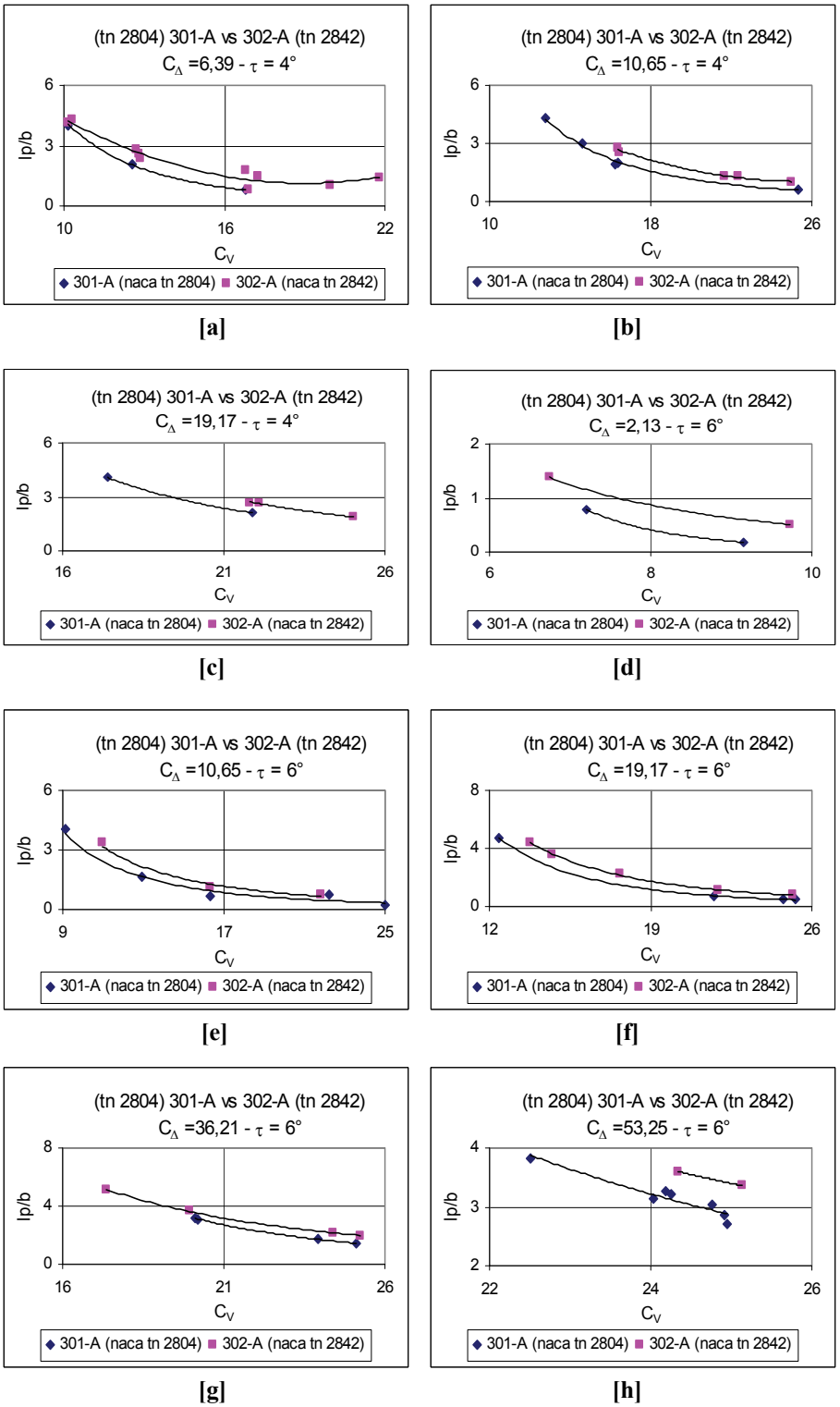

Figure 9.8-7 Deadrise angle effect on longitudinal center pressure position for V-bottom planing surfaces with horizontal chine flared (continue)

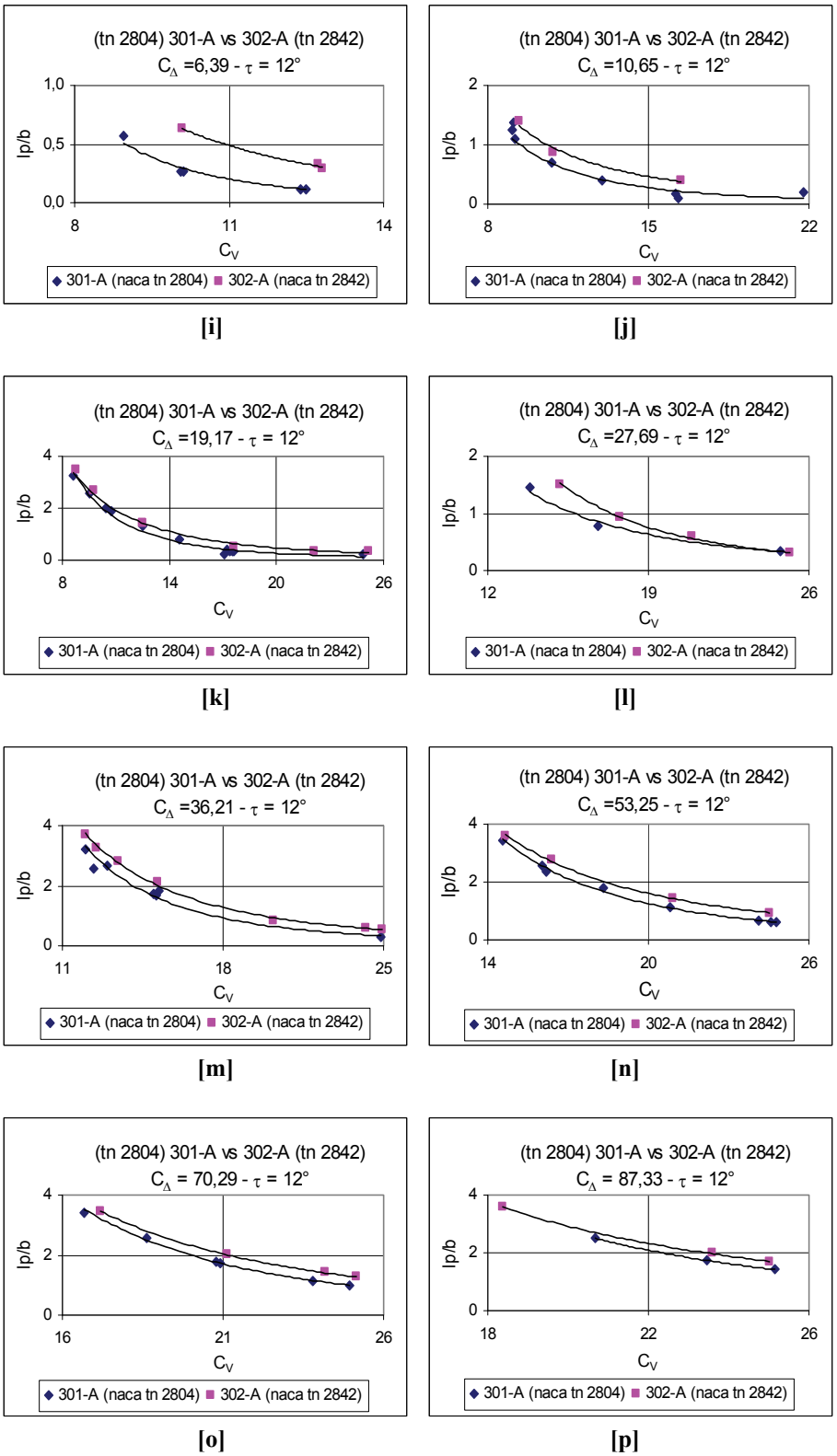

Figure 9.8-7 Deadrise angle effect on longitudinal center pressure position for V-bottom planing surfaces with horizontal chine flared (continue)

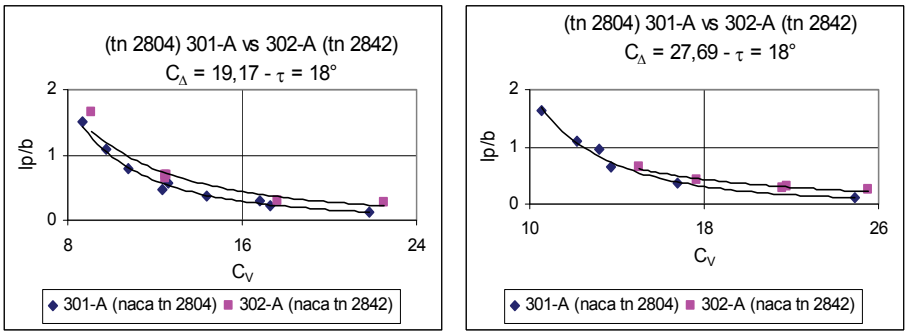

[q]

[r]

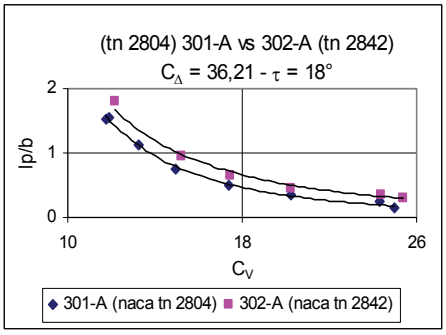

[s]

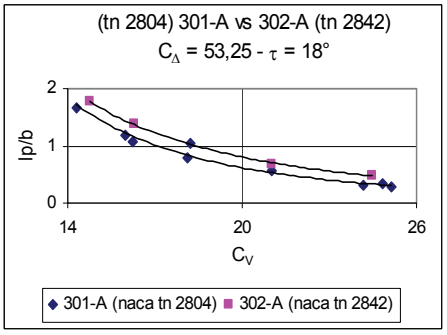

[t]

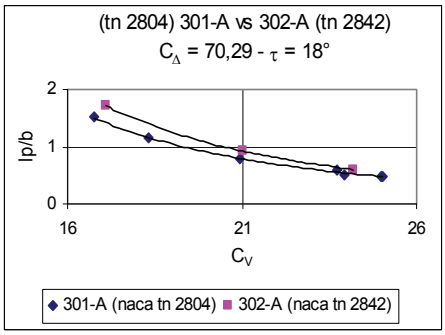

[u]

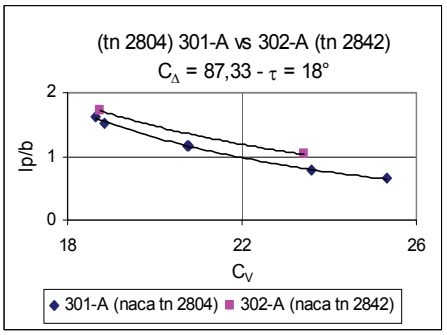

[v]

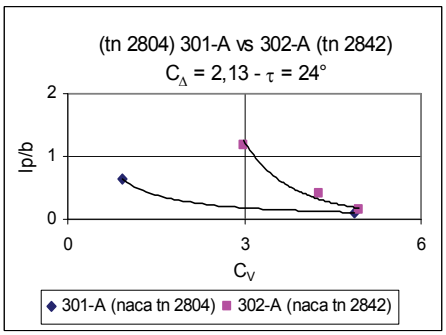

[w]

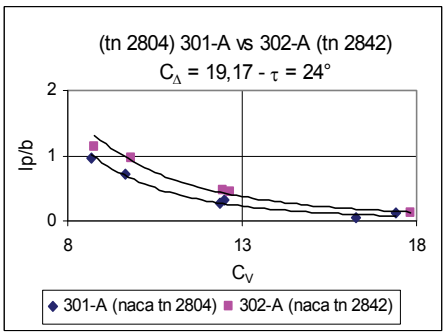

[x]

Figure 9.8-7 Deadrise angle effect on longitudinal center pressure position for V-bottom planing surfaces with horizontal chine flared (continue)

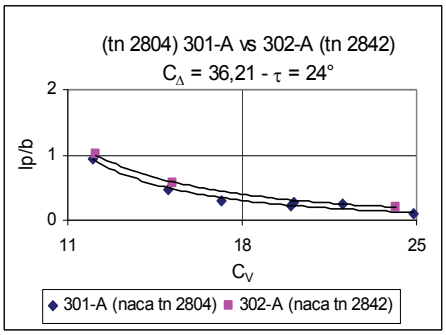

[y]

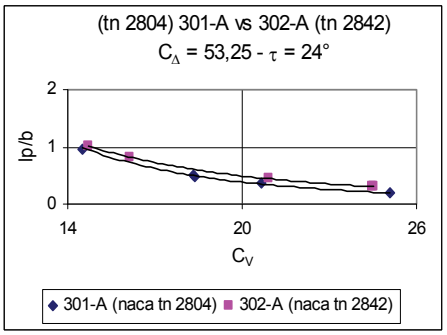

[z]

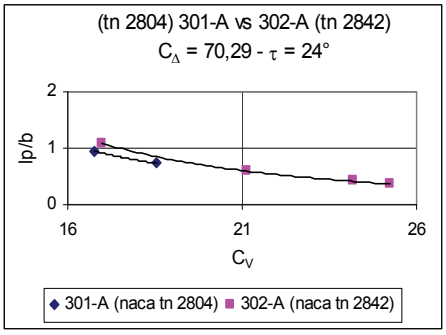

[aa]

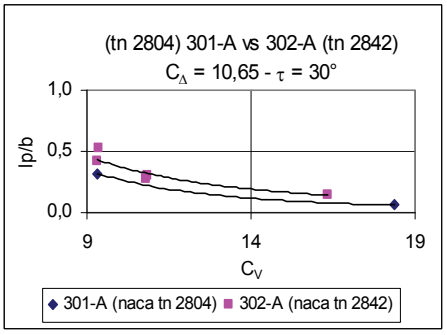

[ab]

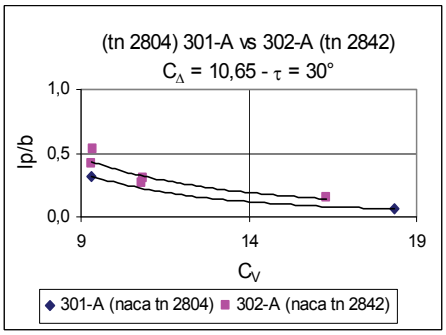

[ac]

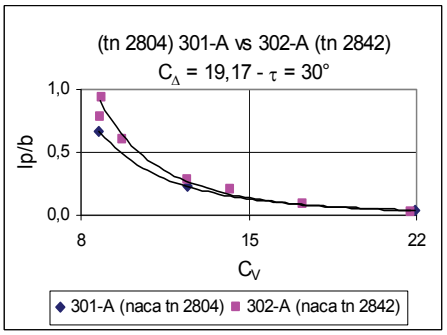

[ad]

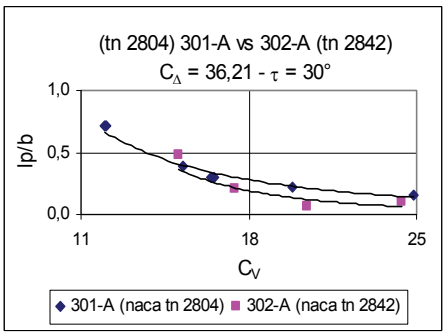

[ae]

(Data sources: [Kapryan & Weinstein 1952] and [Blanchard 1952])

Figure 9.8-7 Deadrise angle effect on longitudinal center pressure position for V-bottom planing surfaces with horizontal chine flared

9.8.8 Center of Pressure: Longitudinal Position Ratio $\frac{l_p}{b}$ vs C_{Lb}

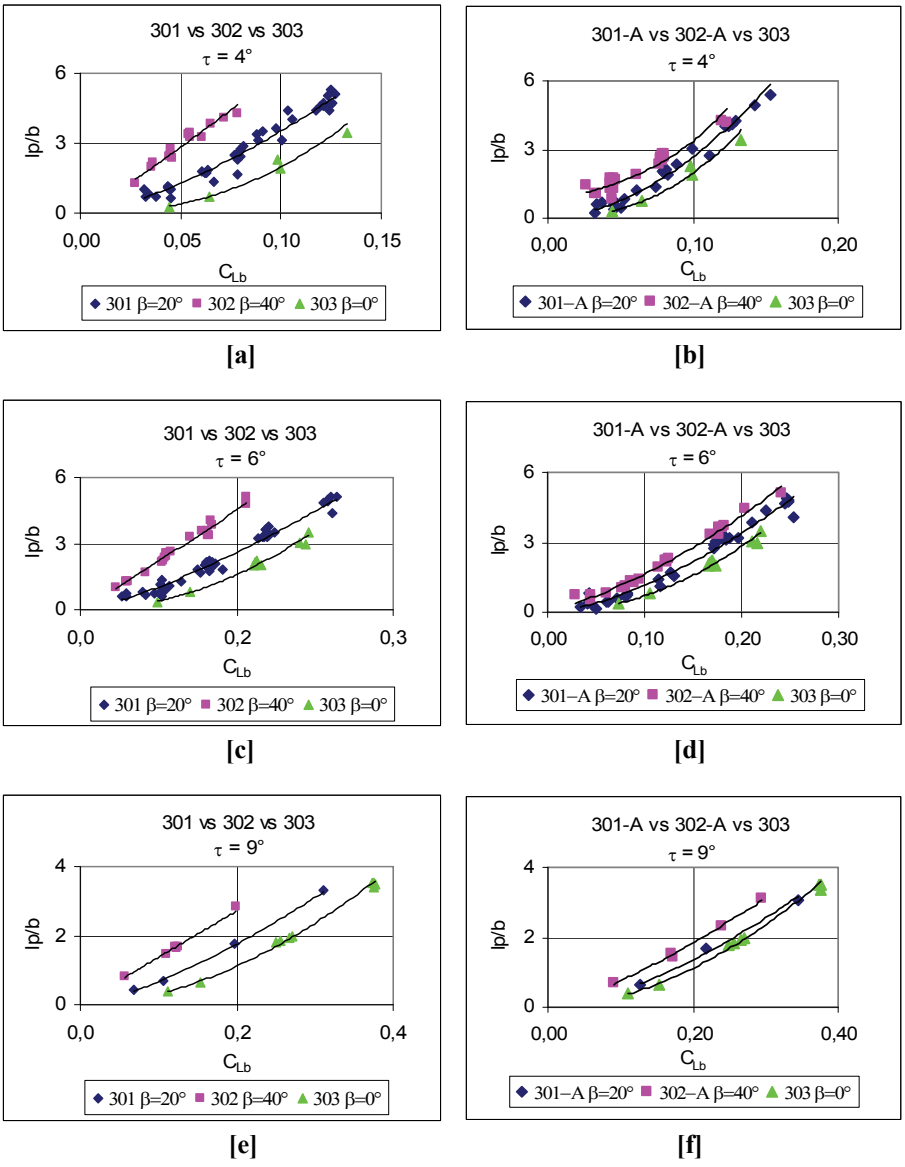

Figure 9.8-8 Deadrise angle effects on longitudinal center pressure location for V-bottom planing surface
(continue)

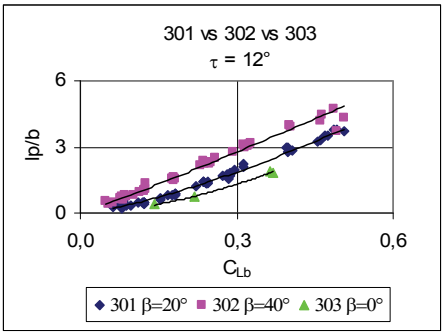

[g]

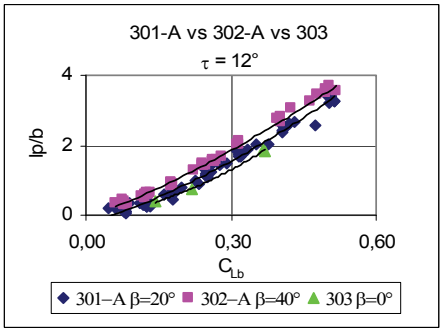

[h]

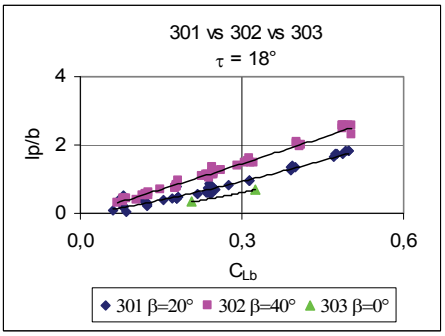

[i]

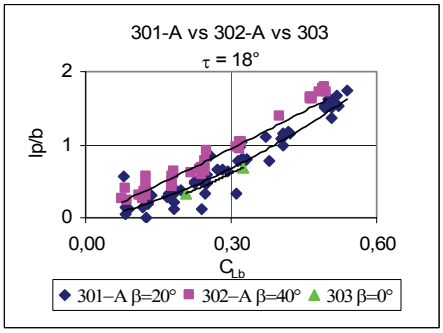

[j]

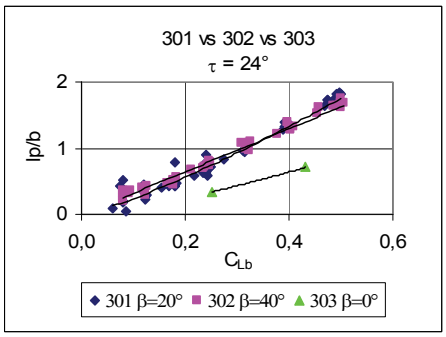

[k]

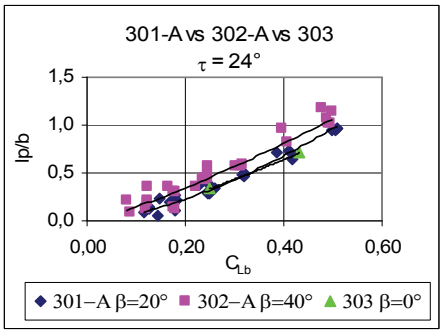

[l]

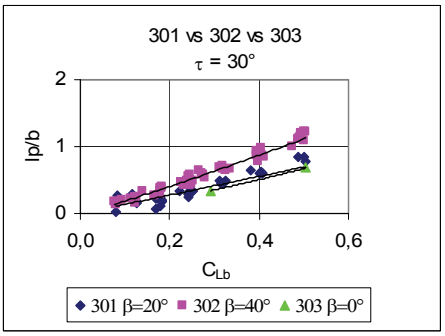

[m]

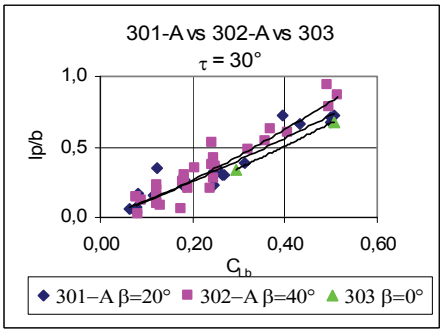

[n]

(Data sources: [Blanchard 1952], [Kapryan & Weinstein 1952]

[Kapryan & Boyd 1955])

Figure 9.8-8 Deadrise angle effects on longitudinal center pressure location for V-bottom planing surface

9.8.9 Stagnation and Spray Edges Lines Position λ vs C_Δ, without Horizontal Chine Flared and with $C_V = 12.2$

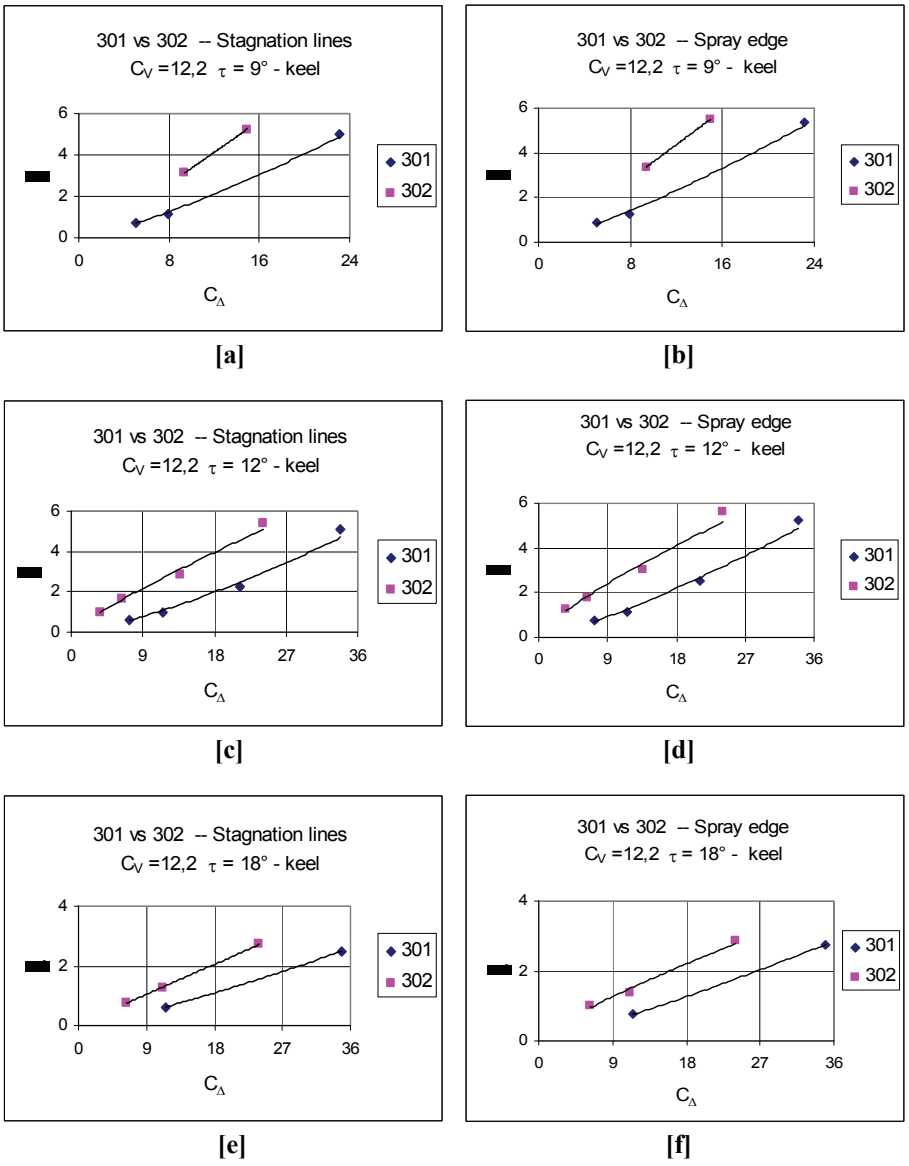

[a] **[b]**

[c] **[d]**

[e] **[f]**

Figure 9.8-9 Deadrise angle effects on stagnation and spray edge lines for V-bottom planing surface without horizontal chine flared and with $C_V = 12.2$ (continue)

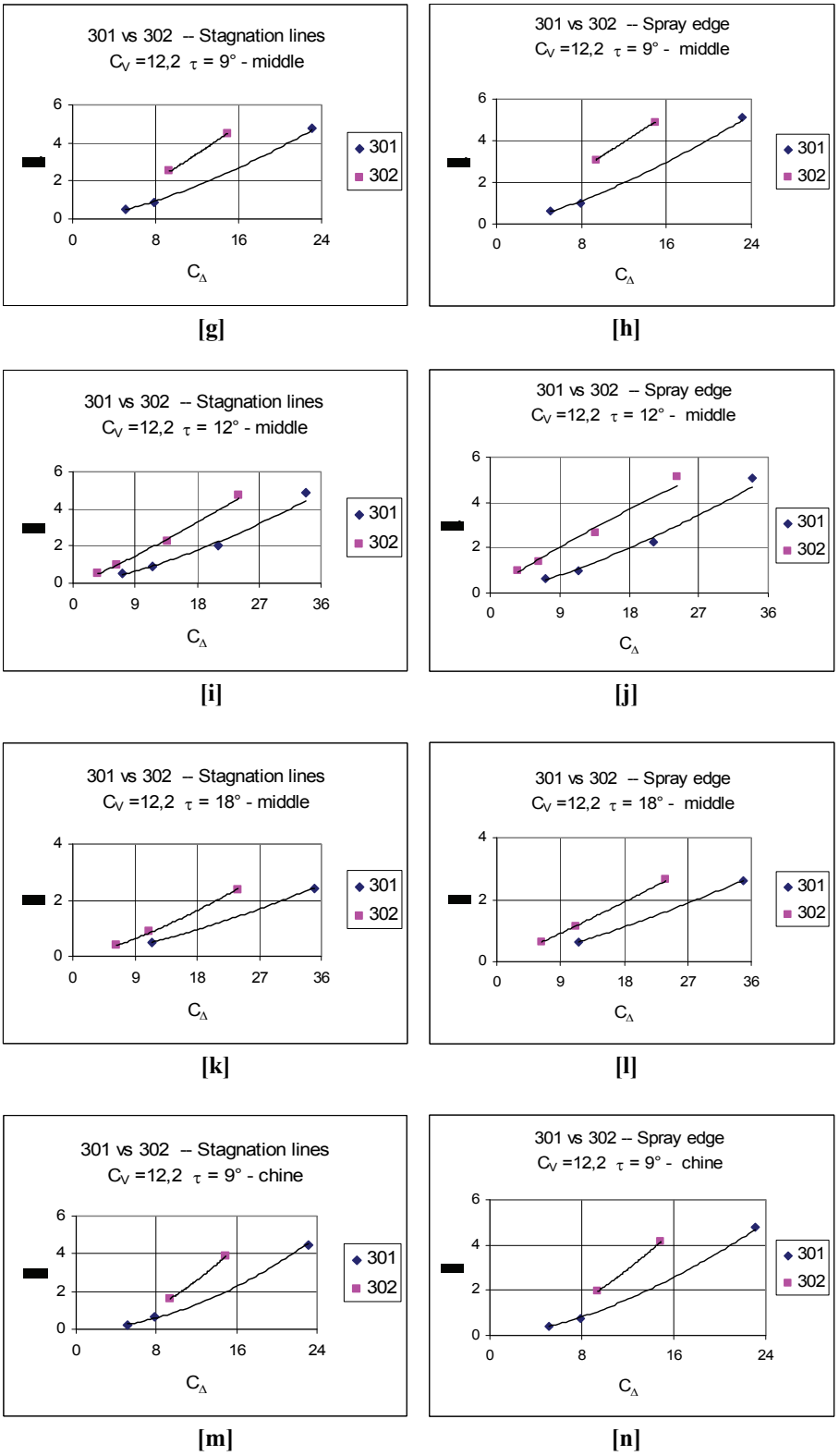

Figure 9.8-9 Deadrise angle effects on stagnation and spray edge lines for V-bottom planing surface without horizontal chine flared and with CV = 12.2 (continue)

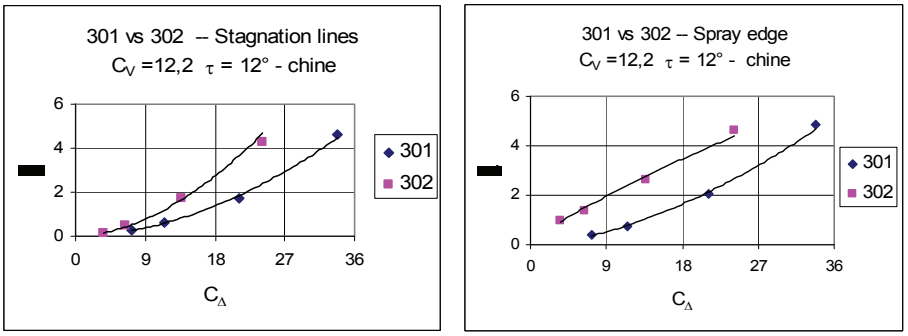

[o]

[p]

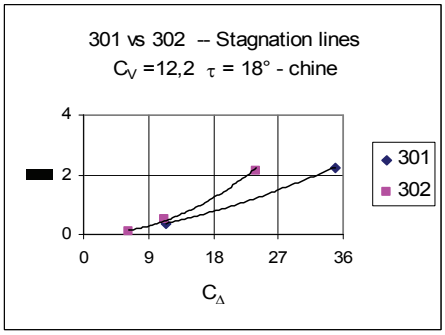

[q]

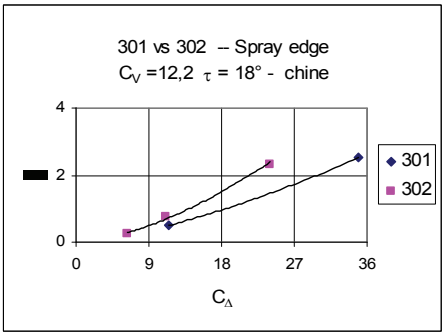

[r]

(Data source: [Kapryan & Boyd 1955])

Figure 9.8-9 Deadrise angle effects on stagnation and spray edge lines for V-bottom planing surface without horizontal chine flared and with CV = 12.2

9.8.10 Stagnation and Spray Edges Lines Position λ vs C_Δ, with Horizontal Chine Flared and $C_V = 12.2$

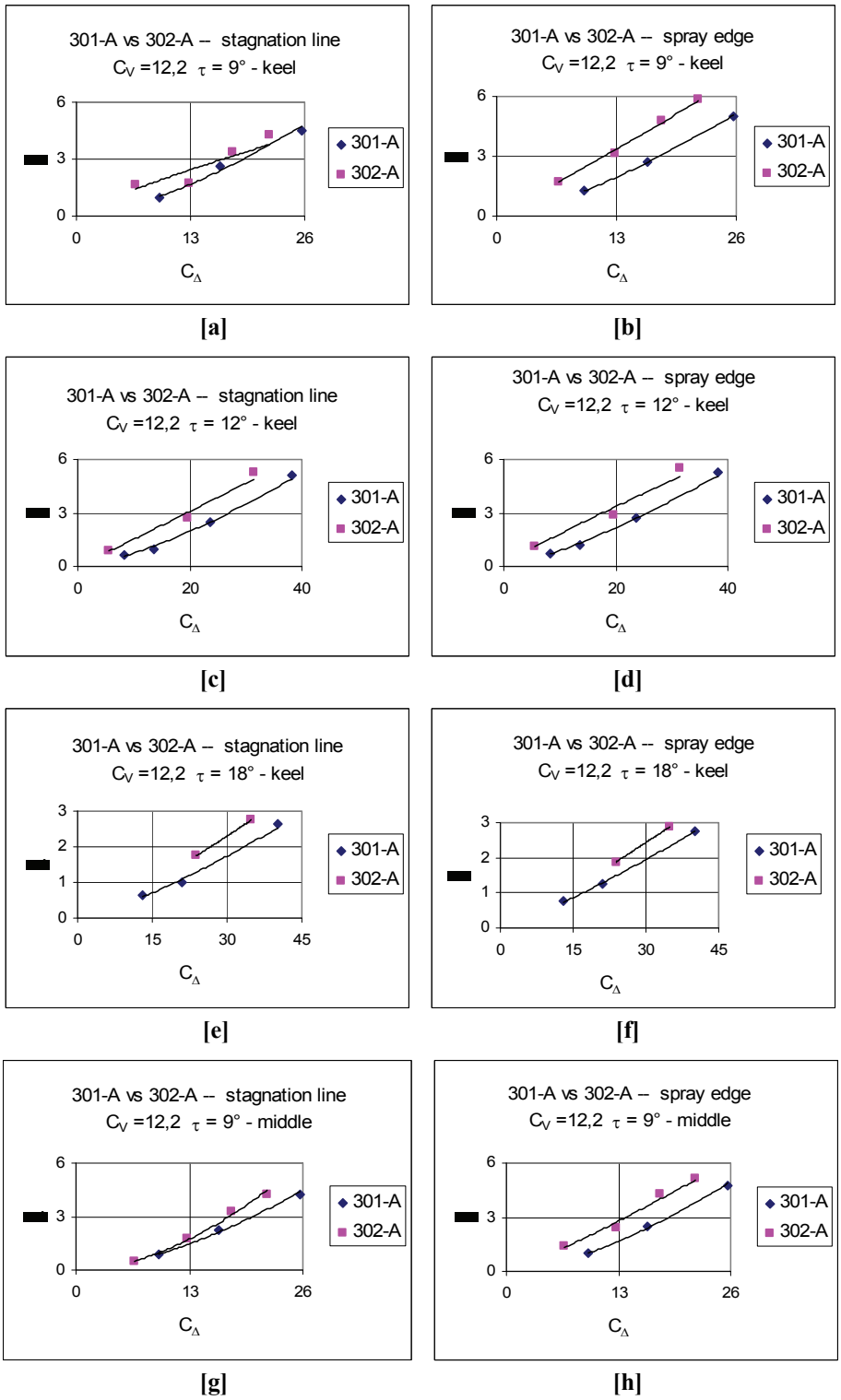

Figure 9.8-10 Deadrise angle effects on stagnation and spray edge lines for V-bottom planing surface with horizontal chine flared and $C_V = 12.2$ (continue)

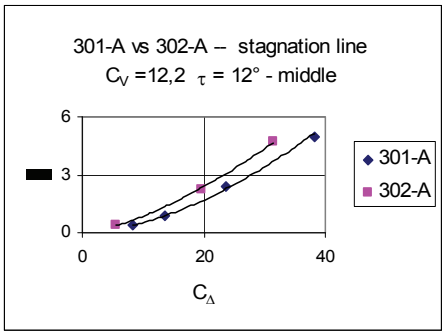

[i]

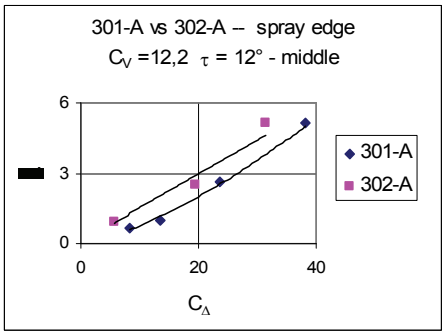

[j]

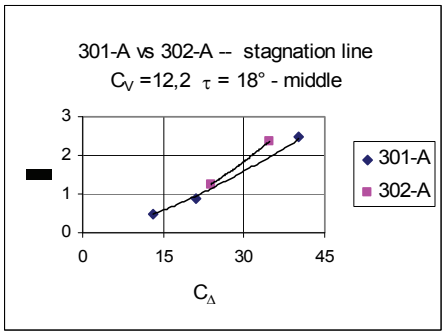

[k]

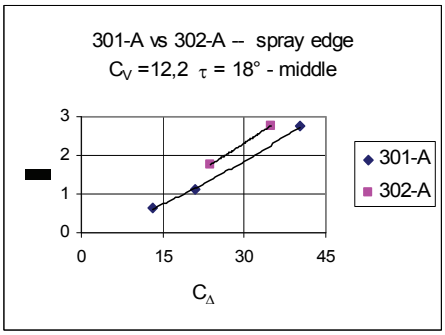

[l]

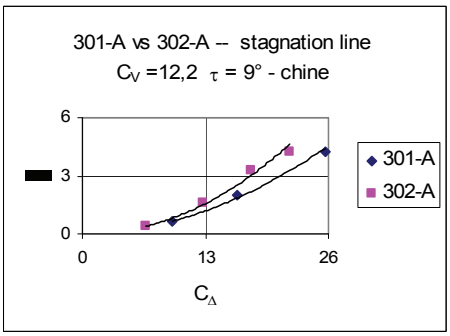

[m]

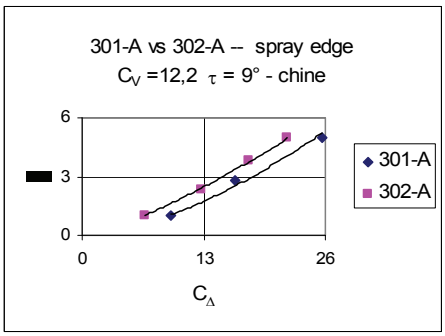

[n]

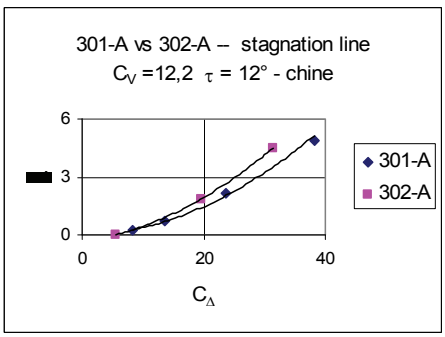

[o]

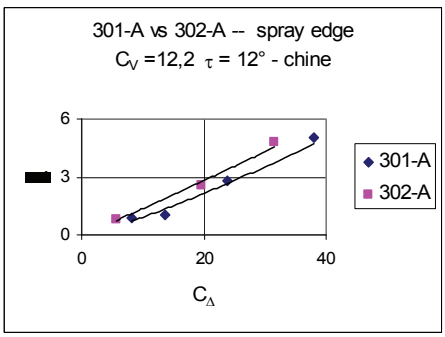

[p]

Figure 9.8-10 Deadrise angle effects on stagnation and spray edge lines for V-bottom planing surface with horizontal chine flared and CV = 12.2 (continue)

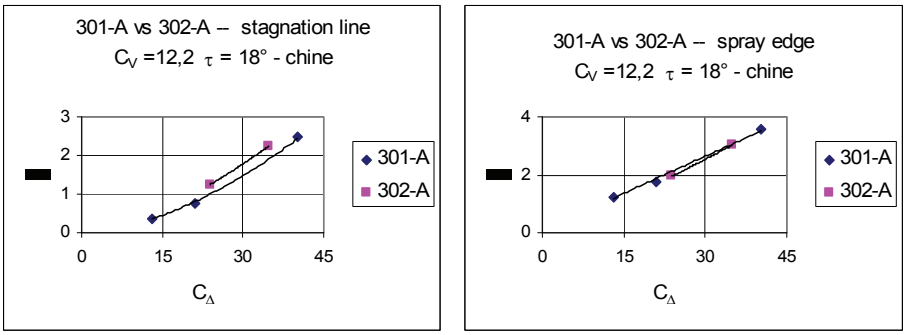

[q] **[r]**

(Data source: [Kapryan & Boyd 1955])

Figure 9.8-10 Deadrise angle effects on stagnation and spray edge lines for V-bottom planing surface with horizontal chine flared and CV = 12.2

9.8.11 Stagnation and Spray Edges Lines Position λ vs C_{Lb} without Horizontal Chine Flared

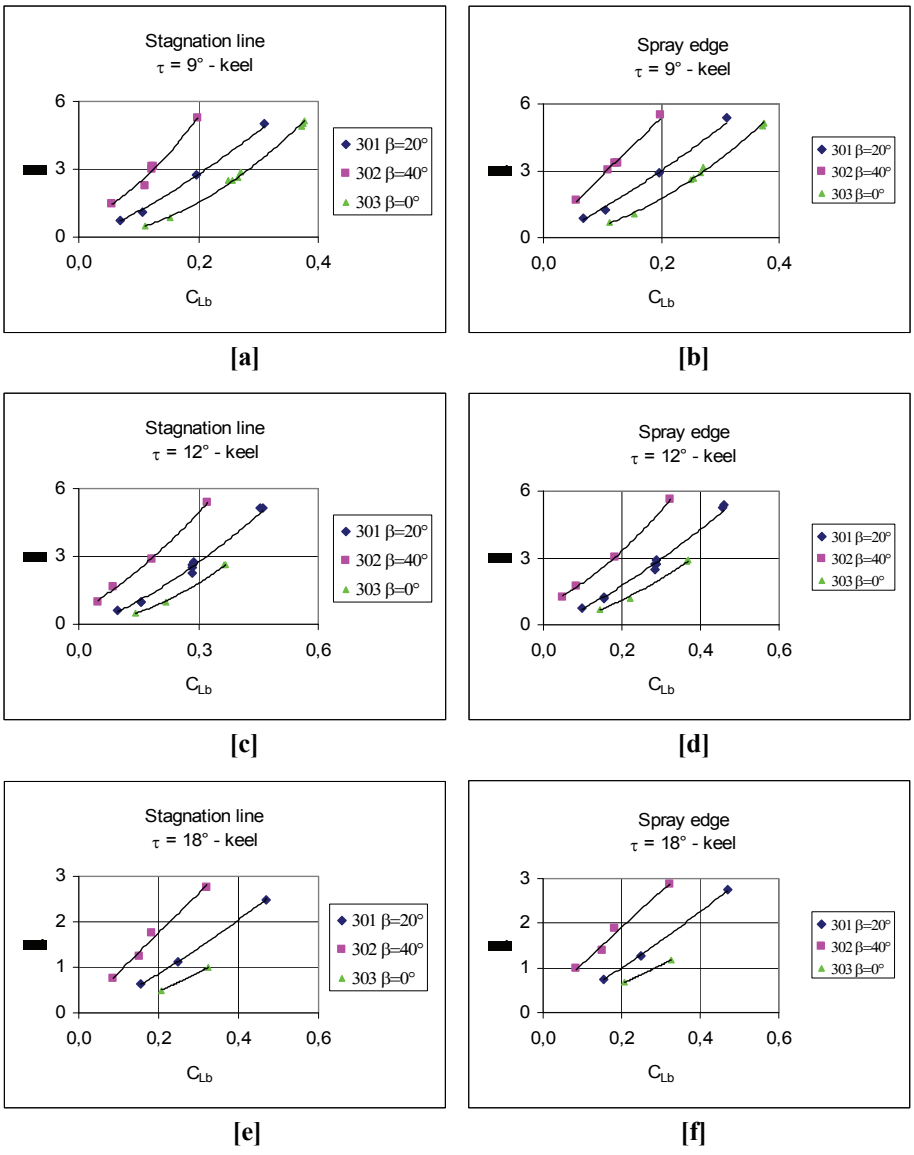

Figure 9.8-11 Deadrise angle effects on stagnation and spray edge lines for V-bottom planing surface without horizontal chine flared (continue)

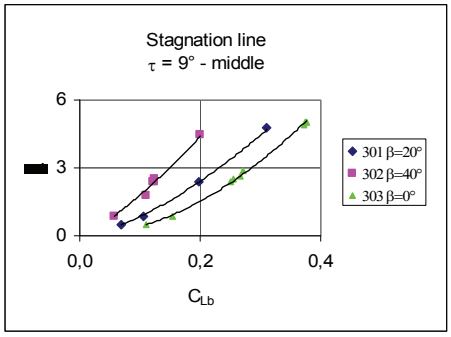

[g]

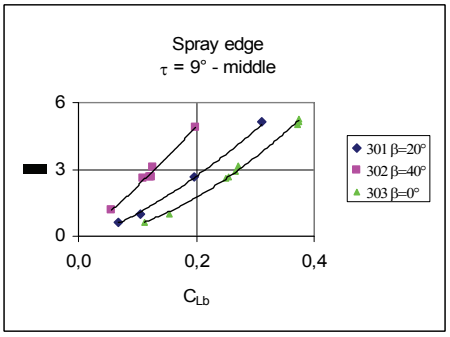

[h]

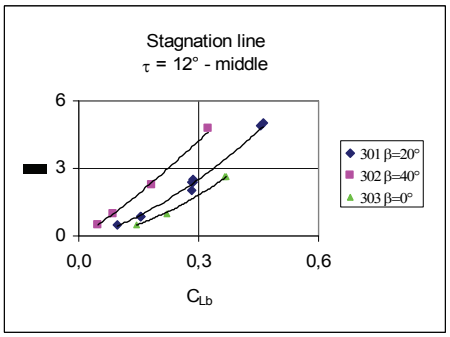

[i]

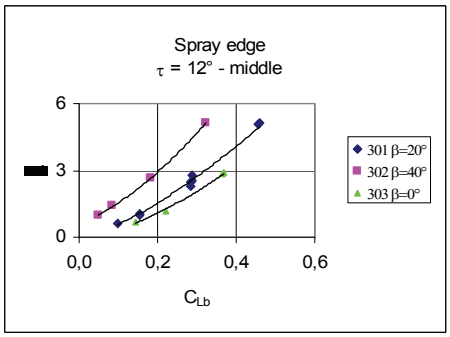

[j]

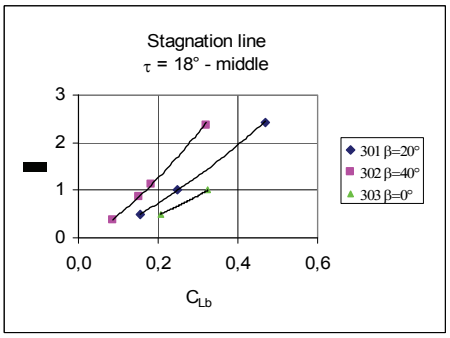

[k]

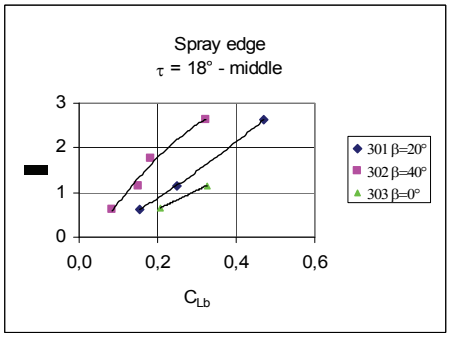

[l]

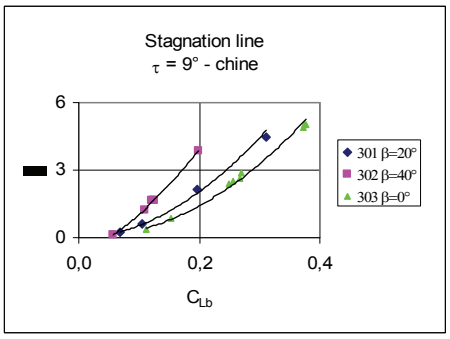

[m]

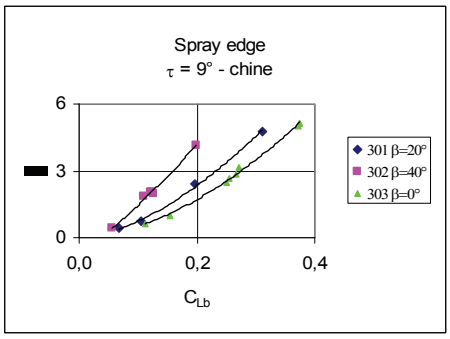

[n]

Figure 9.8-11 Deadrise angle effects on stagnation and spray edge lines for V-bottom planing surface without horizontal chine flared (continue)

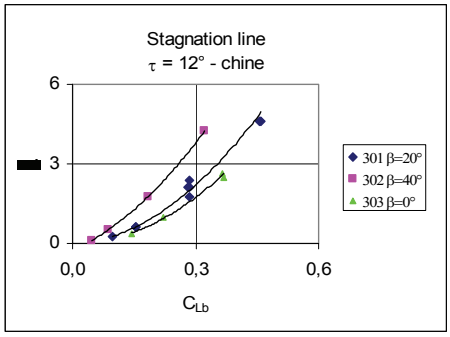

[o]

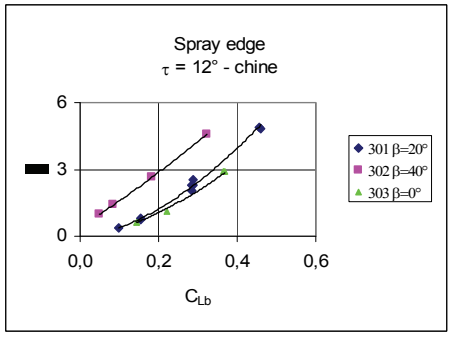

[p]

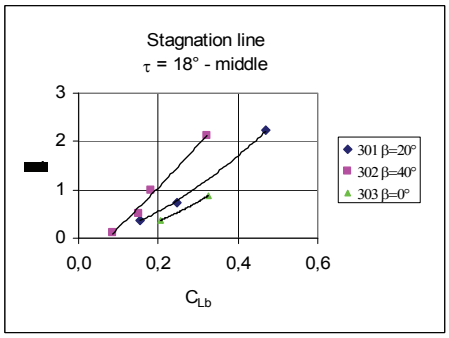

[q]

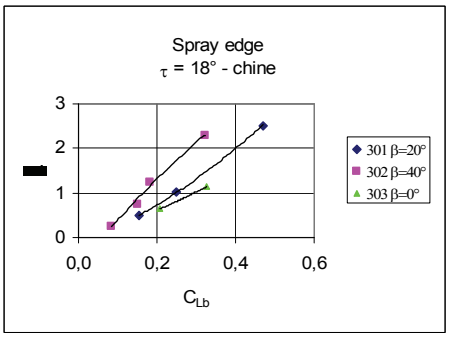

[r]

(Data source: [Kapryan & Boyd 1955])

Figure 9.8-11 Deadrise angle effects on stagnation and spray edge lines for V-bottom planing surface without horizontal chine flared

9.8.12 Stagnation and Spray Edges Lines Position λ vs C_{Lb} with Horizontal Chine Flared

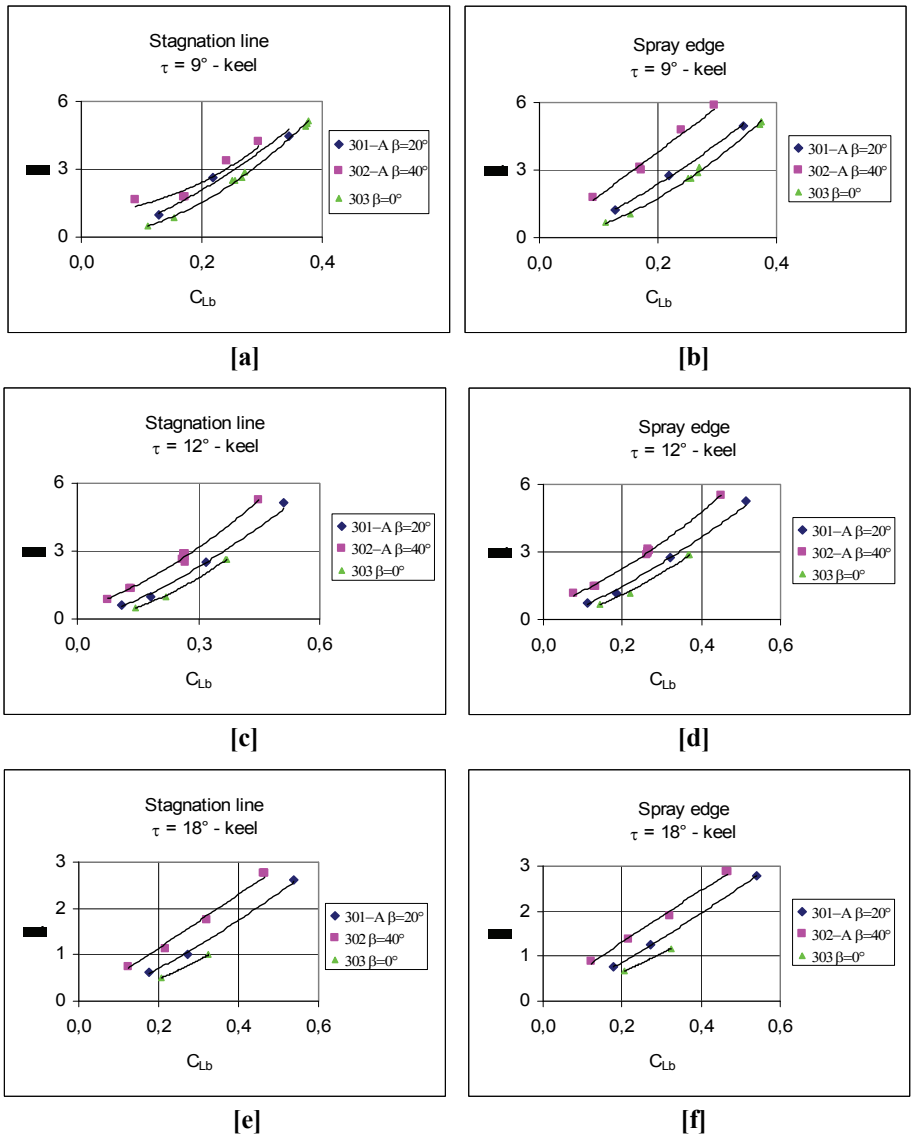

Figure 9.8-12 Deadrise angle effects on stagnation and spray edge lines for V-bottom planing surface with horizontal chine flared (continue)

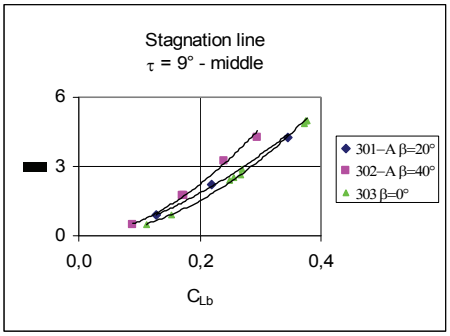

[g]

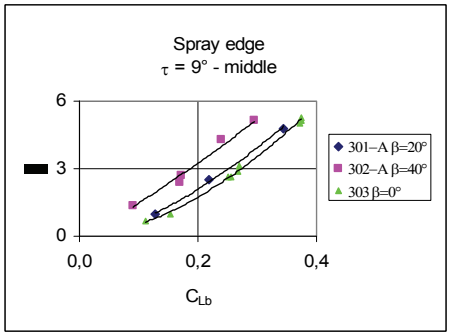

[h]

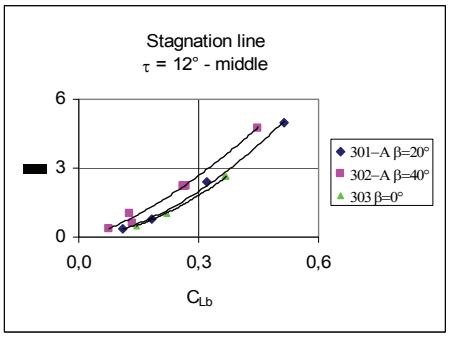

[i]

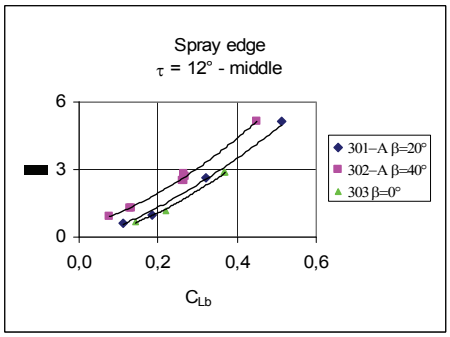

[j]

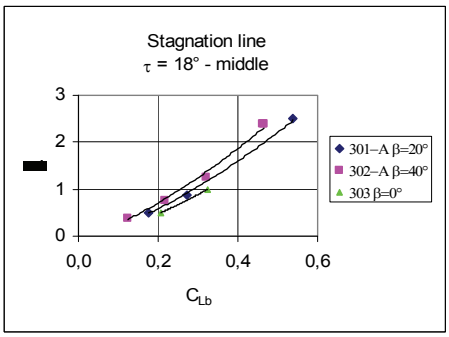

[k]

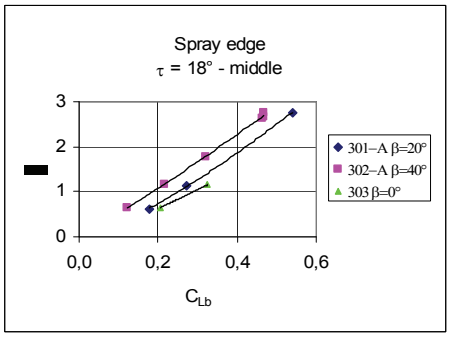

[l]

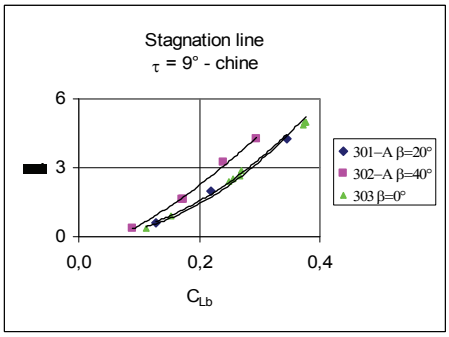

[m]

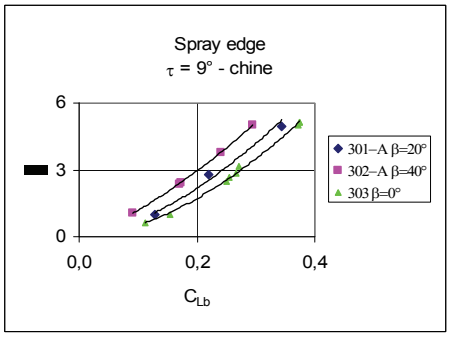

[n]

Figure 9.8-12 Deadrise angle effects on stagnation and spray edge lines for V-bottom planing surface with horizontal chine flared (continue)

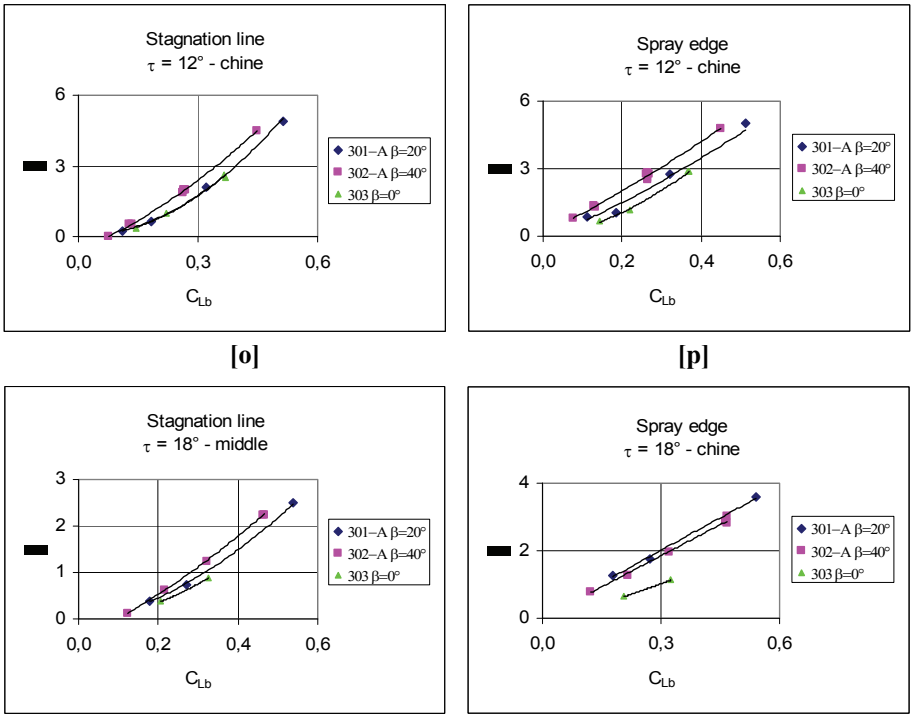

[o] **[p]**

[q] **[r]**

(Data source: [Kapryan & Boyd 1955])

Figure 9.8-12 Deadrise angle effects on stagnation and spray edge lines for V-bottom planing surface with horizontal chine flared

9.9 Diagrams: Horizontal Chine Effects

9.9.1 Mean Wetted Length Ratio $\frac{l_m}{b}$ vs C_Δ with $\beta = 20°$ and $C_V = 12.2$

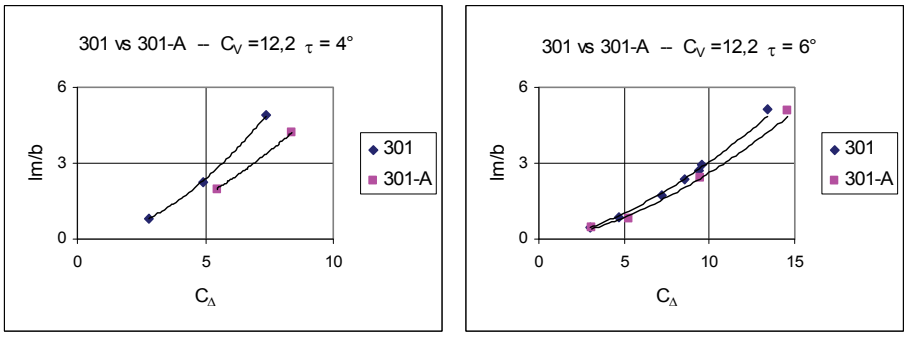

Figure 9.9-1 Effect of horizontal chine flared angle on mean wetted line ratio trend for prismatic planing surfaces with deadrise angle β = 20° and C_V = 12.2 (continue)

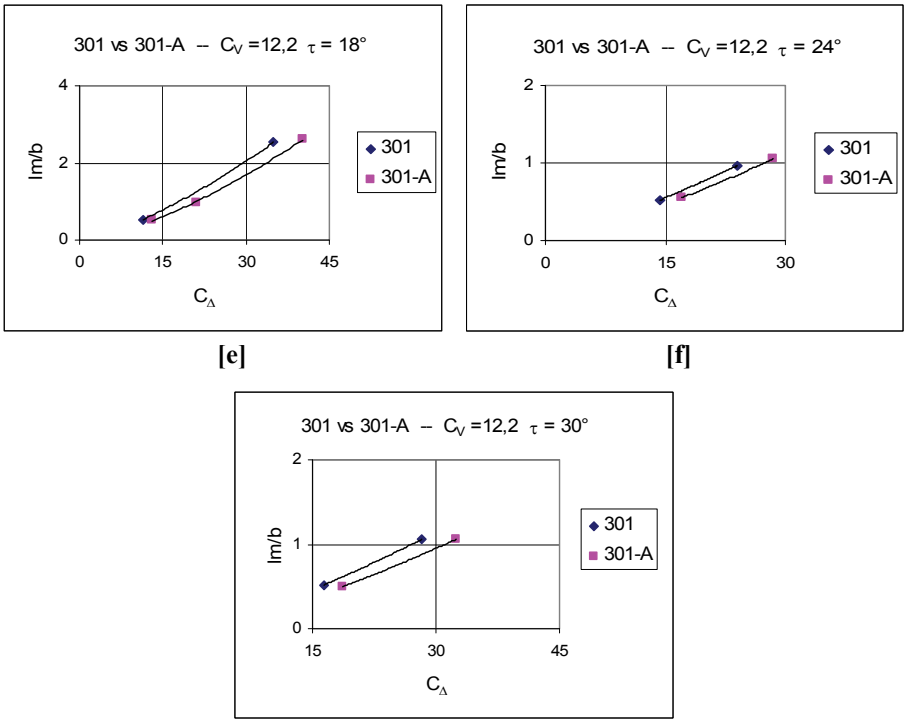

[e] **[f]**

[g]

(Data source: [Kapryan & Boyd 1955])

Figure 9.9-1 Effect of horizontal chine flared angle on mean wetted line ratio trend for prismatic planing surfaces with deadrise angle $\beta = 20°$ and $C_V = 12.2$

9.9.2 Mean Wetted Length Ratio $\frac{l_m}{b}$ vs C_V with $\beta = 20°$

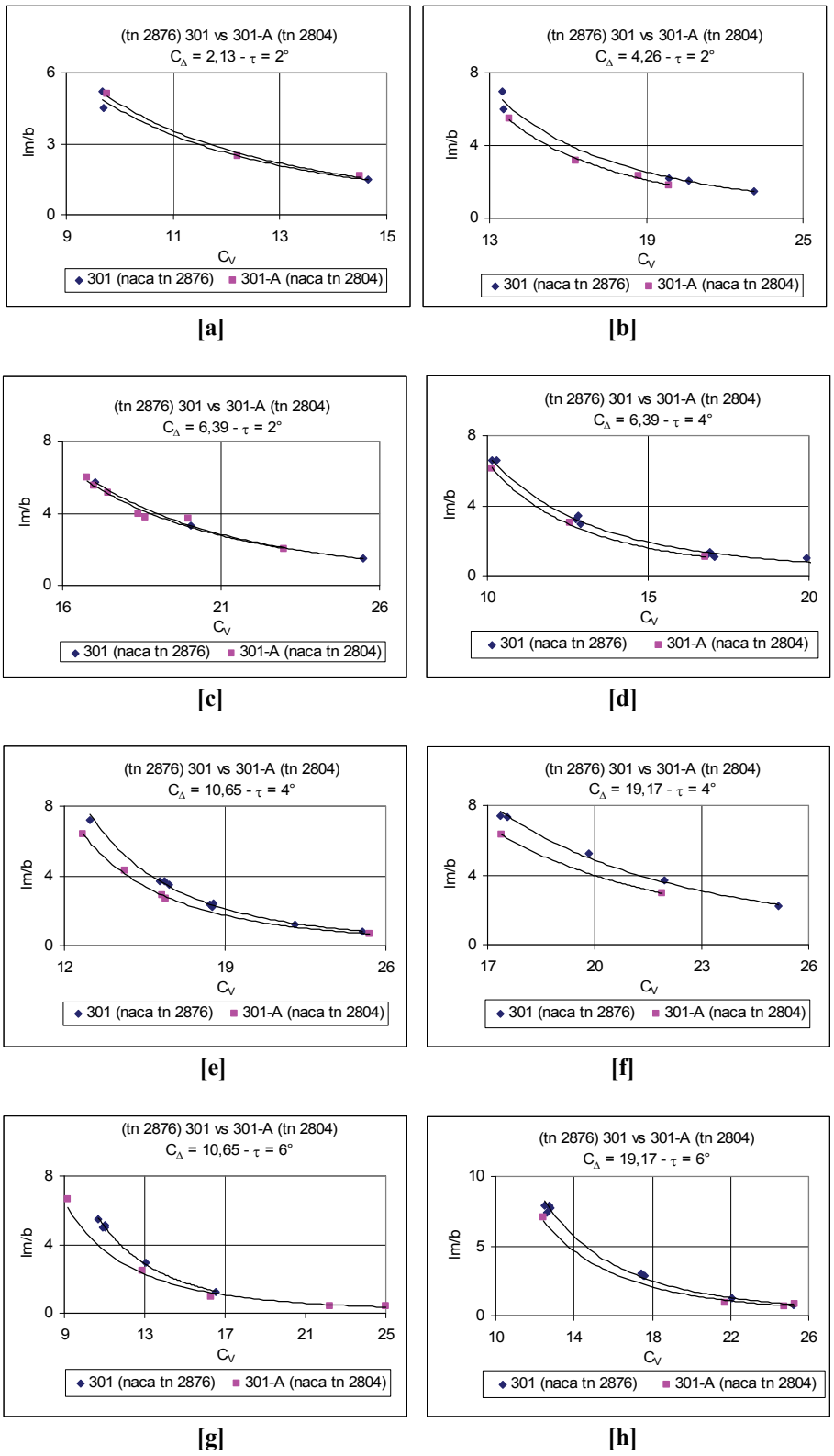

Figure 9.9-2 Effect of horizontal chine flared angle on mean wetted line ratio trend for prismatic planing surfaces with deadrise angle β = 20°
(continue)

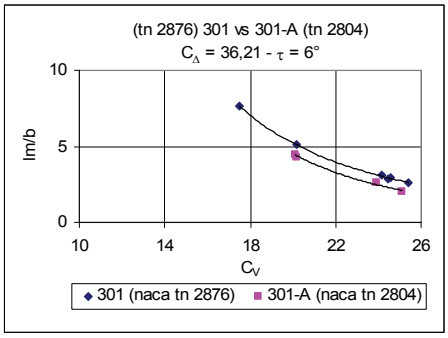

[i]

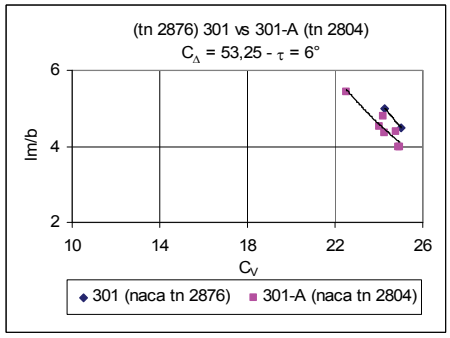

[j]

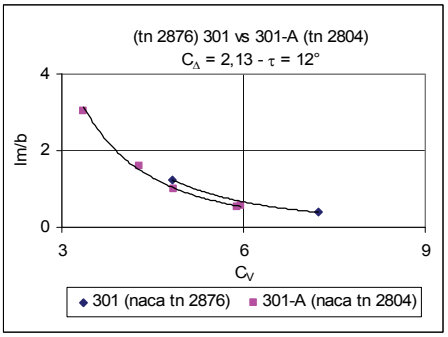

[k]

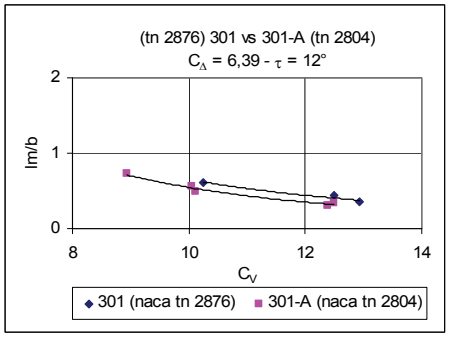

[l]

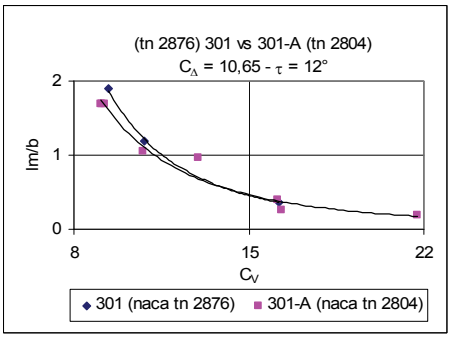

[m]

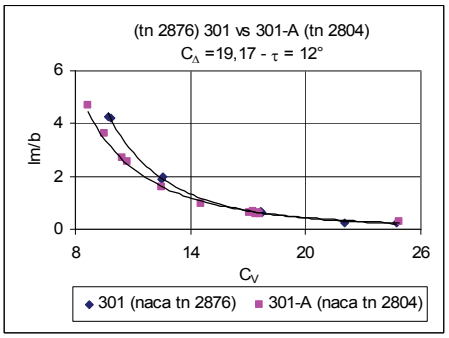

[n]

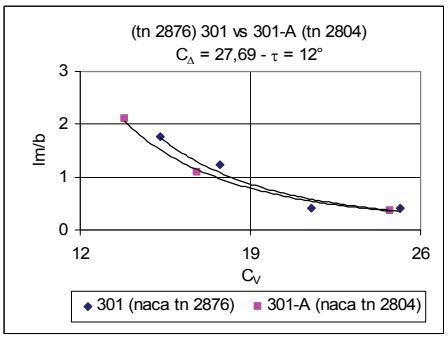

[o]

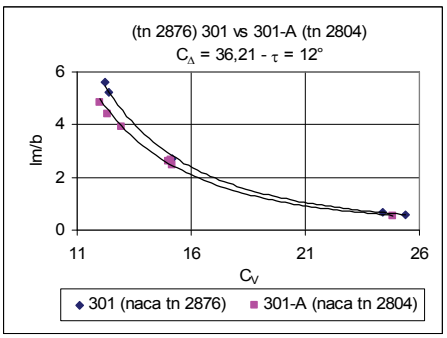

[p]

Figure 9.9-2 Effect of horizontal chine flared angle on mean wetted line ratio trend for prismatic planing surfaces with deadrise angle β = 20° (continue)

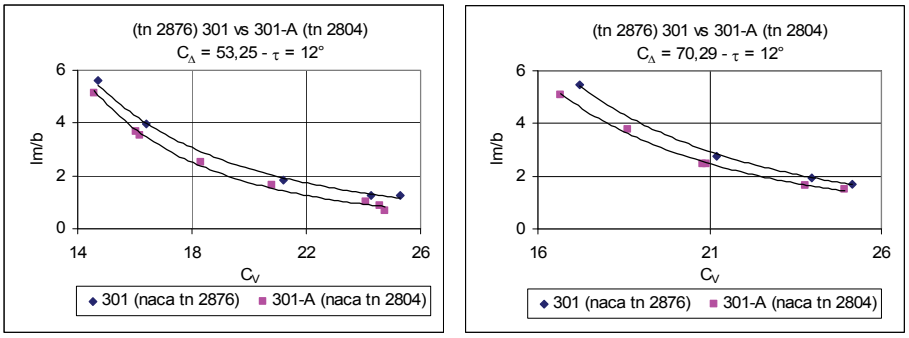

[q]

[r]

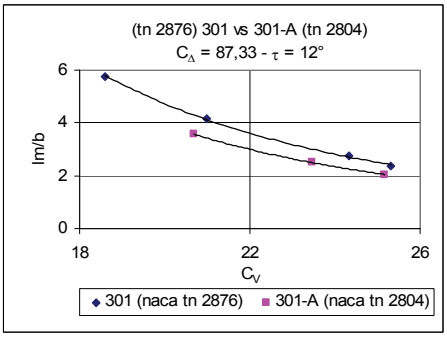

[s]

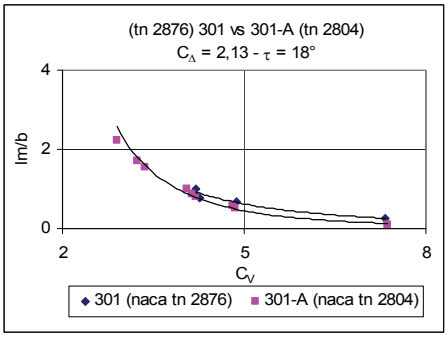

[t]

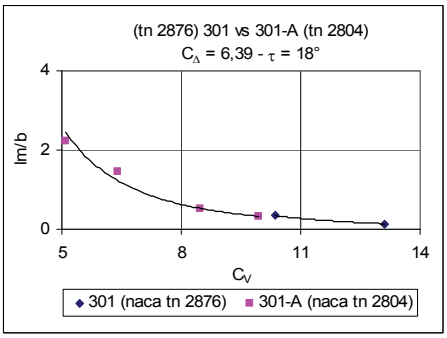

[u]

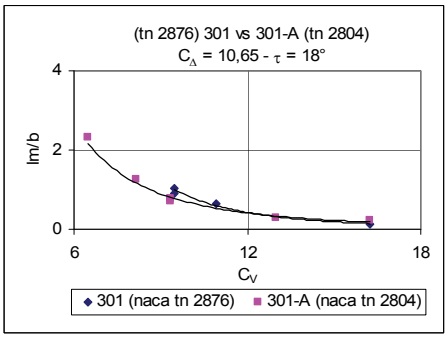

[v]

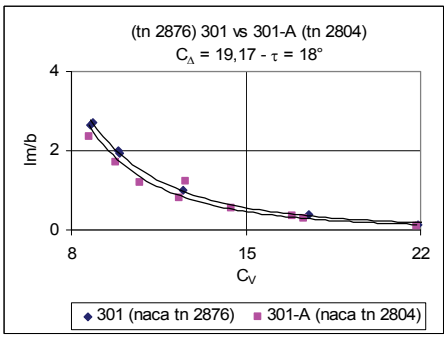

[w]

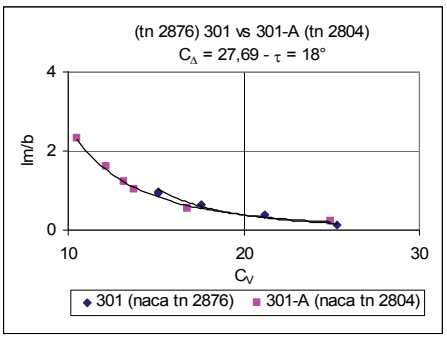

[x]

Figure 9.9-2 Effect of horizontal chine flared angle on mean wetted line ratio trend for prismatic planing surfaces with deadrise angle β = 20° (continue)

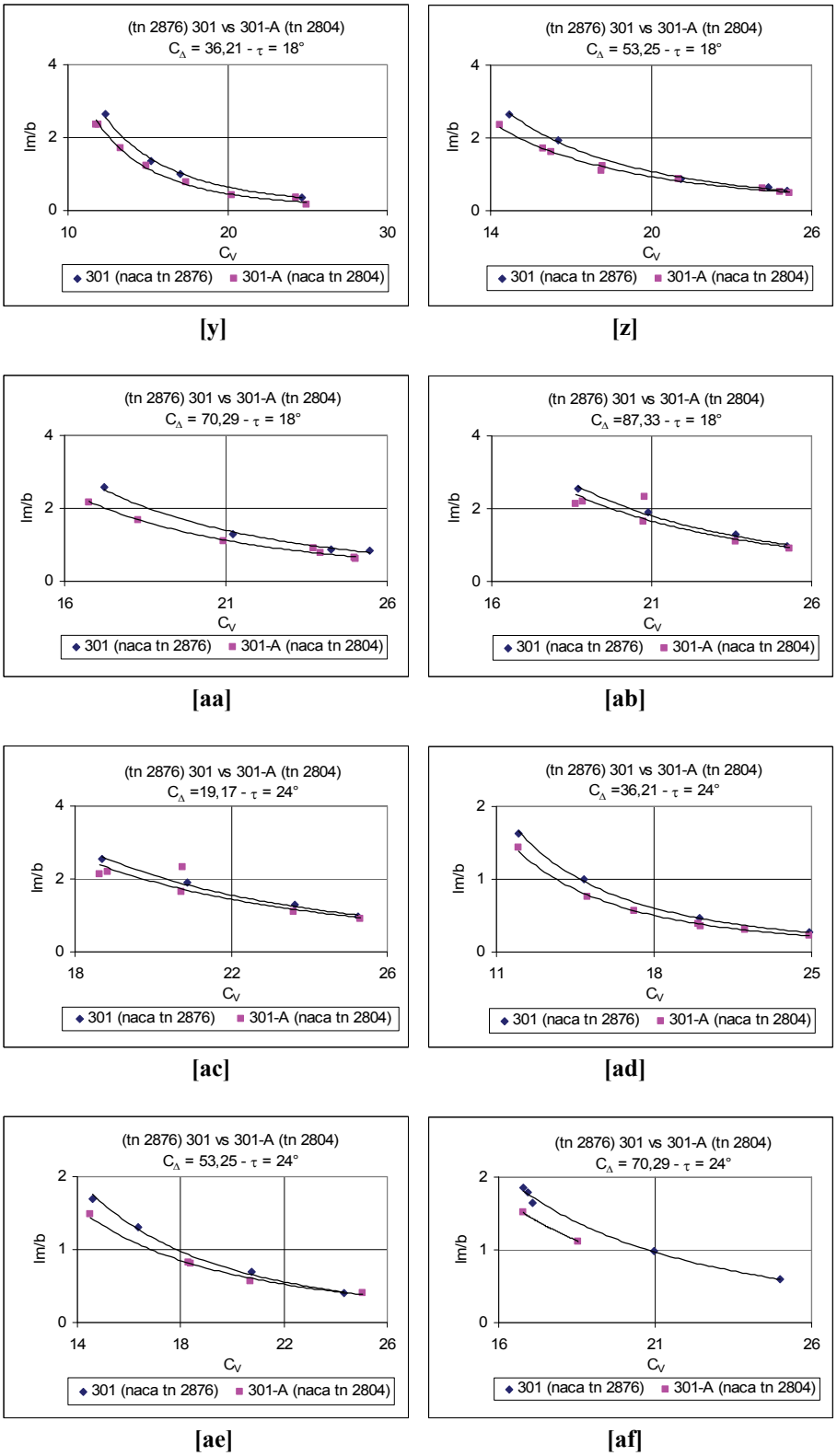

Figure 9.9-2 Effect of horizontal chine flared angle on mean wetted line ratio trend for prismatic planing surfaces with deadrise angle β = 20° (continue)

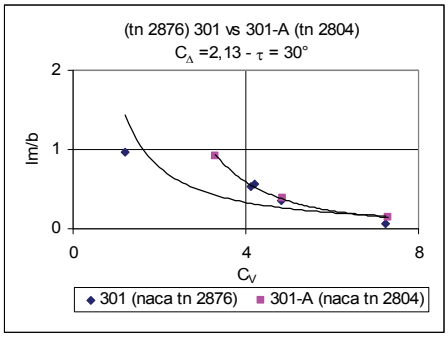

[ag]

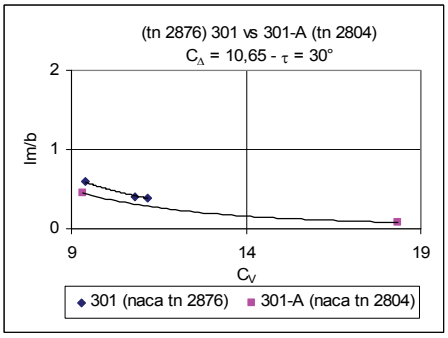

[ah]

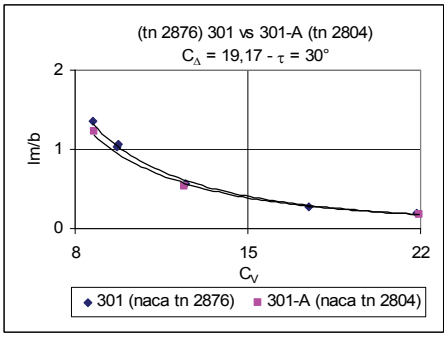

[ai]

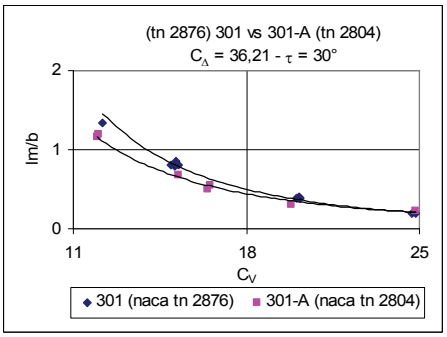

[aj]

(Data sources: [Kapryan & Weinstein 1952] and [Chambliss & Boyd 1953])

Figure 9.9-2 Effect of horizontal chine flared angle on mean wetted line ratio trend for prismatic planing surfaces with deadrise angle β = 20°

9.9.3 Mean wetted length ratio $\frac{l_m}{b}$ vs C_{Lb} with $\beta = 20°$

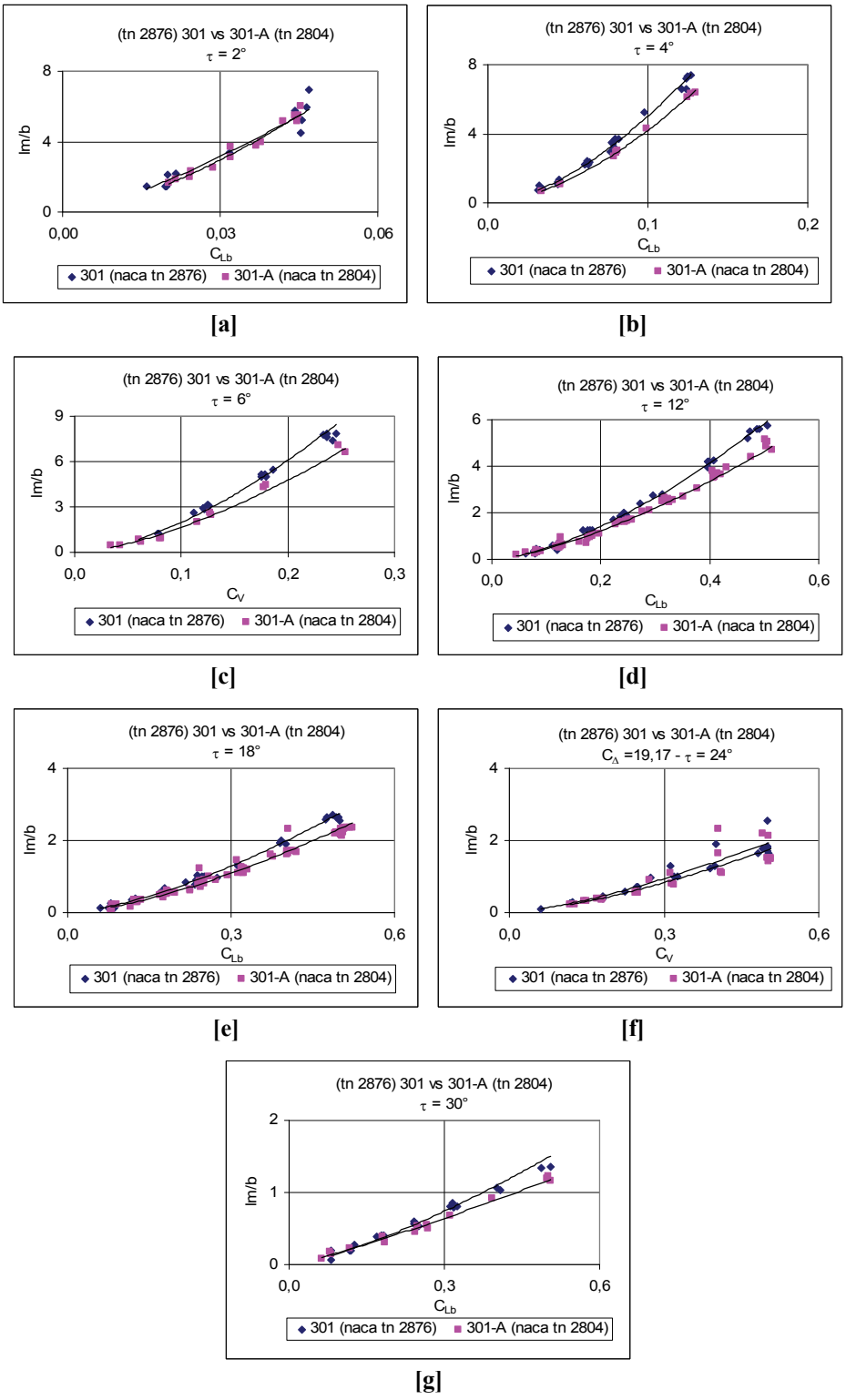

(Data sources: [Kapryan & Weinstein 1952] and [Chambliss & Boyd 1953])

Figure 9.9-3 Effect of horizontal chine flared on mean wetted line ratio trend for V-bottom surfaces with deadrise angle β = 20°

9.9.4 Mean Wetted Length Ratio $\frac{l_m}{b}$ vs C_Δ with $\beta = 40°$ and $C_V = 12.2$

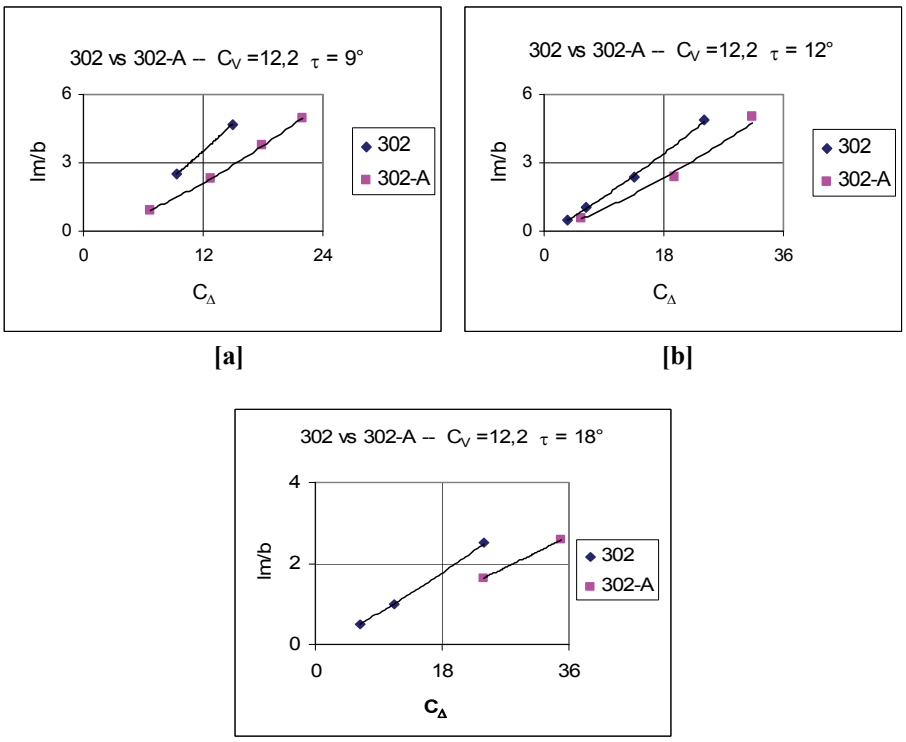

[a] **[b]**

[c]

(Data source: [Kapryan & Boyd 1955])

Figure 9.9-4 Effect of horizontal chine flared angle on mean wetted line ratio trend for prismatic planing surfaces with deadrise angle β = 40° and C_V = 12.2

9.9.5 Mean Wetted Length Ratio $\frac{l_m}{b}$ vs C_V with $\beta = 40°$

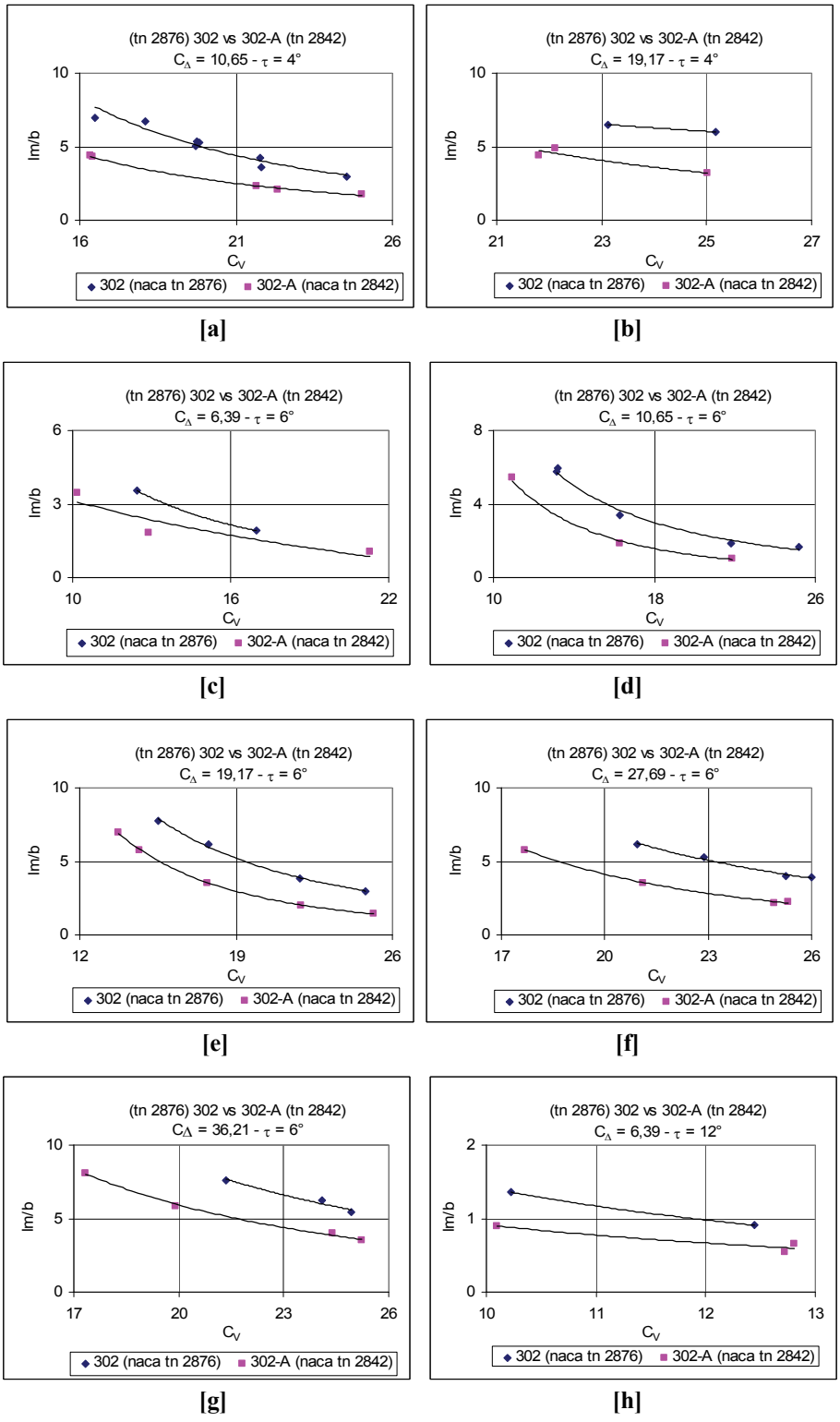

Figure 9.9-5 Effect of horizontal chine flared angle on mean wetted line ratio trend for prismatic planing surfaces with deadrise angle β = 40°
(continue)

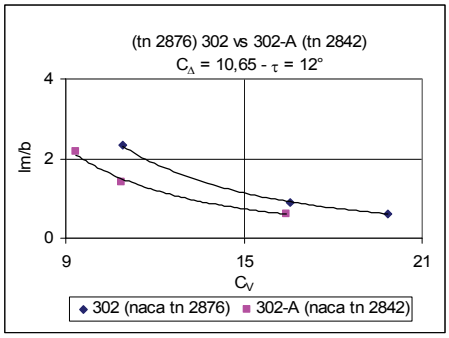

[i]

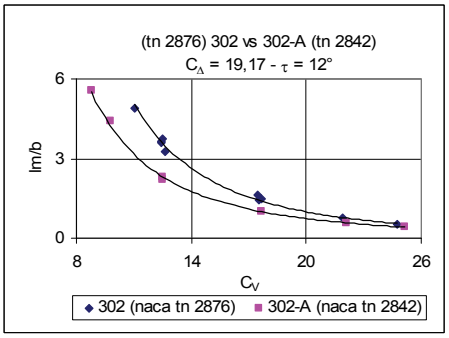

[j]

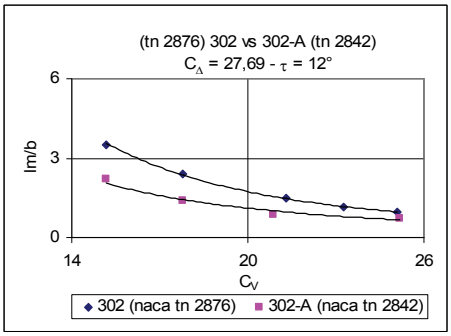

[k]

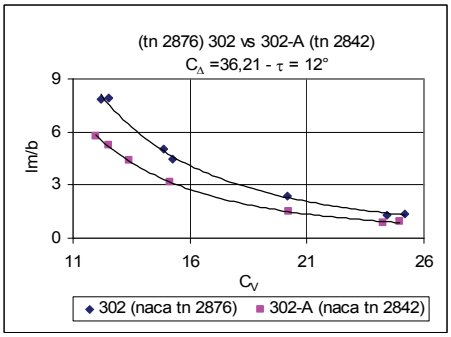

[l]

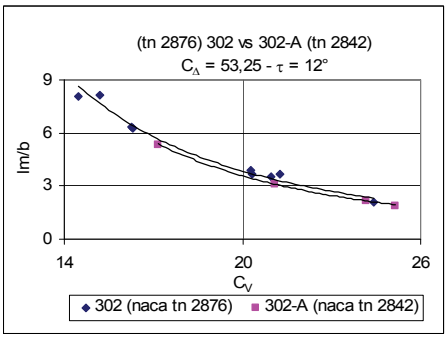

[m]

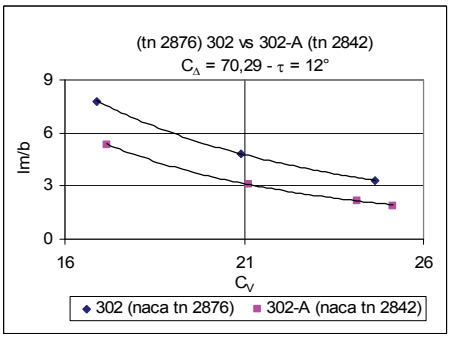

[n]

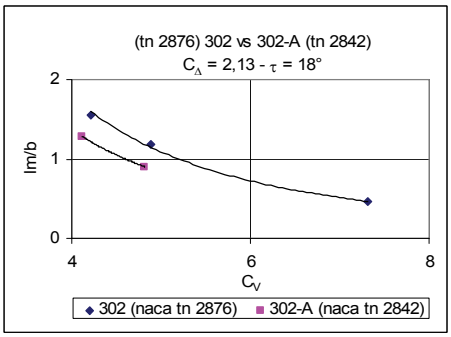

[o]

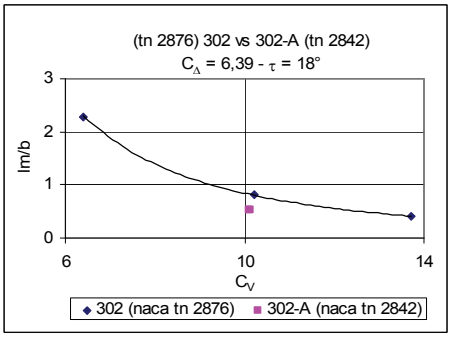

[p]

Figure 9.9-5 Effect of horizontal chine flared angle on mean wetted line ratio trend for prismatic planing surfaces with deadrise angle β = 40° (continue)

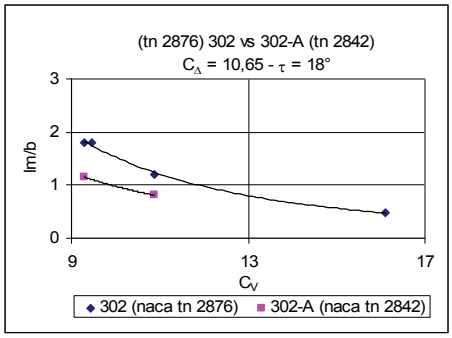

[q]

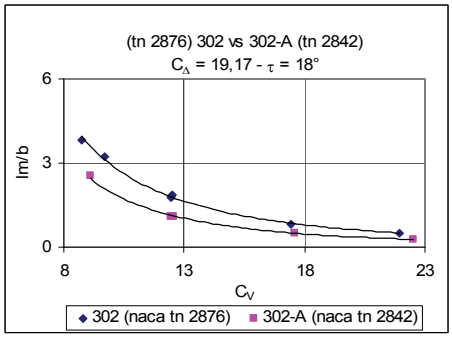

[r]

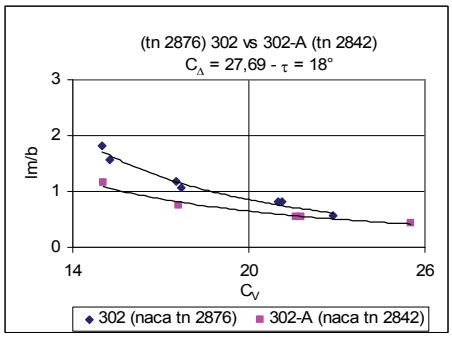

[s]

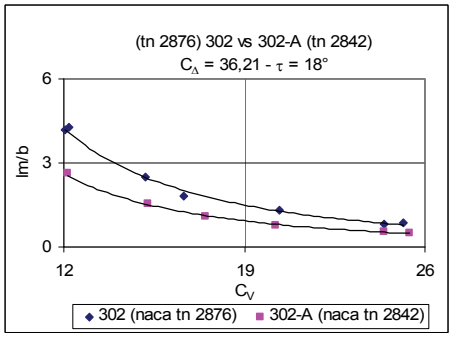

[t]

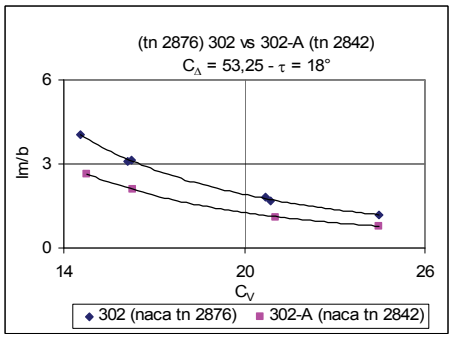

[u]

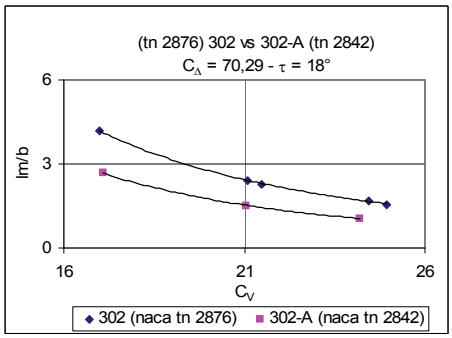

[v]

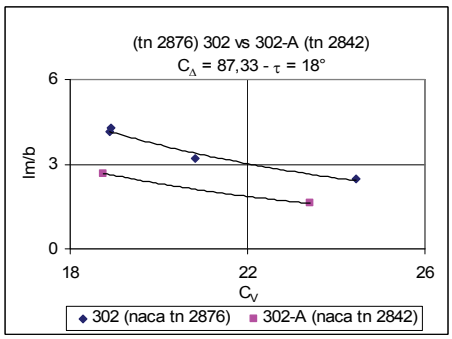

[w]

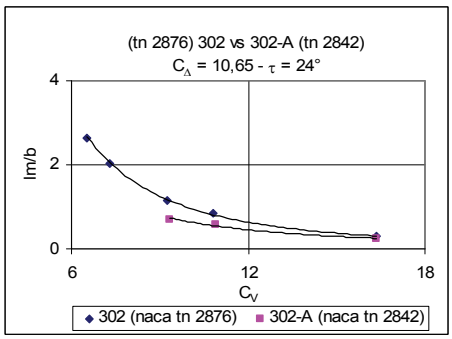

[x]

Figure 9.9-5 Effect of horizontal chine flared angle on mean wetted line ratio trend for prismatic planing surfaces with deadrise angle β = 40° (continue)

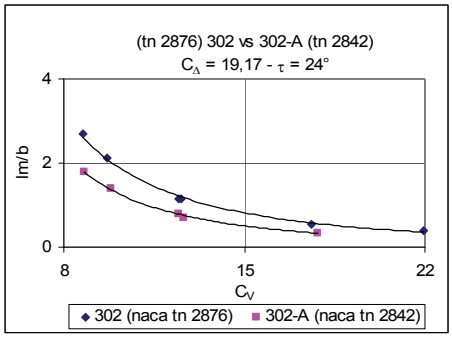

[y]

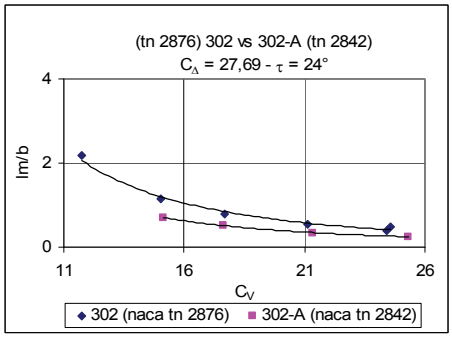

[z]

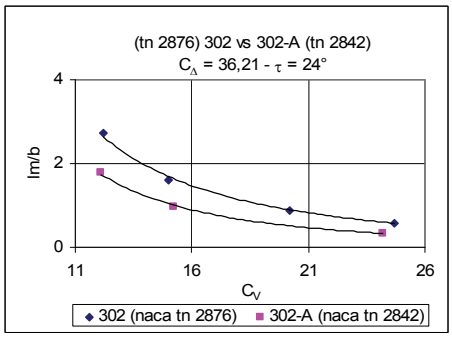

[aa]

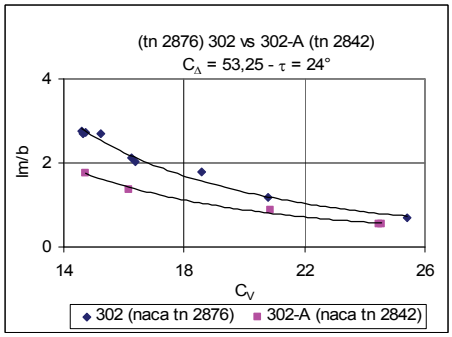

[ab]

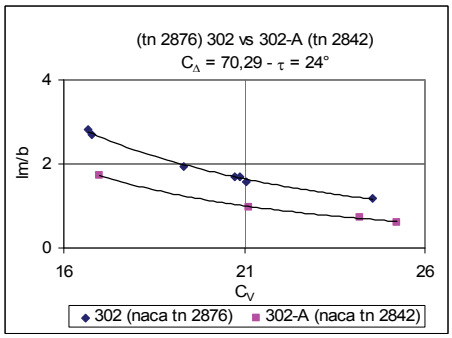

[ac]

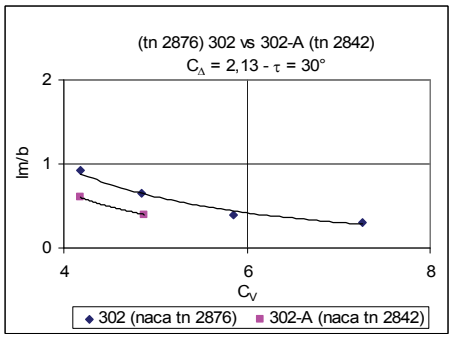

[ad]

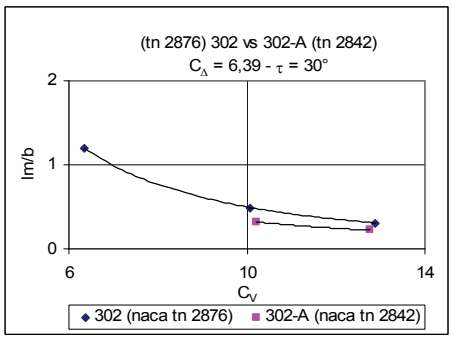

[ae]

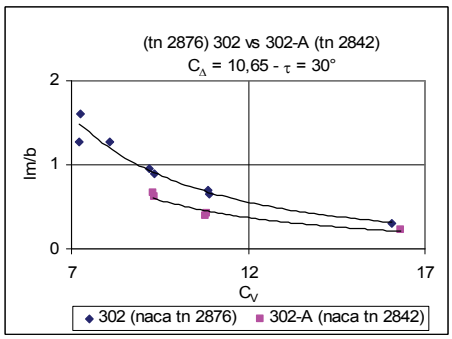

[af]

Figure 9.9-5 Effect of horizontal chine flared angle on mean wetted line ratio trend for prismatic planing surfaces with deadrise angle β = 40° (continue)

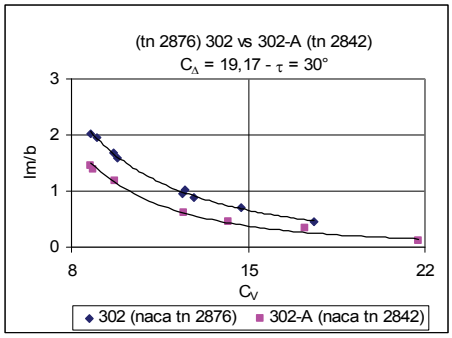

[ag]

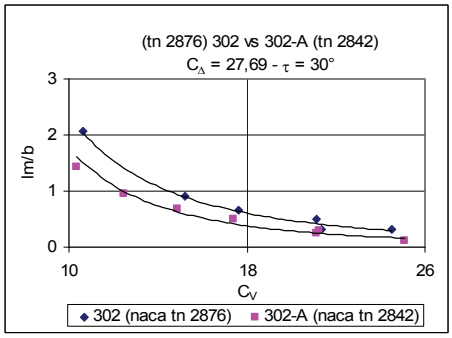

[ah]

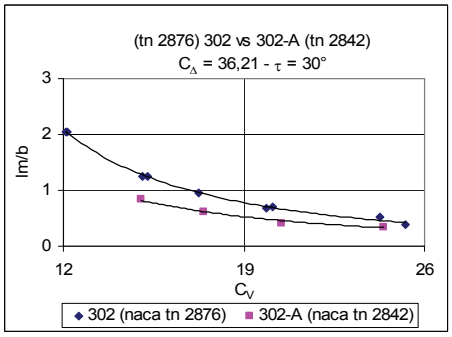

[ai]

(Data sources: [Blanchard 1952] and [Chambliss & Boyd 1953])

Figure 9.9-5 Effect of horizontal chine flared angle on mean wetted line ratio trend for prismatic planing surfaces with deadrise angle β = 40°

9.9.6 Mean Wetted Length Ratio $\frac{l_m}{b}$ vs C_{Lb} with $\beta = 40°$

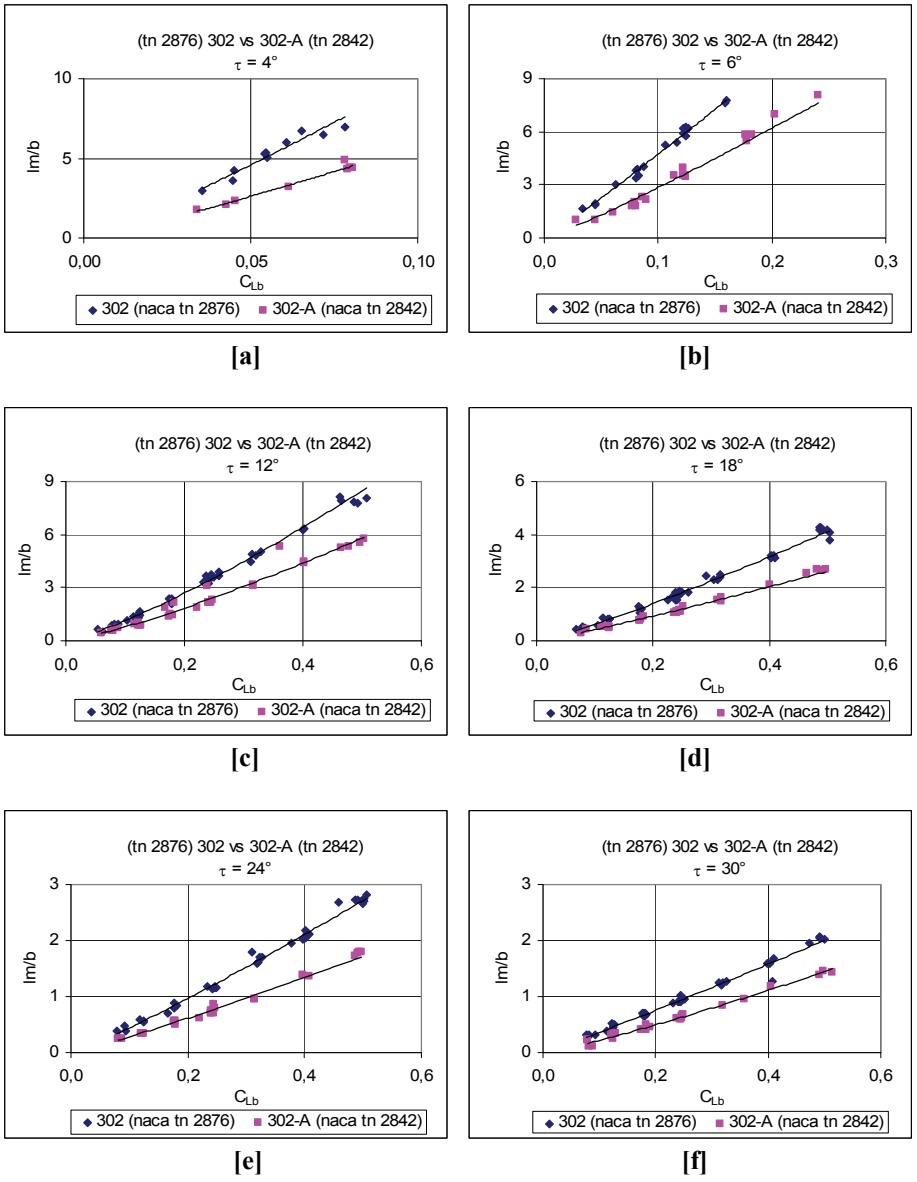

(Data sources: [Blanchard 1952] and [Chambliss & Boyd 1953])

Figure 9.9-6 Effect of horizontal chine flared on mean wetted line ratio trend for V-bottom planing surfaces with deadrise angle β = 40°

9.9.7 Center of Pressure: Longitudinal Position Ratio $\frac{l_p}{b}$ vs C_Δ with $\beta = 20°$ and $C_V = 12.2$

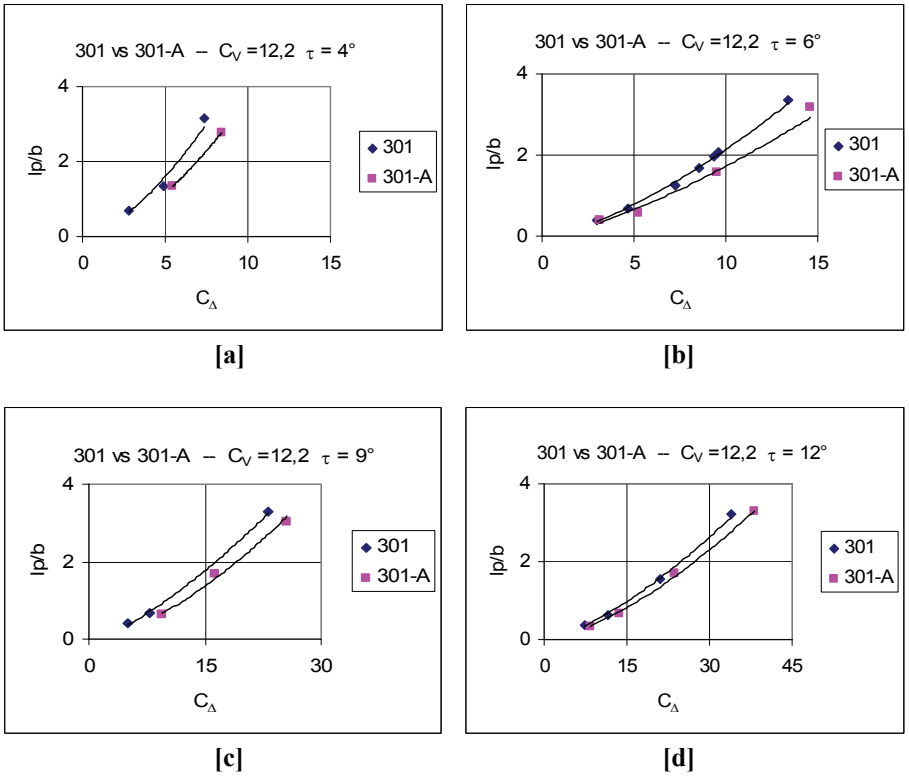

Figure 9.9-7 Effect of horizontal chine flared on longitudinal center pressure position for prismatic planing surfaces with deadrise angle β = 20° and C_V = 12.2 (continue)

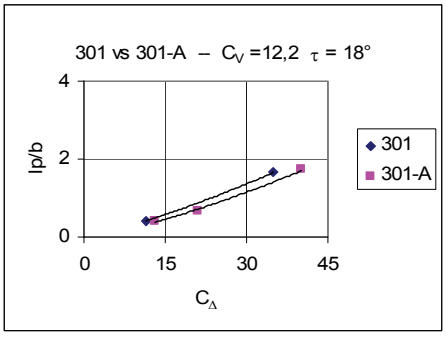

[e]

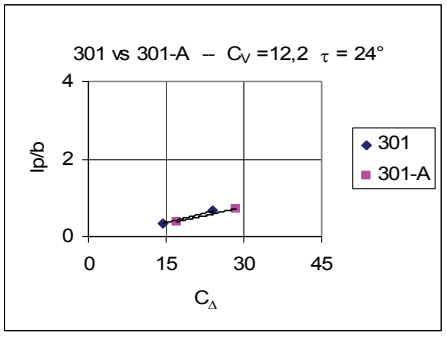

[f]

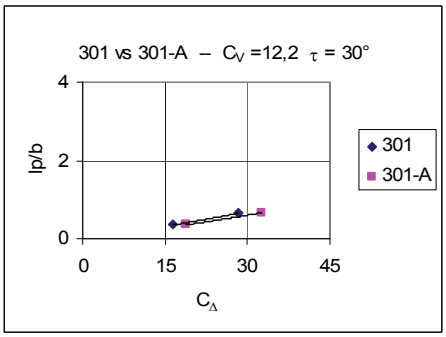

[g]

(Data source: [Kapryan & Boyd 1955])

Figure 9.9-7 Effect of horizontal chine flared on longitudinal center pressure position for prismatic planing surfaces with deadrise angle β = 20° and CV = 12.2

9.9.8 Center of Pressure: Longitudinal Position Ratio $\frac{l_p}{b}$ vs C_V with $\beta = 20°$

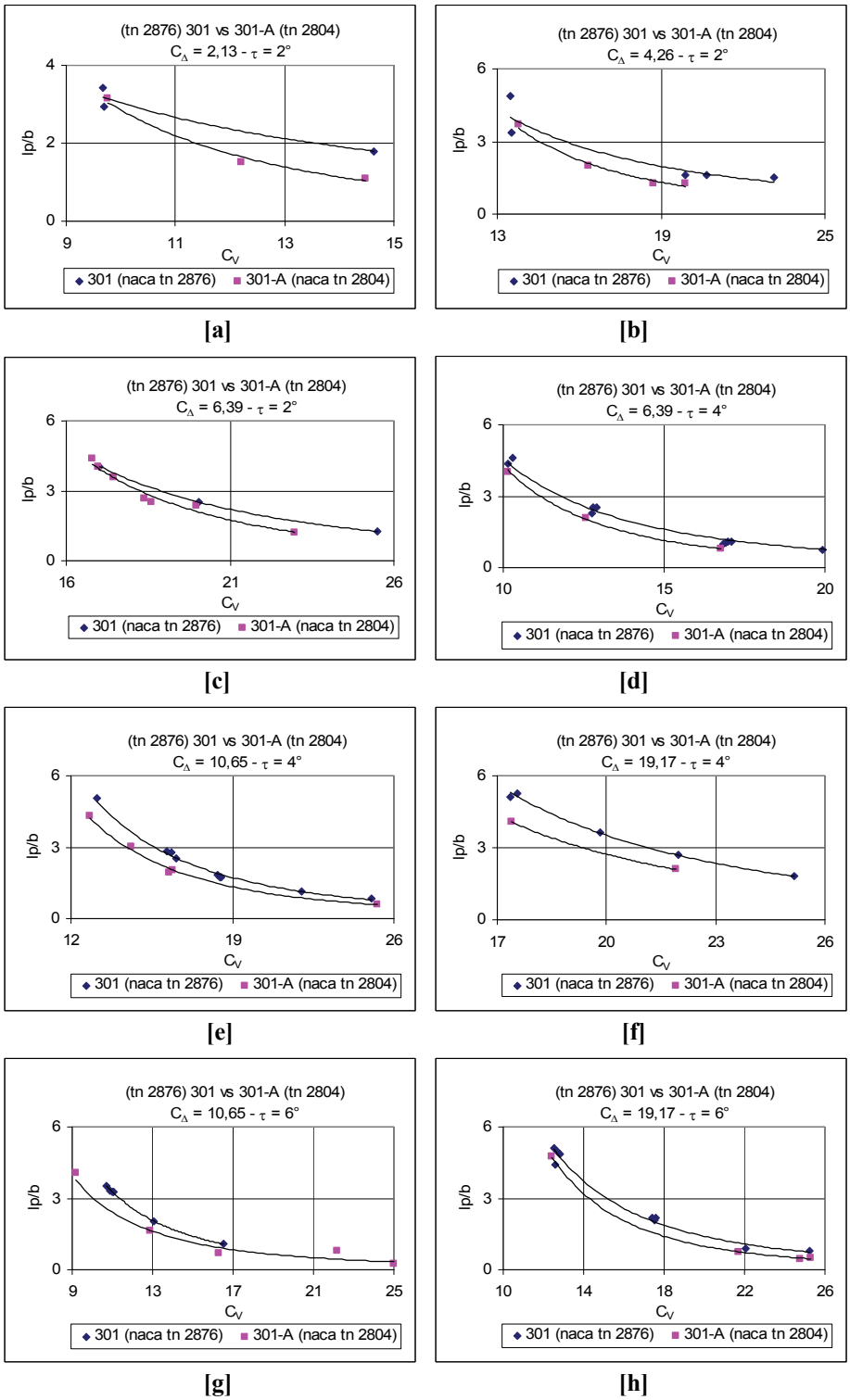

Figure 9.9-8 Effect of horizontal chine flared on longitudinal center pressure position for prismatic planing surfaces with deadrise angle β = 20° (continue)

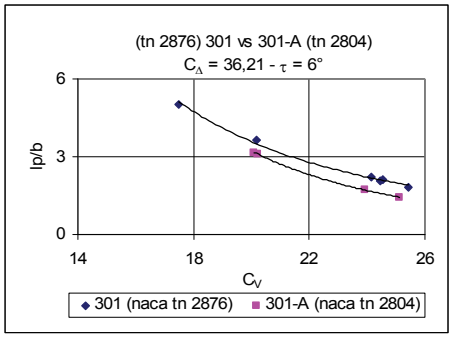

[i]

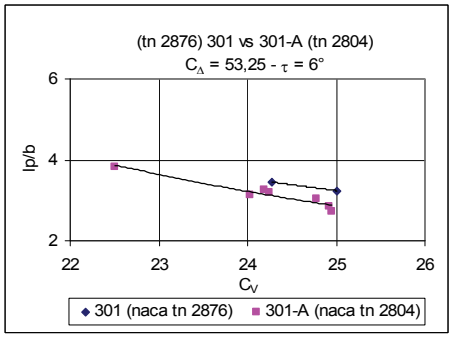

[j]

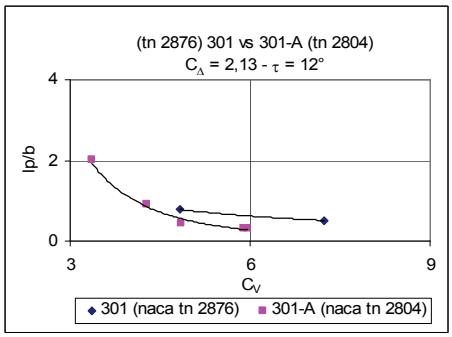

[k]

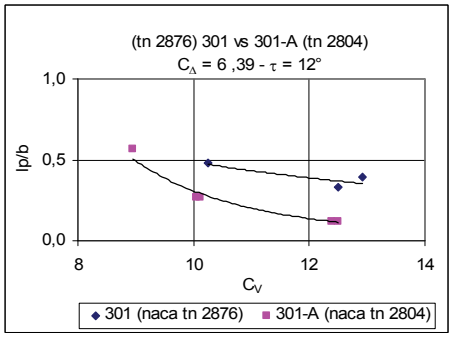

[l]

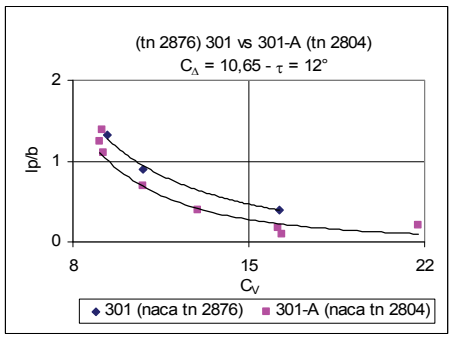

[m]

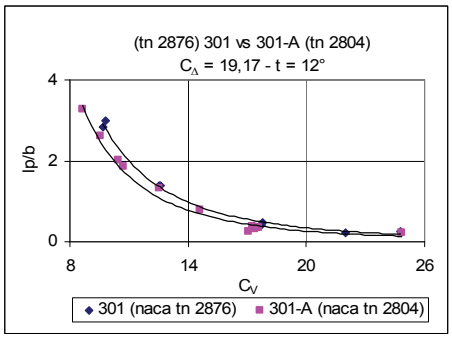

[n]

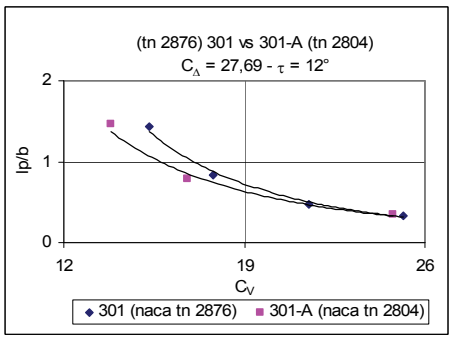

[o]

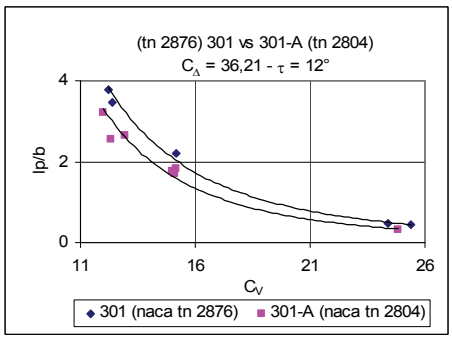

[p]

Figure 9.9-8 Effect of horizontal chine flared on longitudinal center pressure position for prismatic planing surfaces with deadrise angle β = 20° (continue)

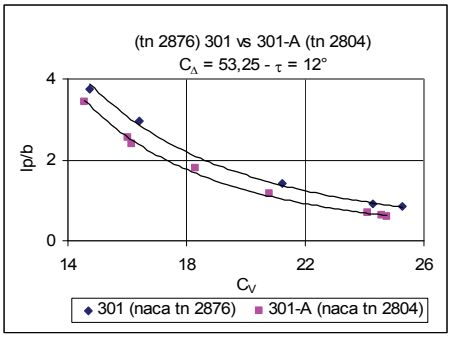

[q]

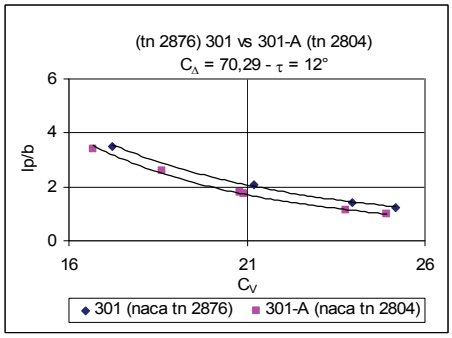

[r]

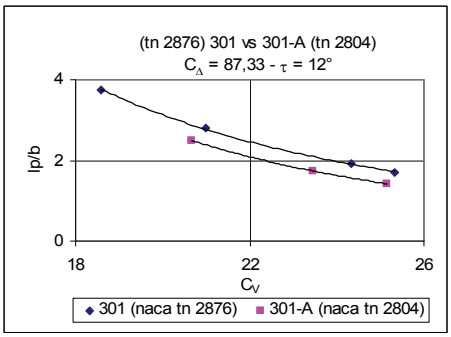

[s]

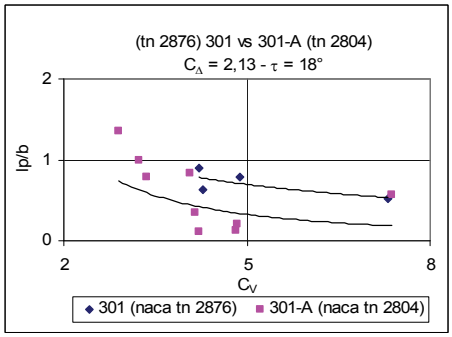

[t]

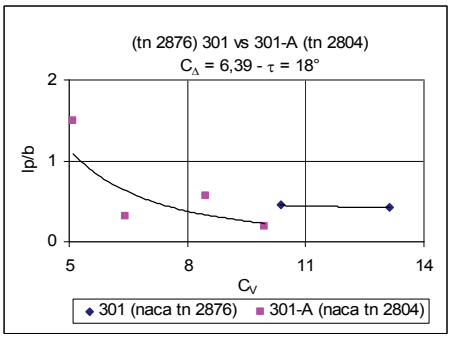

[u]

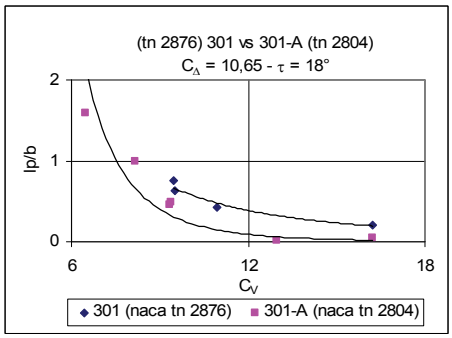

[v]

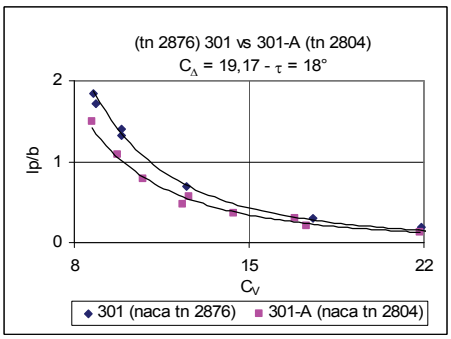

[w]

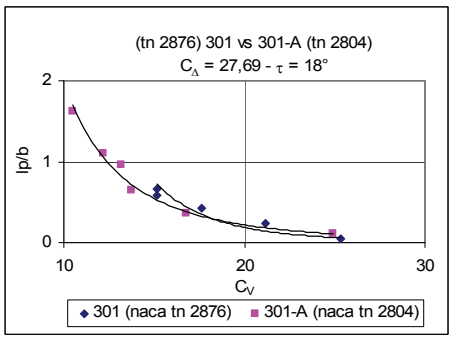

[x]

Figure 9.9-8 Effect of horizontal chine flared on longitudinal center pressure position for prismatic planing surfaces with deadrise angle β = 20° (continue)

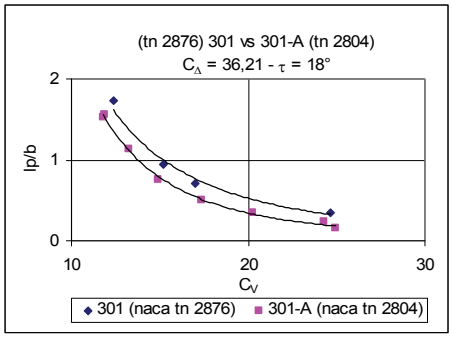

[y]

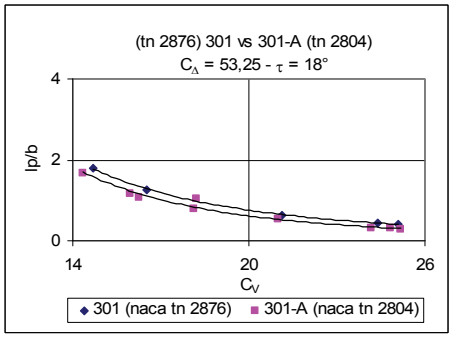

[z]

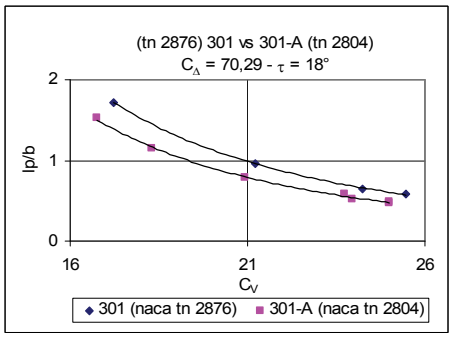

[aa]

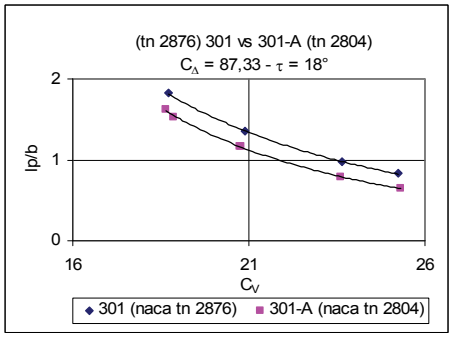

[ab]

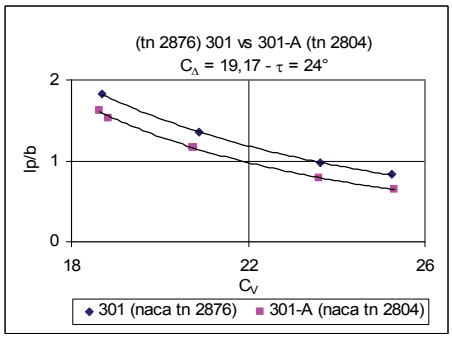

[ac]

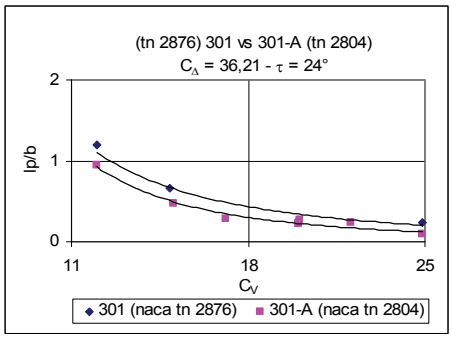

[ad]

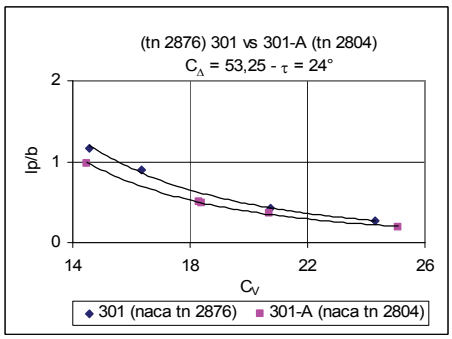

[ae]

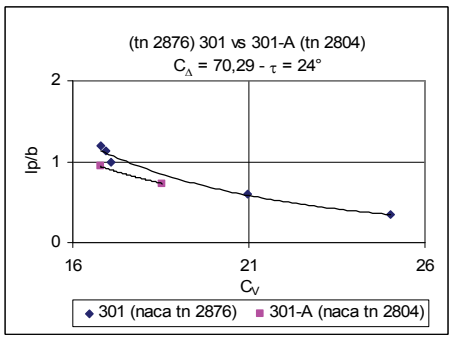

[af]

Figure 9.9-8 Effect of horizontal chine flared on longitudinal center pressure position for prismatic planing surfaces with deadrise angle β = 20° (continue)

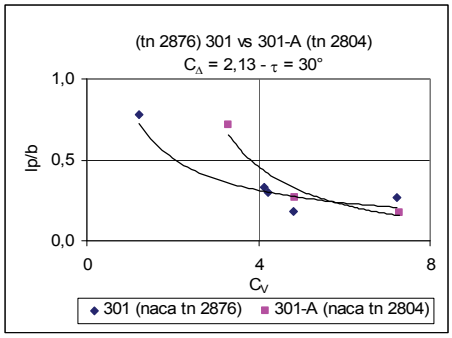

[ag]

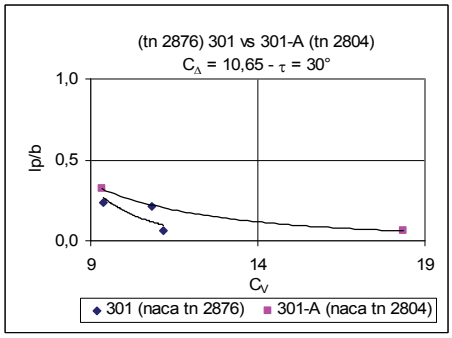

[ah]

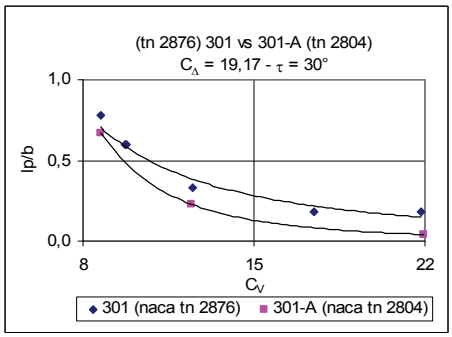

[ai]

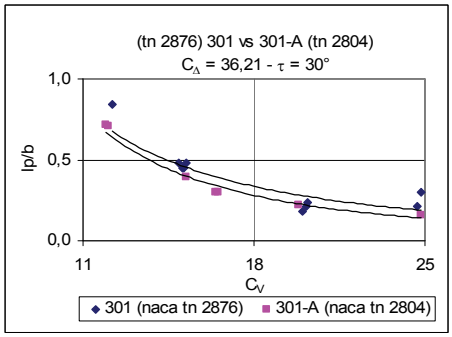

[aj]

(Data sources: [Kapryan & Weinstein 1952] and [Chambliss & Boyd 1953])

Figure 9.9-8 Effect of horizontal chine flared on longitudinal center pressure position for prismatic planing surfaces with deadrise angle β = 20°

9.9.9 Center of Pressure: Longitudinal Position Ratio $\frac{l_p}{b}$ vs C_{Lb} with $\beta = 20°$

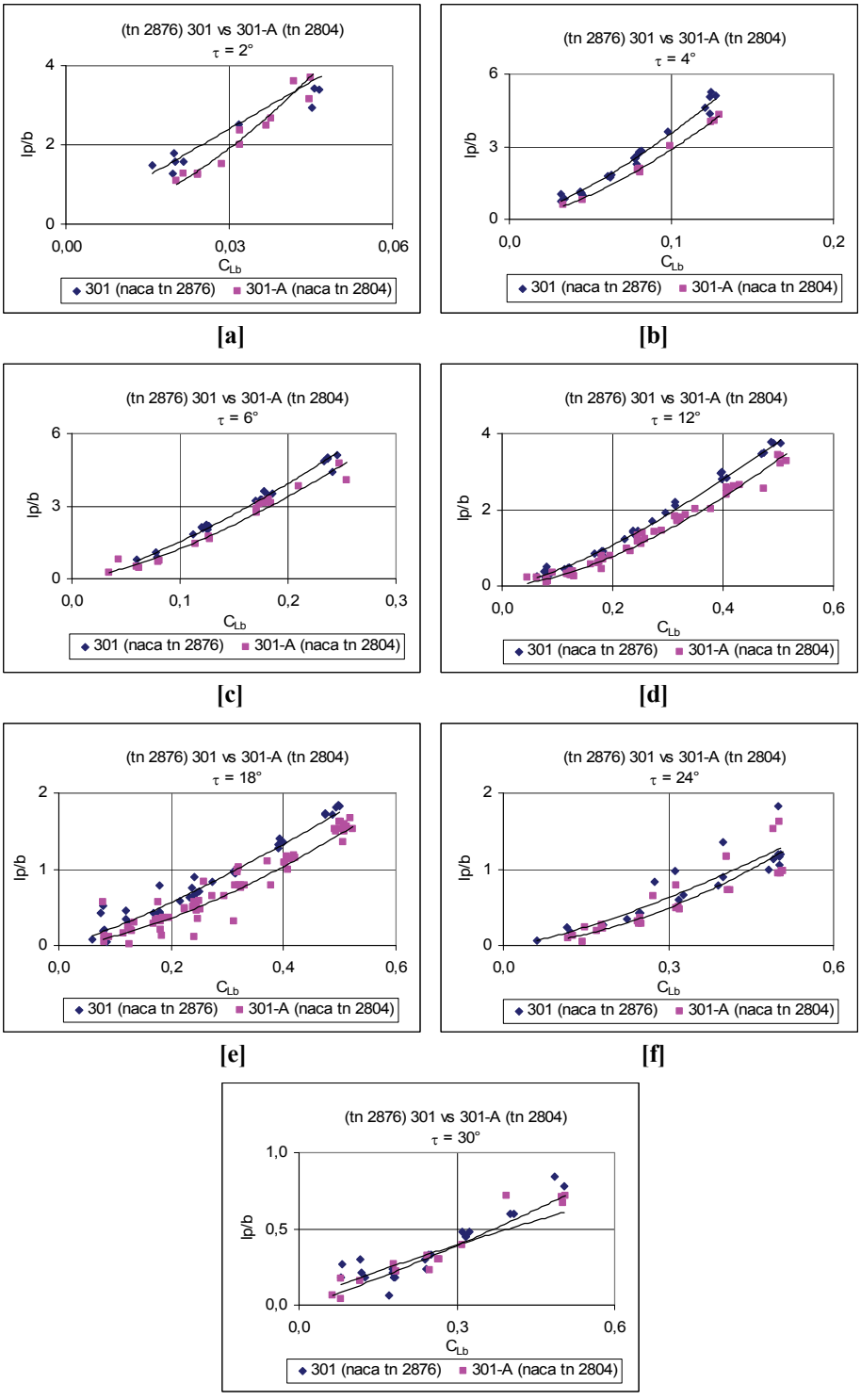

(Data sources: [Kapryan & Weinstein 1952] and [Chambliss & Boyd 1953])

Figure 9.9-9 Effect of horizontal chine flared on longitudinal center pressure position for V-bottom planing surfaces with deadrise angle β = 20°

9.9.10 Center of Pressure: Longitudinal Position Ratio $\frac{l_p}{b}$ vs C_Δ with $\beta = 40°$ and $C_V = 12.2$

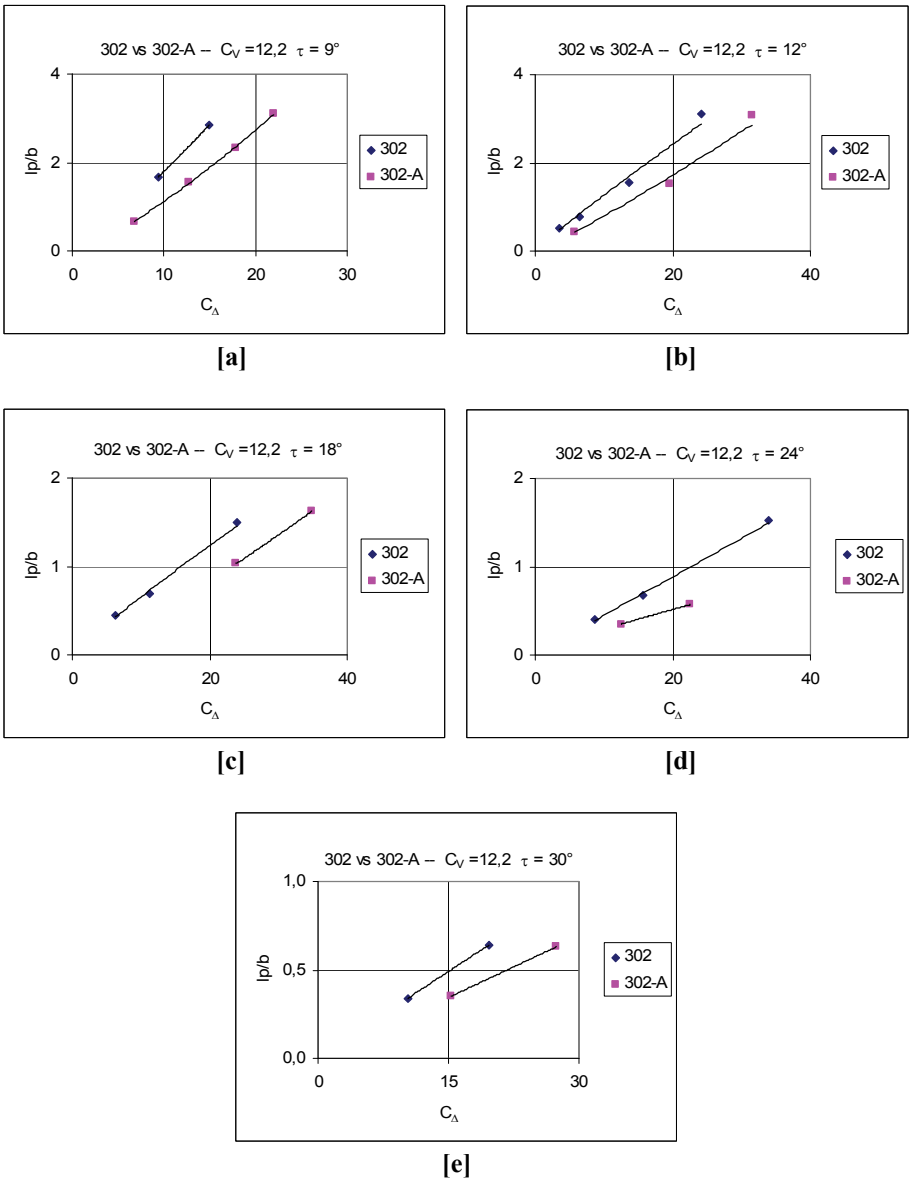

(Data source: [Kapryan & Boyd 1955])

Figure 9.9-10 Effect of horizontal chine flared on longitudinal center pressure position for prismatic planing surfaces with deadrise angle β = 40° and C_V = 12.2

9.9.11 Center of Pressure: Longitudinal Position Ratio $\frac{l_p}{b}$ vs C_V with $\beta = 40°$

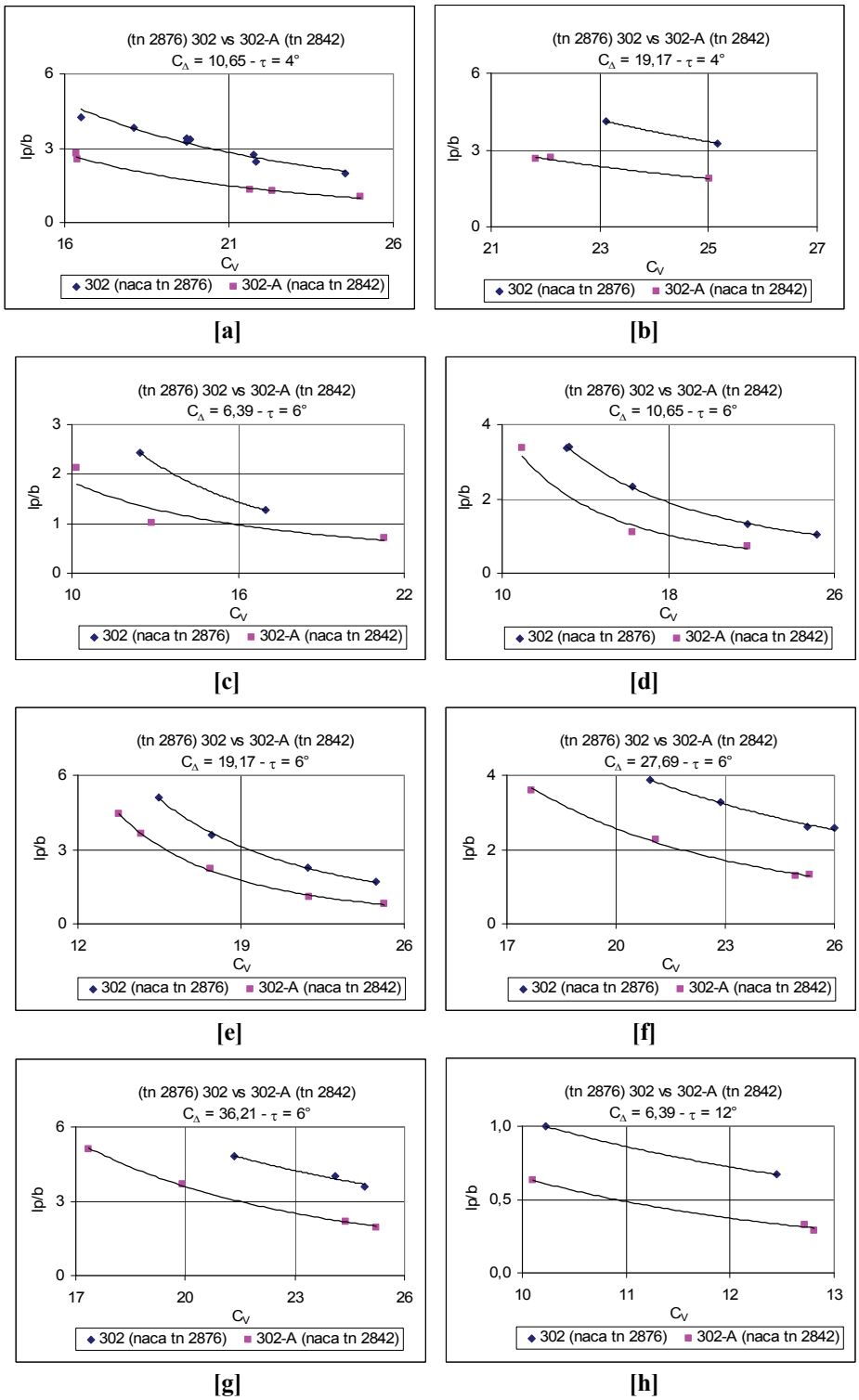

Figure 9.9-11 Effect of horizontal chine flared on longitudinal center pressure position for prismatic planing surfaces with deadrise angle β = 40° (continue)

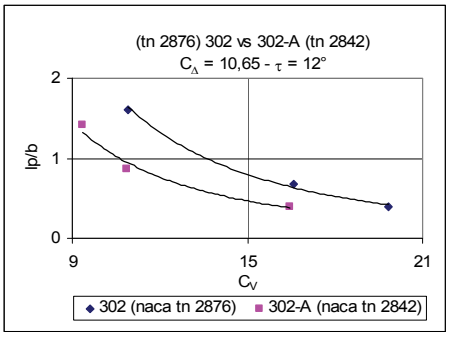

[i]

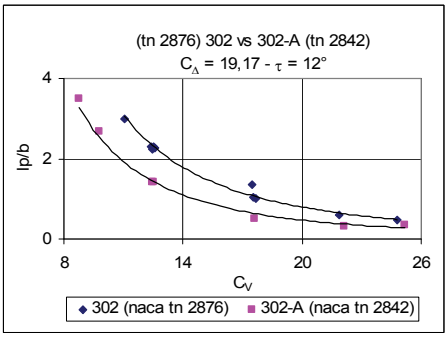

[j]

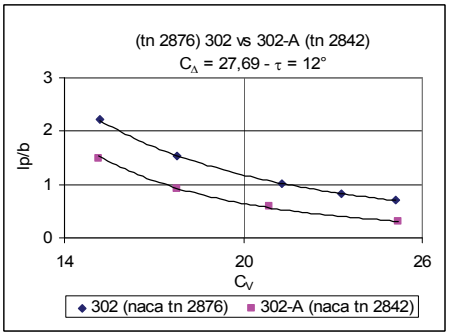

[k]

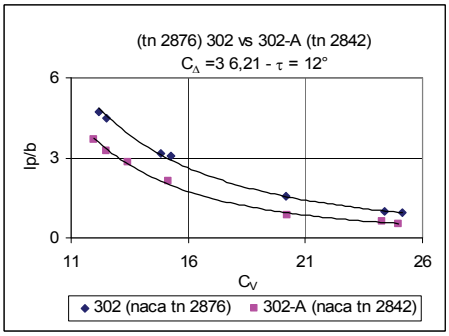

[l]

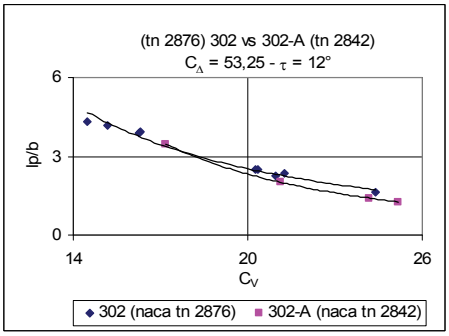

[m]

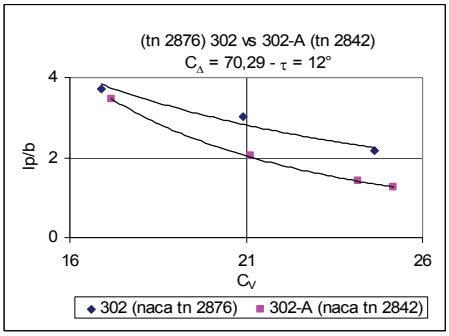

[n]

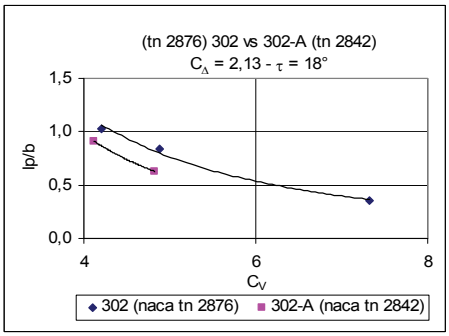

[o]

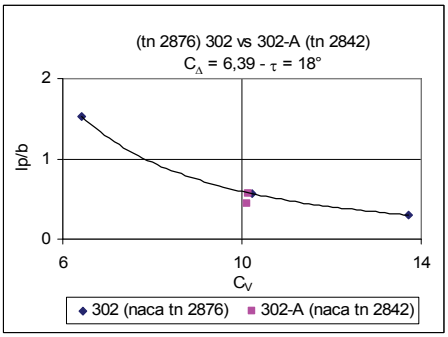

[p]

Figure 9.9-11 Effect of horizontal chine flared on longitudinal center pressure position for prismatic planing surfaces with deadrise angle β = 40° (continue)

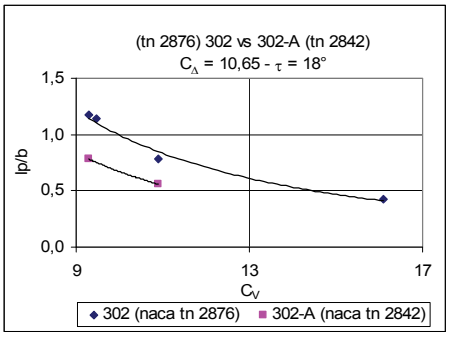

[q]

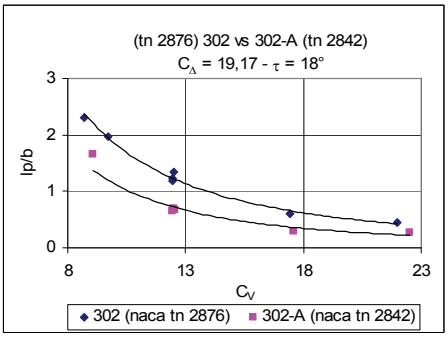

[r]

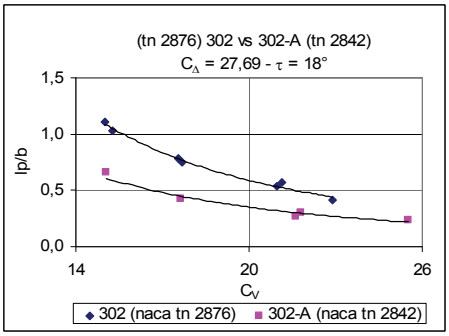

[s]

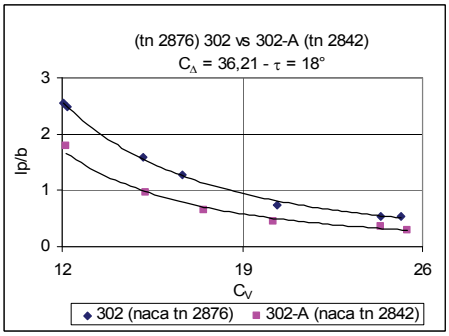

[t]

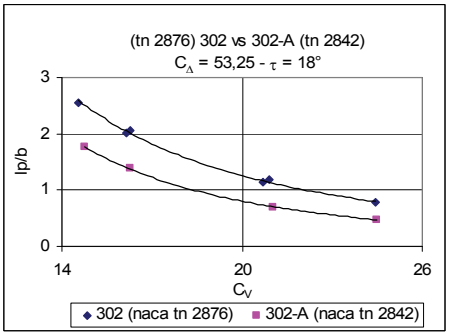

[u]

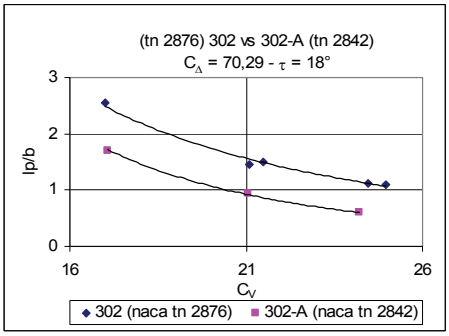

[v]

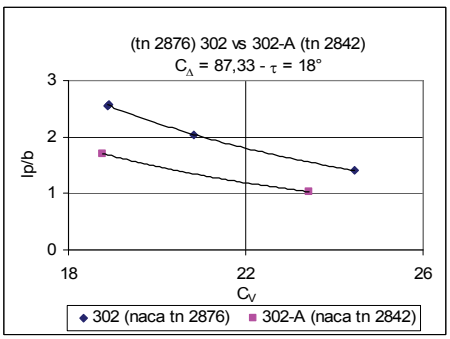

[w]

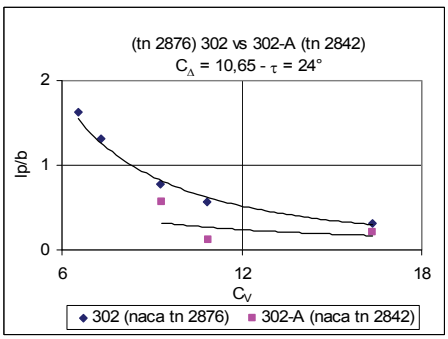

[x]

Figure 9.9-11 Effect of horizontal chine flared on longitudinal center pressure position for prismatic planing surfaces with deadrise angle β = 40° (continue)

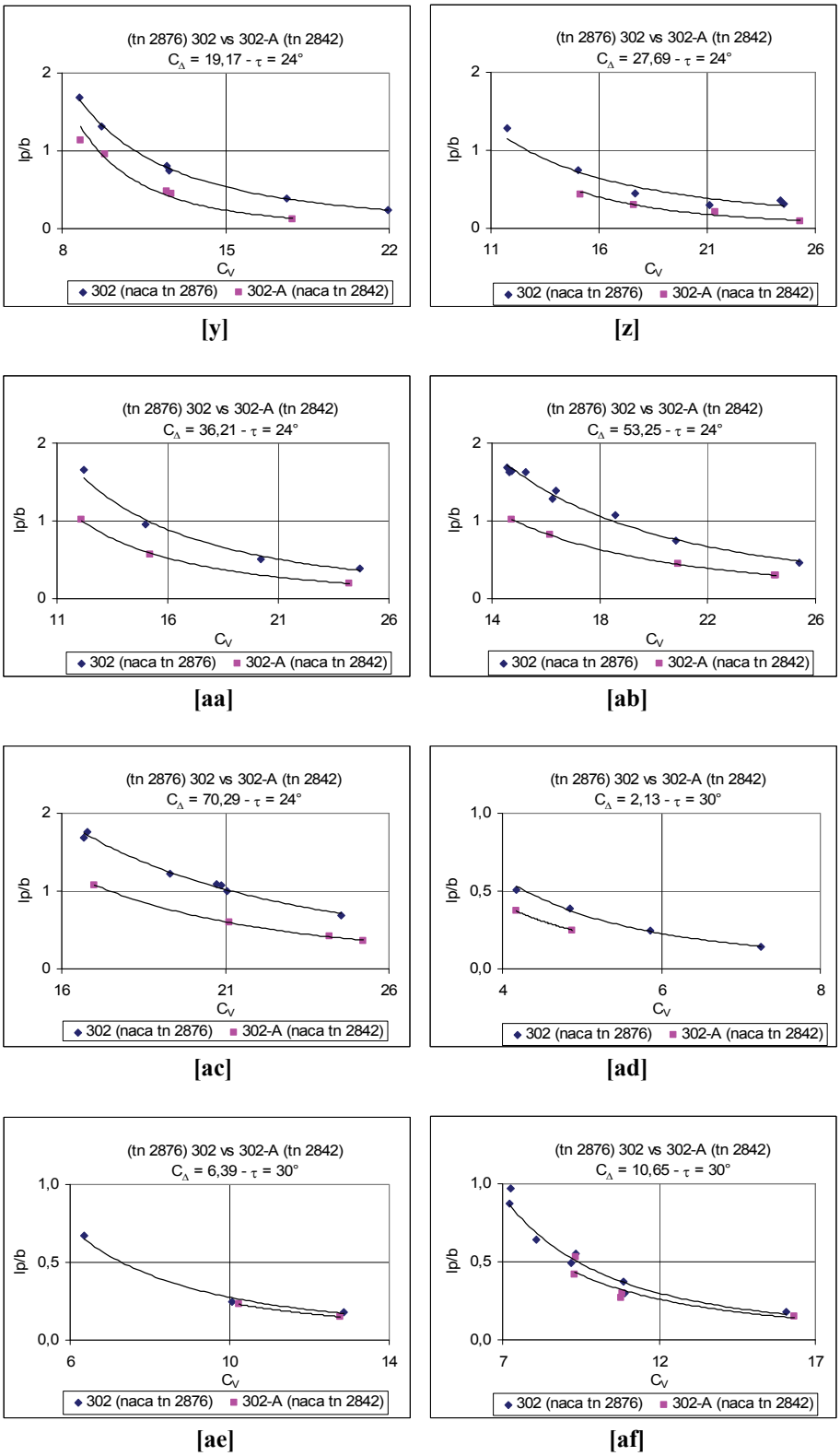

Figure 9.9-11 Effect of horizontal chine flared on longitudinal center pressure position for prismatic planing surfaces with deadrise angle β = 40° (continue)

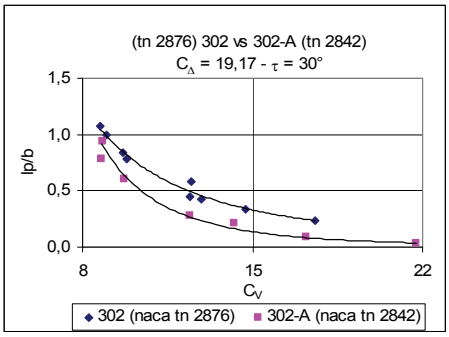

[ag]

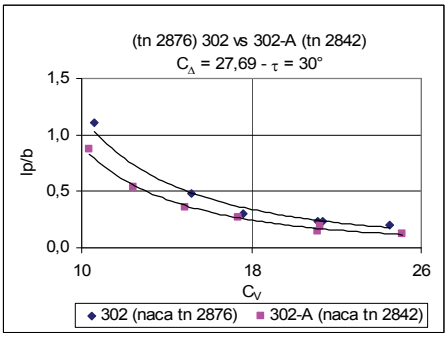

[ah]

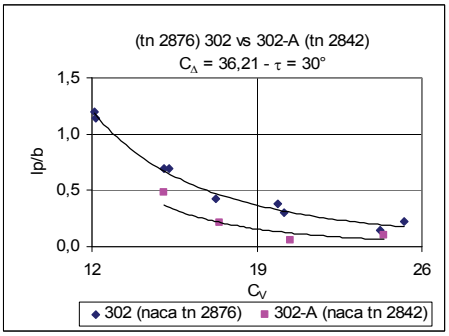

[ai]

(Data sources: [Blanchard 1952] and [Chambliss & Boyd 1953])

Figure 9.9-11 Effect of horizontal chine flared on longitudinal center pressure position for prismatic planing surfaces with deadrise angle β = 40°

9.9.12 Center of Pressure: Longitudinal Position Ratio $\frac{l_p}{b}$ vs C_{Lb} with $\beta = 40°$

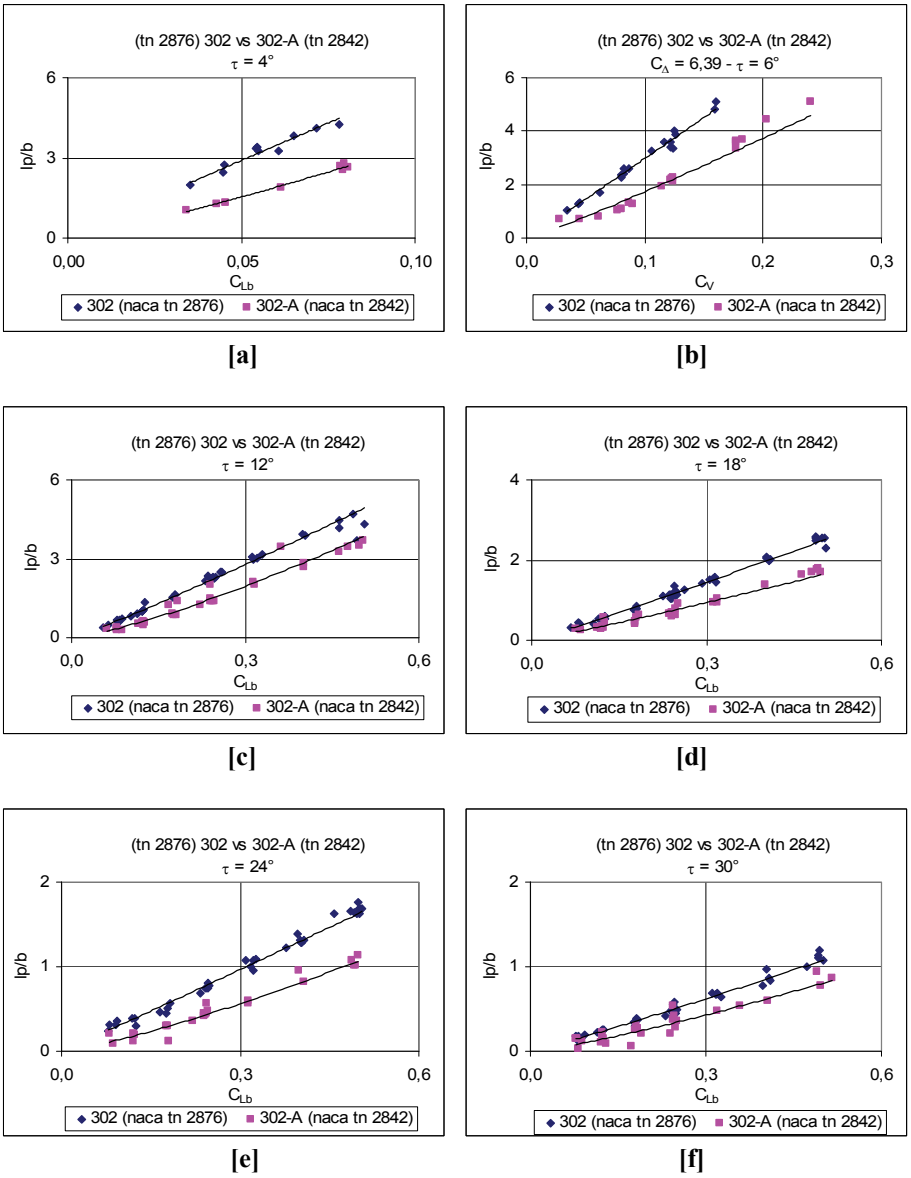

(Data sources: [Blanchard 1952] and [Chambliss & Boyd 1953])

Figure 9.9-12 Effect of horizontal chine flared on longitudinal center pressure position for V-bottom planing surfaces with deadrise angle β = 40°

9.9.13 Stagnation and Spray Edges Lines Position λ vs C_Δ with $\beta = 20°$ and $C_V = 12.2$

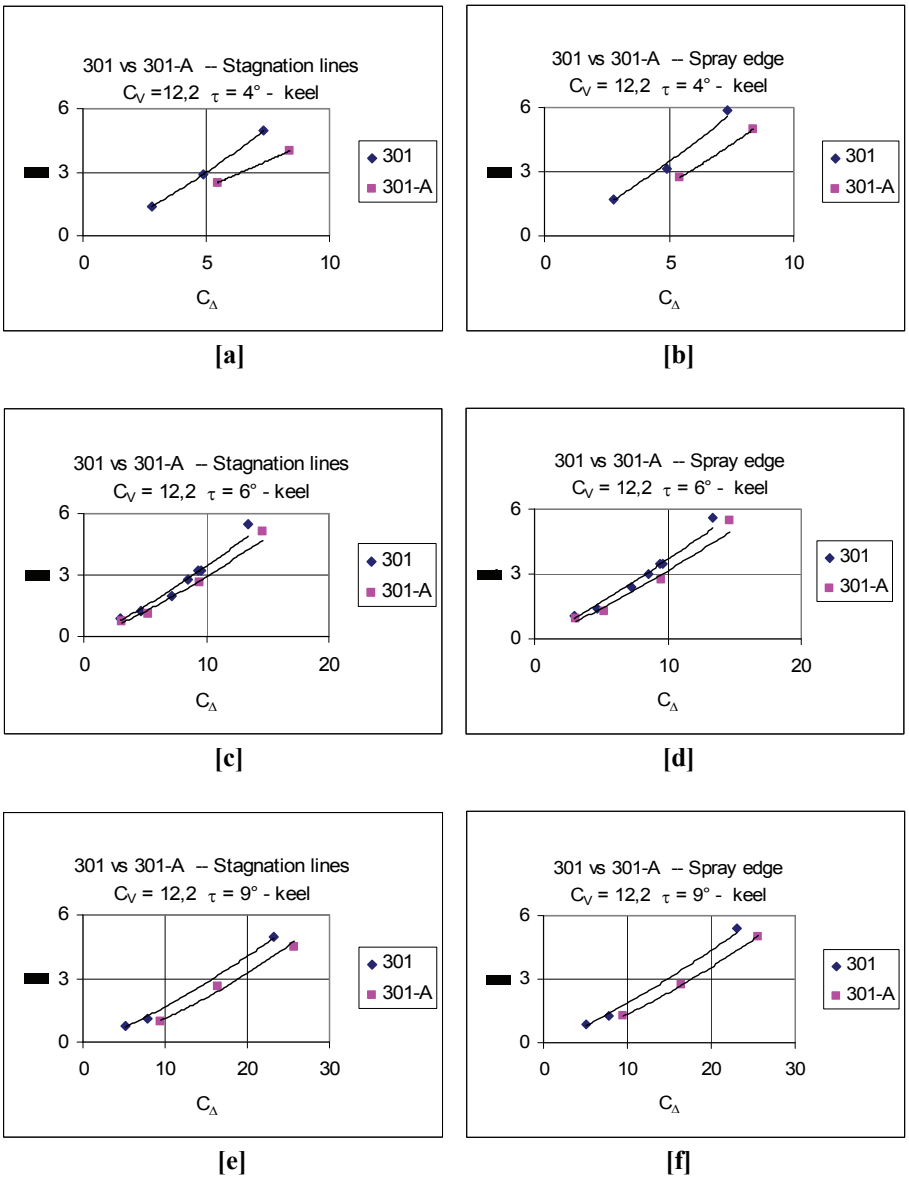

Figure 9.9-13 Effect of horizontal chine flared on stagnation and spray edge lines for V-bottom planing surface with β = 20° and C_V = 12.2 (continue)

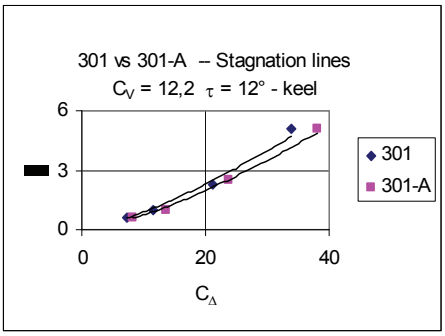

[g]

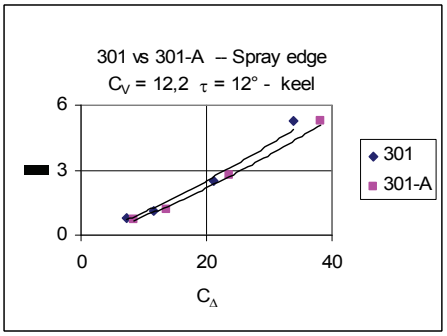

[h]

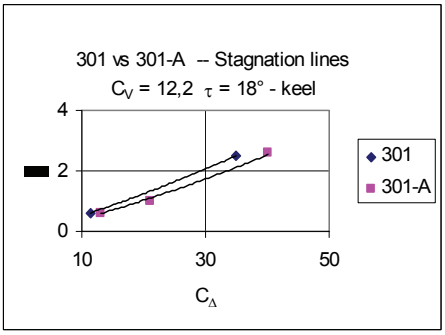

[i]

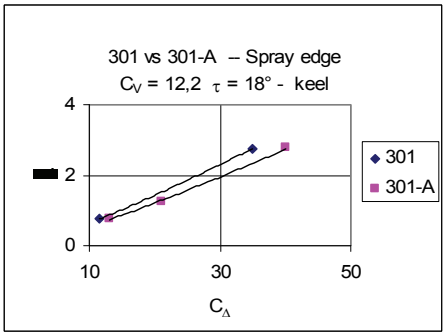

[j]

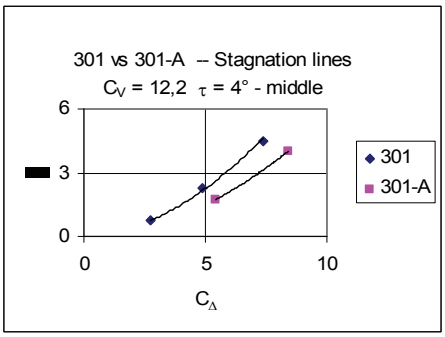

[k]

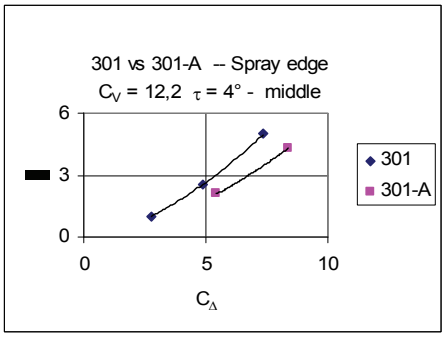

[l]

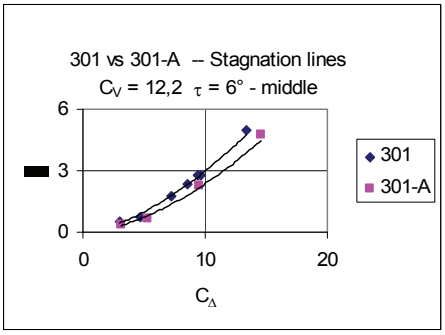

[m]

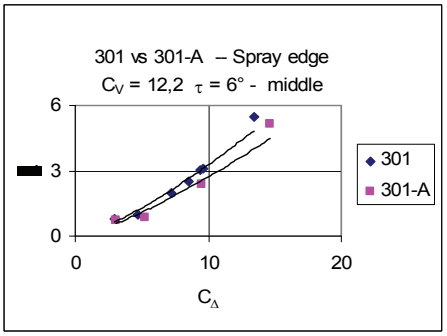

[n]

Figure 9.9-13 Effect of horizontal chine flared on stagnation and spray edge lines for V-bottom planing surface with β = 20° and CV = 12.2 (continue)

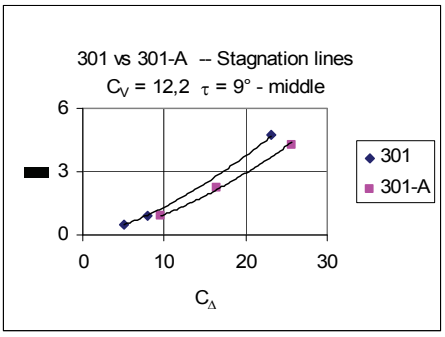

[o]

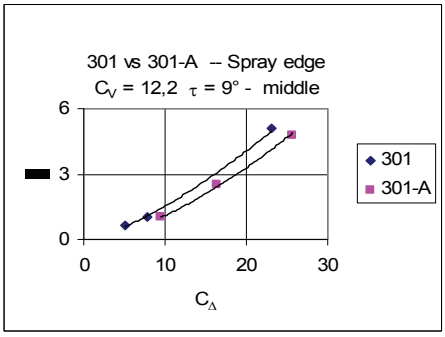

[p]

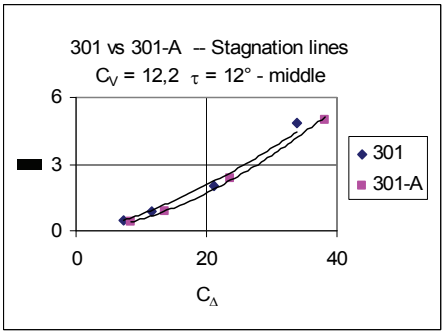

[q]

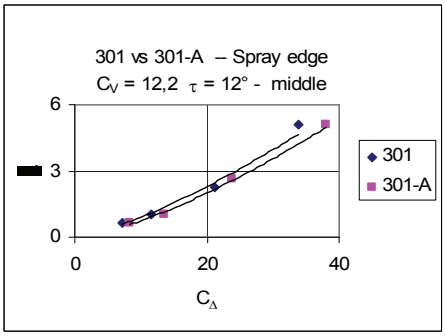

[r]

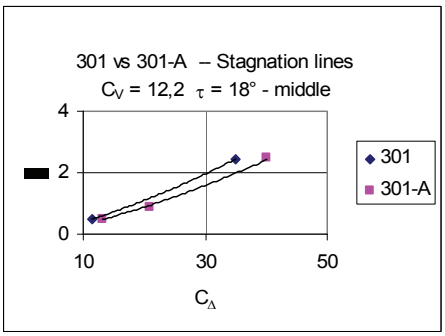

[s]

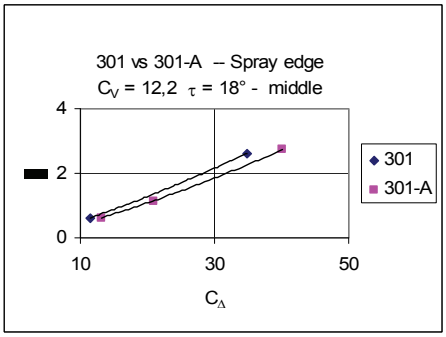

[t]

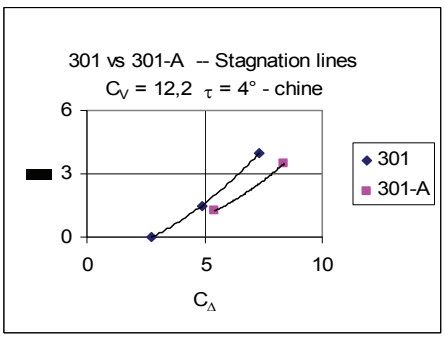

[u]

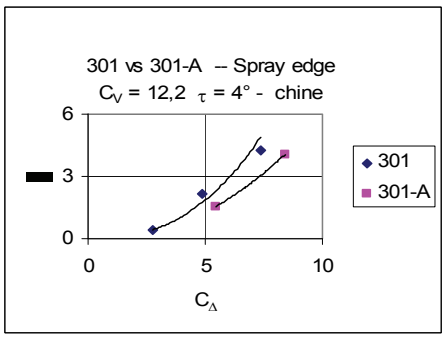

[v]

Figure 9.9-13 Effect of horizontal chine flared on stagnation and spray edge lines for V-bottom planing surface with β = 20° and CV = 12.2 (continue)

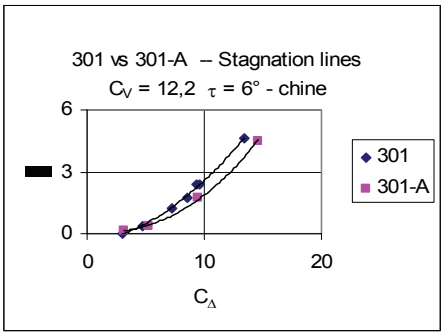

[w]

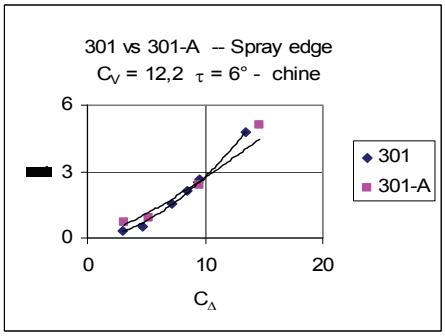

[x]

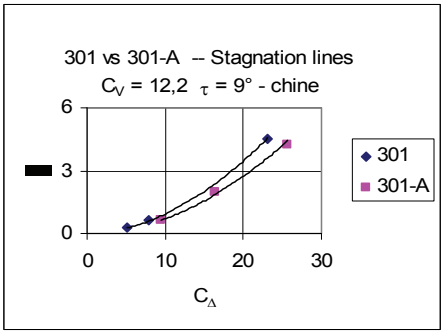

[y]

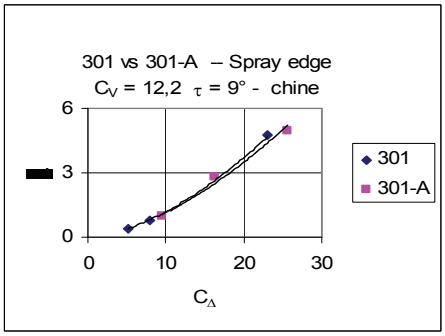

[z]

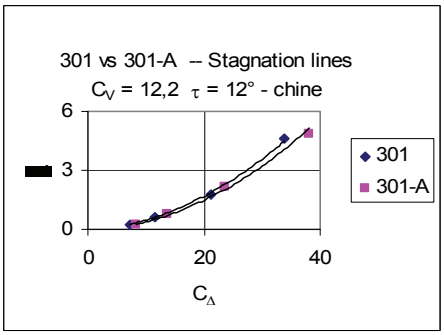

[aa]

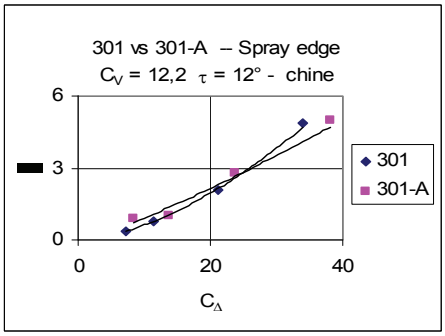

[ab]

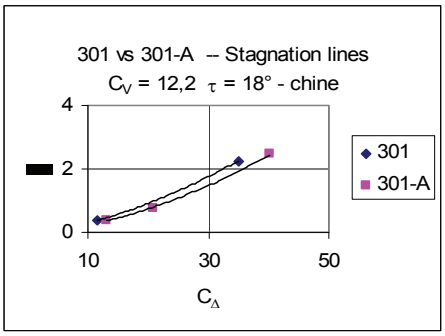

[ac]

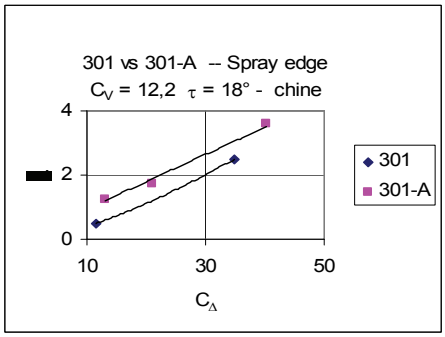

[ad]

(Data source: [Kapryan & Boyd 1955])

Figure 9.9-13 Effect of horizontal chine flared on stagnation and spray edge lines for V-bottom planing surface with β = 20° and CV = 12.2

9.9.14 Stagnation and Spray Edges Lines Position λ vs C_{Lb} with $\beta = 20°$

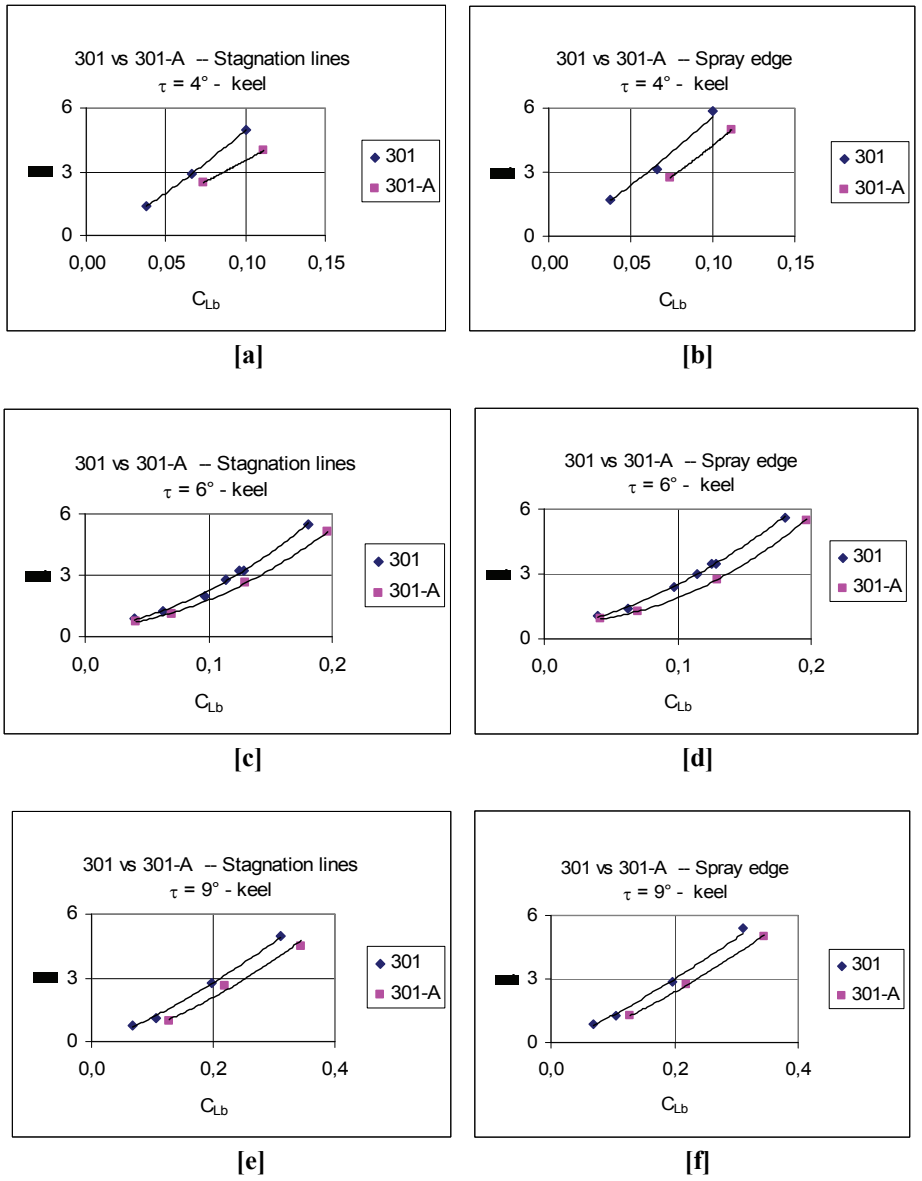

Figure 9.9-14 Effect of horizontal chine flared on stagnation and spray edge lines for V-bottom planing surface with β = 20°
(continue)

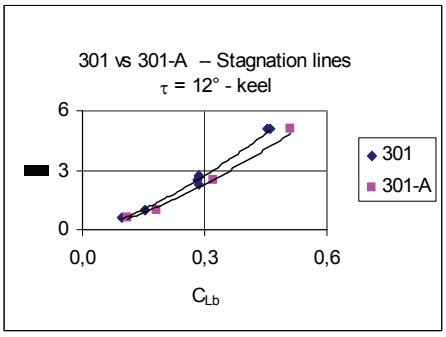

[g]

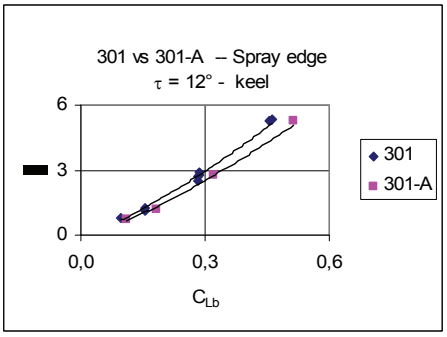

[h]

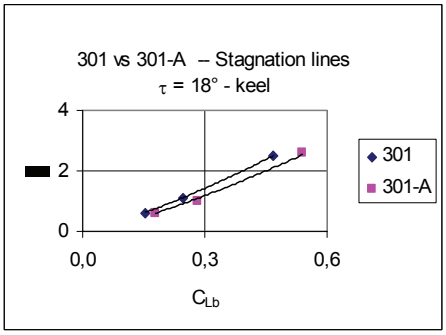

[i]

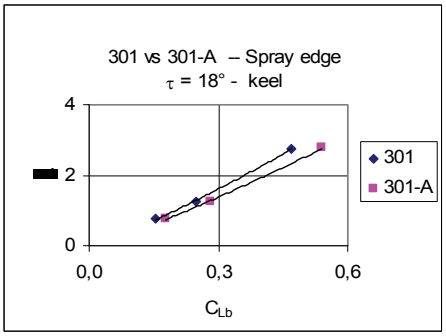

[j]

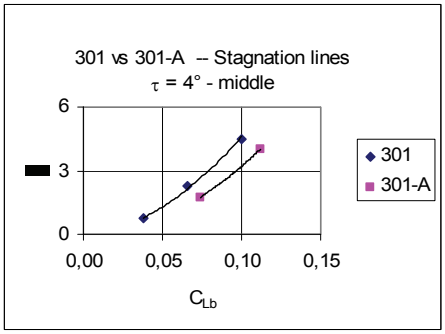

[k]

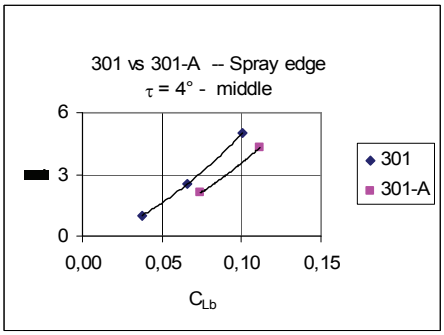

[l]

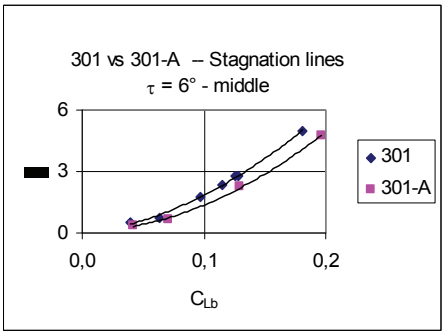

[m]

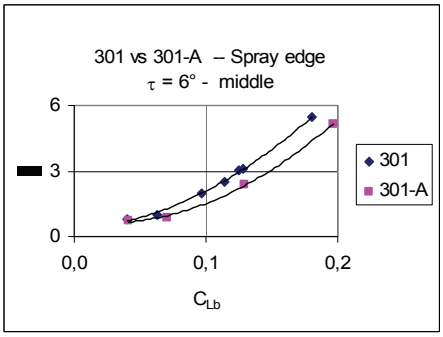

[n]

Figure 9.9-14 Effect of horizontal chine flared on stagnation and spray edge lines for V-bottom planing surface with β = 20° (continue)

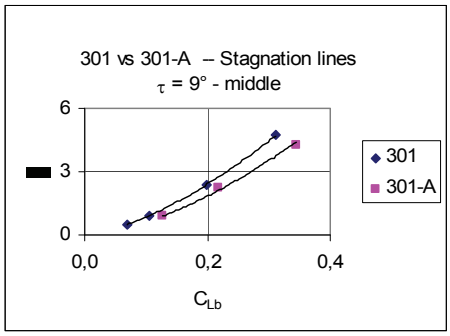

[o]

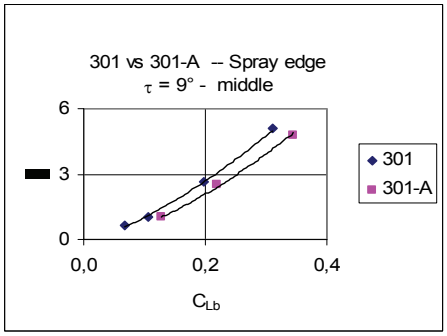

[p]

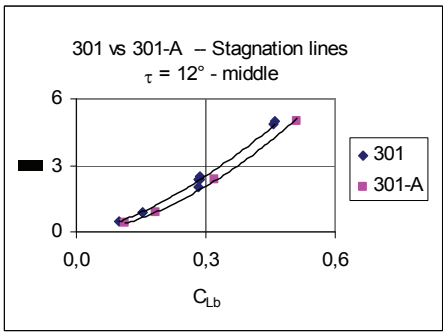

[q]

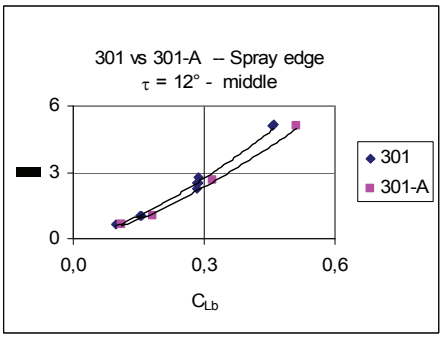

[r]

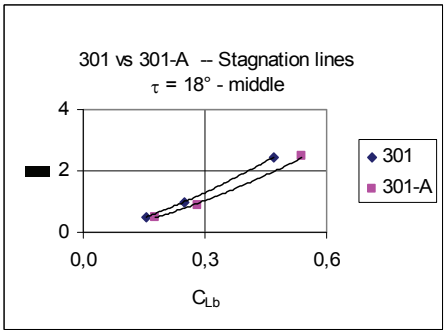

[s]

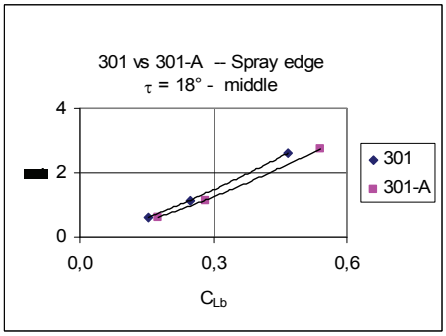

[t]

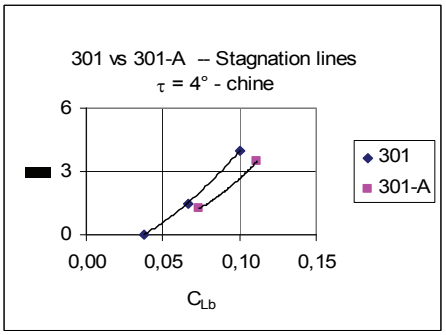

[u]

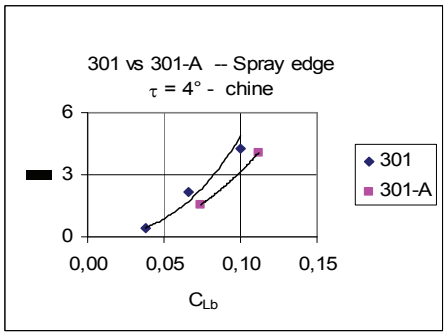

[v]

Figure 9.9-14 Effect of horizontal chine flared on stagnation and spray edge lines for V-bottom planing surface with β = 20° (continue)

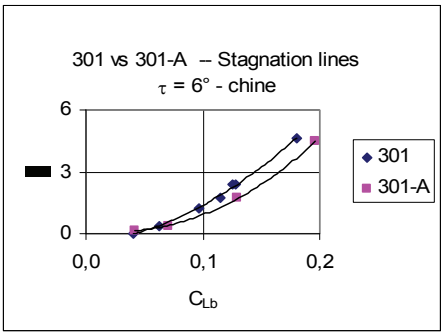

[w]

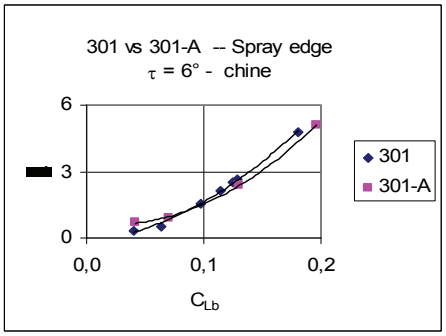

[x]

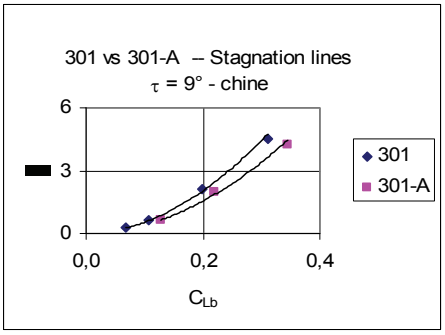

[y]

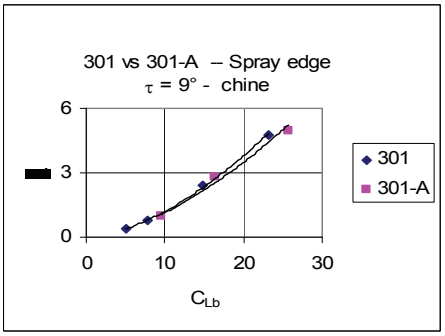

[z]

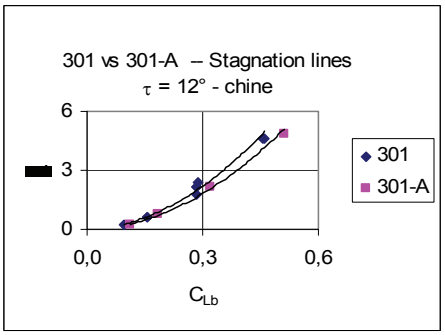

[aa]

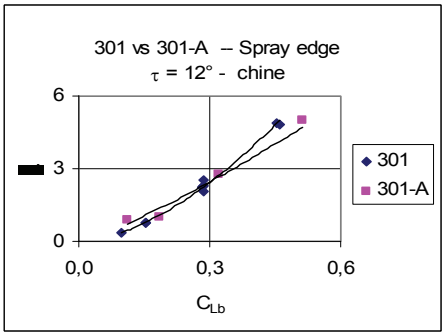

[ab]

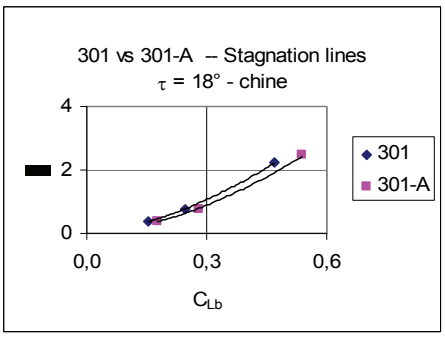

[ac]

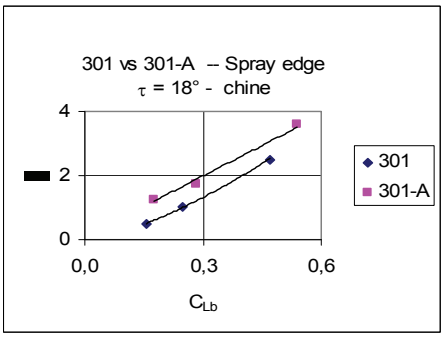

[ad]

(Data source: [Kapryan & Boyd 1955])

Figure 9.9-14 Effect of horizontal chine flared on stagnation and spray edge lines for V-bottom planing surface with β = 20°

9.9.15 Stagnation and Spray Edges Lines Position λ vs C_Δ with $\beta = 40°$ and $C_V = 12.2$

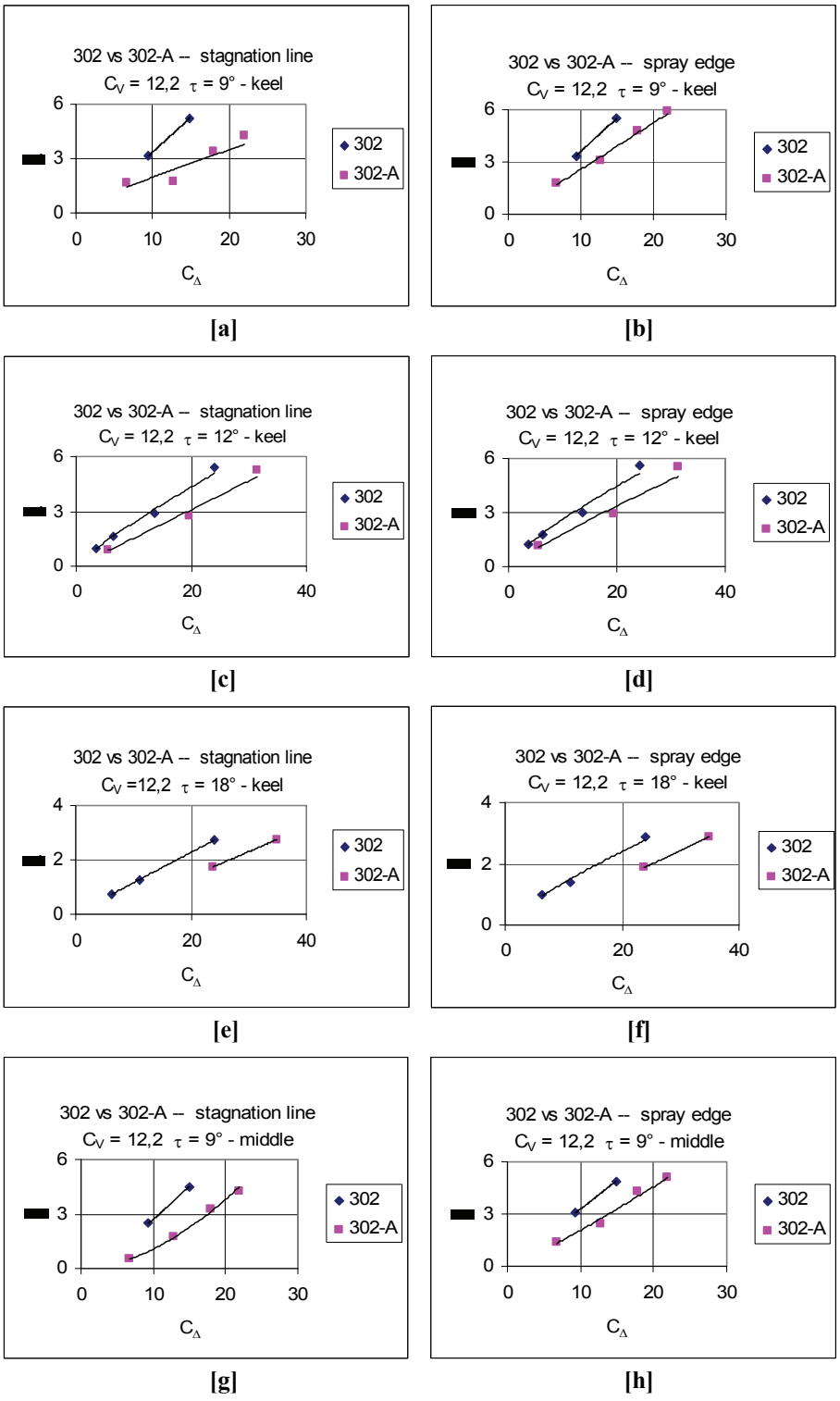

Figure 9.9-15 Effect of horizontal chine flared on stagnation and spray edge lines for V-bottom planing surface with β = 40° and C_V = 12.2 (continue)

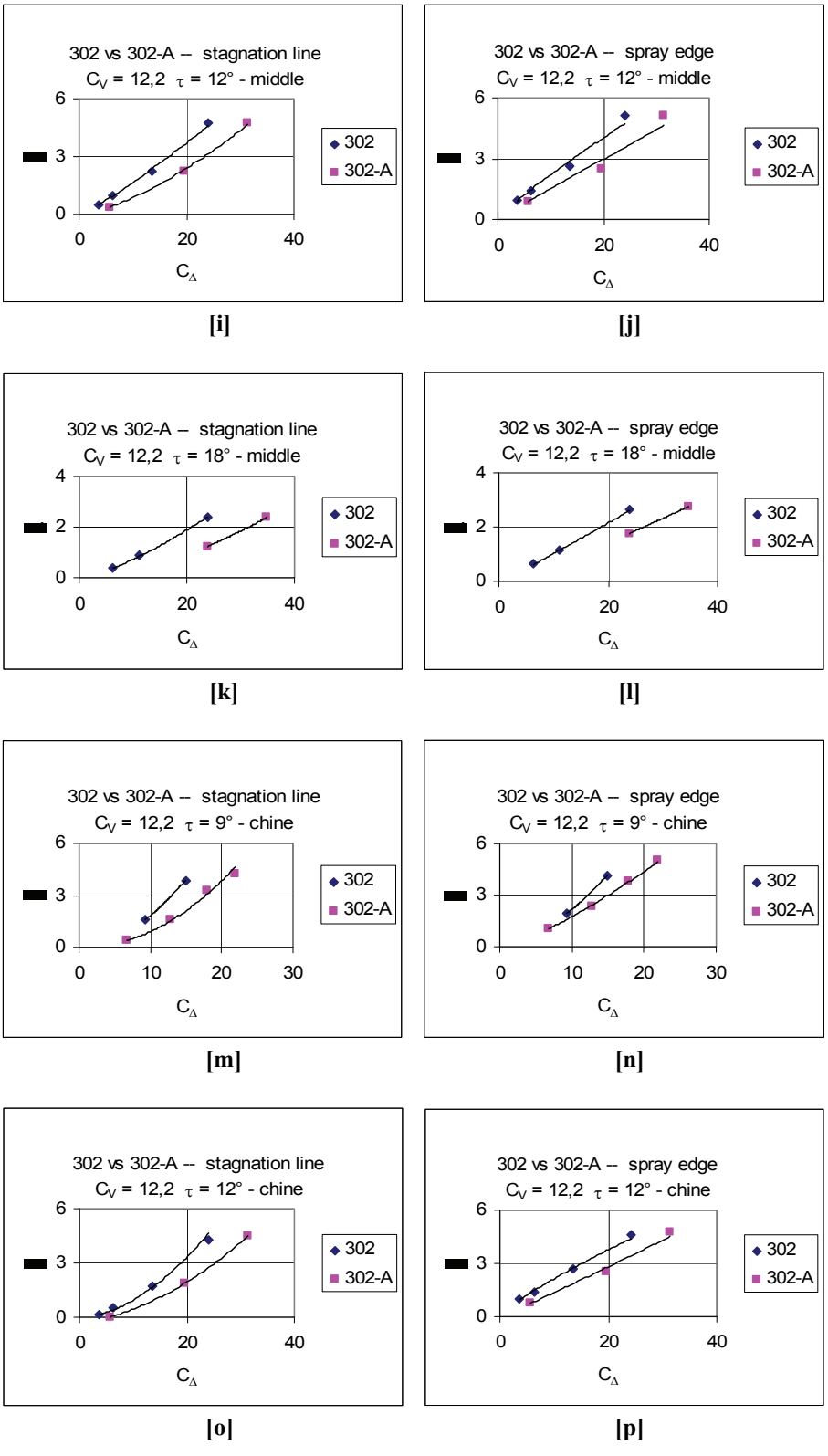

Figure 9.9-15 Effect of horizontal chine flared on stagnation and spray edge lines for V-bottom planing surface with β = 40° and CV = 12.2 (continue)

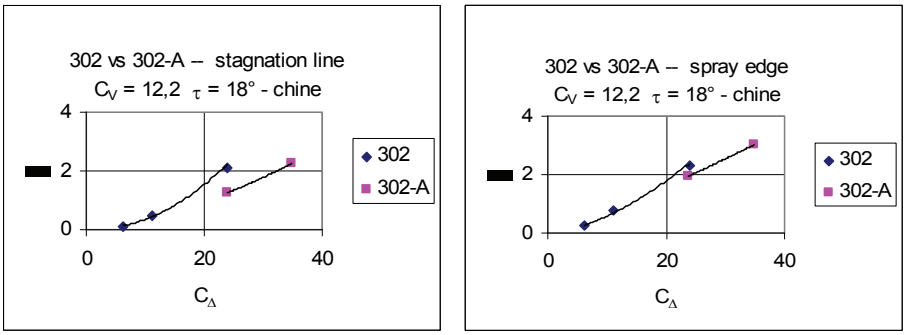

[q] **[r]**

(Data source: [Kapryan & Boyd 1955])

Figure 9.9-15 Effect of horizontal chine flared on stagnation and spray edge lines for V-bottom planing surface with β = 40° and CV = 12.2

9.9.16 Stagnation and Spray Edges Lines Position λ vs C_{Lb} with $\beta = 40°$

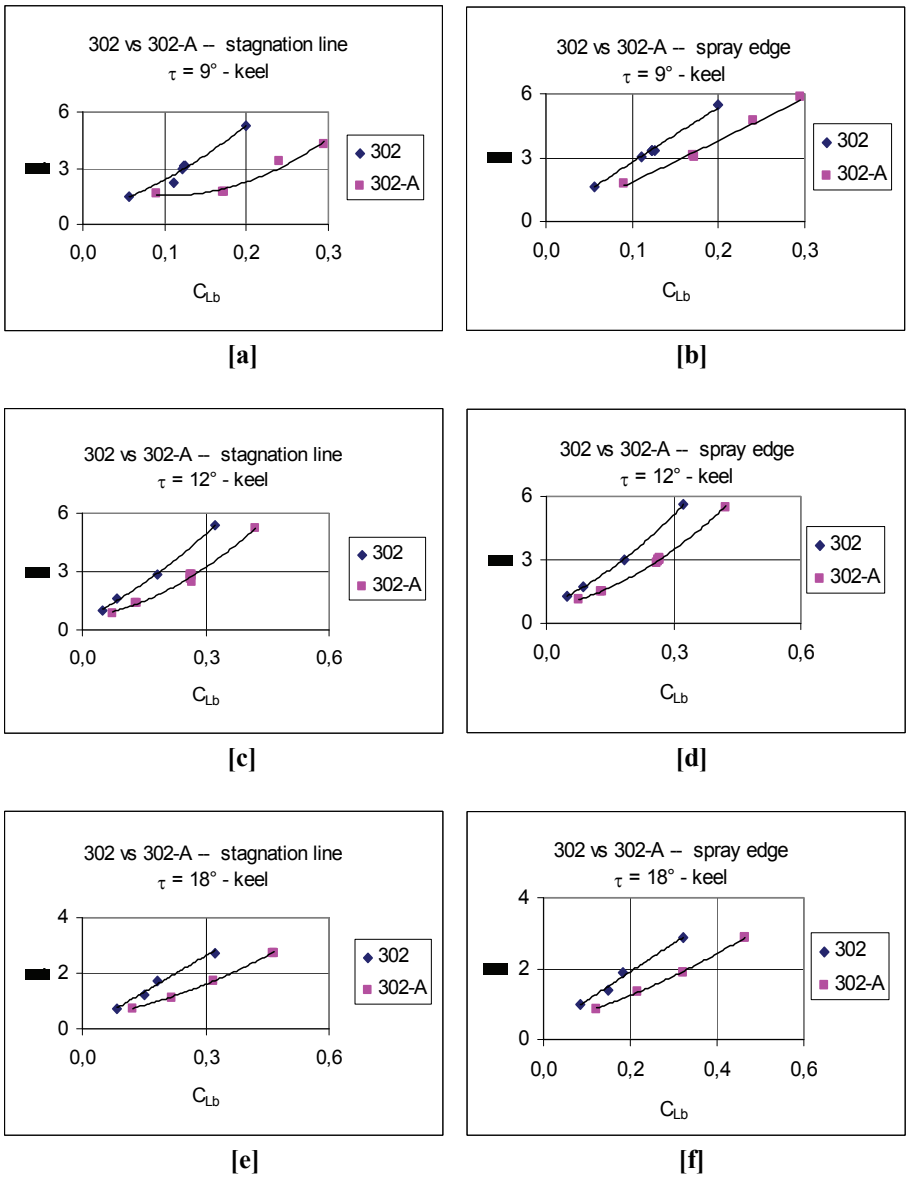

Figure 9.9-16 Effect of horizontal chine flared on stagnation and spray edge lines for V-bottom planing surface with β = 40°
(continue)

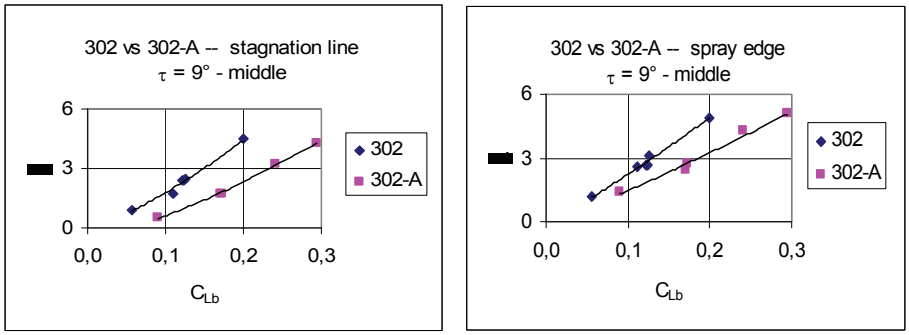

[g]

[h]

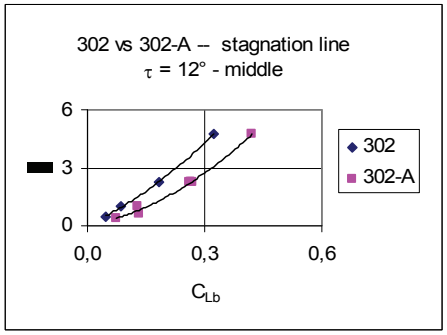

[i]

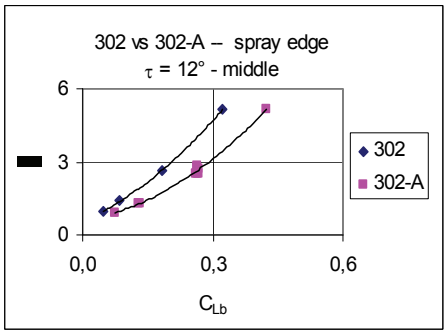

[j]

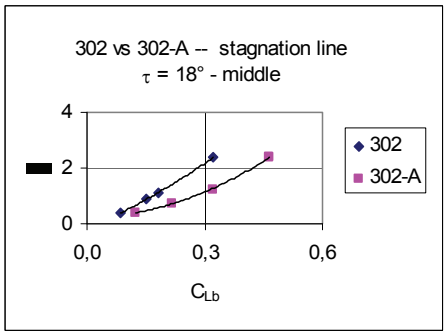

[k]

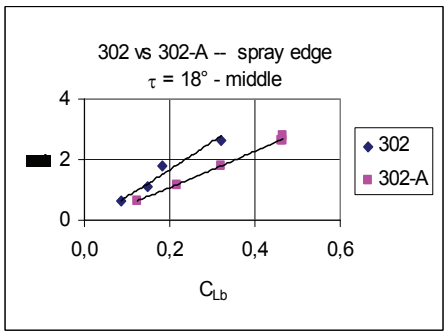

[l]

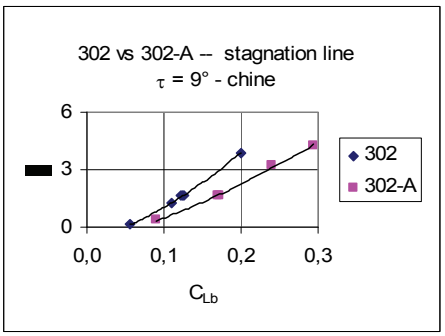

[m]

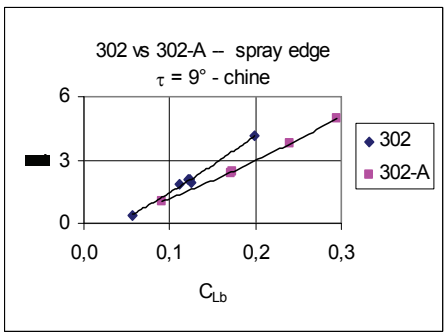

[n]

Figure 9.9-16 Effect of horizontal chine flared on stagnation and spray edge lines for V-bottom planing surface with β = 40° (continue)

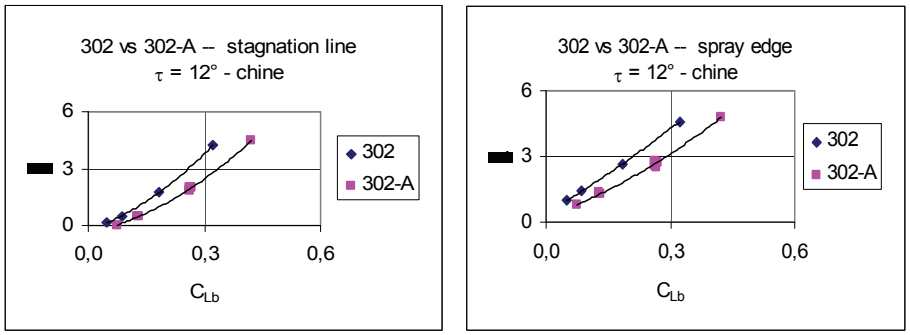

[o]

[p]

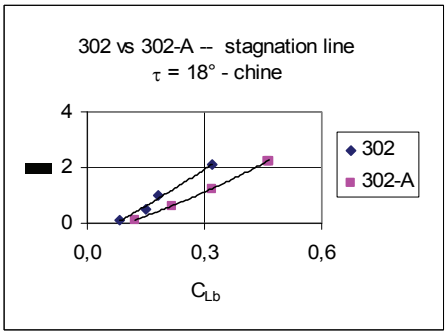

[q]

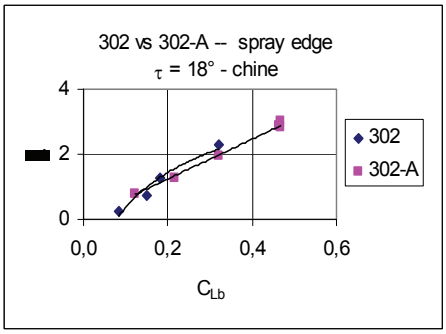

[r]

(Data source: [Kapryan & Boyd 1955])

Figure 9.9-16 Effect of horizontal chine flared on stagnation and spray edge lines for V-bottom planing surface with β = 40°

9.10 Diagrams: Stagnation Line Trends

9.10.1 Model 301 - $\beta = 20°$

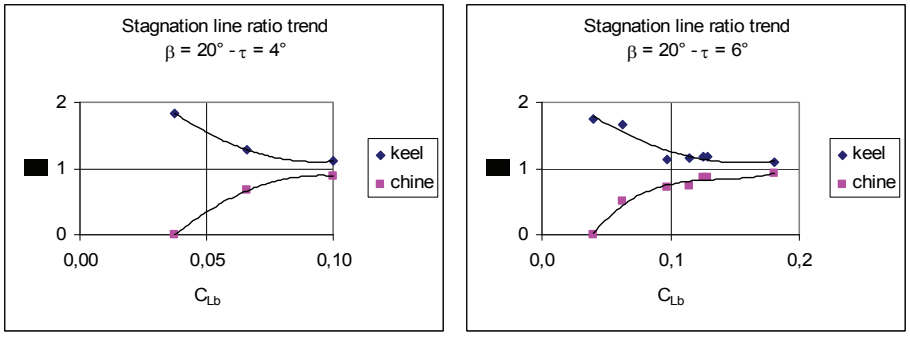

[a]

[b]

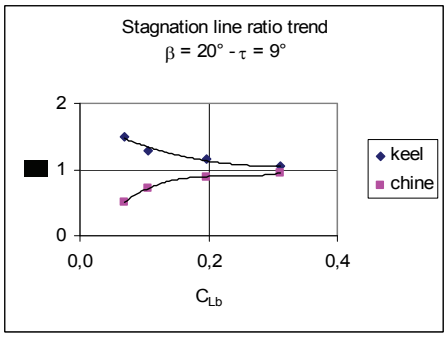

[c]

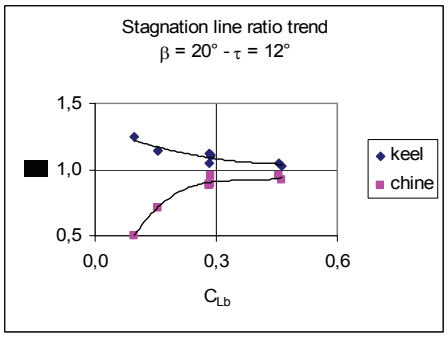

[d]

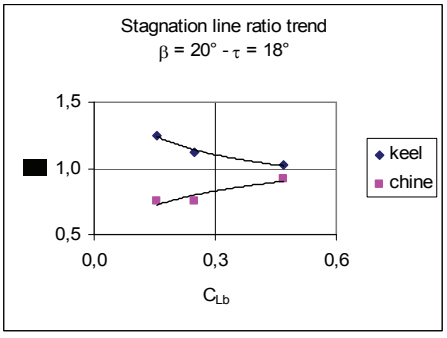

[e]

(Data source: [Kapryan & Boyd 1955])

Figure 9.10-1 Stagnation line ratio trend for β = 20° without horizontal chine flared

9.10.2 Model 301-A - $\beta = 20°$ with Horizontal Chine Flared

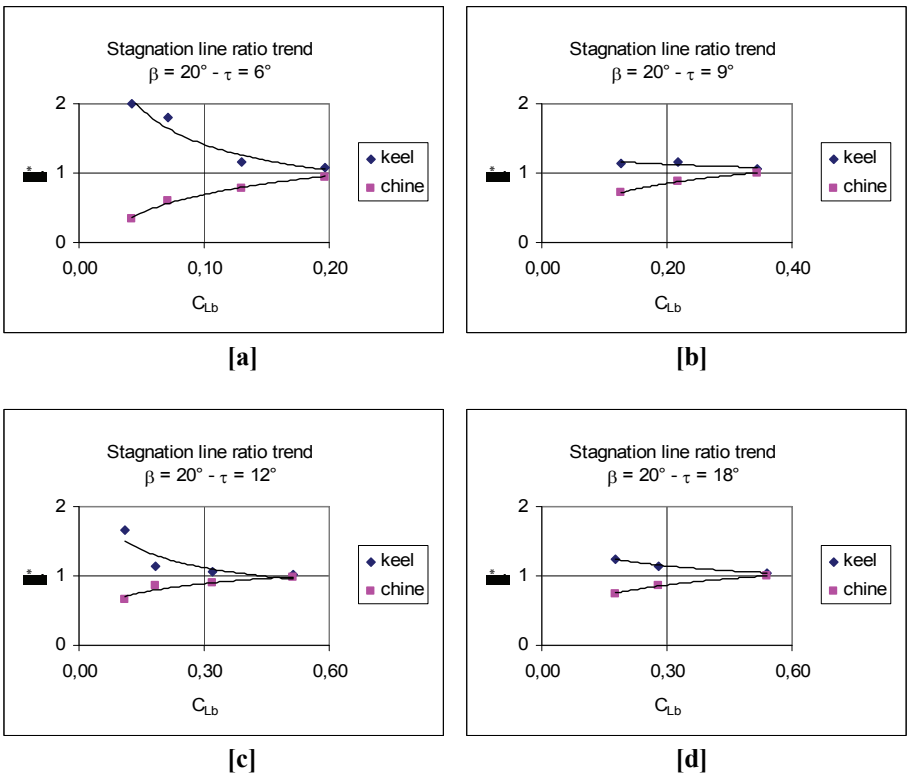

(Data source: [Kapryan & Boyd 1955])

Figure 9.10-2 Stagnation line ratio trend for β = 20° with horizontal chine flared

9.10.3 Model 302 - $\beta = 40°$

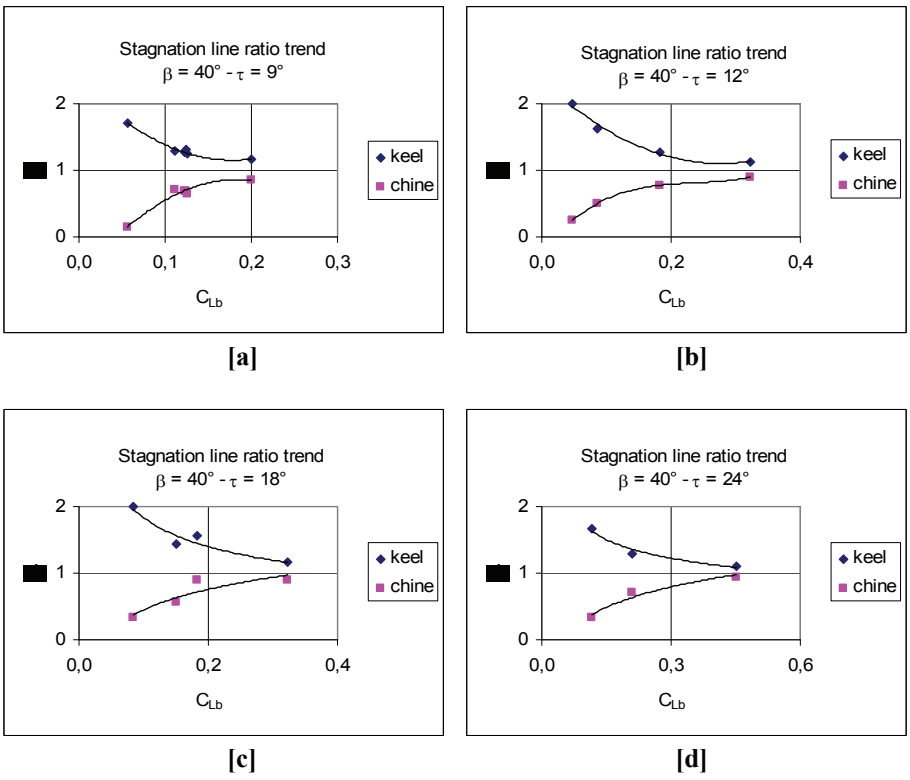

(Data source: [Kapryan & Boyd 1955])

Figure 9.10-3 Stagnation line ratio trend for β = 40° without horizontal chine flared

9.10.4 Model 302-A - $\beta = 40°$ with Horizontal Chine Flared

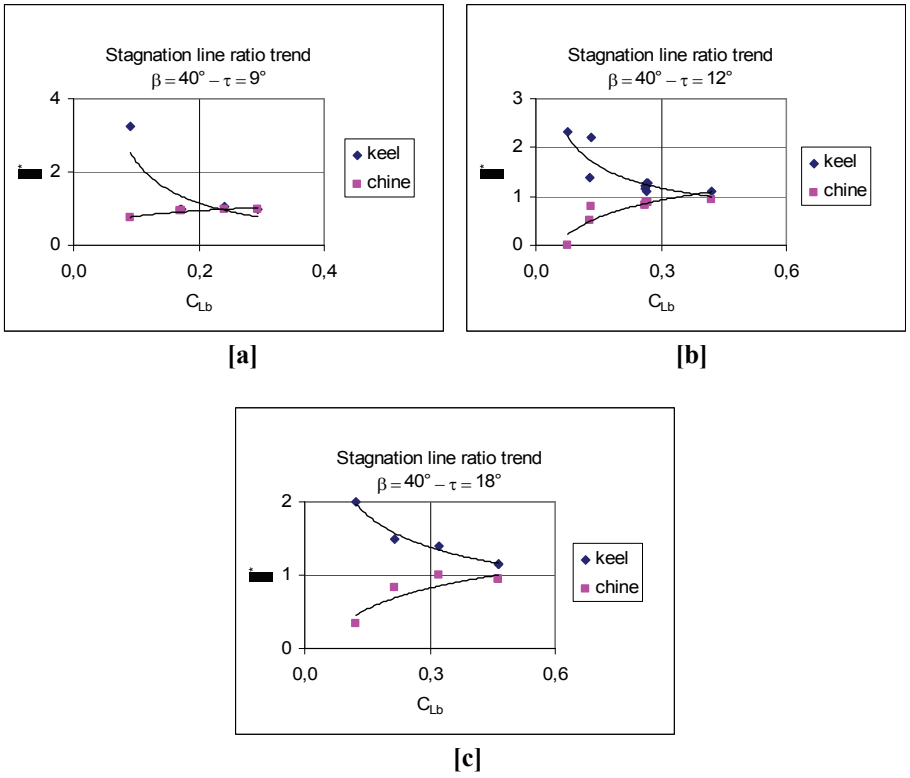

(Data source: [Kapryan & Boyd 1955])

Figure 9.10-4 Stagnation line ratio trend for β = 40° with horizontal chine flared

9.10.5 Deadrise Effects: λ^* vs C_Δ with $C_V = 12.2$

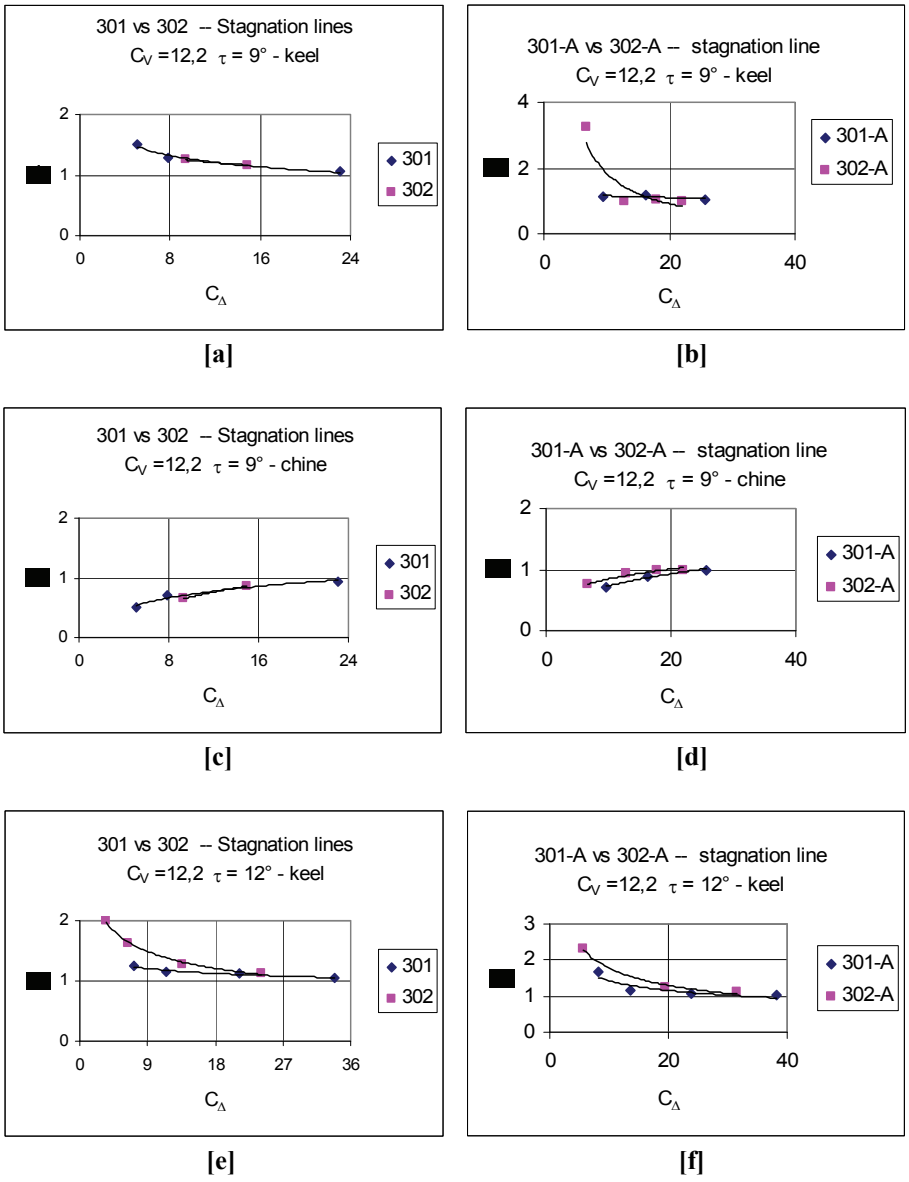

Figure 9.10-5 Deadrise angle effects on stagnation line ratio trend for V-bottom planing surface with $C_V = 12.2$ (continue)

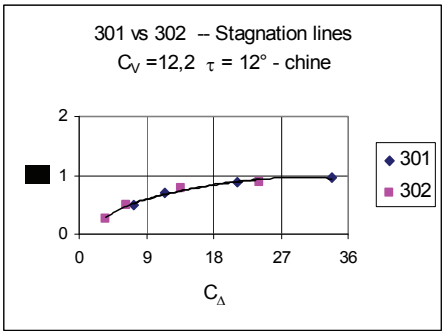

[g]

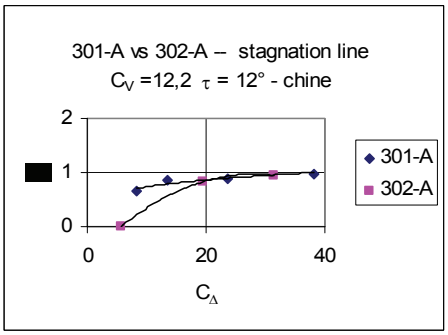

[h]

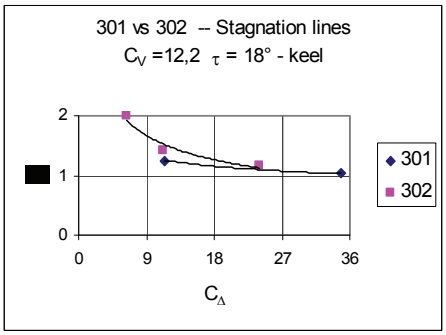

[i]

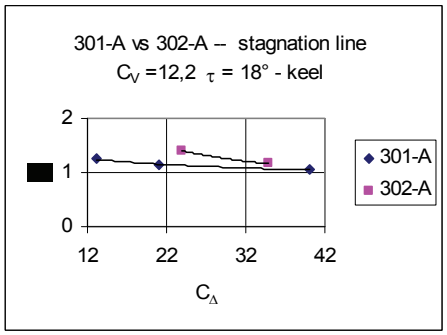

[l]

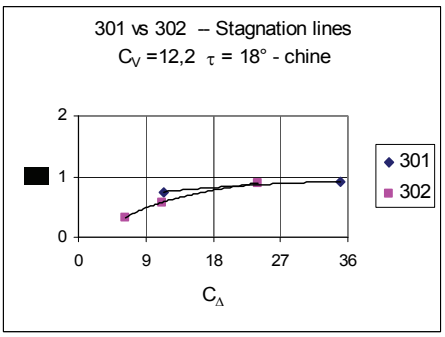

[m]

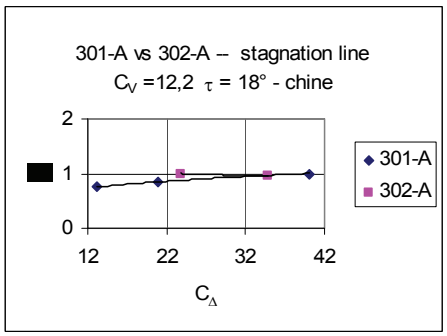

[n]

(Data source: [Kapryan & Boyd 1955])

Figure 9.10-5 Deadrise angle effects on stagnation line ratio trend for V-bottom planing surface with C_V = 12.2

9.10.6 Deadrise Effects: λ^* vs C_{Lb}

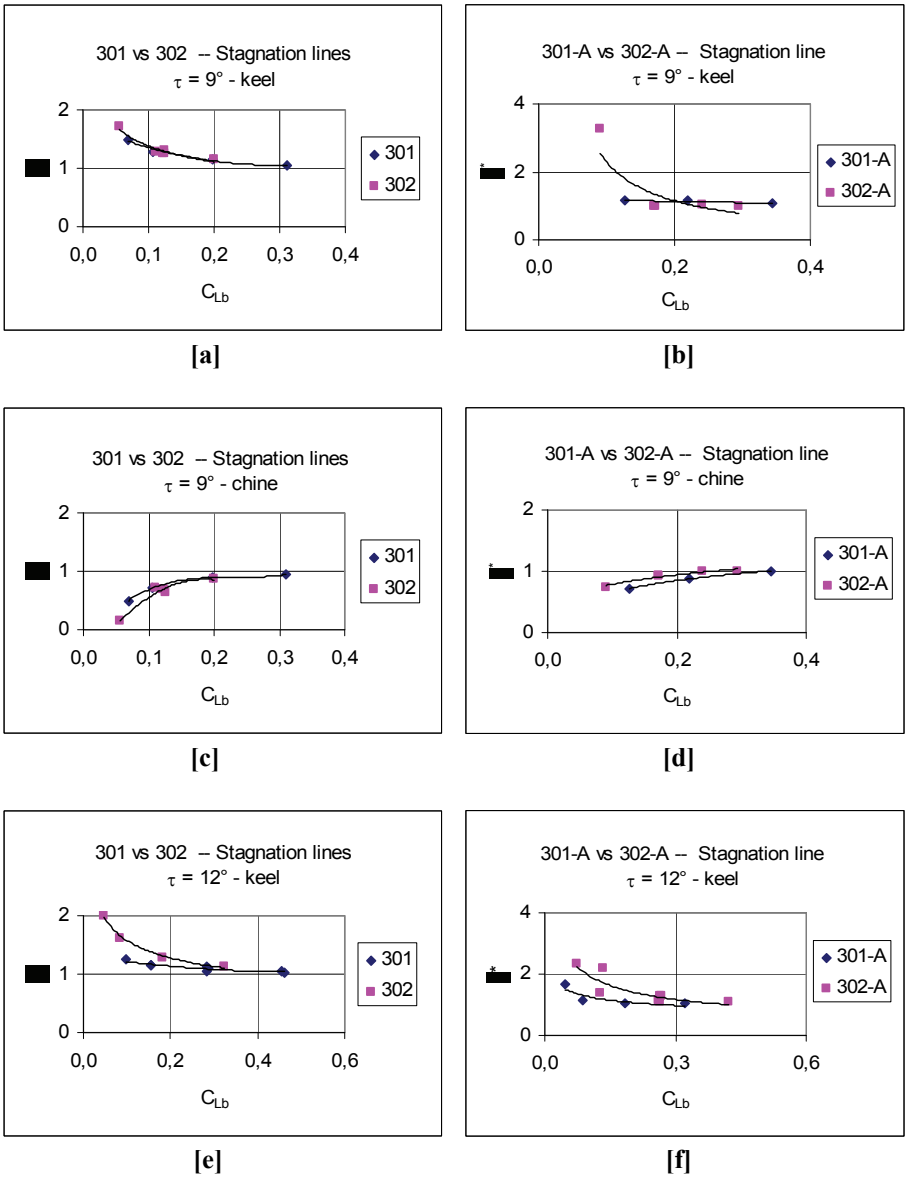

Figure 9.10-6 Deadrise angle effects on stagnation line ratio trend for V-bottom planing surface
(continue)

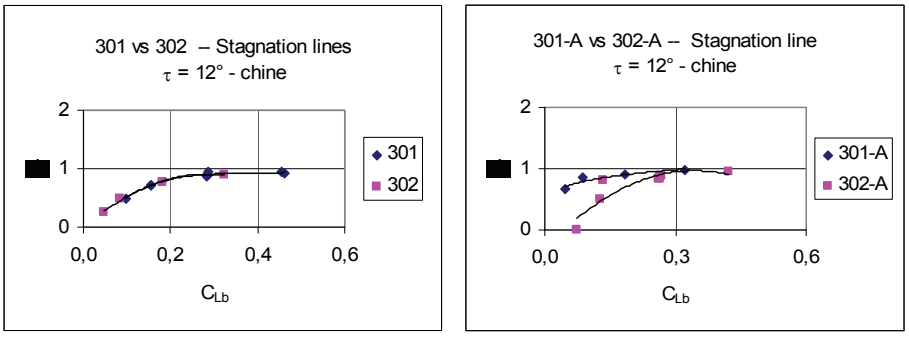

[g]

[h]

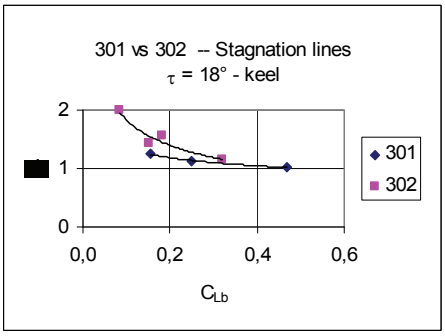

[i]

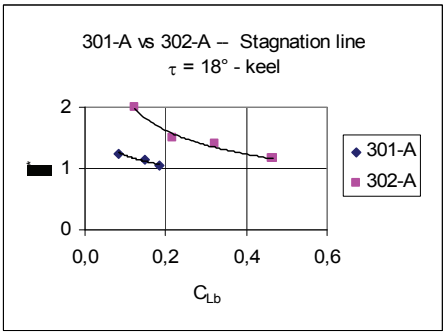

[j]

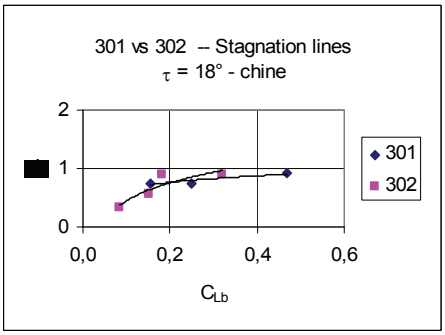

[k]

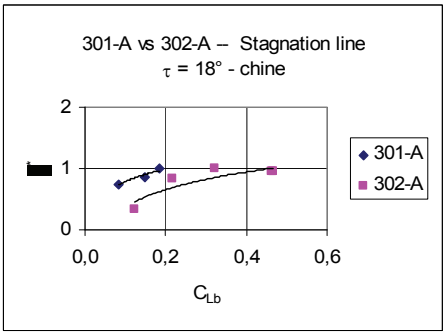

[l]

(Data source: [Kapryan & Boyd 1955])

Figure 9.10-6 Deadrise angle effects on stagnation line ratio trend for V-bottom planing surface

9.10.7 Horizontal Chine Effects for $\beta = 20°$

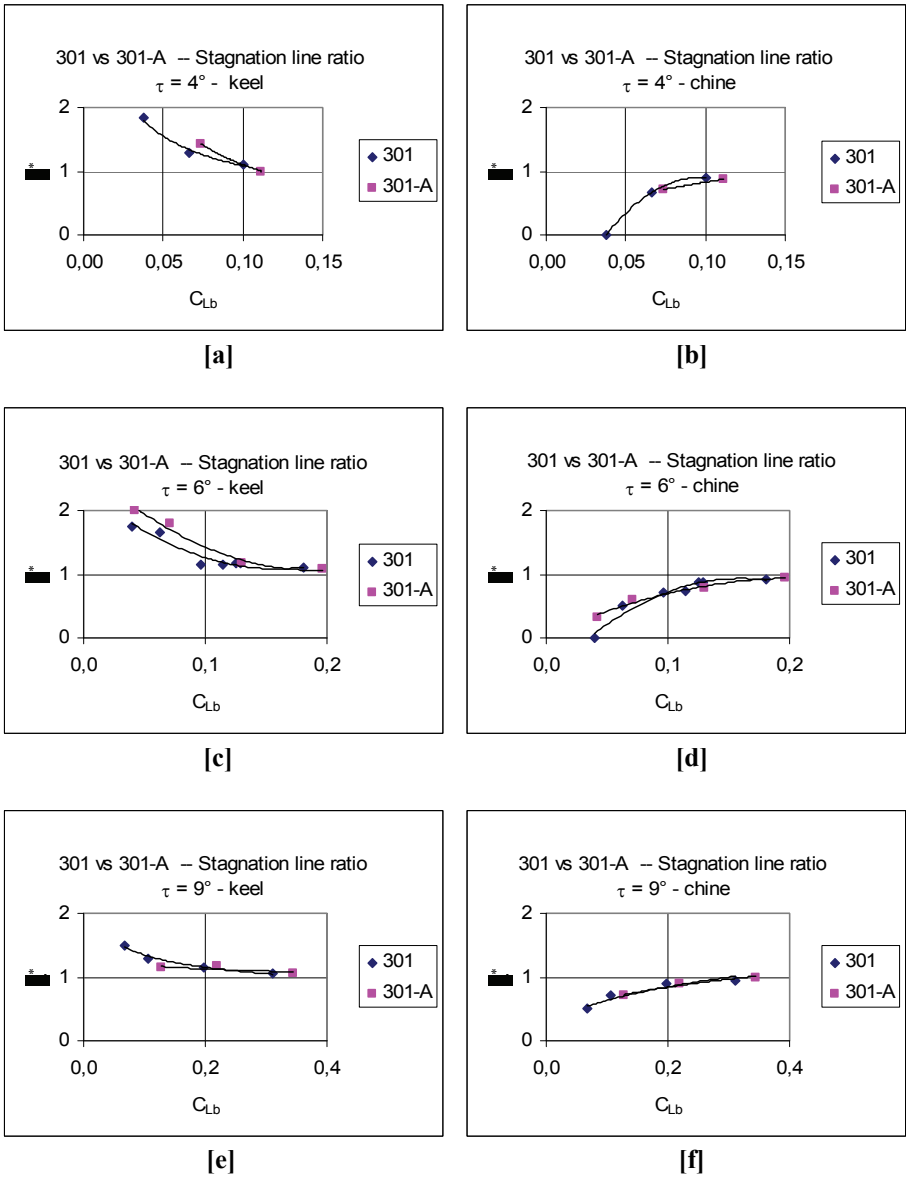

Figure 9.10-7 Horizontal Chine Effects on stagnation line ratio trend for V-bottom planing surface with β = 20° (continue)

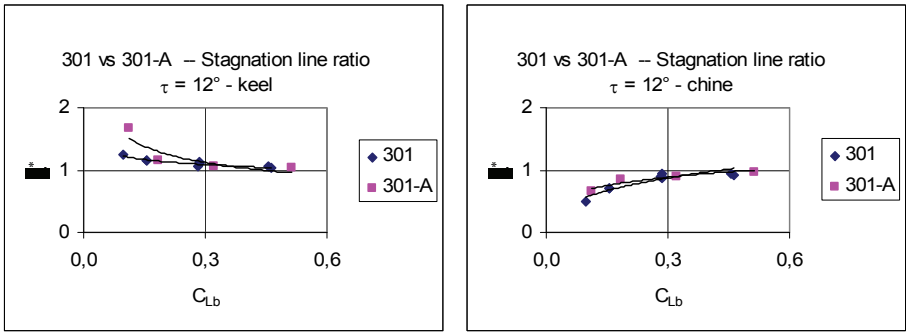

[g]

[h]

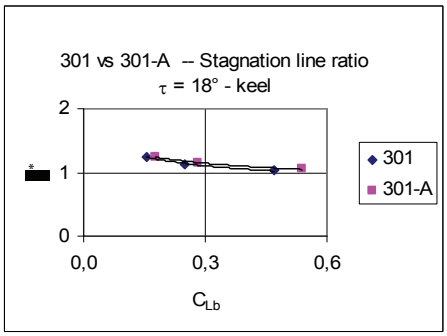

[i]

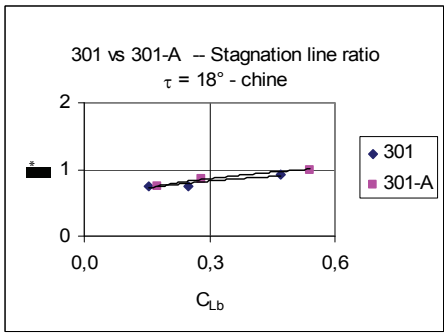

[j]

(Data source: [Kapryan & Boyd 1955])

Figure 9.10-7 Horizontal Chine Effects on stagnation line ratio trend for V-bottom planing surface with β = 20°

9.10.8 Horizontal Chine Effects for $\beta = 40°$

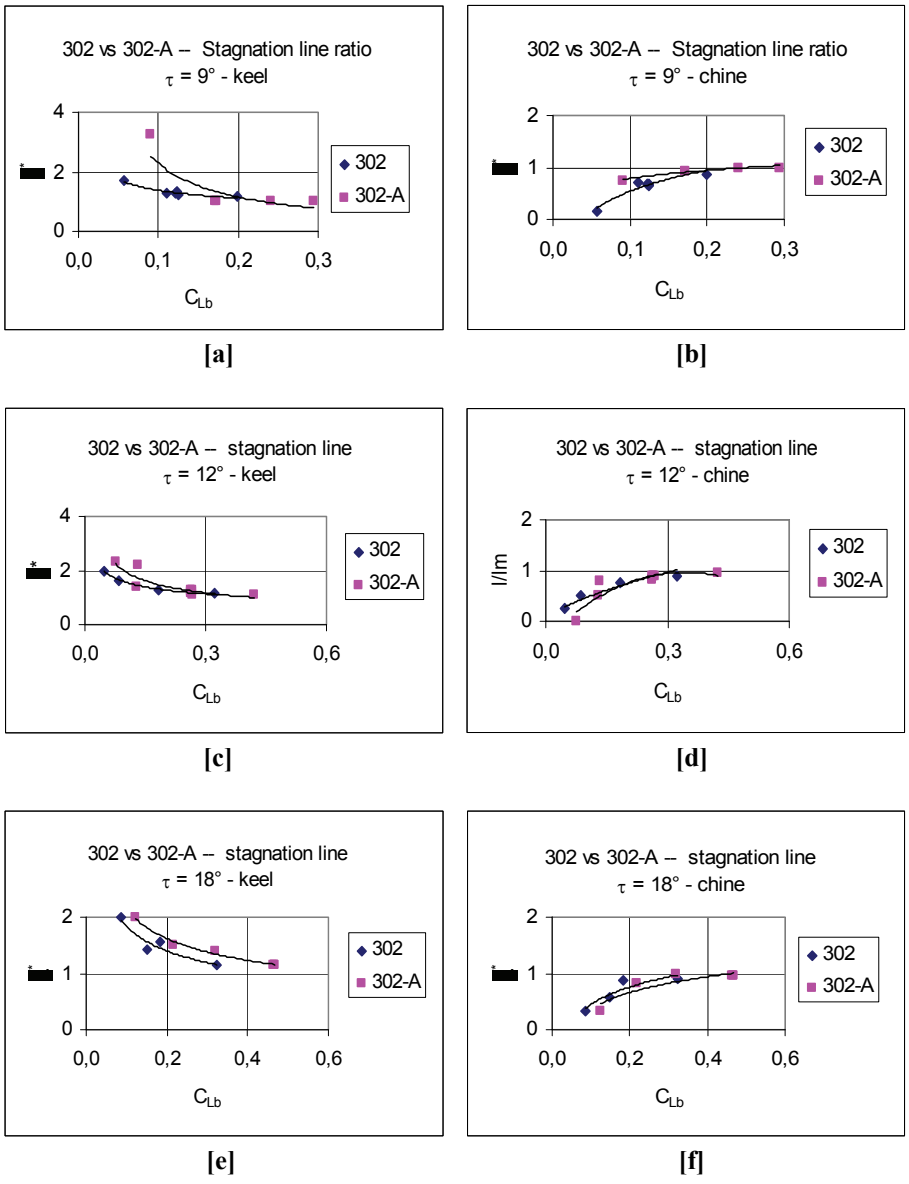

(Data source: [Kapryan & Boyd 1955])

Figure 9.10-8 Horizontal Chine Effects on stagnation line ratio trend for V-bottom planing surface with β = 40°

9.11 Diagrams: Spray Edges Trends

9.11.1 Model 301 - $\beta = 20°$

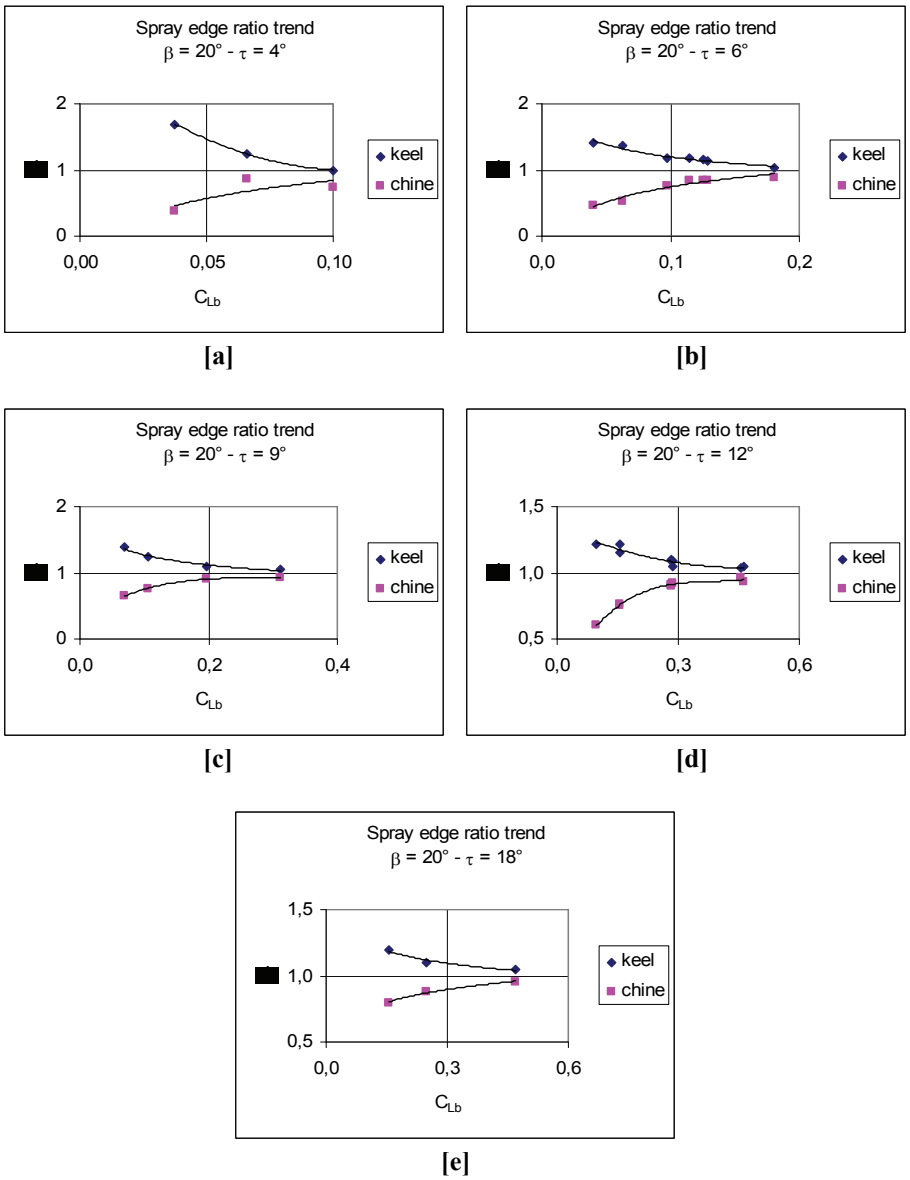

(Data source: [Kapryan & Boyd 1955])

Figure 9.11-1 Spray edge ratio trend for β = 20° without horizontal chine flared

9.11.2 Model 301-A - $\beta = 20°$ with Horizontal Chine Flared

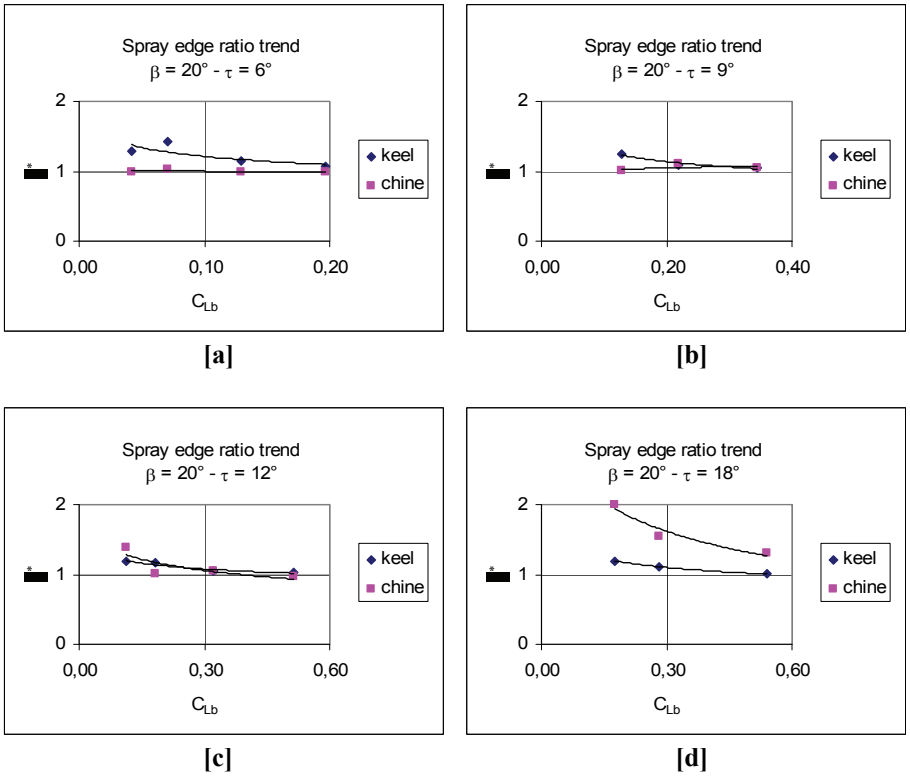

(Data source: [Kapryan & Boyd 1955])

Figure 9.11-2 Spray edge ratio trend for β = 20° with horizontal chine flared

9.11.3 Model 302 - $\beta = 40°$

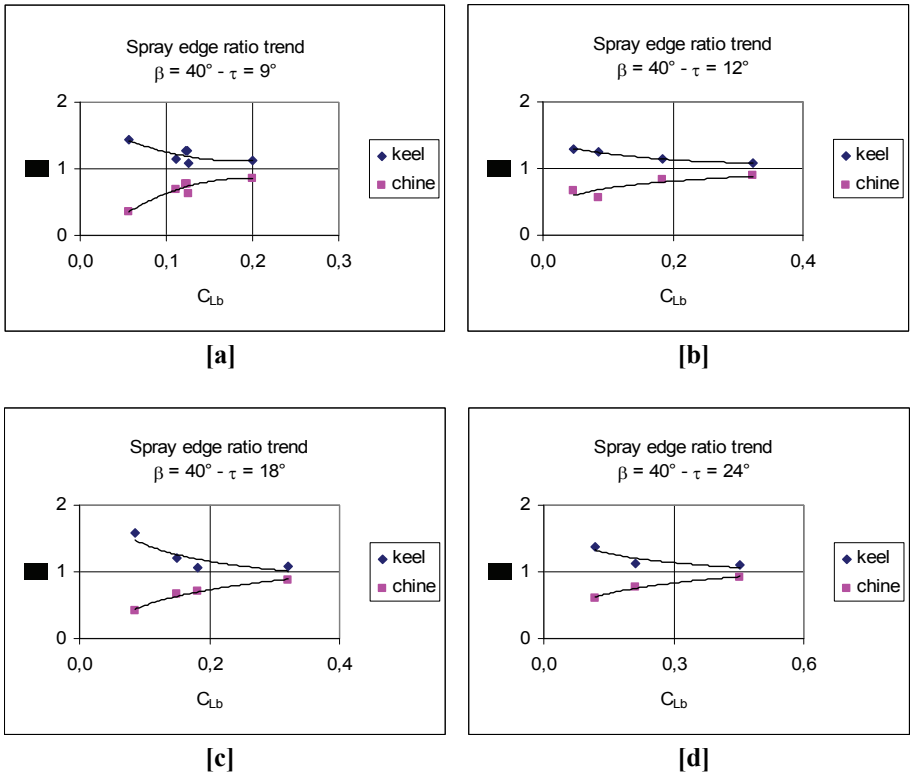

(Data source: [Kapryan & Boyd 1955])

Figure 9.11-3 Spray edge ratio trend for β = 40° without horizontal chine flared

9.11.4 Model 302-A - $\beta = 40°$ with Horizontal Chine Flared

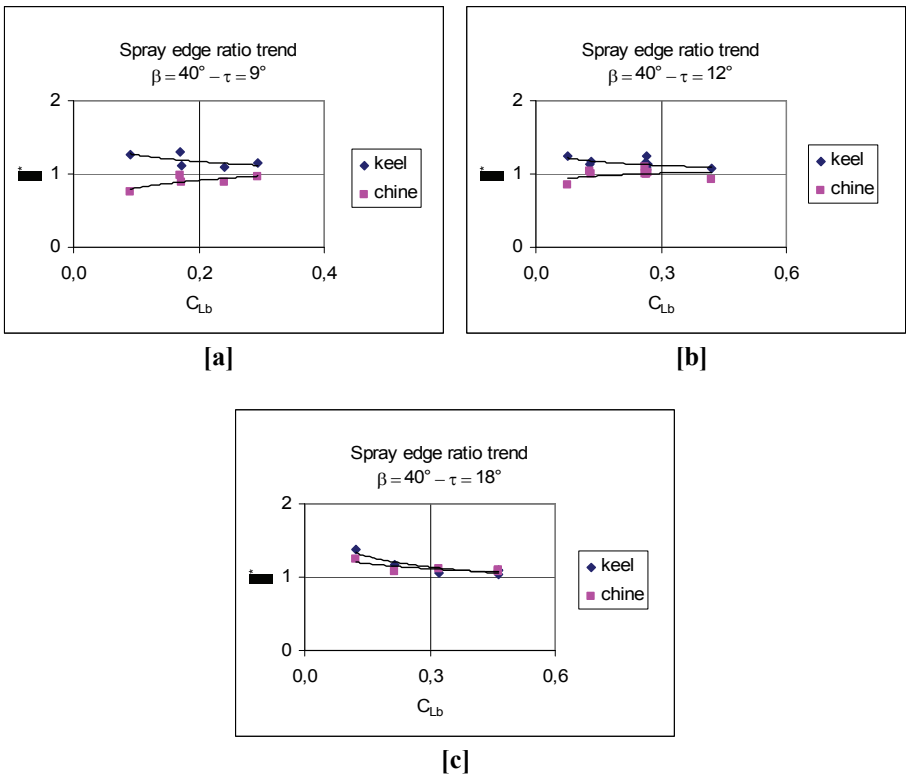

(Data source: [Kapryan & Boyd 1955])

Figure 9.11-4 Spray edge ratio trend for β = 40° with horizontal chine flared

9.11.5 Deadrise Effects: λ^* vs C_Δ with $C_V = 12.2$

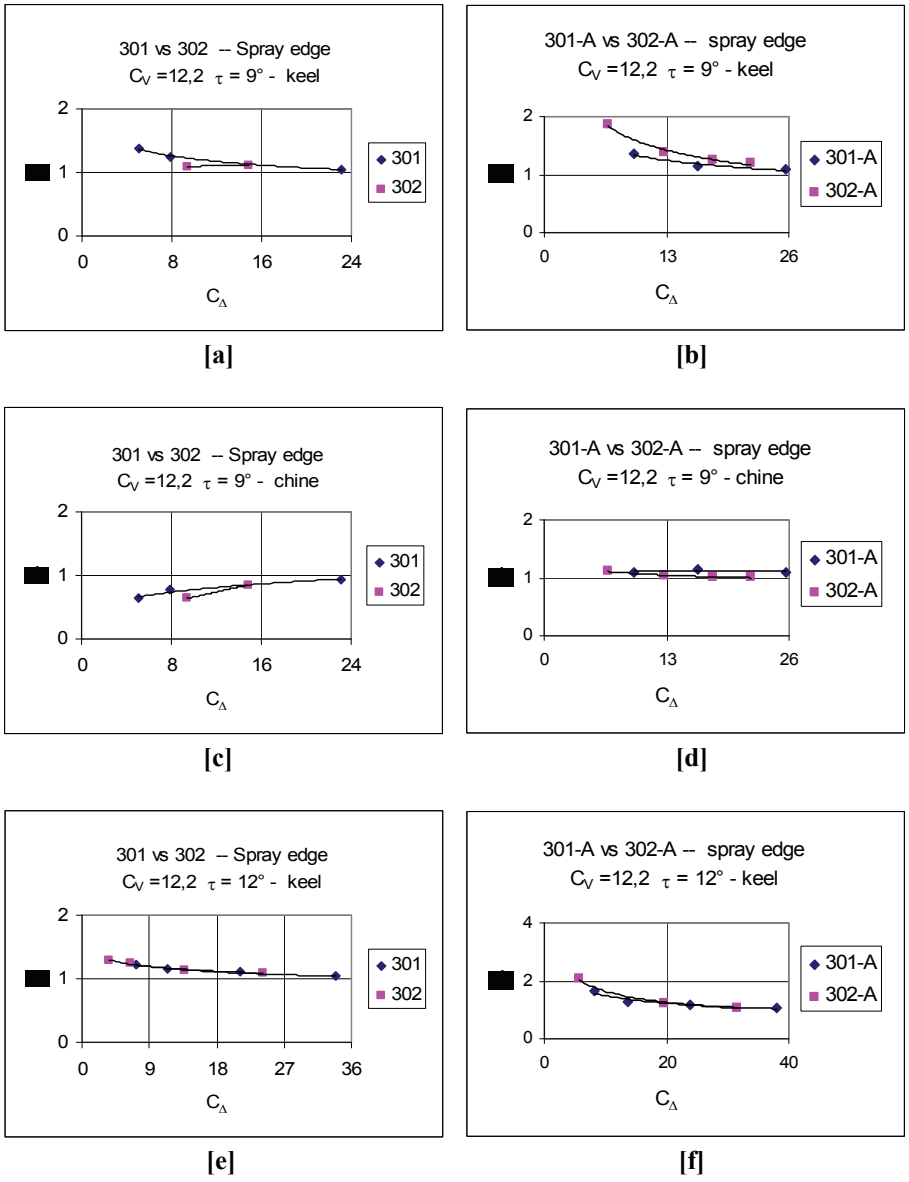

Figure 9.11-5 Deadrise variation effects on spray edge ratio trend for V-bottom planing surface with $C_V = 12.2$ (continue)

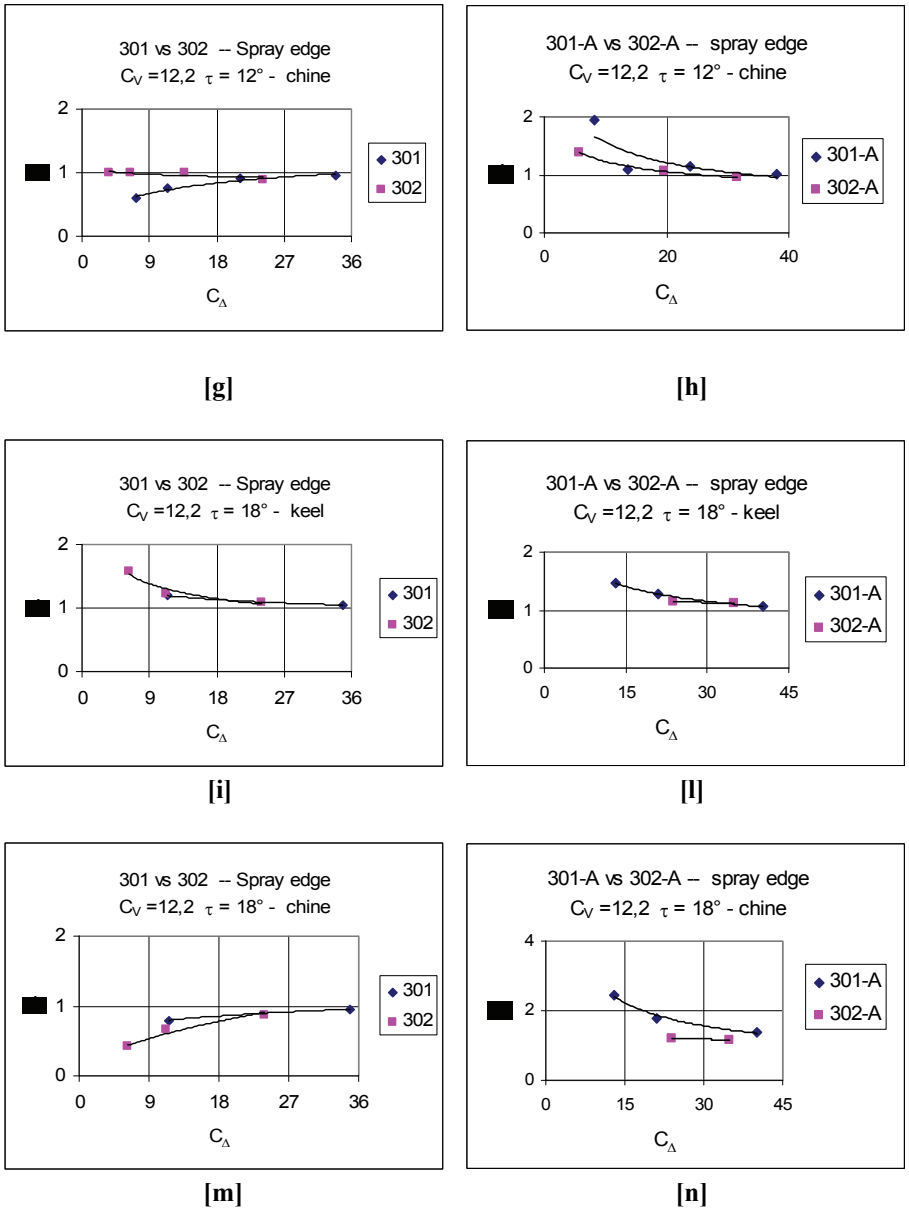

(Data source: [Kapryan & Boyd 1955])

Figure 9.11-5 Deadrise variation effects on spray edge ratio trend for V-bottom planing surface with C_V = 12.2

9.11.6 Deadrise Effects: λ^* vs C_{Lb}

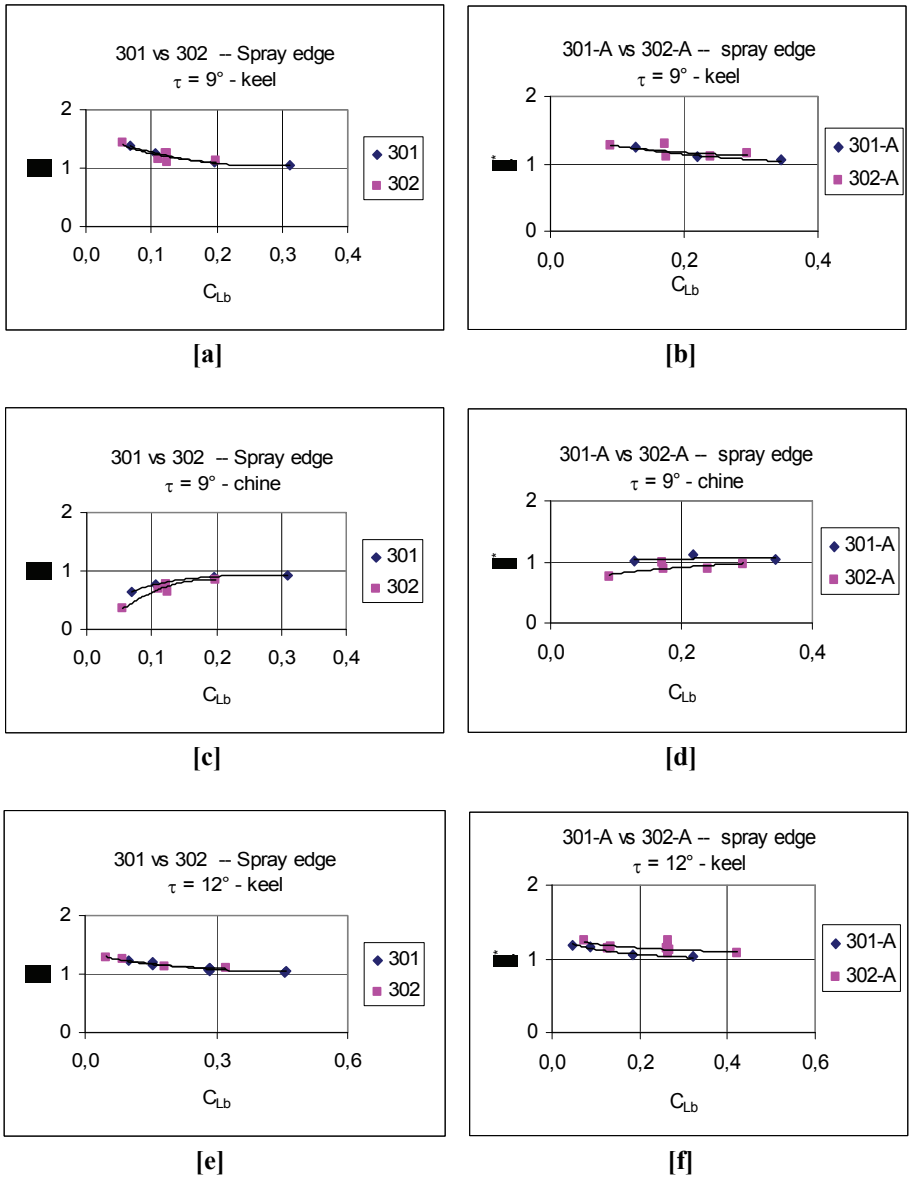

Figure 9.11-6 Deadrise variation effects on spray edge ratio trend for V-bottom planing surface (continue)

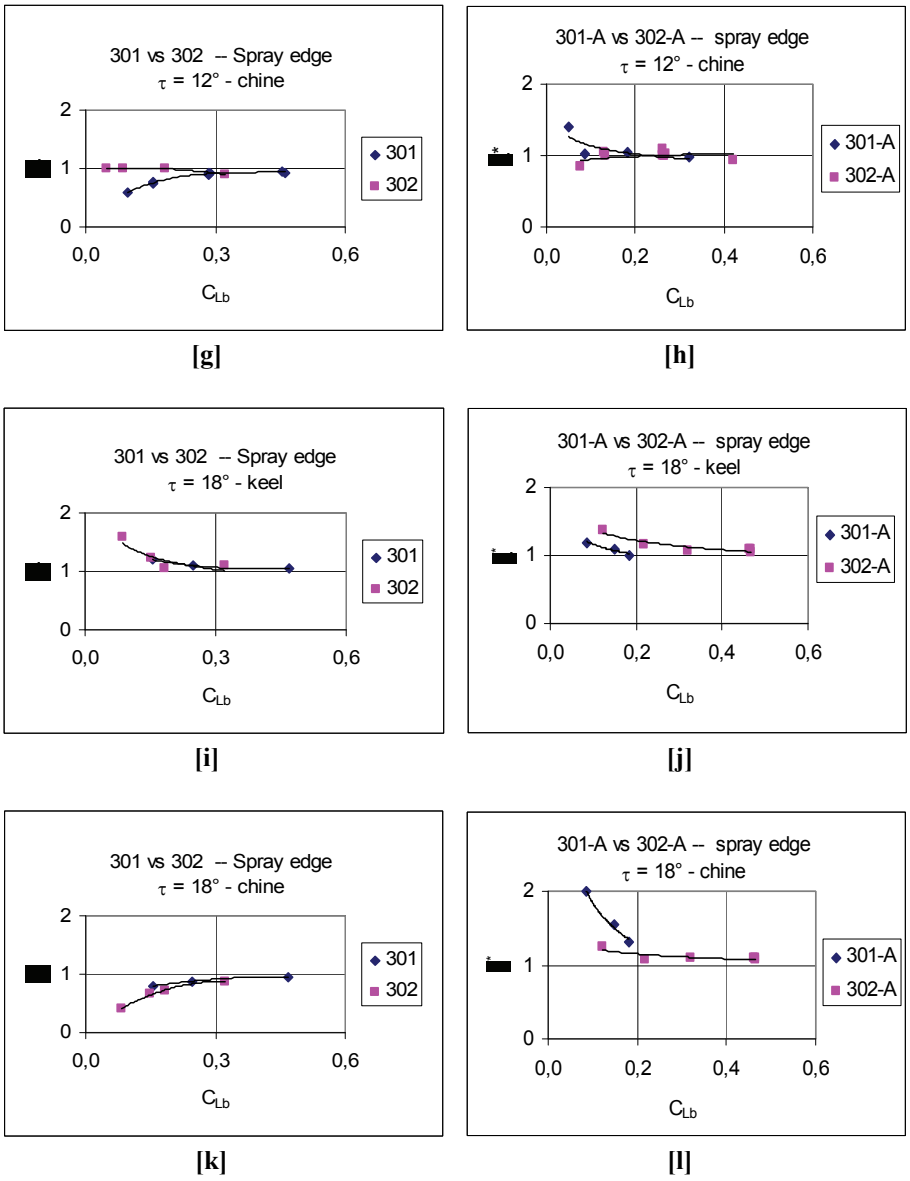

(Data source: [Kapryan & Boyd 1955])

Figure 9.11-6 Deadrise variation effects on spray edge ratio trend for V-bottom planing surface

9.11.7 Horizontal Chine Effects for $\beta = 20°$

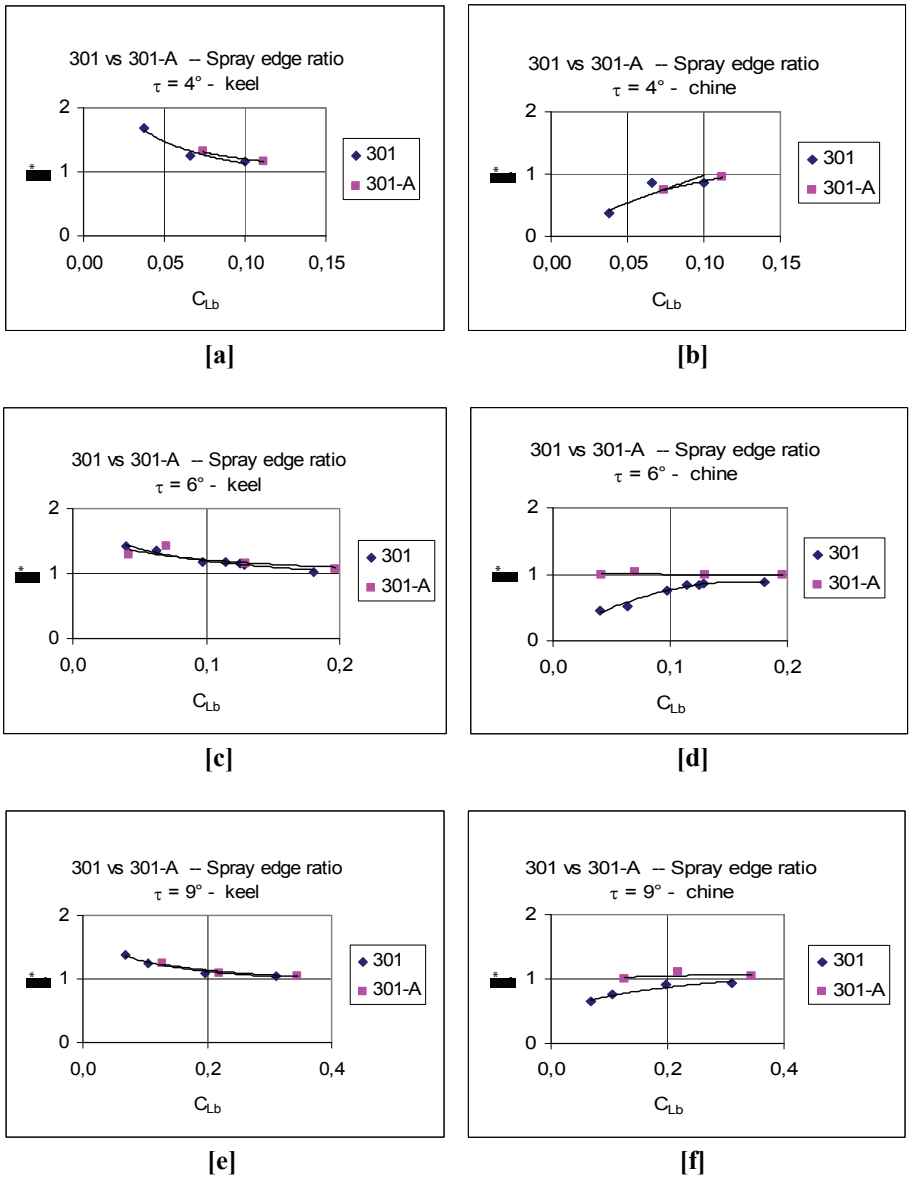

Figure 9.11-7 Horizontal Chine Effects on stagnation line ratio trend for V-bottom planing surface with β = 20° (continue)

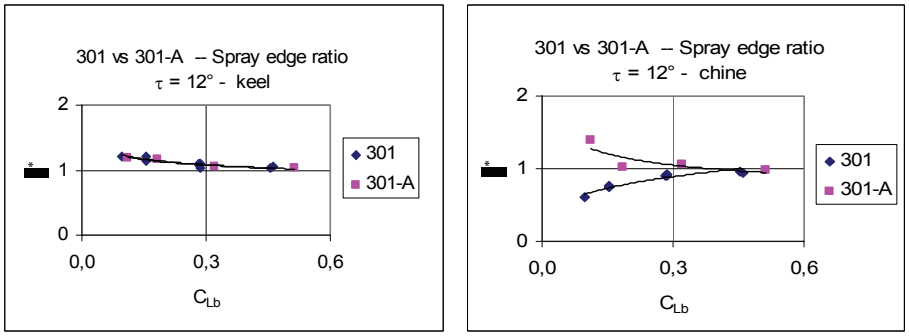

[g]

[h]

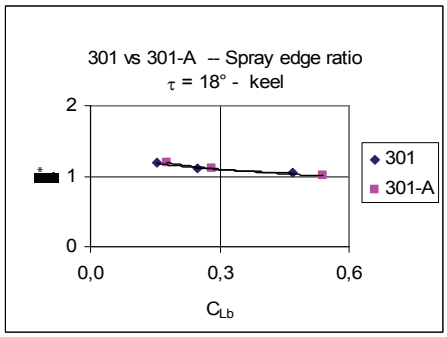

[i]

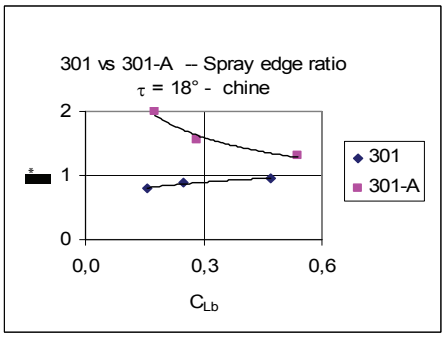

[j]

(Data source: [Kapryan & Boyd 1955])

Figure 9.11-7 Horizontal Chine Effects on stagnation line ratio trend for V-bottom planing surface with β = 20°

9.11.8 Horizontal Chine Effects for $\beta = 40°$

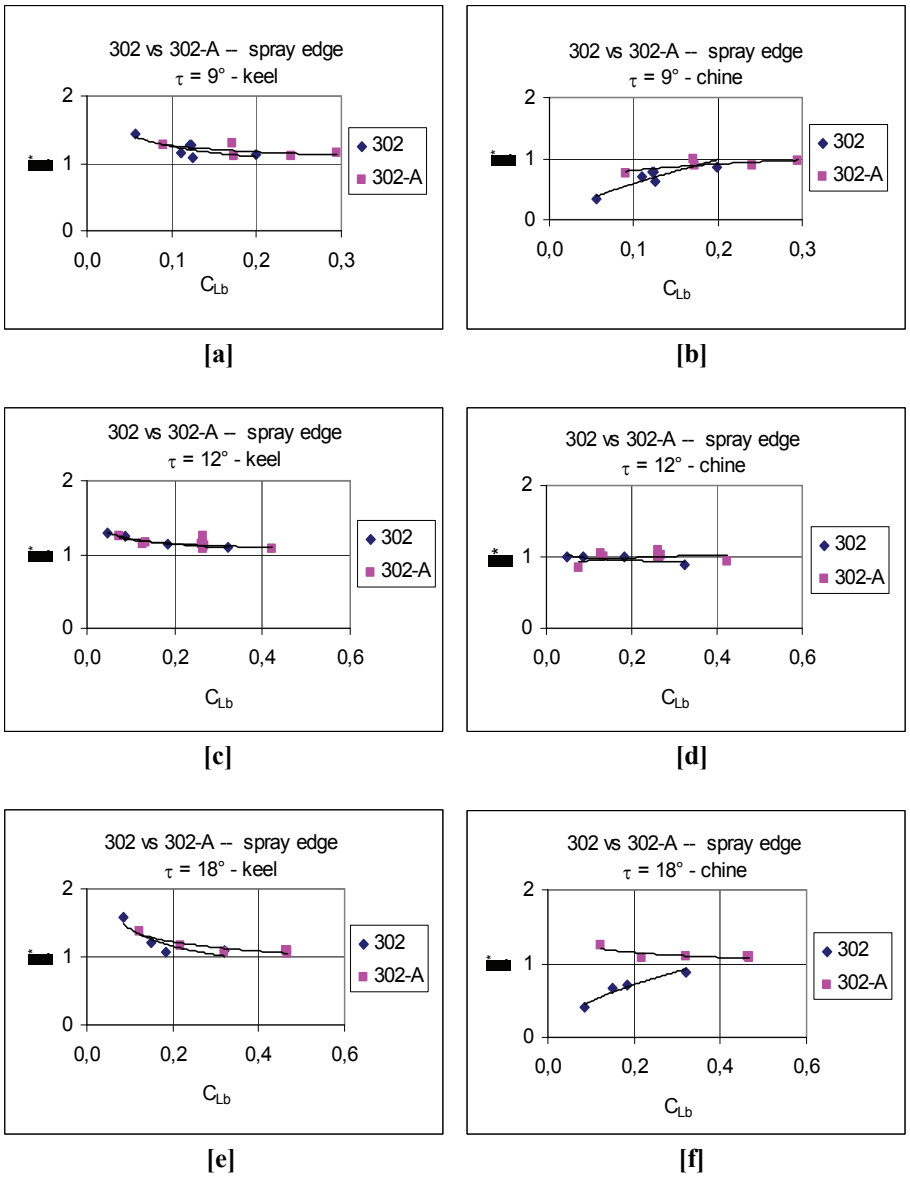

(Data source: [Kapryan & Boyd 1955])

Figure 9.11-8 Horizontal Chine Effects on stagnation line ratio trend for V-bottom planing surface with β = 40°

9.12 Global Trends

9.12.1 Center Pressure Location $\frac{l_p}{b}$ vs Mean Wetted Length $\frac{l_m}{b}$

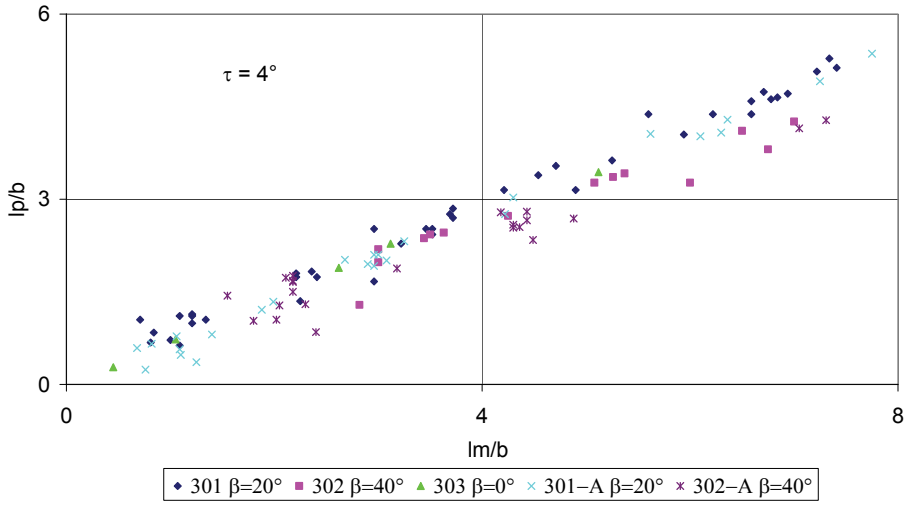

[a]

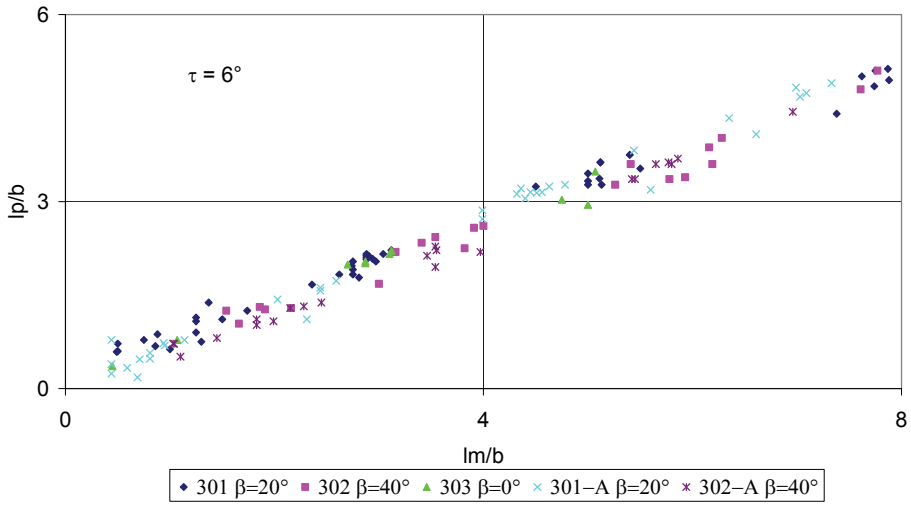

[b]

Figure 9.12-1 Center Pressure Location versus Mean Wetted Length (continue)

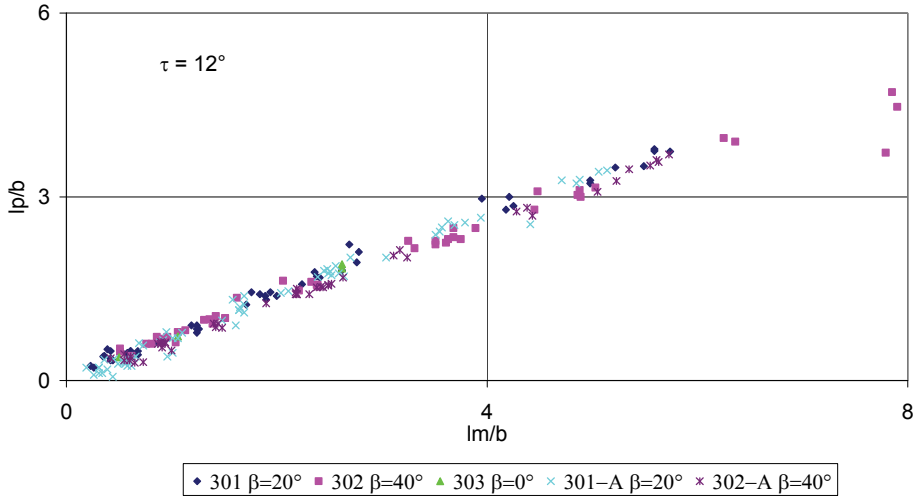

[c]

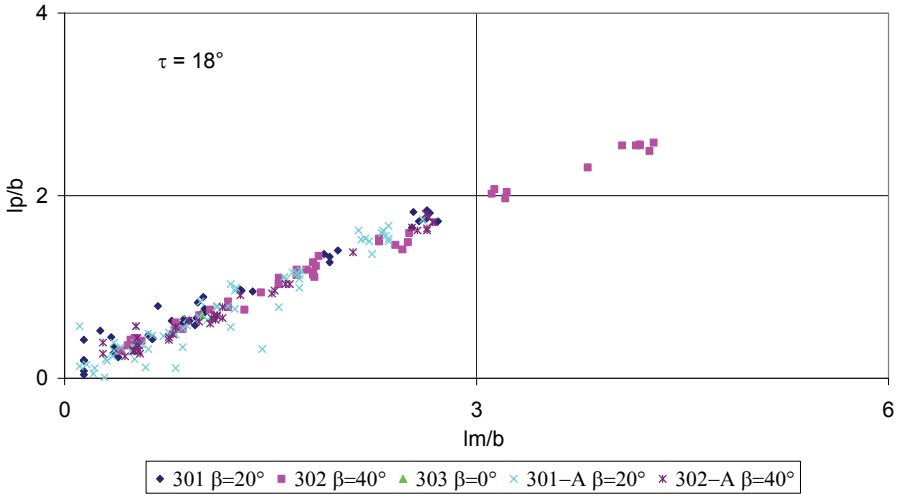

[d]

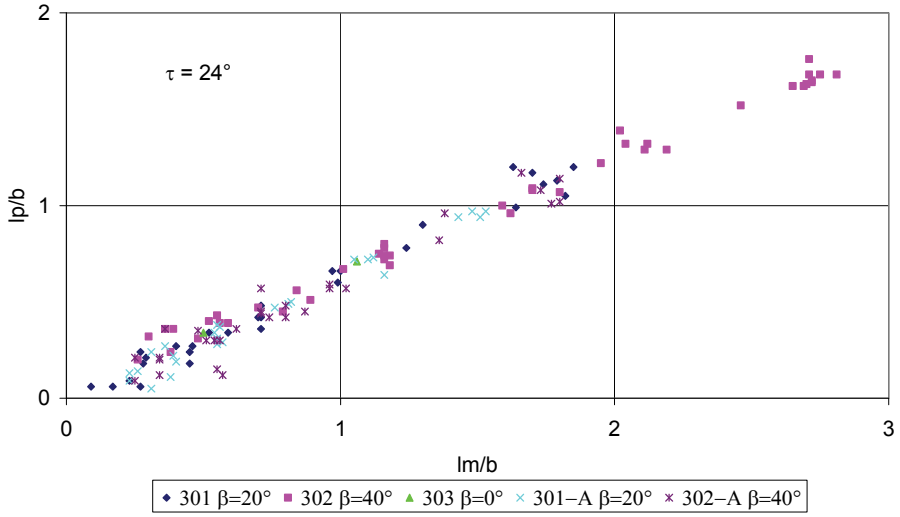

[e]

Figure 9.12-1 Center Pressure Location versus Mean Wetted Length (continue)

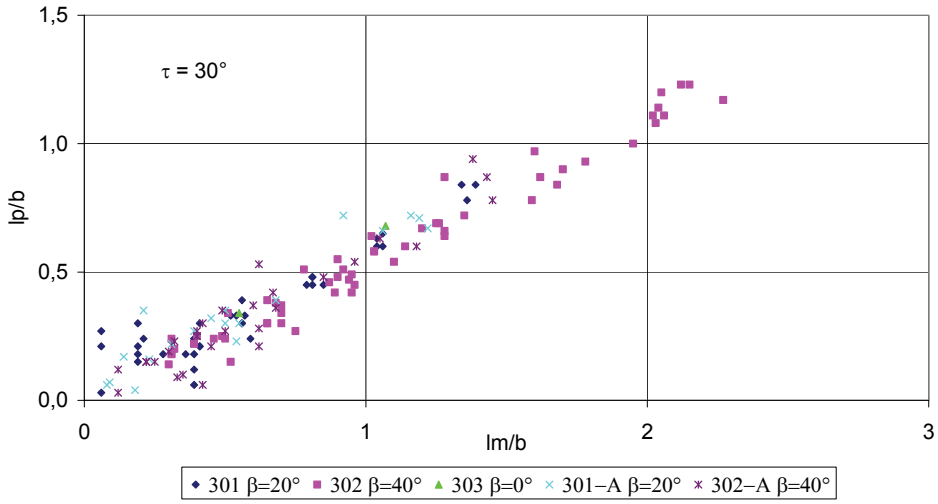

[f]

(Data sources: [Kapryan & Boyd 1955], [Kapryan & Weinstein 1952], [Blanchard 1952] [Chambliss & Boyd 1953])

Figure 9.12-1 Center Pressure Location versus Mean Wetted Length

9.12.2 Center Pressure Location to Mean Wetted Length Ratio

$\frac{l_p}{l_m}$ **vs** C_{Lb}

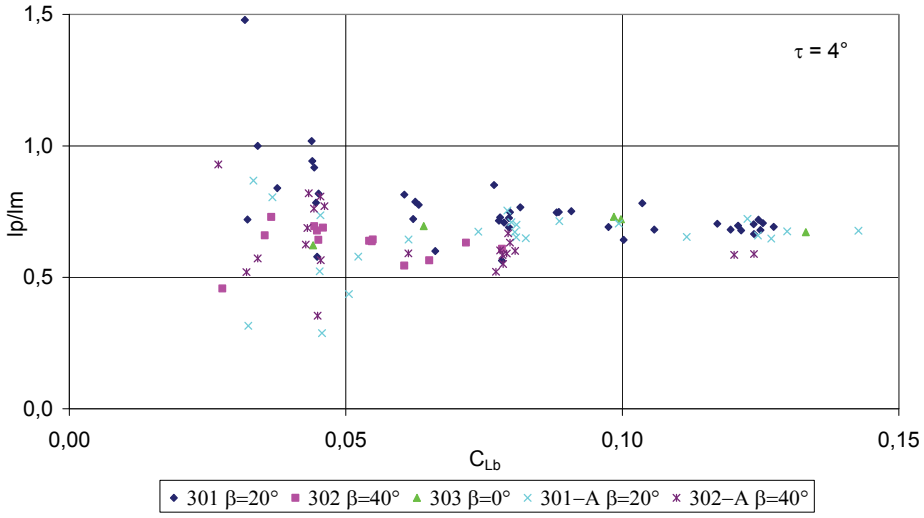

[a]

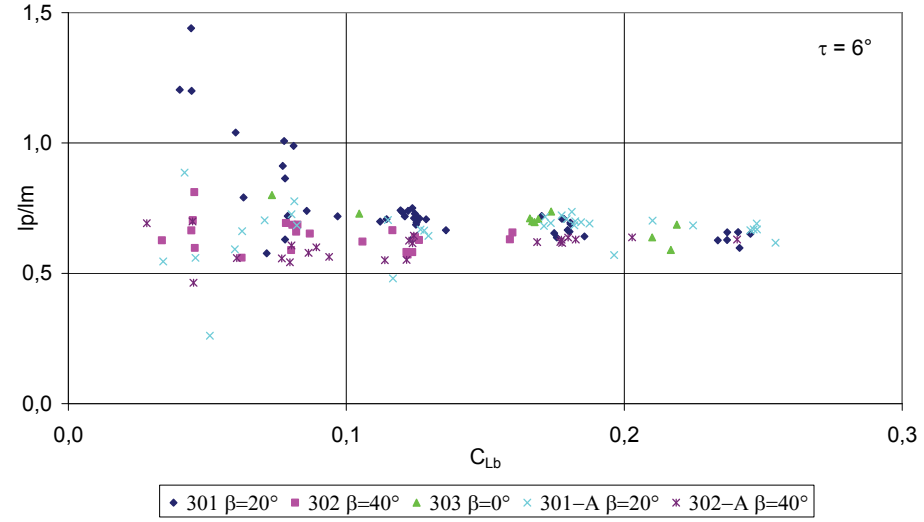

[b]

Figure 9.12-2 Center Pressure Location to Mean Wetted Length Ratio versus Lift Coefficient

(continue)

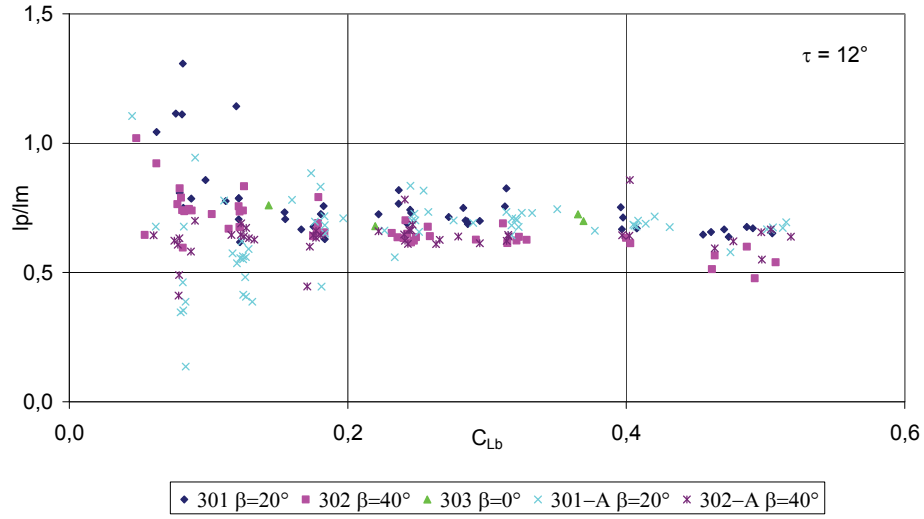

[c]

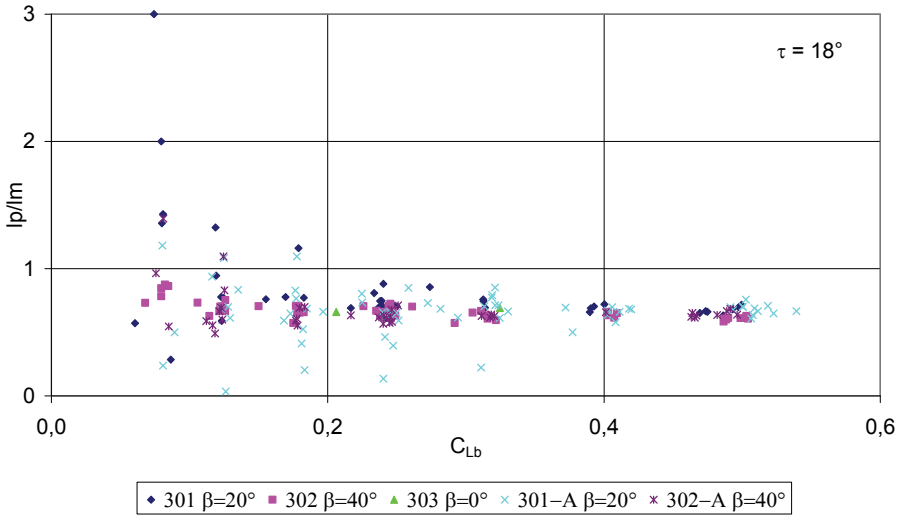

[d]

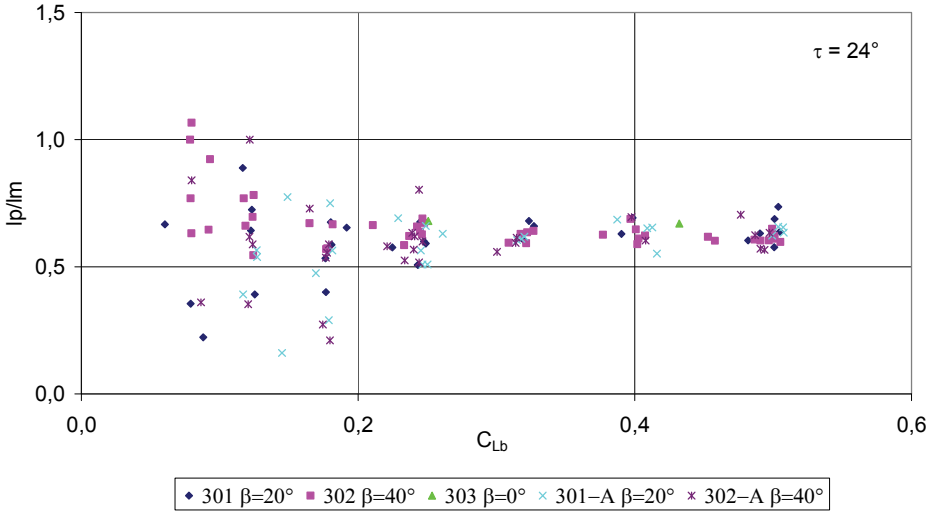

[e]

Figure 9.12-2 Center Pressure Location to Mean Wetted Length Ratio versus Lift Coefficient

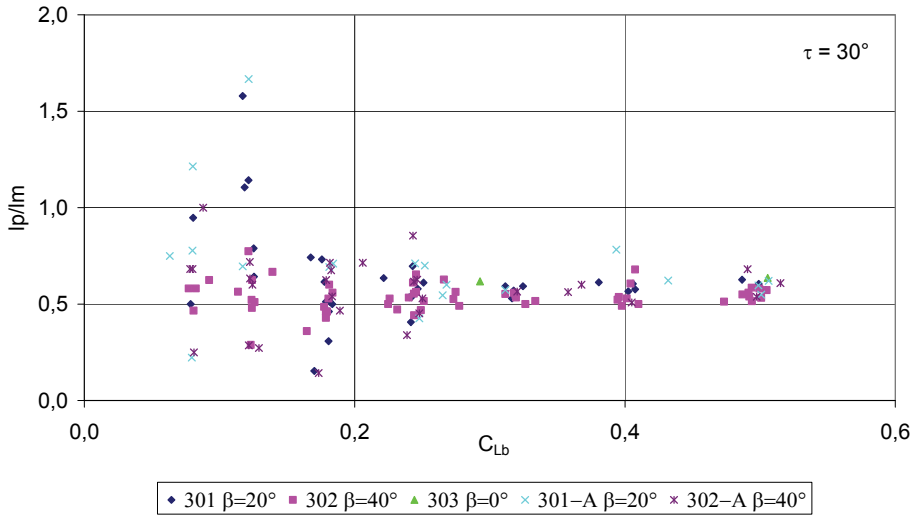

[f]

(Data sources: [Kapryan & Boyd 1955], [Kapryan & Weinstein 1952], [Blanchard 1952], [Chambliss & Boyd 1953])

Figure 9.12-2 Center Pressure Location to Mean Wetted Length Ratio versus Lift Coefficient

9.12.3 Stagnation Lines and Spray Edge Lines Trends

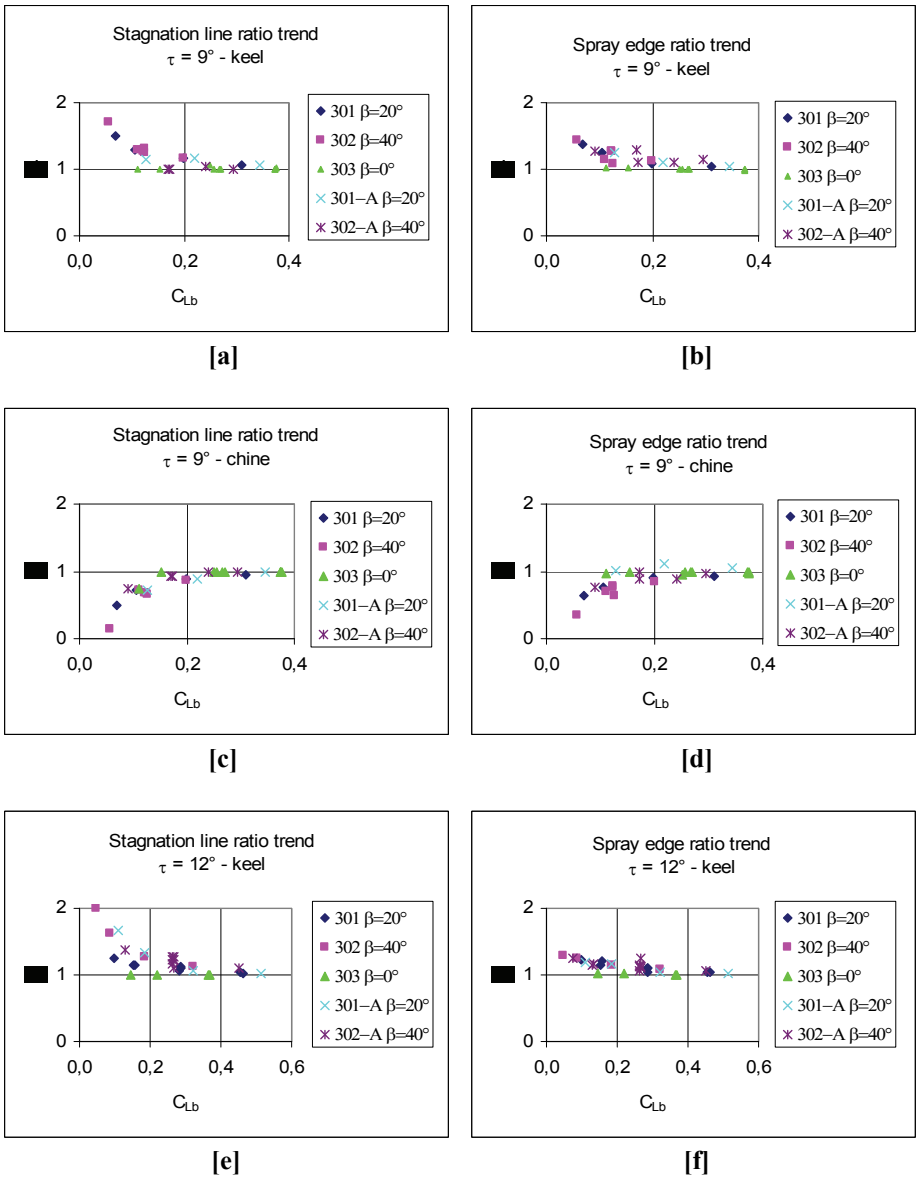

Figure 9.12-3 Stagnation Lines and Spray Edge Lines Trends versus Coefficient Lift (continue)

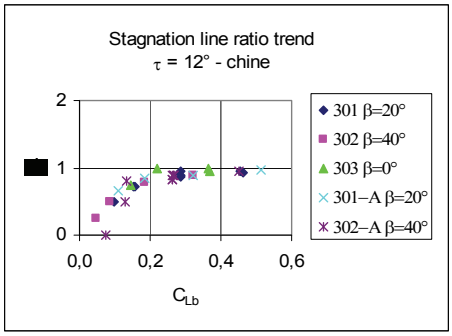

[g]

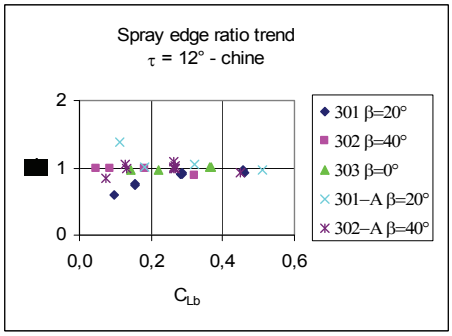

[h]

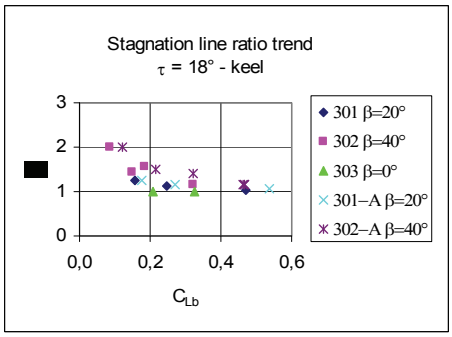

[i]

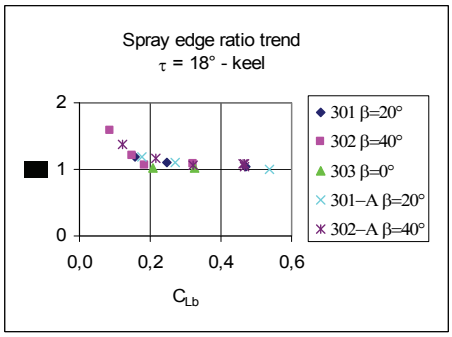

[j]

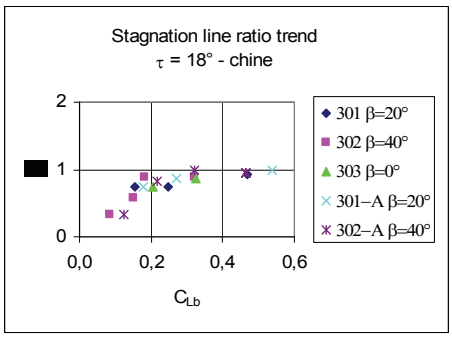

[k]

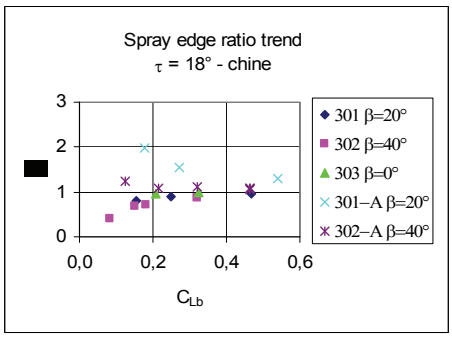

[l]

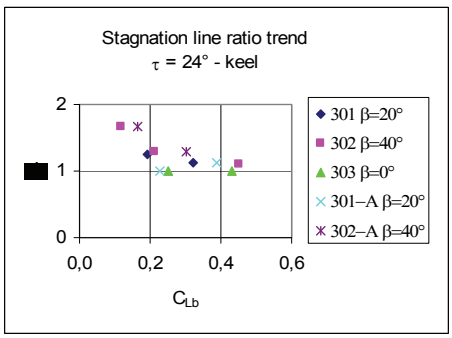

[m]

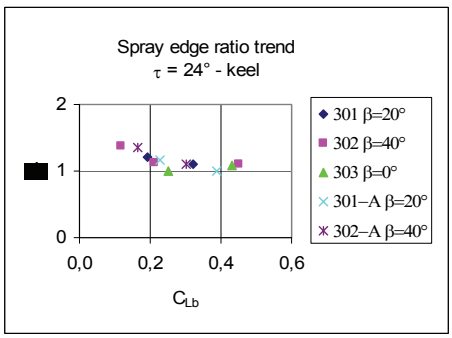

[n]

Figure 9.12-3 Stagnation Lines and Spray Edge Lines Trends versus Coefficient Lift (continue)

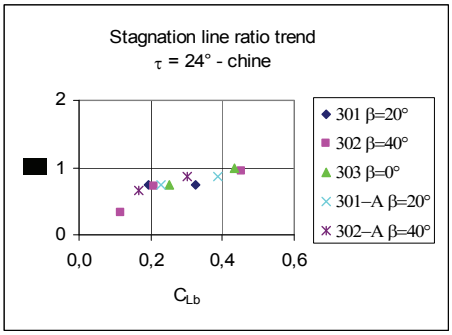

[o]

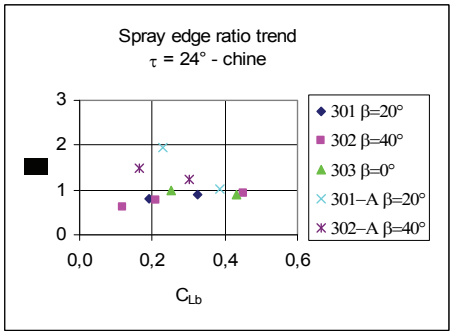

[p]

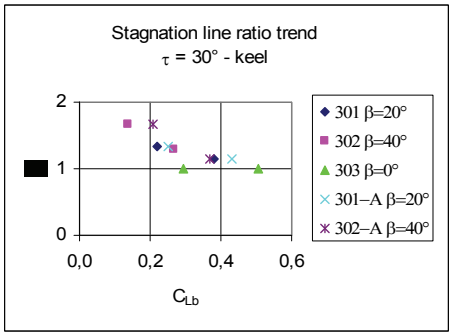

[q]

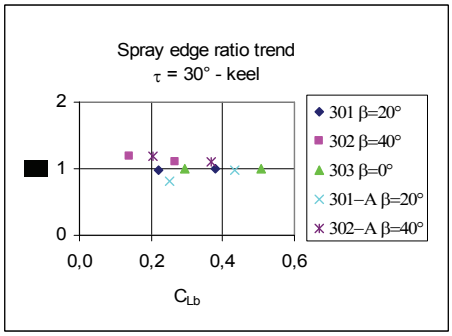

[r]

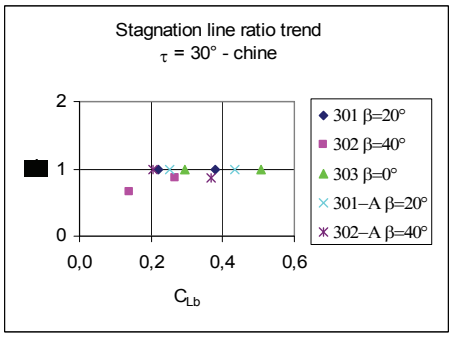

[s]

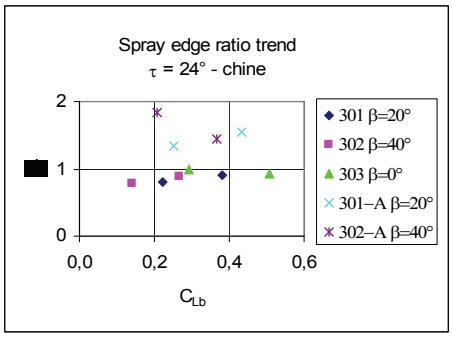

[t]

(Data sources: [Kapryan & Boyd 1955], [Kapryan & Weinstein 1952], [Blanchard 1952], [Chambliss & Boyd 1953])

Figure 9.12-3 Stagnation Lines and Spray Edge Lines Trends versus Coefficient Lift

9.13 Symbols

b	Beam	[inch]
b_w	Wetted beam	[inch]
C_{Lb}	Lift coefficient, based on beam	$C_{Lb} = \frac{\Delta}{\frac{\rho}{2} V^2 b^2} = 2\left(\frac{\sqrt{C_\Delta}}{C_V}\right)^2$
$C_{L\beta}$	Lift coefficient, based on beam, alias C_{Lb}	$C_{L\beta} \equiv C_{Lb}$
$C^*_{Lb,SL}$	Lift coefficient value associated to the invariance of the Stagnation Line position to the deadrise angle β	[-]
$C^*_{Lb,SE}$	Lift coefficient value pertinent to the invariance of the Spray Edge position to the deadrise angle β	[-]
C^*_{Lb}	Lift coefficient value related to the invariance of both Spray Edge and Stagnation Line position to the deadrise angle β	$C^*_{Lb} = \max\left\{C^*_{Lb,SL}; C^*_{Lb,SE}\right\}$
C_{L0}	Lift coefficient of a flat planing plate	[-]
C_V	Froude number, or speed coefficient, related to the beam	$C_V = \frac{V}{\sqrt{gb}}$
C_Δ	Beam loading, or load coefficient	$C_\Delta = \frac{\Delta}{\gamma b^3}$
dF	Elementary Force on a surface	[lb]
dS	Elementary area	$[sq\,inch]$
F	Force on a surface	[lb]
Fz	Vertical component of F	[lb]
g	Acceleration of gravity	$\left[ft/s^2\right]$
lm	Mean wetted length	[inch]
L_{OA}	Length Overall	[inch]
lp	Center pressure location (measured along the keel forward of trailing edge)	[inch]
l_{SE}	Spray edge position (measured along a buttock forward of trailing edge)	[inch]
l_{SL}	Stagnation line position (measured along a buttock forward of trailing edge)	[inch]
l_{Tm}	Mean transverse wetted perimeter	[inch]
l_{TW}	Transverse wetted perimeter	[inch]
$\hat{n}$	Normal unit vector to a surface	[-]

p	Dynamic pressure, measured at the orifice	$\left[lb/ft^2\right]$
p_{dyn}	Dynamic pressure	$\left[lb/ft^2\right]$
q	Dynamic pressure, based on the speed of the towing carriage	$\left[lb/ft^2\right]$
Sw	Wetted surface	$\left[sq\,inch\right]$
$S_{W,norm}$	Wetted surface projected on the horizontal plane	$\left[sq\,inch\right]$
V	Speed	$\left[ft/s\right]$
β	Deadrise angle	[deg]
Δ	Vertical load (displacement plus inertial vertical loads)	[lb]
γ	Unit weight of water	$\gamma = \rho g$
λ	Length ratio to beam	$\lambda = l/b$
λ_m	Mean wetted length ratio	$\lambda_m = l_m/b$
λ_p	Center pressure location ratio	$\lambda_p = l_p/b$
λ^*_{SE}	Spray edge ratio	$\lambda^*_{SE}\big\vert_X = \frac{l_{SE}\vert_X}{l_{SE}\vert_{middle}}$; (X = keel or chine)
λ^*_{SL}	Stagnation line ratio	$\lambda^*_{SL}\big\vert_X = \frac{l_{SL}\vert_X}{l_{SL}\vert_{middle}}$; (X = keel or chine)
ρ	Density of water	$\left[lb/ft^3\right]$
τ	Trim	[deg]

9.14 References

Blanchard; U.J. 1952. The Planing Characteristics of a Surface Having a Basic Angle of Dead Rise of 40° and Horizontal Chine Flare. *Report NACA TN 2842.* Washington, D.C. (USA). (web site: http://ntrs.nasa.gov/search.jsp)

Chambliss, D.B. & Boyd, G.M. Jr. 1953. The Planing Characteristics of Two V-Shaped Prismatic Surfaces Having Angles of Dead Rise of 20° and 40°. *Report NACA TN 2876.* Washington, D.C. (USA). (web site: http://ntrs.nasa.gov/search.jsp)

Kapryan, W.J. & Boyd, G.M. Jr. 1955. Hydrodynamic Pressure Distributions Obtained During a Planing Investigation of Five Related Prismatic Surfaces. *Report NACA TN 3477.* Washington, D.C. (USA). (web site: http://ntrs.nasa.gov/search.jsp)

Kapryan, W.J. & Weinstein, I. Jr. 1952. The Planing Characteristics of a Surface Having a Basic Angle of Dead Rise of 20° and Horizontal Chine Flare. *Report NACA TN 2804.* Washington, D.C. (USA). (web site: http://ntrs.nasa.gov/search.jsp)

Korvin-Kroukovsky B.V., Savitsky D., Lehman W.F. 1949. Wetted Area and Center of Pressure of Planing Surfaces. *Report SIT-DL-49-9-360 Davidson Laboratory* Stevens Institute of Technology. Hoboken, New Jersey (USA)

Mori, A. 1940. *Manuale di Tecnica Aeronautica*. Roma (Italy): Editoriale Aeronautica.

Sottorf, W. 1937. Analyse experimenteller Untersuchungon über den Gleitvorgang an der Wasseroberfläche. *Jahrbuch der deutschen Luftfahrtforschung,* pp 320-339. [English version: Analysis of Experimental Investigations of the Planing Process on the Surface of the Water. *Report NACA TM 1061*, 1944. Washington, D.C. (USA). (web site: http://ntrs.nasa.gov/search.jsp)]

Luciano OLIVIERO

viale CASTELLUCCIO 26F
80059 Torre del Greco (NA) - ITALY

+39 081 882 68 23
+39 347 186 76 21 (mobile)

luciano.oliviero@tin.it
luciano.oliviero@gmail.com

UNIVERSITÀ DEGLI STUDI DI NAPOLI
FEDERICO II

DOCTORATE SCHOOL OF INDUSTRIAL
ENGINEERING

DOCTORATE PROGRAM IN
AEROSPACE, NAVAL AND TOTAL QUALITY MANAGMENT
ENGINEERING

XXII CYCLE

PhD THESIS

APPENDICES
Volume II - No. 1

HYDRODYNAMICS OF PLANING HULLS

A POWER PREDICTION METHOD FOR WARPED V-BOTTOM HULL FORMS

Tutors
Chiar.mo Prof. Ing. Francesco Saverio
MARULO
Prof. Ing. Carlo Francesco Mario
BERTORELLO

Candidate
Ing. Luciano OLIVIERO

CONTENTS

VOLUME I

APPENDIXES
VOLUME II -NO. 1

VOLUME II -NO. 2

APPENDIX F

SAVITSKY'S METHOD

APPROXIMATIONS

10.1 Table of Contents

10.2 Figure Index

10.3 Introduction

The most diffused method to predict the speed-resistance relationships for planing hulls, was proposed by Savitsky, and has been known as Savitsky's method since 1964.

Nowadays, many versions of Savitsky's method are available [Savitsky 1964], [Savitsky & Brown 1976], [Savitsky & Koebel 1993], as well as there are other methods which are related to, as Hadler's method [Hadler 1966].

From a timeline point of view, a first attempt to develop a procedure for predicting the planing performance of a monohedral hull was developed by Murray [Murray 1950].

Murray's method was based on Sottorf's work [Sottorf 1932] and Korvin-Kroukovsky's work [Korvin-Kroukovsky et al 1949] on planing surfaces.

Some years later, Savitsky [Savitsky 1964] proposed an improved version of Murray's prediction method.

The two main differences between the methods are related to the lift coefficient and to the Center of pressure position formulas.

The lift coefficient formula was improved taking in account the splash up phenomena: during the planing the water rises above the still-water level in the fore part of the planing surface, and this rise is greatest for a flat planing plate [Payne 1994].

Meanwhile a new Center of pressure position formula was developed "forcing" airfoil results, flat planing plate results, as well as V-bottom planing surface results.

This formula shows that the center of pressure of a planing hull is beyond the theoretical position for an airfoil: this gap is related to the hull geometry as well as the kinematic characteristics of the motion.

All these methods are based on regression formulas, which have been based on prismatic hull form model tests, as well as on planing surfaces test results. [Savander et al. 2002]

All the above mentioned methods can be classified as:

- Short Form Method (SF),
- Long Form Method (LF).

In the SF methods, per each value of trim τ, all forces involved pass through the Center of Gravity and the equilibrium equation of the pitching moment is an identity always satisfied.

In the LF methods the gravity is the only force that passes through the Center of Gravity for each trim τ , meanwhile there is one and only one value of the trim angle τ. corresponding to all forces pass through the Center of Gravity and the equilibrium equation of the pitching moment is satisfied. Thereby, in order to get the equilibrium planing conditions per each speed V, designers have to iterate a series of steps of the procedure, and this require a great computational effort.

It is interesting to point out that Long Form methods have been usefully applied thanks to the introduction of computer machines in design process and the most common used is the Savitsky's one.

Savitsky's methods have advantages and disadvantages, and the most of all are common to LF as well as SF procedure: so we are use to speak about advantage/disadvantage of Savitsky's method.

The first major advantage of Savitsky's method is that it is simple to perform.[Akers 1999]

This method accounts for a small number of the design parameters, maximum beam of chine at transom, a single characteristic value for the deadrise angle, ship weight and longitudinal position of the centre of gravity. [Barry et al. 2002]

Savitsky's method has a second major advantage: it is accurate for many commonly used prismatic hull forms.

There are a number of disadvantages to Savitsky's method. Spray resistance component and viscous resistance due to the wetted surface of hull sides are neglected.

Further, deadrise angle variation either longitudinal or transversal is not considered.

In addition, the method is quasi-static and it does not directly predict transient behaviour.

Finally, the method lumps all forces into a series of empirical relationships so point or panel hydrodynamic loads cannot be predicted using the method [Akers 1999].

In despite of these Savitsky's methods are the most used resistance prediction methods in the design process of a planing small craft.

The description of the Savitsky's methods is not the goal of this Appendix work[130]: the approximations of the formulas used are highlighted.

This choice is useful in order to give evidence of the approximations which burden on the method proposed in this Thesis work.

[130] For a description of Savitsky's methods, see Chapter 2, Paragraph 3, Sub-Paragraph 3.2 of this Thesis work.

10.4 Savitsky's approximations

Hereinafter the formulas of Savitsky's method taken in account are that ones exposed in paper of 1964.

10.4.1 Wave rise in the spray-root area

"*The wave rise in the spray-root area is accounted for by the following consideration. Wagner computed the wave rise for a two-dimensional wedge penetrating a fluid surface vertically, and found that the actual wetted width of the wedge was* $\pi/2$ *times the wetted width defined by the calm-water intersection with the bottom.*

The motion of a deadrise planing surfaces can be represented as a two-dimensional problem by considering the water flow between two vertical planes normal to the plane of symmetry of the planing surface.

To an observer located between these two planes, the passage of the prismatic Vee planing surface will appear identical to the vertical immersion of a wedge.

This being the case, the $\pi/2$ *wave-rise factor computed by Wagner is applicable, and the difference between actual wetted keel length and chine length for a prismatic planing surface is given by:*

$$L_K - L_C = \frac{b}{\pi}\frac{\tan\beta}{\tan\tau} \qquad (3)"$$

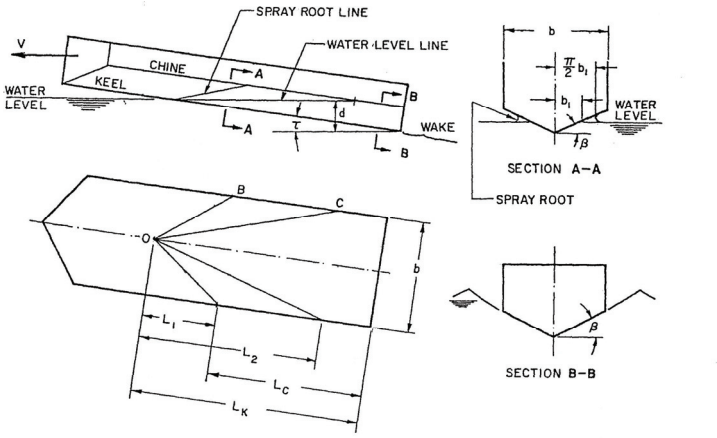

Figure 10.4-1 Waterline intersection for constant deadrise surface[131] [Savitsky 1964]

As first step let explain the above formula.

Let A-A the transversal section of a monohedral hull passing through the waterline intersection with the chines, as shown:

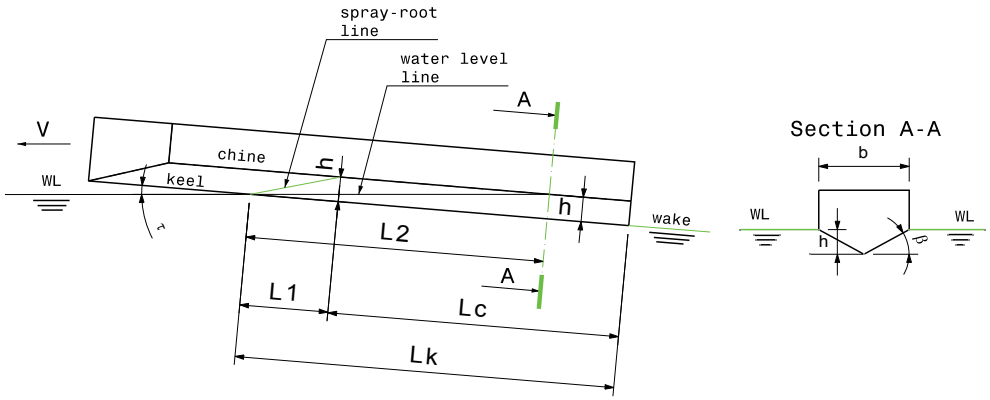

Figure 10.4-2 Waterline intersection for a monohedral hull form

and h the distance between the water level line and the keel, we have:

$$h = L2 \tan\tau \quad \text{and} \quad h = \frac{b}{2}\tan\beta$$

[131] LEGEND

b	beam of planing surfaces;
d	vertical depth of trailing edge of boat (at keel) below level water surface;
Lc	wetted chine length;
Lk	wetted keel length;
L1	difference between wetted keel and chine lengths;
L2	difference between keel and chine lengths wetted by level water surface;
β	deadrise angle of planing surface;
τ	trim angle of planing area

hence:

$$L2 = \frac{b}{2}\frac{\tan\beta}{\tan\tau} \qquad \text{(F. 1)}$$

Let A'-A' the transversal section of a monohedral hull passing through the spray root line intersection with the chines, as shown

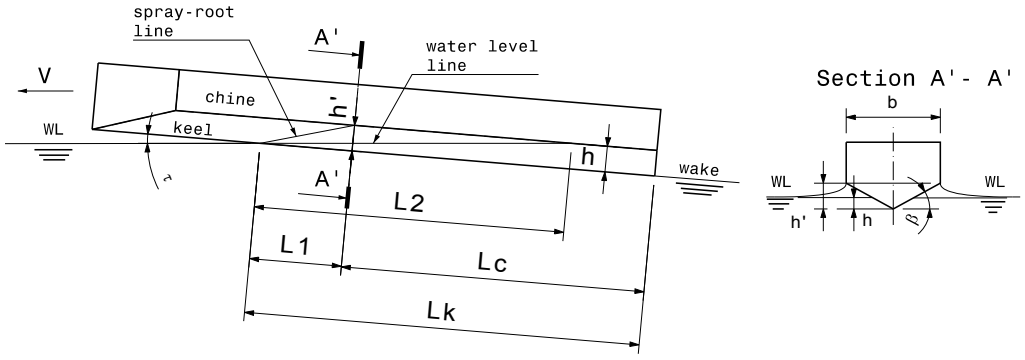

Figure 10.4-3 Spray root line intersection for a monohedral hull form

and h' the distance between the spray root line intersection with the chines and the keel, we have:

$$L1 = Lk - Lc$$

$$h' = \frac{b}{2}\tan\beta$$

and

$$h = L1\tan\tau \quad \text{or} \quad h = (Lk - Lc)\tan\tau$$

In order to take in account the splash up phenomena, Savitsky introduced Wagner's theoretical results on the wave rise of an impacting wedge, and with reference to the symbols in Figure 10.4-3 we have:

$$h' = \frac{\pi}{2}h$$

so

$$\begin{cases} h' = \dfrac{b}{2}\tan\tau \\ h' = \dfrac{\pi}{2}\left[\left(Lk - Lc\right)\tan\tau\right] \end{cases}$$

hence:

$$Lk - Lc = \frac{b}{\pi}\frac{\tan\beta}{\tan\tau} \qquad \text{(F. 2)}$$

This formula has been developed introducing a result related to a two dimensional model (wedge impacting) into a three dimensional model (monohedral hull planing).

Thereby, the application of 2D results to a 3D model is an approximation and there is no evidence of experimental tests on the matter in order to confirm this assumption sound and effective.

10.4.2 Lift coefficient C_L as function of the trim angle τ

"*It will be recalled that the fluid-flow directions over the pressure area of a planing surface were a combination of longitudinal flow and transverse flow across both chine lines.*

From aerodynamic theory it is known that lifting surfaces of high aspect ratio (small λ) have a predominantly longitudinal (chordwise) flow and that the lift is directly proportional to τ. For surfaces of very small span and infinite length, i.e. $\lambda = \infty$, the flow is in transverse direction and the lift is proportional to τ^2.

Hence for a normal low aspect-ratio planing surface, the lift can be expressed in the form

$$C_L = A\tau + B\tau^2$$

For the range of l-values applicable to planing surfaces, the second term takes the form of a small correction to the first term and it is found that equation can be approximated by using t to the 1.1 power.

Hence

$$C_L \Big/ \tau^{1.1} = f(\lambda, C_V) \qquad \text{“}$$

The choice to power the trim angle to 1.1 has not been demonstrated as the best one. It has been introduced by Korvin-Kroukovsky [Korvin-Kroukovsky 1949] in order to reduce the scattering between the theoretical and experimental values of C_L as function of τ, λ and C_V. Thereby this choice represents an approximation.

10.4.3 Hydrostatic component of the lift for a planing surface

"*The lift on a planing surface (at fixed draft and trim) can be attributed to two separate effects; i.e., one is the dynamic reaction of the fluid against the moving surface, and the second is the so-called buoyant contribution to lift which is associated with the static pressures corresponding to a given draft and hull trim.*"

"*Sottorf's analysis of high-speed planing data, where the hydrostatic term is negligible, showed that for a given trim angle, the dynamic component of the lift coefficient varied as* $\lambda^{1/2}$.

Hence we can consider this component to be of the form:

$$C_{Ld} = c\lambda^{1/2}\tau^{1.1} \qquad (10)$$

where c is a constant to be determined.

The hydrostatic component of lift for a flat plate of beam, b, mean wetted length-beam ratio, λ*, and angle of trim* τ *can be written as follows:*

$$L_b = \frac{1}{2}\rho g b^3 (\lambda - 0.30)^2 \tan\tau \qquad (11)$$

Dividing both sides by $\frac{1}{2}\rho V^2 b^2$ *and assuming that* $(\lambda - 0.30)^2$ *can be replaced by* $D\lambda^n$ *where D and n are constants to be determined, results in*

$$C_{Lb} = \frac{D\lambda^n}{C_V^2}\tan\tau \qquad (12)$$

If the difference between $\tan\tau$ *and* $\tau^{1.1}$ *is neglected* C_{Lb} *can be rewritten*

$$C_{Lb} = \frac{D\lambda^n}{C_V^2}\tau^{1.1} \qquad (13)$$

Combining equations of C_{Ld} *and* C_{Lb} *gives a form of an empirical equation for the lift coefficient of a planing surface, i.e.*

$$C_L = \tau^{1.1}\left(c\lambda^{1/2} + \frac{D\lambda^n}{C_V^2}\right) \qquad (14)"$$

"*The constant c, D and n are evaluated by applying the foregoing formula to the large collection of planing data contained in the existing literature.*"

"*As a result of this analysis the empirical planing lift equation for a zero deadrise surface takes the following final form.*

$$C_L = \tau^{1.1}\left[0.0120\lambda^{1/2} + \frac{0.0055\lambda^{5/2}}{C_V^2}\right] \qquad (15)$$

where τ *is in degrees.*"

A first observation is related to the numerical factor in the equation (11): there is no explanation about the choice of the value 0.30.

The second observation is related to the approximation:

$$(\lambda - 0.30)^2 \cong D\lambda^n$$

there is no evidence neither of the range of λ within this assumption is valid nor the error associated to.

The thirst observation is pertinent to the approximation:

$$\tan\tau = \tau^{1.1}$$

there is no evidence neither of the range of τ within this assumption is valid nor the error associated to.

10.4.4 Lift coefficient of deadrise planing surface

"*For a given trim and mean wetted length-beam ratio, the effect of increasing the deadrise angle is to reduce the planing lift. This lift reduction is caused primarily from a reduction in the stagnation pressure at the leading edge of the wetted area.*"

"*When* $\beta = 0$ *the stagnation line is normal to the keel and normal to the free-stream velocity so that full stagnation pressure* $\frac{1}{2}\rho V^2$ *is developed.*"

"*The presence of deadrise causes the stagnation line to be "swept" aft and leads to a lift reduction not unlike that on a swept-back wing.*

To formulate an empirical equation for the planing lift of a deadrise surface, the lift coefficient of a Vee surface was compared with that of a flat plate at identical values of τ, λ, C_V .

It was found that the lift of a deadrise surface can be represented by following equation:

$$C_{L\beta} = C_{L0} - 0.0065\beta C_{L0}^{0.6} \qquad (16)$$

where

$C_{L\beta}$ *= lift coefficient for a deadrise surface*

β *= deadrise, deg*

C_{L0} *= lift coefficient of a flat plate operating at the same* τ, λ *and* C_V *as deadrise surface* "

In the Appendix E "Hydrodynamic Pressure Distribution Trends on a V-Bottom Planing Surface" test results on prismatic planing surfaces have been reexamined.

Sources data adopted are tests results on prismatic planing surfaces, available on four NACA Reports[(132)].

[(132)] The complete list is reported in References of the Appendix E.

This analysis has highlighted an interesting physical phenomena: there is a movement of Stagnation and Spray edge lines related to the growing up of the Lift coefficient; in detail:

3. the lines rotate becoming closer perpendicular to the fluid flow direction;
4. the lines translate forward in the opposite direction of the fluid flow.

Furthermore, the ratio of the center of pressure location to the mean wetted length l_p / l_m appears to be almost constant whereas, as function of $C_{L\beta}$, decreases to a lower limit value, increasing the lift coefficient.

All these phenomena are common to all V-bottom hull, with or without horizontal chine flared, and give us the evidence that, raising up the lift coefficient, the fluid flow field comes close to the planing flat plate ones and, thereby, the effects of the deadrise angle and the chine shape (e.g.: with or without horizontal chine flared) decrease.

According to these observations, the above formula cannot be applied for every value of $C_{L\beta}$, as a matter of fact the deadrise angle has the same influence for each value of $C_{L\beta}$ and this denies the above remarks.

10.4.5 Fluid flow velocity on the bottom of the planing surface

"*The average bottom velocity (V_1) is less than the forward planing velocity (V) owing to the fact that the planing bottom pressure is larger than the free-stream pressure.*"

"*Taking first, the case of a zero deadrise hull, the dynamic contribution to planing lift is given by the first term in (15) to be*

$$C_{Ld} = 0.0120\lambda^{1/2}\tau^{1.1} \qquad (20)$$

The dynamic load on the bottom is

$$\Delta_d = \frac{1}{2}\rho V^2 b^2\left(0.0120\lambda^{1/2}\tau^{1.1}\right) \qquad (21)$$

The average dynamic pressure is

$$p_d = \frac{\Delta}{\lambda b^2\cos\tau} = \frac{0.0120\tau^{1.1}V^2\rho}{2\lambda^{1/2}\cos\tau} \qquad (22)$$

Applying Bernoulli's equation between the free-stream conditions and the average pressure and velocity conditions on the bottom of the planing surface:

$$V_1 = V\left(1-\frac{2p_d}{\rho V^2}\right)^{1/2} \qquad (23)$$

substituting (22) into (23) gives

$$V_1 = V\left(1-\frac{0.0120\tau^{1.1}}{\lambda^{1/2}\cos\tau}\right)^{1/2} \text{ for } \beta = 0° \qquad (24)$$

The average bottom velocity for specific deadrise angle is computed in an analogous manner using the lift coefficient for deadrise surfaces given by (16)."

Bernoulli's equation is the energy balance equation of a perfect fluid flow, hence viscous effects are neglected.

Bernoulli's equation has been applied neglecting the term related to the elevation (gravitational term).

The average pressure has been computed by the formula (15) which is approximated, as shown in the paragraph 10.4.3

Hence the average bottom velocity, computed by the formula (24), is affected by the following approximations:

- viscous effect neglected,
- elevation variation effect neglected,
- numerical approximation in coefficient lift formula used.

10.4.6 Center of pressure of planing surfaces

"*It has been shown that the resultant center of pressure of planing surfaces can be fairly accurately evaluated by separate considerations of the buoyant and dynamic force components of the lift.*

The center of pressure of the dynamic component is taken to be at 75 percent of the mean wetted length forward of the transom, while the center of pressure of the buoyant force is assumed to be 33 percent forward of the transom.

These distances are, of course, approximations but are acceptable in the empirical development of this paper."

The pressure center of planing surfaces can be taken, as suggested, at 75 percent of the mean wetted length forward of the transom for flat planing plate or for planing surface with low longitudinal curvature and, for all of them, at low trim angle.

The choice to take the hydrostatic pressure center at 33 percent forward of the transom is not true at all.

This choice is true in the hypothesis:

- monohedral hull, single chine with deadrise and beam constant,
- transverse wetted area distribution linear, along the keel.

Let draw the transverse wetted area distribution on the symmetry plane of the hull: in each point of the wetted keel let draw a segment, normal to the keel, which length is proportional to the wetted area of the transversal hull section in that point.

If the above second hypothesis is satisfied the transverse wetted area distribution can have a right-angle triangle shape, which sides are: the wetted keel, the wetted transom and the waterline.

In this triangle the wetted transom is the smallest side and the waterline is the hypotenuse.

Reminding that:

- the center of the transverse wetted area distribution is the center of the hydrostatic pressure distribution,
- the center of a triangle is at 1/3 of the high,

the hydrostatic pressure center is at 33 percent of the wetted length from the transom or at 33 percent of the wetted transom from the water line level.

In the most of cases one or both of the above hypothesis are not satisfied at all.

In the hypothesis of monohedral hull in dynamic equilibrium condition, the transverse wetted area distribution is not linear at all but is locally linear: the wetted keel length can be divided in parts and in each one the transverse wetted area distribution is linear. For example, with reference to the Figure 10.4-4 related to a monohedral hull form, we have two different transverse wetted area distribution:

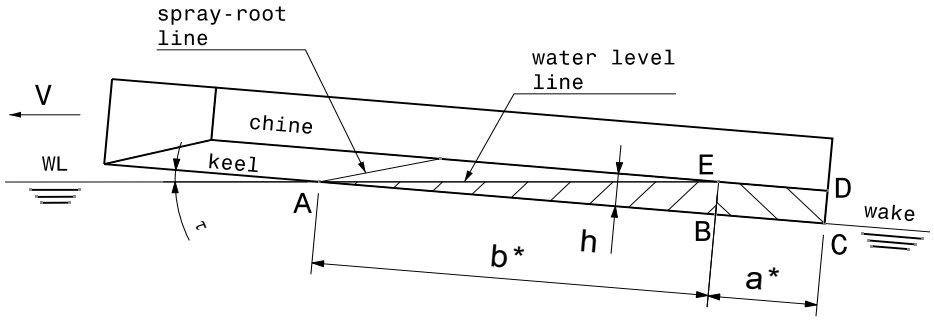

Figure 10.4-4 Transverse wetted area distribution

the area (ABE) is triangular as well as the area (BCDE) is rectangular.

Thereby the distance of the hydrostatic pressure center from the transom is more than the 33 percent of the keel wetted length.

If the hull is not monohedral this effect is amplified.

10.5 Conclusion

Savitsky's methods, SF as well as LF, are based on a large amount of theoretical equations, hydrodynamics as well as aerodynamics, "forced" to describe the fluid flow field under a planing surface by the introduction of empirical coefficient, which have been computed on the bases of model basin test results.

These equations have been developed, step by step, in more than thirty years of research in different countries.

Savitsky's method is the summary of these researches and is affected by the approximations related to.

Taking in account that planing surfaces phenomena are deeply non linear, and computer machines have been introduced in the second half of the twenty century as well as the CFD methods, this method was the only effective way to attack the planing surfaces problem.

Another important point is that results obtained by Savitsky's methods are quiet lower than the other ones measured in towing tests. This is due to the approximations above mentioned and to neglect the spray resistance component of some areas of the wetted surface. [Bertorello & Oliviero 2007]

Nowadays design requirements, as better seakeeping performances and lower structural weight, as well as new materials and shipbuilding technologies available, have led to choose also non-monohedral hull forms with deadrise angle varying along to the hull length and with multi V transverse sections.

In despite of the application of Savitsky's method to these hull drives to results affected by additional approximations and in despite of the other methods available to predict the speed-resistance relationships for planing hulls, this method is still widely and successfully used.

This is due to the fact that Savitsky's method is user-friendly, effective, not patented and, in addition, it not requires too many input data.

10.6 Symbols

A, B, c, D, n	Numerical coefficient	
a^*	Chine immersed length	$[m]$
b	Beam of planing surfaces	$[m]$
b^*	Dry chine length	$[m]$
C_L	Lift coefficient	
C_{Lb}	Component of the coefficient lift due to the static pressure (buoyant)	
C_{Ld}	Component of the coefficient lift due to the dynamic pressure	
$C_{L\beta}$	Lift coefficient for a deadrise surface	
C_{L0}	Lift coefficient of a flat plate operating at the same τ, λ and C_V as deadrise surface	
C_V	Froude number related to the beam	$C_V = \frac{V}{\sqrt{gb}}$
d	Vertical depth of trailing edge of boat (at keel) below level water surface	$[m]$
g	Acceleration of gravity	$g = 9.81 m/s^2$
h	Distance between the water level line and the keel	$[m]$
h'	Distance between the spray root line intersection with the chines and the keel	$[m]$
L_b	Component of the lift due to the buoyant	$[N]$
L_c	Wetted chine length	$[m]$
L_k	Wetted keel length	$[m]$
l_m	Mean wetted length	$[m]$
l_p	Longitudinal position of the center of pressure measured from the transom	$[m]$
$L1$	Difference between wetted keel and chine lengths	$[m]$
$L2$	Difference between keel and chine lengths wetted by	$[m]$

	level water surface	
p_d	Average dynamic pressure	MPa
V	Hull speed	$[m/s]$
V_1	Average bottom velocity	$[m/s]$
β	Angle of deadrise of planing surface	$[\text{deg}]$
Δ_d	Dynamic load on the bottom	$[N]$
ρ	Water density	$[kg/m^3]$
λ	Mean wetted length to beam ratio	
τ	Trim angle	$[\text{deg}]$
τ^*	Dynamic equilibrium trim angle	$[\text{deg}]$

10.7 References

Akers, R.H. 1999. Dynamic Analysis of Planing Hulls in Vertical Plane. *New England SNAME Meeting 1999.* Jersey City (USA): SNAME

Barry, C.R., Gosh D., Akers R., Ulak A. 2002. Implementation, Application and Validation of the Zarnick Strip Theory Analysis Technique for Planing Boats. *Proceeding of first High Performance Yacht Design Conference (HPYD1),* Auckland, Australia.

Bertorello, C. & Oliviero, L. 2007. Hydrodynamic Resistance Assessment of Non-Monohedral Planing Hull Forms based on Savitsky's Method. *Australian Journal of Mechanical Engineer,* Vol. 4 No.2, pp 209-224. Engineers Media, CROWS NEST, Australia. (ACN001311511).

Hadler, J.B. 1966. The prediction of power performance on planing craft. *SNAME Transactions,* Vol. 74. pp563-610. Jersey City (USA): SNAME

Korvin-Kroukovsky B.V., Savitsky D., Lehman W.F. 1949. Wetted Area and Center of Pressure of Planing Surfaces. *Report SIT-DL-49-9-360 Davidson Laboratory* Stevens Institute of Technology. Hoboken, New Jersey (USA)

Murray, A.B. 1950. The hydrodynamic of Planing Hulls. *New England SNAME Meeting 1950.* Jersey City (USA): SNAME

Payne P.R. 1994. The water rise in front of a model planing hull. *Experiments in Fluids,* Vol.17, Issue 1-2, pp. 96-104. Berlin (Germany): Springer-Verlag. ISSN 0723-4864.

Savander, B.R., Scorpio, S.M., Taylor, R.K. 2002. Steady Hydrodynamic Analysis of Planing Surfaces. *Journal of Ship Research* Vol.46 No. 4. Jersey City (USA): SNAME

Savitsky, D. 1964. Hydrodynamic Design of Planing Hull. *Marine Technology*, Vol.1, No.1, Jersey City (USA): SNAME

Savitsky, D. & Brown, P.W. 1976. Procedures for Hydrodynamic Evaluation of Planing Hulls in Smooth and Rough Water. *Marine Technology*, Vol.13, No.4, pp381-400, Jersey City (USA): SNAME

Savitsky, D., Koebel, J. G. 1993. Seakeeping Considerations in Design and Operation of Hard Chine Planing Hulls, *Technical Research Bulletin* R-42, pp124 Jersey City (USA): SNAME

Sottorf, W. 1932. Versuche mit Gleitflächen. *Werft-Reederei-Hafen,* pp 285-290 October 1932; pp 43-47 February 1933; pp 61-66 March 1933. [English version: Experiments with Planing Surfaces. *Report NACA TM 739*, 1934. Washington, D.C. (USA). (web site: http://ntrs.nasa.gov/search.jsp)]

Wagner, H. 1932. Über Stoss und Gleitvorgänge an der Oberfläche von Flüssigkeiten. *Z.A.M.M*. No.4 Vol.12. [English version: Phenomena associated with Impacts and Sliding on liquid surfaces. *Report NACA TR N-23507*, 1936. Washington, D.C. (USA). (web site: http://ntrs.nasa.gov/search.jsp)]

APPENDIX G

COMPARISON RESULTS:

ASEM VS SERIES 62

11.1 Table of Contents

11.2 Figure Index

11.3 Table Index

11.4 Introduction

Analytical Semi-Empirical Method (ASEM) has been developed in order to predict Resistance and Power performance versus hull speed related to a warped bare monohull. [Bertorello & Oliviero 2007]

In this chapter ASEM will be applied to the models of the Systematic Series 62, in order to check reliability and efficiency.

In order to achieve this goal, geometrical and physical data related to Series 62 have been here reported in International System Units.

Further, Savitsky‘s method [Savitsky 1964] will be applied too, in order to get an overall comparison.

11.5 Models: Geometry and Tests [Clement & Blount 1963]

Series 62 is composed by five hull models with different length-beam ratio.

The parent model (Model 4667-1) has been developed improving steering qualities and rough-water performance of the hull form of Series 50.

In order to achieve these goals following improvements of hull form Series 50 have been adopted:

- an high deadrise angle value at transom,
- the deadrise angle constant in the afterward part of the hull,
- the stern narrow, with transom width equal to 65% of max chine width,
- the bow sections convex.

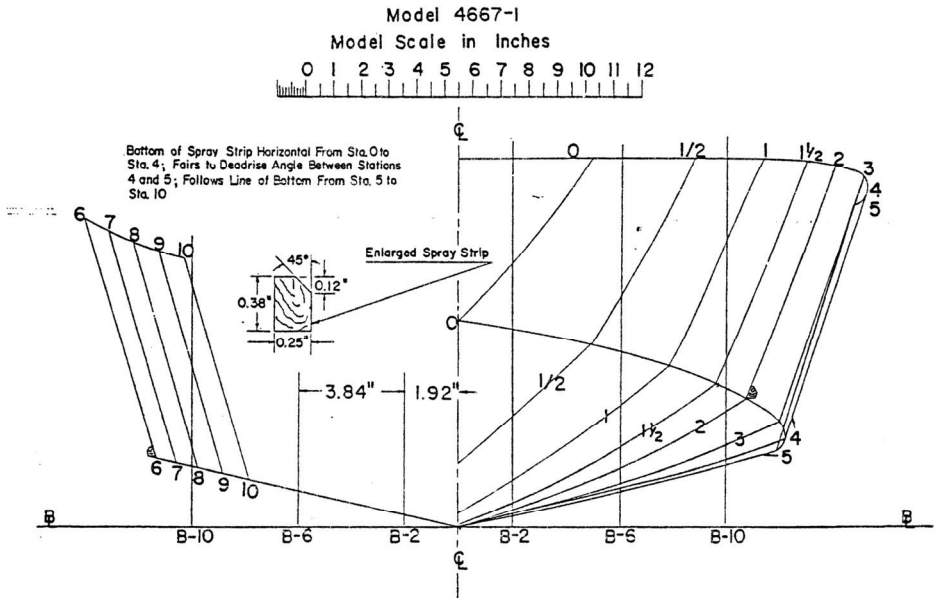

Figure 11.5-1 Body Plans: Parent Model 4667-1

The four additional models of the series were derived from the parent by maintaining the same body plan shape but adjusting the station spacing and the body plan size to give the different length-beam ratio desired.

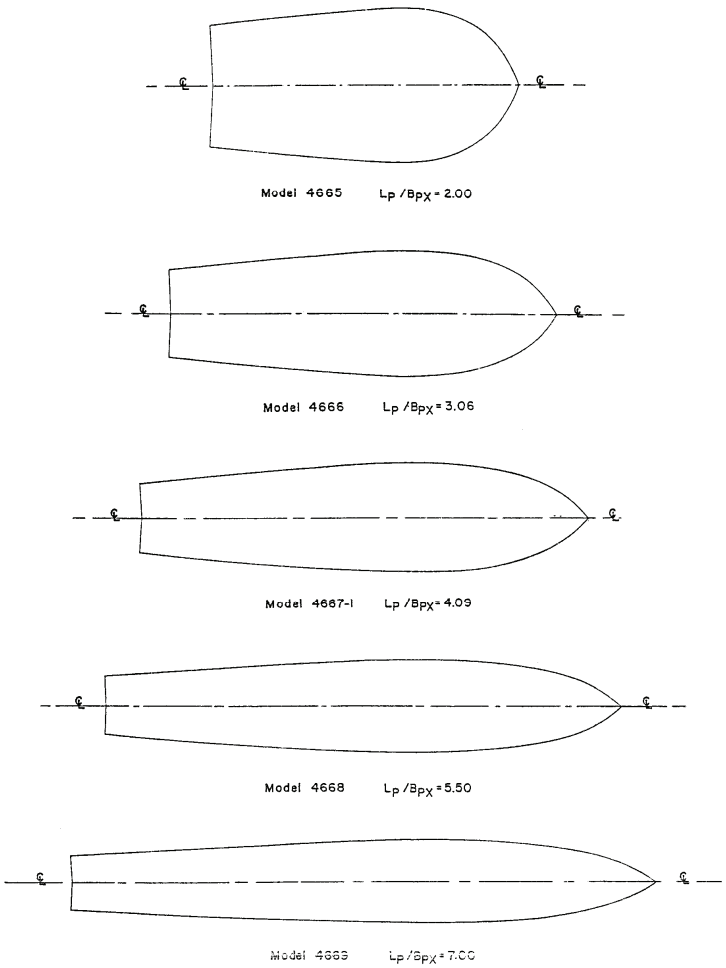

Fig. 3 Chine lines in plan view of five models of series

Figure 11.5-2 Chine lines in plan view

In order to keep the models widths within the limits imposed by the carriage bay used for the tests, the length of models were:

Table 11.5-1 Models length

Model	**L_{OA}**	
4665	1.219 m	4 ft
4666	1.829 m	6 ft
4667-1	2.438 m	8 ft
4668		
4669		

Hereinafter tables of models coordinates and dimensions are reported:

Table 11.5-2 Models coordinates: Model 4665 & Model 4666

Model		4665			4666		
	station	**x**	**y**	**z**	**x**	**y**	**z**
		[m]	[m]	[m]	[m]	[m]	[m]
stern	10	0,000	0,000	0,000	0,000	0,000	0,000
			0,192	0,043		0,192	0,043
	9	0,119	0,000	0,000	0,182	0,000	0,000
			0,224	0,050		0,224	0,050
	8	0,238	0,000	0,000	0,365	0,000	0,000
			0,240	0,053		0,240	0,053
	7	0,357	0,000	0,000	0,547	0,000	0,000
			0,260	0,058		0,260	0,058
	6	0,477	0,000	0,000	0,729	0,000	0,000
			0,276	0,061		0,276	0,061
	5	0,596	0,000	0,000	0,912	0,000	0,000
			0,292	0,071		0,292	0,071
	4	0,715	0,000	0,000	1,094	0,000	0,000
			0,298	0,080		0,298	0,080
	3	0,834	0,000	0,000	1,277	0,000	0,000
			0,295	0,096		0,295	0,096
	2	0,953	0,000	0,000	1,459	0,000	0,000
			0,266	0,131		0,266	0,131
	1,5	1,013	0,000	0,003	1,550	0,000	0,003
			0,237	0,135		0,237	0,135
	1	1,072	0,000	0,013	1,641	0,000	0,013
			0,192	0,151		0,192	0,151
	0,5	1,132	0,000	0,054	1,733	0,000	0,054
			0,122	0,167		0,122	0,167
bow	0	1,219	0,000	0,000	1,829	0,000	0,000
			0,000	0,192		0,000	0,192

Table 11.5-3 Models coordinates: Model 4667-1, Model 4668 and Model 4669

Model		4667-1			4668			4669		
	station	x	y	z	x	y	z	x	y	z
		[m]	[m]	[m]	[m]	[m]	[m]	[m]	[m]	[m]
stern	10	0,000	0,000	0,000	0,000	0,000	0,000	0,000	0,000	0,000
			0,192	0,043		0,143	0,032		0,112	0,025
	9	0,244	0,000	0,000	0,244	0,000	0,000	0,244	0,000	0,000
			0,224	0,050		0,167	0,037		0,131	0,029
	8	0,488	0,000	0,000	0,488	0,000	0,000	0,488	0,000	0,000
			0,240	0,053		0,179	0,040		0,140	0,031
	7	0,732	0,000	0,000	0,732	0,000	0,000	0,732	0,000	0,000
			0,260	0,058		0,193	0,043		0,152	0,034
	6	0,975	0,000	0,000	0,975	0,000	0,000	0,975	0,000	0,000
			0,276	0,061		0,205	0,045		0,161	0,036
	5	1,219	0,000	0,000	1,219	0,000	0,000	1,219	0,000	0,000
			0,292	0,071		0,217	0,052		0,170	0,041
	4	1,463	0,000	0,000	1,463	0,000	0,000	1,463	0,000	0,000
			0,298	0,080		0,222	0,060		0,174	0,047
	3	1,707	0,000	0,000	1,707	0,000	0,000	1,707	0,000	0,000
			0,295	0,096		0,219	0,072		0,172	0,056
	2	1,951	0,000	0,000	1,951	0,000	0,000	1,951	0,000	0,000
			0,266	0,131		0,198	0,098		0,155	0,077
	1,5	2,073	0,000	0,003	2,073	0,000	0,002	2,073	0,000	0,001
			0,237	0,135		0,176	0,100		0,139	0,079
	1	2,195	0,000	0,013	2,195	0,000	0,010	2,195	0,000	0,007
			0,192	0,151		0,143	0,112		0,112	0,088
	0,5	2,316	0,000	0,054	2,316	0,000	0,041	2,316	0,000	0,032
			0,122	0,167		0,091	0,124		0,071	0,097
bow	0	2,438	0,000	0,000	2,438	0,000	0,000	2,438	0,000	0,000
			0,000	0,192		0,000	0,143		0,000	0,112

Models have been tested in order to evaluate the influence of some hull form parameters on planing hull performance:

- L_P / B_{PX} a length to beam ratio,
- $A_P / \nabla^{2/3}$ a relationship between hull size and gross weight,
- $\left(1 - \frac{L_{CG}}{L_P}\right)$ the distance between the center of gravity and the centroid of the area A_P in term of longitudinal position of the centroid L_P.

In detail:

- the speed range, in term of Fn_{∇}, was about 0.2 up to 6.0;
- L_P/B_{PX} values were 2.00, 3.06, 4.09, 5.50, 7.00;
- $\left(1-\frac{L_{CG}}{L_P}\right)$ values were 0, 4, 8 and 12 percent;
- $A_P/\nabla^{2/3}$ values were 4.0, 5.5, 7.0, 8.5.

with 85 test cases developed: 17 per each model.

In order to get a comparison among data related to planing condition, tests developed only up to semi-displacement condition $(Fn_{\nabla} \le 3)$ have not been taken in account. Thereby only 48 test cases have been taken in account.

In the following five tables, one per each model, planing test conditions considered are reported:

Table 11.5-4 Planing Test Conditions: Model 4665

Model 4665 - $L_P/B_{PX} = 2.00$					
Test n.	**W**	α_0	**L_{CG} Fwd of Station 10**	**L_{CG} Aft of Centroid of A_P**	$A_P/\nabla^{2/3}$
	[N]	[deg]	[m]	[%L_P]	[-]
1	242,5	0,00	0,494	6	7.1
6	356,3	-2,65	0,573	0	5.5
7	356,3	-0,63	0,518	4	5.5
10	248,2	-2,19	0,567	0	7.0
11	242,5	-0,76	0,518	4	7.1
12	242,5	0,80	0,472	8	7.1
14	184,0	-2,05	0,567	0	8.5
15	184,0	-0,82	0,518	4	8.5
16	184,0	0,42	0,472	8	8.5
17	184,0	0,64	0,424	12	8.5

Table 11.5-5 Planing Test Conditions: Model 4666

Model 4666 - $L_P/B_{PX} = 3.06$					
Test n.	**W**	α_0	**L_{CG} Fwd of Station 10**	**L_{CG} Aft of Centroid of A_P**	$A_P/\nabla^{2/3}$
	[N]	[deg]	[m]	[%L_P]	[-]
1	453,0	0,02	0,771	6	7.0
6	650,6	-1,70	0,881	0	5.5
7	650,6	-0,30	0,808	4	5.5
10	453,0	-1,53	0,881	0	7.0
14	338,6	-1,47	0,881	0	8.5
15	338,6	-0,62	0,808	4	8.5
16	338,6	0,28	0,735	8	8.5
17	338,6	1,23	0,661	12	8.5

Table 11.5-6 Planing Test Conditions: Model 4667-1

Model 4667-1 - $L_P/B_{PX} = 4.09$					
Test n.	**W**	α_0	**L_{CG} Fwd of Station 10**	**L_{CG} Aft of Centroid of A_P**	$A_P/\nabla^{2/3}$
	[N]	[deg]	[m]	[%L_P]	[-]
1	685,3	0,10	1,045	6	7.0
7	983,8	-0,32	1,094	4	5.5
8	983,8	0,85	0,997	8	5.5
10	685,3	-1,42	1,192	0	7.0
11	685,3	-0,50	1,094	4	7.0
12	685,3	0,50	0,997	8	7.0
13	685,3	1,50	1,094	12	7.0
14	512,2	-1,18	1,192	0	8.5
15	512,2	-0,50	1,094	4	8.5
16	512,2	0,22	0,997	8	8.5
17	512,2	1,00	0,899	12	8.5

Table 11.5-7 Planing Test Conditions: Model 4668

Model 4668 - $L_P/B_{PX} = 5.50$					
Test n.	**W**	α_0	**L_{CG} Fwd of Station 10**	**L_{CG} Aft of Centroid of A_P**	$A_P/\nabla^{2/3}$
	[N]	[deg]	[m]	[%L_P]	[-]
1	439,2	-0,15	1,058	5	7.0
7	631,0	-0,30	1,094	4	5.5
8	631,0	0,70	0,997	8	5.5
9	631,0	1,87	0,899	12	5.5
10	439,2	-1,10	1,192	0	7.0
11	439,2	-0,48	1,094	4	7.0
12	439,2	0,44	0,997	8	7.0
13	439,2	1,09	0,899	12	7.0
14	328,4	-1,00	1,192	0	8.5

Table 11.5-8 Planing Test Conditions: Model 4669

Model 4669 - $L_P/B_{PX} = 7.00$					
Test n.	**W**	α_0	**L_{CG} Fwd of Station 10**	**L_{CG} Aft of Centroid of A_P**	$A_P/\nabla^{2/3}$
	[N]	[deg]	[m]	[%L_P]	[-]
1	306,1	0,05	1,045	6	7.0
7	453,0	-0,10	1,094	4	5.5
8	453,0	0,82	0,997	8	5.5
9	453,0	1,75	0,899	12	5.5
10	306,1	-0,82	1,192	0	7.0
11	306,1	-0,25	1,094	4	7.0
12	306,1	0,42	0,997	8	7.0
13	306,1	1,15	0,899	12	7.0
14	228,7	-0,80	1,192	0	8.5
15	228,7	-0,35	1,094	4	8.5

where α_0 is the trim angle at rest[(133)].

[(133)] In their paper, Clement and Blount defined α as "*angle of attack of after portion of planing bottom, deg*". [Clement & Blount 1963]

11.6 Data Comparison

Data comparison has been developed with reference to Resistance and Power trends related to hull speed. Power data pertinent to the models of Series 62 have been derived by measurements of hull speed and resistance.

Hereinafter ASEM and Savitsky's results without physical meaning have not been taken in account (i.e.: results related to a mean wetted length higher than hull length overall), meanwhile results with physical meaning coupled with data out of range have been reported with dash line (i.e.: results related to a mean wetted length/beam ratio higher than four times).

11.6.1 Model 4665

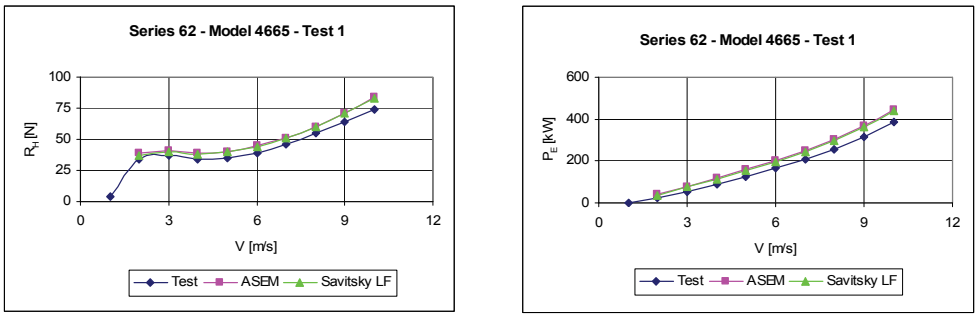

[a] **[b]**

Figure 11.6-1 Data Comparison: Model 4665 - Test 1

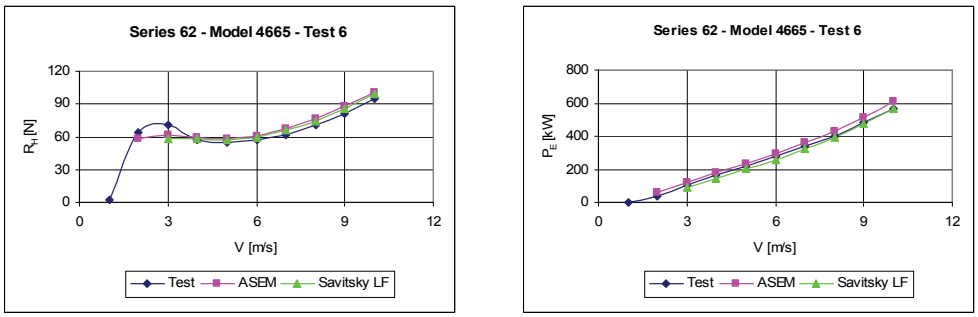

[a] **[b]**

Figure 11.6-2 Data Comparison: Model 4665 - Test 6

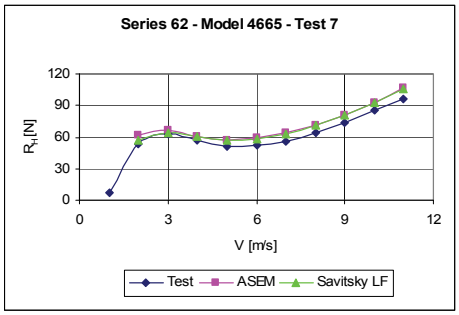

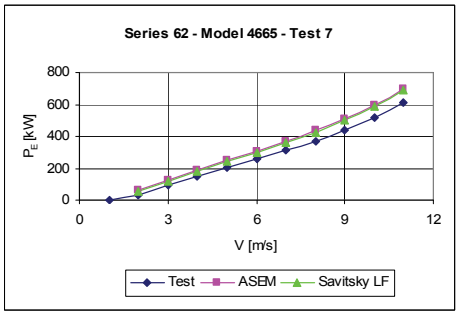

[a] **[b]**

Figure 11.6-3 Data Comparison: Model 4665 - Test 7

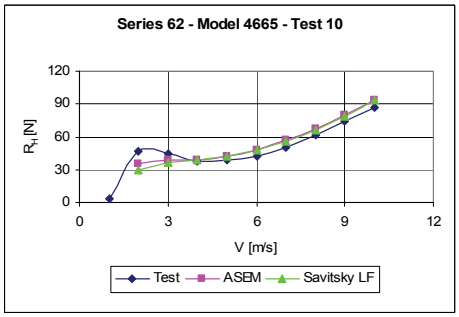

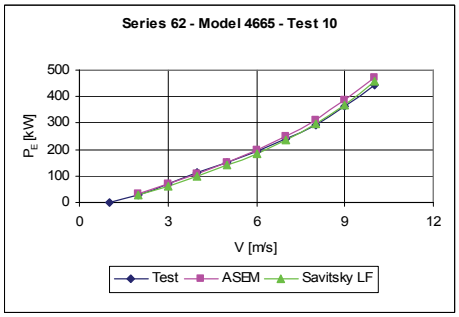

[a] **[b]**

Figure 11.6-4 Data Comparison: Model 4665 - Test 10

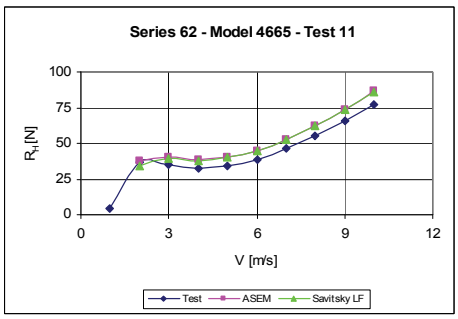

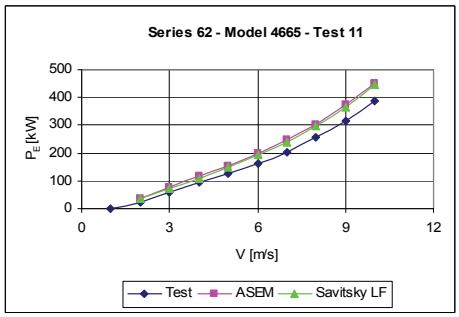

[a] **[b]**

Figure 11.6-5 Data Comparison: Model 4665 - Test 11

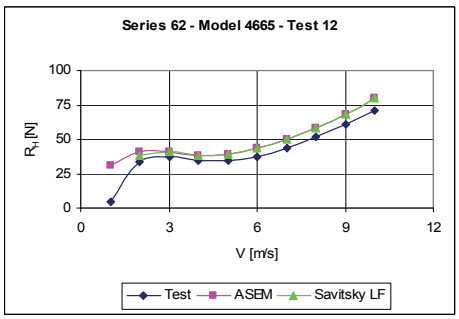

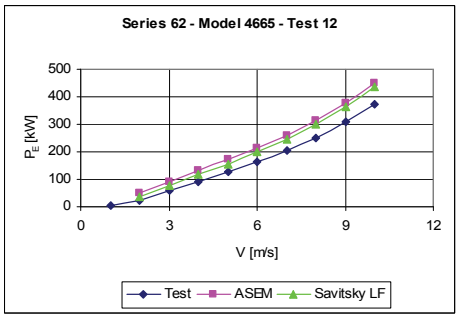

[a] **[b]**

Figure 11.6-6 Data Comparison: Model 4665 - Test 12

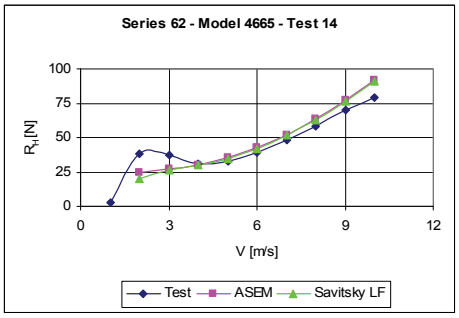

[a]

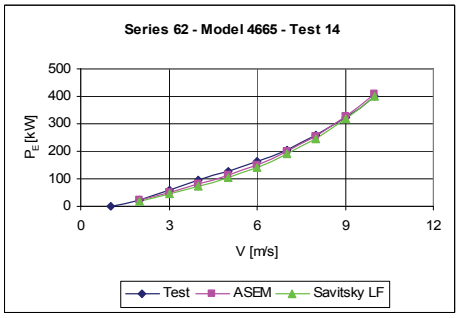

[b]

Figure 11.6-7 Data Comparison: Model 4665 - Test 14

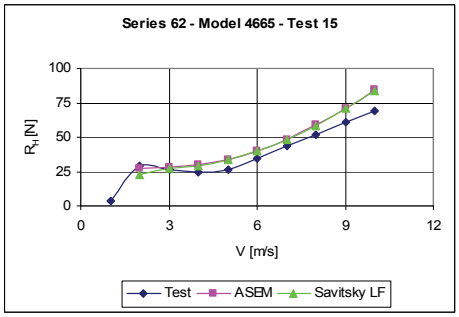

[a]

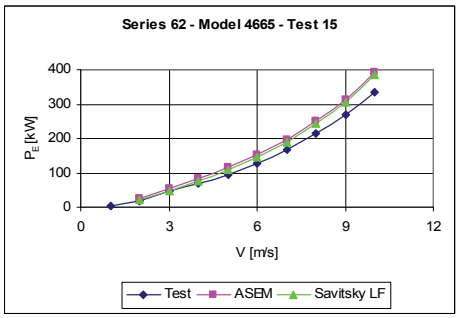

[b]

Figure 11.6-8 Data Comparison: Model 4665 - Test 15

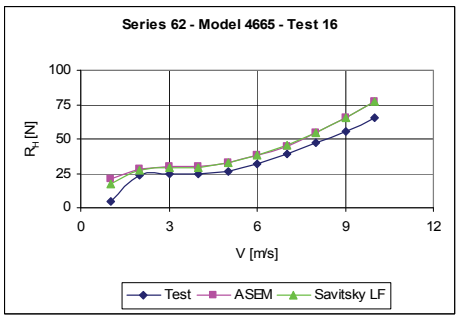

[a]

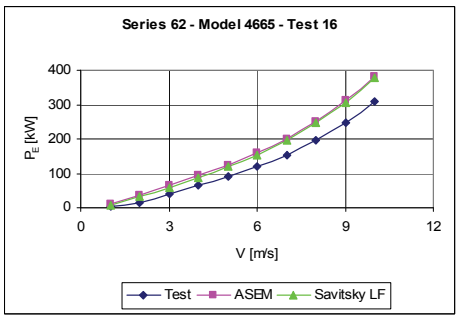

[b]

Figure 11.6-9 Data Comparison: Model 4665 - Test 16

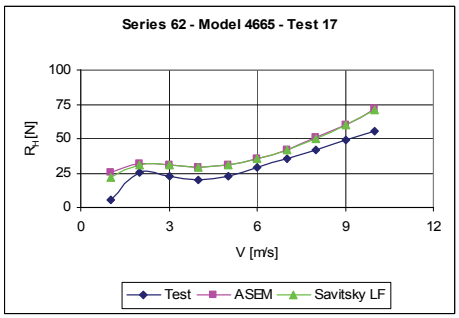

[a]

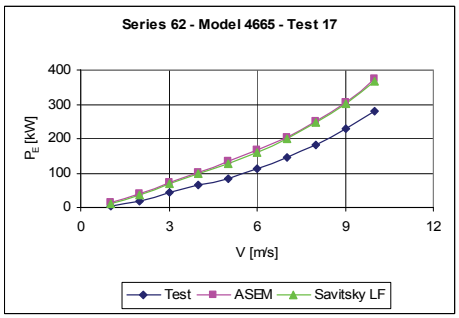

[b]

Figure 11.6-10 Data Comparison: Model 4665 - Test 17

11.6.2 Model 4666

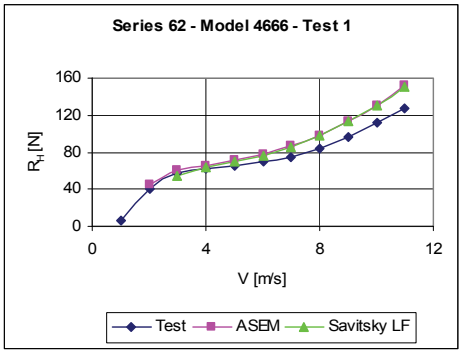

[a]

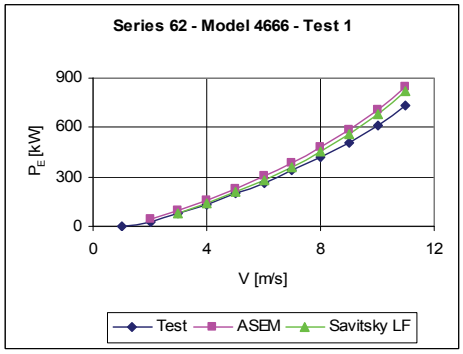

[b]

Figure 11.6-11 Data Comparison: Model 4666 - Test 1

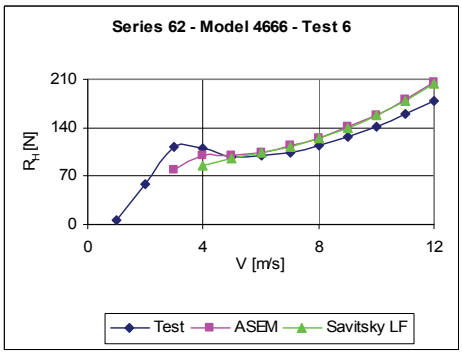

[a]

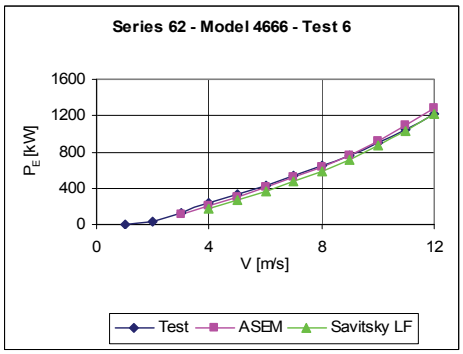

[b]

Figure 11.6-12 Data Comparison: Model 4666 - Test 6

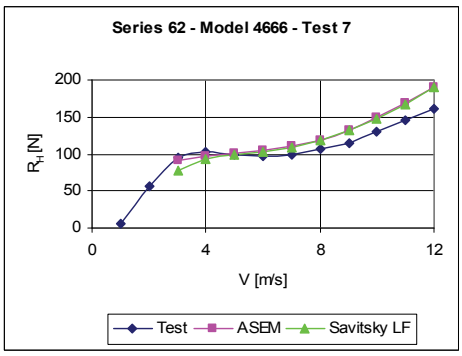

[a]

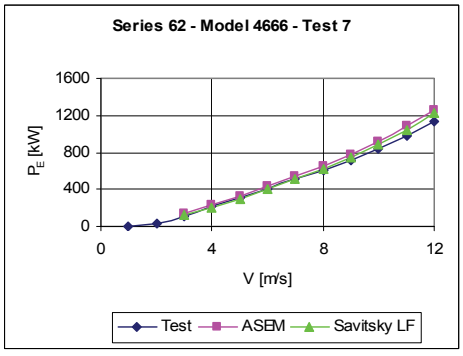

[b]

Figure 11.6-13 Data Comparison: Model 4666 - Test 7

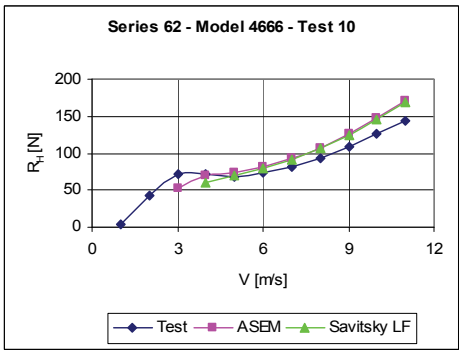

[a]

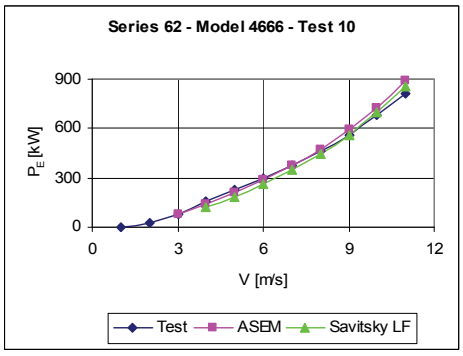

[b]

Figure 11.6-14 Data Comparison: Model 4666 - Test 10

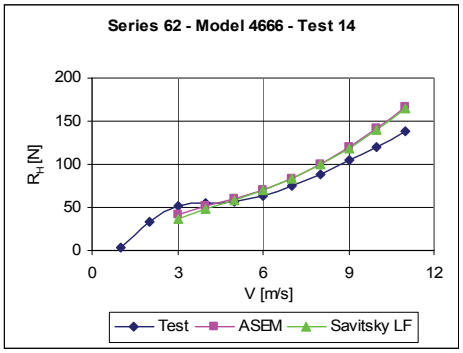

[a]

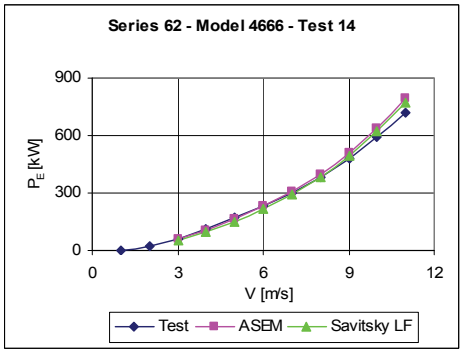

[b]

Figure 11.6-15 Data Comparison: Model 4666 - Test 14

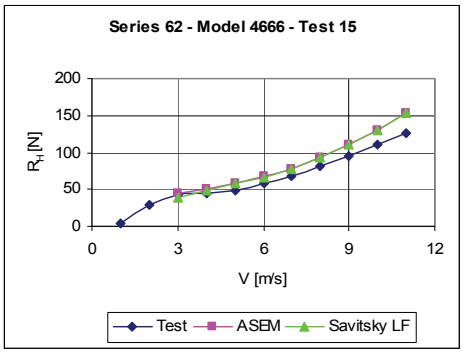

[a]

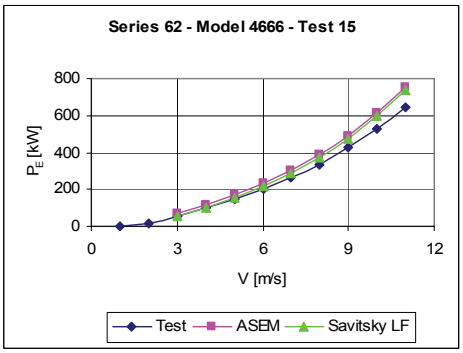

[b]

Figure 11.6-16 Data Comparison: Model 4666 - Test 15

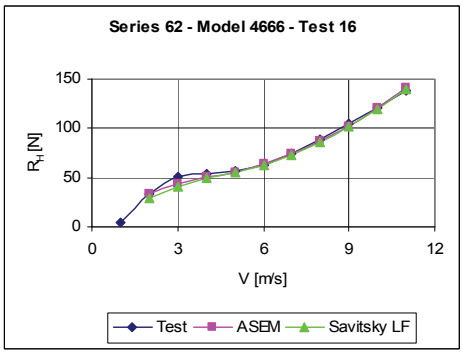

[a]

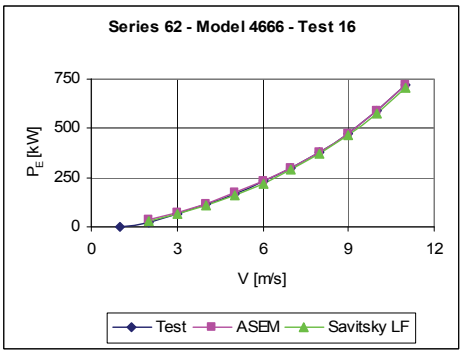

[b]

Figure 11.6-17 Data Comparison: Model 4666 - Test 16

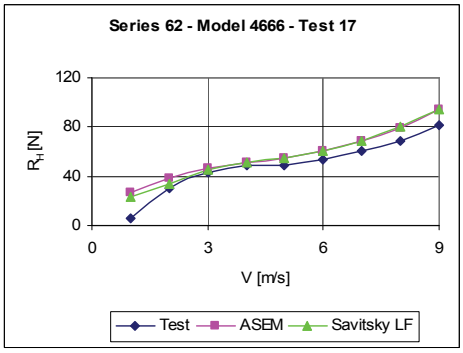

[a]

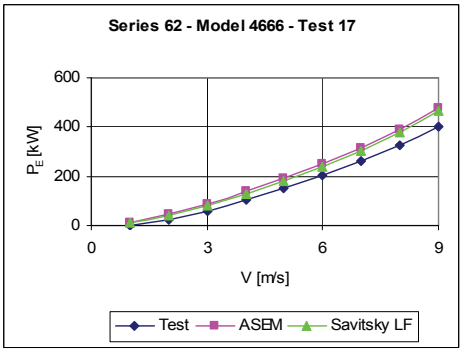

[b]

Figure 11.6-18 Data Comparison: Model 4666 - Test 17

11.6.3 Model 4667-1

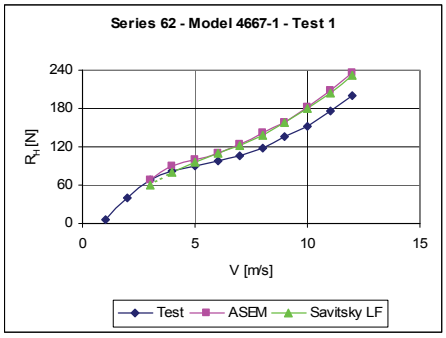

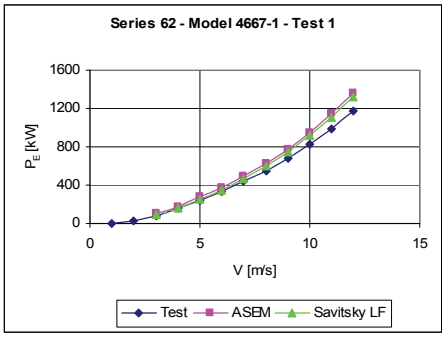

[a] **[b]**

Figure 11.6-19 Data Comparison: Model 4667-1 - Test 1

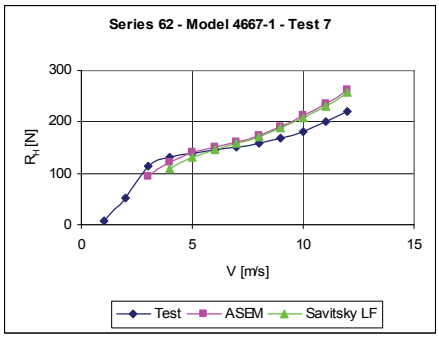

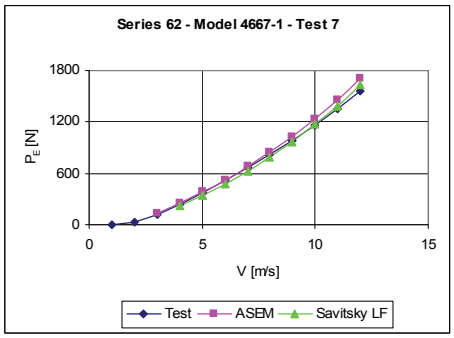

[a] **[b]**

Figure 11.6-20 Data Comparison: Model 4667-1 - Test 7

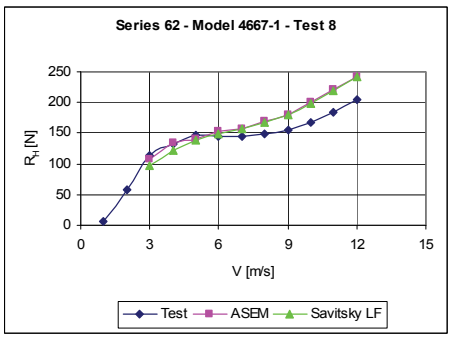

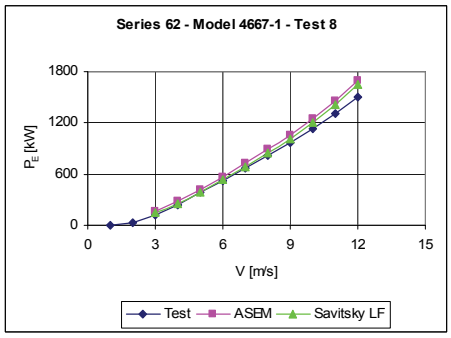

[a] **[b]**

Figure 11.6-21 Data Comparison: Model 4667-1 - Test 8

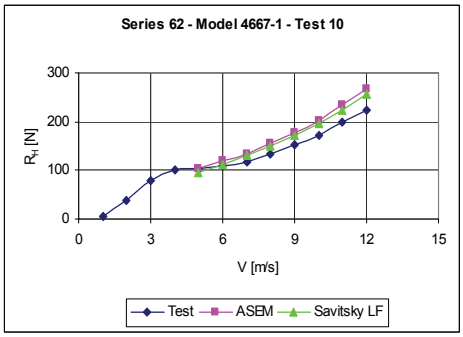

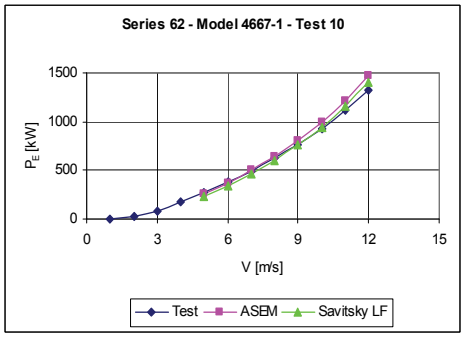

[a] **[b]**

Figure 11.6-22 Data Comparison: Model 4667-1 - Test 10

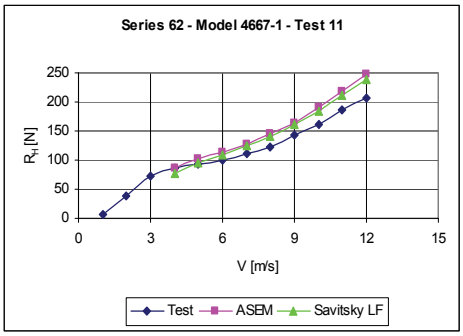

[a]

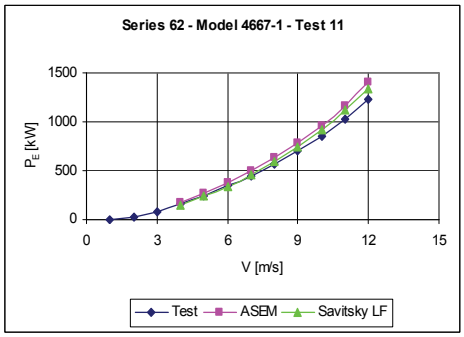

[b]

Figure 11.6-23 Data Comparison: Model 4667-1 - Test 11

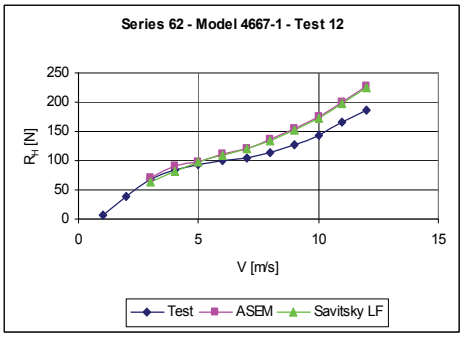

[a]

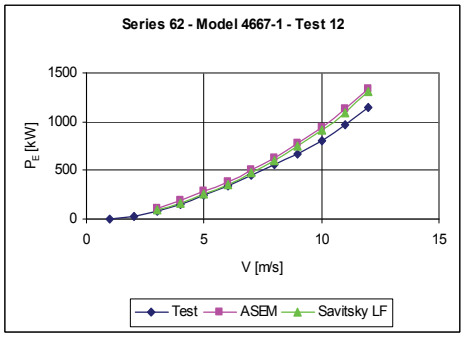

[b]

Figure 11.6-24 Data Comparison: Model 4667-1 - Test 12

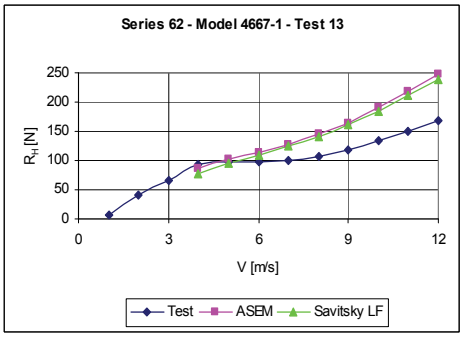

[a]

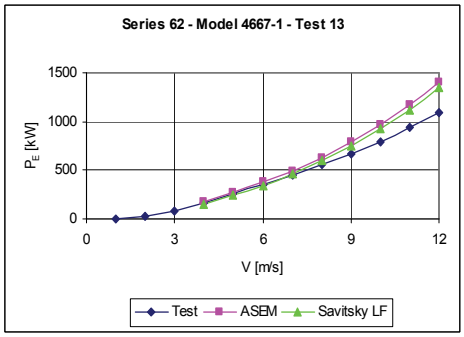

[b]

Figure 11.6-25 Data Comparison: Model 4667-1 - Test 13

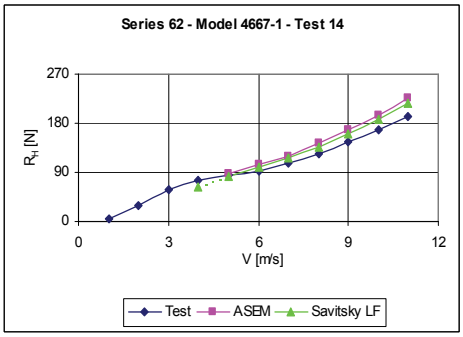

[a]

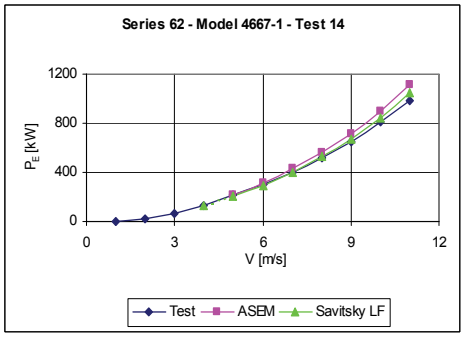

[b]

Figure 11.6-26 Data Comparison: Model 4667-1 - Test 14

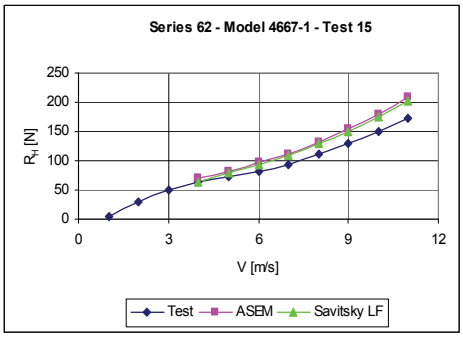

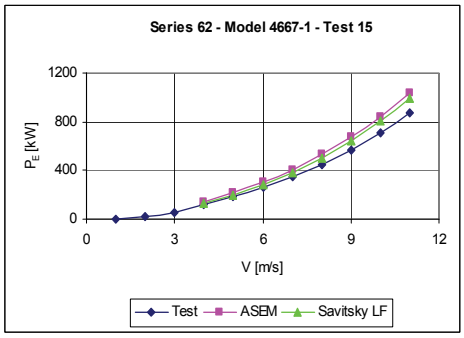

[a] **[b]**

Figure 11.6-27 Data Comparison: Model 4667-1 - Test 15

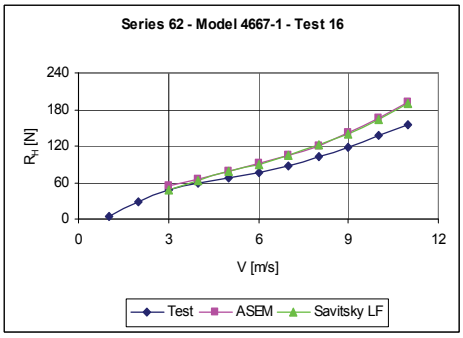

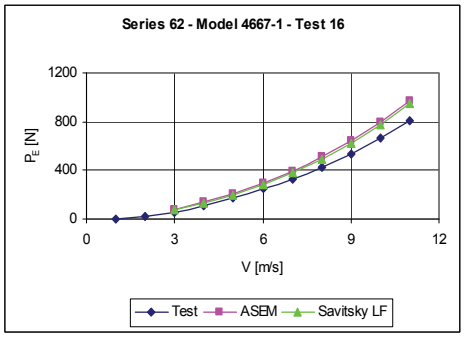

[a] **[b]**

Figure 11.6-28 Data Comparison: Model 4667-1 - Test 16

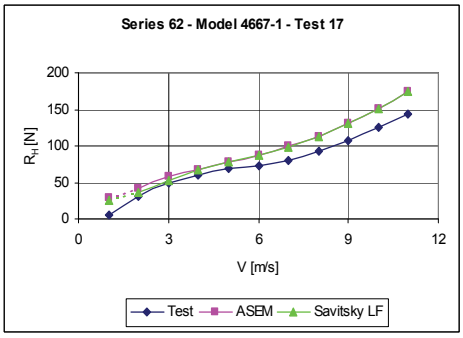

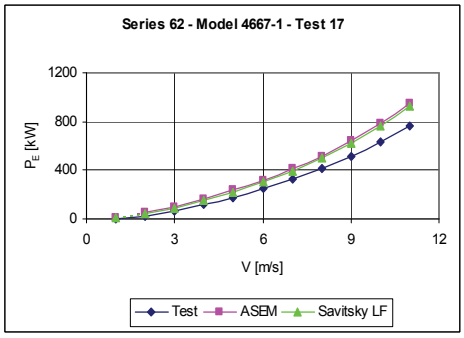

[a] **[b]**

Figure 11.6-29 Data Comparison: Model 4667-1 - Test 17

11.6.4 Model 4668

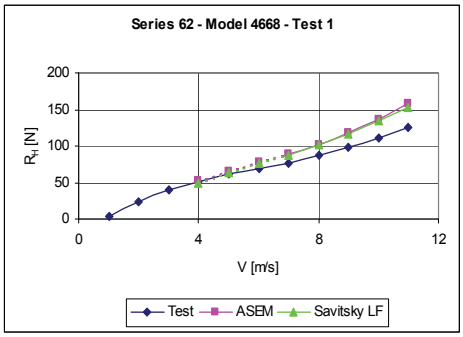

[a]

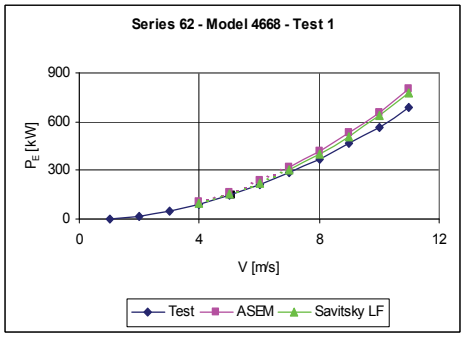

[b]

Figure 11.6-30 Data Comparison: Model 4668 - Test 1

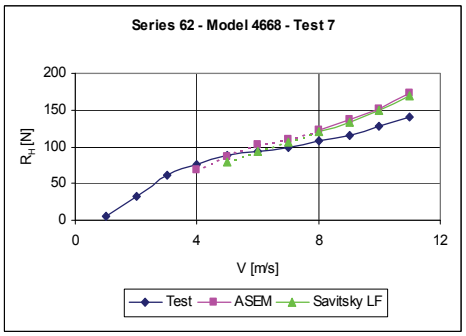

[a]

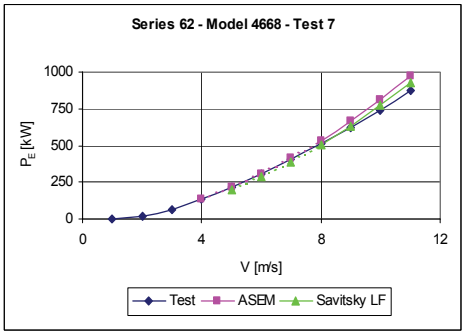

[b]

Figure 11.6-31 Data Comparison: Model 4668 - Test 7

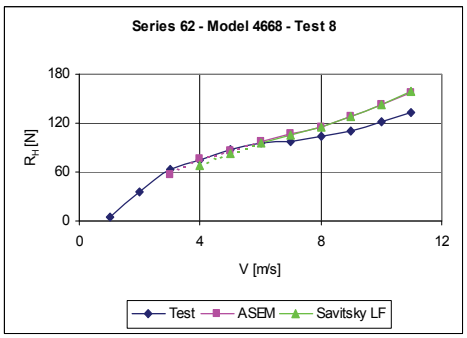

[a]

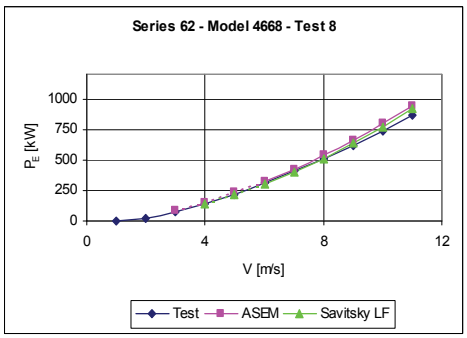

[b]

Figure 11.6-32 Data Comparison: Model 4668 - Test 8

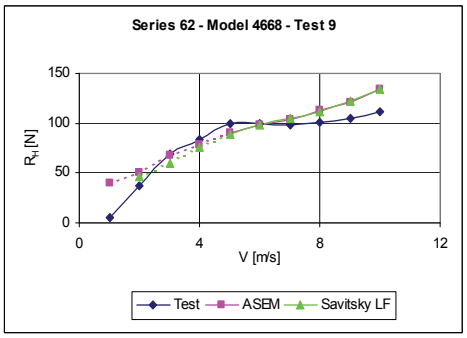

[a]

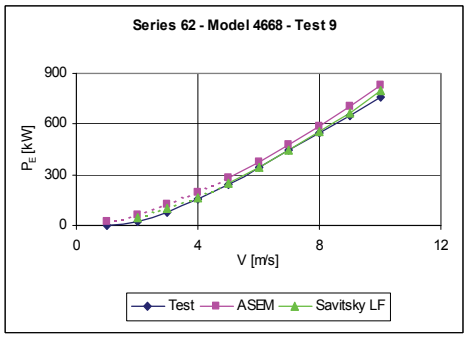

[b]

Figure 11.6-33 Data Comparison: Model 4668 - Test 9

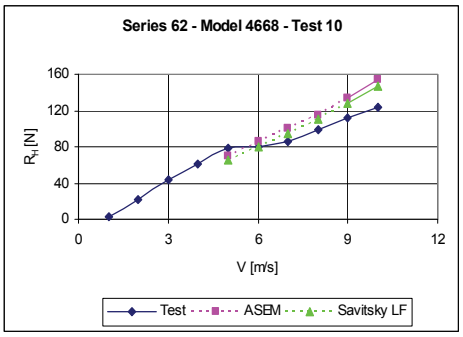

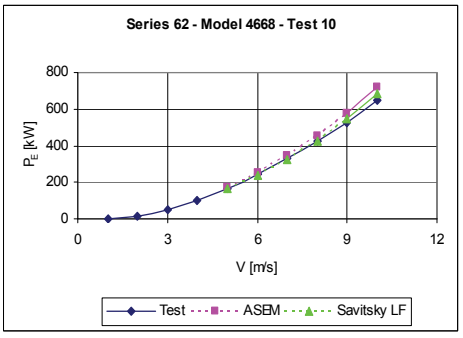

[a] **[b]**

Figure 11.6-34 Data Comparison: Model 4668 - Test 10

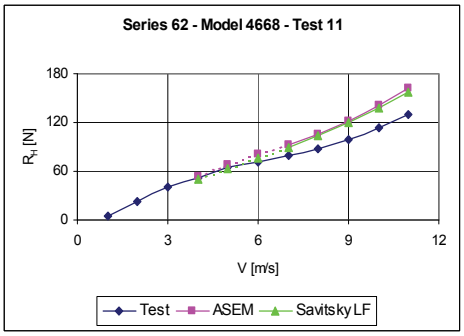

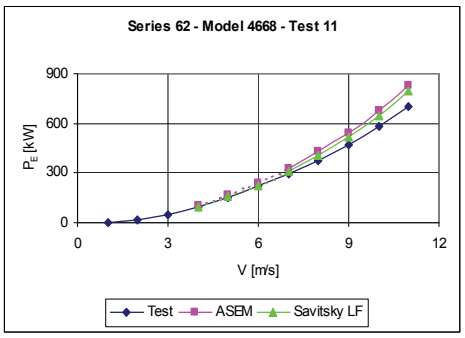

[a] **[b]**

Figure 11.6-35 Data Comparison: Model 4668 - Test 11

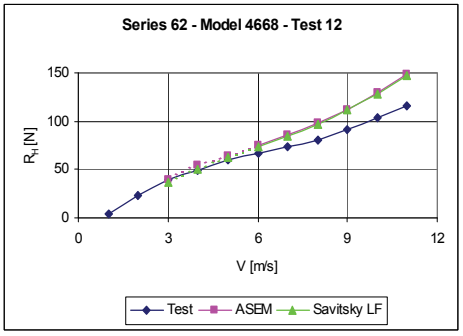

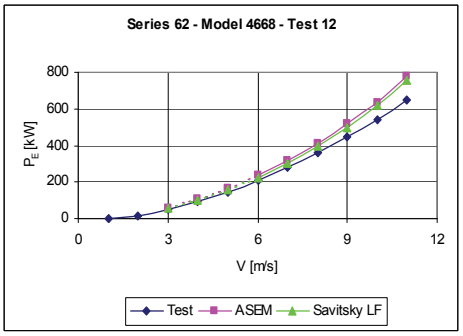

[a] **[b]**

Figure 11.6-36 Data Comparison: Model 4668 - Test 12

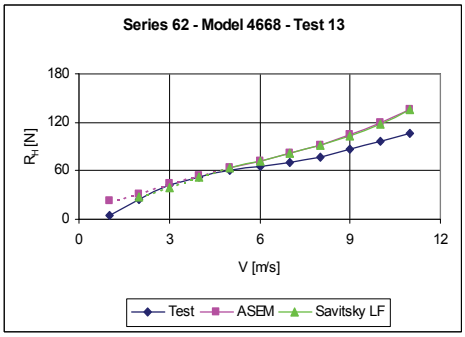

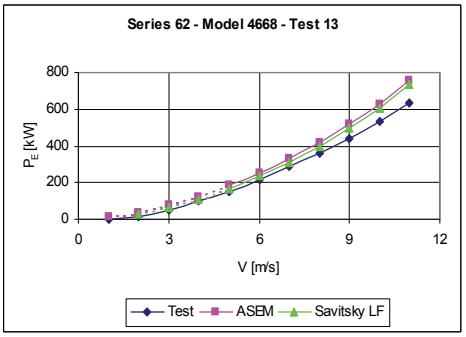

[a] **[b]**

Figure 11.6-37 Data Comparison: Model 4668 - Test 13

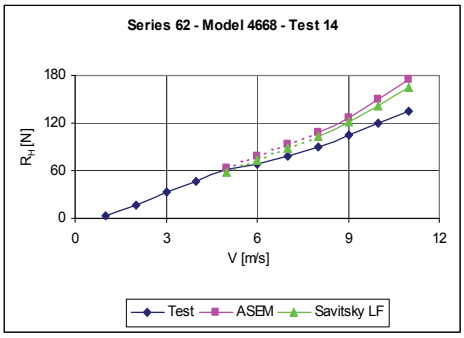

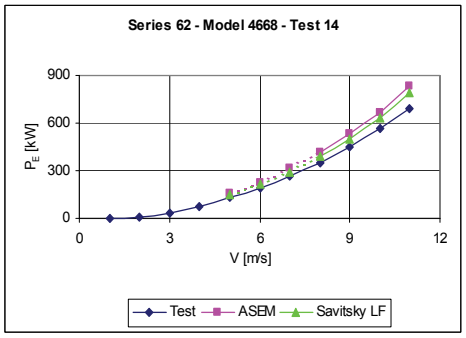

[a] **[b]**

Figure 11.6-38 Data Comparison: Model 4668 - Test 14

11.6.5 Model 4669

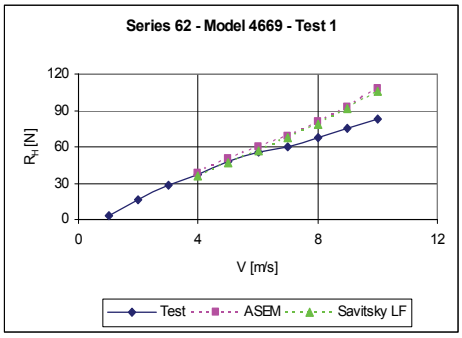

[a]

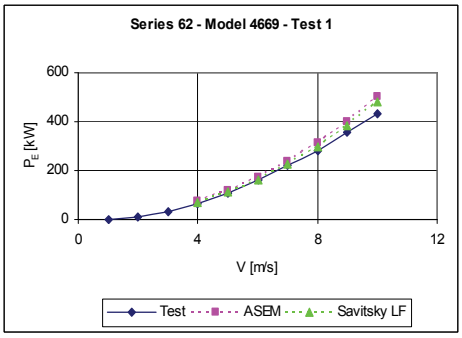

[b]

Figure 11.6-39 Data Comparison: Model 4669 - Test 1

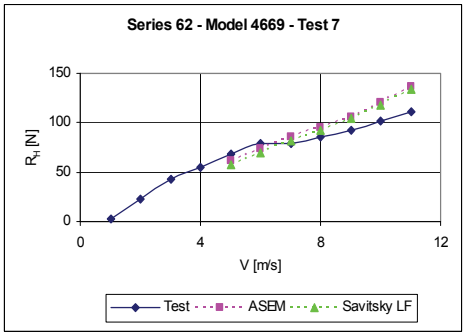

[a]

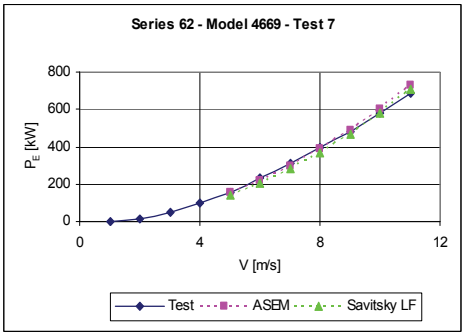

[b]

Figure 11.6-40 Data Comparison: Model 4669 - Test 7

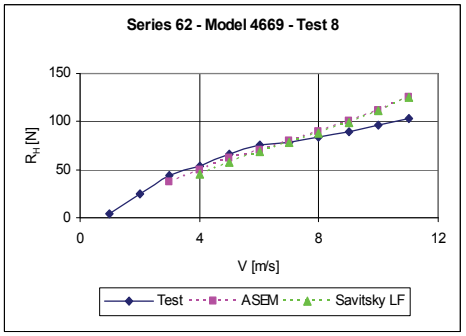

[a]

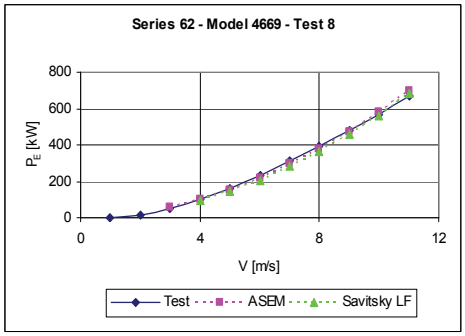

[b]

Figure 11.6-41 Data Comparison: Model 4669 - Test 8

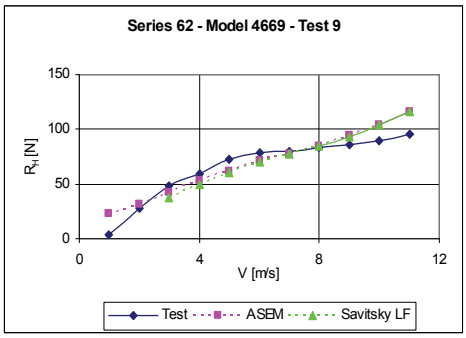

[a]

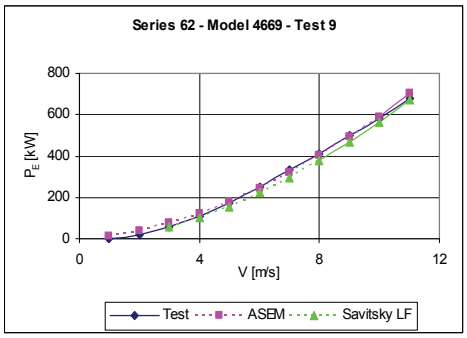

[b]

Figure 11.6-42 Data Comparison: Model 4669 - Test 9

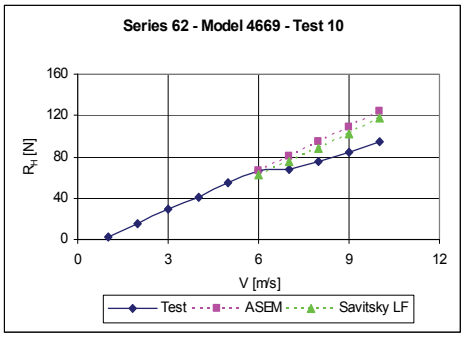

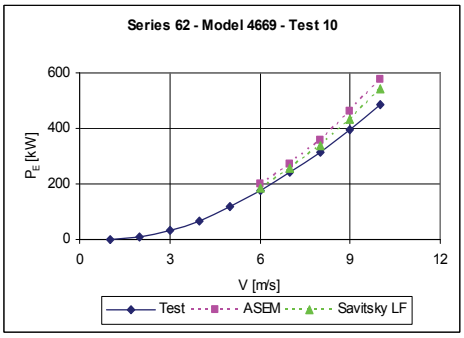

[a] **[b]**

Figure 11.6-43 Data Comparison: Model 4669 - Test 10

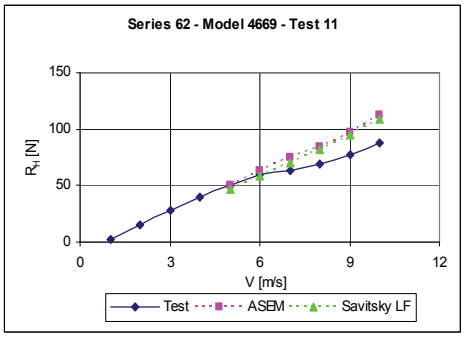

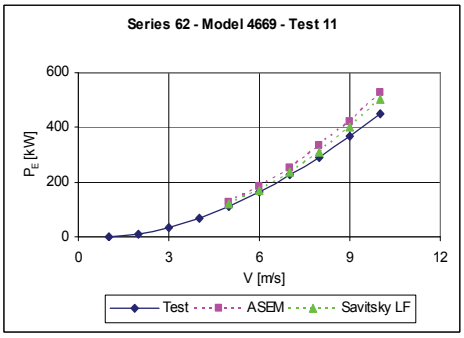

[a] **[b]**

Figure 11.6-44 Data Comparison: Model 4669 - Test 11

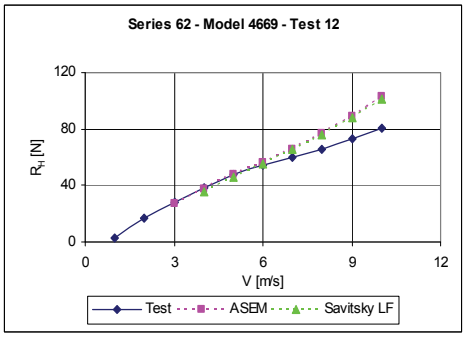

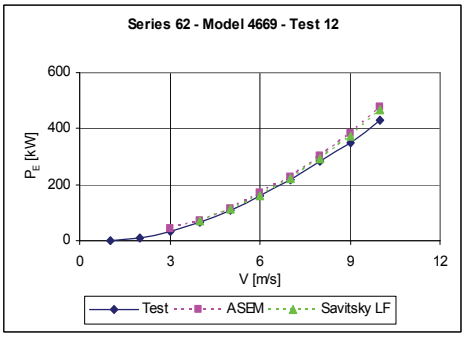

[a] **[b]**

Figure 11.6-45 Data Comparison: Model 4669 - Test 12

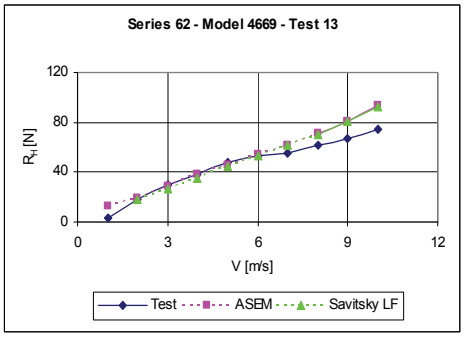

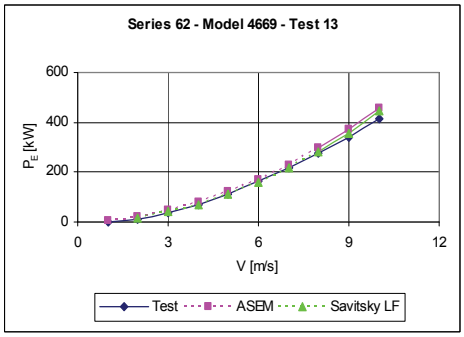

[a] **[b]**

Figure 11.6-46 Data Comparison: Model 4669 - Test 13

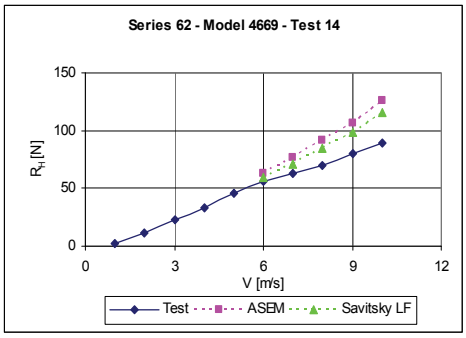

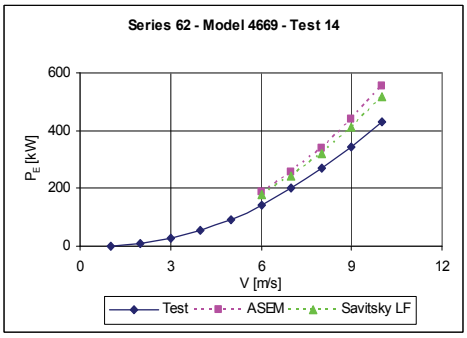

[a] **[b]**

Figure 11.6-47 Data Comparison: Model 4669 - Test 14

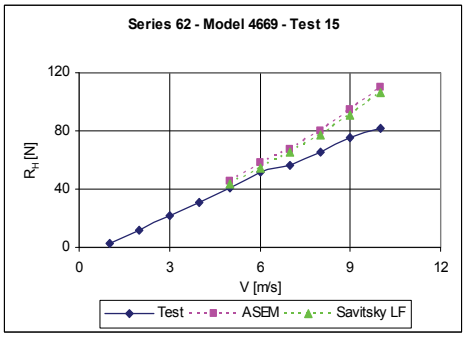

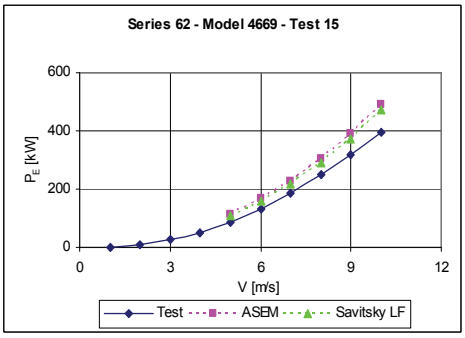

[a] **[b]**

Figure 11.6-48 Data Comparison: Model 4669 - Test 15

11.7 Data Comparison Analysis

Analysis of data comparison have been developed computing dimensionless variation of resistance and power versus hull speed.

In detail, these dimensionless variation have been computed adopting Test results as benchmark, as shown:

$$\Delta R_H = \frac{R_{H,\mathrm{Predicted}} - R_{H,Series\,62}}{R_{H,Sereis\,62}} \qquad \textbf{(G. 1)}$$

and

$$\Delta P_E = \frac{P_{E,\mathrm{Predicted}} - P_{E,Series\,62}}{P_{E,Sereis\,62}} \qquad \textbf{(G. 2)}$$

where *Predicted* stands for ASEM as well as Savitsky's LF results.

Further ASEM results have been compared to Savitsky's LF results in term of dimensionless variation:

$$\Delta R_H = \frac{R_{H,ASEM} - R_{H,Savitsky}}{R_{H,Savitsky}} \qquad \textbf{(G. 3)}$$

and

$$\Delta P_E = \frac{P_{E,ASEM} - P_{E,Savitsky}}{P_{E,Savitsky}} \qquad \textbf{(G. 4)}$$

These dimensionless data give us the measurement of reliability and efficiency of ASEM and Savitsky's method related to model test results as well as ASEM results related to Savitsky's ones.

Results comparison, reported in up listed diagrams with dash line, have been hereinafter reported with dash line too.

11.7.1 Model 4665

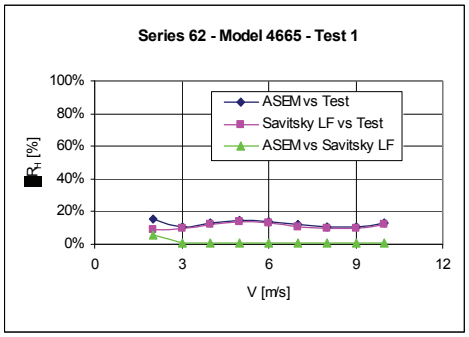

[a]

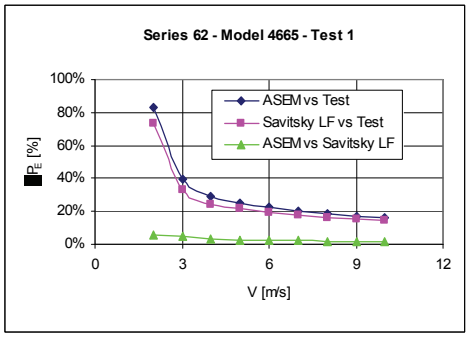

[b]

Figure 11.7-1 Data Comparison Analysis: Model 4665 - Test 1

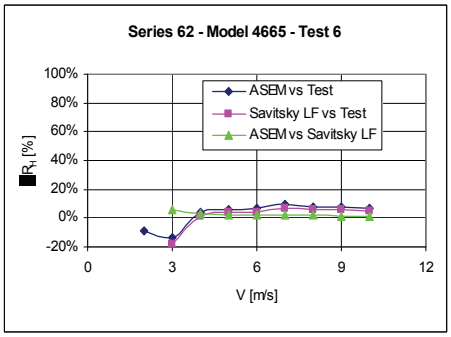

[a]

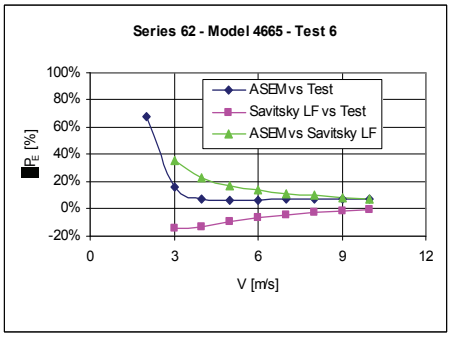

[b]

Figure 11.7-2 Data Comparison Analysis: Model 4665 - Test 6

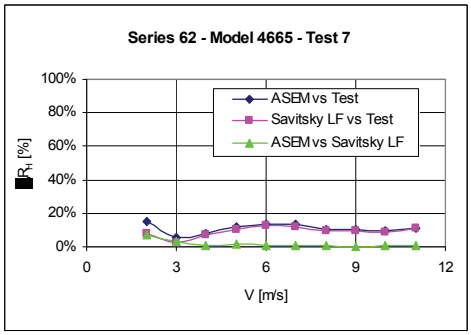

[a]

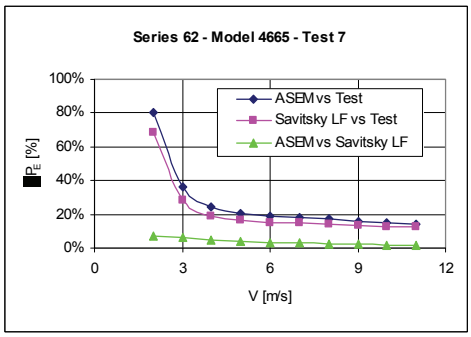

[b]

Figure 11.7-3 Data Comparison Analysis: Model 4665 - Test 7

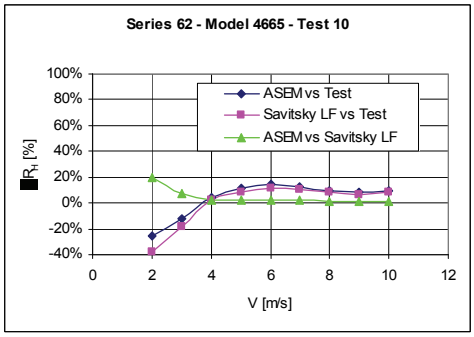

[a]

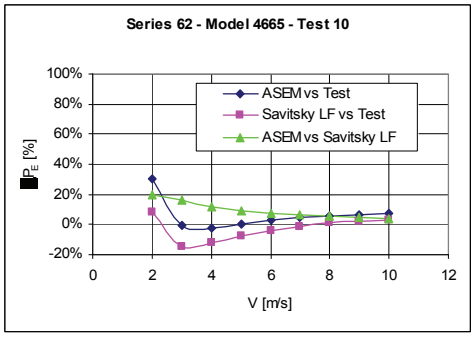

[b]

Figure 11.7-4 Data Comparison Analysis: Model 4665 - Test 10

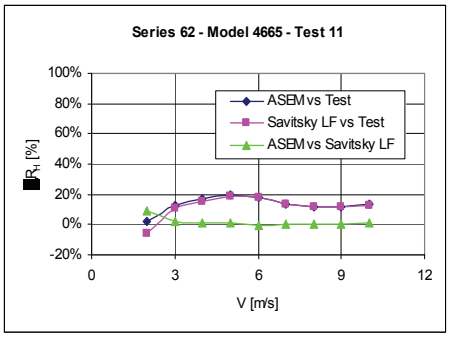

[a]

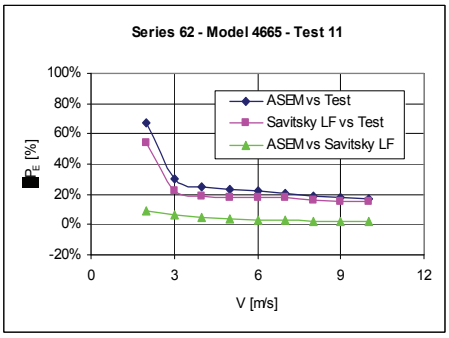

[b]

Figure 11.7-5 Data Comparison Analysis: Model 4665 - Test 11

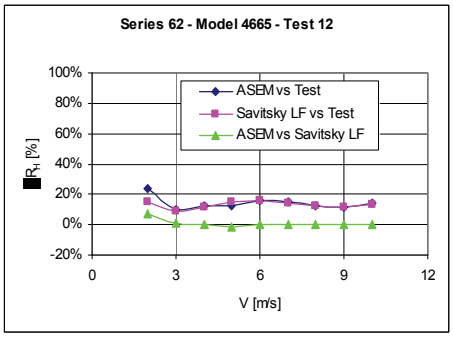

[a]

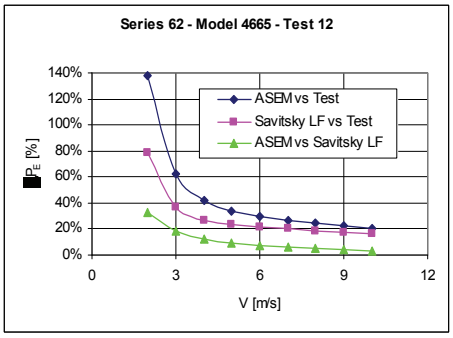

[b]

Figure 11.7-6 Data Comparison Analysis: Model 4665 - Test 12

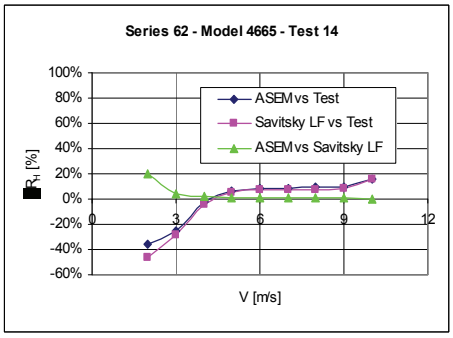

[a]

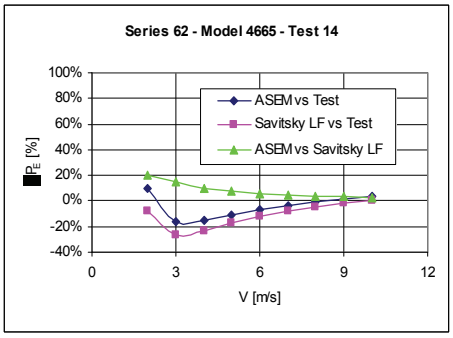

[b]

Figure 11.7-7 Data Comparison Analysis: Model 4665 - Test 14

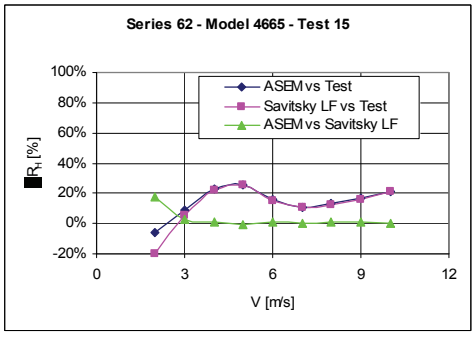

[a]

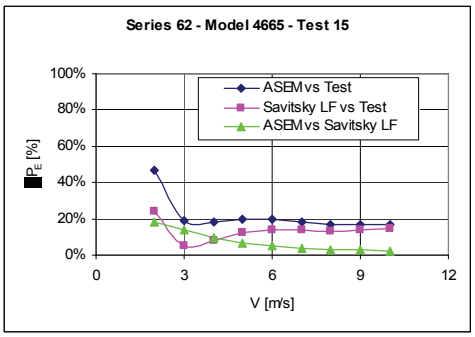

[b]

Figure 11.7-8 Data Comparison Analysis: Model 4665 - Test 15

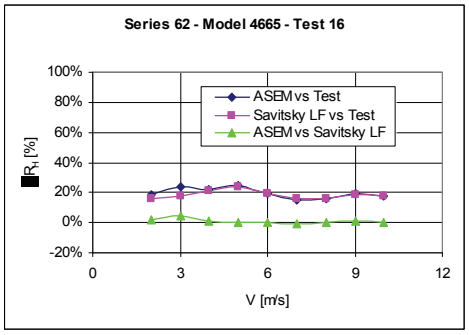

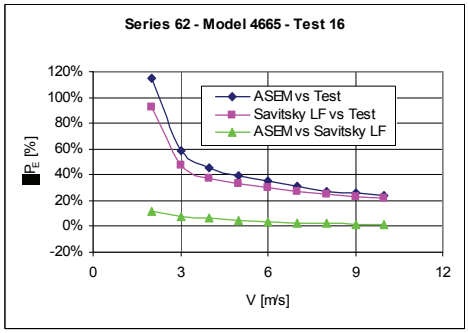

[a] **[b]**

Figure 11.7-9 Data Comparison Analysis: Model 4665 - Test 16

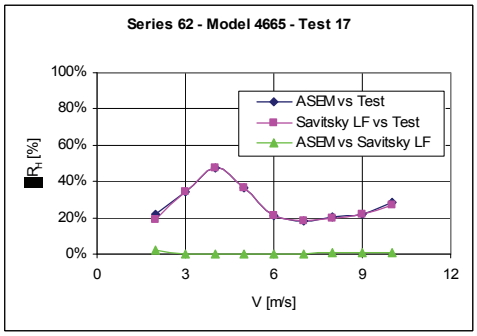

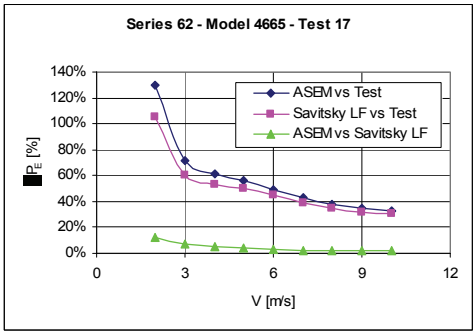

[a] **[b]**

Figure 11.7-10 Data Comparison Analysis: Model 4665 - Test 17

11.7.2 Model 4666

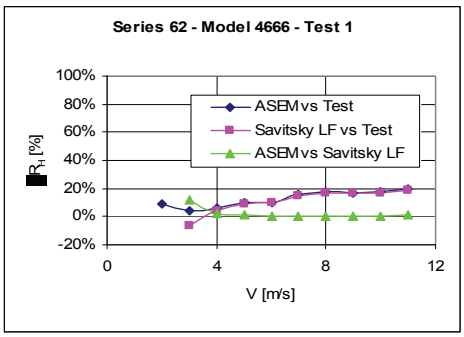

[a]

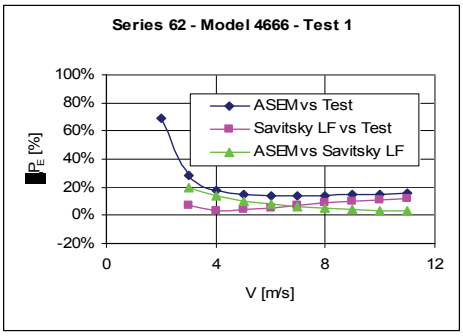

[b]

Figure 11.7-11 Data Comparison Analysis: Model 4666 - Test 1

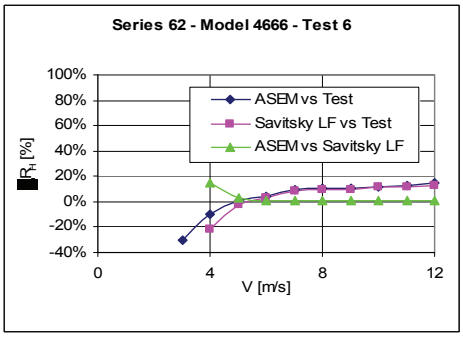

[a]

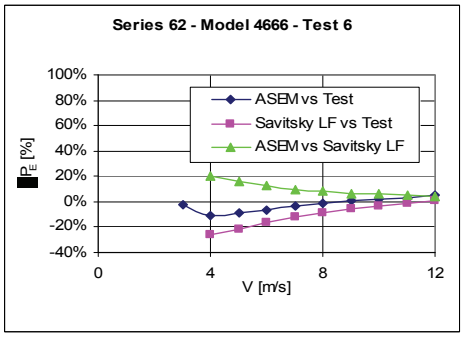

[b]

Figure 11.7-12 Data Comparison Analysis: Model 4666 - Test 6

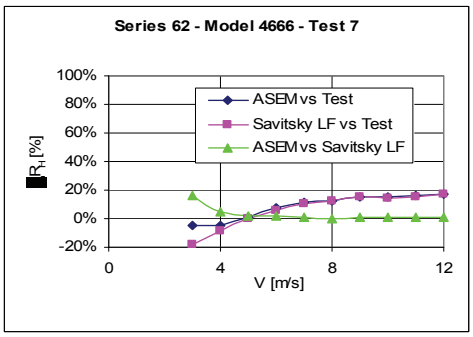

[a]

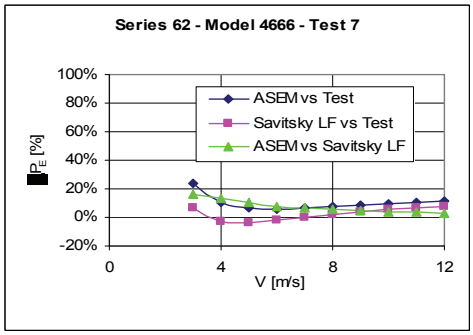

[b]

Figure 11.7-13 Data Comparison Analysis: Model 4666 - Test 7

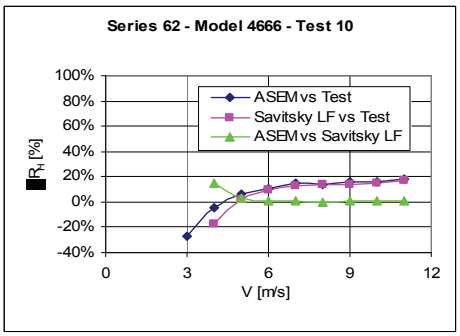

[a]

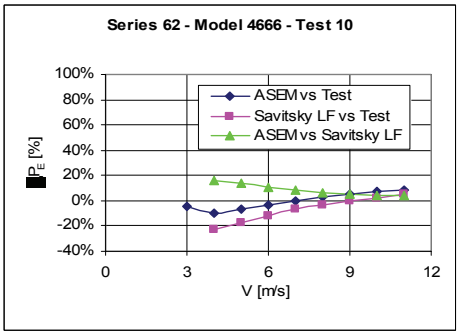

[b]

Figure 11.7-14 Data Comparison Analysis: Model 4666 - Test 10

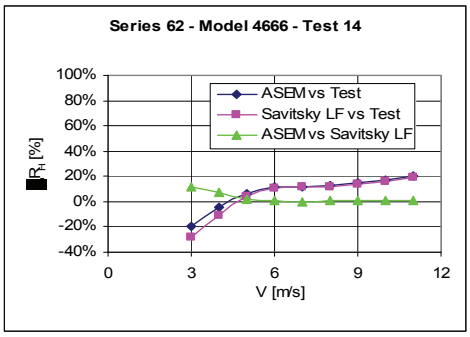

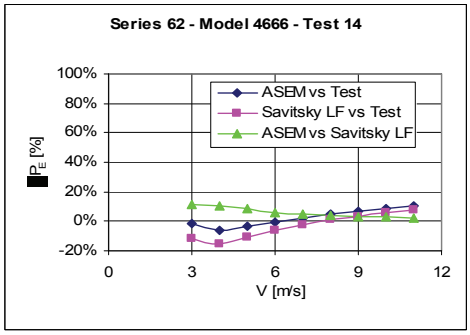

[a] **[b]**

Figure 11.7-15 Data Comparison Analysis: Model 4666 - Test 14

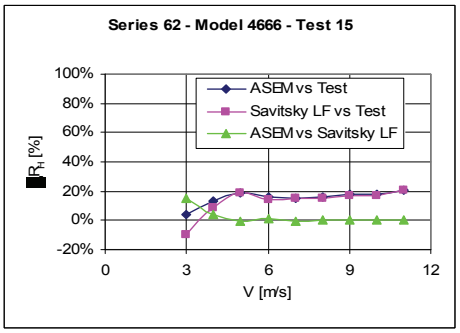

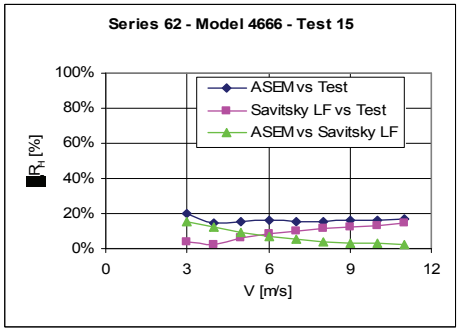

[a] **[b]**

Figure 11.7-16 Data Comparison Analysis: Model 4666 - Test 16

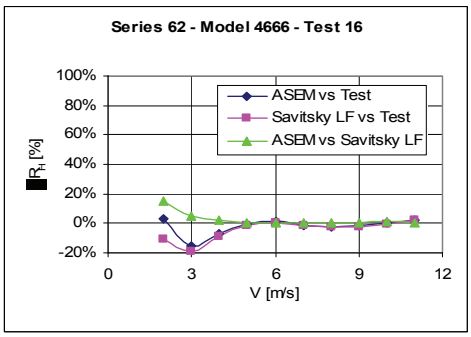

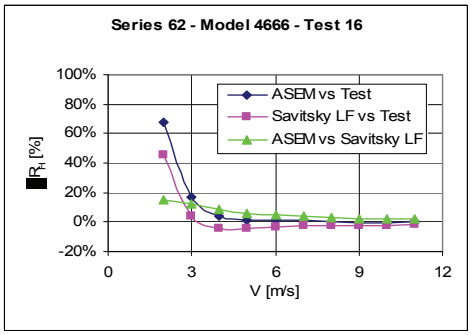

[a] **[b]**

Figure 11.7-17 Data Comparison Analysis: Model 4666 - Test 17

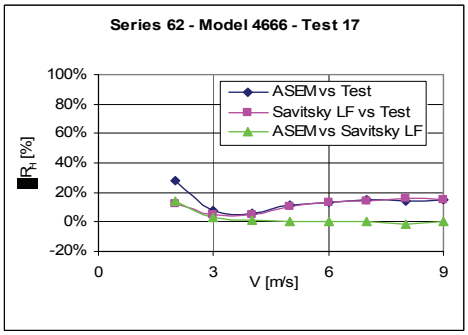

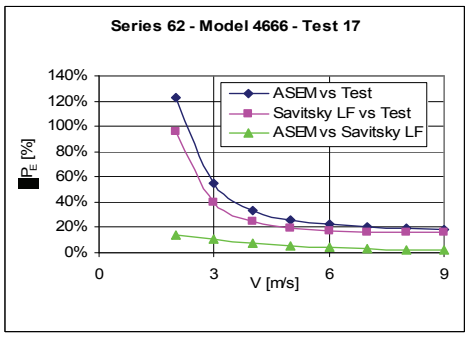

[a] **[b]**

Figure 11.7-18 Data Comparison Analysis: Model 4666 - Test 17

11.7.3 Model 4667-1

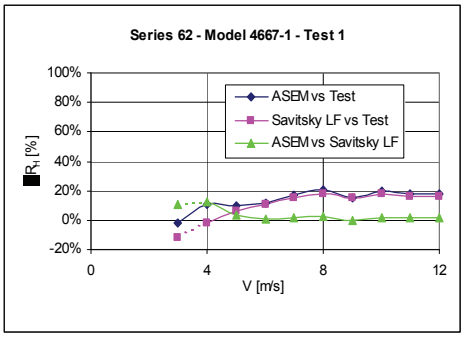

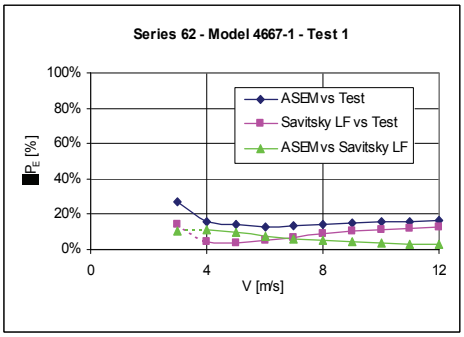

[a] **[b]**

Figure 11.7-19 Data Comparison Analysis: Model 4667-1 - Test 1

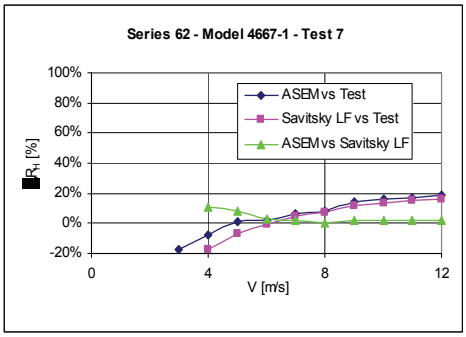

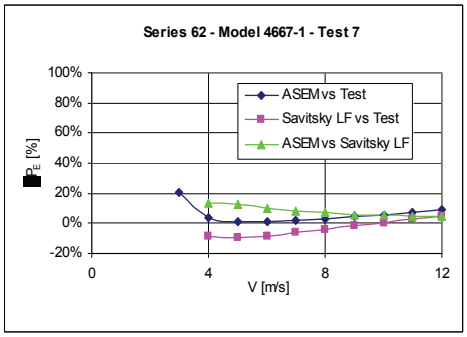

[a] **[b]**

Figure 11.7-20 Data Comparison Analysis: Model 4667-1 - Test 7

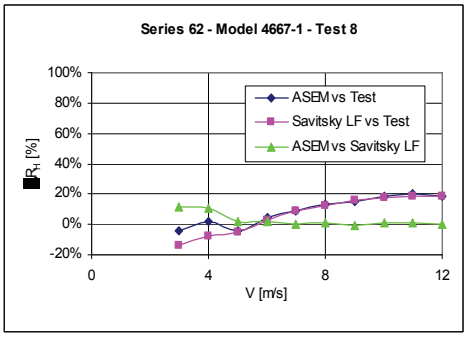

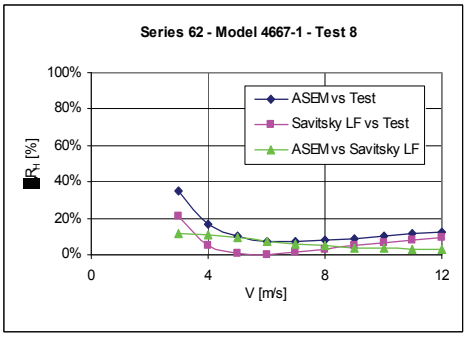

[a] **[b]**

Figure 11.7-21 Data Comparison Analysis: Model 4667-1 - Test 8

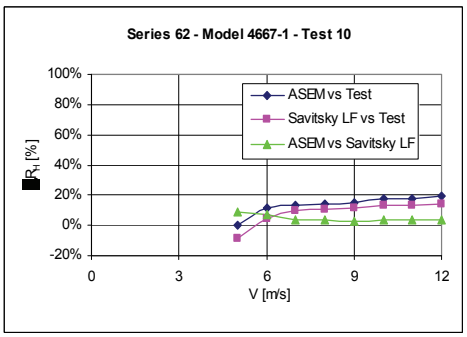

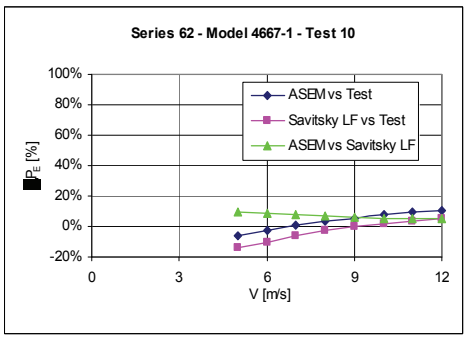

[a] **[b]**

Figure 11.7-22 Data Comparison Analysis: Model 4667-1 - Test 10

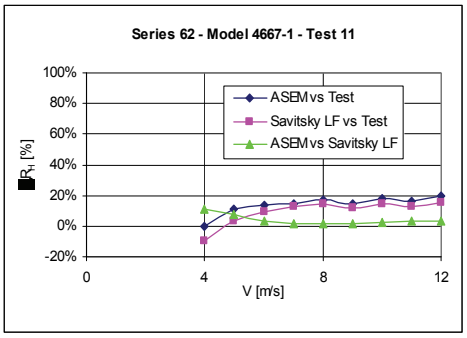

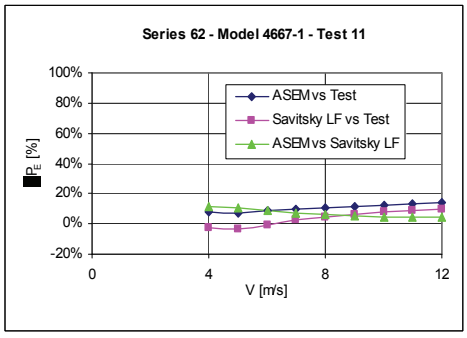

[a] **[b]**

Figure 11.7-23 Data Comparison Analysis: Model 4667-1 - Test 11

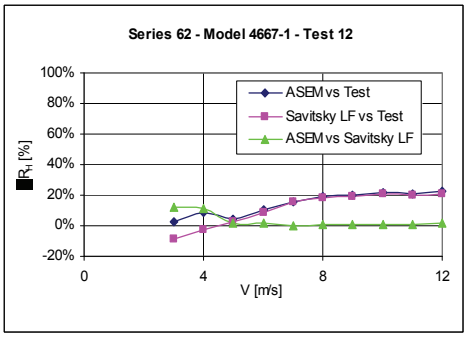

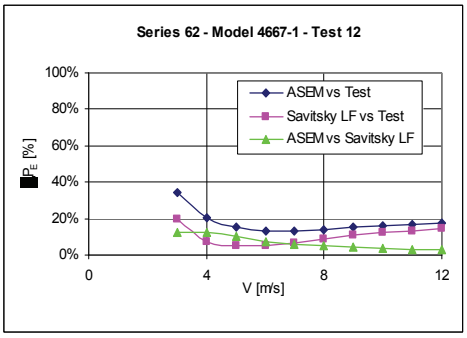

[a] **[b]**

Figure 11.7-24 Data Comparison Analysis: Model 4667-1 - Test 12

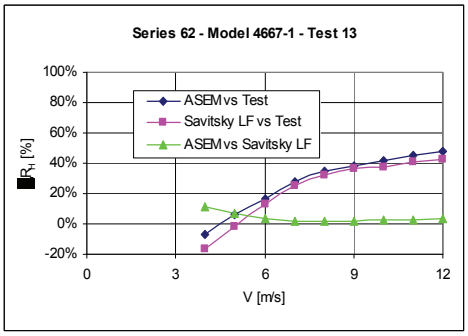

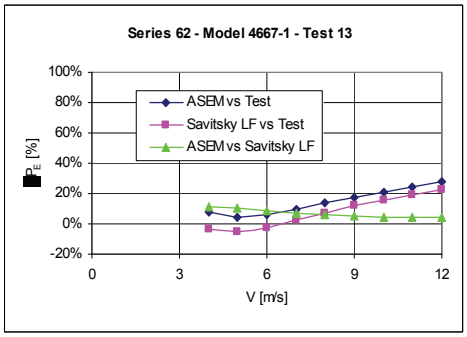

[a] **[b]**

Figure 11.7-25 Data Comparison Analysis: Model 4667-1 - Test 13

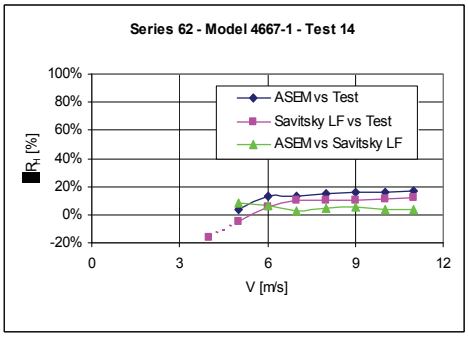

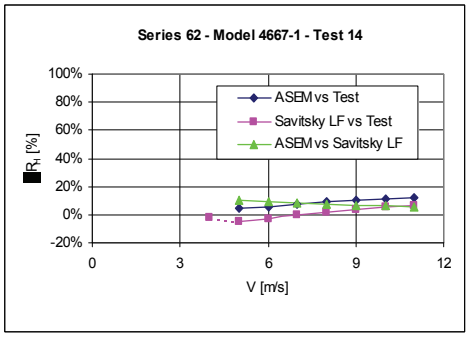

[a] **[b]**

Figure 11.7-26 Data Comparison Analysis: Model 4667-1 - Test 14

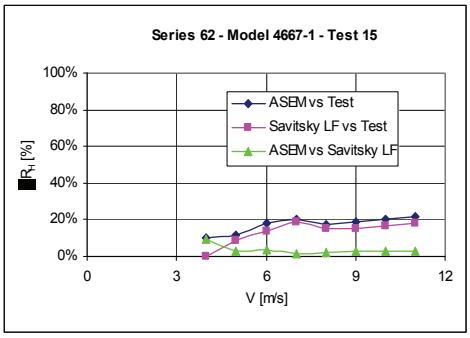

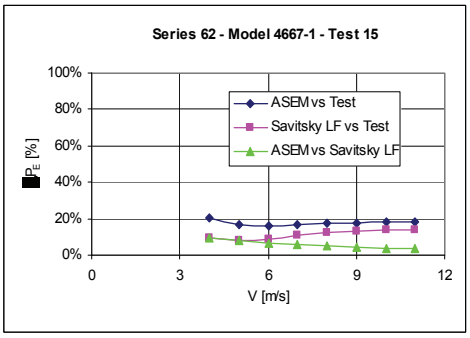

[a] **[b]**

Figure 11.7-27 Data Comparison Analysis: Model 4667-1 - Test 15

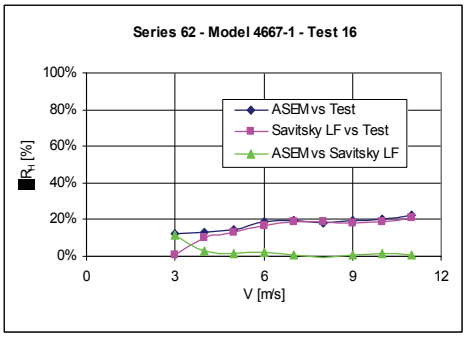

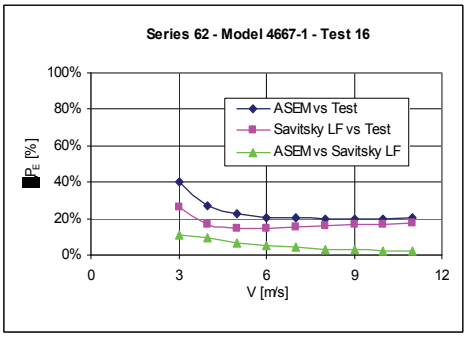

[a] **[b]**

Figure 11.7-28 Data Comparison Analysis: Model 4667-1 - Test 16

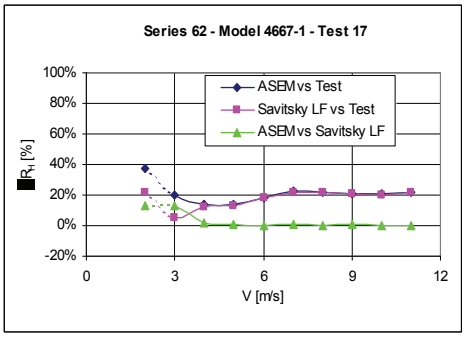

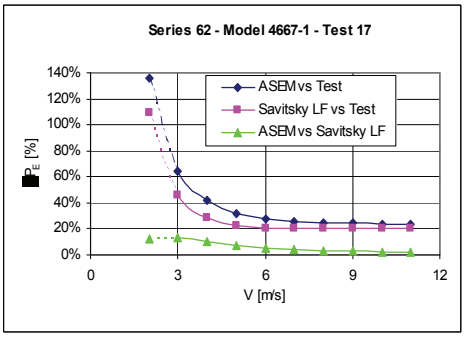

[a] **[b]**

Figure 11.7-29 Data Comparison Analysis: Model 4667-1 - Test 17

11.7.4 Model 4668

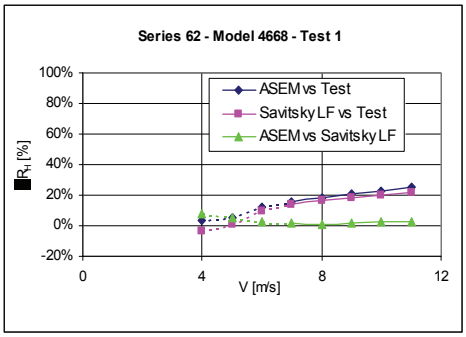

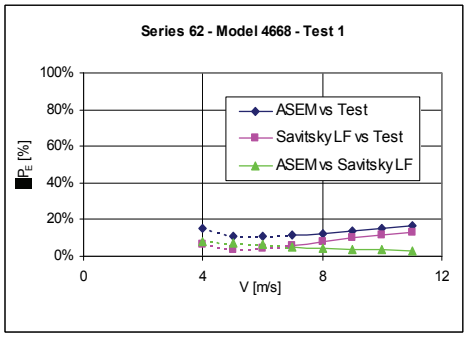

[a] **[b]**

Figure 11.7-30 Data Comparison Analysis: Model 4668 - Test 1

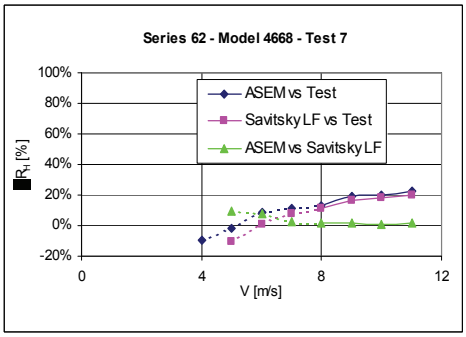

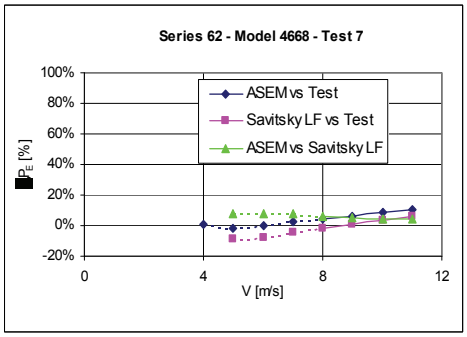

[a] **[b]**

Figure 11.7-31 Data Comparison Analysis: Model 4668 - Test 7

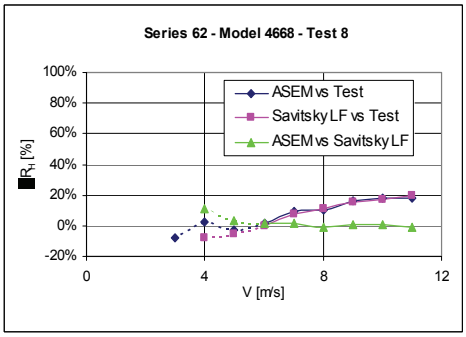

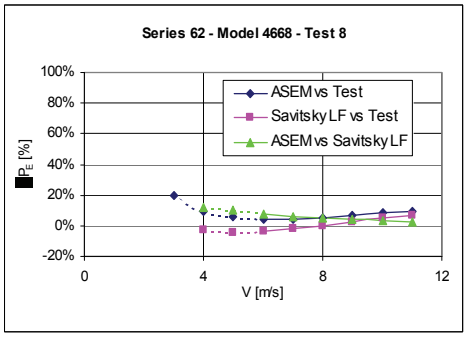

[a] **[b]**

Figure 11.7-32 Data Comparison Analysis: Model 4668 - Test 8

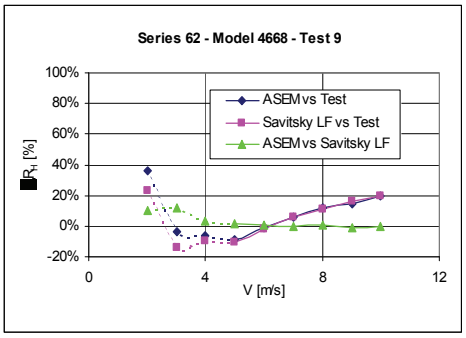

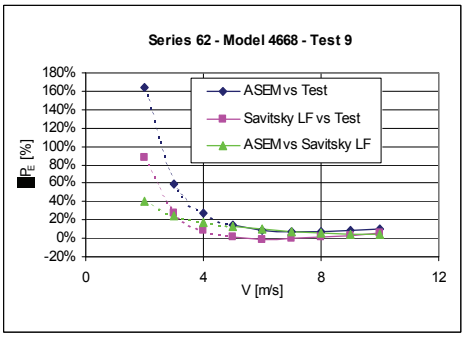

[a] **[b]**

Figure 11.7-33 Data Comparison Analysis: Model 4668 - Test 9

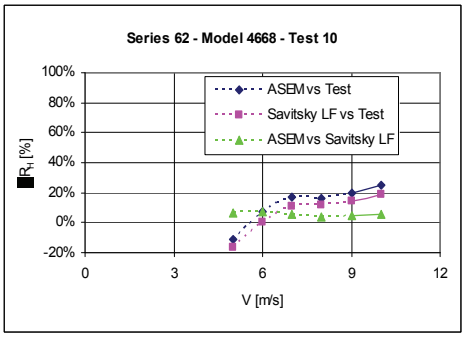

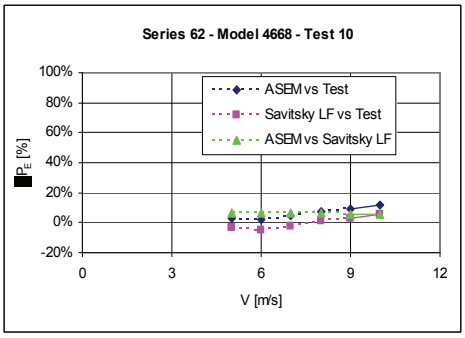

[a] **[b]**

Figure 11.7-34 Data Comparison Analysis: Model 4668 - Test 10

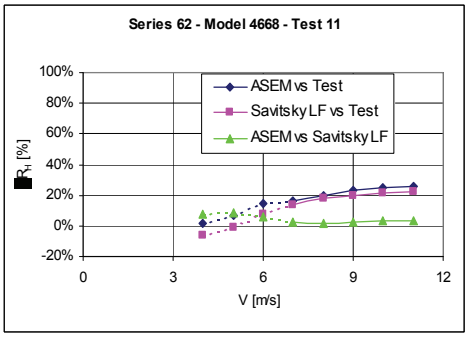

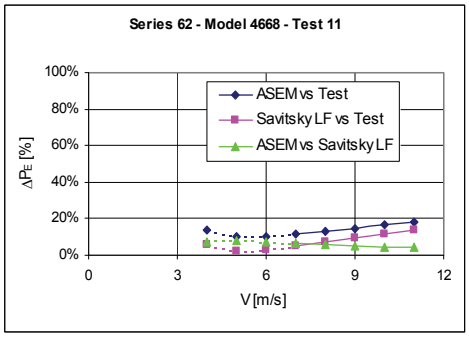

[a] **[b]**

Figure 11.7-35 Data Comparison Analysis: Model 4668 - Test 11

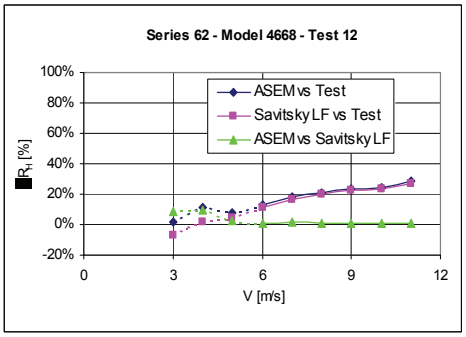

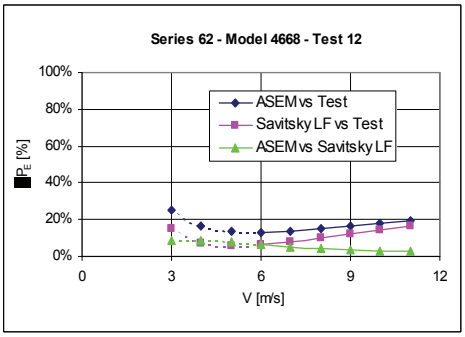

[a] **[b]**

Figure 11.7-36 Data Comparison Analysis: Model 4668 - Test 12

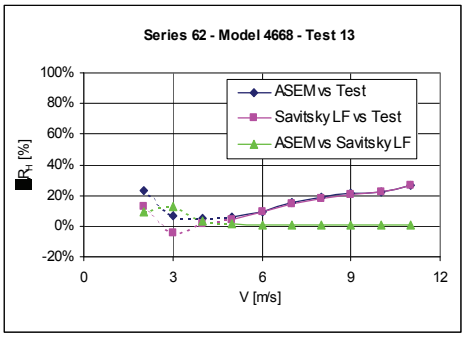

[a]

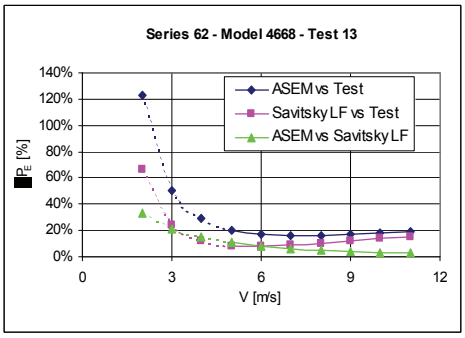

[b]

Figure 11.7-37 Data Comparison Analysis: Model 4668 - Test 13

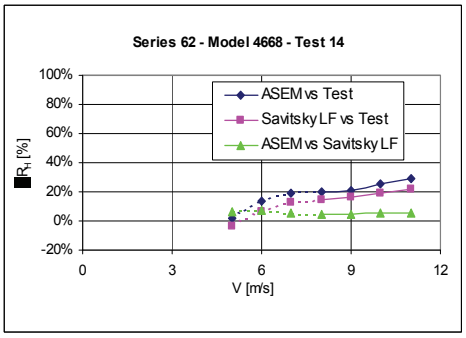

[a]

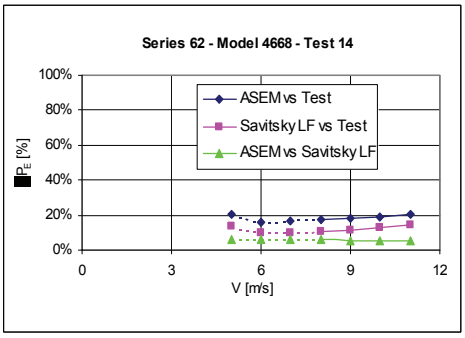

[b]

Figure 11.7-38 Data Comparison Analysis: Model 4668 - Test 14

11.7.5 Model 4669

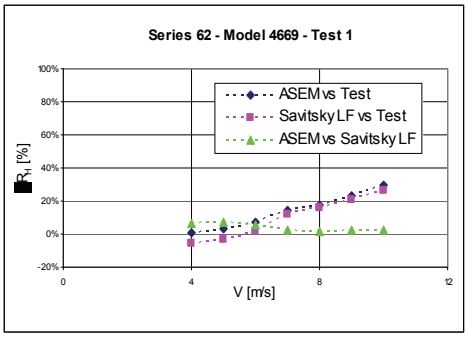

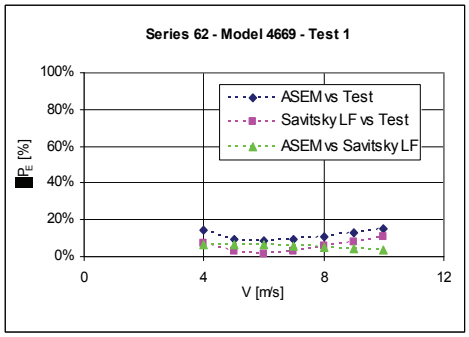

[a] **[b]**

Figure 11.7-39 Data Comparison Analysis: Model 4669 - Test 1

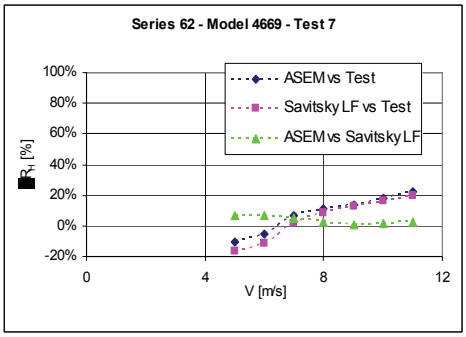

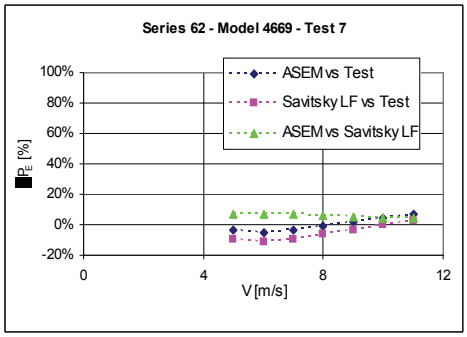

[a] **[b]**

Figure 11.7-40 Data Comparison Analysis: Model 4669 - Test 7

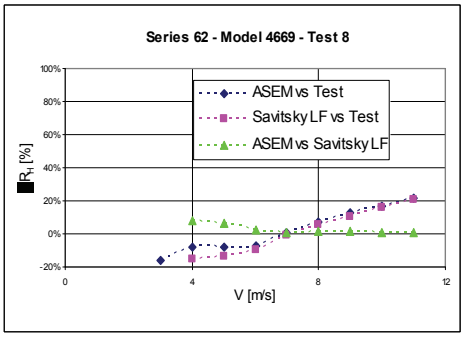

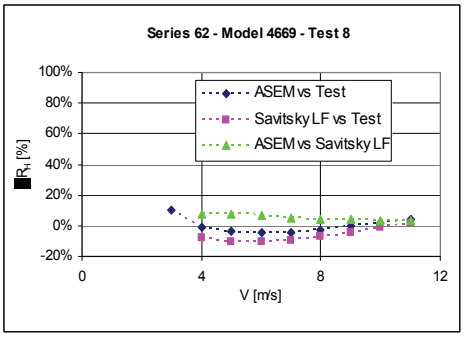

[a] **[b]**

Figure 11.7-41 Data Comparison Analysis: Model 4669 - Test 8

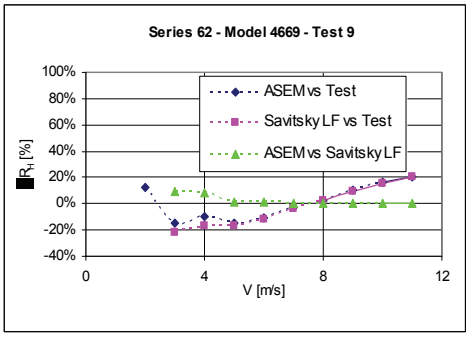

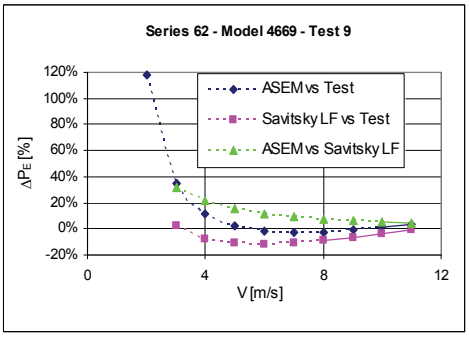

[a] **[b]**

Figure 11.7-42 Data Comparison Analysis: Model 4669 - Test 9

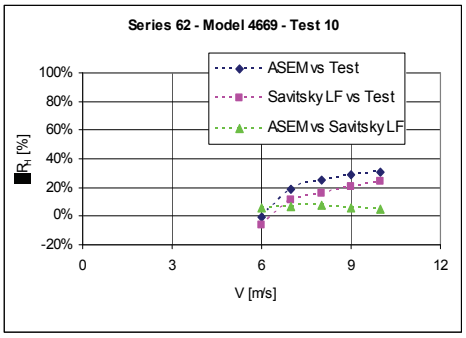

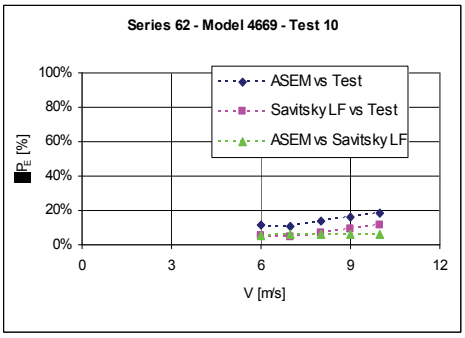

[a] **[b]**

Figure 11.7-43 Data Comparison Analysis: Model 4669 - Test 10

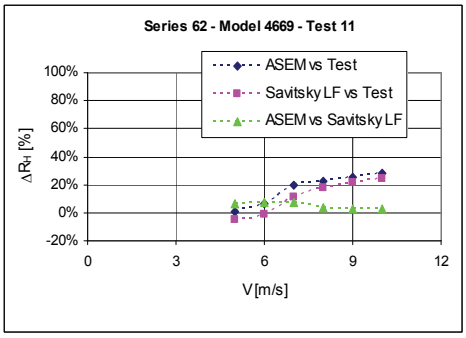

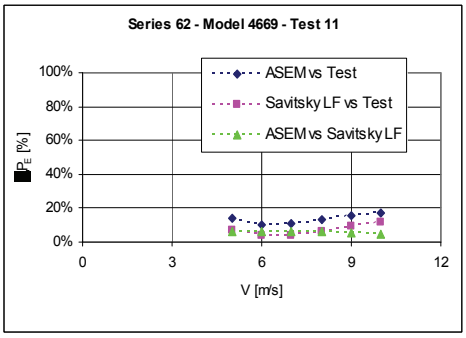

[a] **[b]**

Figure 11.7-44 Data Comparison Analysis: Model 4669 - Test 11

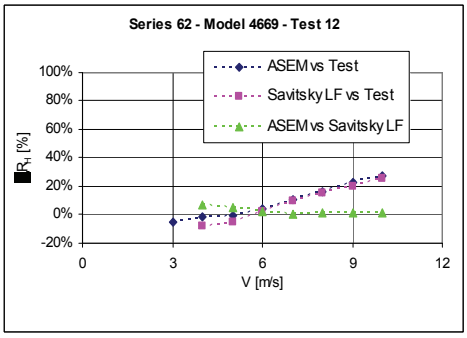

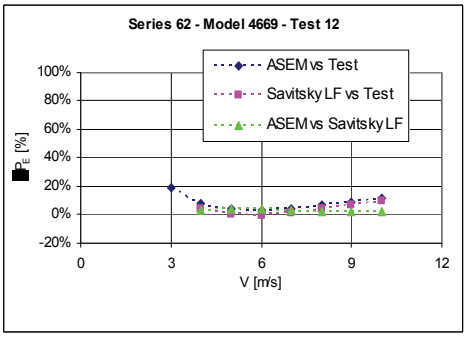

[a] **[b]**

Figure 11.7-45 Data Comparison Analysis: Model 4669 - Test 12

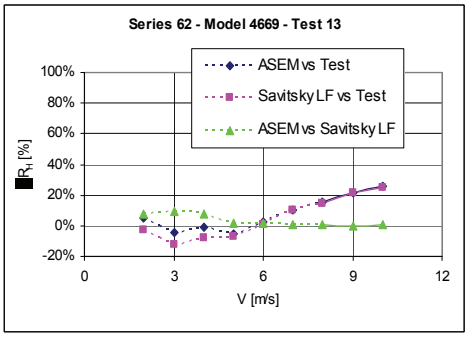

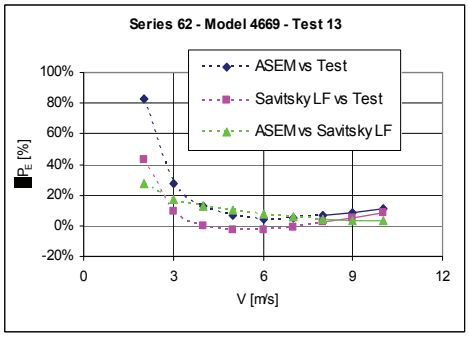

[a] **[b]**

Figure 11.7-46 Data Comparison Analysis: Model 4669 - Test 13

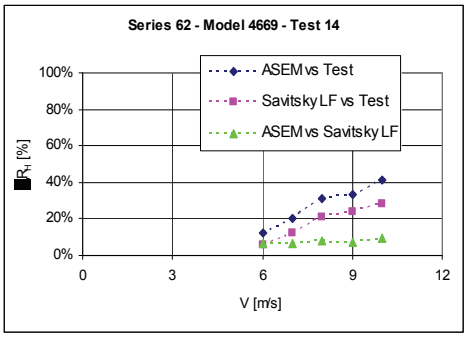

[a]

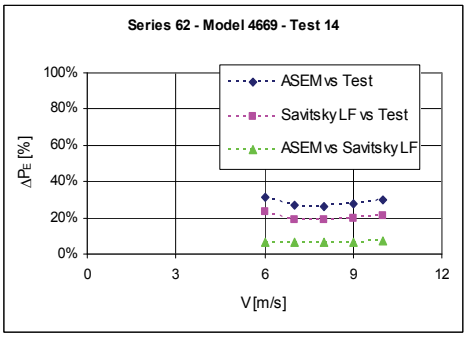

[b]

Figure 11.7-47 Data Comparison Analysis: Model 4669 - Test 14

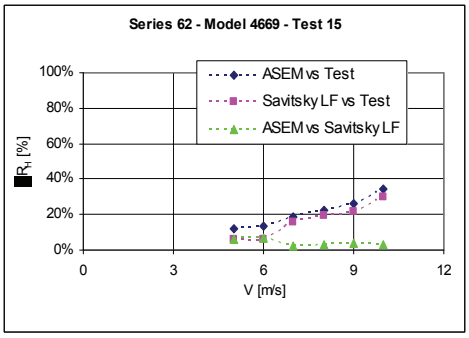

[a]

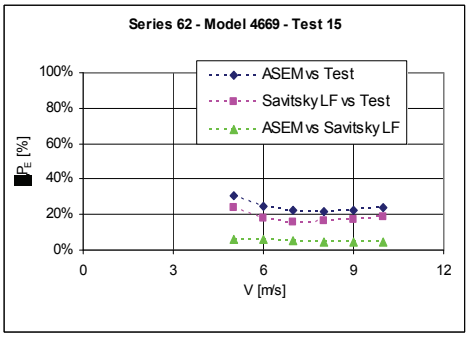

[b]

Figure 11.7-48 Data Comparison Analysis: Model 4669 - Test 15

11.8 Data Correlation Analysis

Hereinafter max dimensionless variations of resistance, as well as power, per each Model and Test case are reported.

Table 11.8-1 Max dimensionless variations: Model 4665

Model 4665				
Test n.	$\max\{\Delta R_H\}$	**Note**	$\max\{\Delta P_E\}$	**Note**
1	≤ 20%		≤ 20%	for V > 5 m/s
6	≤ 20%		≤ 20%	for V > 4 m/s
7	≤ 20%		≤ 20%	for V > 4 m/s
10	≤ 20%	for V > 3 m/s	≤ 20%	for V > 2 m/s
11	≤ 20%		≤ 20%	for V > 3 m/s
12	≤ 20%	for V > 2 m/s	≤ 40%	for V > 3 m/s
14	≤ 20%	for V > 3 m/s	≤ 20%	for V > 3 m/s
15	≤ 20%	for V > 5 m/s	≤ 20%	for V > 2 m/s
16	≤ 25%		≤ 40%	
17	≤ 20%	for V > 5 m/s	≤ 40%	for V > 6 m/s

Table 11.8-2 Max dimensionless variations: Model 4666

Model 4666				
Test n.	$\max\{\Delta R_H\}$	**Note**	$\max\{\Delta P_E\}$	**Note**
1	≤ 20%		≤ 20%	for V > 3 m/s
6	≤ 20%	for V > 3 m/s	≤ 20%	
7	≤ 20%		≤ 20%	
10	≤ 20%	for V > 4 m/s	≤ 20%	
14	≤ 20%	for V > 4 m/s	≤ 20%	
15	≤ 20%		≤ 20%	
16	≤ 20%		≤ 20%	for V > 2 m/s
17	≤ 20%	for V > 3 m/s	≤ 25%	for V > 5 m/s

Table 11.8-3 Max dimensionless variations: Model 4667-1

Model 4667-1				
Test n.	$\max\{\Delta R_H\}$	**Note**	$\max\{\Delta P_E\}$	**Note**
1	≤ 20%		≤ 20%	
7	≤ 20%		≤ 20%	
8	≤ 20%		≤ 20%	for V > 3 m/s
10	≤ 20%		≤ 20%	
11	≤ 20%		≤ 20%	
12	≤ 20%		≤ 20%	for V > 3 m/s
13	≤ 50%		≤ 30%	
14	≤ 20%		≤ 20%	
15	≤ 20%		≤ 20%	
16	≤ 20%		≤ 20%	for V > 4 m/s
17	≤ 20%	for V > 2 m/s	≤ 30%	for V > 5 m/s

Table 11.8-4 Max dimensionless variations: Model 4668

Model 4668				
Test n.	$\max\{\Delta R_H\}$	**Note**	$\max\{\Delta P_E\}$	**Note**
1	≤ 25%		≤ 20%	
7	≤ 20%		≤ 20%	
8	≤ 20%		≤ 20%	for V > 5 m/s
9	≤ 20%		≤ 20%	for V > 4 m/s
10	≤ 25%		≤ 20%	
11	≤ 25%		≤ 20%	
12	≤ 30%		≤ 25%	for V > 5 m/s
13	≤ 30%		≤ 20%	for V > 4 m/s
14	≤ 30%		≤ 20%	

Table 11.8-5 Max dimensionless variations: Model 4669

Model 4669				
Test n.	$\max\{\Delta R_H\}$	**Note**	$\max\{\Delta P_E\}$	**Note**
1	≤ 30%		≤ 20%	
7	≤ 20%		≤ 20%	
8	≤ 20%		≤ 20%	
9	≤ 20%		≤ 20%	for V > 4 m/s
10	≤ 30%		≤ 20%	
11	≤ 30%		≤ 20%	
12	≤ 30%		≤ 20%	
13	≤ 30%		≤ 25%	for V > 4 m/s
14	≤ 40%		≤ 40%	
15	≤ 40%		≤ 40%	

In the most of case, the max dimensionless variation has a value less than 20%, within the overall range of hull speed. The few test cases with dimensionless variations higher than 20% are associated to both positive value of α_0, and value of $\left(1-\frac{L_{CG}}{L_P}\right)$ higher than 6 percent.

Thereby goodness of ASEM results, as well as Savitsky's ones, is related to the mutual longitudinal position of the Center of Gravity both the Center of Buoyancy and the centroid of A_P: higher the forward longitudinal position of Center of Gravity (versus the Center of Buoyancy as well as the centroid of A_P), higher the error related to drives to of ASEM results.

This trend cannot be confirmed by tests data pertinent to the Model 4669, due to their state of uncertainty.

11.9 Remarks on Data Analysis

A first look shows us the common trends of ASEM results versus Savitsky's LF results: higher hull speed closer results.

This is due to the geometry of the models tested. For all models of Series 62, the large part of the hull has a constant deadrise angle: the afterward part of the hull looks like a monohedral hull form. Despite at low speed, ASEM takes in account also the contribution of forward transversal section -which deadrise angle is different versus the transom ones- there is no great difference in term of results due to the low speed value. Increasing the speed the wetted surface is reduced and, in planing condition, the afterward part of the hull is the only one interested by the pressure distribution. Thereby, in planing condition, models of Series 62 work as monohedral hull form does. For monohedral hull forms ASEM and Savitsky's results are quite the same: the presence of little differences are due to approximations in computing flows.

A second remark is pertinent to Power dimensionless variations: dimensionless variation magnitude has a decreasing trend at all, with a steeply downsizing at low hull speed. As matter of fact, per each test case analyzed Power grows up with the hull speed meanwhile difference between predicted value (with ASEM as well as Savitsky's LF method) and computed ones, by test results, is quite constant with the hull speed. Thereby Power dimensionless variation decreases with the hull speed: lower hull speed higher dimensionless variation magnitude.

A third observation is related to Froude numbers and the different motion fields pointed out for the same value of hull speed achieved. These differences are due to the "geometric term" present in the Froude number formula. For the Froude number linked to the beam C_V,

$$C_V = \frac{V}{\sqrt{gB_C}} \qquad \textbf{(G. 5)}$$

the geometric term is connected to an hull dimension: the beam between the chines B_C. This is a constant data that characterize the geometry of each model tested. Thereby this geometric term is constant whatever the hull speed value has been achieved and for

each test developed: the Froude number is linear with the hull speed, and has the same trend with all tests related to the same model.

For the Froude number related to the "volume "length Fn_{∇} ,

$$Fn_{\nabla} = \frac{V}{\sqrt{g \cdot \sqrt[3]{\frac{W}{\gamma}}}} \qquad \textbf{(G. 6)}$$

the geometric term is associated to an hull mechanical parameter: the weight W. This data is related to the model test developed: the Froude number is linear with the hull speed, but his trend is pertinent to the weight value adopted in towing test.

For the Froude number related to the mean wetted length Fn ,

$$Fn = \frac{V}{\sqrt{gL_W}} \qquad \textbf{(G. 7)}$$

the geometric term is connected to a data related to all test parameters: the mean wetted length L_W. This geometric term is not constant with the hull speed and his value is further in relation to the model test developed: the Froude number is not linear with the hull speed, and his trend is pertinent to the towing test parameters.

As matter of fact motion fields related to Froude numbers are quit different.

Table 11.9-1 Motion Fields Range

Motion Fields	**Fn**	**C_V**	**F_d**
displacement field	< 0,4	< 1,5	< 3
semidisplacement field	0,4 ÷ 1,2	1,5 ÷ 3	3 ÷ 5
planing field	> 1,2	> 3	> 5

Table 11.9-2 Model 4665: Motion Fields

Model 4665																					
V [m/s]	C_V	Test n.1		Test n.6		Test n.7		Test n.10		Test n.11		Test n.12		Test n.14		Test n.15		Test n.16		Test n.17	
		F_d	Fn	F_d	Fn	F_d	Fn	F_d	Fn	F_d	Fn	F_d	Fn	F_d	Fn	F_d	Fn	F_d	Fn	F_d	Fn
1	0,4	0,6	0,3	0,6	0,3	0,6	0,3	0,6	0,3	0,6	0,3	0,6	0,3	0,6	0,3	0,6	0,3	0,6	0,3	0,6	0,3
2	0,8	1,2	0,6	1,1	0,6	1,1	0,6	1,2	0,6	1,2	0,6	1,2	0,7	1,2	0,6	1,2	0,6	1,2	0,7	1,2	0,7
3	1,2	1,8	1,1	1,7	1,0	1,7	1,0	1,8	1,0	1,8	1,0	1,8	1,1	1,9	1,0	1,9	1,0	1,9	1,1	1,9	1,2
4	1,7	2,4	1,6	2,2	1,4	2,2	1,5	2,4	1,4	2,4	1,5	2,4	1,6	2,5	1,4	2,5	1,5	2,5	1,6	2,5	1,7
5	2,1	3,0	2,0	2,8	1,8	2,8	2,0	2,9	1,8	3,0	1,9	3,0	2,0	3,1	1,9	3,1	1,9	3,1	2,1	3,1	2,2
6	2,5	3,6	2,5	3,3	2,2	3,3	2,4	3,5	2,3	3,6	2,4	3,6	2,5	3,7	2,3	3,7	2,4	3,7	2,5	3,7	2,7
7	2,9	4,1	2,9	3,9	2,6	3,9	2,8	4,1	2,7	4,1	2,8	4,1	2,9	4,3	2,8	4,3	2,9	4,3	3,0	4,3	3,2
8	3,3	4,7	3,4	4,4	3,1	4,4	3,2	4,7	3,2	4,7	3,3	4,7	3,3	5,0	3,3	5,0	3,4	5,0	3,6	5,0	3,9
9	3,7	5,3	3,9	5,0	3,6	5,0	3,7	5,3	3,7	5,3	3,8	5,3	4,0	5,6	3,9	5,6	4,0	5,6	4,1	5,6	4,4
10	4,1	5,9	4,5	5,8	4,0	5,5	4,3	5,9	4,2	5,9	4,4	5,9	4,6	6,2	4,4	6,2	4,5	6,2	4,6	6,2	4,9

Table 11.9-3 Model 4666: Motion Fields

Model 4666																	
V [m/s]	C_V	Test n.1		Test n.6		Test n.7		Test n.10		Test n.14		Test n.15		Test n.16		Test n.17	
		F_d	Fn	F_d	Fn	F_d	Fn	F_d	Fn	F_d	Fn	F_d	Fn	F_d	Fn	F_d	Fn
1	0,6	0,5	0,3	0,5	0,2	0,5	0,3	0,5	0,3	0,6	0,3	0,6	0,3	0,6	0,3	0,6	0,3
2	1,2	1,1	0,5	1,0	0,5	1,0	0,5	1,1	0,5	1,1	0,5	1,1	0,5	1,1	0,5	1,1	0,6
3	1,8	1,6	0,8	1,5	0,7	1,5	0,8	1,6	0,7	1,7	0,8	1,7	0,8	1,7	0,8	1,7	0,9
4	2,3	2,1	1,1	2,0	1,0	2,0	1,1	2,1	1,0	2,2	1,1	2,2	1,1	2,2	1,2	2,2	1,3
5	2,9	2,7	1,5	2,5	1,4	2,5	1,5	2,7	1,4	2,8	1,4	2,8	1,5	2,8	1,5	2,8	1,7
6	3,5	3,2	1,9	3,0	1,7	3,0	1,8	3,2	1,7	3,4	1,7	3,4	1,8	3,5	1,9	3,4	2,0
7	4,1	3,7	2,2	3,5	2,0	3,5	2,2	3,7	2,0	3,9	2,1	3,9	2,1	3,9	2,3	3,9	2,4
8	4,7	4,3	2,6	4,0	2,4	4,0	2,5	4,3	2,3	4,5	2,4	4,5	2,5	4,5	2,6	4,5	2,8
9	5,3	4,8	2,9	4,5	2,7	4,4	2,8	4,8	2,7	5,0	2,8	5,0	2,9	5,0	3,0	5,0	3,2
10	5,8	5,3	3,2	5,1	3,0	5,0	3,2	5,3	3,0	5,6	3,1	5,6	3,2	5,6	3,4		

Table 11.9-4 Model 4667-1: Motion Fields

Model 4667-1																					
V [m/s]	C_V	Test n.1		Test n.7		Test n.8		Test n.10		Test n.11		Test n.12		Test n.13		Test n.14		Test n.15		Test n.16		Test n.17	
		F_d	Fn	F_d	Fn	F_d	Fn	F_d	Fn	F_d	Fn	F_d	Fn	F_d	Fn	F_d	Fn	F_d	Fn	F_d	Fn	F_d	Fn
1	0,6	0,5	0,2	0,5	0,2	0,5	0,2	0,5	0,2	0,5	0,2	0,5	0,2	0,5	0,2	0,5	0,2	0,5	0,2	0,5	0,2	0,5	0,2
2	1,2	1,0	0,4	0,9	0,4	0,9	0,4	1,0	0,4	1,0	0,4	1,0	0,4	1,0	0,4	1,0	0,4	1,0	0,5	1,0	0,5	1,0	0,4
3	1,8	1,5	0,7	1,4	0,6	1,4	0,7	1,5	0,6	1,5	0,6	1,5	0,7	1,5	0,7	1,6	0,7	1,6	0,6	1,6	0,6	1,6	0,7
4	2,3	2,0	0,9	1,9	0,9	1,9	0,9	2,0	0,9	2,0	0,9	2,0	0,9	2,0	1,0	2,1	0,8	2,1	0,8	2,1	0,9	2,1	1,0
5	2,9	2,5	1,2	2,3	1,2	2,3	1,3	2,5	1,1	2,5	1,2	2,5	1,3	2,5	1,3	2,6	1,1	2,6	1,1	2,6	1,2	2,6	1,3
6	3,5	3,0	1,5	2,8	1,5	2,8	1,6	3,0	1,4	3,0	1,5	3,0	1,6	3,0	1,6	3,1	1,3	3,1	1,4	3,1	1,5	3,1	1,6
7	4,1	3,5	1,8	3,3	1,8	3,3	1,9	3,5	1,7	3,5	1,8	3,5	1,9	3,5	2,0	3,7	1,5	3,7	1,7	3,7	1,8	3,6	1,9
8	4,7	4,0	2,1	3,7	2,1	3,8	2,2	4,0	2,0	4,0	2,0	4,0	2,2	4,0	2,3	4,2	1,8	4,2	1,9	4,2	2,1	4,2	2,3
9	5,3	4,6	2,4	4,2	2,4	4,2	2,5	4,5	2,2	4,5	2,3	4,5	2,5	4,5	2,6	4,7	2,0	4,7	2,2	4,7	2,3	4,7	2,6
10	5,8	5,0	2,7	4,7	2,6	4,7	2,8	5,0	2,5	5,0	2,6	5,0	2,8	5,0	3,0	5,2	2,3	5,2	2,4	5,2	2,6	5,2	2,9

Table 11.9-5 Model 4668: Motion Fields

Model 4668																			
V [m/s]	C_V	Test n.1		Test n.7		Test n.8		Test n.9		Test n.10		Test n.11		Test n.12		Test n.13		Test n.14	
		F_d	Fn	F_d	Fn	F_d	Fn	F_d	Fn	F_d	Fn	F_d	Fn	F_d	Fn	F_d	Fn	F_d	Fn
1	0,6	0,5	0,2	0,5	0,2	0,5	0,2	0,5	0,2	0,5	0,2	0,5	0,2	0,5	0,2	0,5	0,2	0,6	0,2
2	1,2	1,1	0,4	1,0	0,4	1,0	0,4	1,0	0,4	1,1	0,4	1,1	0,4	1,1	0,4	1,1	0,4	1,1	0,5
3	1,8	1,6	0,6	1,5	0,6	1,5	0,6	1,5	0,7	1,6	0,6	1,6	0,6	1,6	0,7	1,6	0,7	1,7	0,6
4	2,3	2,1	0,9	2,0	0,9	2,0	0,9	2,0	1,0	2,1	0,9	2,1	0,9	2,1	0,9	2,1	0,9	2,2	0,9
5	2,9	2,7	1,1	2,5	1,1	2,5	1,2	2,5	1,3	2,7	1,1	2,7	1,1	2,7	1,2	2,7	1,3	2,8	1,1
6	3,5	3,2	1,4	3,0	1,4	3,0	1,5	3,0	1,7	3,2	1,3	3,2	1,4	3,2	1,5	3,2	1,6	3,4	1,4
7	4,1	3,8	1,8	3,5	1,7	3,5	1,8	3,5	2,0	3,8	1,6	3,8	1,7	3,8	1,9	3,8	2,0	3,9	1,6
8	4,7	4,3	2,1	4,0	2,1	4,0	2,2	4,0	2,3	4,3	1,9	4,3	2,0	4,3	2,2	4,3	2,3	4,5	2,0
9	5,3	4,8	2,4	4,5	2,4	4,5	2,5	4,6	2,7	4,8	2,2	4,8	2,3	4,8	2,5	4,8	2,6	5,1	2,2
10	5,8	5,4	2,7	5,1	2,6	5,1	2,8	5,1	3,0	5,4	2,6	5,4	2,6	5,4	2,8	5,4	2,9	5,6	2,5

Table 11.9-6 Model 4669: Motion Fields

Model 4669																					
V [m/s]	C_V	Test n.1		Test n.7		Test n.8		Test n.9		Test n.10		Test n.11		Test n.12		Test n.13		Test n.14		Test n.15	
		F_d	Fn	F_d	Fn	F_d	Fn	F_d	Fn	F_d	Fn	F_d	Fn	F_d	Fn	F_d	Fn	F_d	Fn	F_d	Fn
1	0,6	0,6	0,2	0,5	0,2	0,5	0,2	0,5	0,2	0,6	0,2	0,6	0,2	0,6	0,2	0,6	0,2	0,6	0,2	0,6	0,2
2	1,2	1,1	0,4	1,1	0,4	1,1	0,4	1,1	0,4	1,1	0,4	1,1	0,4	1,1	0,4	1,1	0,4	1,2	0,4	1,2	0,4
3	1,8	1,7	0,6	1,6	0,6	1,6	0,6	1,6	0,7	1,7	0,6	1,7	0,6	1,7	0,6	1,7	0,7	1,8	0,6	1,8	0,6
4	2,3	2,3	0,8	2,1	0,8	2,1	0,9	2,1	0,9	2,3	0,8	2,3	0,8	2,3	0,9	2,3	0,9	2,4	0,8	2,4	0,8
5	2,9	2,9	1,1	2,7	1,0	2,7	1,1	2,7	1,2	2,8	1,0	2,8	1,1	2,8	1,1	2,8	1,2	3,0	1,0	3,0	1,1
6	3,5	3,4	1,4	3,2	1,3	3,2	1,4	3,2	1,6	3,4	1,3	3,4	1,3	3,4	1,4	3,4	1,6	3,6	1,3	3,6	1,3
7	4,1	4,0	1,7	3,7	1,7	3,7	1,7	3,7	1,9	4,0	1,6	4,0	1,6	4,0	1,8	4,0	1,9	4,2	1,5	4,2	1,6
8	4,7	4,4	2,0	4,3	2,0	4,3	2,1	4,3	2,2	4,6	1,8	4,6	1,9	4,6	2,1	4,6	2,2	4,8	1,8	4,8	1,9
9	5,3	4,1	2,3	4,8	2,3	4,8	2,3	4,8	2,6	5,1	2,1	5,1	2,3	5,1	2,4	5,1	2,6	5,4	2,1	5,4	2,3
10	5,8	5,1	2,6	5,3	2,5	5,3	2,7	5,3	2,9	5,7	2,4	5,7	2,6	5,7	2,7	5,7	2,9	6,0	2,4	6,0	2,6

It is easy to show that there is an high uncertain degree on the motion field nature achieved per each value of hull speed.

In the writer opinion, this uncertain is not acceptable: further researches on the matter should be developed in order to define univocally what motion field is on.

11.10 Conclusion

Analytical Semi-Empirical Method (ASEM) has been applied to models of the Systematic Series 62. Further, Savitsky‘s method has been applied too, in order to get an overall comparison.

On 85 test cases developed, only 48 tests have been taken in account in order to get a comparison among data related to planing condition.

Data comparison has been developed with reference to Resistance and Power trends related to hull speed. ASEM and Savitsky’s results without physical meaning have not been taken in account meanwhile results with physical meaning and relate to data out of range have been reported.

There is a common trends of ASEM results versus Savitsky’s LF results: higher hull speed closer results. This is due to the geometry of the models tested: the afterward part of the hull has a constant deadrise angle and, in planing condition, this is the only part interested by the pressure distribution. Thereby, in planing condition, models of Series 62 work as monohedral hull form does.

Further, analysis of data comparison have been developed computing dimensionless variation of both resistance and power versus hull speed.

These dimensionless data give us the measurement of ASEM reliability and efficiency.

In the most of case, the max dimensionless variation has a value less than 20%, within the overall range of hull speed. The few test cases with dimensionless variations higher than 20% are related to both positive value of α_0, and value of $\left(1-\frac{L_{CG}}{L_P}\right)$ higher than 6 percent.

Thereby ASEM reliability and efficiency results are related to the longitudinal position of Center of Gravity: higher the forward longitudinal position of Center of Gravity (versus the Center of Buoyancy as well as the centroid of A_P), higher the error on results related to.

Accordingly to the above remarks, ASEM results, as well as Savitsky's ones, are in good agreement with tests results.

11.11 Symbols

A_P	Projected planing bottom area, excluding area of external spray strips	$[m^2]$
B_C	Beam between chines	$[m]$
B_{PX}	Maximum breadth over chines, excluding external spray strips	$[m]$
C_V	Froude number related to the beam	
Fn	Froude number related to the mean wetted length	
Fn_∇	Froude number based on volume displaced	
g	Gravity Acceleration	$g = 9.81 m/s^2$
L_{CG}	Longitudinal center of gravity location	$[m]$
LF	Long Form	
L_{OA}	Length over all	$[m]$
L_P	Projected chine length	$[m]$
L_W	Mean wetted length	$[m]$
P_E	Effective Power of bare hull	$[W]$
R_H	Bare hull resistance	$[N]$
V	Hull speed	$[m/s]$
W	Hull weight	$[N]$
$\{x, y, z\}$	Geometrical coordinates	
α_0	Angle of attack of after portion of planing bottom	$[\text{deg}]$
ΔP_E	Power dimensionless variation	
ΔR_H	Resistance dimensionless variation	
γ	Unit weight of water	$[N/m^3]$
∇	Volume of displacement at rest	$[m^3]$

11.12 References

Bertorello, C. & Oliviero, L. 2007. Hydrodynamic Resistance Assessment of Non-Monohedral Planing Hull Forms based on Savitsky's Method. *Australian Journal of Mechanical Engineering,* Vol. 4 No.2, pp 209-224. Engineers Media, CROWS NEST, Australia. (ACN001311511).

Clement, E.P. & Blount, D.L. 1963. Resistance Tests of a Systematic Series of Planing Hull Forms. *Transactions SNAME,* pages 491-579. Jersey City (USA): SNAME

Savitsky, D. 1964. Hydrodynamic Design of Planing Hull. *Marine Technology*, Vol.1, No.1, Jersey City (USA): SNAME

APPENDIX H

COMPARISON RESULTS:

ASEM VS BK SERIES

12.1 Table of Contents

12.2 Figure Index

12.3 Table Index

12.4 Introduction

Analytical Semi-Empirical Method (ASEM) has been developed in order to predict Resistance and Power performance versus hull speed related to a warped bare monohull. [Bertorello & Oliviero 2007]

BK Series hull forms represent a first attempt to highlight the influence of some hull form geometry variations on resistance. Among these, hull form with longitudinal variation of the deadrise angle has been tested. This hull form has been recorded as Model BK-1.

Despite nowadays BK Series hull forms are not used and test results are not available in the original form anymore, some data are released in literature yet [Radojcic 1985], and the most of them data are related to the Model BK-1.

In this chapter ASEM will be applied to the model BK-1 of the BK Series, in order to check reliability and efficiency.

Further, Savitsky‘s method [Savitsky 1964] as well as Egorov’s method [Voitkounski 1985] will be applied too, in order to get an overall comparison.

12.5 Models: Geometry and Tests

[Voitkounski 1985]

Series BK is composed by nine hull models with the same dimensions and different shapes.

Model BK-1 has a single chine per side: a sharp edge chine at each intersection of the bottom and side; this single chine is developed throughout the length of the hull itself.

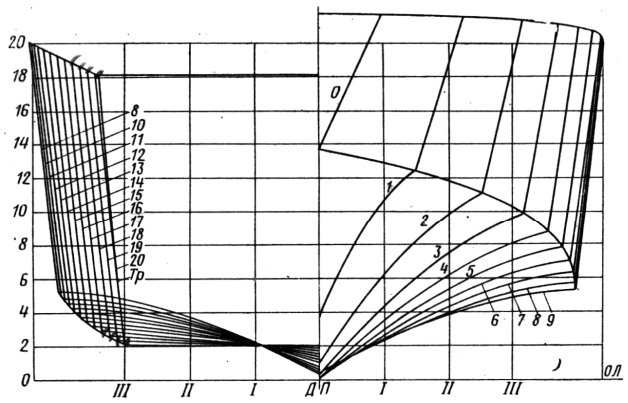

Рис. II.7а. Корпус модели БК-1.

Figure 12.5-1 Transversal sections of Model BK-1 [Voitkounski 1985]

Model BK-2 has the same shape of model BK-1: the distinctive feature of the model BK-2 is the rounding to the keel.

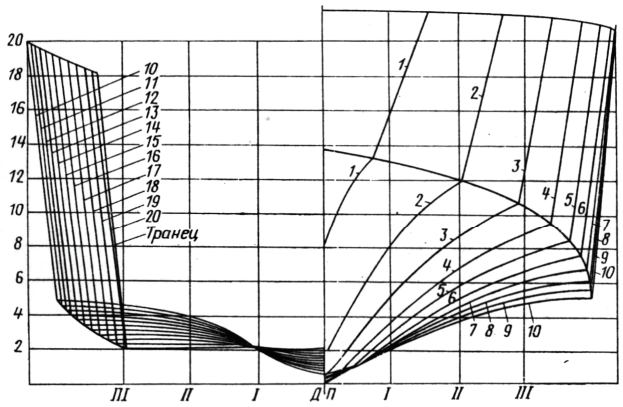

Рис. II.7б. Корпус модели БК-2.

Figure 12.5-2 Transversal sections of Model BK-2

[Voitkounski 1985]

In the model BK-3 the hull shape between the transom and the 5th section is the same of BK-1, meanwhile sections foreword the 5th section (bow direction) are "rounded" on the template.

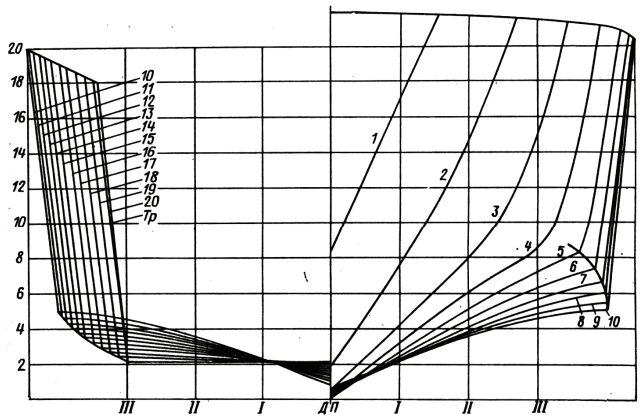

Рис. II.7в. Корпус модели БК-3.

Figure 12.5-3 Transversal sections of Model BK-3
[Voitkounski 1985]

Model BK-4 is derived from the model BK-1 by the introduction of a step in the central trunk of the hull: the transverse height of the step is constant.

Model BK-5 is a mixed hull: there are two single chines (one per each side), present from the transom to the 5th section, then softening towards the bow. This model has been developed in order to operate in semi-displacement field.

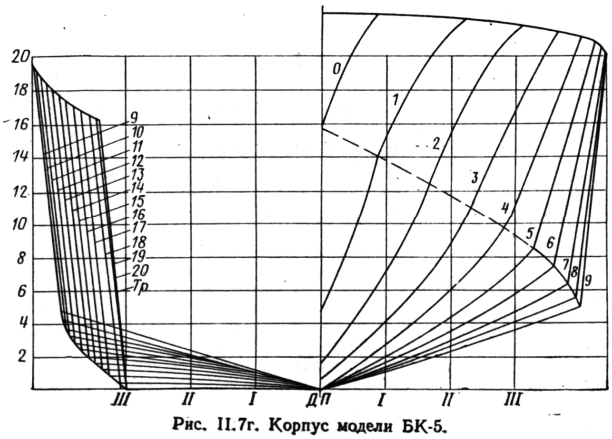

Рис. II.7г. Корпус модели БК-5.

Figure 12.5-4 Transversal sections of Model BK-5
[Voitkounski 1985]

Model BK-6 has a step in the central part of the hull and an high deadrise angle value along the hull.

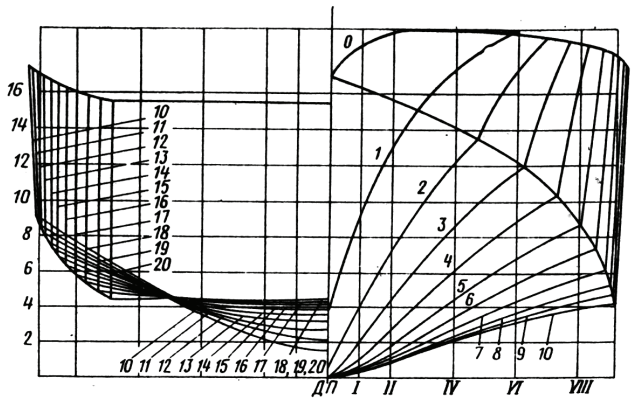

Рис. II.7д. Корпус модели БК-6.

Figure 12.5-5 Transversal sections of Model BK-6 [Voitkounski 1985]

Model BK-7 has monohedral shape in the aft part of the hull, meanwhile model BK-8 has edges like “Cissoid”.

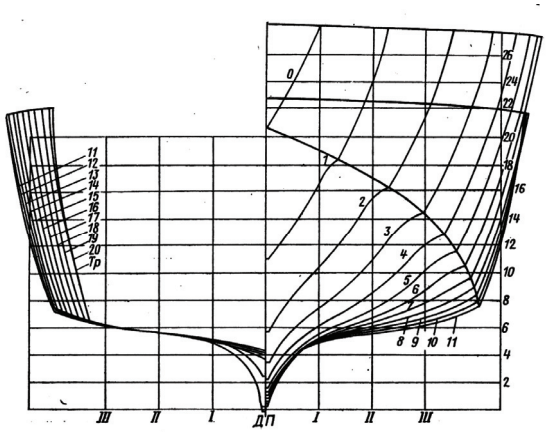

Рис. II.7е. Корпус модели БК-7.

Figure 12.5-6 Transversal sections of Model BK-7 [Voitkounski 1985]

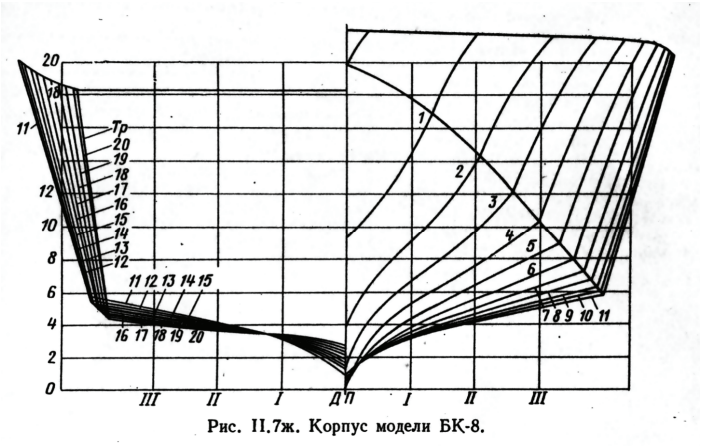

Рис. II.7ж. Корпус модели БК-8.

Figure 12.5-7 Transversal sections of Model BK-8 [Voitkounski 1985]

Model BK-9 is characterized by a line break that is located above the knee

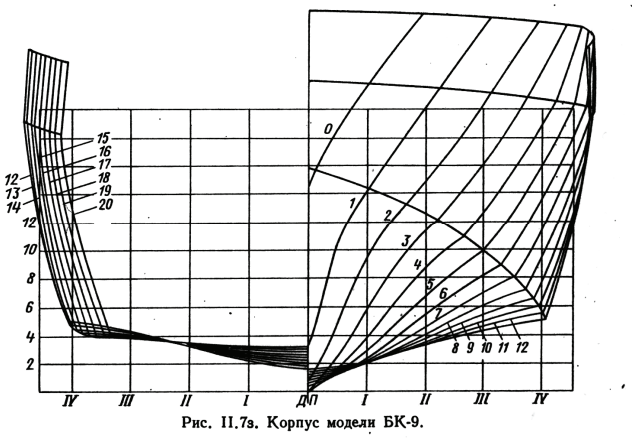

Рис. II.7з. Корпус модели БК-9.

Figure 12.5-8 Transversal sections of Model BK-9 [Voitkounski 1985]

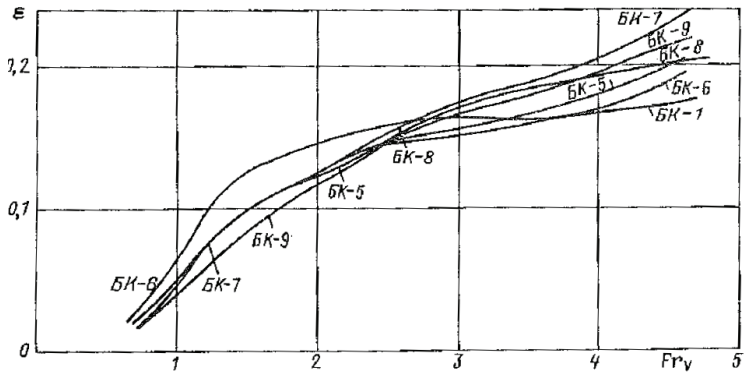

Figure 12.5-9 Dimensionless resistances ε versus volumetric Froude number Fn_{∇} [134]

[134] In the Russian symbols, the volumetric Froude number is reported as Fr_V.

[Voitkounski 1985]

For $Fn_{\nabla} \leq 2.2$ test results related to models BK-1 to BK-4 are quite similar and models BK-7 to BK-9 present the lower resistance value.

For $Fn_{\nabla} \geq 2.7$ performance of models BK-7 to BK-9 drops down meanwhile model BK-1 presents the best performance.

Results, hereafter reported, are related to Model BK-1, which is:

- the Vee-bottom transverse sections with the deadrise increasing towards the bow (not monohedral),
- the sharp edge chines at the intersection of the bottom and sides,
- the wide transom with a sharp trailing edge,
- the straight horizontal buttock lines at the aft end,
- the water entry lines fine with narrow angle at the bow.

Dimensionless coordinates of model BK-1 are hereafter reported:

Table 12.5-1 Model BK-1: dimensionless coordinates

	STATION	x	y	z	STATION	x	y	z	STATION	x	y	z	
		[-]	[-]	[-]		[-]	[-]	[-]		[-]	[-]	[-]	
stern	0	0,000	0,0000	0,0783	8	0,381	0,0000	0,0304	15	0,714	0,0000	0,0000	
			0,6893	0,0799			0,8835	0,1629			0,8859	0,2668	
	1	0,048	0,0000	0,0735	9	0,429	0,0000	0,0256	16	0,762	0,0000	0,0000	
			0,7160	0,0895			0,8932	0,1741			0,8568	0,3003	
	2	0,095	0,0000	0,0687	10	0,476	0,0000	0,0208	17	0,810	0,0000	0,0000	
			0,7451	0,0990			0,9029	0,1837			0,8083	0,3355	
	3	0,143	0,0000	0,0607	11	0,524	0,0000	0,0144	18	0,857	0,0000	0,0000	
			0,7718	0,1086			0,9248	0,1997			0,7184	0,3802	
	4	0,190	0,0000	0,0543	12	0,571	0,0000	0,0144	19	0,905	0,0000	0,0000	
			0,7961	0,1198			0,9053	0,2045			0,5704	0,4233	
	5	0,238	0,0000	0,0543	13	0,619	0,0000	0,0144	20	0,952	0,0000	0,0000	
			0,8228	0,1310			0,9005	0,2188			0,3350	0,4744	
	6	0,286	0,0000	0,0463	14	0,667	0,0000	0,0000	21	1,000	0,0000	0,0000	bow
			0,8495	0,1438			0,8981	0,2428			0,0000	0,5224	
	7	0,333	0,0000	0,0399									
			0,8665	0,1534									

All diagrams available are in terms of dimensionless sizes

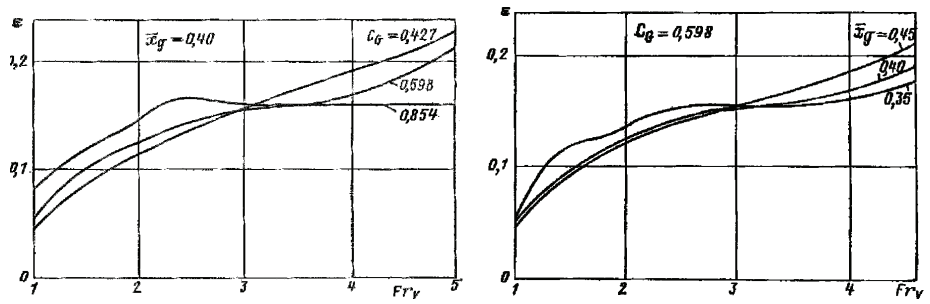

[a] **[b]**

Figure 12.5-10 Dimensionless resistance trends (continue)

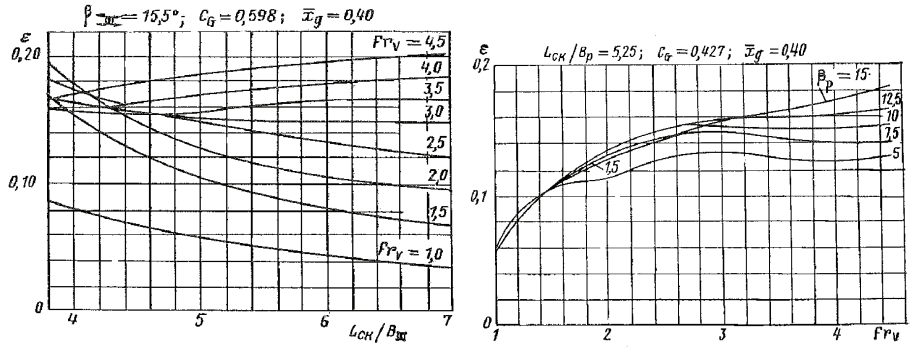

[c] **[d]**

Figure 12.5-10 Dimensionless resistance trends(135)
[Voitkounski 1985]

and in detail:

- the speed, in term of Fn_{∇}, is about 1.0 up to 4.5;
- λ values are about 4.00 up to 7.00;
- $\bar{x}_g$ values are about 0.35 up to 0.45;
- C_{Δ} values are about 0.427 up to 0.854.

by which 12 cases of study have been defined and analyzed, and below reported:

Table 12.5-2 Model BK-1: cases of study

	Cases											
	1	**2**	**3**	**4**	**5**	**6**	**7**	**8**	**9**	**10**	**11**	**12**
λ	4,00	4,50	5,00	5,25	5,50	6,00	6,50	7,00	5,25	5,25	5,25	5,25
C_{Δ}	0,598	0,598	0,598	0,598	0,598	0,598	0,598	0,598	0,427	0,854	0,598	0,598
$\bar{x}_g$	0,40	0,40	0,40	0,40	0,40	0,40	0,40	0,40	0,40	0,40	0,45	0,35

In order to apply the Egorov, Savitsky as well as ASEM method, hull characteristics have been defined imposing a value of 25 meter to the length between the perpendicular, as defined in a benchmark application of Egorov's method [Voitkounski 1985].

This choice have been driven to the following hull characteristics:

---

(135) Russian Symbols:
β deadrise angle in amidships section,
B beam between chines in amidships section,
B_p beam between chines,
C_G weight coefficient $(C_G \equiv C_{\Delta})$,
L_{ck} chines length,
$\bar{x}_g$ longitudinal position of CG to length between perpendicular ratio.

Table 12.5-3 Model BK-1: hull characteristics related to the cases of study

Case	W	B_C	L_{CG}
	[N]	[m]	[m]
1	1441419	6,25	10,00
2	1012355	5,56	10,00
3	738007	5,00	10,00
4	637518	4,76	10,00
5	554475	4,55	10,00
6	427087	4,17	10,00
7	335916	3,85	10,00
8	268953	3,57	10,00
9	455218	4,76	10,00
10	910435	4,76	10,00
11	637518	4,76	11,25
12	637518	4,76	8,75

12.6 Data Comparison

Data comparison has been developed with reference to resistance and power trends related to hull speed. Power data have been computed by values of hull speed and pertinent resistance, reported in literature.

The most of data available in literature are reported in dimensionless form, and in detail: volumetric Froude number instead of hull speed, ratio ε instead of bare hull resistance R_H and ratio μ for the effective power P_E:

$$\varepsilon = \frac{R_H}{\Delta} \qquad \textbf{(G. 8)}$$

$$\mu = \frac{P_E}{\Delta \cdot V} \qquad \textbf{(G. 9)}$$

It is important to highlight that functions $R_H = R_H(V)$ and $\varepsilon = \varepsilon(Fr_V)$ have the same trend, while this is not true for the functions $P_E = P_E(V)$ and $\mu = \mu(Fr_V)$. As matter of fact the ratio R_H/ε, equal to Δ, is constant with the speed V, meanwhile the ratio P_E/μ, equal to $(\Delta \cdot V)$, is linear depending on V.

In order to get a comparison not related to the dimensional choice of the hull length, all results computed have been replaced with their relative dimensionless sizes.

Hereinafter ASEM and Savitsky's results without physical meaning have not been taken in account (i.e.: results related to a mean wetted length higher than hull length overall), meanwhile results with physical meaning coupled with data out of range have been reported with dash line (i.e.: results pertinent to a mean wetted length/beam ratio higher than four times).

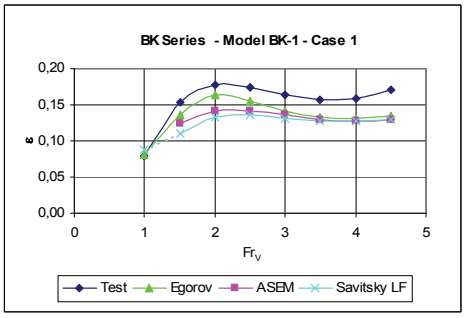

[a]

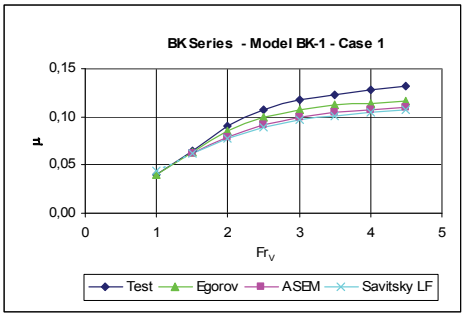

[b]

Figure 12.6-1 Data Comparison: Model BK-1 - Case 1

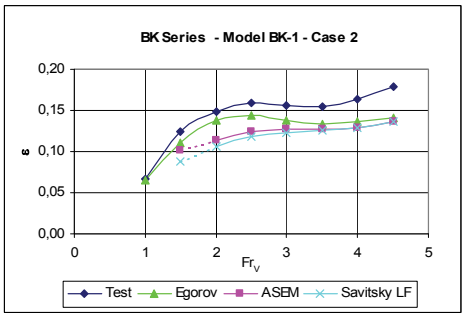

[a]

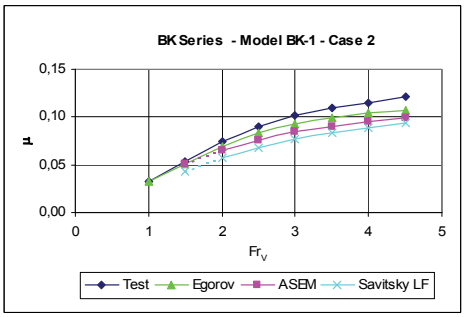

[b]

Figure 12.6-2 Data Comparison: Model BK-1 - Case 2

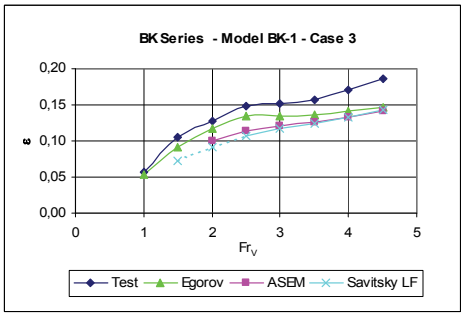

[a]

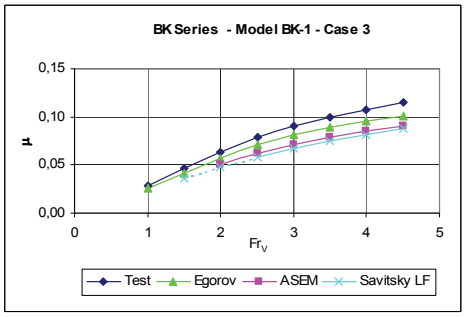

[b]

Figure 12.6-3 Data Comparison: Model BK-1 - Case 3

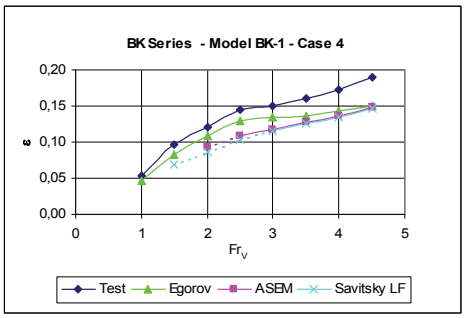

[a]

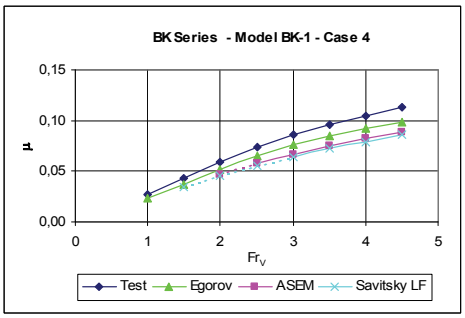

[b]

Figure 12.6-4 Data Comparison: Model BK-1 - Case 4

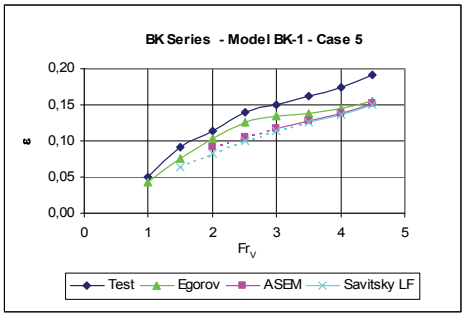

[a]

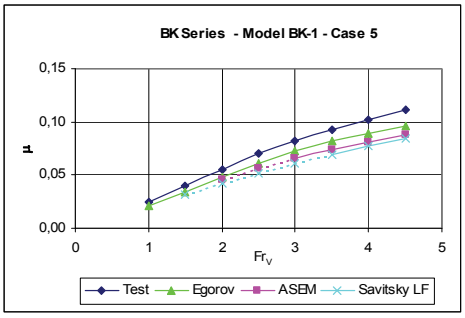

[b]

Figure 12.6-5 Data Comparison: Model BK-1 - Case 5

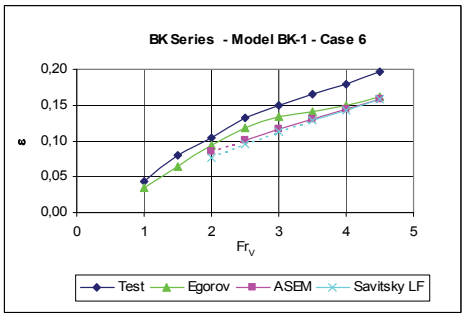

[a]

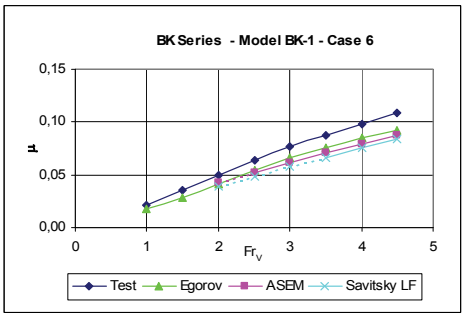

[b]

Figure 12.6-6 Data Comparison: Model BK-1 - Case 6

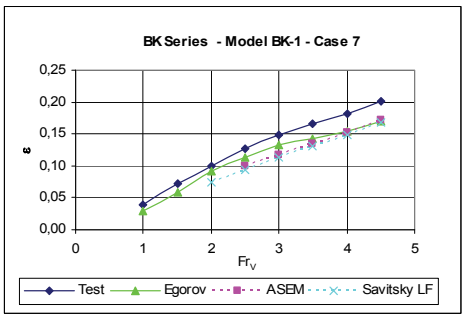

[a]

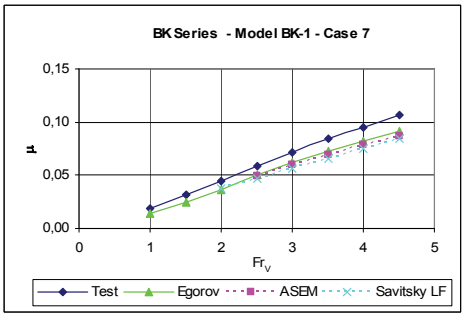

[b]

Figure 12.6-7 Data Comparison: Model BK-1 - Case 7

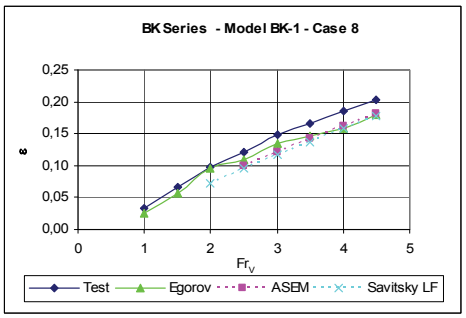

[a]

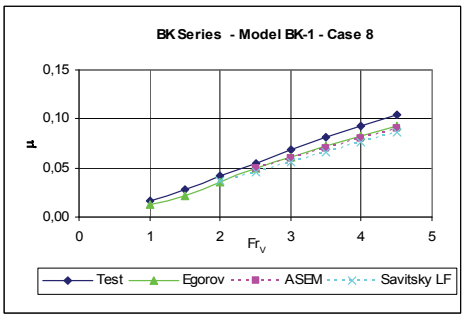

[b]

Figure 12.6-8 Data Comparison: Model BK-1 - Case 8

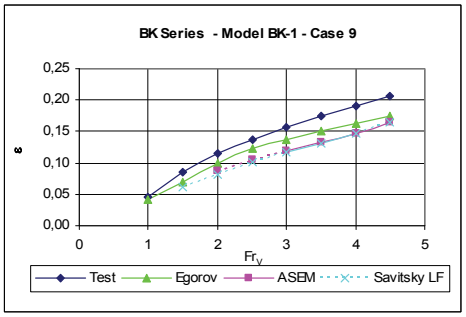

[a]

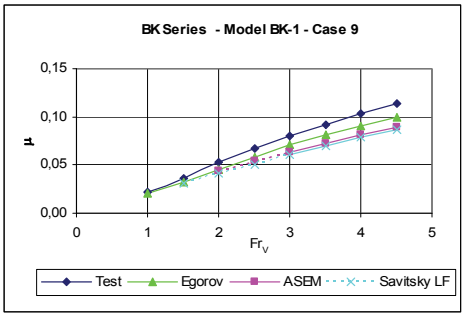

[b]

Figure 12.6-9 Data Comparison: Model BK-1 - Case 9

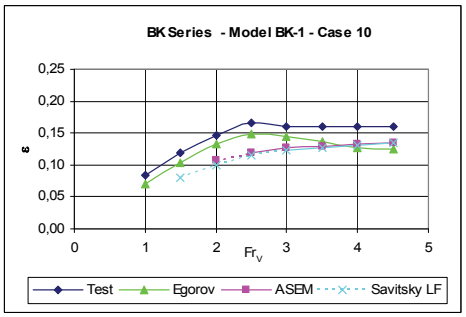

[a]

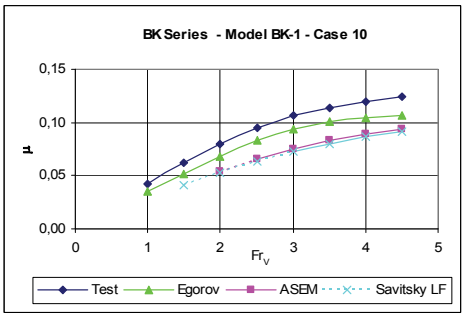

[b]

Figure 12.6-10 Data Comparison: Model BK-1 - Case 10

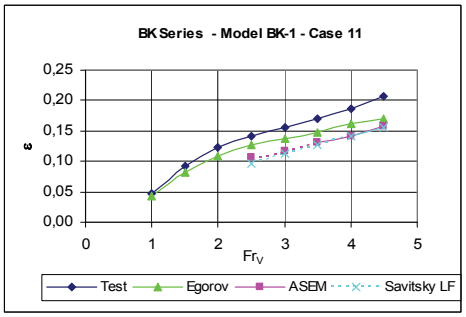

[a]

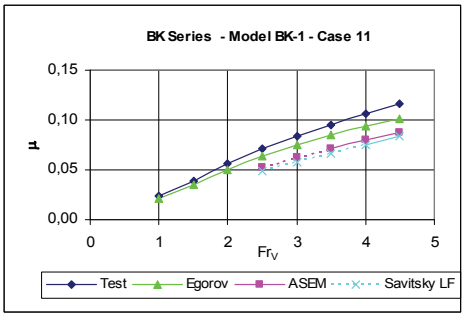

[b]

Figure 12.6-11 Data Comparison: Model BK-1 - Case 11

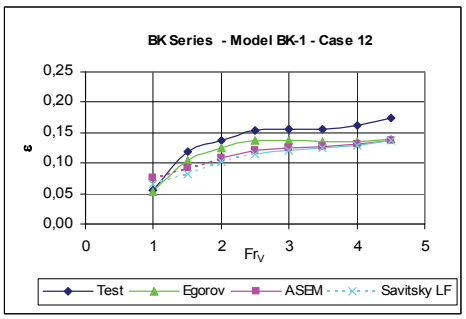

[a]

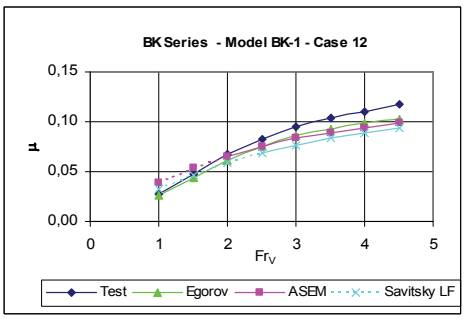

[b]

Figure 12.6-12 Data Comparison: Model BK-1 - Case 12

12.7 Data Comparison Analysis

Analysis of data comparison have been developed computing dimensionless variation of resistance and power versus hull speed.

In detail, these dimensionless variation[136] have been computed adopting Test results as benchmark, as following:

$$\Delta\varepsilon = \Delta R_H = \frac{R_{H,\mathrm{Predicted}} - R_{H,BK-1}}{R_{H,BK-1}} \qquad \textbf{(G. 10)}$$

and

$$\Delta\mu = \Delta P_E = \frac{P_{E,\mathrm{Predicted}} - P_{E,BK-1}}{P_{E,BK-1}} \qquad \textbf{(G. 11)}$$

where *Predicted* stands for Egorov, ASEM as well as Savitsky's LF results.

These dimensionless data give us the measurement of reliability and efficiency of prediction methods used.

Comparison of results, reported in up listed diagrams with dash line, have been hereinafter reported with dash line too.

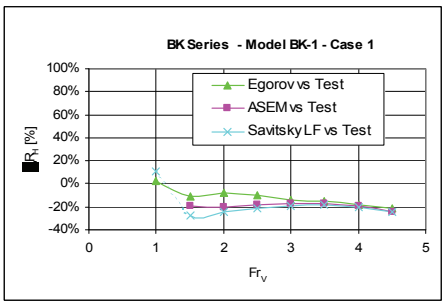

[a]

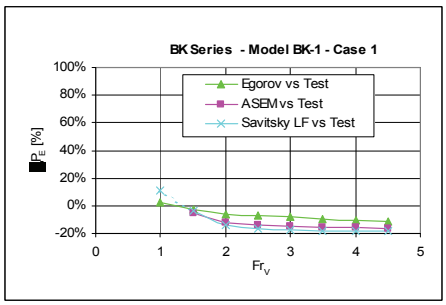

[b]

Figure 12.7-1 Data Comparison Analysis: Model BK-1 - Case 1

([136]) These dimensionless ratios are not affected by the choice of dimensional sizes instead of dimensionless ones; as matter of fact:

$$\Delta\varepsilon = \frac{\varepsilon_{\mathrm{Predicted}} - \varepsilon_{BK-1}}{\varepsilon_{BK-1}} = \frac{\frac{R_{H,\mathrm{Predicted}}}{\Delta} - \frac{R_{H,BK-1}}{\Delta}}{\frac{R_{H,BK-1}}{\Delta}} = \frac{R_{H,\mathrm{Predicted}} - R_{H,BK-1}}{R_{H,BK-1}} = \Delta R_H \quad \Delta\mu = \frac{\mu_{\mathrm{Predicted}} - \mu_{BK-1}}{\mu_{BK-1}} = \frac{\frac{P_{E,\mathrm{Predicted}}}{\Delta\cdot V} - \frac{P_{E,BK-1}}{\Delta\cdot V}}{\frac{P_{E,BK-1}}{\Delta\cdot V}} = \frac{P_{E,\mathrm{Predicted}} - P_{E,BK-1}}{P_{E,BK-1}} = \Delta P_E$$

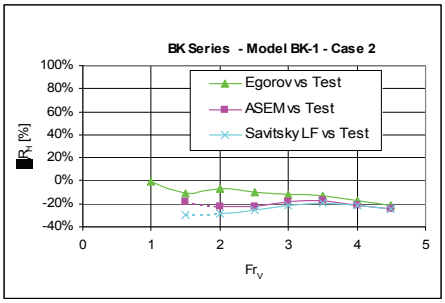

[a]

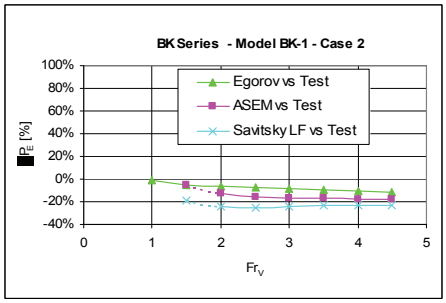

[b]

Figure 12.7-2 Data Comparison Analysis: Model BK-1 - Case 2

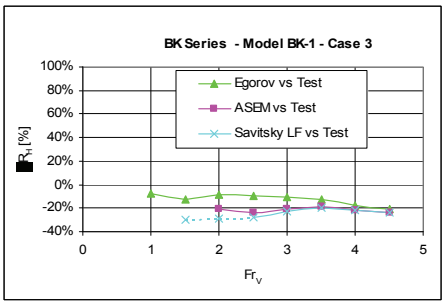

[a]

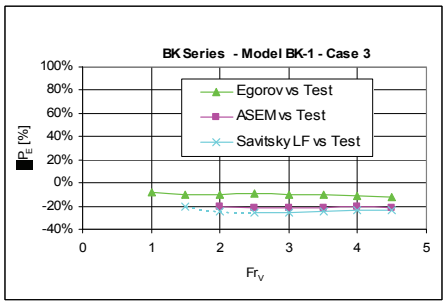

[b]

Figure 12.7-3 Data Comparison Analysis: Model BK-1 - Case 3

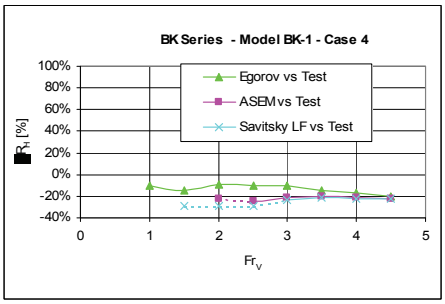

[a]

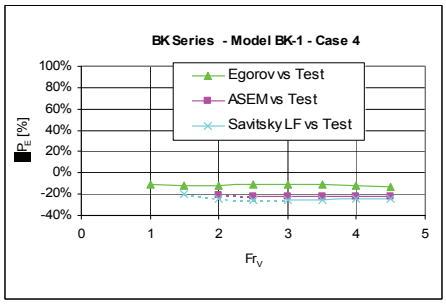

[b]

Figure 12.7-4 Data Comparison Analysis: Model BK-1 - Case 4

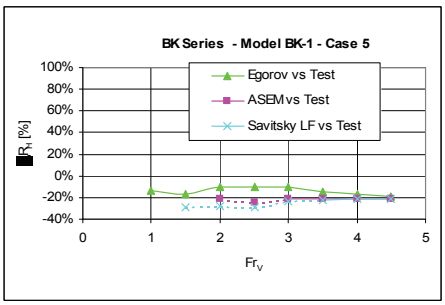

[a]

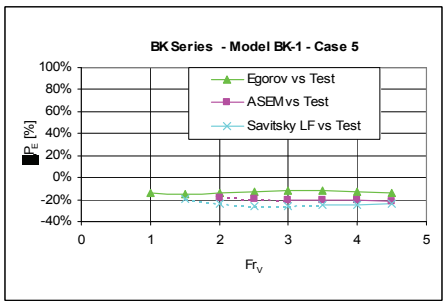

[b]

Figure 12.7-5 Data Comparison Analysis: Model BK-1 - Case 5

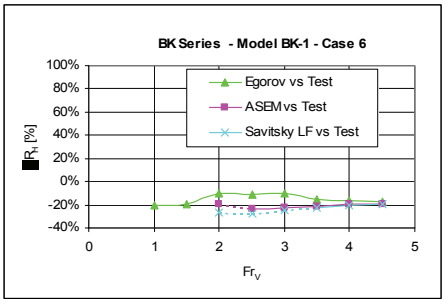

[a]

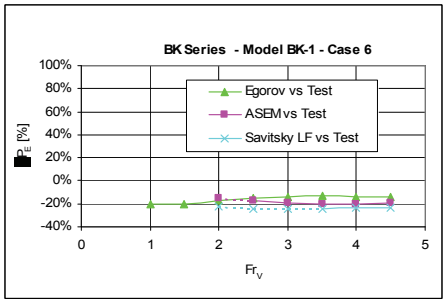

[b]

Figure 12.7-6 Data Comparison Analysis: Model BK-1 - Case 6

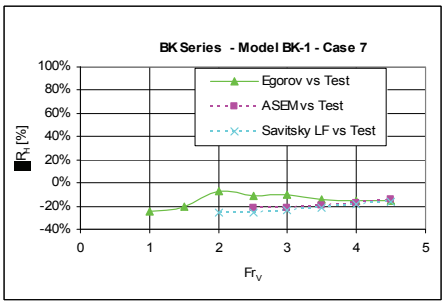

[a]

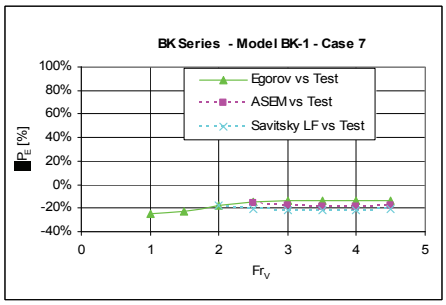

[b]

Figure 12.7-7 Data Comparison Analysis: Model BK-1 - Case 7

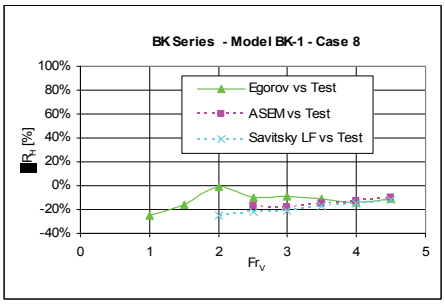

[a]

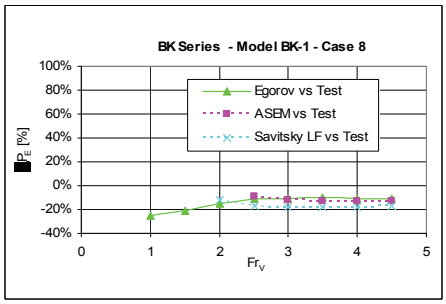

[b]

Figure 12.7-8 Data Comparison Analysis: Model BK-1 - Case 8

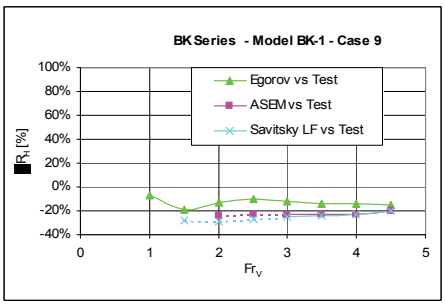

[a]

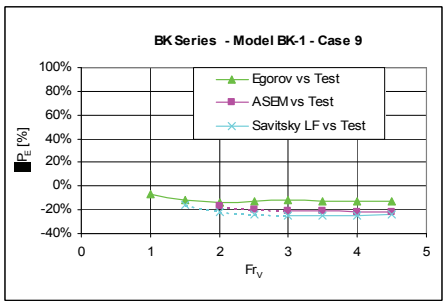

[b]

Figure 12.7-9 Data Comparison Analysis: Model BK-1 - Case 9

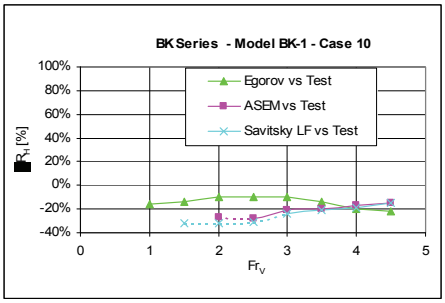

[a]

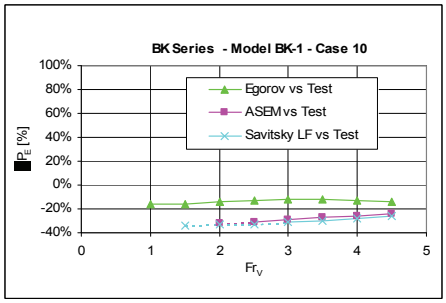

[b]

Figure 12.7-10 Data Comparison Analysis: Model BK-1 - Case 10

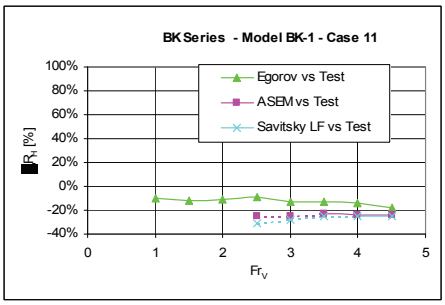

[a]

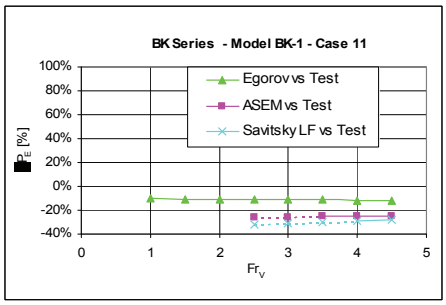

[b]

Figure 12.7-11 Data Comparison Analysis: Model BK-1 - Case 11

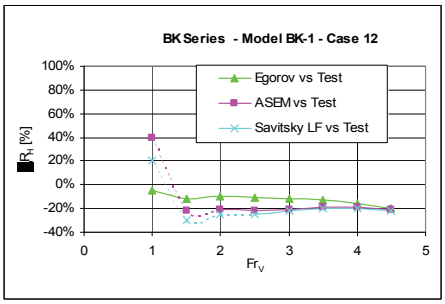

[a]

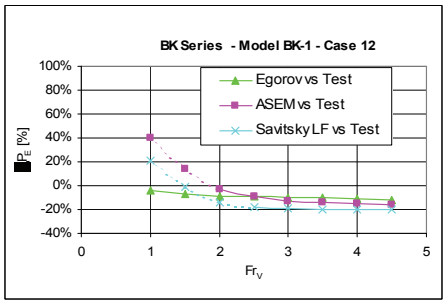

[b]

Figure 12.7-12 Data Comparison Analysis: Model BK-1 - Case 12

In the most of cases, all prediction methods present the max dimensionless variation within the range $[-40\%;0\%]$; further, for ASEM method, the magnitude of dimensionless variations is close to -20% for $Fn_V \geq 2$.

12.8 Data Analysis and Remarks

Egorov's method presents the best results, and this is due to its nature: a regression method which coefficients have been computed by statistical results analysis related to BK as well as MBK Series.

Table 12.8-1 Egorov'method: dimensionless resistance trends

Egorov										
ΔR_H	Fn^d									
Cases	1,5	2	2,5	3	3,5	4	4,5		mean	sd
1	-11%	-8%	-10%	-14%	-15%	-18%	-21%		-14%	0,05
2	-11%	-7%	-10%	-12%	-13%	-17%	-22%		-13%	0,05
3		-8%	-10%	-11%	-13%	-17%	-21%		-13%	0,05
4		-9%	-10%	-10%	-14%	-17%	-20%		-14%	0,04
5		-10%	-11%	-10%	-15%	-17%	-20%		-14%	0,04
6		-10%	-11%	-11%	-15%	-16%	-18%		-13%	0,03
7			-11%	-10%	-14%	-16%	-15%		-13%	0,02
8			-10%	-9%	-11%	-14%	-11%		-11%	0,02
9		-13%	-10%	-12%	-14%	-14%	-15%		-13%	0,02
10		-9%	-10%	-10%	-14%	-20%	-22%		-14%	0,06
11			-9%	-13%	-13%	-14%	-18%		-13%	0,03
12	-12%	-9%	-11%	-12%	-13%	-16%	-20%		-13%	0,04
mean	-11%	-9%	-10%	-11%	-14%	-16%	-19%		-13%	
sd	-	0,02	0,01	0,01	0,01	0,02	0,03			0,04

Table 12.8-2 Egorov'method: dimensionless power trends

Egorov										
ΔP_E	Fn^d									
Cases	1,5	2	2,5	3	3,5	4	4,5		mean	sd
1	-3%	-6%	-7%	-8%	-9%	-10%	-12%		-8%	0,03
2	-5%	-7%	-7%	-8%	-9%	-10%	-12%		-8%	0,02
3		-10%	-10%	-10%	-10%	-11%	-13%		-11%	0,01
4		-12%	-11%	-11%	-11%	-12%	-13%		-12%	0,01
5		-14%	-13%	-12%	-12%	-13%	-14%		-13%	0,01
6		-17%	-15%	-14%	-13%	-14%	-15%		-15%	0,01
7			-15%	-13%	-13%	-14%	-14%		-14%	0,01
8			-11%	-11%	-10%	-11%	-11%		-11%	0,00
9		-14%	-13%	-12%	-12%	-13%	-13%		-13%	0,01
10		-14%	-13%	-12%	-12%	-13%	-14%		-13%	0,01
11			-11%	-11%	-11%	-12%	-12%		-11%	0,01
12	-7%	-9%	-9%	-10%	-10%	-11%	-12%		-10%	0,02
mean	-5%	-11%	-11%	-11%	-11%	-12%	-13%		-11%	
sd	-	0,04	0,03	0,02	0,01	0,01	0,01			0,02

ASEM dimensionless result trends present a little rate upon the volumetric Froude Number Fn_∇.

These low variations allow us to consider dimensionless results constant and close to -20% for $Fn_\nabla \geq 2$.

Table 12.8-3 ASEM: dimensionless resistance trends

ASEM										
ΔR_H	Fn^d									
Cases	1,5	2	2,5	3	3,5	4	4,5		mean	sd
1	-19%	-20%	-18%	-17%	-17%	-20%	-24%		-19%	0,02
2	-18%	-23%	-22%	-18%	-17%	-21%	-24%		-21%	0,03
3		-21%	-23%	-20%	-19%	-21%	-24%		-22%	0,02
4		-22%	-25%	-21%	-20%	-21%	-22%		-22%	0,02
5		-21%	-25%	-21%	-21%	-21%	-21%		-22%	0,01
6		-20%	-24%	-22%	-21%	-19%	-19%		-21%	0,02
7			-22%	-21%	-20%	-17%	-15%		-19%	0,03
8			-17%	-18%	-15%	-13%	-10%		-15%	0,03
9		-24%	-23%	-23%	-23%	-23%	-20%		-23%	0,01
10		-27%	-28%	-21%	-20%	-17%	-15%		-21%	0,05
11			-25%	-25%	-23%	-24%	-24%		-24%	0,01
12	-22%	-21%	-22%	-20%	-19%	-19%	-21%		-21%	0,01
mean	-20%	-22%	-23%	-21%	-20%	-20%	-20%		-21%	
sd	-	0,02	0,03	0,02	0,03	0,03	0,04			0,03

Table 12.8-4 ASEM: dimensionless power trends

ASEM										
ΔP_E	Fn^d									
Cases	1,5	2	2,5	3	3,5	4	4,5		mean	sd
1	-5%	-12%	-14%	-15%	-15%	-16%	-17%		-14%	0,04
2	-6%	-13%	-16%	-17%	-17%	-18%	-18%		-15%	0,04
3		-21%	-21%	-21%	-21%	-21%	-21%		-21%	0,00
4		-21%	-22%	-22%	-22%	-22%	-22%		-22%	0,01
5		-18%	-20%	-21%	-21%	-21%	-21%		-20%	0,01
6		-15%	-17%	-19%	-20%	-20%	-20%		-18%	0,02
7			-15%	-17%	-18%	-18%	-18%		-17%	0,01
8			-9%	-12%	-13%	-13%	-13%		-12%	0,02
9		-17%	-19%	-21%	-21%	-22%	-22%		-20%	0,02
10		-32%	-31%	-29%	-27%	-26%	-24%		-28%	0,03
11			-26%	-26%	-25%	-25%	-25%		-25%	0,01
12	14%	-3%	-9%	-13%	-14%	-15%	-16%		-8%	0,11
mean	1%	-17%	-18%	-19%	-20%	-20%	-20%		-18%	
sd	-	0,08	0,06	0,05	0,04	0,04	0,04			0,07

In the first approximation model results, in term of resistance as well as power, can be obtained by ASEM results, not out of range, multiplied by 1.25[137].

[137] In first approximation, let $\Delta\Psi = -20\%$ per each value of Fn_∇, where Ψ stands for R_H as well as P_E; it follows:

It is not true for the other prediction methods. In detail, despite of Egorov's results are the closest to test results, dimensionless trends related to cannot be approximated as constant through range of the volumetric Froude numbers.

At the same time, despite of Savitsky's dimensionless result trends are quite similar to ASEM's ones, Savitsky's results present an higher "distance" from test results than ASEM.

Table 12.8-5 Savitsky's method: dimensionless resistance trends

Savitsky										
ΔR_H	Fn^d									
Cases	1,5	2	2,5	3	3,5	4	4,5		mean	sd
1	-27%	-25%	-21%	-19%	-18%	-20%	-24%		-22%	0,03
2	-30%	-28%	-25%	-21%	-19%	-21%	-24%		-24%	0,04
3		-29%	-28%	-22%	-20%	-22%	-24%		-24%	0,03
4		-28%	-29%	-23%	-22%	-22%	-23%		-24%	0,03
5		-28%	-29%	-24%	-22%	-22%	-22%		-24%	0,03
6		-27%	-28%	-24%	-23%	-20%	-19%		-24%	0,03
7			-25%	-23%	-21%	-18%	-16%		-21%	0,04
8			-22%	-21%	-17%	-15%	-12%		-17%	0,04
9		-29%	-27%	-25%	-24%	-23%	-20%		-25%	0,03
10		-32%	-31%	-24%	-21%	-18%	-15%		-24%	0,07
11			-31%	-28%	-25%	-25%	-25%		-27%	0,03
12	-30%	-25%	-25%	-22%	-20%	-20%	-21%		-23%	0,04
mean	-29%	-28%	-27%	-23%	-21%	-21%	-21%		-23%	
sd	-	0,02	0,03	0,02	0,02	0,02	0,04			0,04

$$\Delta\Psi = \frac{\Psi_{ASEM} - \Psi_{BK-1}}{\Psi_{BK-1}} = \frac{\Psi_{ASEM}}{\Psi_{BK-1}} - 1 = -0.2$$

and

$$\Psi_{BK-1} = \frac{1}{0.8}\Psi_{ASEM} = 1.25\,\Psi_{ASEM} \cdot$$

Table 12.8-6 Savitsky's method: dimensionless power trends

Savitsky										
ΔP_E	Fn^d									
Cases	1,5	2	2,5	3	3,5	4	4,5		mean	sd
1	-4%	-14%	-17%	-18%	-18%	-18%	-19%		-15%	0,05
2	-19%	-24%	-25%	-24%	-23%	-23%	-23%		-23%	0,02
3		-24%	-26%	-26%	-25%	-24%	-24%		-25%	0,01
4		-24%	-26%	-26%	-25%	-24%	-24%		-25%	0,01
5		-24%	-25%	-26%	-25%	-24%	-24%		-25%	0,01
6		-22%	-24%	-25%	-24%	-24%	-23%		-24%	0,01
7			-20%	-22%	-22%	-21%	-20%		-21%	0,01
8			-17%	-18%	-18%	-18%	-17%		-18%	0,01
9		-22%	-24%	-25%	-25%	-24%	-24%		-24%	0,01
10		-33%	-33%	-31%	-30%	-28%	-26%		-30%	0,03
11			-32%	-31%	-30%	-29%	-28%		-30%	0,02
12	-1%	-14%	-18%	-19%	-20%	-20%	-20%		-16%	0,07
mean	-8%	-22%	-24%	-24%	-24%	-23%	-23%		-23%	
sd	-	0,06	0,05	0,04	0,04	0,03	0,03			0,05

ASEM results are a little bit closer to test results than Savitsky's ones, but at the same time, the computational effort required by ASEM is the highest among prediction methods used.

Thereby, in term of goodness of results versus computational efforts, Savitsky's method is more efficient then ASEM.

12.9 Conclusion

Analytical Semi-Empirical Method (ASEM) has been applied to model BK-1 of the BK Series. Further, Savitsky‘s as well as Egorov’s method have been applied too, in order to get an overall comparison.

By data available, 12 cases have been taken in account in order to get a comparison among data associated to planing condition.

Data comparison has been developed with reference to Resistance and Power trends related to hull speed. In order to get a comparison not pertinent to the dimensional choice of the hull length, all results have been replaced with their relative dimensionless sizes.

ASEM and Savitsky’s results without physical meaning have not been taken in account meanwhile results with physical meaning but out of range have been reported with dash line.

Egorov’s method presents the best results: it is a regression method which coefficients have been computed by statistical results analysis of BK and MBK Series.

ASEM dimensionless result trends present low variations as function of volumetric Froude Number Fn_{∇}. In first approximation model results, in term of resistance as well as power, can be computed by ASEM’s ones multiplied by 1.25, whereas ASEM’s results shall be not out of range.

ASEM results are a little bit closer to test results than Savitsky’s ones, but in term of goodness of results versus computational efforts, Savitsky’s method is more efficient then ASEM.

12.10 Symbols

B⌧	Beam between chines in amidship section - Russian symbol	[m]
Bc	Beam between chines	[m]
$B_{C,ms}$	Beam between chines in mean section	[m]
B_p	Beam between chines	[m]
C_Δ	Weight coefficient	$C_\Delta = \frac{W}{\frac{1}{2}\gamma B_C^3}$
C_G	Weight coefficient - Russian symbol	$\left(C_G \equiv C_\Delta\right)$
Fn_∇	Volumetric Froude number	$Fn_\nabla = \frac{V}{\sqrt{g\sqrt[3]{\nabla}}}$
Fr_V	Volumetric Froude number - Russian symbol	$Fr_V = \frac{V}{\sqrt{g\sqrt[3]{\frac{W}{\gamma}}}}$
g	Acceleration of gravity	$9.81 m/s^2$
L_{CG}	Longitudinal position of CG versus the transom	[m]
L_{ck}	Chines length - Russian symbol	[m]
L_{PP}	Length between perpendicular	[m]
sd	Standard Deviation	
R_H	Bare hull resistance	[N]
V	Hull speed	[m/s]
W	Hull weight - Displacement	[N]
$\bar{x}_g$	Longitudinal position of CG to length between perpendicular ratio - Russian symbol	$\bar{x}_g = \frac{L_{CG}}{L_{PP}}$
$\{x, y, z\}$	Geometrical coordinates	
β ⌧	Deadrise angle in amidship section - Russian symbol	[deg]
ΔP_E	Dimensionless variation of the power	
ΔR_H	Dimensionless variation of the resistance	
ε	Dimensionless resistance - Russian symbol	$\varepsilon = \frac{R_H}{\Delta}$
γ	Unit weight of water	$\left[N/m^3\right]$
λ	Length between perpendicular to beam between chines of mean section ratio	$\lambda = \frac{L_{PP}}{B_{C,ms}}$

μ	Dimensionless power	$\mu = \frac{P_E}{\Delta \cdot V}$
∇	Volume of displacement at rest	$\left[m^3\right]$

12.11 References

Bertorello, C. & Oliviero, L. 2007. Hydrodynamic Resistance Assessment of Non-Monohedral Planing Hull Forms based on Savitsky's Method. *Australian Journal of Mechanical Engineering,* Vol. 4 No.2, pp 209-224. Engineers Media, CROWS NEST, Australia. (ACN001311511).

Radojcic, D. 1985. An Approximate Method For Calculation of Resistance and Trim of the Planing Hulls. *Ship Science Report No.23* University of Southampton (UK)

Savitsky, D. 1964. Hydrodynamic Design of Planing Hull. *Marine Technology*, Vol.1, No.1, Jersey City (USA): SNAME

Voitkounski, Y.I. 1985. *Ship Theory Handbook:. Vol.3. Manoeuvrability of conventional Ships. Hydrodynamics of Gliders Hydrofoils and Hovercrafts.* Leningrad (Russia): Sudostroenie. pp. 277-283 (Russian language)

APPENDIX I

COMPARISON RESULTS: ASEM VS SERIES YP81

13.1 Table of Contents

13.2 Figure Index

13.3 Table Index

13.4 Introduction

Analytical Semi-Empirical Method (ASEM) has been developed in order to predict Resistance and Power performance versus hull speed related to a warped bare monohull. [Bertorello & Oliviero 2007]

In this chapter ASEM will be applied to models of the Series YP81 [Compton 1986], in order to check reliability and efficiency in semi-planing field.

In order to achieve this goal, geometrical and physical data related to Series YP81 have been here reported in International System Units.

Further, Savitsky‘s LF method [Savitsky 1964] will be applied too, in order to get an overall comparison.

13.5 Models: Geometry and Tests [Compton 1986]

Series YP81, also known as Compton Series as well as US Academy Series, is composed by six transom-stern hull models.

Parent model (YP81-1) has been developed applying to the Yard Patrol Craft YP676 the form features of three hull series: Series NPL, Series 63 and Series 64, in order to get a new coastal patrol craft. The other models of the Series YP81 have been developed to study the influence on performance of some hull form characteristics.

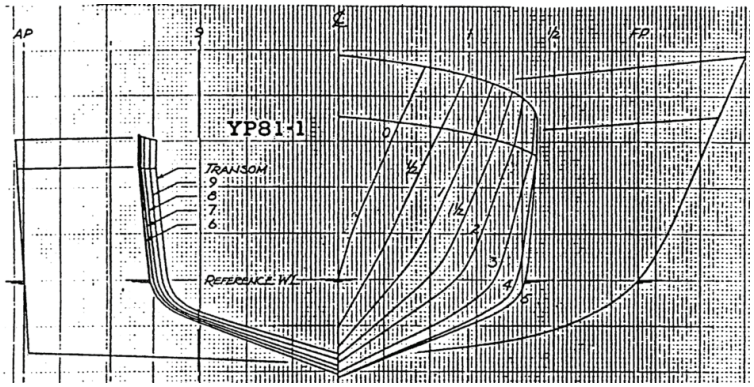

Figure 13.5-1 Body plans & end profiles: Model YP81-1

Models YP81-1 to YP81-3 are soft-chine shapes with different length to beam ratio.

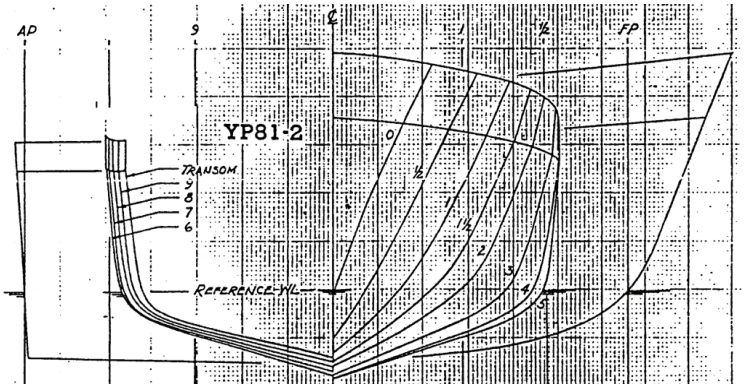

Figure 13.5-2 Body plans & end profiles: Model YP81-2

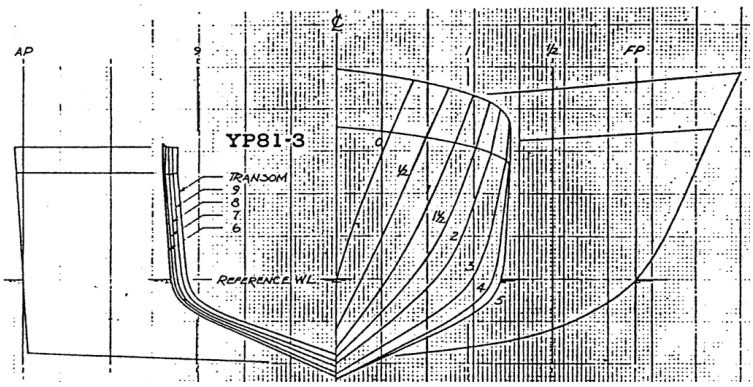

Figure 13.5-3 Body plans & end profiles: Model YP81-3

Models YP81-4 to YP81-6 have been developed respectively from the Models YP81-1 to YP81-3 "*extending bottom and side tangents at each station until they intersected*": the hard-chine counterparts of soft-chine models.

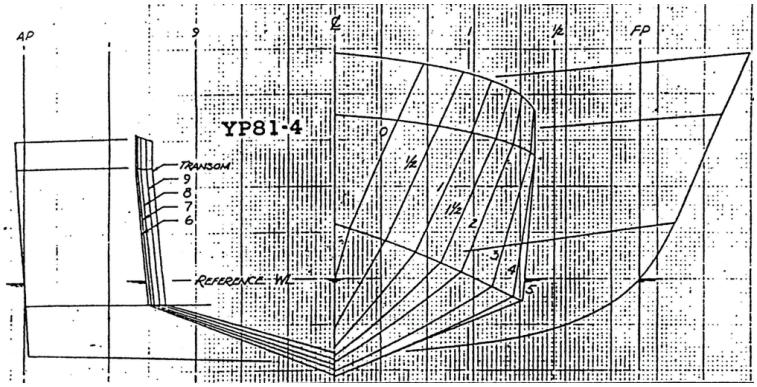

Figure 13.5-4 Body plans & end profiles: Model YP81-4

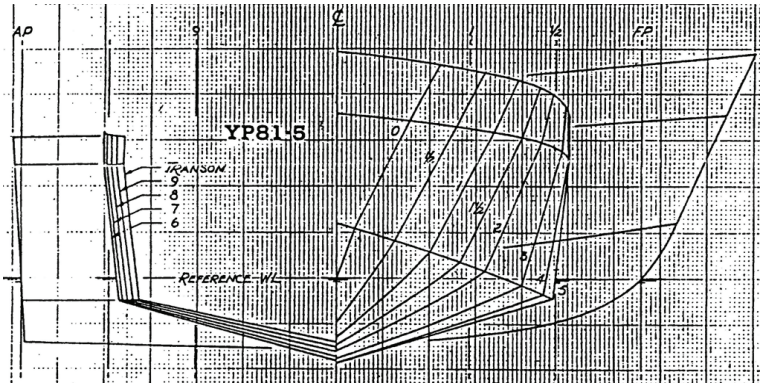

Figure 13.5-5 Body plans & end profiles: Model YP81-5

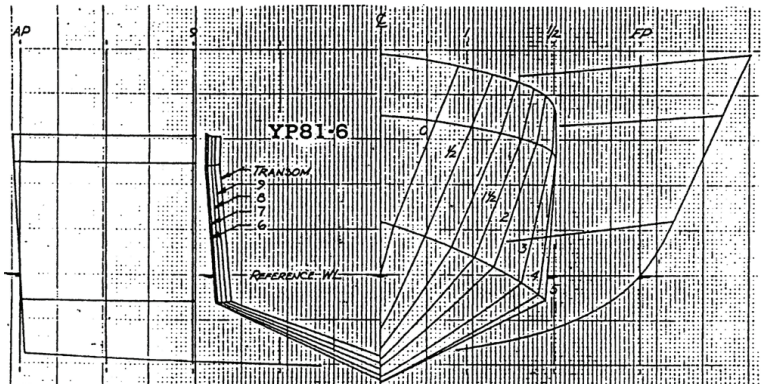

Figure 13.5-6 Body plans & end profiles: Model YP81-6

All six models are 5 ft in length with "*the hypothetical propeller shaft centreline passed through a point 1.95 in. below the lowest point (on ℄) of the most transom and made an angle of 9.75 deg with the design waterline*".

In order to get a comparison among data related to planing condition of hard-chine hull form, models of series YP81 with soft-chines have not been take in account[(138)].

Table 13.5-1 Hull characteristics at reference waterline

	YP81-4	YP81-5	YP81-6
L_{PP}/B_{REF}	4.49	3.86	5.17
B_{REF}/T	3.90	5.25	3.03
∇	158.3	164.7	154.8
S	6.818	7.345	6.513
C_B	0.437	0.452	0.437
C_P	0.721	0.720	0.719
C_{WP}	0.802	0.804	0.809
LCB/L_{PP}	-0.086	-0.086	-0.084
KM_T/B_{REF}	0.684	0.817	0.598
BM_L/L_{PP}	1.986	2.246	1.798
$i_e[\text{deg}]$	17.7	21.5	17.3
$\beta_{10}[\text{deg}]$	16.4	12.4	21.0

(138) This choice is due to the fact that Savitsky's method formulas, and thereby ASEM, are based on results related to tests on planing hull form with hard-chines as well as planing surfaces with sharp edges.

Hereinafter coordinates and dimensions of models are reported:

Table 13.5-2 Models coordinates

Model	Station	YP81-4			YP81-5			YP81-6		
		x	y	z	x	y	z	x	y	z
		[m]	[m]	[m]	[m]	[m]	[m]	[m]	[m]	[m]
Stern	0	0,00	0,000	0,019	0,00	0,000	0,017	0,00	0,000	0,022
			0,150	0,060		0,177	0,052		0,132	0,069
	1	0,15	0,000	0,014	0,15	0,000	0,012	0,15	0,000	0,016
			0,155	0,060		0,182	0,052		0,136	0,068
	2	0,30	0,000	0,009	0,30	0,000	0,009	0,30	0,000	0,011
			0,160	0,060		0,187	0,052		0,141	0,068
	3	0,46	0,000	0,005	0,46	0,000	0,005	0,46	0,000	0,006
			0,163	0,060		0,191	0,052		0,145	0,068
	4	0,61	0,000	0,001	0,61	0,000	0,002	0,61	0,000	0,001
			0,165	0,060		0,194	0,051		0,145	0,068
	5	0,76	0,000	0,000	0,76	0,000	0,000	0,76	0,000	0,000
			0,166	0,063		0,192	0,054		0,145	0,071
	6	0,91	0,000	0,000	0,91	0,000	0,000	0,91	0,000	0,000
			0,158	0,066		0,184	0,057		0,138	0,076
	7	1,07	0,000	0,004	1,07	0,000	0,004	1,07	0,000	0,005
			0,140	0,075		0,165	0,065		0,123	0,086
	8	1,22	0,000	0,012	1,22	0,000	0,010	1,22	0,000	0,014
			0,112	0,087		0,132	0,077		0,099	0,099
	8,5	1,30	0,000	0,017	1,30	0,000	0,015	1,30	0,000	0,021
			0,094	0,094		0,110	0,084		0,082	0,107
	9	1,37	0,000	0,024	1,37	0,000	0,022	1,37	0,000	0,030
			0,072	0,104		0,082	0,092		0,062	0,116
	9,5	1,45	0,000	0,040	1,45	0,000	0,034	1,45	0,000	0,047
			0,046	0,114		0,051	0,101		0,039	0,125
	10	1,52	0,000	0,081	1,52	0,000	0,070	1,52	0,000	0,092
			0,014	0,124		0,015	0,112		0,011	0,134
Bow	10,5	1,60	0,000	0,081	1,60	0,000	0,070	1,60	0,000	0,137
			0,000	0,128		0,000	0,116		0,000	0,092

Models have been tested in order to evaluate the influence of some hull form parameters on planing hull performances:

- the length to beam ratio L_{PP}/B_{REF},
- the displacement to length ratio ∇,
- the longitudinal distance from amidships to center of gravity related to the hull length x_g [139]

Resistance results were processed to draw a set of crossplot diagrams useful for design purposes.

Per each model and per each value of x_g, a set of five curves have been developed: each curve represents the residual resistance coefficient[140] versus Froude number based on waterline length at rest Fn [141] for a fixed value of the displacement to length ratio ∇.

In detail:

- the speed range, in term of Fn, was about 0.1 up to 0.65;
- ∇ values were 110, 120, 130, 140, 150 $[LTSW/ft^3]$;
- x_g values were 0.0244, 0.0778 and 0.1312.

In order to get an overall comparison in International System units and reminding that models were 5-ft long all curves have been redrawn showing, per each model and per each x_g value, the bare hull resistance R_H in term of speed V and weight W.

Table 13.5-3 Series YP81: match data

---

[139] In his paper, Compton used the symbol L_{CG} as longitudinal distance from amidships to center of gravity, positive in stern direction. In order to avoid confusion -in this thesis work L_{CG} indicates the distance between the center of gravity and the hull transom stern of the hull- Compton's symbol L_{CG} here has been replaced with X_g, and thereby: $x_g = X_g / L_{PP}$.

[140] In order to evaluate the residual resistance ITTC 1957 formula has been adopted as friction line.

[141] Compton considered the Froude number based on the waterline length at rest. According to remarks on Froude numbers in paragraph G.9 of Appendix G of this Thesis work, this Froude number (related to the waterline length at rest) is a "mechanical" Froude number. As matter of fact the geometric term (waterline length at rest) is connected mechanical hull parameter: the weight W. Thereby this Froude number is linear with the hull speed, but his trend is related to the weight value adopted in towing test.

$\triangle$	**W**
[LTSW/ft^3]	[N]
110	137
120	150
130	162
140	174
150	187

13.6 Data Comparison

Data comparison has been developed with reference to Resistance and Power trends related to hull speed. Power data related to the models of Series YP have been derived by measurements of hull speed and resistance.

Hereinafter ASEM and Savitsky's results without physical meaning have not been taken in account (i.e.: results related to a mean wetted length higher than hull length overall), meanwhile results with physical meaning coupled with data out of range have been reported with dash line (i.e.: results related to a mean wetted length/beam ratio higher than four times).

13.6.1 Model YP81-4

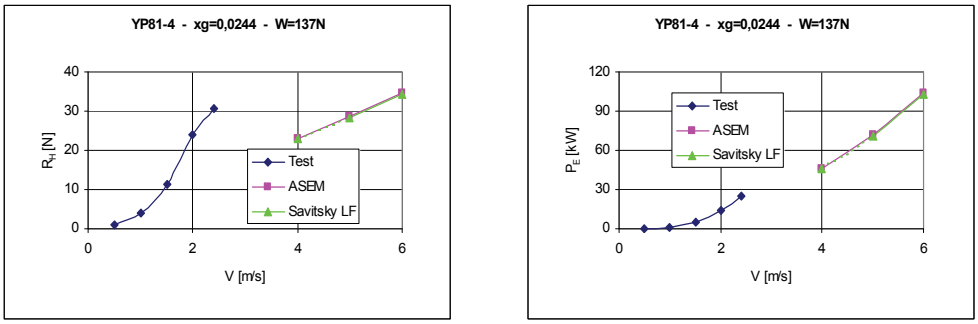

[a] **[b]**

Figure 13.6-1 Data Comparison: Model YP81-4 - xg=0.0244 - W=137N

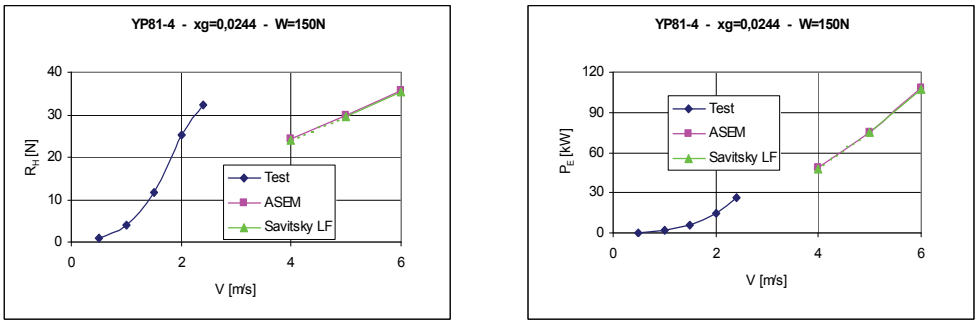

[a] **[b]**

Figure 13.6-2 Data Comparison: Model YP81-4 - xg=0.0244 - W=150N

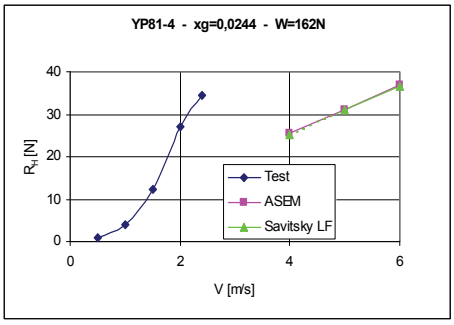

[a]

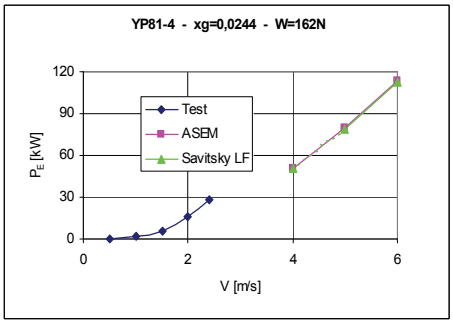

[b]

Figure 13.6-3 Data Comparison: Model YP81-4 - xg=0.0244 - W=162N

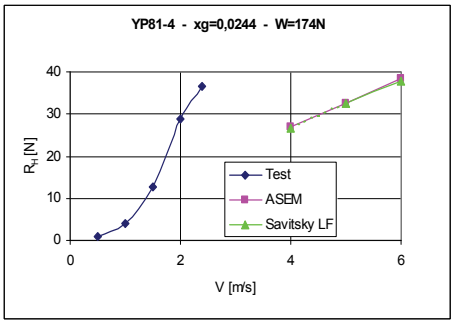

[a]

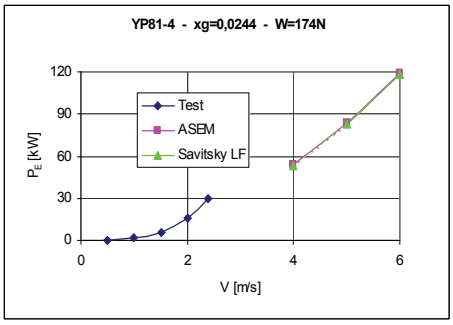

[b]

Figure 13.6-4 Data Comparison: Model YP81-4 - xg=0.0244 - W=174N

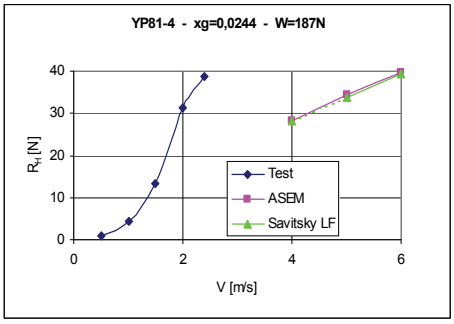

[a]

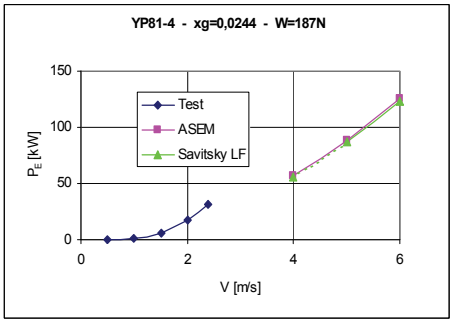

[b]

Figure 13.6-5 Data Comparison: Model YP81-4 - xg=0.0244 - W=187N

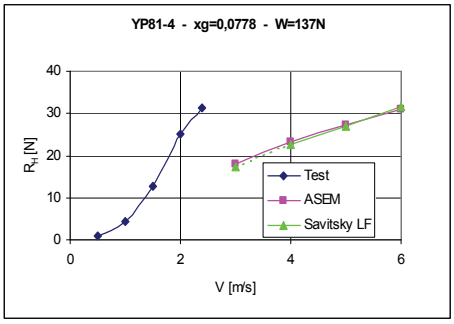

[a]

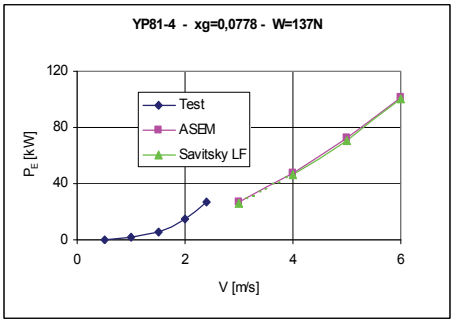

[b]

Figure 13.6-6 Data Comparison: Model YP81-4 - xg=0.0778 - W=137N

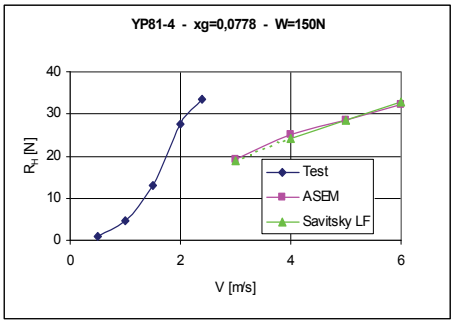

[a]

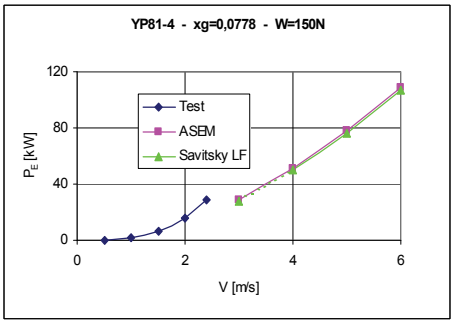

[b]

Figure 13.6-7 Data Comparison: Model YP81-4 - xg=0.0778 - W=150N

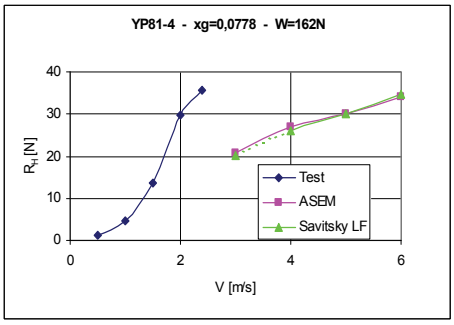

[a]

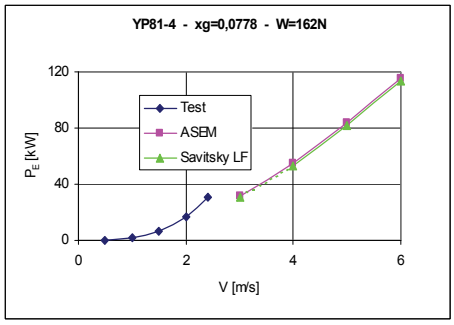

[b]

Figure 13.6-8 Data Comparison: Model YP81-4 - xg=0.0778 - W=162N

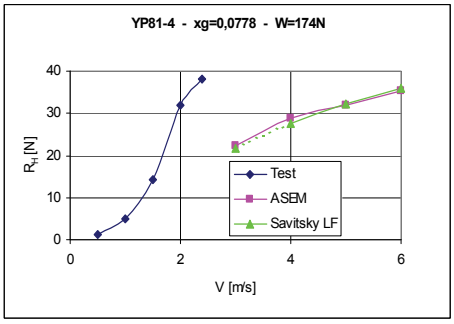

[a]

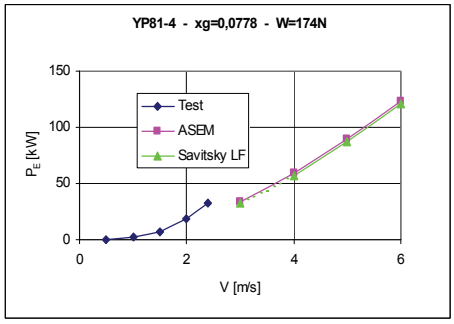

[b]

Figure 13.6-9 Data Comparison: Model YP81-4 - xg=0.0778 - W=174N

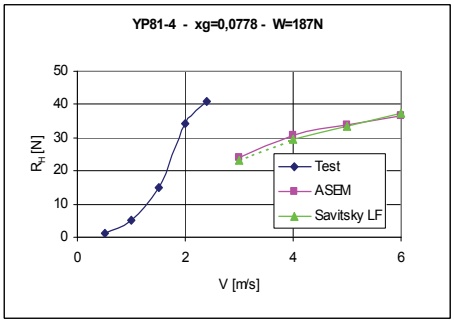

[a]

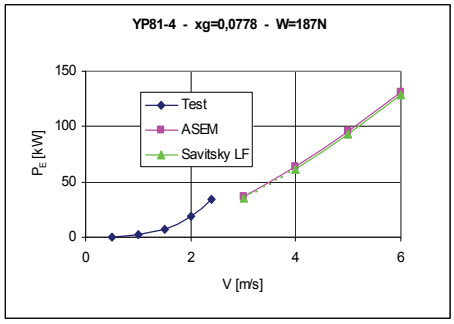

[b]

Figure 13.6-10 Data Comparison: Model YP81-4 - xg=0.0778 - W=187N

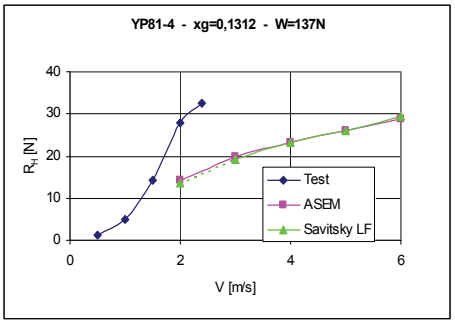

[a]

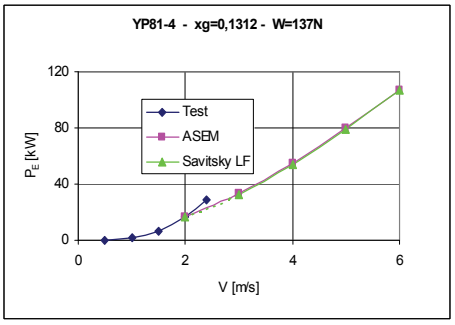

[b]

Figure 13.6-11 Data Comparison: Model YP81-4 - xg=0.1312 - W=137N

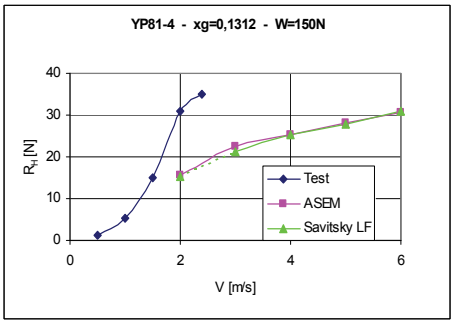

[a]

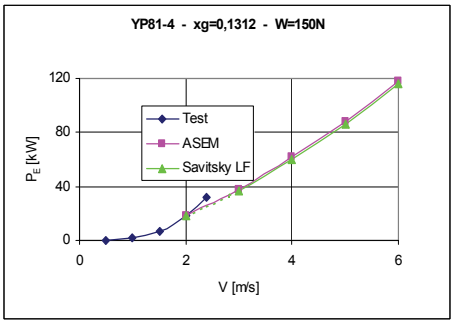

[b]

Figure 13.6-12 Data Comparison: Model YP81-4 - xg=0.1312 - W=150N

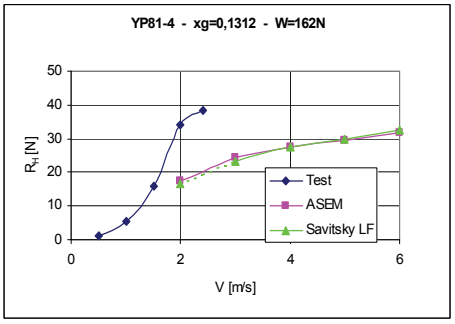

[a]

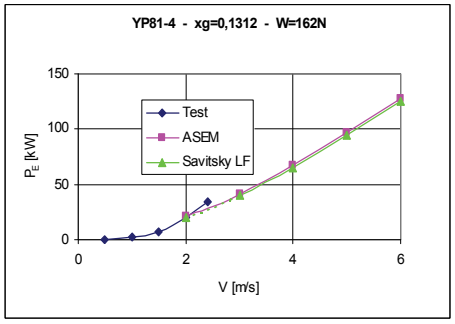

[b]

Figure 13.6-13 Data Comparison: Model YP81-4 - xg=0.1312 - W=162N

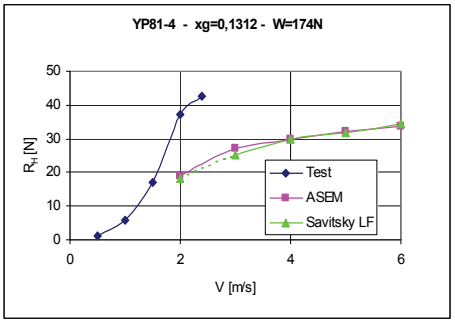

[a]

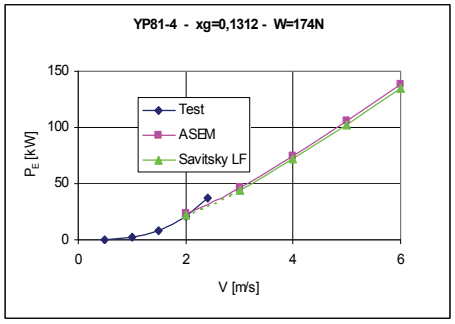

[b]

Figure 13.6-14 Data Comparison: Model YP81-4 - xg=0.1312 - W=174N

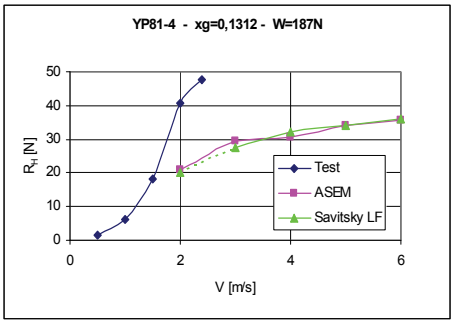

[a]

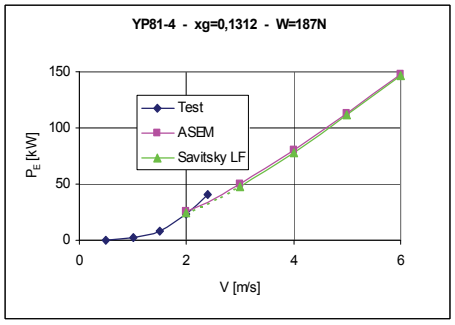

[b]

Figure 13.6-15 Data Comparison: Model YP81-4 - xg=0.1312 - W=187N

13.6.2 Model YP81-5

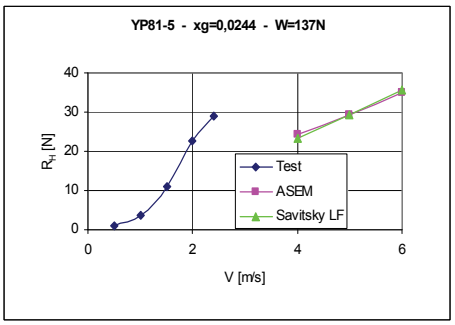

[a]

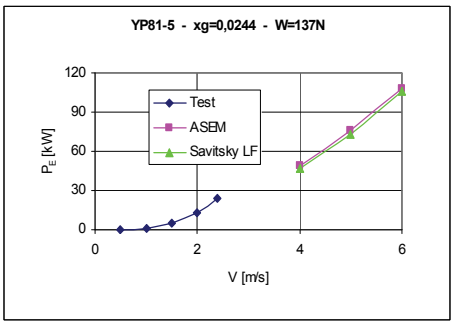

[b]

Figure 13.6-16 Data Comparison: Model YP81-5 - xg=0.0244 - W=137N

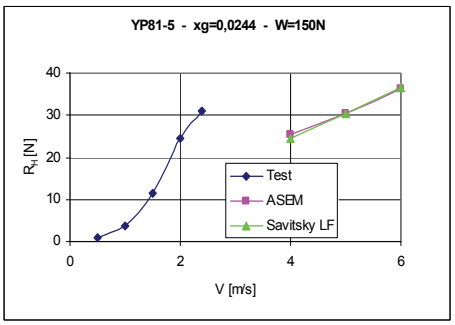

[a]

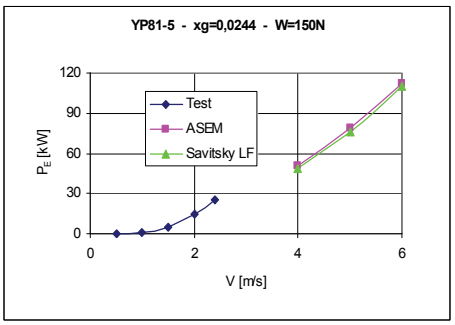

[b]

Figure 13.6-17 Data Comparison: Model YP81-5 - xg=0.0244 - W=150N

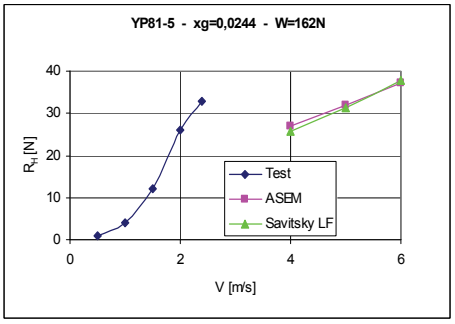

[a]

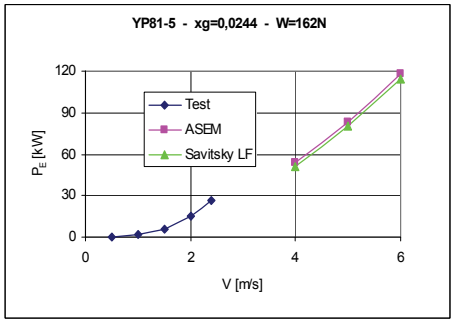

[b]

Figure 13.6-18 Data Comparison: Model YP81-5 - xg=0.0244 - W=162N

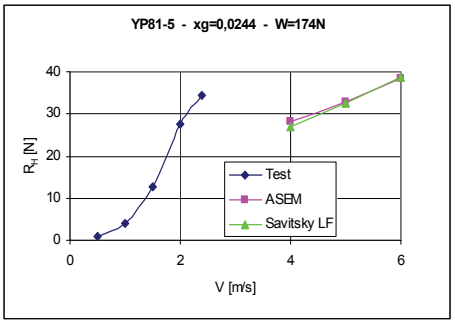

[a]

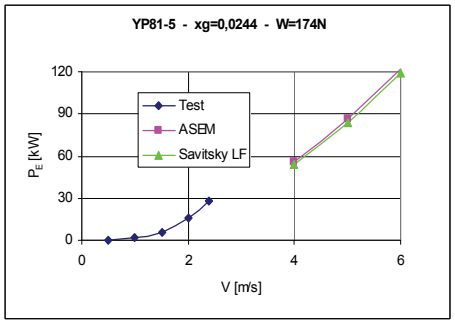

[b]

Figure 13.6-19 Data Comparison: Model YP81-5 - xg=0.0244 - W=174N

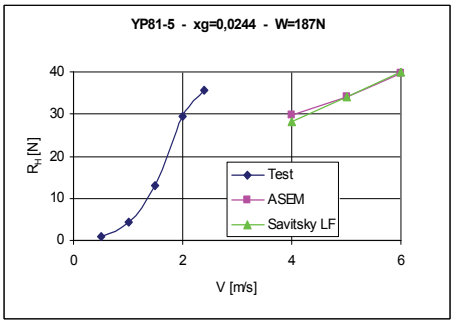

[a]

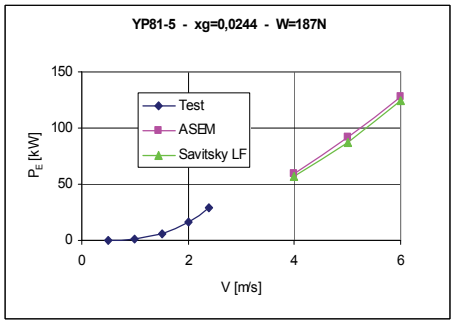

[b]

Figure 13.6-20 Data Comparison: Model YP81-5 - xg=0.0244 - W=187N

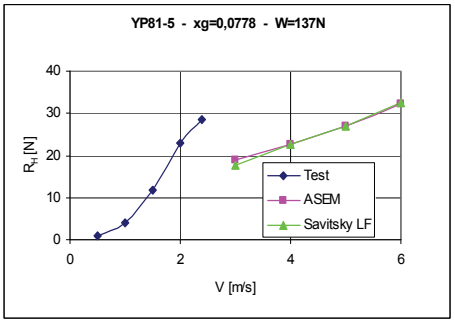

[a]

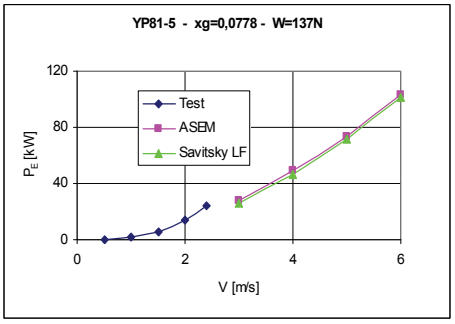

[b]

Figure 13.6-21 Data Comparison: Model YP81-5 - xg=0.0778 - W=137N

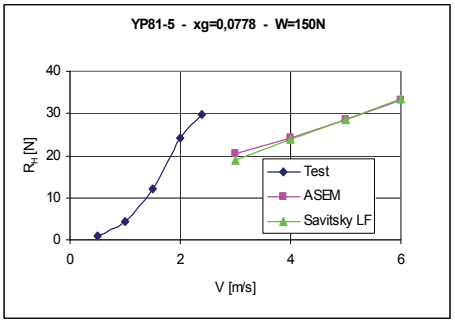

[a]

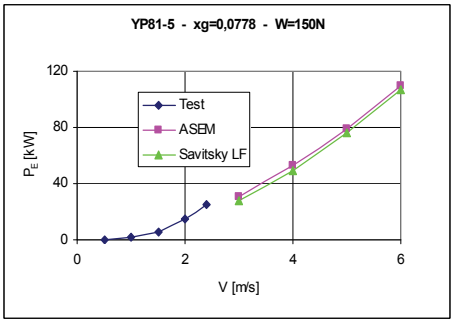

[b]

Figure 13.6-22 Data Comparison: Model YP81-5 - xg=0.0778 - W=150N

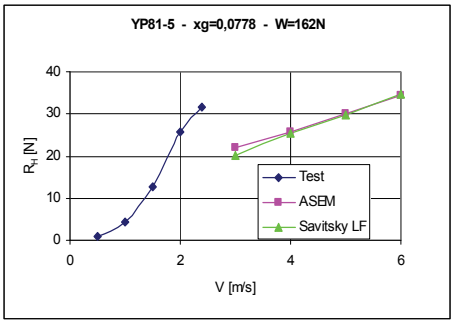

[a]

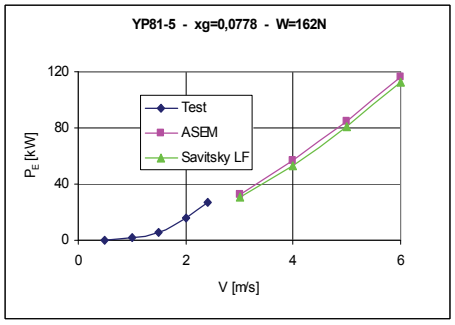

[b]

Figure 13.6-23 Data Comparison: Model YP81-5 - xg=0.0778 - W=162N

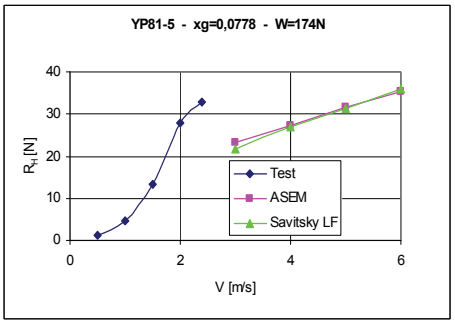

[a]

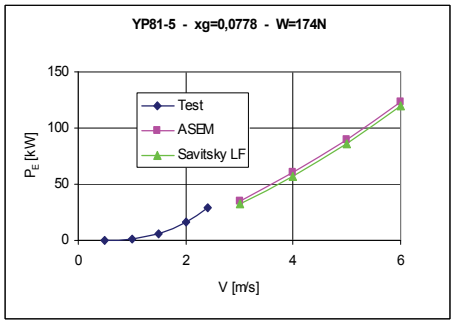

[b]

Figure 13.6-24 Data Comparison: Model YP81-5 - xg=0.0778 - W=174N

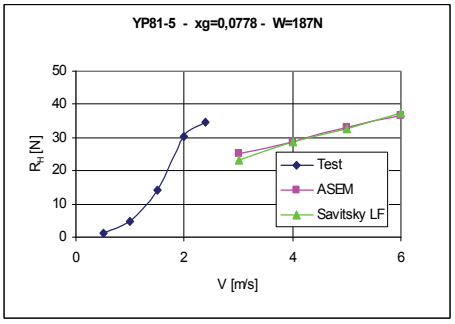

[a]

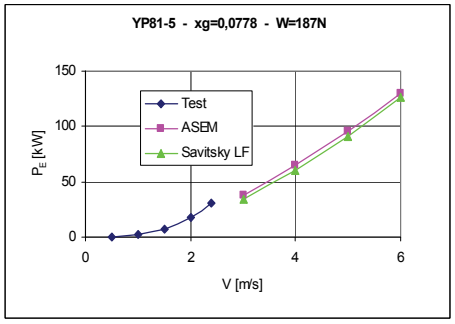

[b]

Figure 13.6-25 Data Comparison: Model YP81-5 - xg=0.0778 - W=187N

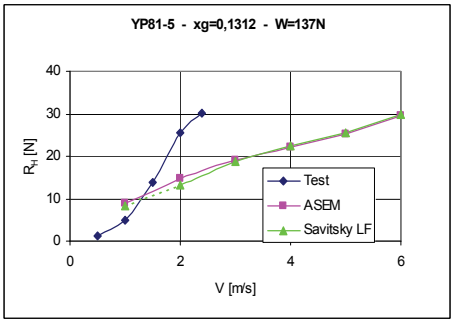

[a]

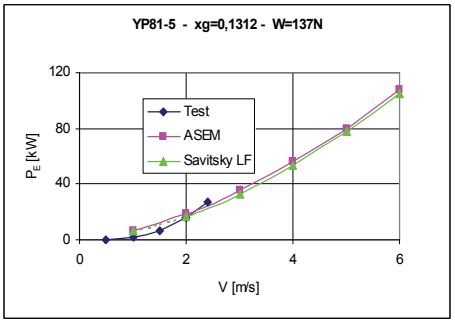

[b]

Figure 13.6-26 Data Comparison: Model YP81-5 - xg=0.1312 - W=137N

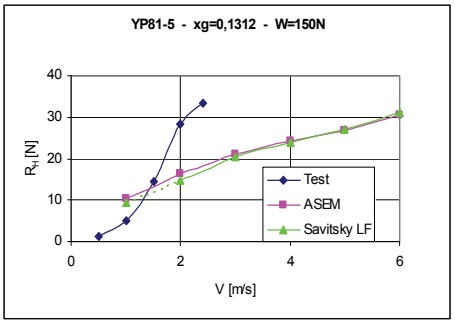

[a]

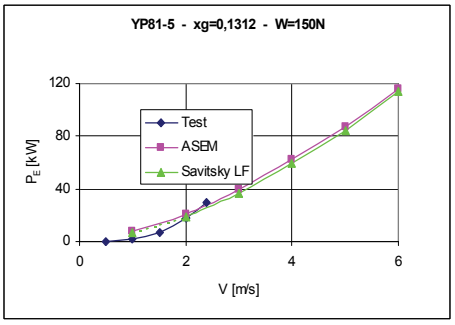

[b]

Figure 13.6-27 Data Comparison: Model YP81-5 - xg=0.1312 - W=150N

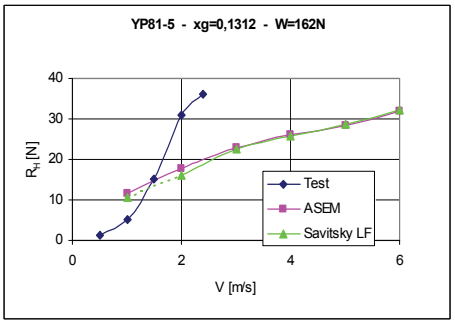

[a]

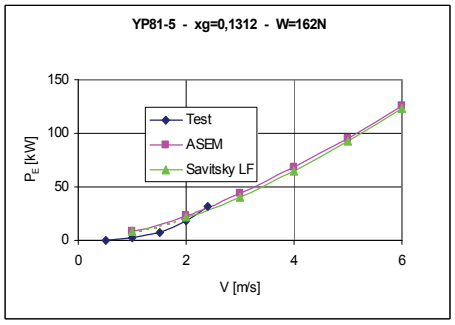

[b]

Figure 13.6-28 Data Comparison: Model YP81-5 - xg=0.1312 - W=162N

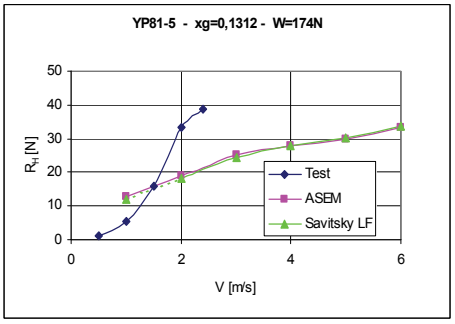

[a]

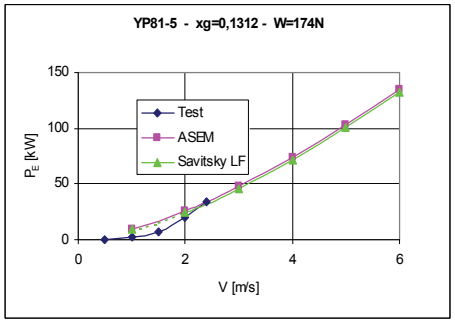

[b]

Figure 13.6-29 Data Comparison: Model YP81-5 - xg=0.1312 - W=174N

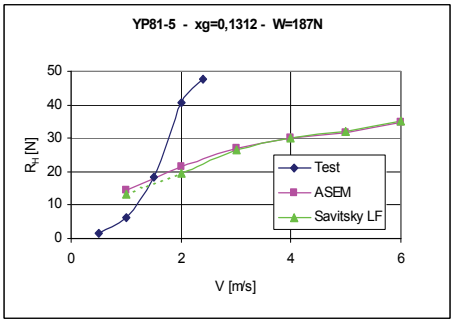

[a]

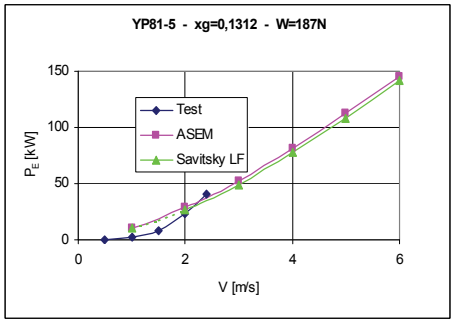

[b]

Figure 13.6-30 Data Comparison: Model YP81-5 - xg=0.1312 - W=187N

13.6.3 Model YP81-6

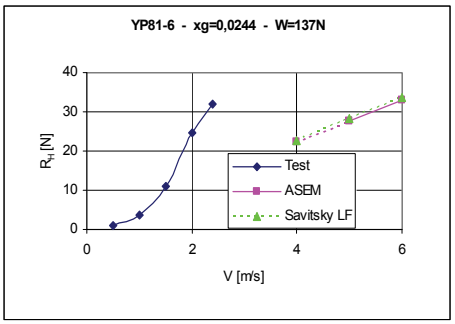

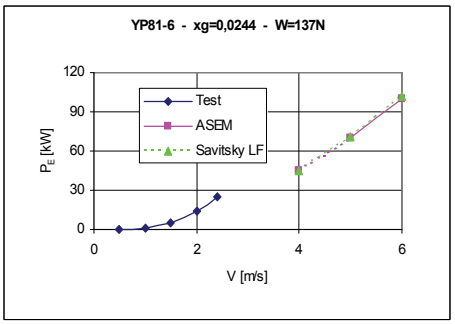

[a] **[b]**

Figure 13.6-31 Data Comparison: Model YP81-6 - xg=0.0244 - W=137N

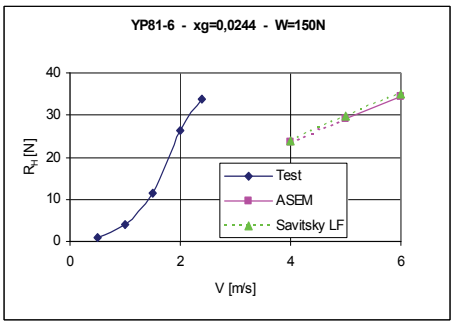

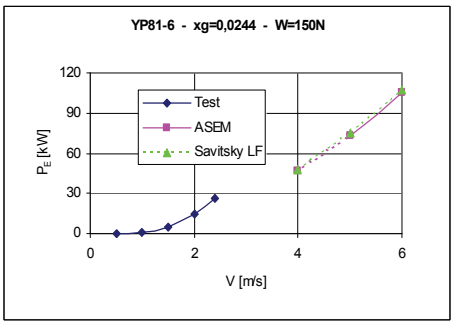

[a] **[b]**

Figure 13.6-32 Data Comparison: Model YP81-6 - xg=0.0244 - W=150N

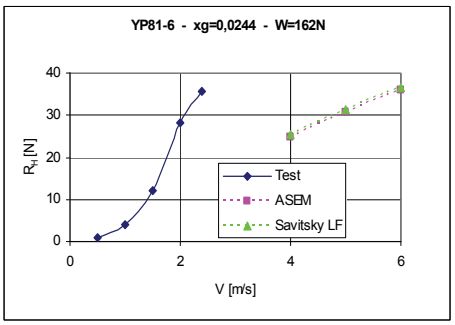

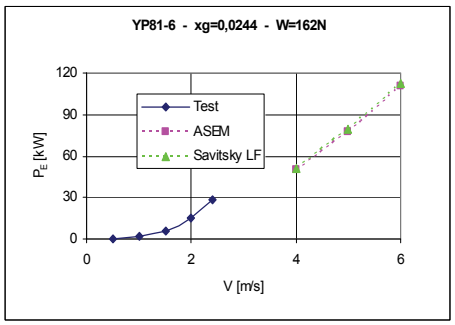

[a] **[b]**

Figure 13.6-33 Data Comparison: Model YP81-6 - xg=0.0244 - W=162N

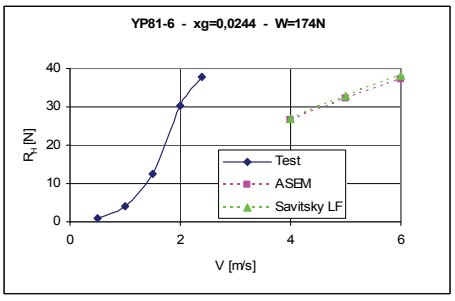

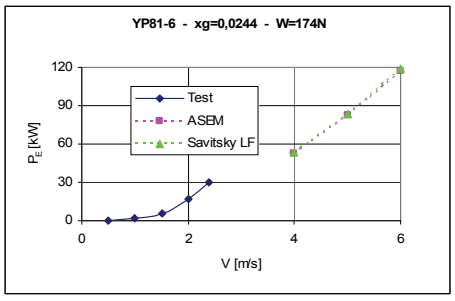

[a] **[b]**

Figure 13.6-34 Data Comparison: Model YP81-6 - xg=0.0244 - W=174N

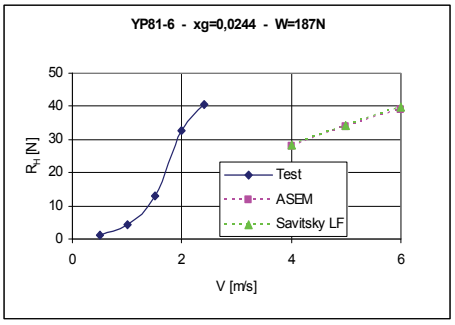

[a]

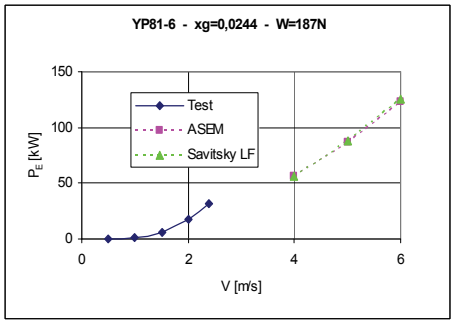

[b]

Figure 13.6-35 Data Comparison: Model YP81-6 - xg=0.0244 - W=187N

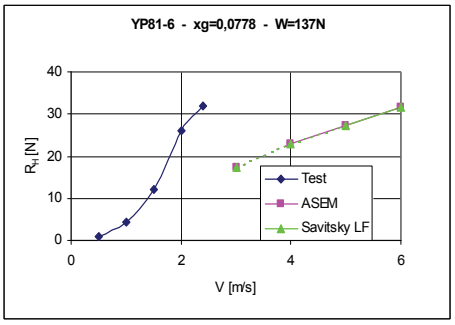

[a]

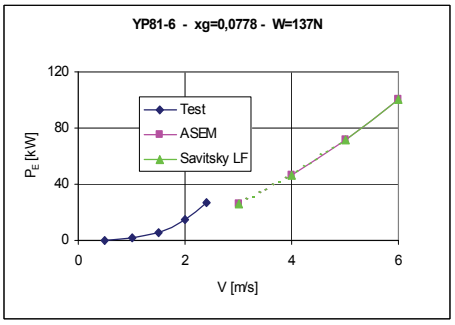

[b]

Figure 13.6-36 Data Comparison: Model YP81-6 - xg=0.0778 - W=137N

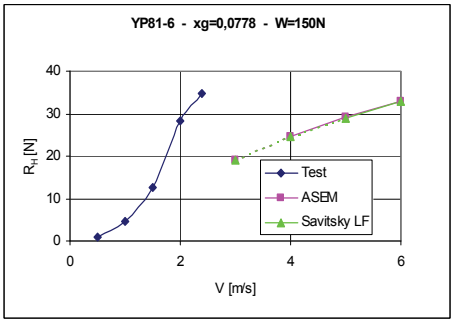

[a]

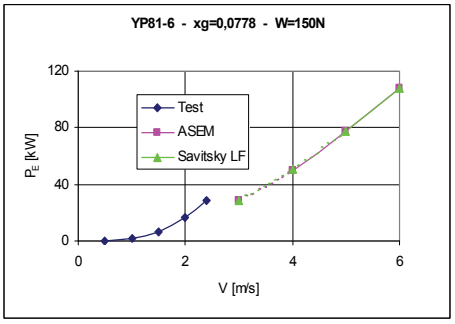

[b]

Figure 13.6-37 Data Comparison: Model YP81-6 - xg=0.0778 - W=150N

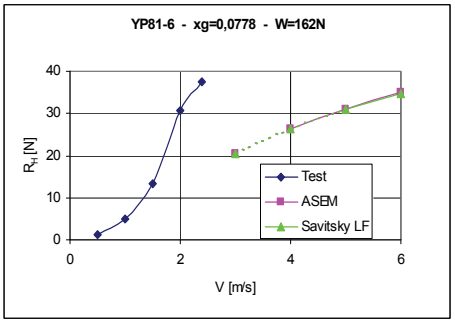

[a]

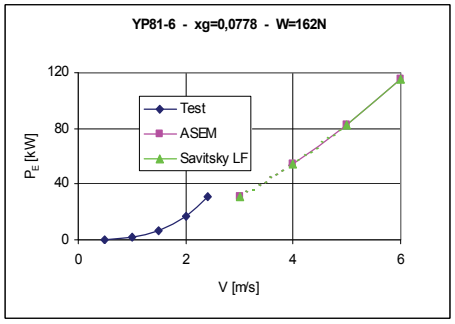

[b]

Figure 13.6-38 Data Comparison: Model YP81-6 - xg=0.0778 - W=162N

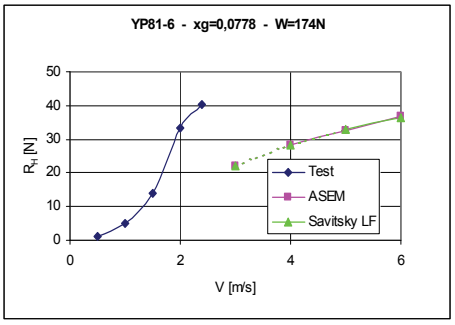

[a]

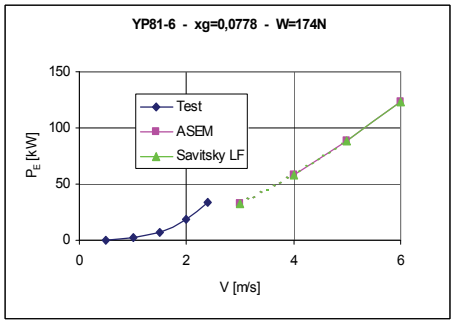

[b]

Figure 13.6-39 Data Comparison: Model YP81-6 - xg=0.0778 - W=174N

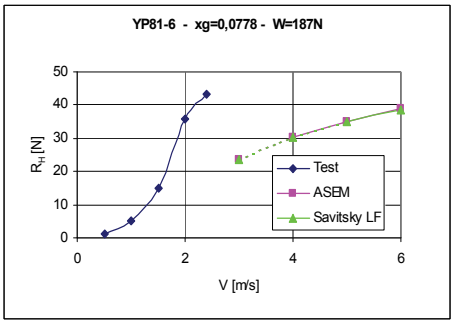

[a]

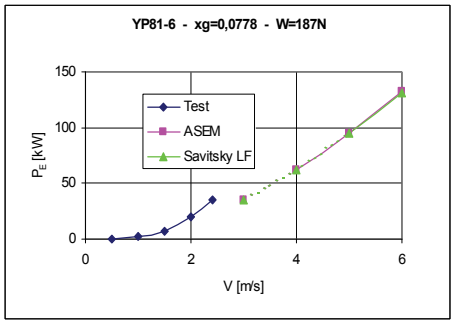

[b]

Figure 13.6-40 Data Comparison: Model YP81-6 - xg=0.0778 - W=187N

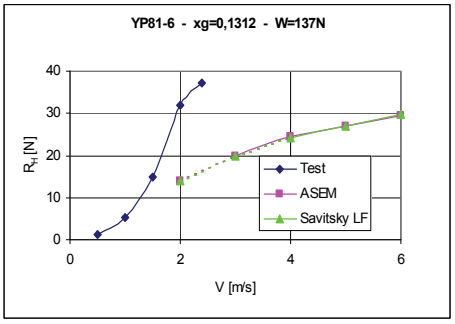

[a]

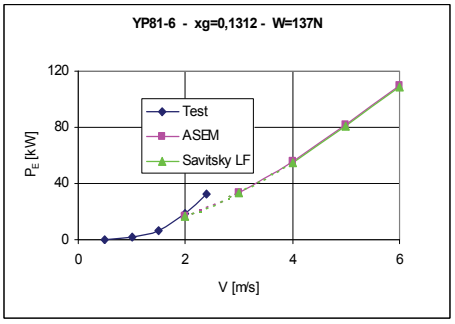

[b]

Figure 13.6-41 Data Comparison: Model YP81-6 - xg=0.1312 - W=137N

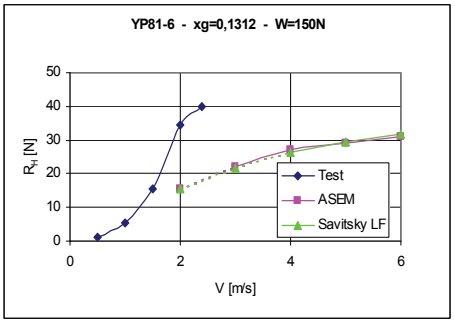

[a]

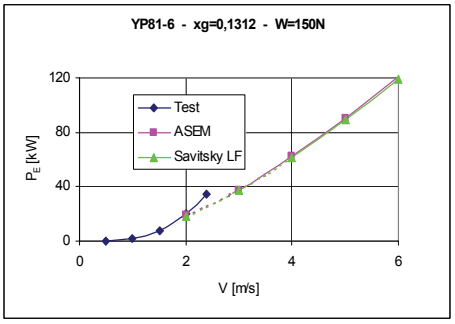

[b]

Figure 13.6-42 Data Comparison: Model YP81-6 - xg=0.1312 - W=150N

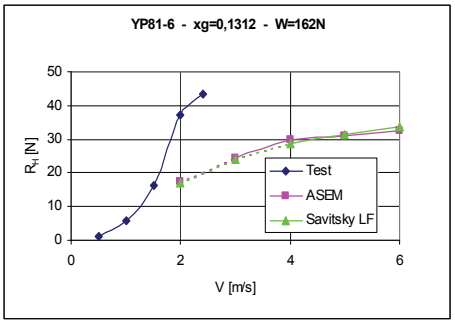

[a]

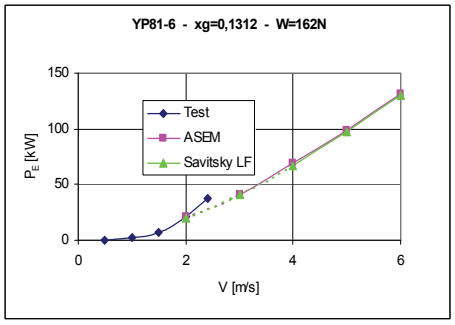

[b]

Figure 13.6-43 Data Comparison: Model YP81-6 - xg=0.1312 - W=162N

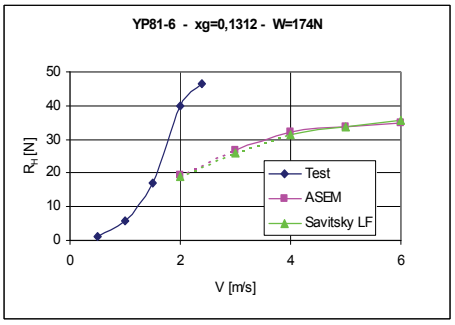

[a]

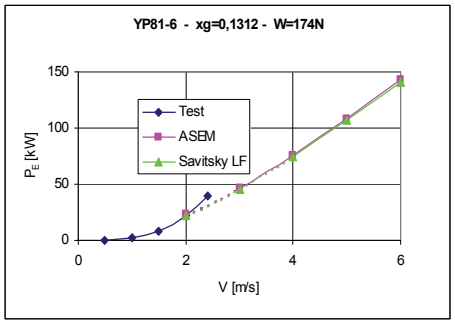

[b]

Figure 13.6-44 Data Comparison: Model YP81-6 - xg=0.1312 - W=174N

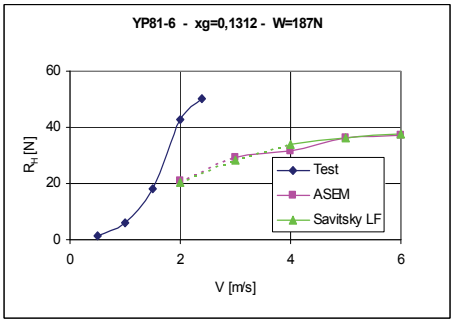

[a]

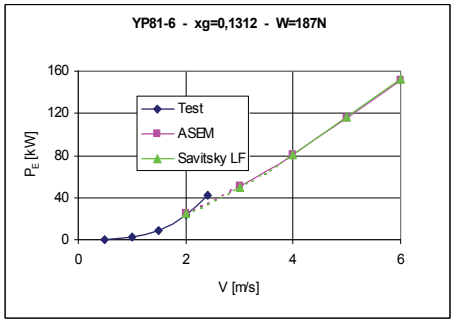

[b]

Figure 13.6-45 Data Comparison: Model YP81-6 - xg=0.1312 - W=187N

13.7 Remarks on Data Comparison

A first look shows us a common trend of ASEM results and Savitsky's ones.

At the same time computed results (ASEM & Savitsky) are quite different versus test results.

For $x_g \leq 0.0778$ no comparison is achievable: max speed of test results is lower than minimum speed of computed results (computed results with no physical meaning have been neglected).

For $x_g = 0.1312$ computed results at low speed are not negligible anymore, but at the same time they are "out of range" (data reported with dash line) and comparison is not achievable too.

13.8 Conclusion

Despite Systematic Series YP81 are not planing hulls, Analytical Semi-Empirical Method (ASEM) has been applied to these non-monohedral models in order to check reliability and efficiency in semi-planing field.

Further, Savitsky‘s method has been applied too, in order to get an overall comparison.

Models of Systematic Series YP81 are semi-planing transom-stern hulls with deadrise variable longitudinally, along the keel. Series YP81 is composed by six hulls: the first three are soft-chines hulls meanwhile the last three are the hard-chine counterparts of soft-chine models.

On a total of 54 test cases developed, only 27 test results, associated to hard-chine hulls, have been taken in account and rearranged in order to achieve a data comparison with computed results related to speed up to planing condition.

In all cases analyzed, at low speed, no comparison among test results and computed results is achievable.

Some remarks on the matters are hereinafter proposed.

Buoyancy, in the Savitsky’s method, is treated as an “add-on” of the dynamic lift: its value has a degree of approximation higher than dynamic lift value[142]. Taking in mind that in the low speed range buoyancy and dynamic lift have the same magnitude, it follows: higher approximation on buoyancy higher error on total lift computed.

A second remark is pertinent to the bare hull resistance. Savitsky’s method does not take in account some components of resistance. One of these is the wave resistance component that is negligible at high speed (planing condition), but at low speed (up to semi-planing condition) it is not negligible too[143].

This drive to a “mismatch” between computed and test results not negligible: Savitsky’s method as well as ASEM are not applicable to hull forms optimized for work only up to semi-planing field.

---

[142] See Appendix F on the matter.
[143] See Chapter 1, Paragraph 1.4.4.2 “Semi-empirical approaches”.

13.9 Symbols

AP	After Perpendicular	
BM_L	Longitudinal metacentric radius	[m]
B_{REF}	Beam at waterline	[m]
C_B	Block coefficient	
C_P	Prismatic coefficient	
C_{WP}	Waterplane coefficient	
	Centerline	
Fn	Froude number related to the waterline length	$Fn = \frac{V}{\sqrt{gL_{WL}}}$
FP	Fore Perpendicular	
g	Acceleration of gravity	$\left[m/s^2\right]$
i_e	Half angle of entrance	[deg]
KM_T	Height of transverse metacenter above keel	[m]
LCB	Longitudinal distance from amidships to center of buoyancy	[m]
L_{CG}	Longitudinal center of gravity location	[m]
LF	Long Form	
L_{PP}	Length between perpendiculars	[m]
L_{WL}	Length on waterline	[m]
P_E	Effective Power of bare hull	[W]
R_H	Bare hull resistance	[N]
T	Draft	[m]
V	Hull speed	$\left[m/s\right]$
W	Weight of hull	[N]
x_g	Longitudinal distance from amidships to center of gravity related to the hull length	$x_g = X_g / L_{PP}$
X_g	Longitudinal distance from amidships to center of gravity, positive in stern direction	[m]
$\{x, y, z\}$	Geometrical coordinates	
β_{10}	Deadrise angle at transom	[deg]
	Displacement-length ratio	$\left[LTWS/ft^3\right]$
d	Volume of displacement at rest	$\left[m^3\right]$
s	Wetted Surface Area - displaced volume ratio	$s = WSA/\nabla^{2/3}$

13.10 References

Bertorello, C. & Oliviero, L. 2007. Hydrodynamic Resistance Assessment of Non-Monohedral Planing Hull Forms based on Savitsky's Method. *Australian Journal of Mechanical Engineering,* Vol. 4 No.2, pp 209-224. Engineers Media, CROWS NEST, Australia. (ACN001311511).

Compton R.H. 1986. Resistance of systematic series of semi-planing transom stern hulls. *Marine Technology*, Vol.23, No.4, Jersey City (USA): SNAME

Savitsky, D. 1964. Hydrodynamic Design of Planing Hull. *Marine Technology*, Vol.1, No.1, Jersey City (USA): SNAME

APPENDIX J

ERROR PROPAGATION

ANALYSIS

14.1 Table of Contents

14.2 Figure Index

14.3 Table Index

14.4 Introduction

Analytical Semi-Empirical Method (ASEM) has been developed in order to predict Resistance and Power performance versus hull speed related to a warped bare monohull. [Bertorello & Oliviero 2007]

In this chapter the Error Propagation Analysis will be applied to ASEM as well as Savitsky's method, in order to check reliability and efficiency in term of magnitude of errors related to results.

Error Propagation Theory explanation is not the goal of this thesis.

The aim of this analysis is to evaluate the sensitivity of these methods. The sensitivity is assessed as relative error on the bare hull resistance ε_{R_H} .

Error formulas will be calculated through Differential Analysis tools.

14.5 Error Propagation Model

Hereinafter the "uncertain size" of a input parameter will be the unit variation of the smallest significant figure. The "uncertain range" is the range within the value of the parameter is included.

Further, the relative error related to a parameter will be defined as the half of the ratio between uncertain and value of the considered parameter.

As example, the relative error related to the speed is:

Parameter value: $V = 25.7\,m/s$

Smallest significant value: $0.7\,m/s$

Uncertainty: $\partial V = 0.1\,m/s$

Uncertain range $25.65\frac{m}{s} \le V \le 25.75\frac{m}{s}$

Relative error: $\varepsilon_V = \frac{0.05\,{}^{m}/_{s}}{25.7\,{}^{m}/_{s}} = 1.95 \cdot 10^{-3}$

According to the above definitions, each parameter has a defined and constant uncertainty, which magnitude is the same for all parameter values, meanwhile the relative error is related to the mean parameter value too.

Thereby two different values of a parameter present the same uncertainty but two different relative errors.

Differential Analysis tools have been applied in order to define the relationships useful to compute the relative error of each computed parameter.

The explanation of these math tools is not the goal of this thesis.

It is important to remark that Differential Analysis formulas are tools useful to compute the max value expected of each relative error. The real value achieved could be quite lower than the above one.

According to this observation both value will be reported.

14.6 Error formulas

14.6.1 Savitsky's LF Method

14.6.1.1 Froude number C_V

$$\boxed{C_V = \frac{V}{\sqrt{gB_C}}}$$

$$(\pm\partial C_V) = \frac{1}{gB_C}\left\{(gB_C)^{1/2}(\pm\partial V) - \frac{V}{2}(gB_C)^{-1/2}\left[B_C(\pm\partial g) + g(\pm\partial B_C)\right]\right\}$$

$$\frac{\pm\partial C_V}{C_V} = \frac{\pm\partial V}{V} - \frac{1}{2}\left(\frac{\pm\partial g}{g} + \frac{\pm\partial B_C}{B_C}\right)$$

$$\pm\varepsilon_{C_V} = (\pm\varepsilon_V) - \frac{1}{2}\left[(\pm\varepsilon_g) + (\pm\varepsilon_{B_C})\right]$$

$$\boxed{\varepsilon_{C_V} = \varepsilon_V + \frac{1}{2}(\varepsilon_g + \varepsilon_{B_C})}$$

14.6.1.2 Lift coefficient $C_{L\beta}$

$$\boxed{C_{L\beta} = \frac{W}{\frac{1}{2}\rho V^2 B_C^2}}$$

$$(\pm\partial C_{L\beta}) = \frac{(\pm\partial W)\left(\frac{1}{2}\rho V^2 B_C^2\right) - \frac{1}{2}W\left[(\pm\partial\rho)V^2 B_C^2 + \rho 2V(\pm\partial V)B_C^2 + \rho V^2 2B_C(\pm\partial B_C)\right]}{\left(\frac{1}{2}\rho V^2 B_C^2\right)^2}$$

$$\frac{\pm\partial C_{L\beta}}{C_{L\beta}} = \frac{\pm\partial W}{W} - \frac{\pm\partial\rho}{\rho} - 2\frac{\pm\partial V}{V} - 2\frac{\pm\partial B_C}{B_C}$$

$$(\pm\varepsilon_{C_{L\beta}}) = (\pm\varepsilon_W) - (\pm\varepsilon_\rho) - 2(\pm\varepsilon_V) - 2(\pm\varepsilon_{B_C})$$

$$\boxed{\varepsilon_{C_{L\beta}} = \varepsilon_W + \varepsilon_\rho + 2\varepsilon_V + 2\varepsilon_{B_C}}$$

14.6.1.3 Lift coefficient zero deadrise C_{L0}

$$\boxed{C_{L\beta} = C_{L0} - 0.0065\,\beta\,C_{L0}^{0.6}}$$

$$\left(\pm\partial C_{L\beta}\right) = \left(\pm\partial C_{L0}\right) - 0.0039\,\beta\,C_{L0}^{-0.4}\left(\pm\partial C_{L0}\right) - 0.0065\,C_{L0}^{0.6}\left(\pm\partial\beta\right)$$

$$\left(\pm\partial C_{L\beta}\right) = \left(1 - 0.0039\,\beta\,C_{L0}^{-0.4}\right)\left(\pm\partial C_{L0}\right) - 0.0065\,C_{L0}^{0.6}\left(\pm\partial\beta\right)$$

$$\left(\pm\partial C_{L0}\right) = \frac{\left(\pm\partial C_{L\beta}\right) + 0.0065\,C_{L0}^{0.6}\left(\pm\partial\beta\right)}{1 - 0.0039\,\beta\,C_{L0}^{-0.4}}$$

$$\left(\pm\varepsilon_{C_{L0}}\right) = \frac{C_{L\beta}\cdot\left(\pm\varepsilon_{C_{L\beta}}\right) + \left(0.0065\,\beta\,C_{L0}^{0.6}\right)\cdot\left(\pm\varepsilon_{\beta}\right)}{C_{L0}\cdot\left(1 - 0.0039\,\beta\,C_{L0}^{-0.4}\right)}$$

$$\boxed{\varepsilon_{C_{L0}} = \frac{C_{L\beta}\cdot\varepsilon_{C_{L\beta}} + \left(0.0065\,\beta\,C_{L0}^{0.6}\right)\cdot\varepsilon_{\beta}}{C_{L0}\cdot\left(1 - 0.0039\,\beta\,C_{L0}^{-0.4}\right)}}$$

14.6.1.4 Length-beam ratio λ

$$\boxed{C_{L0} = \tau^{1.1}\left(0.0120\lambda^{1/2} + 0.0055\frac{\lambda^{2.5}}{C_V^2}\right)}$$

$$\left(\pm\partial C_{L0}\right) = 1.1\tau^{0.1}\left(\pm\partial\tau\right)\left(0.012\,\lambda^{1/2} + 0.0055\frac{\lambda^{2.5}}{C_V{}^2}\right) +$$

$$+\tau^{1.1}\left[0.006\,\lambda^{-1/2}\left(\pm\partial\lambda\right) + \frac{0.0055}{C_V^4}\left(2.5\,\lambda^{1.5}\,C_V^2\left(\pm\partial\lambda\right) - 2\,\lambda^{2.5}\,C_V\left(\pm\partial C_V\right)\right)\right]$$

$$\left(\frac{\pm\partial C_{L0}}{C_{L0}}\right) = 1.1\left(\frac{\pm\partial\tau}{\tau}\right) + \frac{1}{C_{L0}}\tau^{1.1}\left[\left(0.006\,\lambda^{1/2} + \frac{0.01375\,\lambda^{2.5}}{C_V^2}\right)\left(\frac{\pm\partial\lambda}{\lambda}\right) - \frac{0.0110\,\lambda^{2.5}}{C_V^2}\left(\frac{\pm\partial C_V}{C_V}\right)\right]$$

$$\left(\frac{\pm\partial\lambda}{\lambda}\right) = \frac{\left[\left(\frac{\pm\partial C_{L0}}{C_{L0}}\right) - 1.1\left(\frac{\pm\partial\tau}{\tau}\right)\right]\frac{C_{L0}}{\tau^{1.1}} + \frac{0.0110\,\lambda^{2.5}}{C_V^2}\left(\frac{\pm\partial C_V}{C_V}\right)}{0.006\,\lambda^{1/2} + \frac{0.01375\,\lambda^{2.5}}{C_V^2}}$$

$$\left(\pm\varepsilon_{\lambda}\right) = \frac{\left[\left(\pm\varepsilon_{C_{L0}}\right) - 1.1\cdot\left(\pm\varepsilon_{\tau}\right)\right]\frac{C_{L0}}{\tau^{1.1}} + \frac{0.0110\,\lambda^{2.5}}{C_V^2}\left(\pm\varepsilon_{C_V}\right)}{0.006\,\lambda^{1/2} + \frac{0.01375\,\lambda^{2.5}}{C_V^2}}$$

$$\varepsilon_\lambda = \frac{\left(\varepsilon_{C_{L0}} + 1.1 \cdot \varepsilon_\tau\right)\frac{C_{L0}}{\tau^{1.1}} + \frac{0.0110\,\lambda^{2.5}}{C_V^2}\varepsilon_{C_V}}{0.006\,\lambda^{1/2} + \frac{0.01375\,\lambda^{2.5}}{C_V^2}}$$

14.6.1.5 Corrected length-beam ratio λ_F

$$\lambda_F = \lambda + \Delta\lambda$$

$$\left(\pm\partial\lambda_F\right) = \partial\lambda + \partial\Delta\lambda$$

$$\frac{\left(\pm\partial\lambda_F\right)}{\lambda_F} = \frac{\lambda}{\lambda_F}\left(\frac{\pm\partial\lambda}{\lambda}\right) + \frac{\Delta\lambda}{\lambda_F}\left(\frac{\pm\partial\Delta\lambda}{\Delta\lambda}\right)$$

$$\left(\pm\varepsilon_{\lambda_F}\right) = \frac{\lambda}{\lambda_F}\left(\pm\varepsilon_\lambda\right) + \frac{\Delta\lambda}{\lambda_F}\left(\pm\varepsilon_{\Delta\lambda}\right)$$

$$\varepsilon_{\lambda_F} = \frac{\lambda}{\lambda_F}\varepsilon_\lambda + \frac{\Delta\lambda}{\lambda_F}\varepsilon_{\Delta\lambda}$$

14.6.1.6 Mean wetted length L_{WS}

$$L_{WS} = \lambda_F\, B_C$$

$$\left(\pm\partial\mathrm{L_{WS}}\right) = \left(\pm\partial\lambda_F\right)B_C + \lambda_F\left(\pm\partial B_C\right)$$

$$\frac{\left(\pm\partial\mathrm{L_{WS}}\right)}{\mathrm{L_{WS}}} = \frac{\left(\pm\partial\lambda_F\right)}{\lambda_F} + \frac{\left(\pm\partial B_C\right)}{B_C}$$

$$\left(\pm\varepsilon_{L_{WS}}\right) = \left(\pm\varepsilon_{\lambda_F}\right) + \left(\pm\varepsilon_{B_C}\right)$$

$$\varepsilon_{L_{WS}} = \varepsilon_{\lambda_F} + \varepsilon_{B_C}$$

14.6.1.7 Mean velocity over bottom of hull V_m

$$V_m = \left(\frac{V_m}{V}\right)V$$

$$\left(\pm\partial V_m\right) = V\left[\pm\partial\left(\frac{V_m}{V}\right)\right] + \frac{V_m}{V}\left(\pm\partial V\right)$$

$$\frac{\partial V_m}{V_m} = \frac{\left[\pm\partial\left(V_m \diagup V\right)\right]}{V_m \diagup V} + \frac{(\pm\partial V)}{V}$$

$$\left(\pm\varepsilon_{V_m}\right) = \left(\pm\varepsilon_{\frac{V_m}{V}}\right) + \left(\pm\varepsilon_V\right)$$

$$\boxed{\varepsilon_{V_m} = \varepsilon_{\frac{V_m}{V}} + \varepsilon_V}$$

14.6.1.8 Reynolds number R_n

$$\boxed{R_n = \frac{V_m B_C \lambda_F}{\nu}}$$

$$\left(\pm\partial R_n\right) = \frac{1}{\nu^2}\left\{\left[B_C\lambda_F\left(\pm\partial V_m\right) + V_m\lambda_F\left(\pm\partial B_C\right) + V_m B_C\left(\pm\partial\lambda_F\right)\right]\nu - V_m B_C\lambda_F\left(\pm\partial\nu\right)\right\}$$

$$\frac{\left(\pm\partial R_n\right)}{R_n} = \frac{\left(\pm\partial V_m\right)}{V_m} + \frac{\left(\pm\partial B_C\right)}{B_C} + \frac{\left(\pm\partial\lambda_F\right)}{\lambda_F} - \frac{\left(\pm\partial\nu\right)}{\nu}$$

$$\left(\pm\varepsilon_{R_n}\right) = \left(\pm\varepsilon_{V_m}\right) + \left(\pm\varepsilon_{B_C}\right) + \left(\pm\varepsilon_{\lambda_F}\right) - \left(\pm\varepsilon_\nu\right)$$

$$\boxed{\varepsilon_{R_n} = \varepsilon_{V_m} + \varepsilon_{B_C} + \varepsilon_\nu + \varepsilon_{\lambda_F}}$$

14.6.1.9 Schoenherr friction line C_f

$$\boxed{\frac{0.242}{C_f^{1/2}} = Log\left(R_n C_f\right)}$$

$$-0.121\frac{\left(\pm\partial C_f\right)}{C_f^{3/2}} = \frac{1}{\lg 10}\left[\frac{\left(\pm\partial R_n\right)}{R_n} + \frac{\left(\pm\partial C_f\right)}{C_f}\right]$$

$$\frac{-0.121}{C_f^{1/2}}\left(\pm\varepsilon_{C_f}\right) = \frac{1}{\lg 10}\left[\left(\pm\varepsilon_{R_n}\right) + \left(\pm\varepsilon_{C_f}\right)\right]$$

$$\left(\pm\varepsilon_{C_f}\right) = \frac{1}{-1 - \frac{0.121\cdot\lg 10}{C_f^{1/2}}}\left(\pm\varepsilon_{R_n}\right)$$

$$\boxed{\varepsilon_{C_f} = \frac{C_f^{1/2}}{C_f^{1/2} + 0.121\cdot\lg 10}\varepsilon_{R_n}}$$

14.6.1.10 Corrected friction coefficient C_F

$$\boxed{C_F = C_f + \Delta C_F}$$

$$\left(\pm \partial C_F\right) = \left(\pm \partial C_f\right) + \left(\pm \partial \Delta C_F\right)$$

$$\frac{\pm \partial C_F}{C_F} = \frac{C_f}{C_F}\left(\frac{\pm \partial C_f}{C_f}\right) + \frac{\Delta C_F}{C_F}\left(\frac{\pm \partial \Delta C_F}{\Delta C_F}\right)$$

$$\left(\pm \varepsilon_{C_F}\right) = \frac{C_f}{C_F}\left(\pm \varepsilon_{C_f}\right) + \frac{\Delta C_F}{C_F}\left(\pm \varepsilon_{\Delta C_F}\right)$$

$$\boxed{\varepsilon_{C_F} = \frac{C_f}{C_F}\varepsilon_{C_f} + \frac{\Delta C_F}{C_F}\varepsilon_{\Delta C_F}}$$

14.6.1.11 Viscous component of drag D_F

$$\boxed{D_F = \frac{1}{2}\rho V_m^2 \frac{\lambda_F B_C^2}{\cos\beta} C_F}$$

$$\pm \partial D_F = \frac{1}{4\cos^2\beta}\left\{2\cos\beta\left(\rho\lambda_F V_m^2 B_C^2 C_F\right)\left[\frac{\pm\partial\rho}{\rho} + \frac{\pm\partial\lambda_F}{\lambda_F} + 2\frac{\pm\partial V_m}{V_m} + 2\frac{\pm\partial B_C}{B_C} + \frac{\pm\partial C_F}{C_F}\right]\right\} +$$

$$-\frac{1}{4\cos^2\beta}\left\{2\cos\beta\left(\rho\lambda_F V_m^2 B_C^2 C_F\right)\left[\beta\cdot tg\beta\frac{\pm\partial\beta}{\beta}\right]\right\}$$

$$\left(\pm \varepsilon_{D_F}\right) = \left(\pm \varepsilon_\rho\right) + \left(\pm \varepsilon_{\lambda_F}\right) + 2\left(\pm \varepsilon_{V_m}\right) + 2\left(\pm \varepsilon_{B_C}\right) + \left(\pm \varepsilon_{C_F}\right) - \left[\left(\beta\cdot tg\beta\right)\left(\pm \varepsilon_\beta\right)\right]$$

$$\boxed{\varepsilon_{D_F} = \varepsilon_\rho + \varepsilon_{\lambda_F} + 2\varepsilon_{V_m} + 2\varepsilon_{B_C} + \varepsilon_{C_F} + \left(\beta\cdot tg\beta\right)\varepsilon_\beta}$$

14.6.1.12 Bare hull resistance R_H

$$\boxed{R_H = \frac{D_F}{\cos\beta} + W tg\tau}$$

$$\left(\pm \partial R_H\right) = \frac{\left(\pm \partial D_F\right)\cos\beta + D_F\, sen\beta\left(\pm\partial\beta\right)}{\cos^2\beta} + \left(\pm\partial W\right)tg\tau + \frac{W}{\cos^2\tau}\left(\pm\partial\tau\right)$$

$$\frac{\left(\pm \partial R_H\right)}{R_H} = \frac{D_F \diagup \cos\beta}{R_H}\left[\frac{\left(\pm\partial D_F\right)}{D_F} + tg\beta\left(\pm\partial\beta\right)\right] + \frac{W}{R_H}\left[tg\tau\frac{\left(\pm\partial W\right)}{W} + \frac{\left(\pm\partial\tau\right)}{\cos^2\tau}\right]$$

$$\left(\pm \varepsilon_{R_H}\right) = \frac{D_F \diagup \cos\beta}{R_H}\left[\left(\pm \varepsilon_{D_F}\right) + \beta\, tg\beta\cdot\left(\pm\varepsilon_\beta\right)\right] + \frac{W}{R_H}\left[tg\tau\cdot\left(\pm\varepsilon_W\right) + \frac{\tau}{\cos^2\tau}\left(\pm\varepsilon_\tau\right)\right]$$

$$\varepsilon_{R_H} = \frac{D_F / \cos\beta}{R_H}\left(\varepsilon_{D_F} + \beta\, tg\beta \cdot \varepsilon_\beta\right) + \frac{W}{R_H}\left(tg\tau \cdot \varepsilon_W + \frac{\tau}{\cos^2\tau}\varepsilon_\tau\right)$$

14.6.2 ASEM

14.6.2.1 Froude number C_V

$$C_V = \frac{V}{\sqrt{gB_C}}$$

$$\varepsilon_{C_V} = \varepsilon_V + \frac{1}{2}\left(\varepsilon_g + \varepsilon_{B_C}\right)$$

14.6.2.2 Lift coefficient $C_{L\beta}$

$$C_{L\beta} = \frac{W}{\frac{1}{2}\rho V^2 B_C^2}$$

$$\varepsilon_{C_{L\beta}} = \varepsilon_W + \varepsilon_\rho + 2\varepsilon_V + 2\varepsilon_{B_C}$$

14.6.2.3 Lift coefficient zero deadrise C_{L0} of i^{th} strip

$$C_{L\beta} = \left({}^iC_{L0}\right) - 0.0065 \cdot \left({}^i\beta\right) \cdot \left({}^iC_{L0}\right)^{0.6}$$

$${}^i\varepsilon_{C_{L0}} = \frac{\left({}^iC_{L0} - C_{L\beta}\right) \cdot \left({}^i\varepsilon_\beta\right) + C_{L\beta} \cdot \varepsilon_{C_{L\beta}}}{0.4 \cdot \left({}^iC_{L0}\right) + 0.6 \cdot C_{L\beta}}$$

14.6.2.4 Length-beam ratio λ of i^{th} strip

$${}^i\left(\frac{C_{L0}}{\tau^{1.1}}\right) = \left(0.0120 \cdot \left({}^i\lambda\right)^{1/2} + 0.0055 \cdot \frac{\left({}^i\lambda\right)^{2.5}}{C_V^2}\right)$$

$${}^i\varepsilon_\lambda = \frac{\left[\left({}^i\varepsilon_{C_{L0}}\right) + 1.1 \cdot \left({}^i\varepsilon_\tau\right)\right] \cdot {}^i\left(\frac{C_{L0}}{\tau^{1.1}}\right) + \frac{0.0110\left({}^i\lambda\right)^{2.5}}{C_V^2}\varepsilon_{C_V}}{0.006 \cdot \left({}^i\lambda\right)^{1/2} + \frac{0.01375 \cdot \left({}^i\lambda\right)^{2.5}}{C_V^2}}$$

14.6.2.5 Longitudinal Center of Pressure position to mean wetted length ratio L_{CP}/L_{WS} of i^{th} strip

$$ {}^{i}\left(\frac{L_{CP}}{L_{WS}}\right) = 0.75 - \frac{1}{5.21\cdot\left[\frac{C_V}{\left({}^{i}\lambda\right)}\right]^2 + 2.39} $$

$$ {}^{i}\varepsilon_{\frac{L_{CP}}{L_{WS}}} = \frac{10.42\cdot\left(\frac{C_V}{{}^{i}\lambda}\right)^2}{\left\{5.21\cdot\left[\frac{C_V}{\left({}^{i}\lambda\right)}\right]^2 + 2.39\right\}\cdot\left\{3.91\cdot\left[\frac{C_V}{\left({}^{i}\lambda\right)}\right]^2 + 0.79\right\}}\left[\varepsilon_{C_V} + \left({}^{i}\varepsilon_{\lambda}\right)\right] $$

14.6.2.6 Wagner's Pressure Coefficient C_P of i^{th} strip

$$ {}^{i}C_P(\xi) = 1 - \left[\frac{\xi - \cos\left({}^{i}\tau\right)}{1 - \xi\cos\left({}^{i}\tau\right) + \sin\left({}^{i}\tau\right)\sqrt{1-\xi^2}}\right]^2 $$

$$ {}^{i}\varepsilon_{C_P} = \sqrt{1-{}^{i}C_P}\left\{\left[\frac{1}{1-\xi^2} + \frac{\sqrt{1-\left({}^{i}C_P\right)}}{\xi - \cos\left({}^{i}\tau\right)}\right]\cdot\xi\cdot\varepsilon_{\xi} + \frac{\left({}^{i}\tau\right)}{\sin\left({}^{i}\tau\right)}\left({}^{i}\varepsilon_{\tau}\right)\right\} $$

14.6.2.7 Normalized Pressure Coefficient C_P^n of i^{th} strip

$$ {}^{i}C_P^n(\xi) = \frac{{}^{i}C_P(\xi)}{{}^{i}C_{P,\max}} $$

$$ {}^{i}\varepsilon_{C_P^n} = \left({}^{i}\varepsilon_{C_P}\right) + \left({}^{i}\varepsilon_{C_{P,\max}}\right) $$

14.6.2.8 Longitudinal Center of Pressure position to mean wetted length ratio L_{CP}/L_{WS}

$$ \frac{L_{CP}}{L_{WS}} = \frac{\sum_i\left[{}^{i}\left(\frac{L_{CP}}{L_{WS}}\right)\left({}^{i}C_P^{\,n}\right)\right]}{\sum_i\left({}^{i}C_P^{\,n}\right)} $$

$$\varepsilon_{\frac{L_{CP}}{L_{WS}}} = \frac{\sum_i \left[{}^i\left(\frac{L_{CP}}{L_{WS}}\right)\left({}^iC_P^n\right)\left({}^i\varepsilon_{L_{CP}/L_{WS}}\right)\right] + \sum_i \left[{}^i\left(\frac{L_{CP}}{L_{WS}}\right)\left({}^iC_P^n\right)\left({}^i\varepsilon_{C_P^n}\right)\right]}{\sum_i \left[{}^i\left(\frac{L_{CP}}{L_{WS}}\right)\left({}^iC_P^n\right)\right]} + \frac{\sum_i \left[\left({}^iC_P^n\right)\left({}^i\varepsilon_{C_P^n}\right)\right]}{\sum_i \left({}^iC_P^n\right)}$$

14.6.2.9 Length-beam ratio λ

$$\left(\frac{L_{CP}}{L_{WS}}\right) = 0.75 - \frac{1}{5.21 \cdot \left(\frac{C_V}{\lambda}\right)^2 + 2.39}$$

$$\varepsilon_\lambda = \frac{\left[5.21 \cdot \left(\frac{C_V}{\lambda}\right)^2 + 2.39\right] \cdot \left[3.91 \cdot \left(\frac{C_V}{\lambda}\right)^2 + 0.79\right]}{10.42 \cdot \left(\frac{C_V}{\lambda}\right)^2} \cdot \varepsilon_{L_{CP}/L_{WS}} + \varepsilon_{C_V}$$

14.6.2.10 $C_{L0}/\tau^{1.1}$ ratio

$$\frac{C_{L0}}{\tau^{1.1}} = 0.012\lambda^{1/2} + 0.0055\frac{\lambda^{2.5}}{C_V^2}$$

$$\varepsilon_{\left(\frac{C_{L0}}{\tau^{1.1}}\right)} = \frac{\left(0.006\lambda^{1/2} + 0.01375\frac{\lambda^{2.5}}{C_V^2}\right)\varepsilon_\lambda + 0.011\frac{\lambda^{2.5}}{C_V^2}\varepsilon_{C_V}}{\left(C_{L0}/\tau^{1.1}\right)}$$

14.6.2.11 Lift coefficient zero deadrise C_{L0}

$$C_{L0} = \left(\frac{C_{L0}}{\tau^{1.1}}\right) \cdot \tau^{1.1}$$

$$\varepsilon_{C_{L0}} = \varepsilon_{C_{L0}/\tau^{1.1}} + 1.1 \cdot \varepsilon_\tau$$

14.6.2.12 Deadrise angle β

$$C_{L\beta} = C_{L0} - 0.0065\,\beta\,C_{L0}^{0.6}$$

$$\varepsilon_\beta = \frac{1}{C_{L0} - C_{L\beta}} \left[\left(0.4 C_{L0} + 0.6 C_{L\beta} \right) \varepsilon_{C_{L0}} + C_{L\beta} \varepsilon_{C_{L\beta}} \right]$$

14.6.2.13 Corrected length-beam ratio λ_F

$$\lambda_F = \lambda + \Delta\lambda$$

$$\varepsilon_{\lambda_F} = \frac{\lambda}{\lambda_F} \varepsilon_\lambda + \frac{\Delta\lambda}{\lambda_F} \varepsilon_{\Delta\lambda}$$

14.6.2.14 Mean wetted length L_{WS}

$$L_{WS} = \lambda_F \, B_C$$

$$\varepsilon_{L_{WS}} = \varepsilon_{\lambda_F} + \varepsilon_{B_C}$$

14.6.2.15 Mean velocity over bottom of hull V_m

$$V_m = \left(\frac{V_m}{V} \right) V$$

$$\varepsilon_{V_m} = \varepsilon_{\frac{V_m}{V}} + \varepsilon_V$$

14.6.2.16 Reynolds number R_n

$$R_n = \frac{V_m B_C \lambda_F}{\nu}$$

$$\varepsilon_{R_n} = \varepsilon_{V_m} + \varepsilon_{B_C} + \varepsilon_\nu + \varepsilon_{\lambda_F}$$

14.6.2.17 Schoenherr friction line C_f

$$\frac{0.242}{C_f^{1/2}} = Log\left(R_n C_f \right)$$

$$\varepsilon_{C_f} = \frac{C_f^{1/2}}{C_f^{1/2} + 0.121 \cdot \lg 10} \varepsilon_{R_n}$$

14.6.2.18 Corrected friction coefficient C_F

$$C_F = C_f + \Delta C_F$$

$$\varepsilon_{C_F} = \frac{C_f}{C_F}\varepsilon_{C_f} + \frac{\Delta C_F}{C_F}\varepsilon_{\Delta C_F}$$

14.6.2.19 Viscous component of drag D_F

$$D_F = \frac{1}{2}\rho V_m^2 \frac{\lambda_F B_C^2}{\cos\beta} C_F$$

$$\varepsilon_{D_F} = \varepsilon_\rho + \varepsilon_{\lambda_F} + 2\varepsilon_{V_m} + 2\varepsilon_{B_C} + \varepsilon_{C_F} + (\beta \cdot tg\beta)\varepsilon_\beta$$

14.6.2.20 Bare hull resistance R_H

$$R_H = \frac{D_F}{\cos\beta} + W tg\tau$$

$$\varepsilon_{R_H} = \frac{D_F / \cos\beta}{R_H}\left(\varepsilon_{D_F} + \beta\, tg\beta \cdot \varepsilon_\beta\right) + \frac{W}{R_H}\left(tg\tau \cdot \varepsilon_W + \frac{\tau}{\cos^2\tau}\varepsilon_\tau\right)$$

14.7 Errors, Uncertainties and Results

Hereinafter diagrams of bare hull resistance (R_H), uncertainties (∂R_H) and relative errors (εR_H), versus hull speed V, are presented. ASEM results are reported in black as well as Savitsky's results in red. In diagrams of results, minimum value points as well as maximum ones represent the border lines of the uncertain field.

ASEM and Savitsky's results without physical meaning have not been taken in account (i.e.: results related to a mean wetted length higher than hull length overall), meanwhile results with physical meaning coupled with data out of range have been reported with tiny dash line (i.e.: results related to a mean wetted length/beam ratio higher than four times).

Per each Series, geometrical and mechanical data input are reported in the Appendix pertinent to, as shown in following table:

Table 14.7-1 Series Analyzed

SERIES	APPENDIX
62	G
BK	H
YP81	I

Test results available related to Series BK, and reported in Appendix H, are presented in dimensionless form. This is not useful to a direct match with data here available. Consequently, for only Series BK, test results in dimensional will be here reported.

14.7.1 Series 62

14.7.1.1 Model 4665

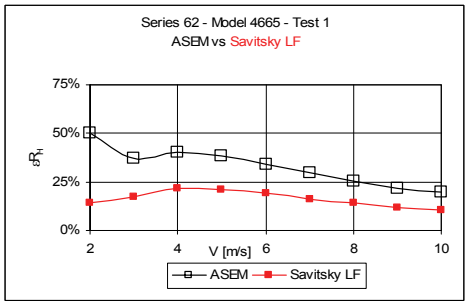

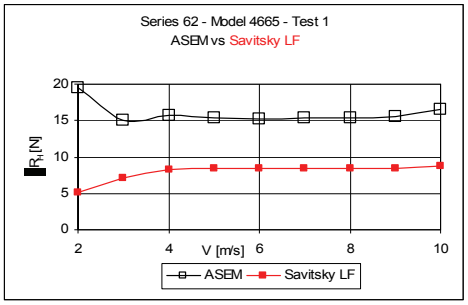

[a]

[b]

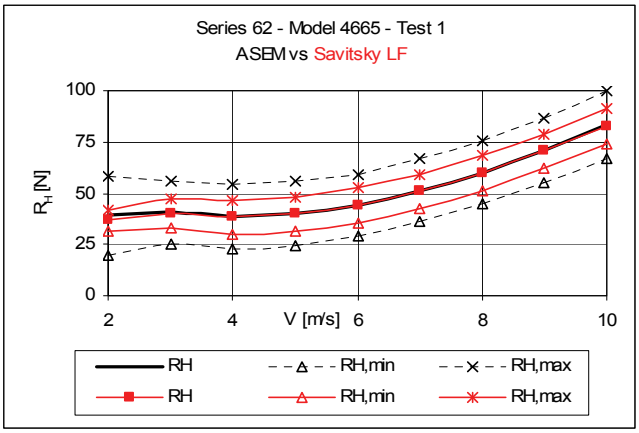

[c]

Figure 14.7-1 Model 4665 - Test 1

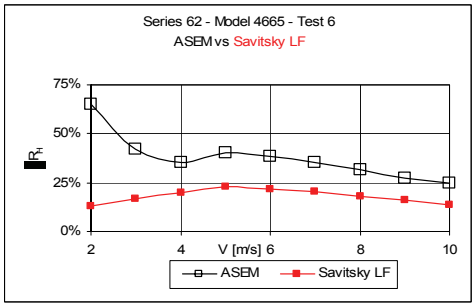

[a]

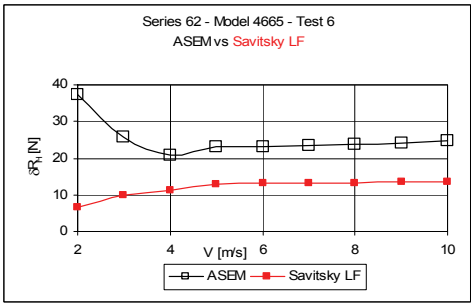

[b]

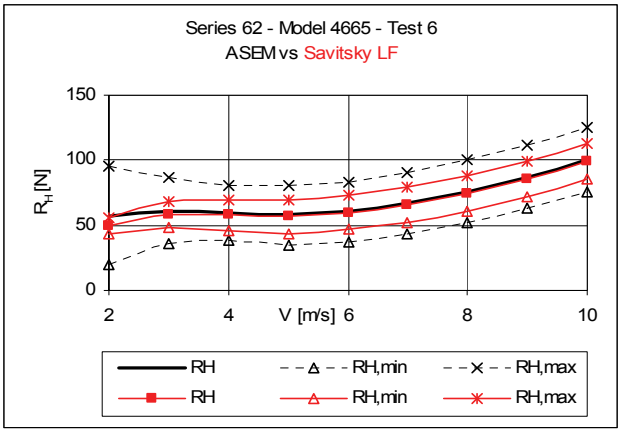

[c]

Figure 14.7-2 Model 4665 - Test 6

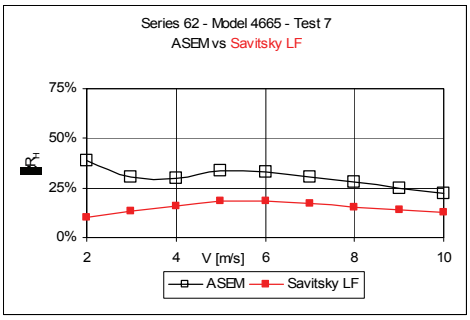

[a]

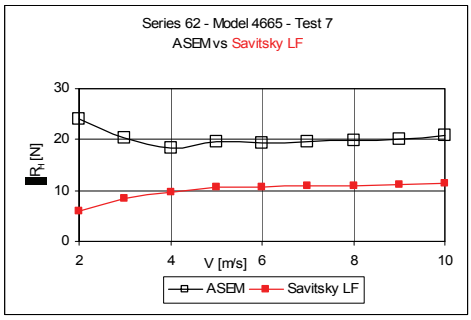

[b]

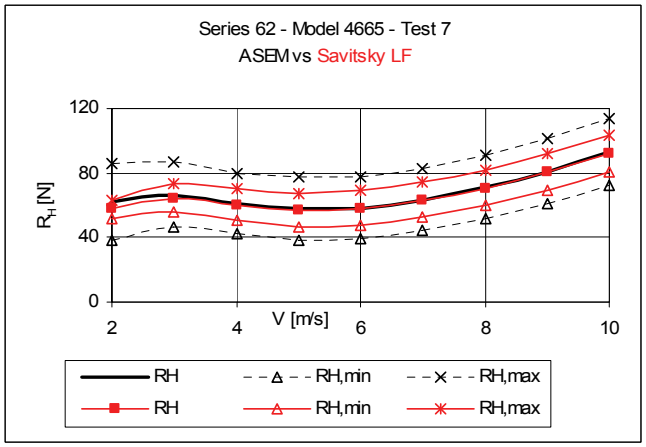

[c]

Figure 14.7-3 Model 4665 - Test 7

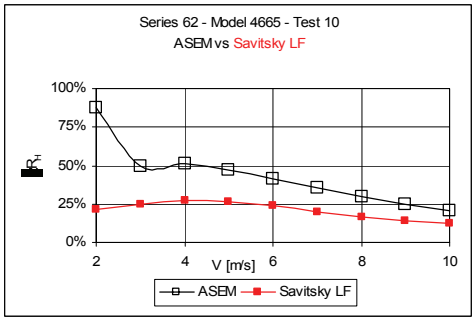

[a]

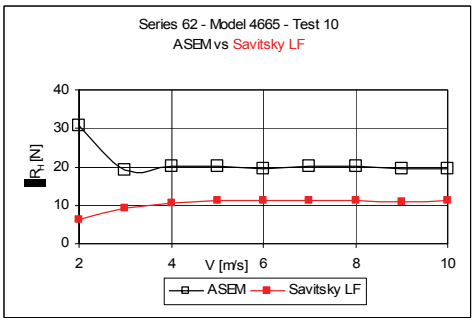

[b]

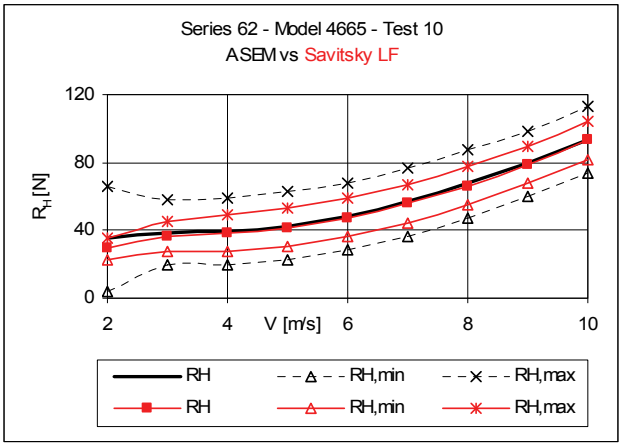

[c]

Figure 14.7-4 Model 4665 - Test 10

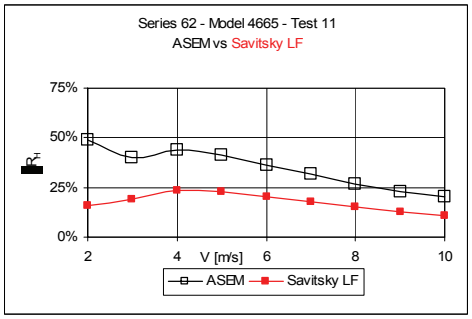

[a]

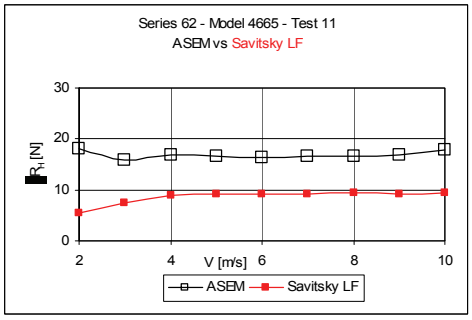

[b]

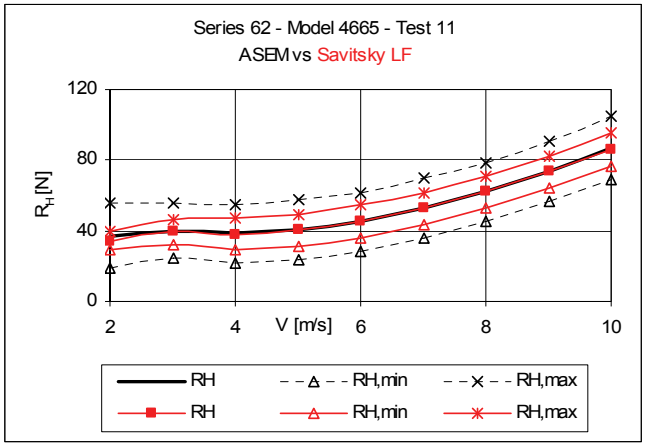

[c]

Figure 14.7-5 Model 4665 - Test 11

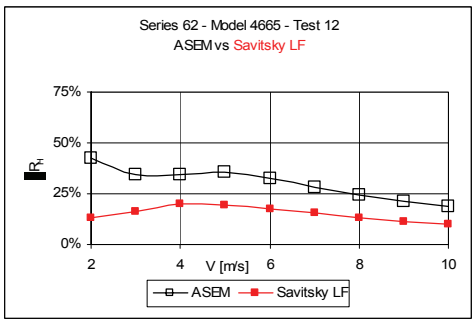

[a]

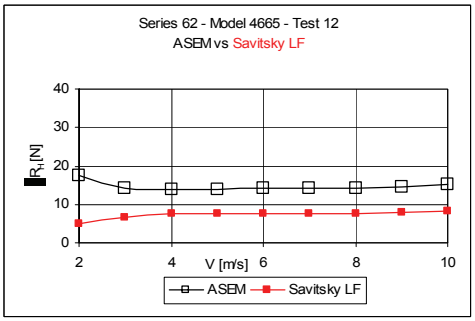

[b]

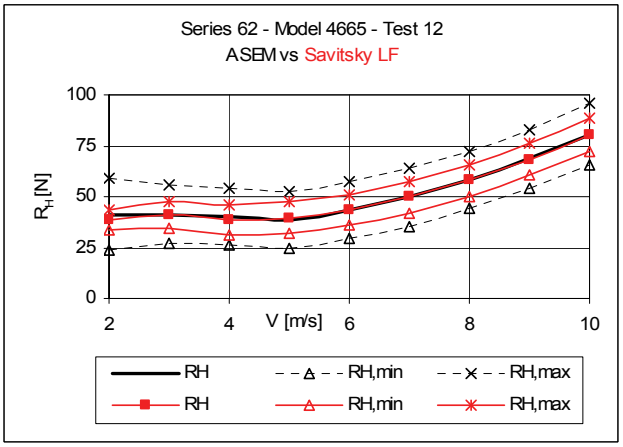

[c]

Figure 14.7-6 Model 4665 - Test 12

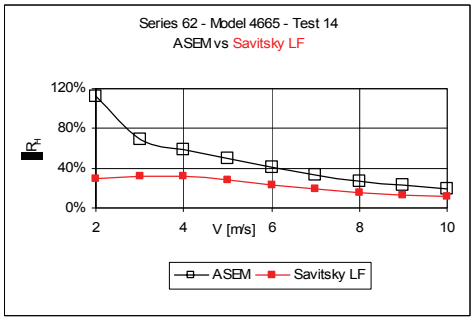

[a]

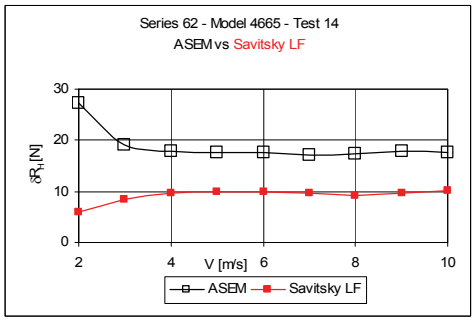

[b]

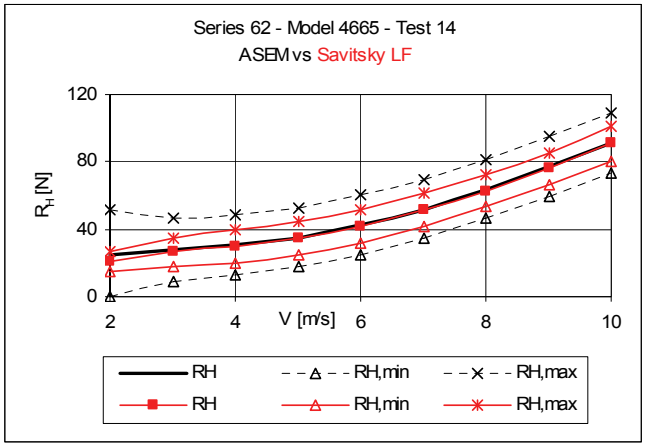

[c]

Figure 14.7-7 Model 4665 - Test 14

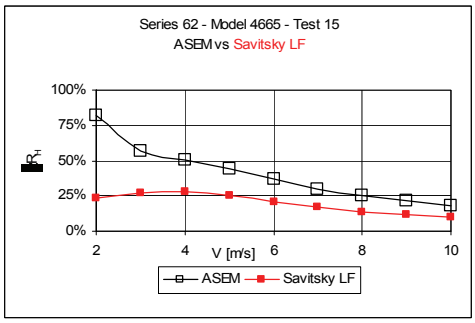

[a]

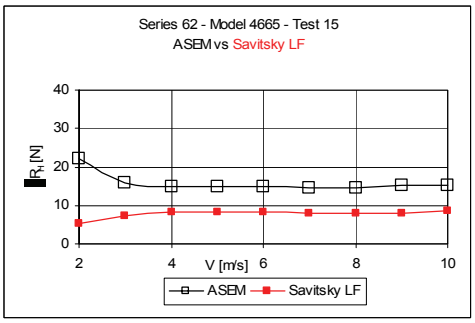

[b]

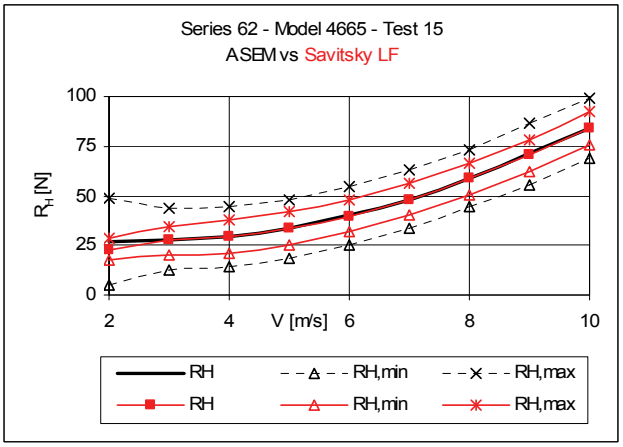

[c]

Figure 14.7-8 Model 4665 - Test 15

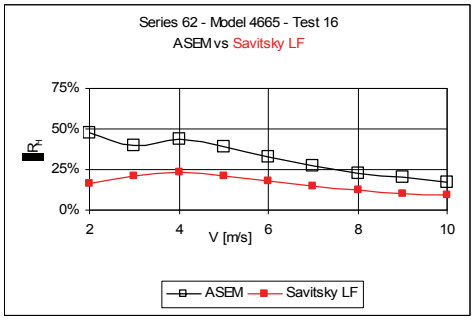

[a]

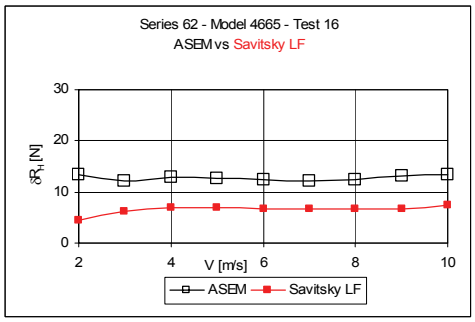

[b]

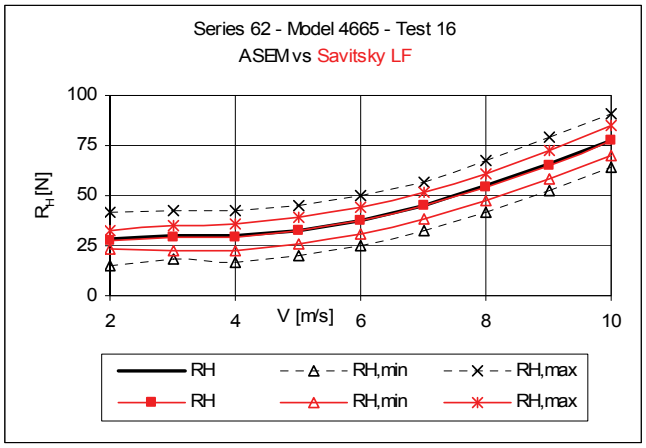

[c]

Figure 14.7-9 Model 4665 - Test 16

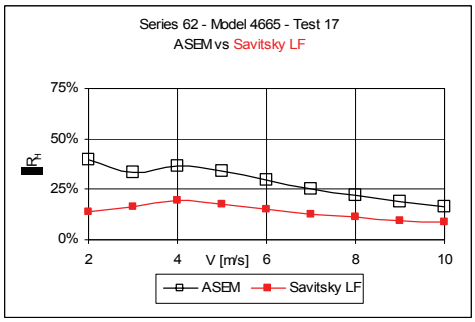

[a]

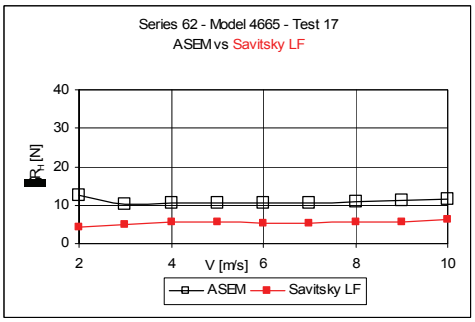

[b]

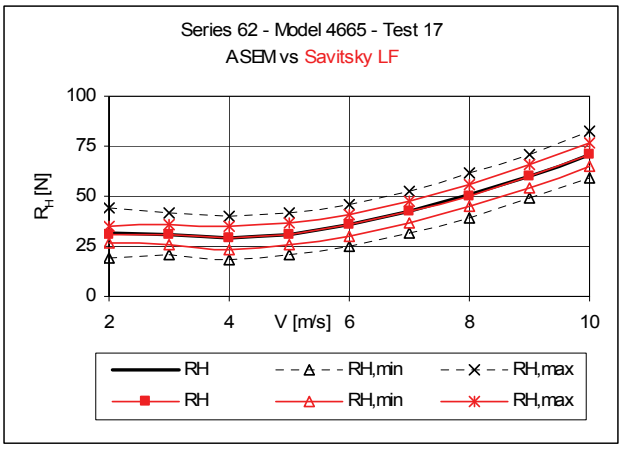

[c]

Figure 14.7-10 Model 4665 - Test 17

14.7.1.2 Model 4666

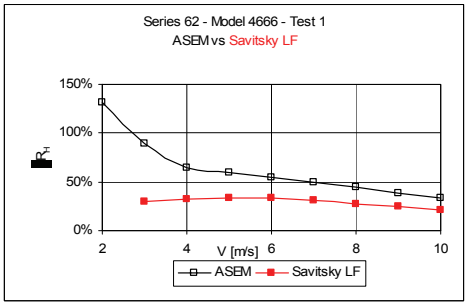

[a]

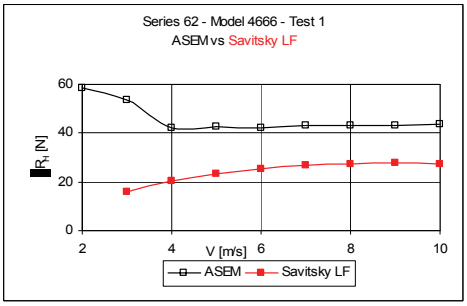

[b]

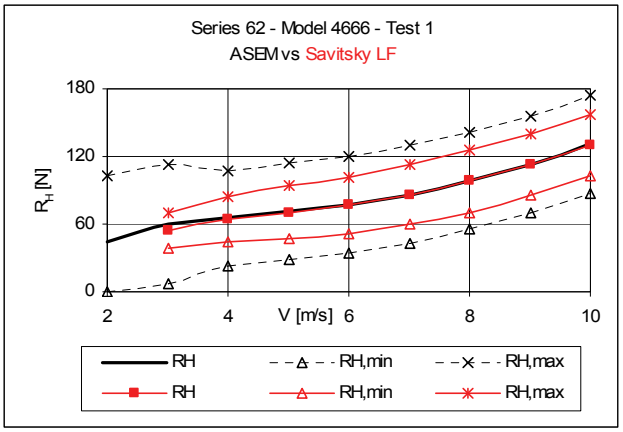

[c]

Figure 14.7-11 Model 4666 - Test 1

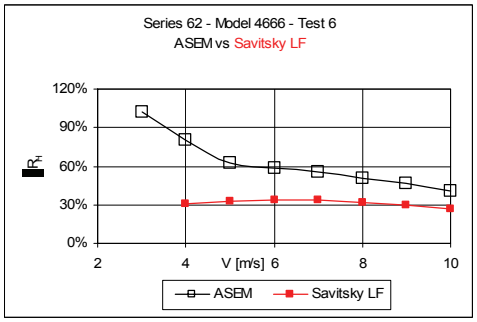

[a]

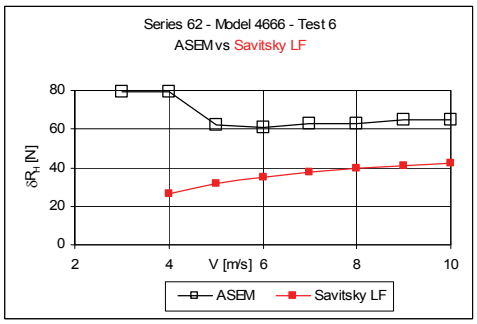

[b]

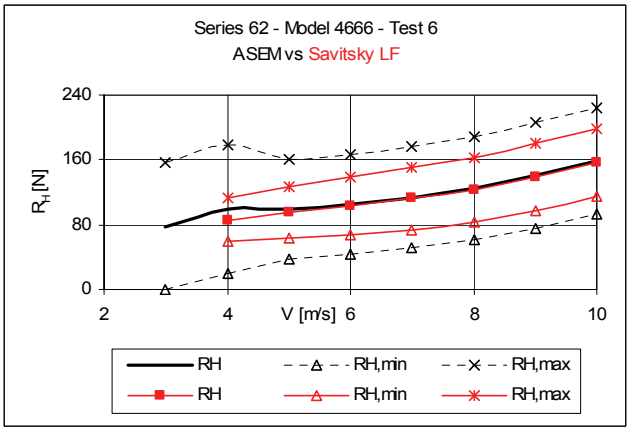

[c]

Figure 14.7-12 Model 4666 - Test 6

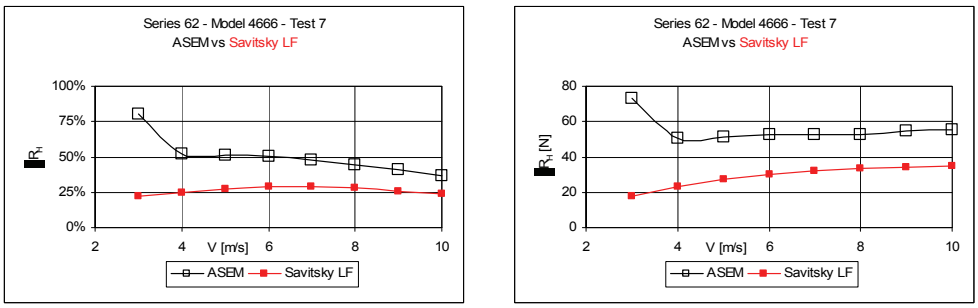

[a] **[b]**

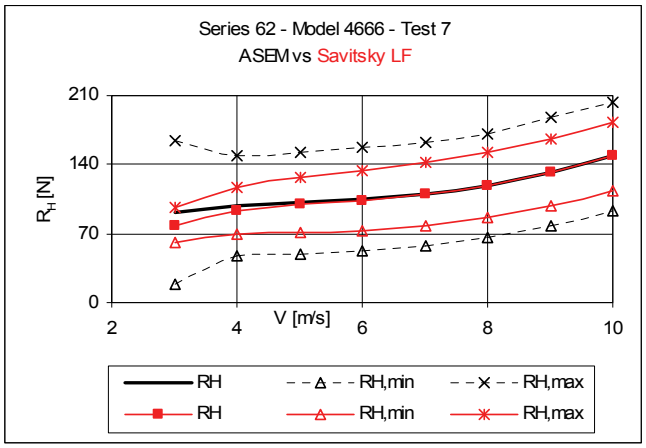

[c]

Figure 14.7-13 Model 4666 - Test 7

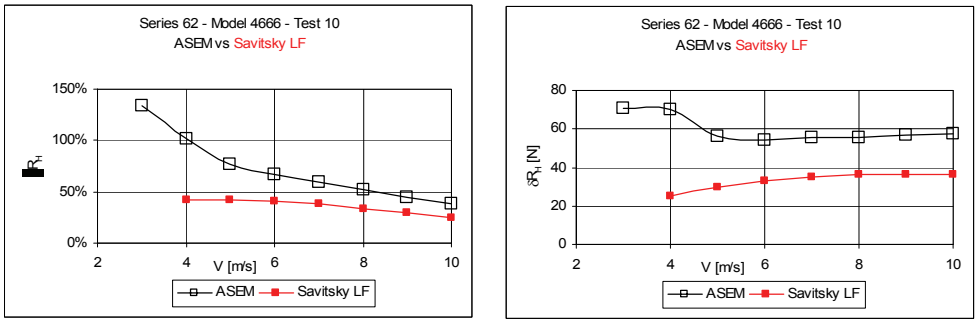

[a] **[b]**

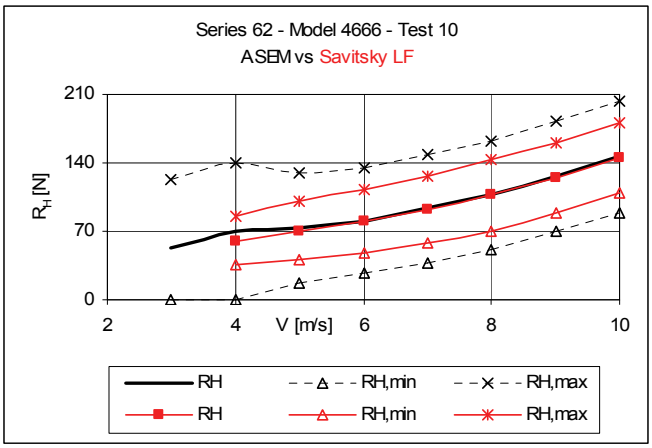

[c]

Figure 14.7-14 Model 4666 - Test 10

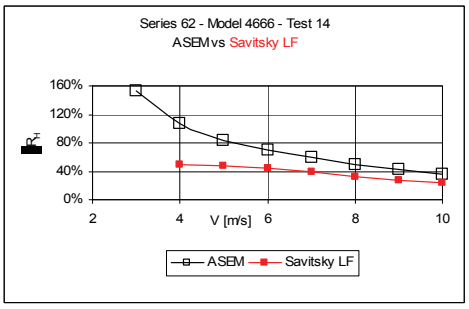

[a]

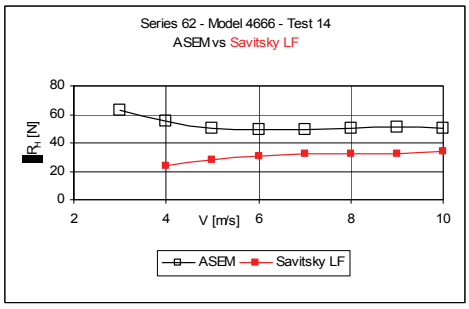

[b]

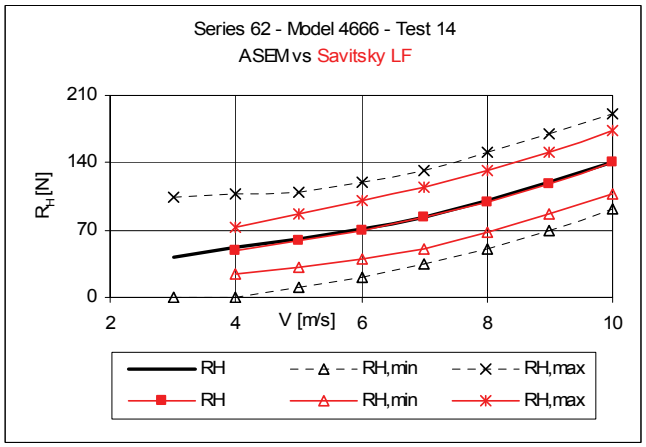

[c]

Figure 14.7-15 Model 4666 - Test 14

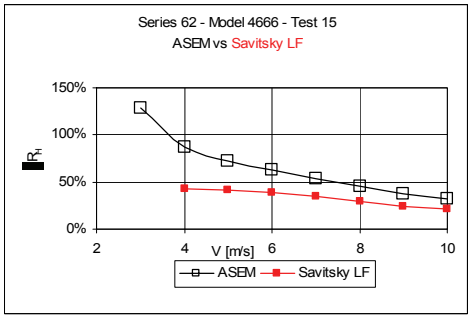

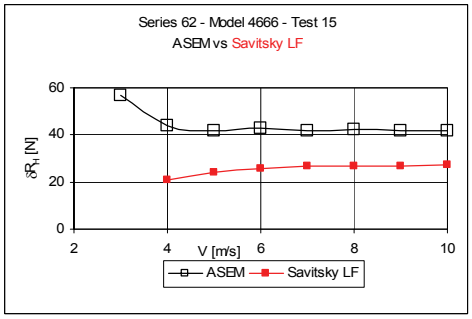

[a]

[b]

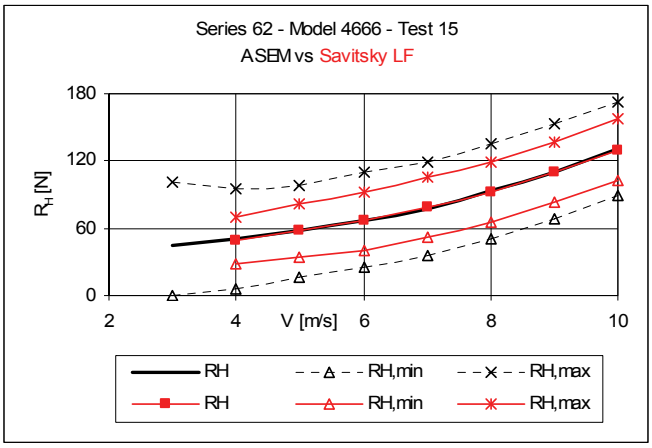

[c]

Figure 14.7-16 Model 4666 - Test 15

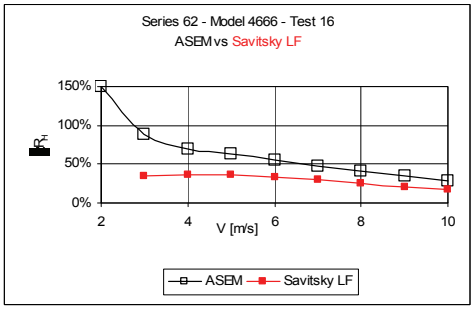

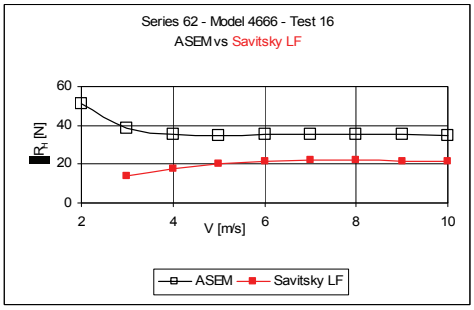

[a]

[b]

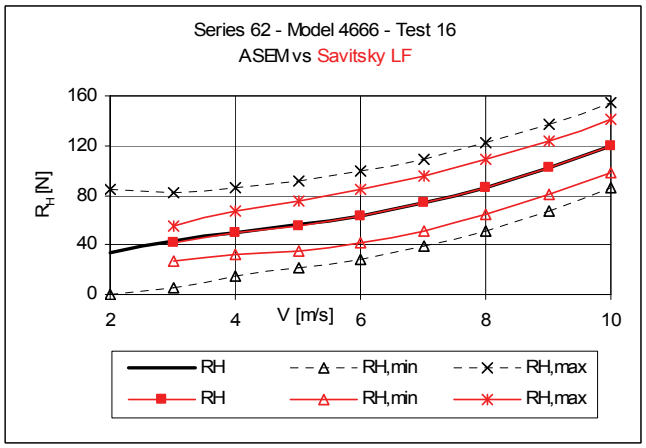

[c]

Figure 14.7-17 Model 4666 - Test 16

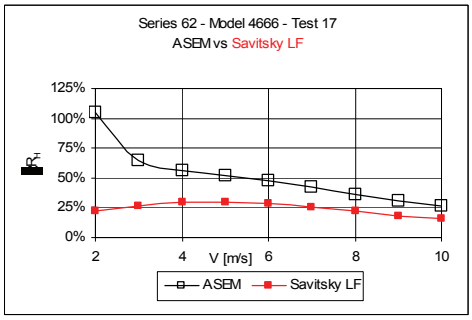

[a]

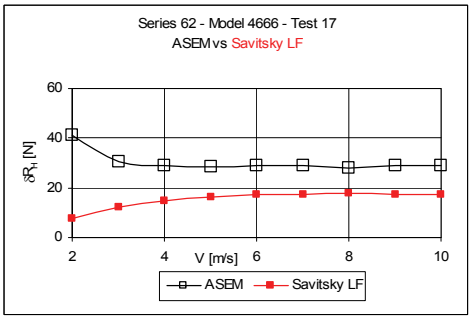

[b]

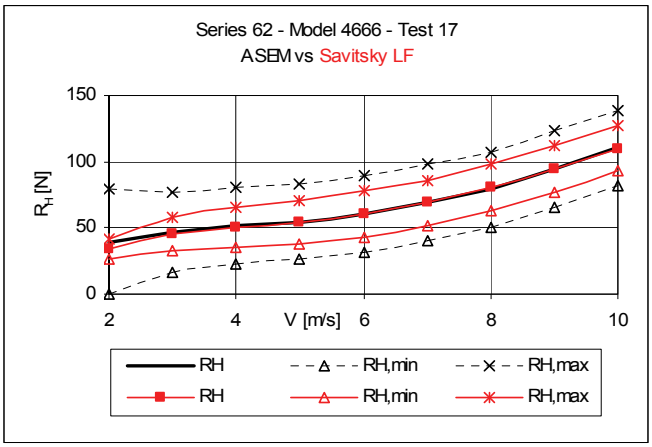

[c]

Figure 14.7-18 Model 4666 - Test 17

14.7.1.3 Model 4667-1

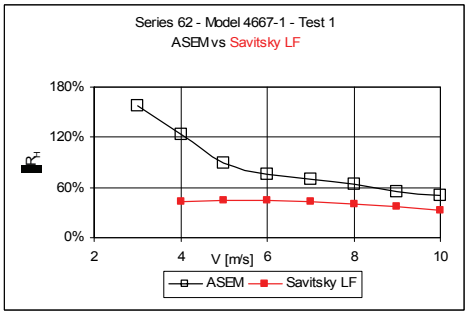

[a]

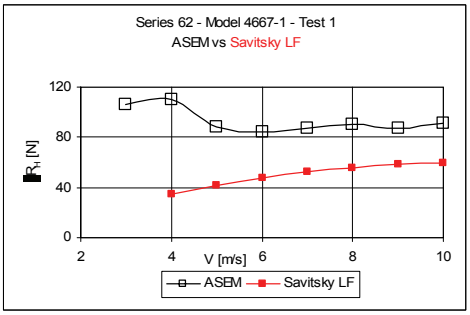

[b]

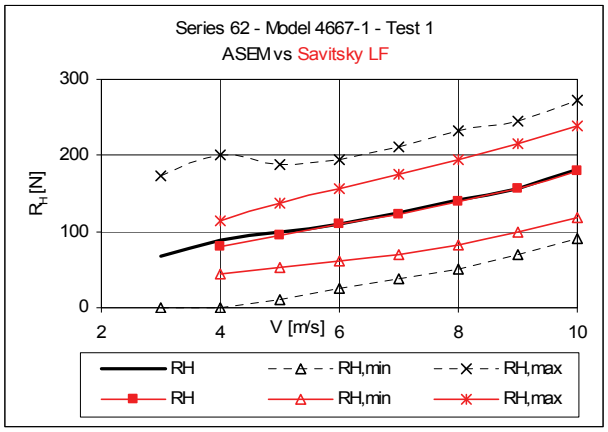

[c]

Figure 14.7-19 Model 4667-1 - Test 1

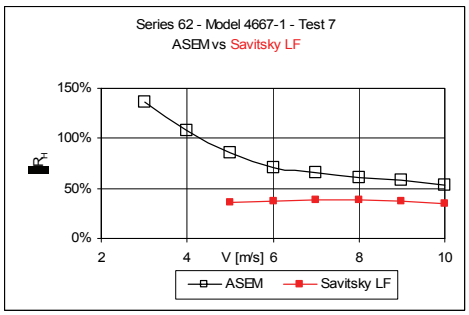

[a]

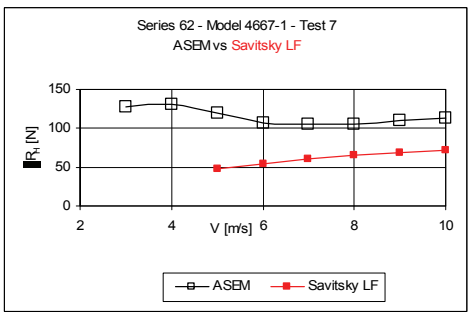

[b]

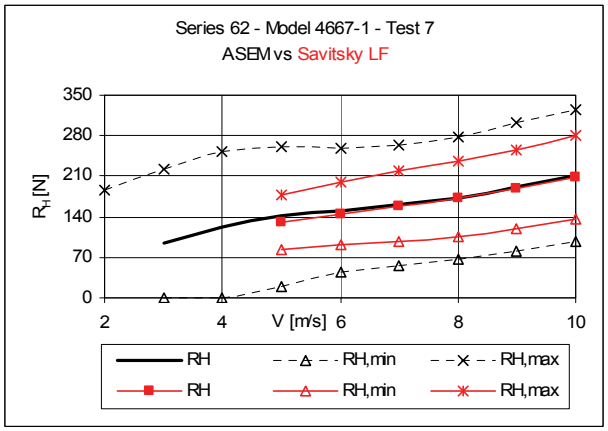

[c]

Figure 14.7-20 Model 4667-7 - Test 1

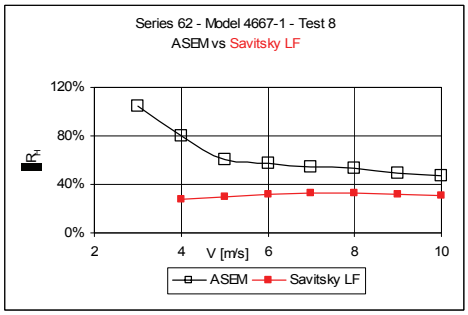

[a]

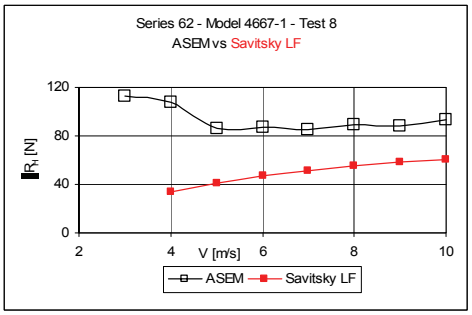

[b]

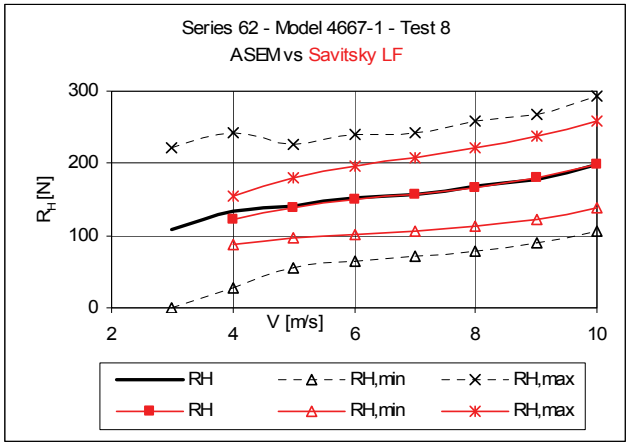

[c]

Figure 14.7-21 Model 4667-1 Test 8

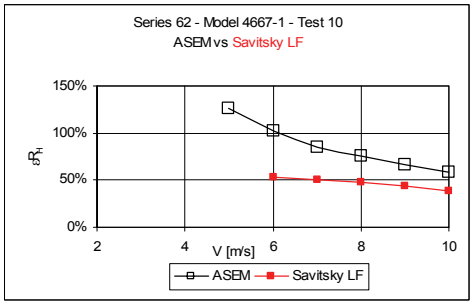

[a]

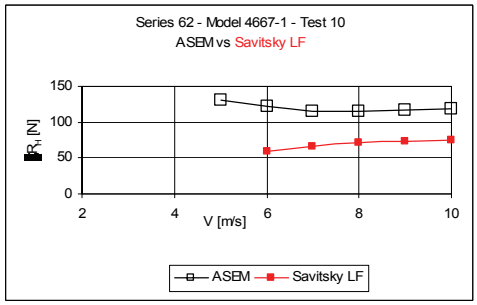

[b]

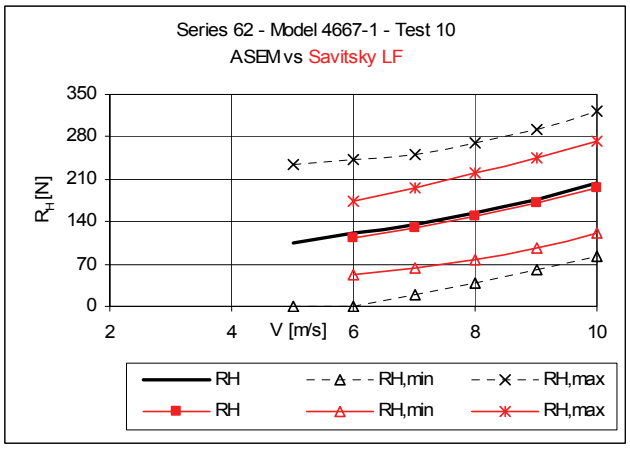

[c]

Figure 14.7-22 Model 4667-1 Test 10

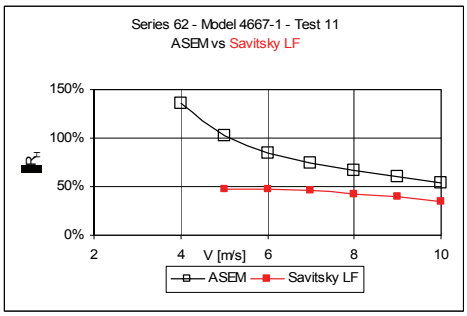

[a]

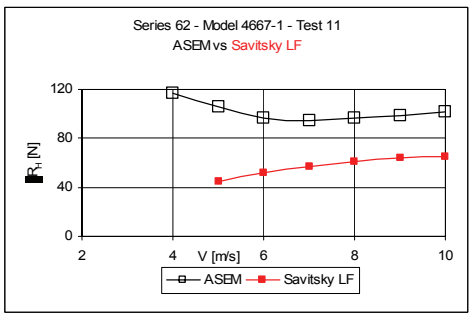

[b]

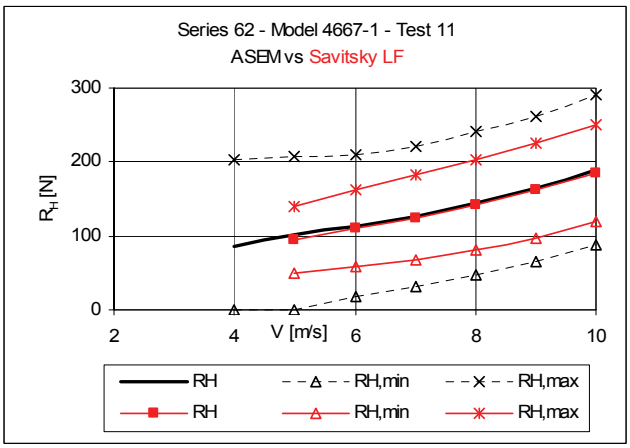

[c]

Figure 14.7-23 Model 4667-1 Test 11

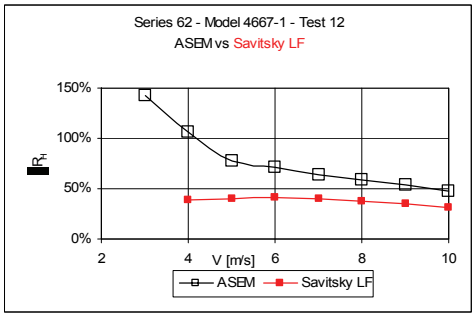

[a]

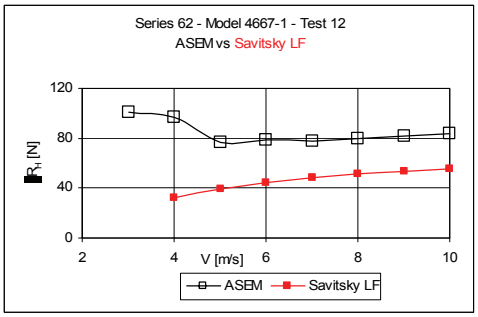

[b]

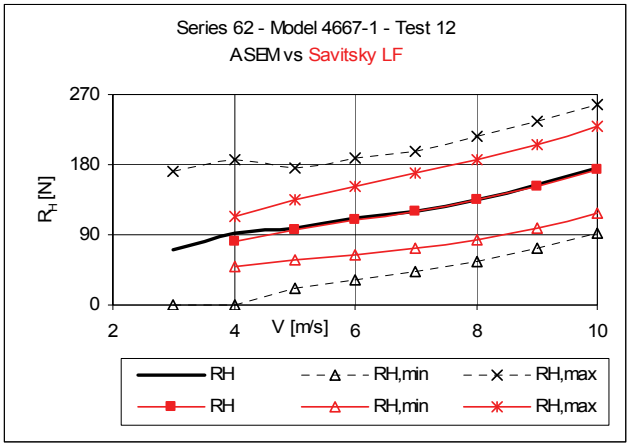

[c]

Figure 14.7-24 Model 4667-1 Test 12

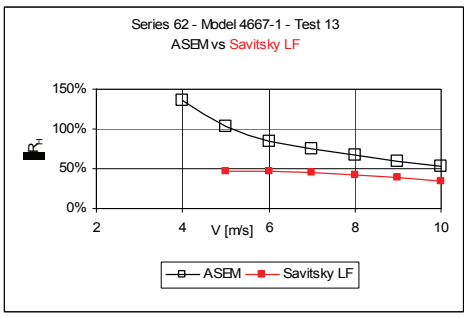

[a]

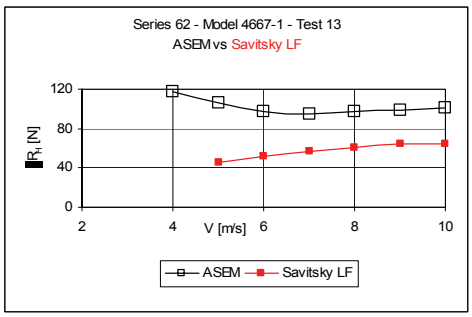

[b]

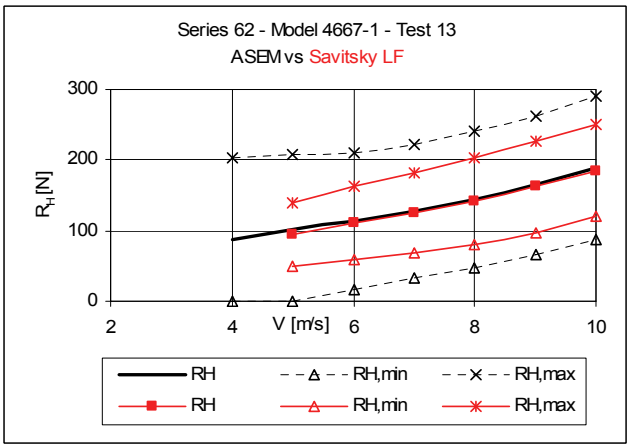

[c]

Figure 14.7-25 Model 4667-1 Test 13

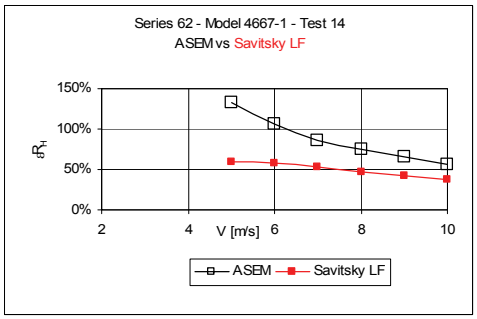

[a]

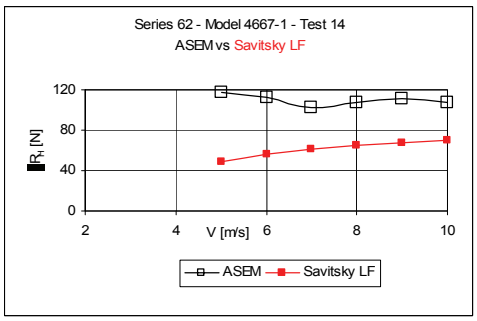

[b]

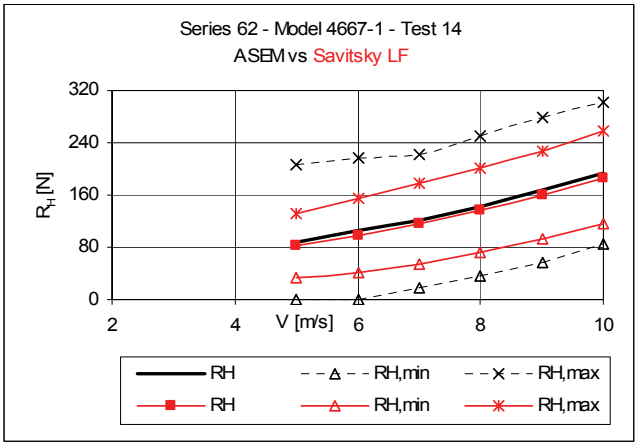

[c]

Figure 14.7-26 Model 4667-1 Test 14

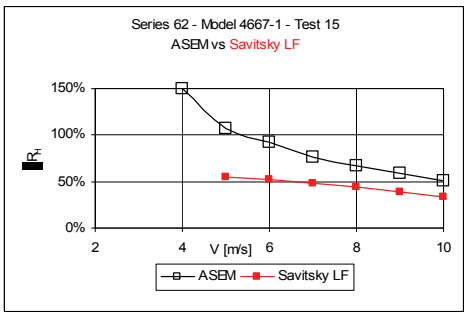

[a]

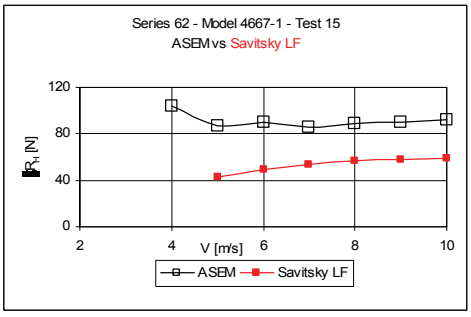

[b]

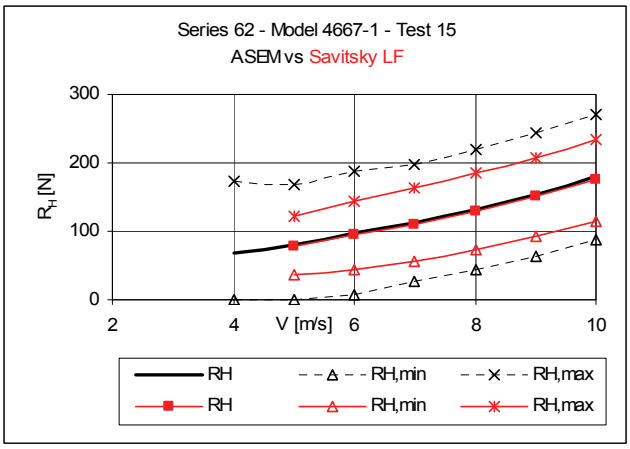

[c]

Figure 14.7-27 Model 4667-1 Test 15

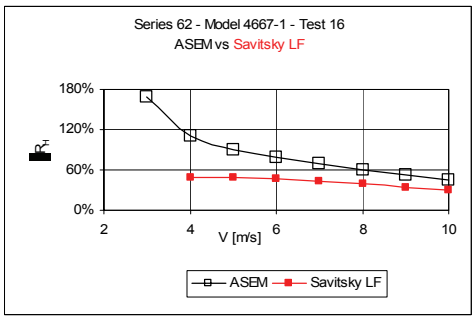

[a]

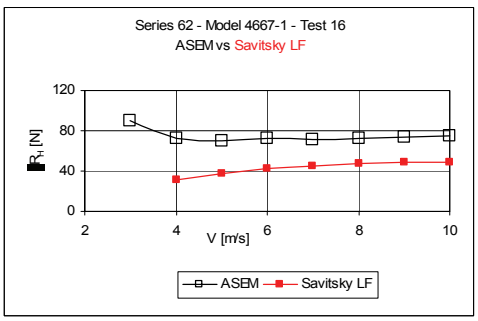

[b]

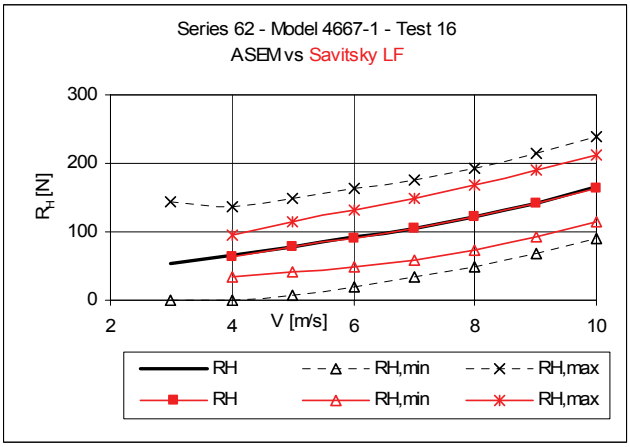

[c]

Figure 14.7-28 Model 4667-1 Test 16

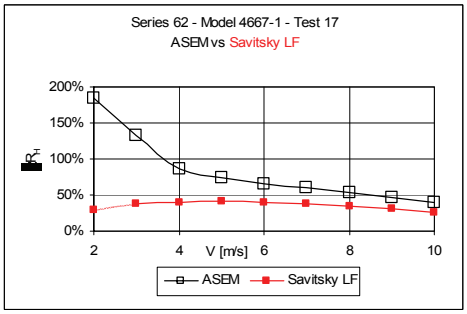

[a]

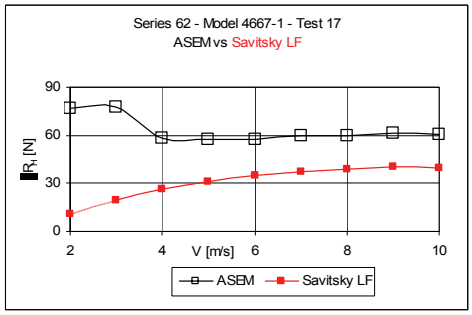

[b]

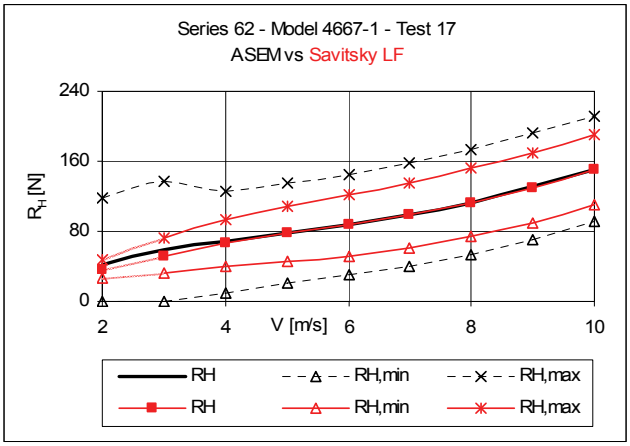

[c]

Figure 14.7-29 Model 4667-1 Test 17

14.7.1.4 Model 4668

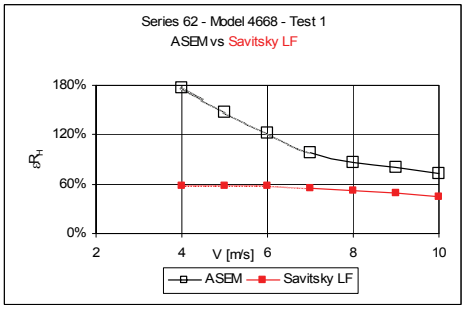

[a]

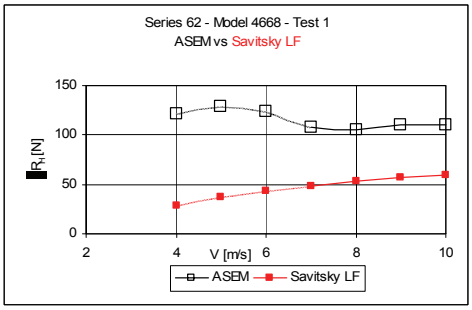

[b]

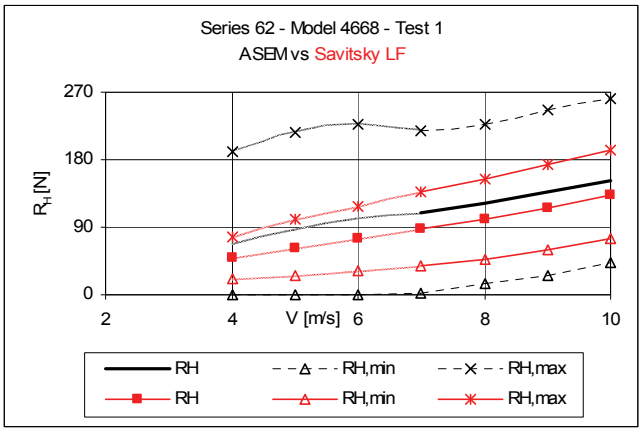

[c]

Figure 14.7-30 Model 4668 - Test 1

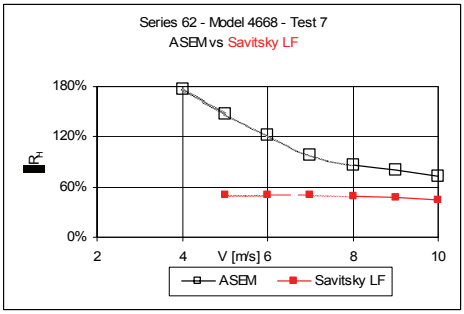

[a]

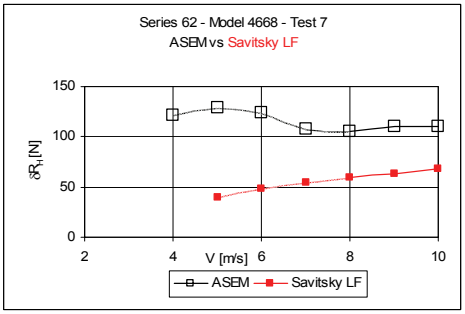

[b]

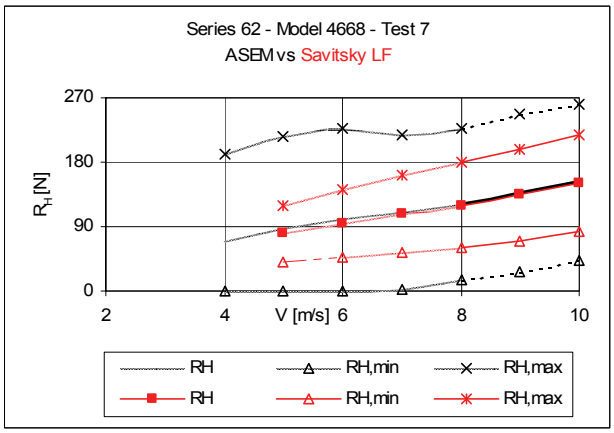

[c]

Figure 14.7-31 Model 4668 - Test 7

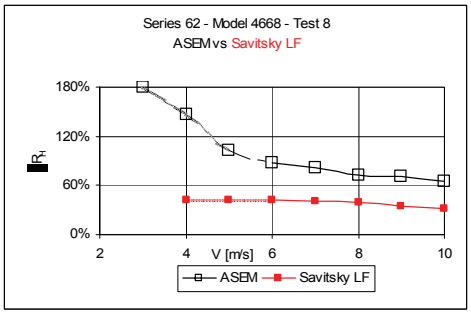

[a]

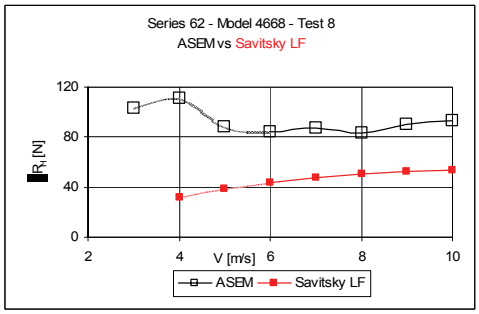

[b]

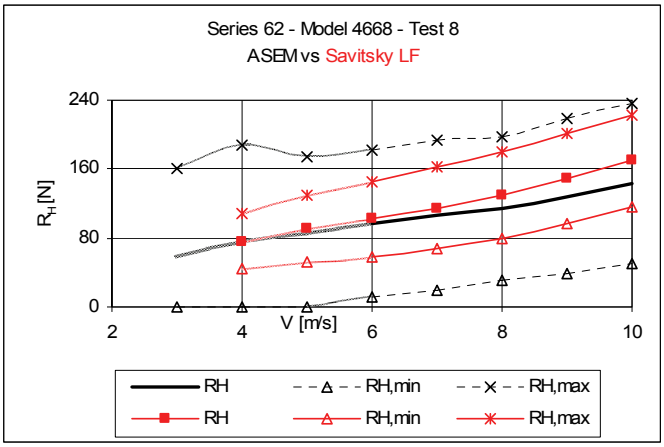

[c]

Figure 14.7-32 Model 4668 - Test 8

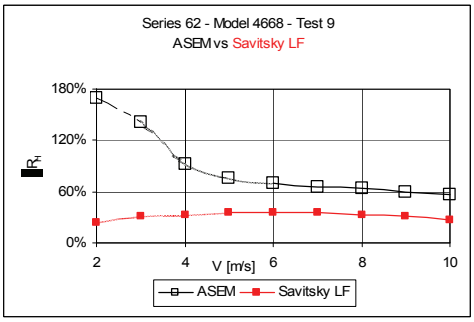

[a]

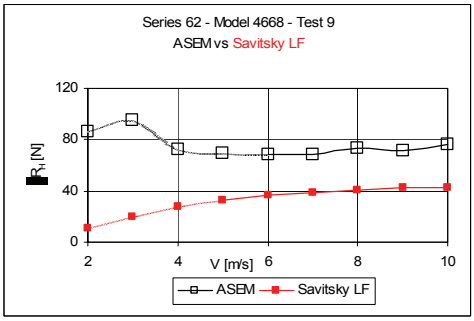

[b]

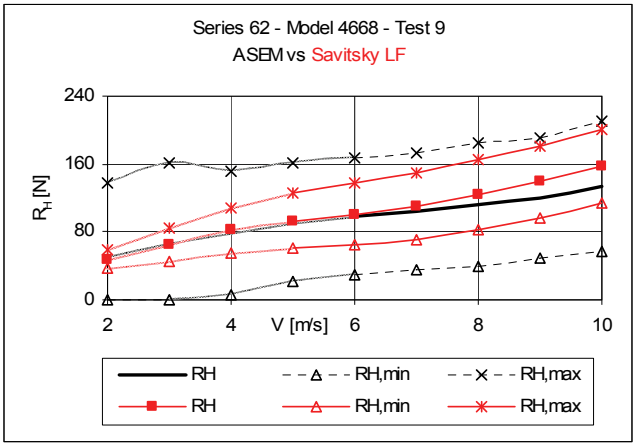

[c]

Figure 14.7-33 Model 4668 - Test 9

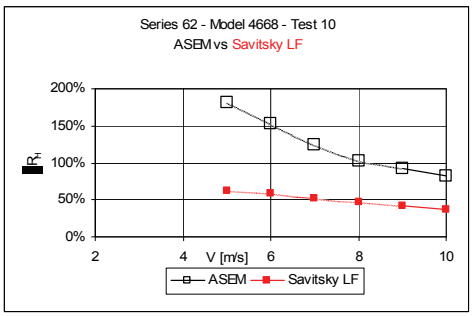

[a]

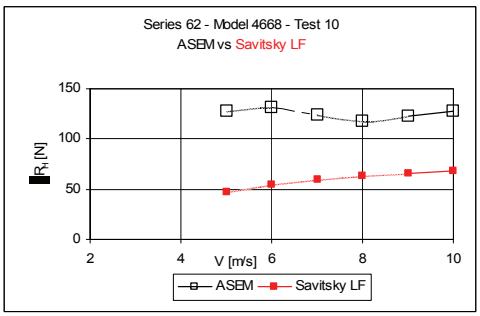

[b]

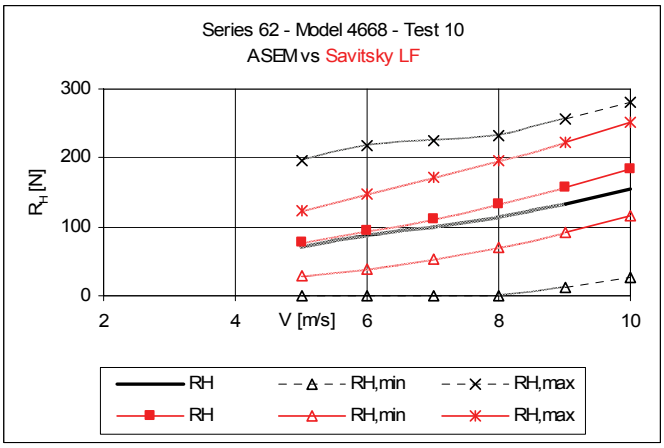

[c]

Figure 14.7-34 Model 4668 - Test 10

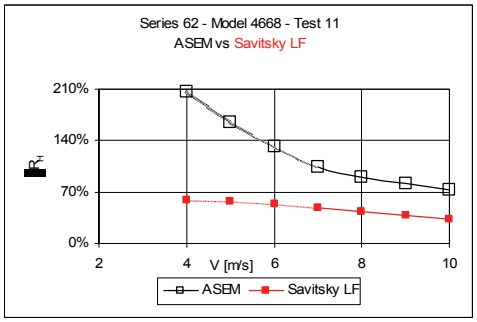

[a]

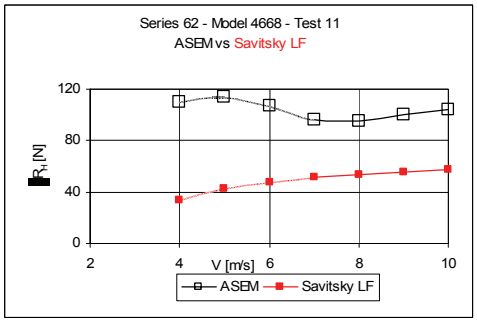

[b]

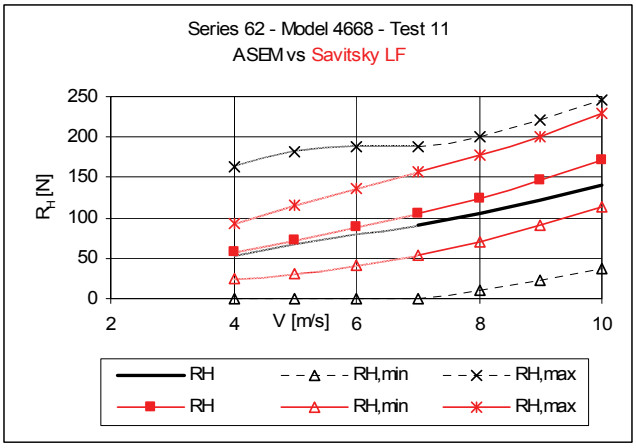

[c]

Figure 14.7-35 Model 4668 - Test 11

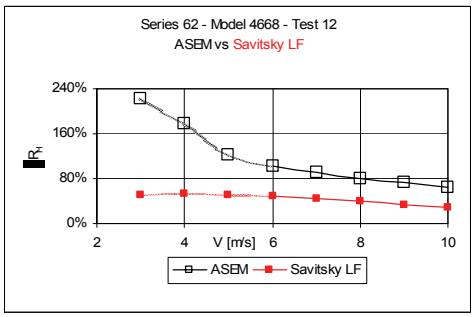

[a]

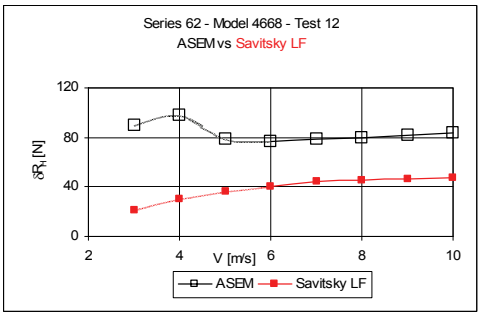

[b]

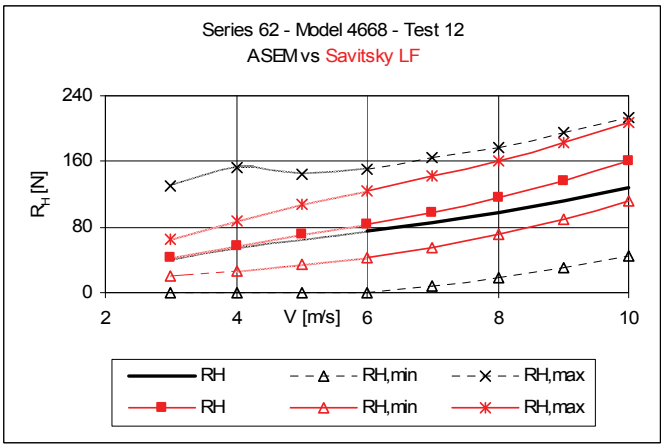

[c]

Figure 14.7-36 Model 4668 - Test 12

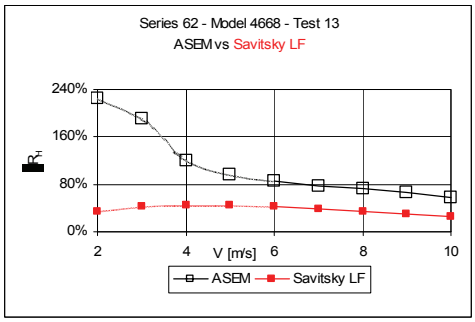

[a]

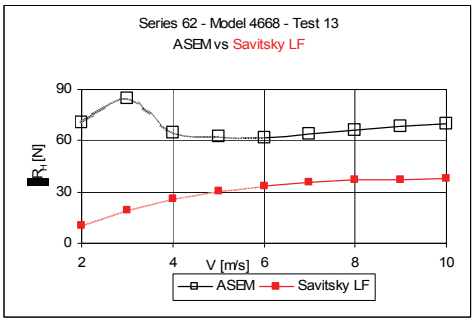

[b]

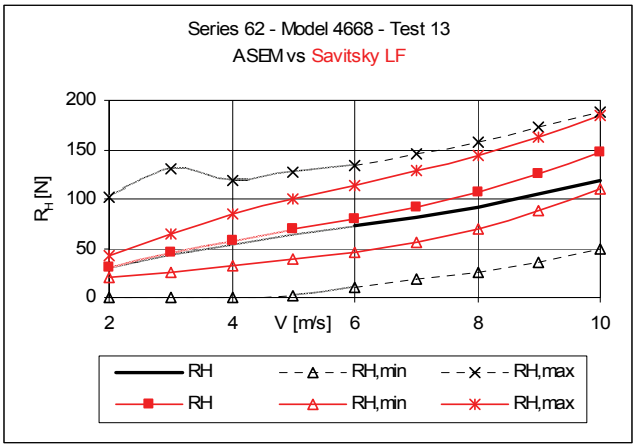

[c]

Figure 14.7-37 Model 4668 - Test 13

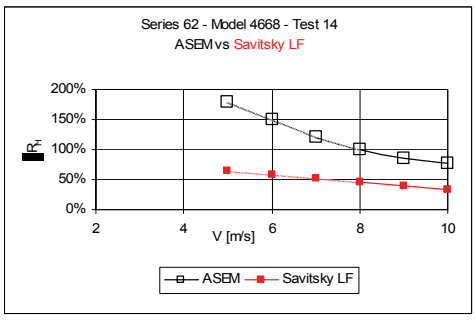

[a]

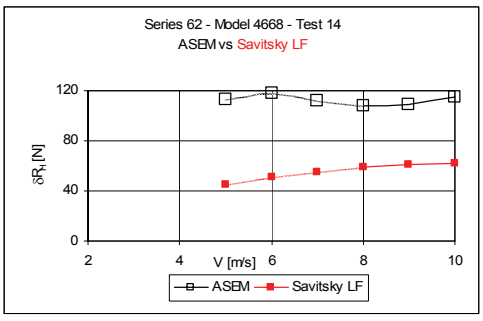

[b]

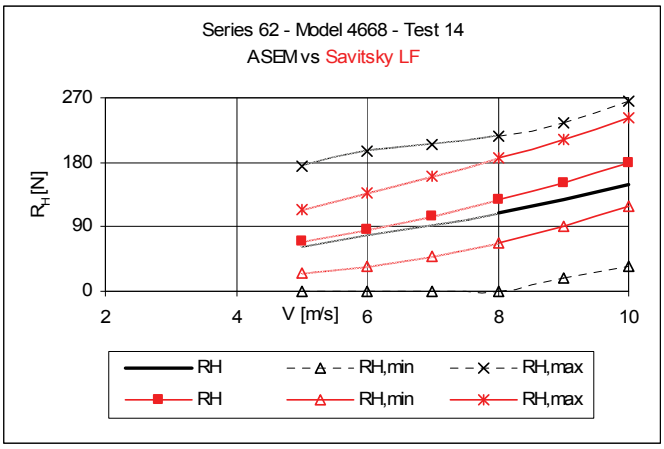

[c]

Figure 14.7-38 Model 4668 - Test 14

14.7.1.5 Model 4669

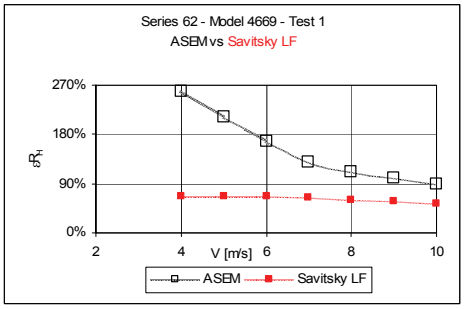

[a]

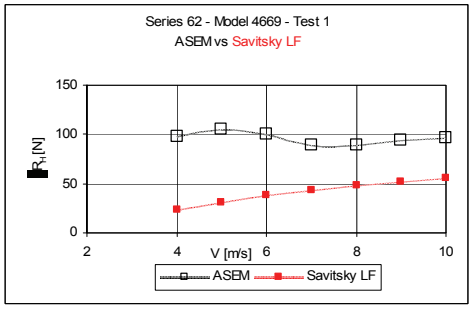

[b]

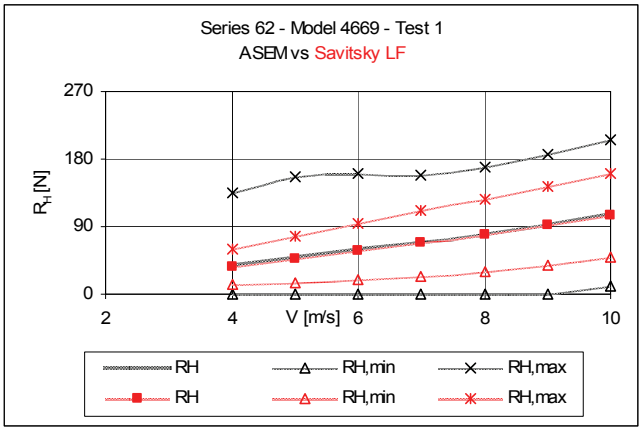

[c]

Figure 14.7-39 Model 4669 - Test 1

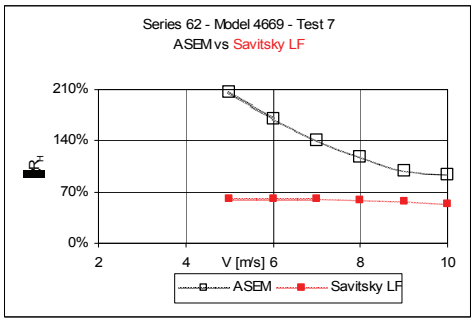

[a]

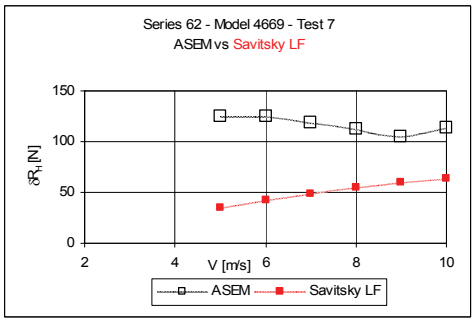

[b]

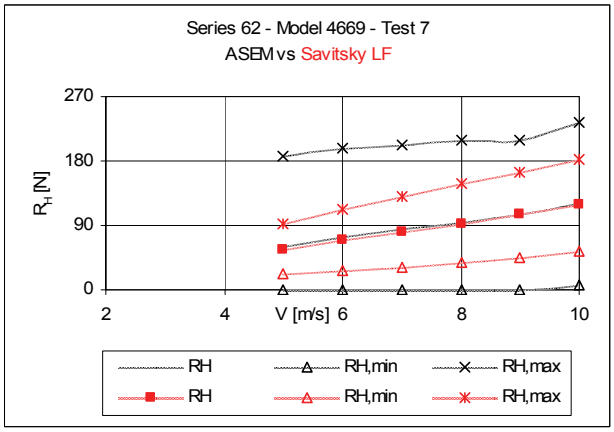

[c]
Figure 14.7-40 Model 4669 - Test 7

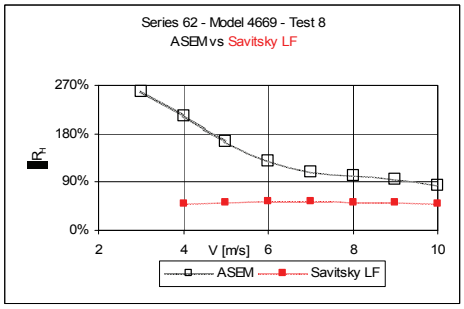

[a]

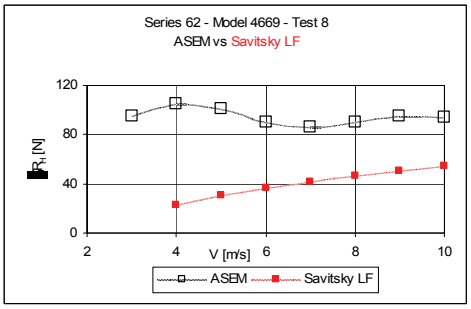

[b]

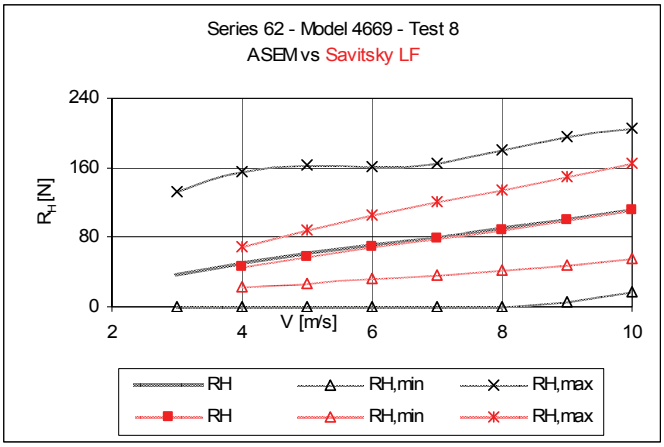

[c]

Figure 14.7-41 Model 4669 - Test 8

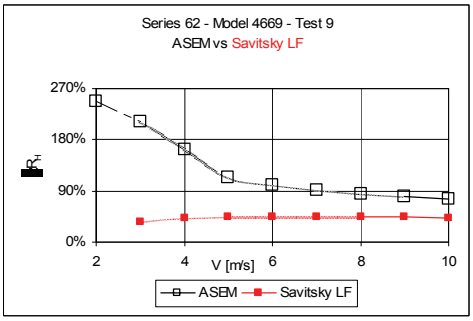

[a]

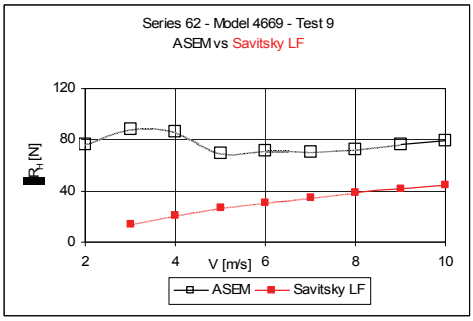

[b]

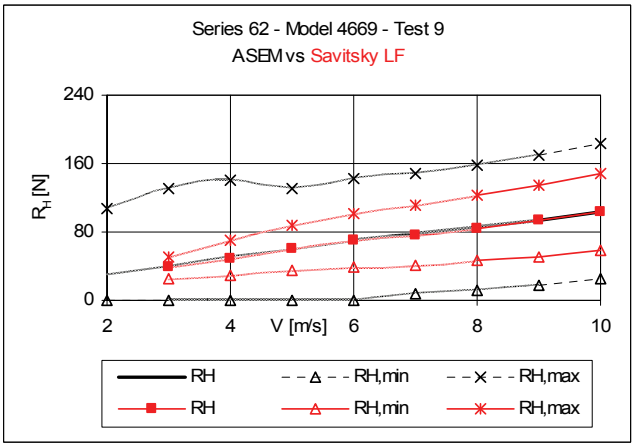

[c]

Figure 14.7-42 Model 4669 - Test 9

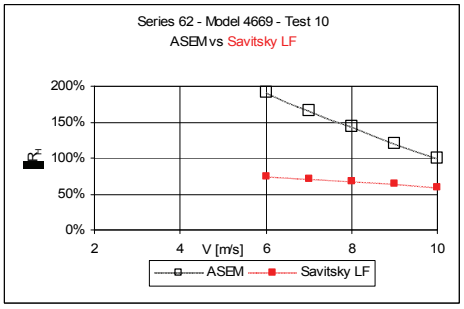

[a]

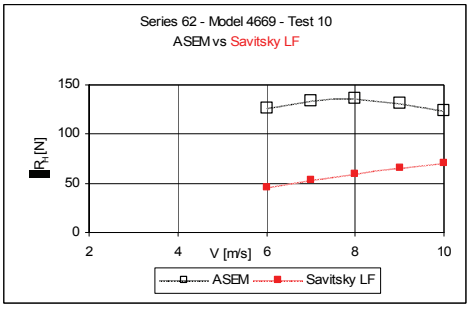

[b]

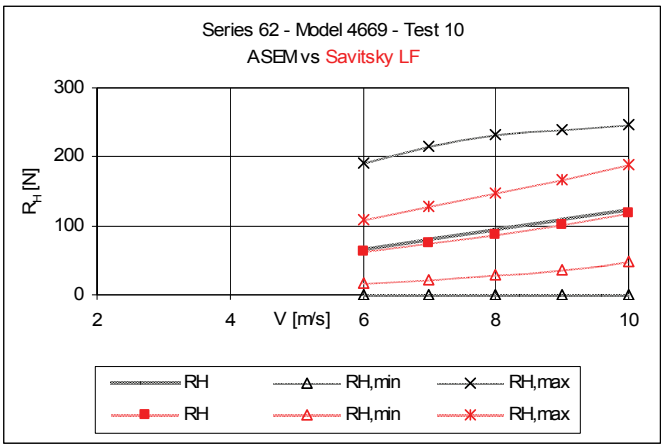

[c]

Figure 14.7-43 Model 4669 - Test 10

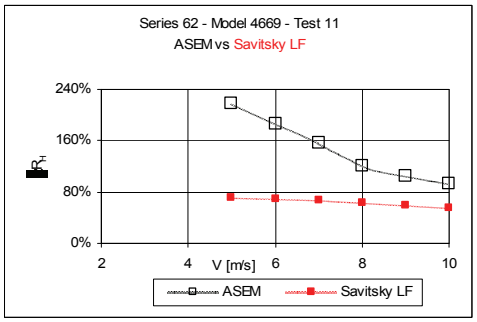

[a]

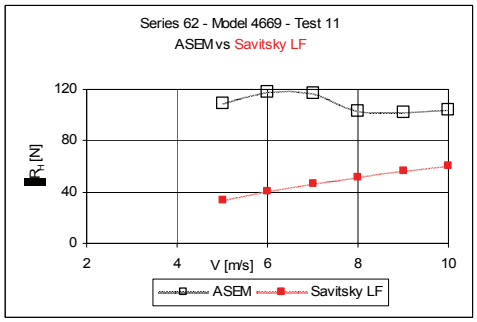

[b]

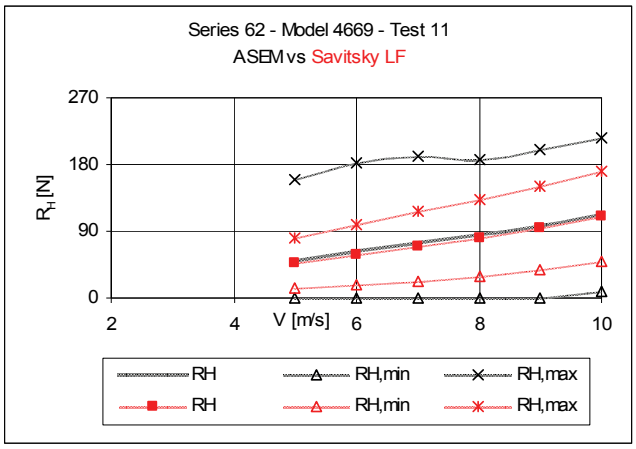

[c]

Figure 14.7-44 Model 4669 - Test 11

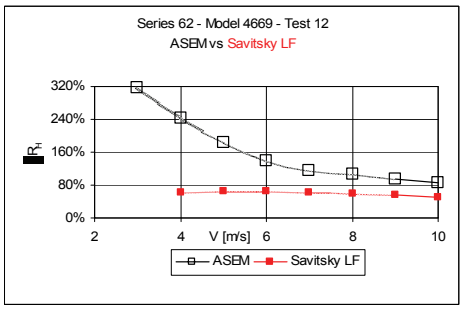

[a]

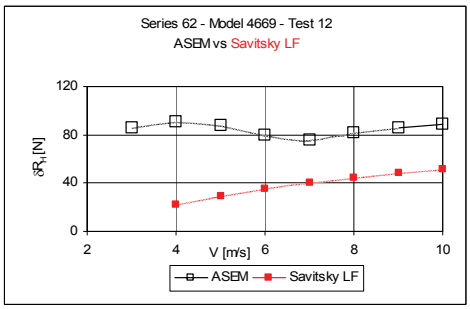

[b]

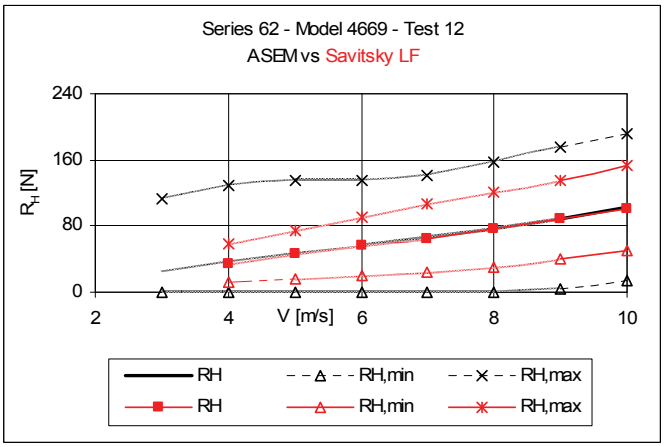

[c]

Figure 14.7-45 Model 4669 - Test 12

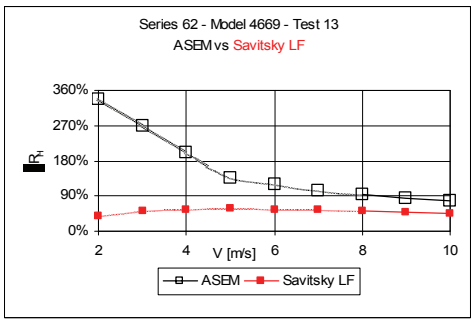

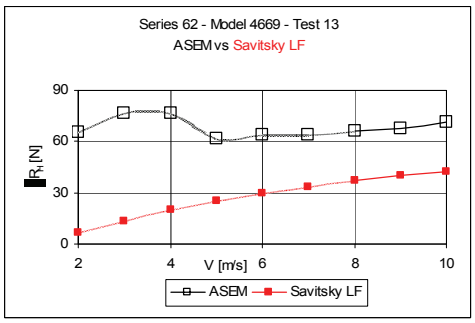

[a]

[b]

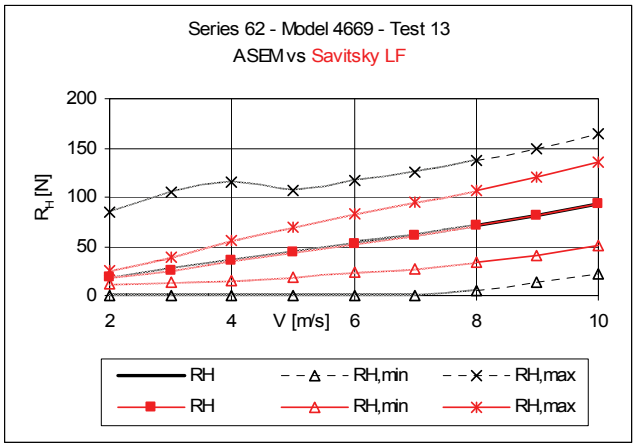

[c]

Figure 14.7-46 Model 4669 - Test 13

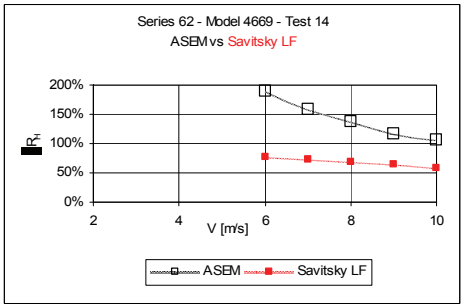

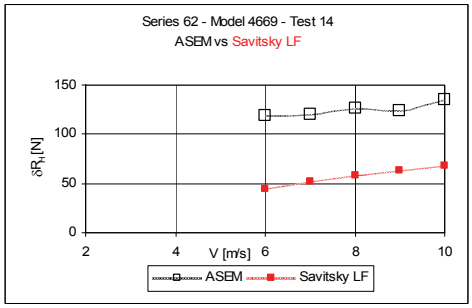

[a]

[b]

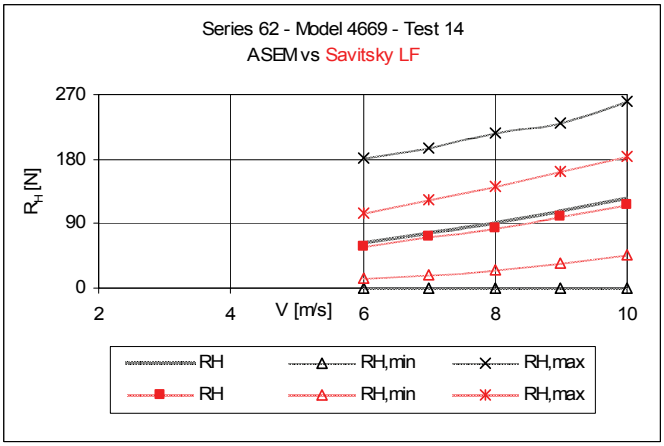

[c]

Figure 14.7-47 Model 4669 - Test 14

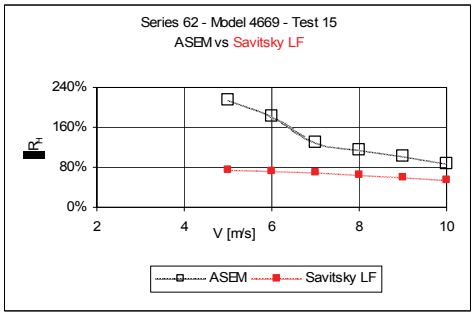

[a]

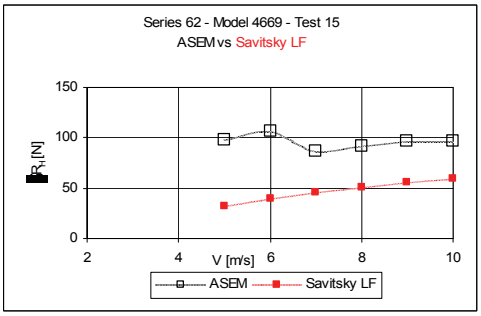

[b]

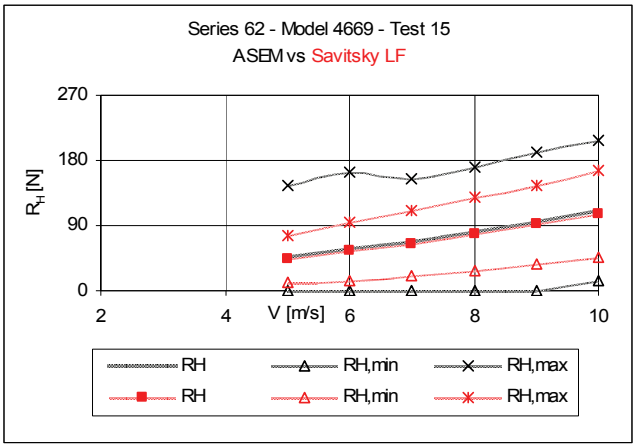

[c]

Figure 14.7-48 Model 4669 - Test 15

14.7.2 Series BK

14.7.2.1 Model BK-1

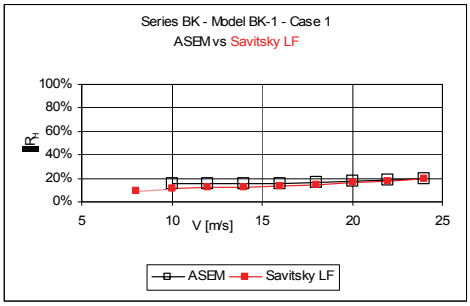

[a]

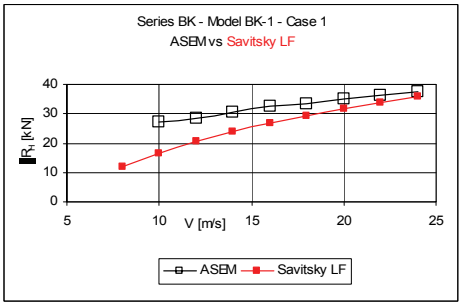

[b]

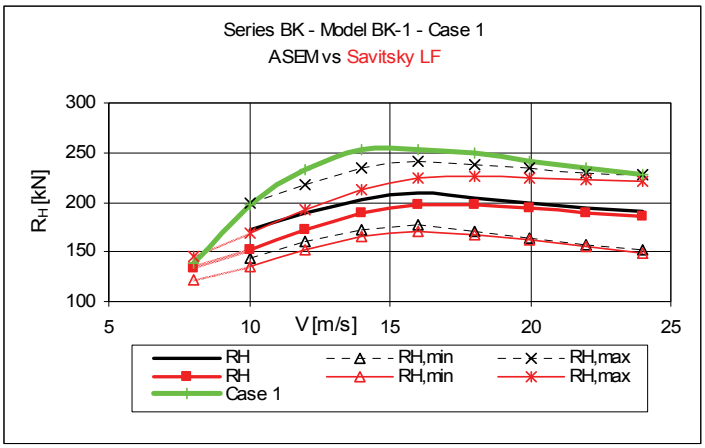

[c]

Figure 14.7-49 Model BK-1 - Case 1

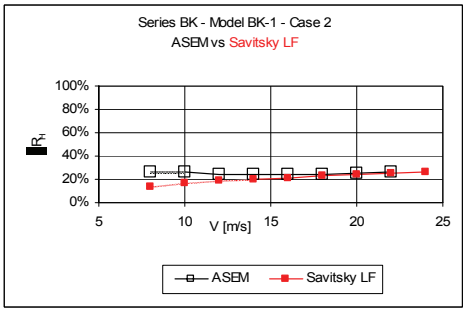

[a]

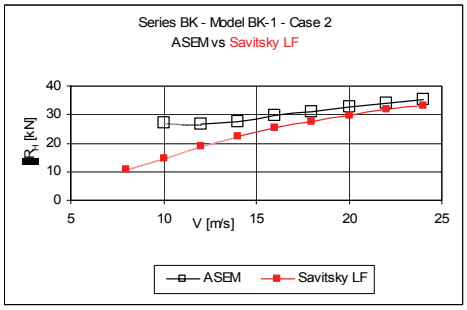

[b]

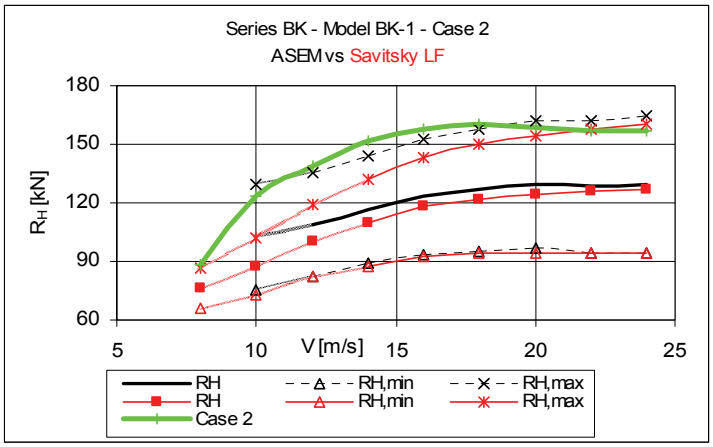

[c]

Figure 14.7-50 Model BK-1 - Case 2

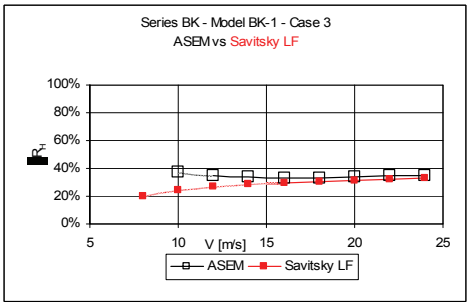

[a]

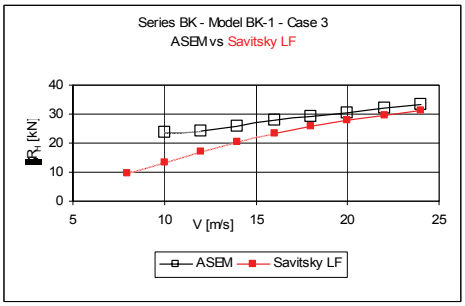

[b]

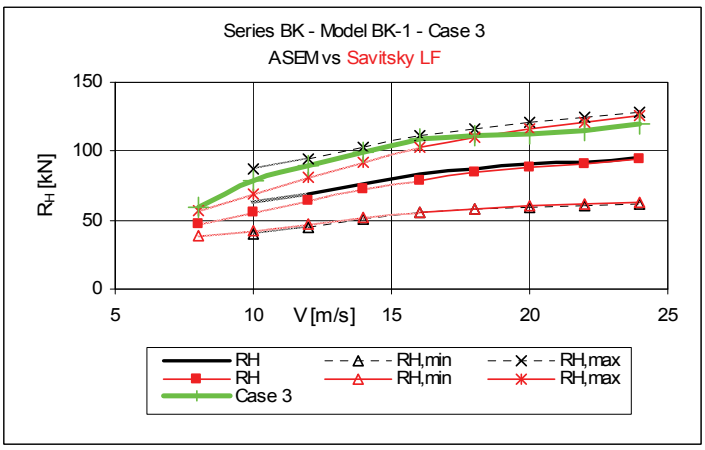

[c]

Figure 14.7-51 Model BK-1 - Case 3

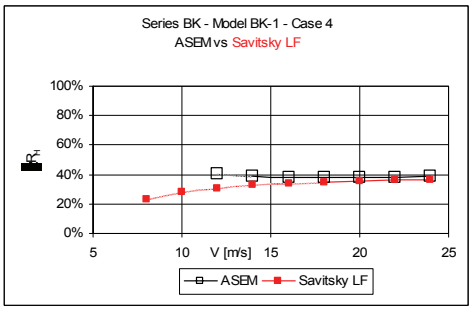

[a]

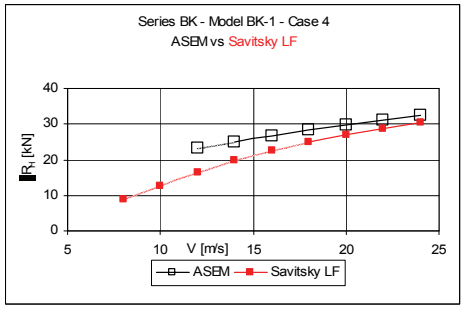

[b]

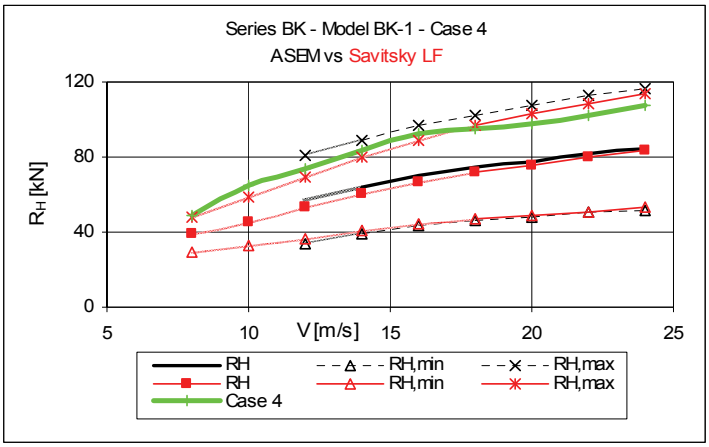

[c]

Figure 14.7-52 Model BK-1 - Case 4

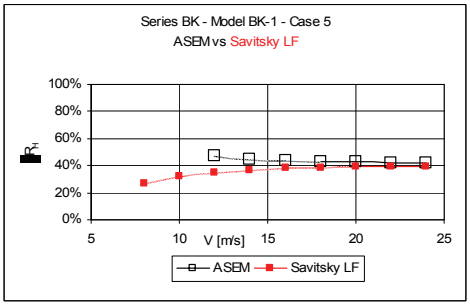

[a]

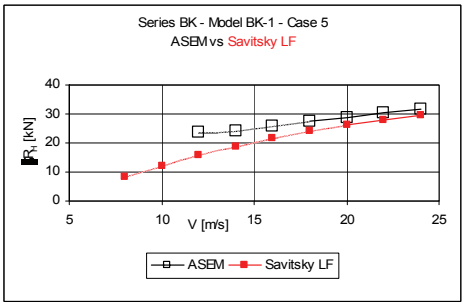

[b]

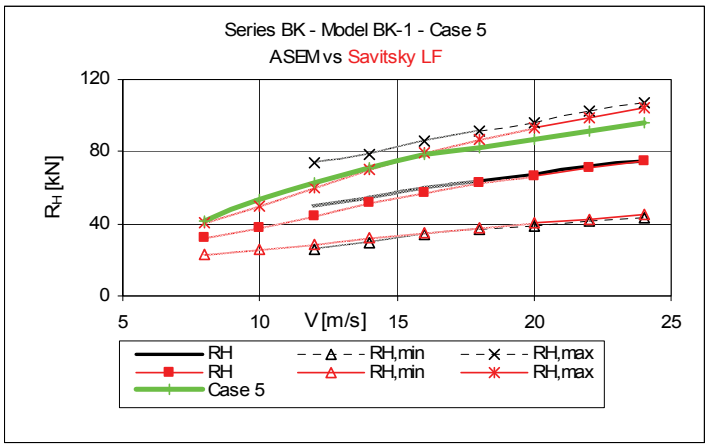

[c]

Figure 14.7-53 Model BK-1 - Case 5

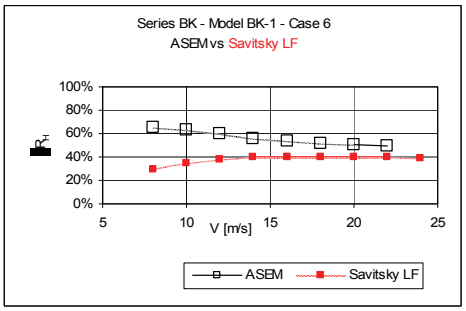

[a]

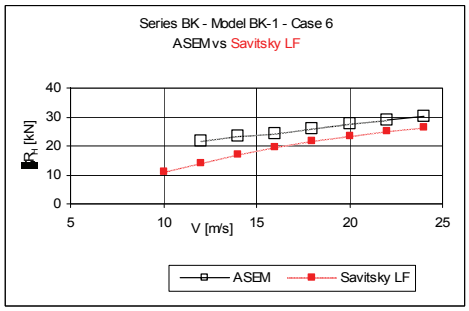

[b]

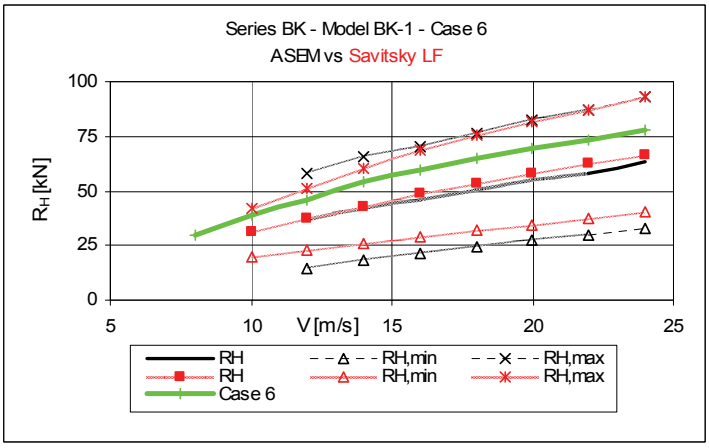

[c]

Figure 14.7-54 Model BK-1 - Case 6

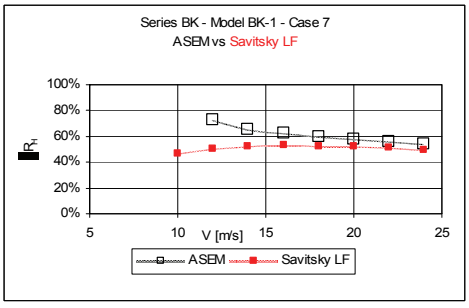

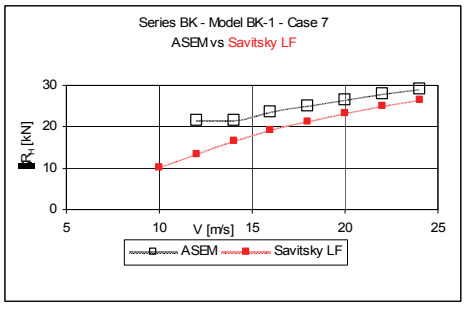

[a]

[b]

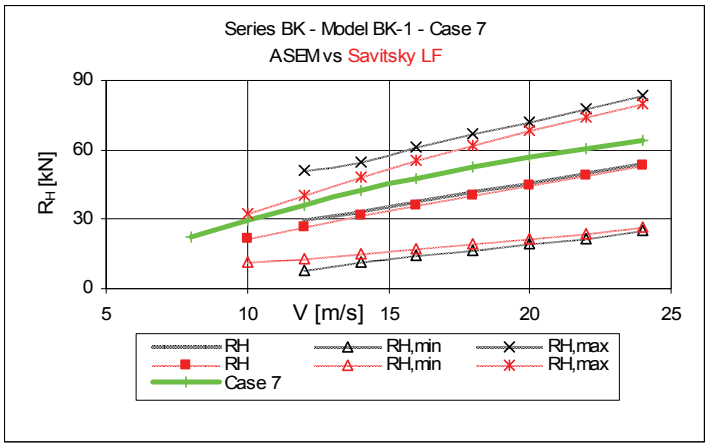

[c]

Figure 14.7-55 Model BK-1 - Case 7

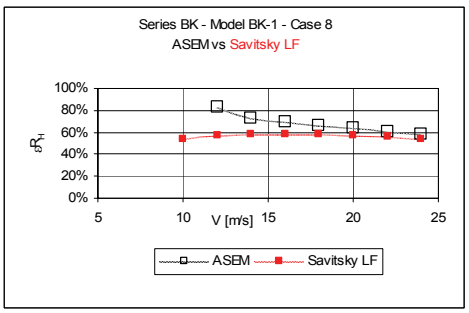

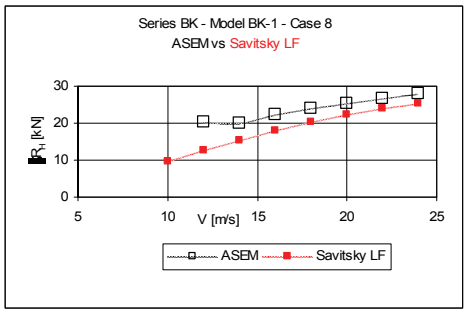

[a]

[b]

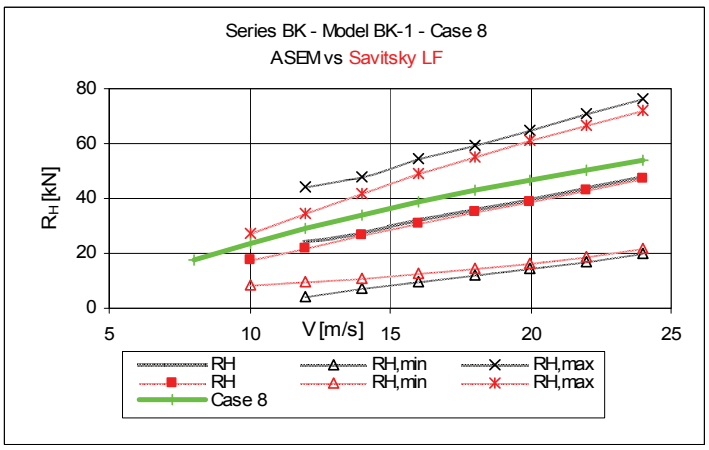

[c]

Figure 14.7-56 Model BK-1 - Case 8

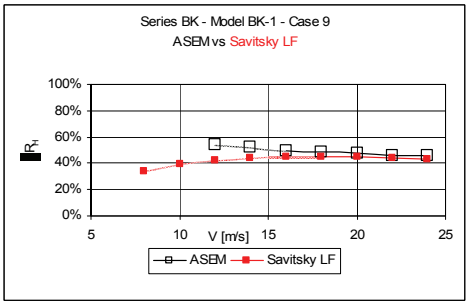

[a]

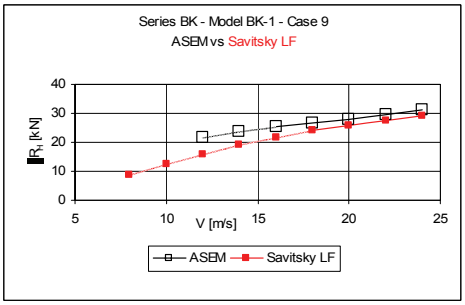

[b]

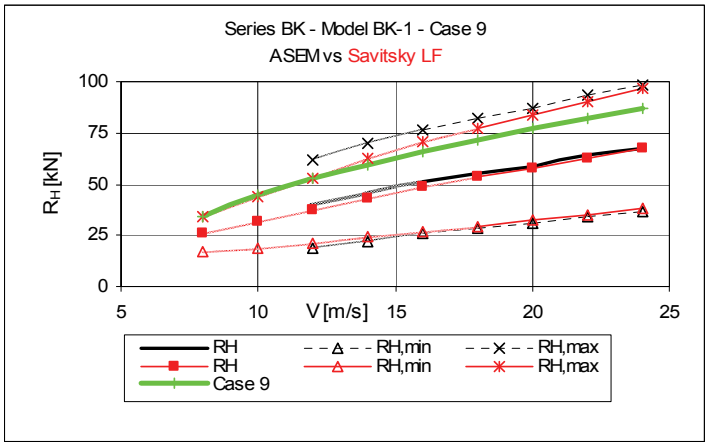

[c]

Figure 14.7-57 Model BK-1 - Case 9

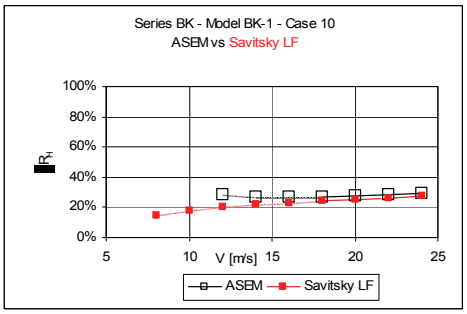

[a]

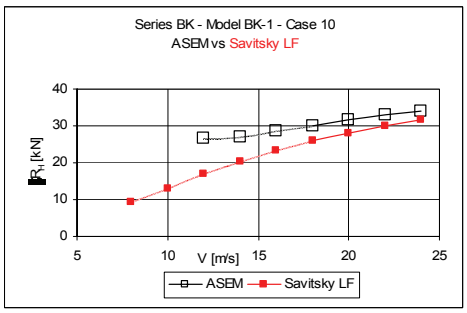

[b]

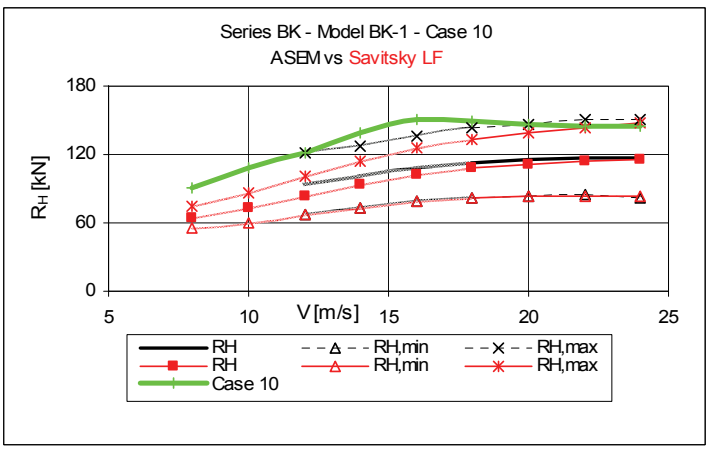

[c]

Figure 14.7-58 Model BK-1 - Case 10

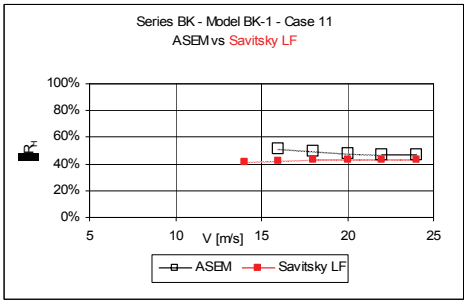

[a]

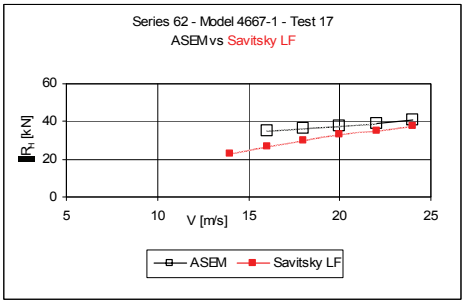

[b]

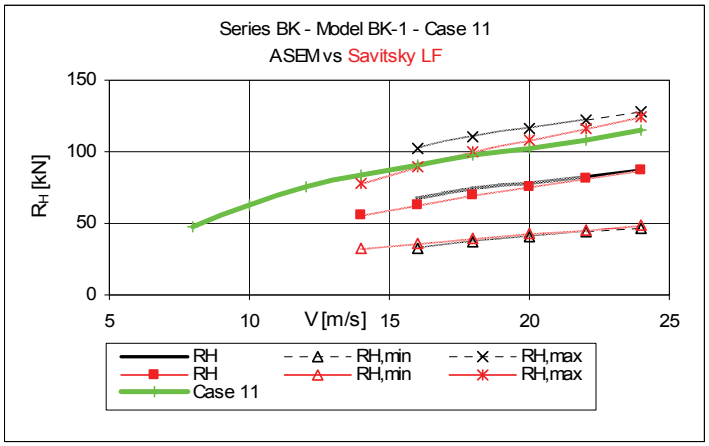

[c]

Figure 14.7-59 Model BK-1 - Case 11

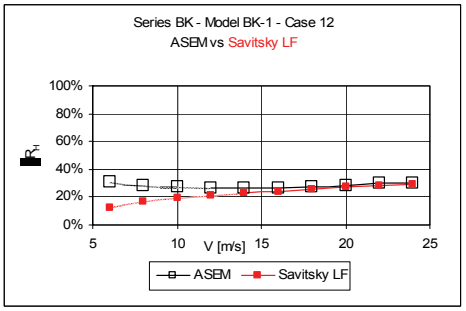

[a]

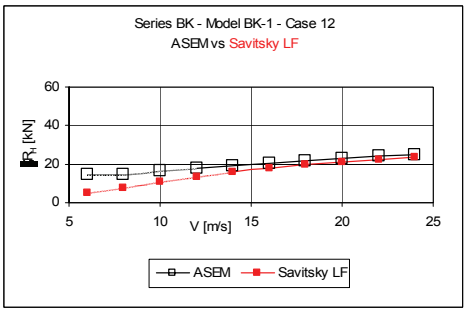

[b]

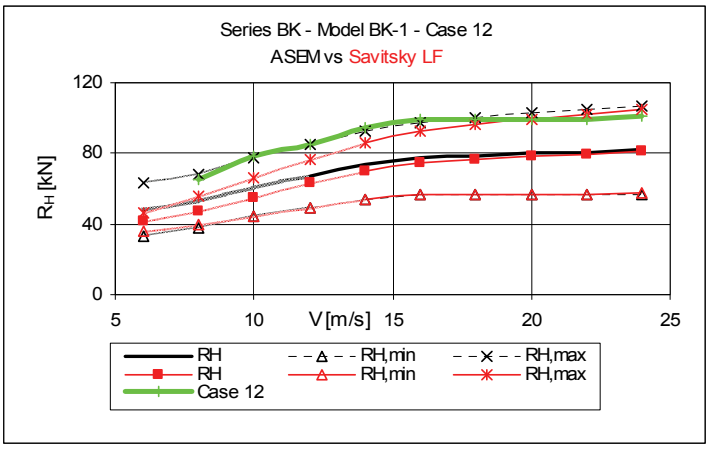

[c]

Figure 14.7-60 Model BK-1 - Case 12

14.7.3 Series YP81

14.7.3.1 Model YP81-4

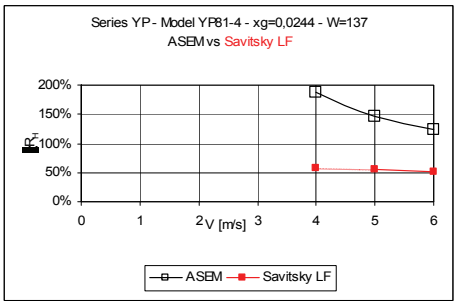

[a]

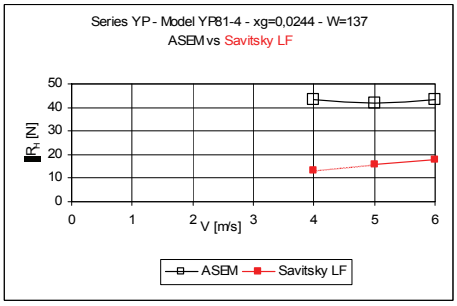

[b]

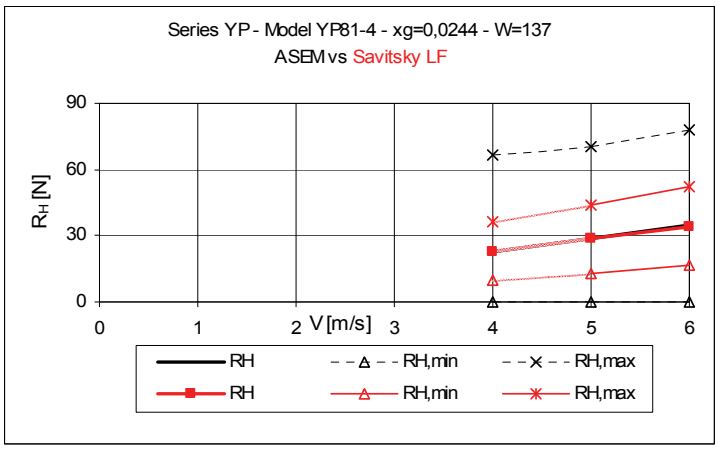

[c]

Figure 14.7-61 Model YP81-4 - xg=0,0244 - W=137

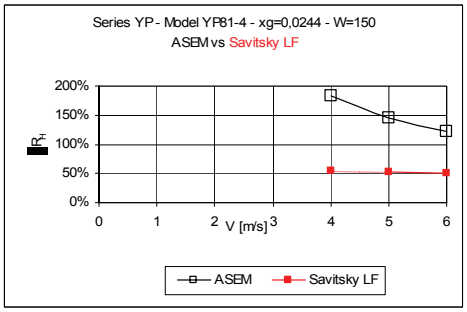

[a]

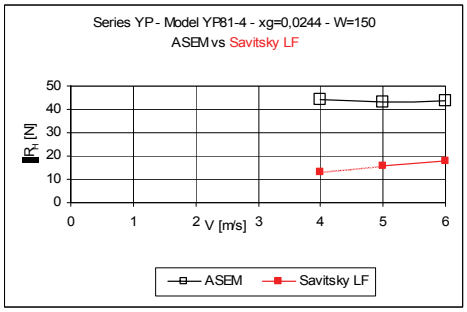

[b]

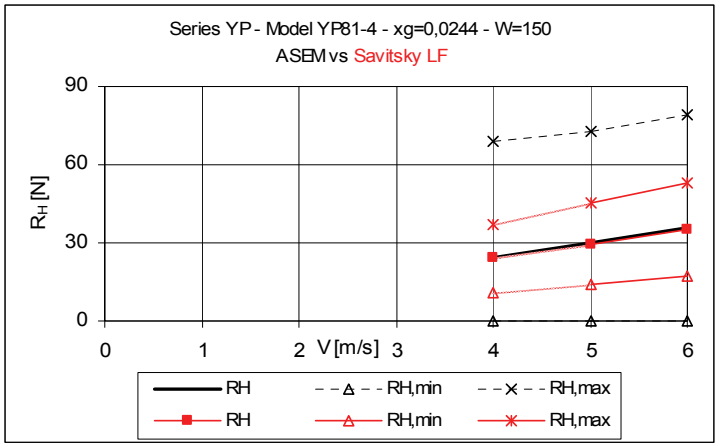

[c]

Figure 14.7-62 Model YP81-4 - xg=0,0244 - W=150

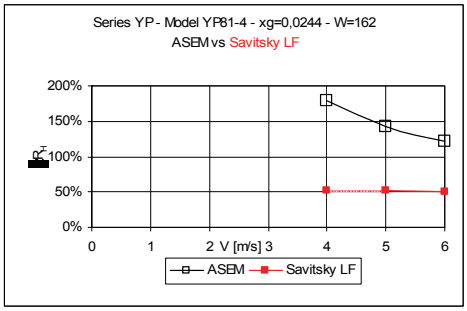

[a]

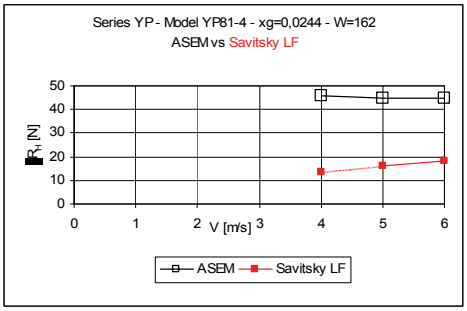

[b]

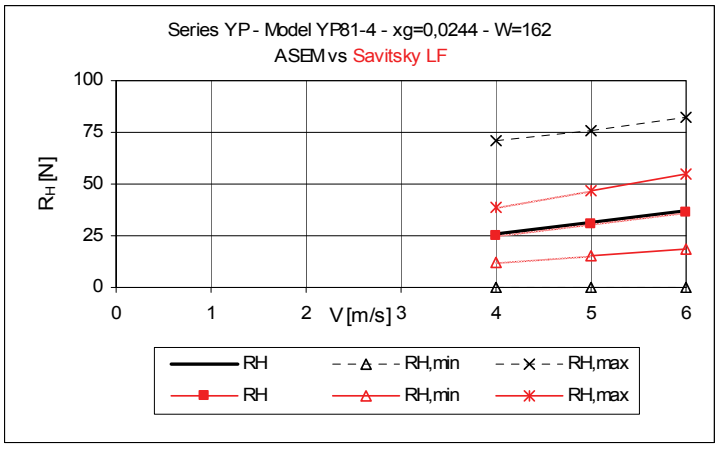

[c]

Figure 14.7-63 Model YP81-4 - xg=0,0244 - W=162

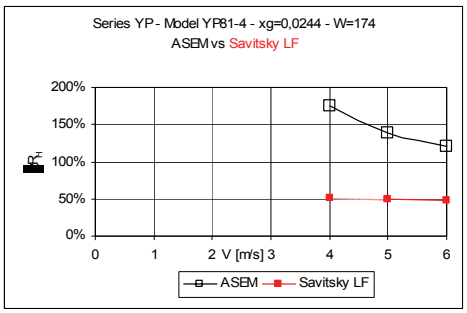

[a]

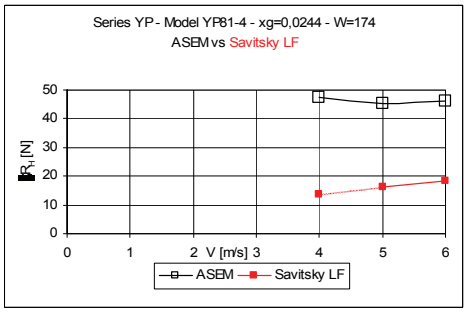

[b]

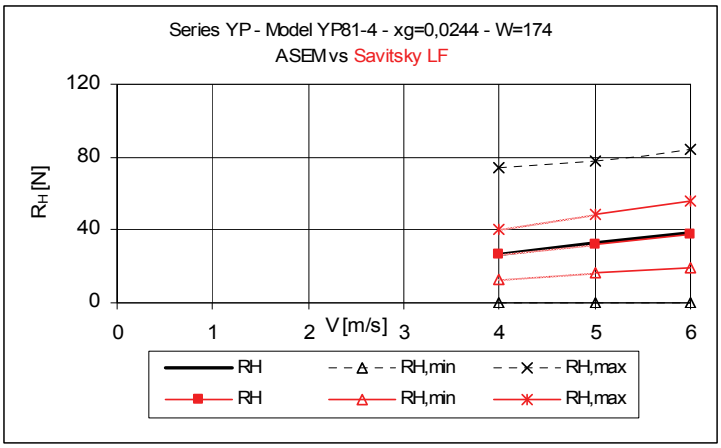

[c]

Figure 14.7-64 Model YP81-4 - xg=0,0244 - W=174

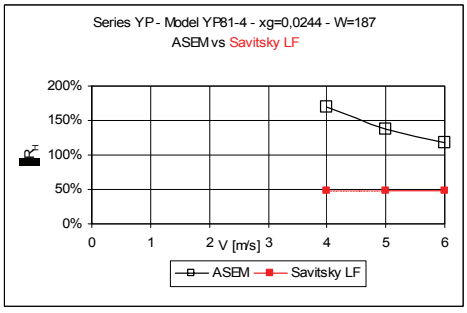

[a]

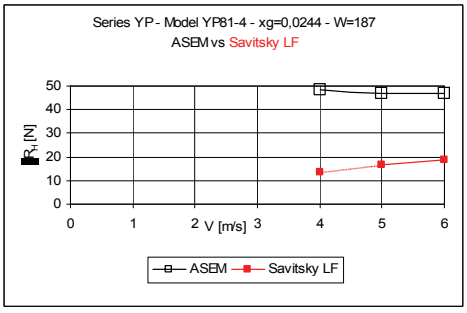

[b]

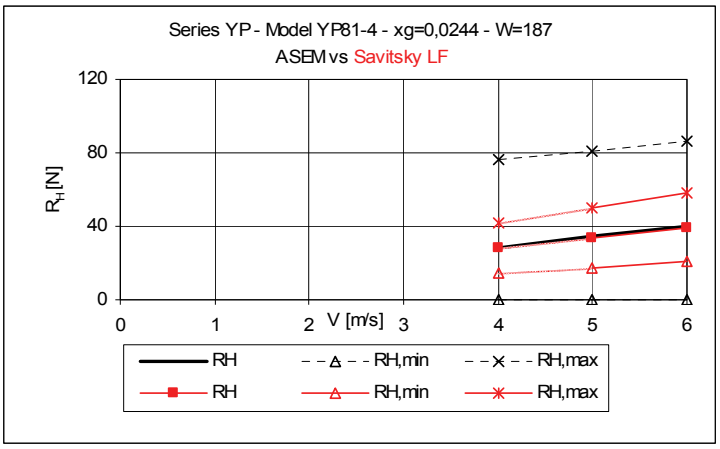

[c]

Figure 14.7-65 Model YP81-4 - xg=0,0244 - W=187

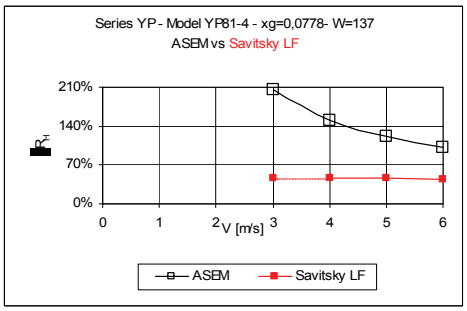

[a]

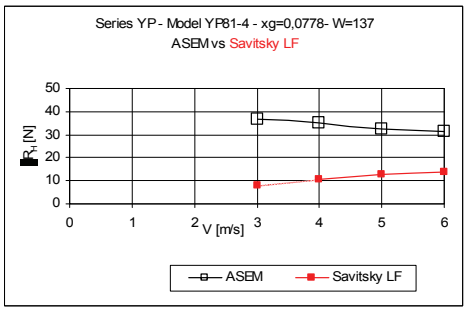

[b]

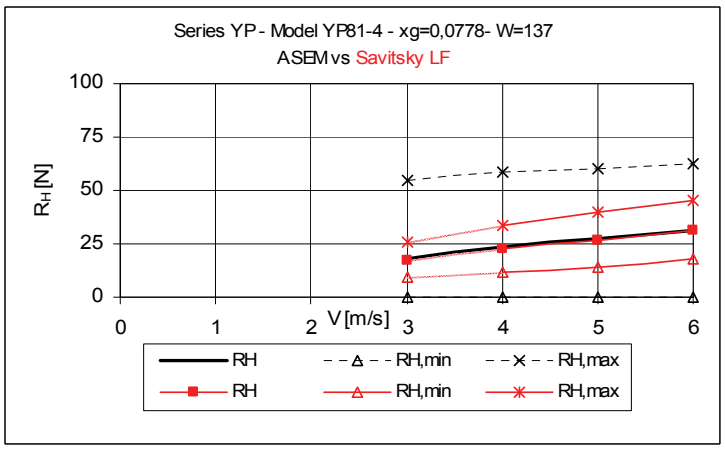

[c]

Figure 14.7-66 Model YP81-4 - xg=0,0778 - W=137

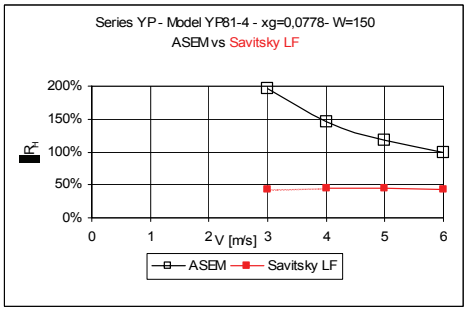

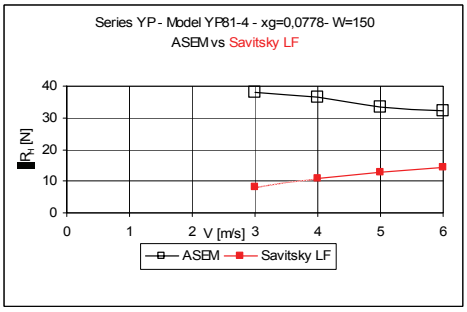

[a]

[b]

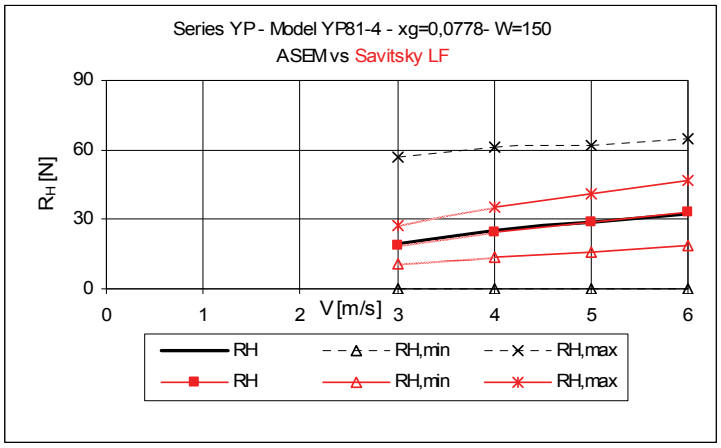

[c]

Figure 14.7-67 Model YP81-4 - xg=0,0778 - W=150

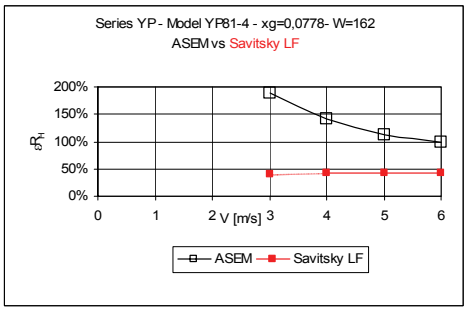

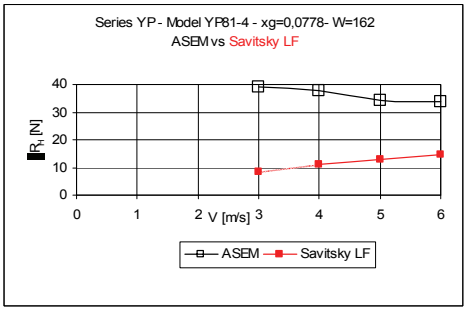

[a]

[b]

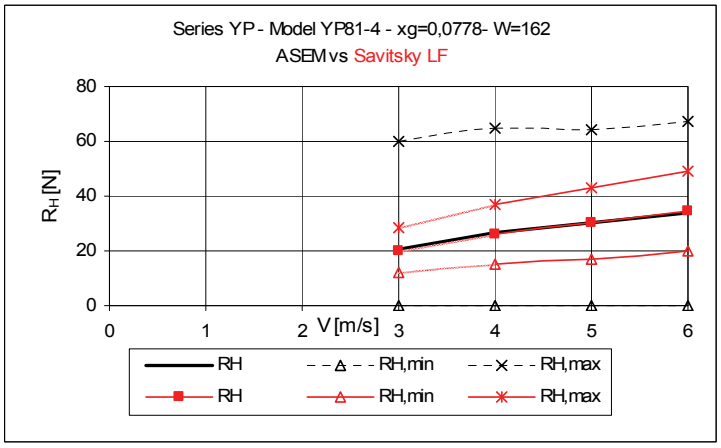

[c]

Figure 14.7-68 Model YP81-4 - xg=0,0778 - W=162

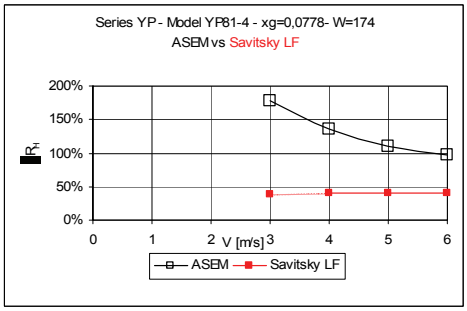

[a]

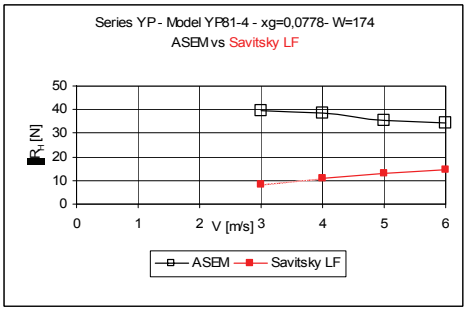

[b]

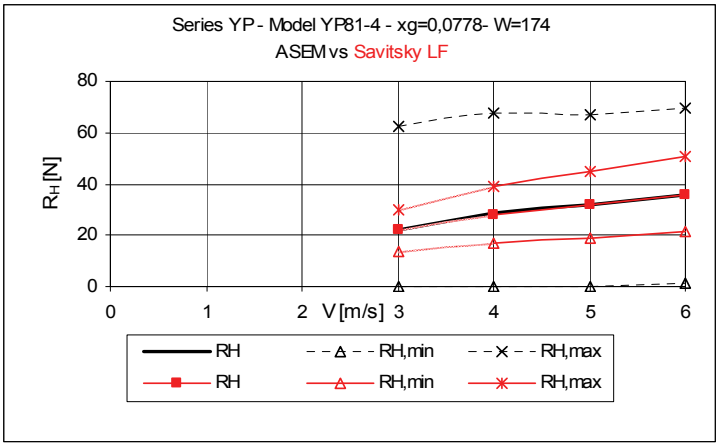

[c]

Figure 14.7-69 Model YP81-4 - xg=0,0778 - W=174

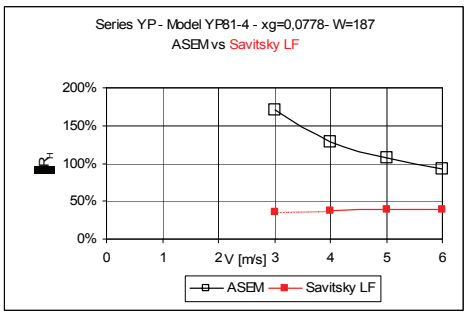

[a]

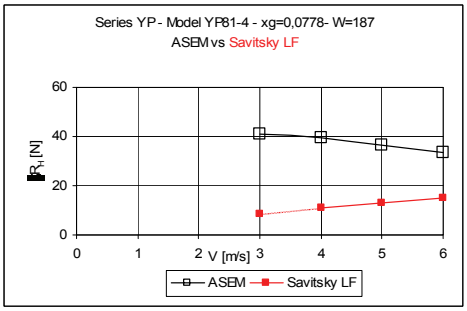

[b]

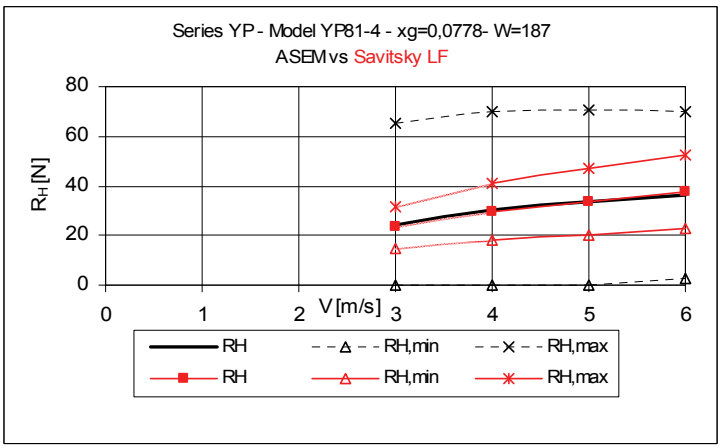

[c]

Figure 14.7-70 Model YP81-4 - xg=0,0778 - W=187

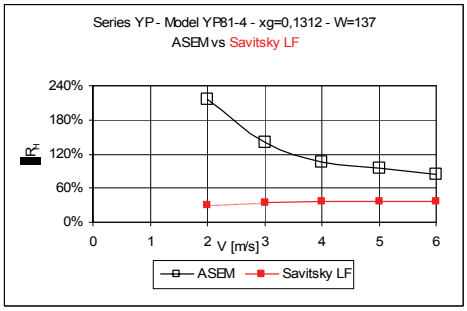

[a]

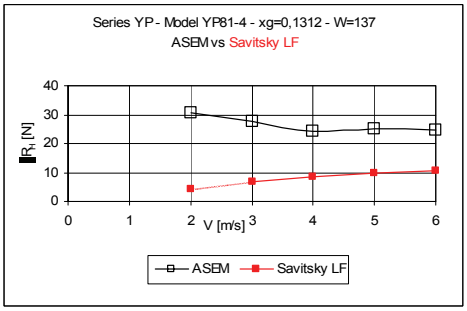

[b]

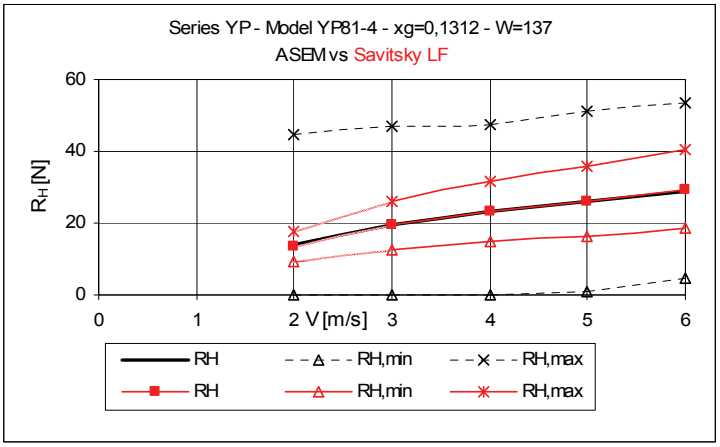

[c]

Figure 14.7-71 Model YP81-4 - xg=0,1312 - W=137

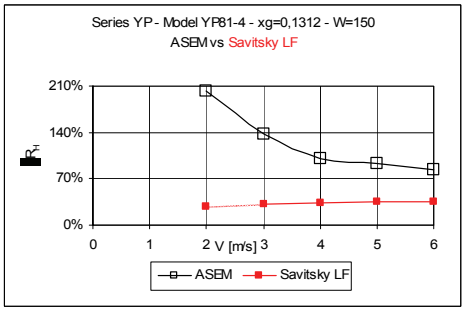

[a]

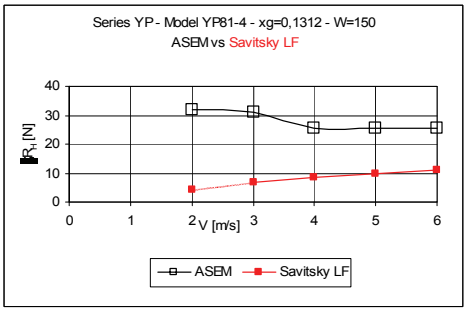

[b]

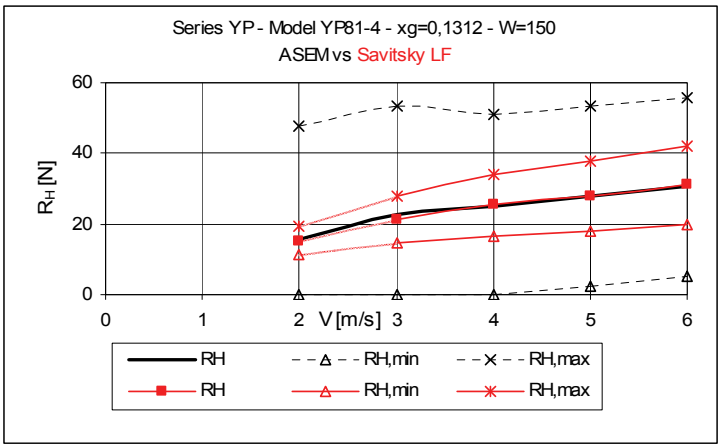

[c]

Figure 14.7-72 Model YP81-4 - xg=0,1312 - W=150

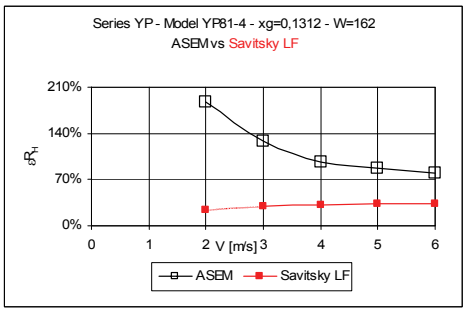

[a]

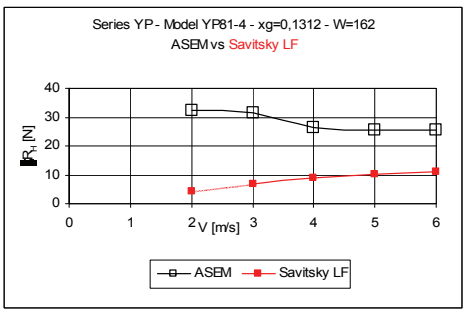

[b]

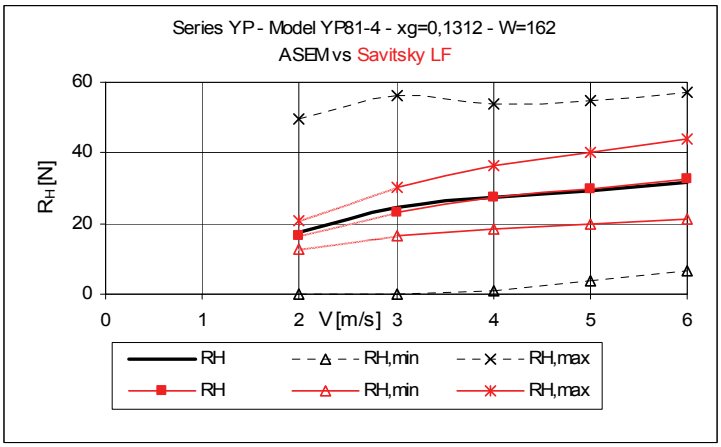

[c]

Figure 14.7-73 Model YP81-4 - xg=0,1312 - W=162

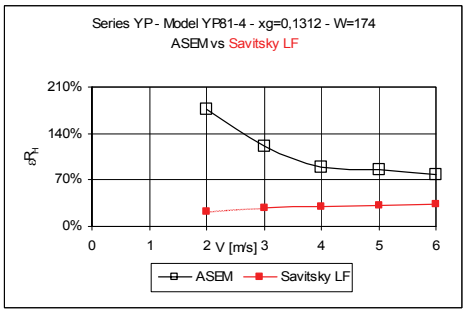

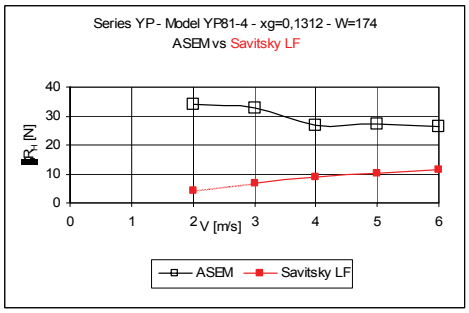

[a]

[b]

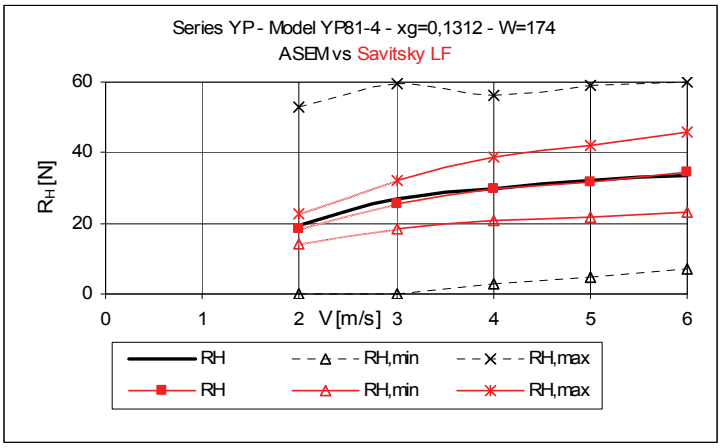

[c]

Figure 14.7-74 Model YP81-4 - xg=0,1312 - W=174

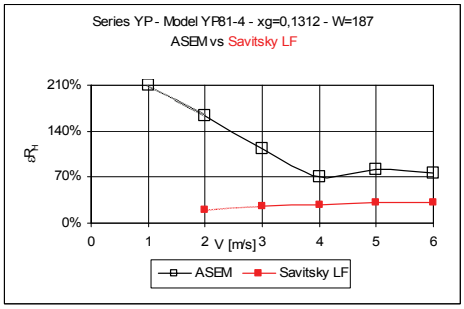

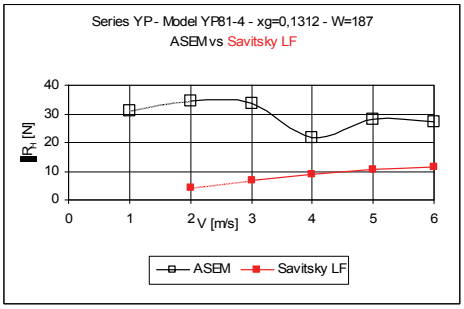

[a]

[b]

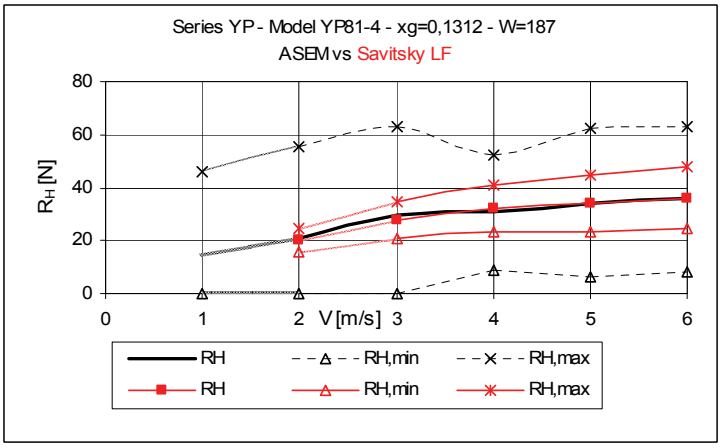

[c]

Figure 14.7-75 Model YP81-4 - xg=0,1312 - W=187

14.7.3.2 Model YP81-5

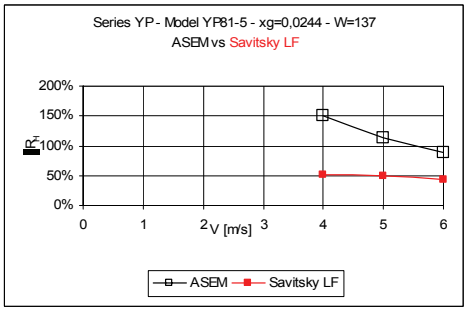

[a]

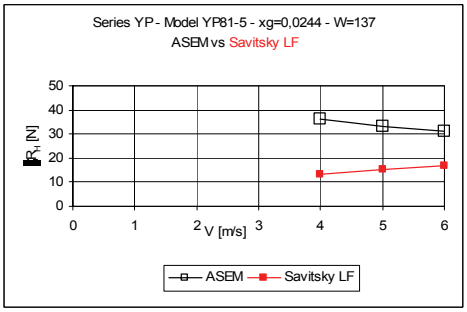

[b]

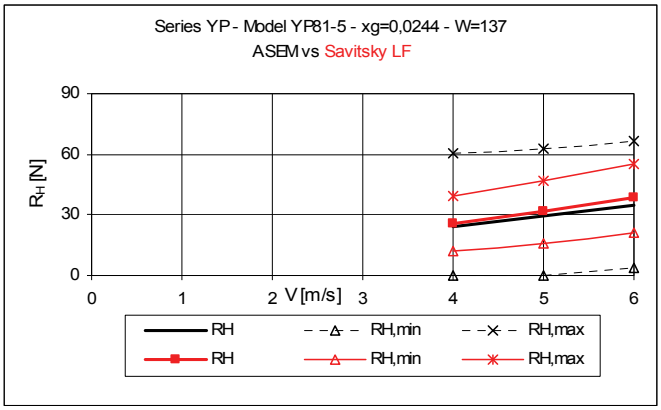

[c]

Figure 14.7-76 Model YP81-5 - xg=0,0244 - W=137

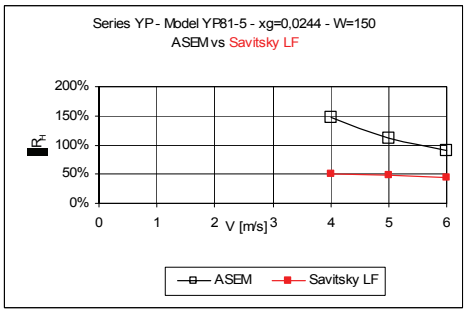

[a]

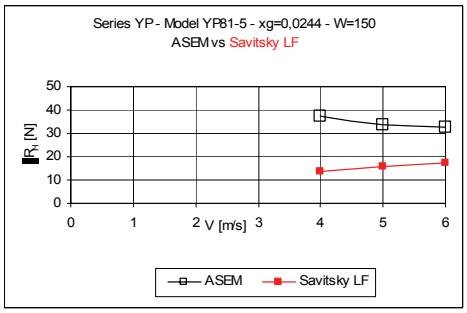

[b]

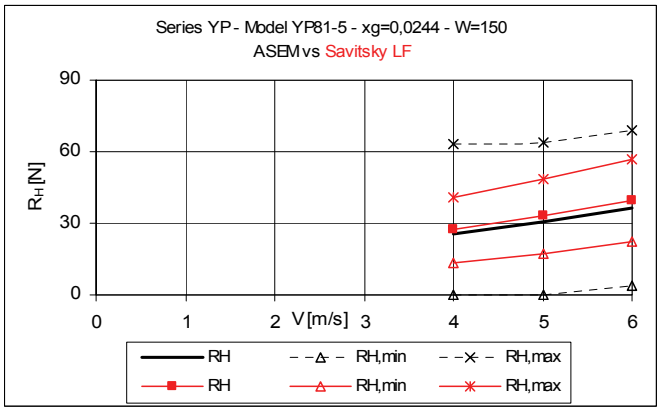

[c]

Figure 14.7-77 Model YP81-5 - xg=0,0244 - W=150

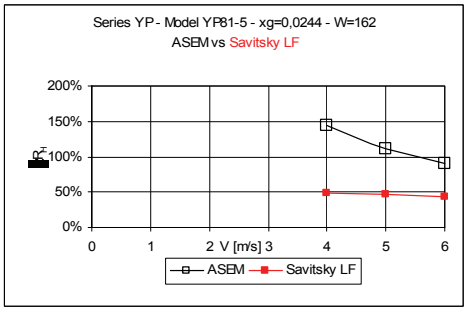

[a]

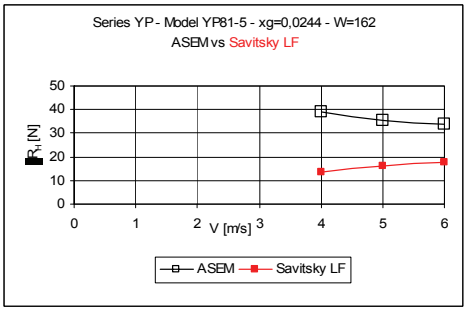

[b]

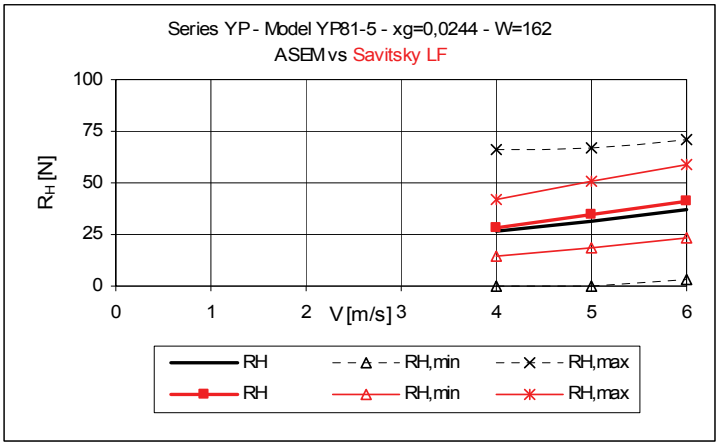

[c]

Figure 14.7-78 Model YP81-5 - xg=0,0244 - W=162

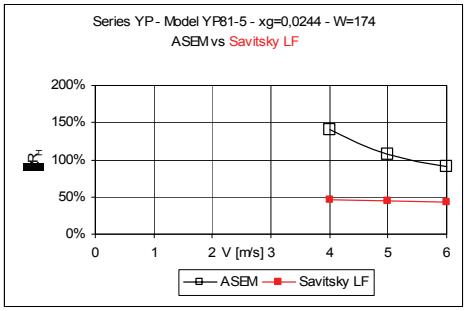

[a]

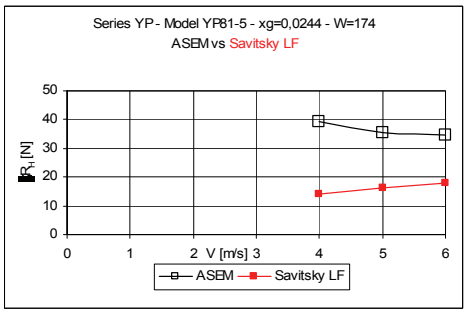

[b]

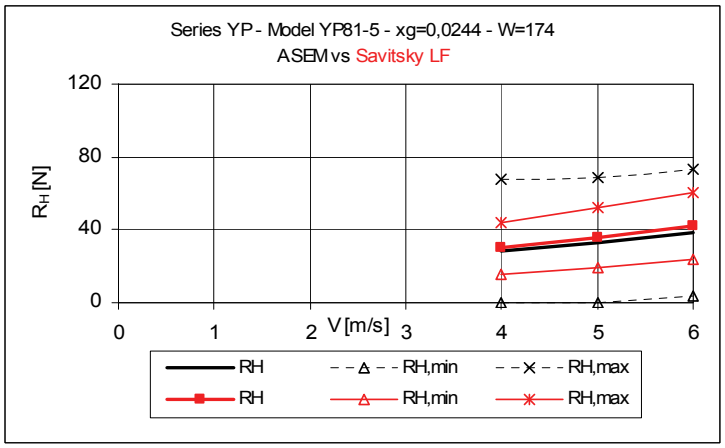

[c]

Figure 14.7-79 Model YP81-5 - xg=0,0244 - W=174

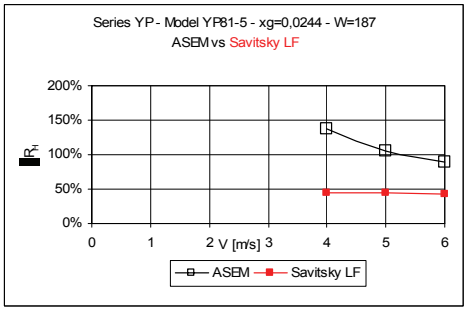

[a]

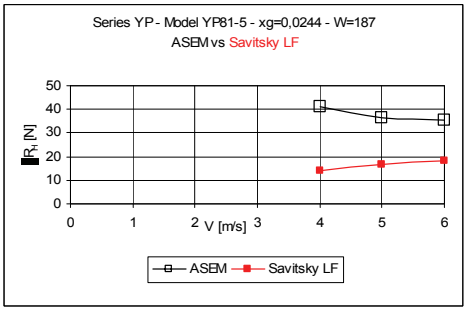

[b]

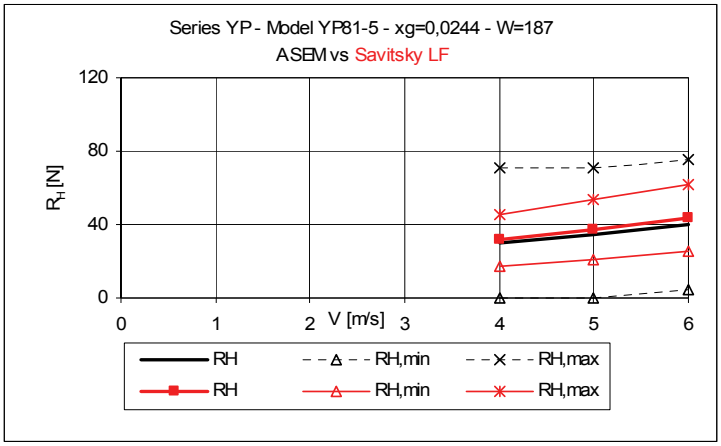

[c]

Figure 14.7-80 Model YP81-5 - xg=0,0244 - W=187

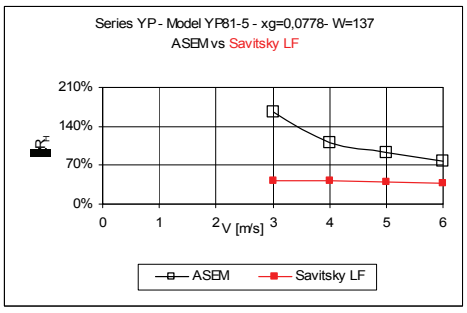

[a]

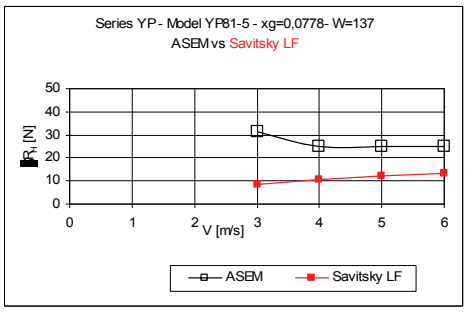

[b]

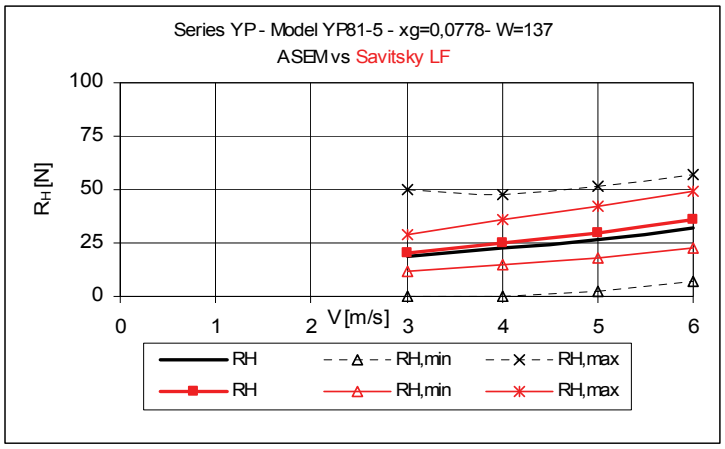

[c]

Figure 14.7-81 Model YP81-5 - xg=0,0778 - W=137

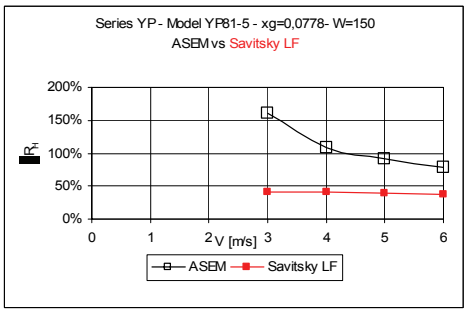

[a]

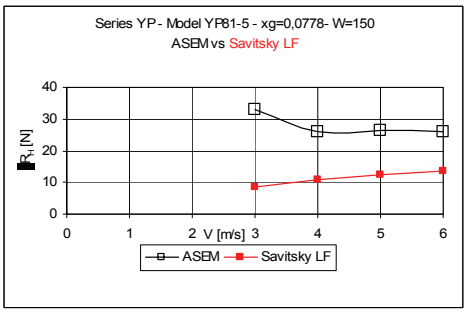

[b]

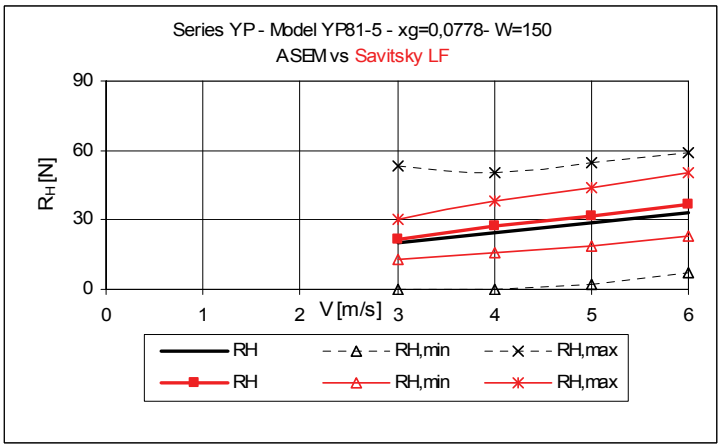

[c]

Figure 14.7-82 Model YP81-5 - xg=0,0778 - W=150

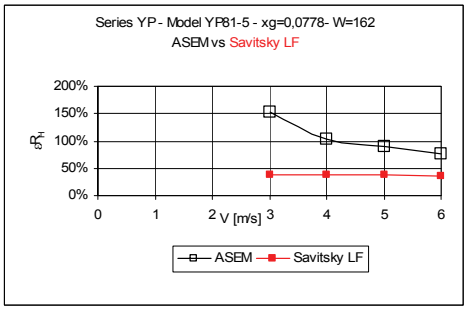

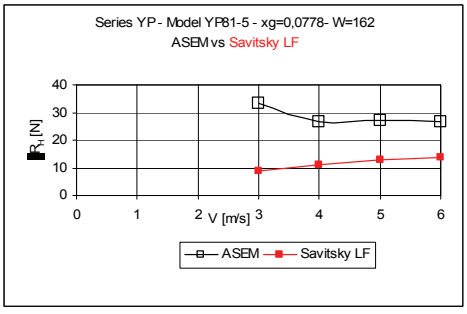

[a]

[b]

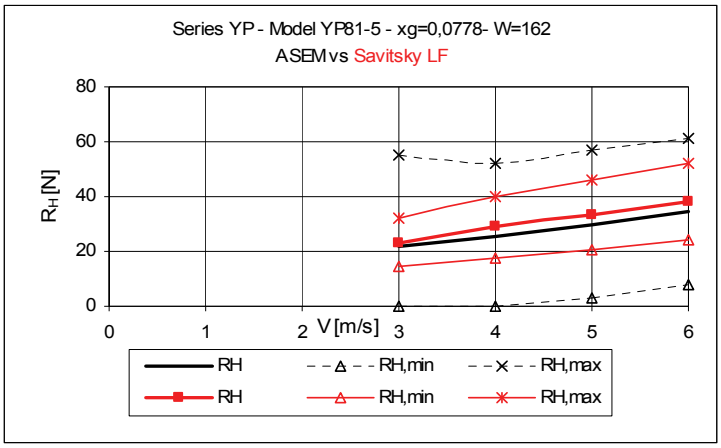

[c]

Figure 14.7-83 Model YP81-5 - xg=0,0778 - W=162

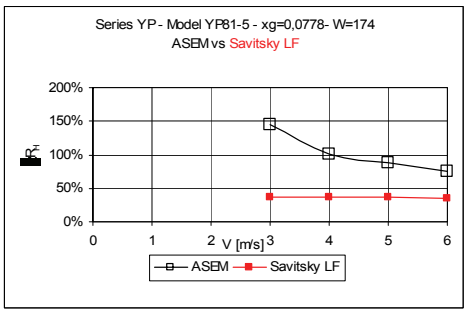

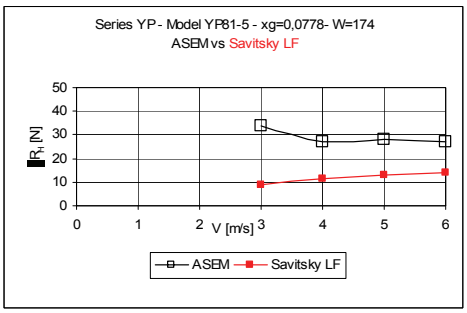

[a]

[b]

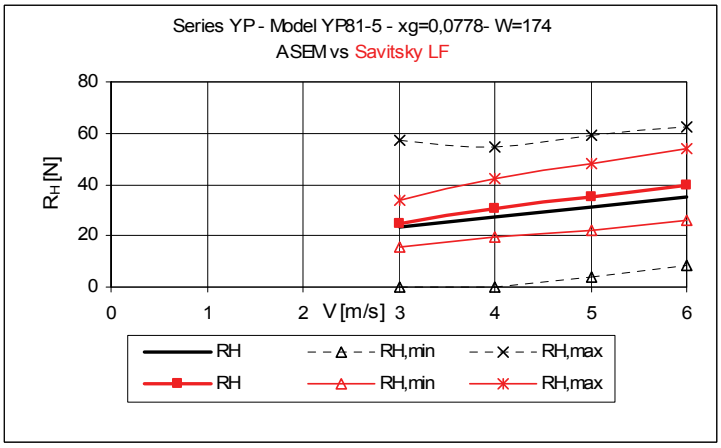

[c]

Figure 14.7-84 Model YP81-5 - xg=0,0778 - W=174

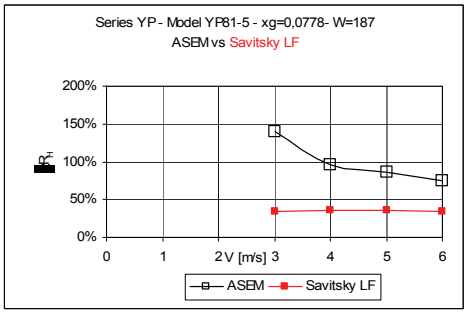

[a]

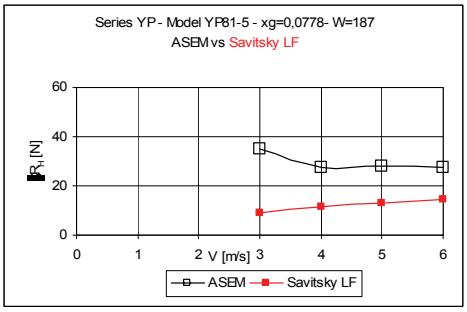

[b]

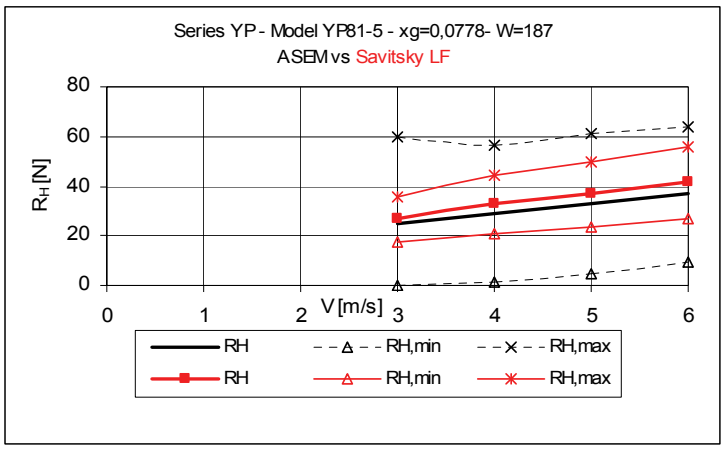

[c]

Figure 14.7-85 Model YP81-5 - xg=0,0778 - W=187

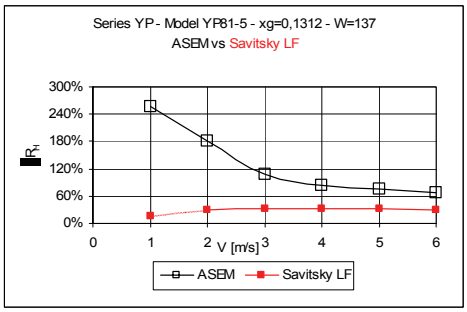

[a]

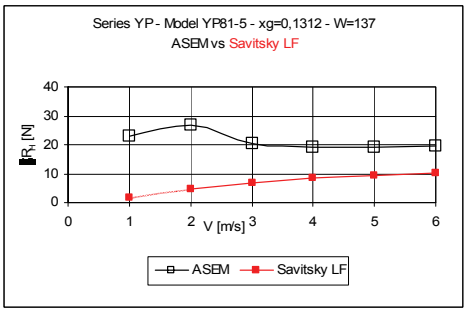

[b]

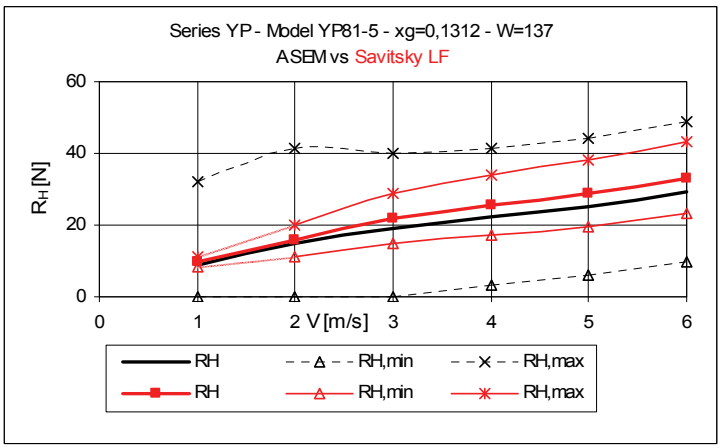

[c]

Figure 14.7-86 Model YP81-5 - xg=0,1312 - W=137

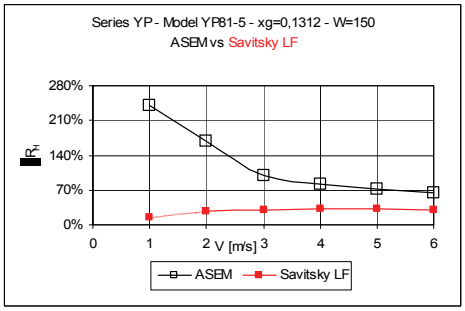

[a]

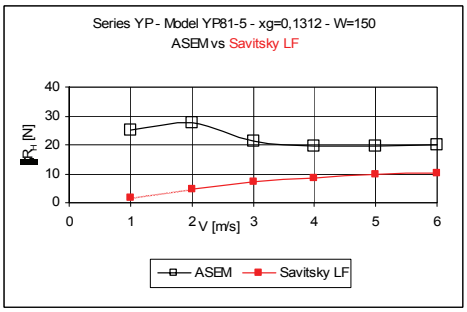

[b]

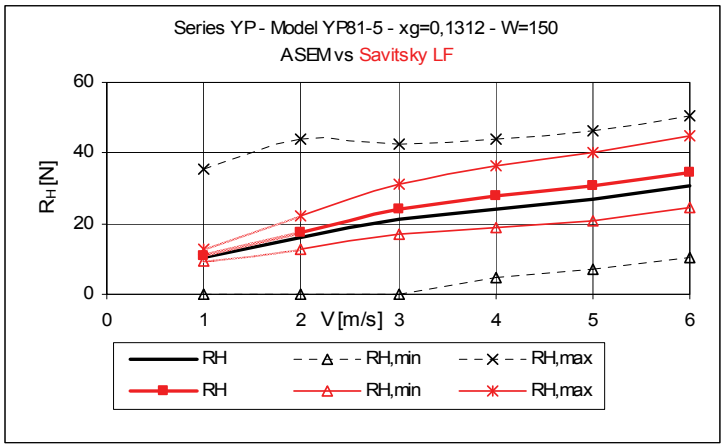

[c]

Figure 14.7-87 Model YP81-5 - xg=0,1312 - W=150

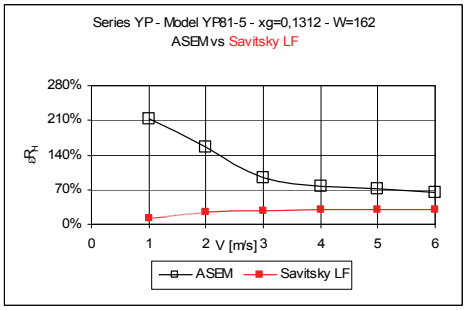

[a]

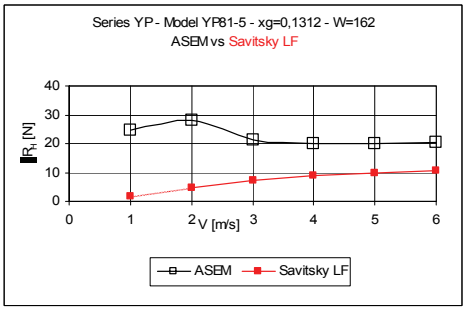

[b]

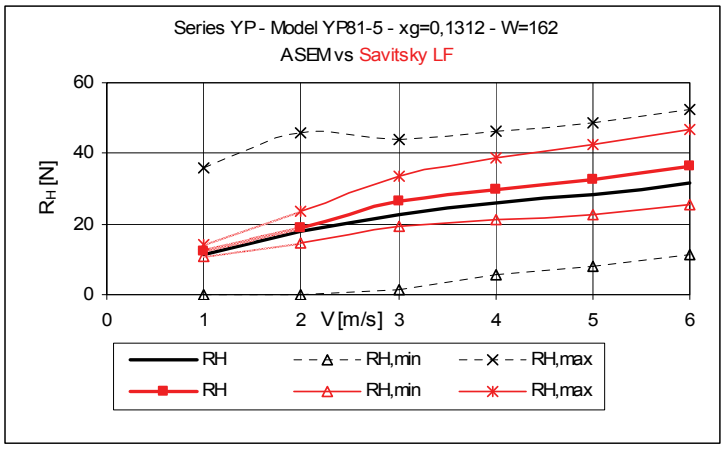

[c]

Figure 14.7-88 Model YP81-5 - xg=0,1312 - W=162

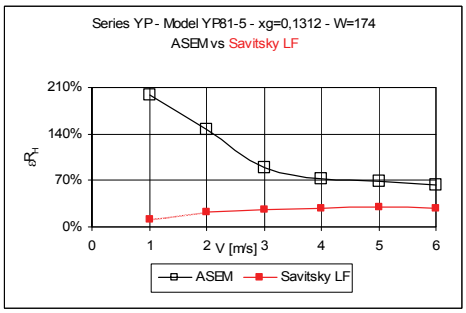

[a]

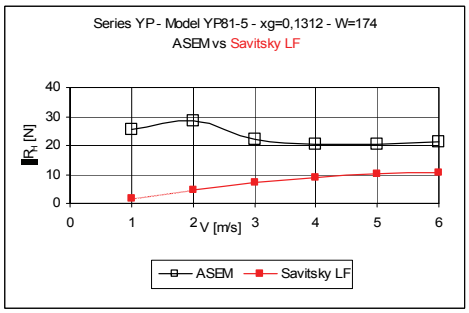

[b]

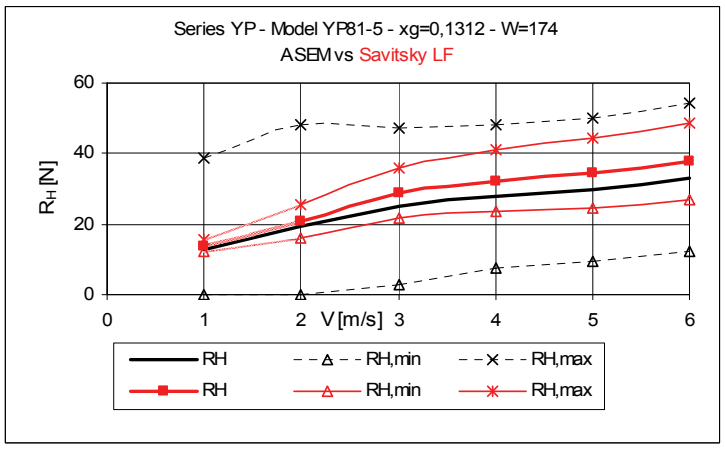

[c]

Figure 14.7-89 Model YP81-5 - xg=0,1312 - W=174

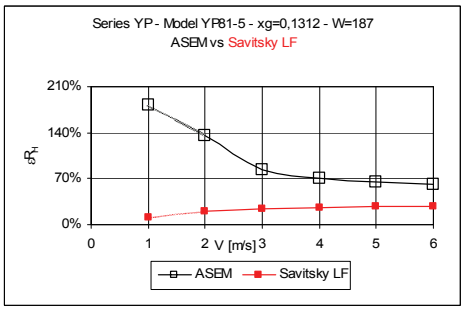

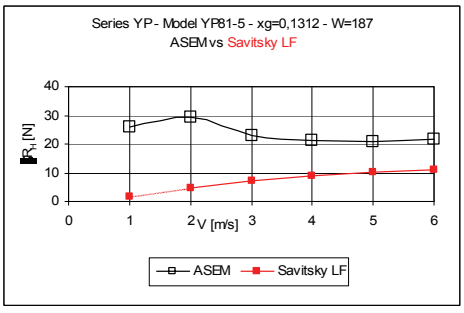

[a]

[b]

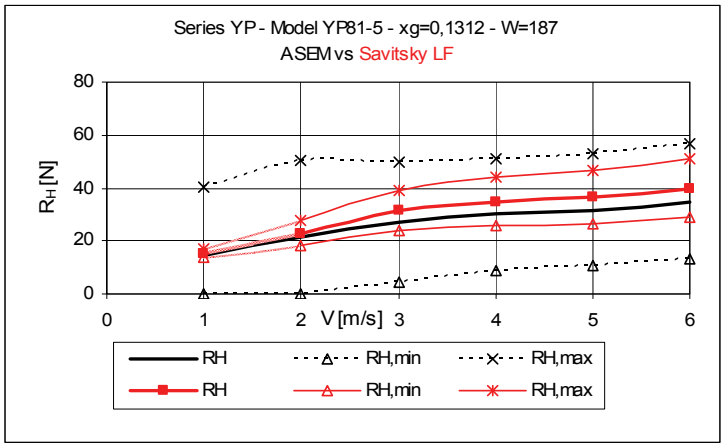

[c]

Figure 14.7-90 Model YP81-5 - xg=0,1312 - W=187

14.7.3.3 Model YP81-6

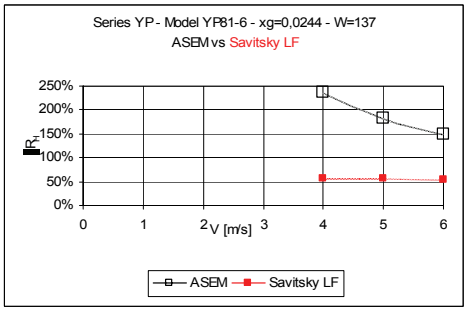

[a]

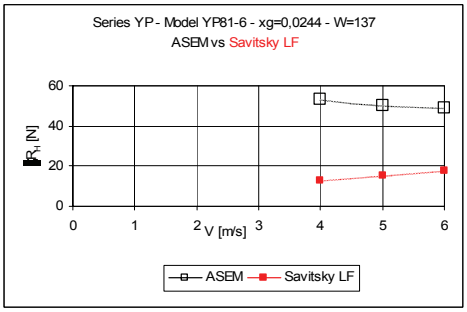

[b]

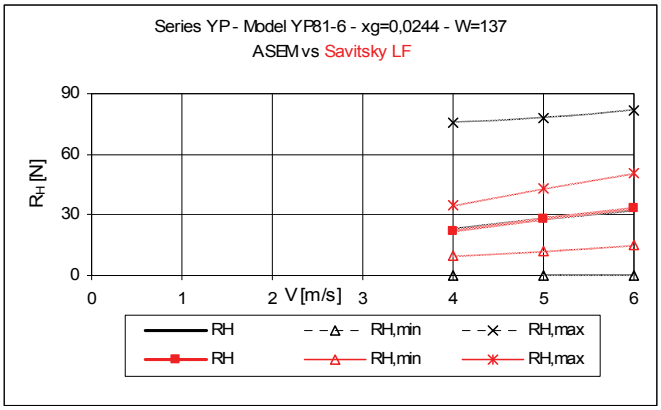

[c]

Figure 14.7-91 Model YP81-6 - xg=0,0244 - W=137

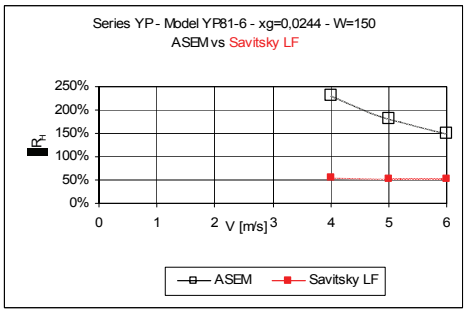

[a]

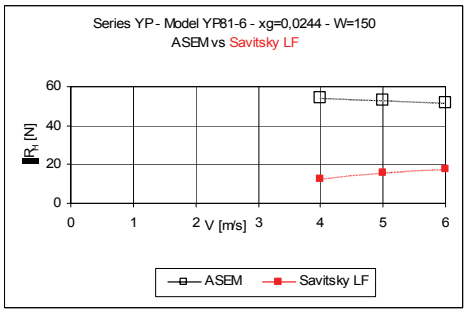

[b]

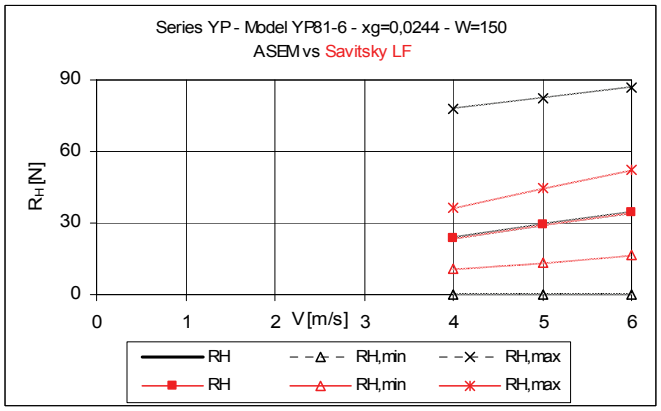

[c]

Figure 14.7-92 Model YP81-6 - xg=0,0244 - W=150

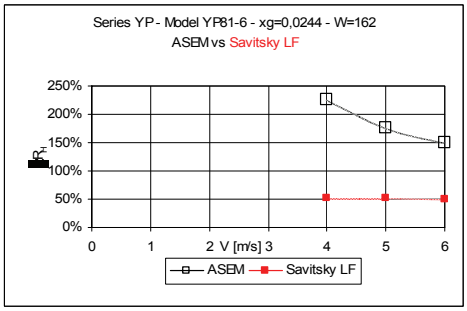

[a]

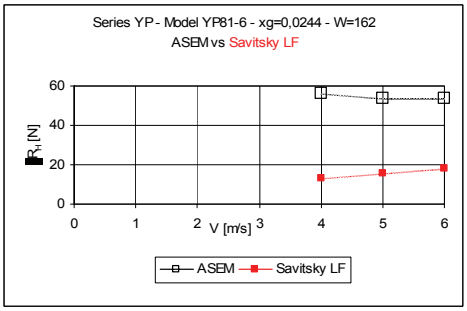

[b]

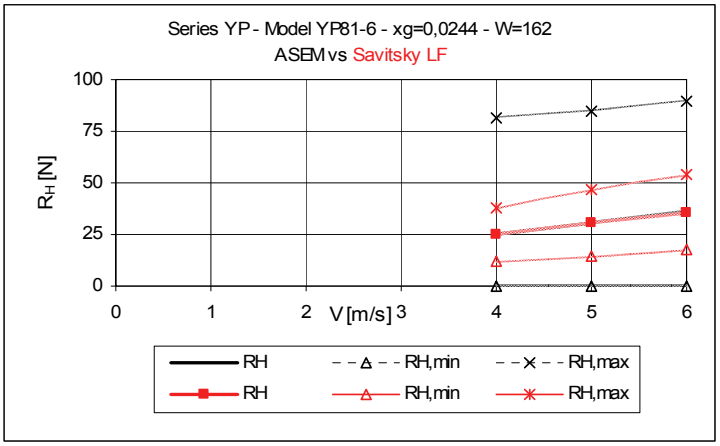

[c]

Figure 14.7-93 Model YP81-6 - xg=0,0244 - W=162

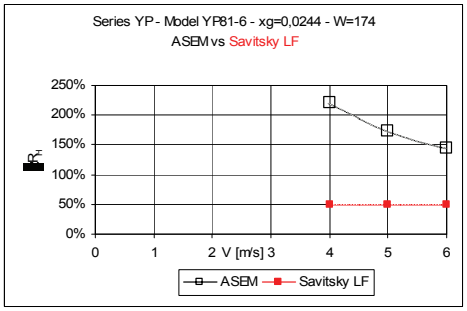

[a]

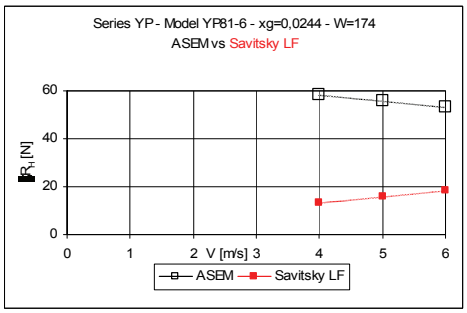

[b]

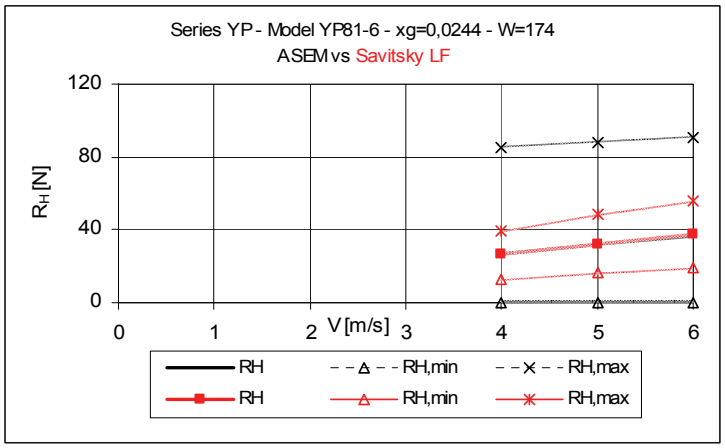

[c]

Figure 14.7-94 Model YP81-6 - xg=0,0244 - W=174

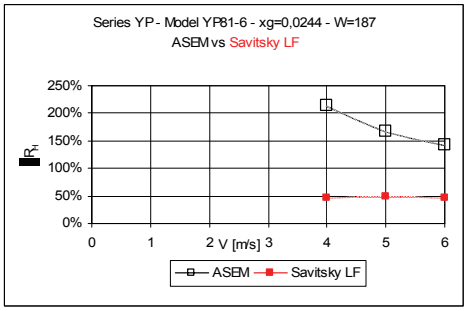

[a]

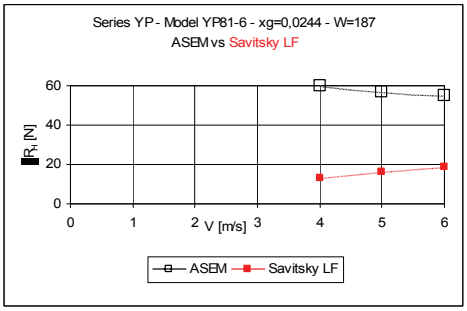

[b]

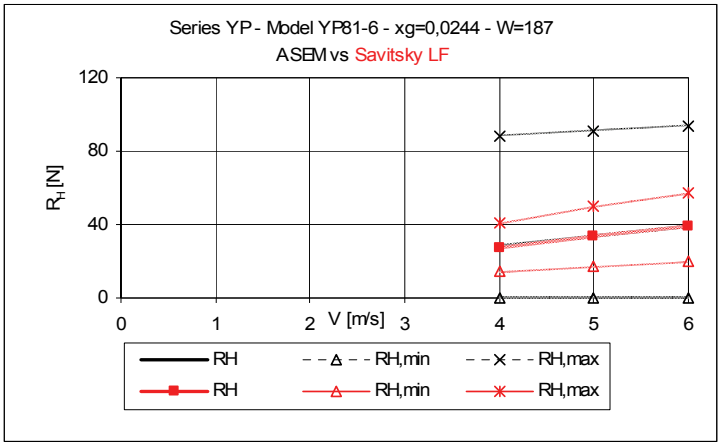

[c]

Figure 14.7-95 Model YP81-6 - xg=0,0244 - W=187

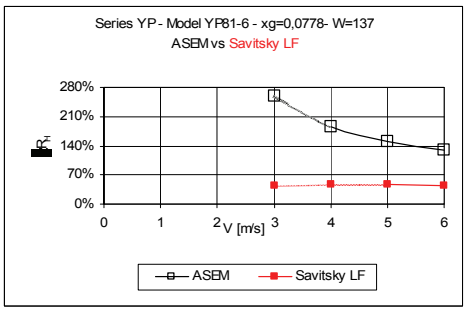

[a]

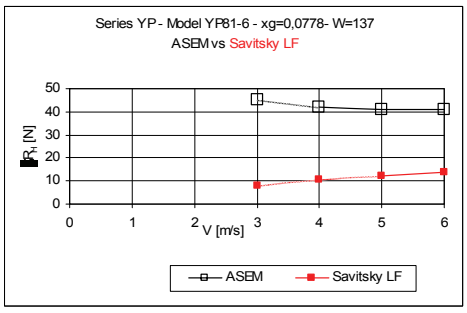

[b]

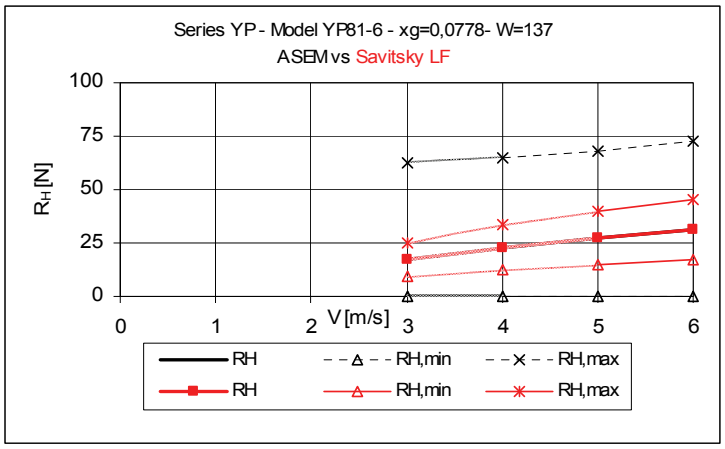

[c]

Figure 14.7-96 Model YP81-6 - xg=0,0778 - W=137

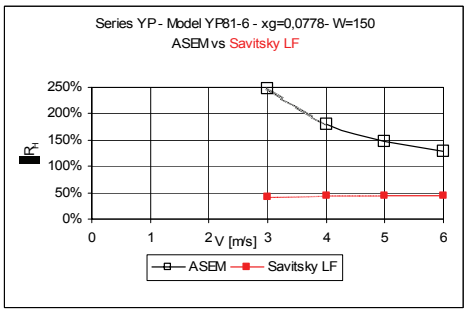

[a]

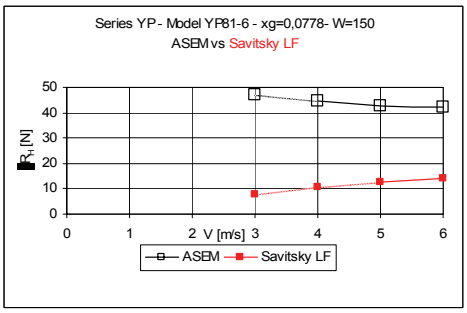

[b]

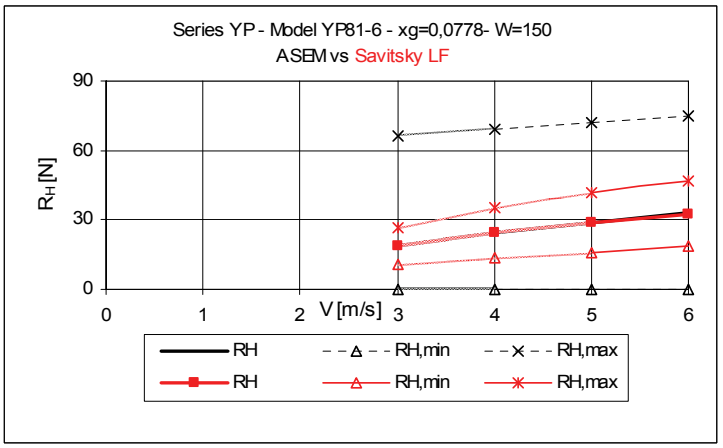

[c]

Figure 14.7-97 Model YP81-6 - xg=0,0778 - W=150

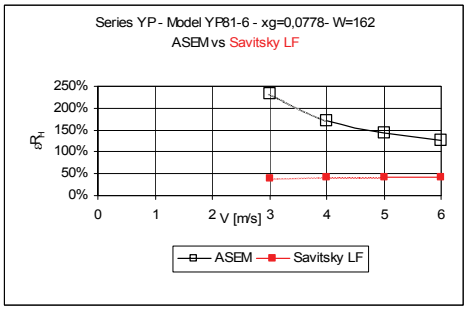

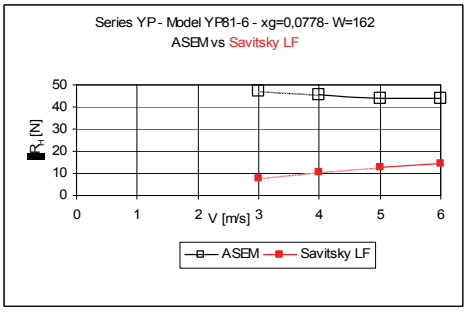

[a]

[b]

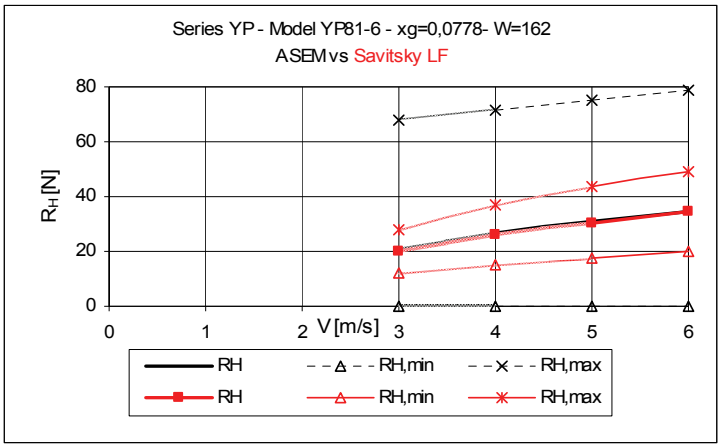

[c]

Figure 14.7-98 Model YP81-6 - xg=0,0778 - W=162

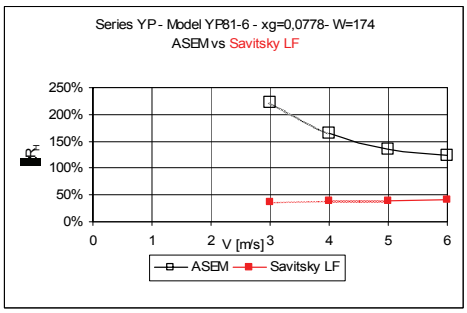

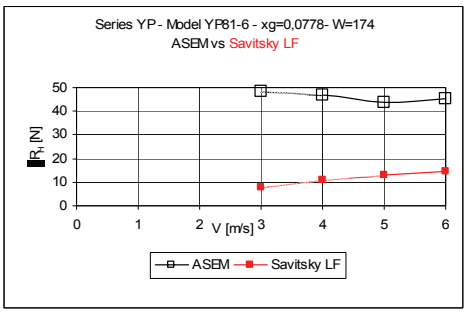

[a]

[b]

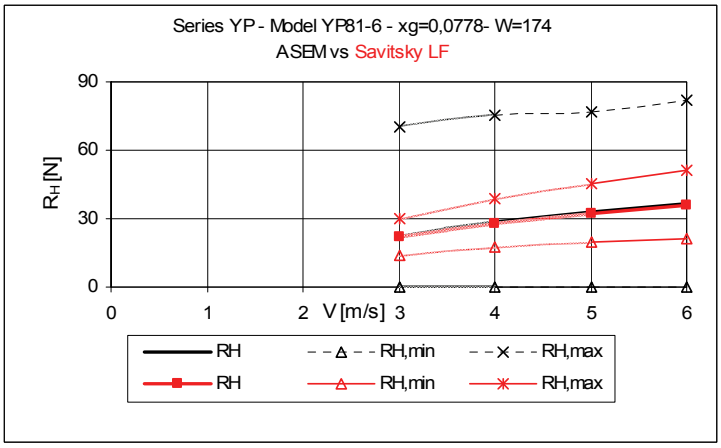

[c]

Figure 14.7-99 Model YP81-6 - xg=0,0778 - W=174

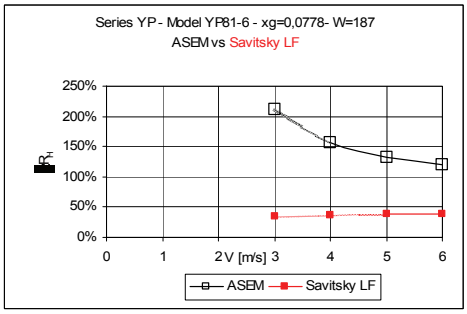

[a]

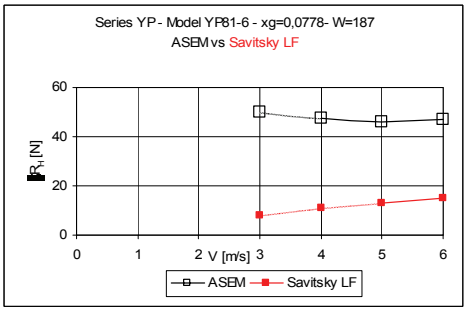

[b]

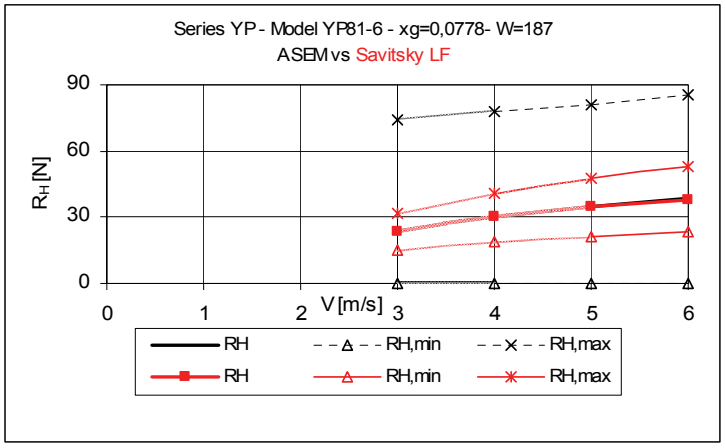

[c]

Figure 14.7-100 Model YP81-6 - xg=0,0778 - W=187

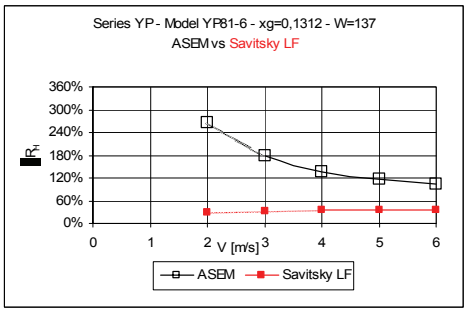

[a]

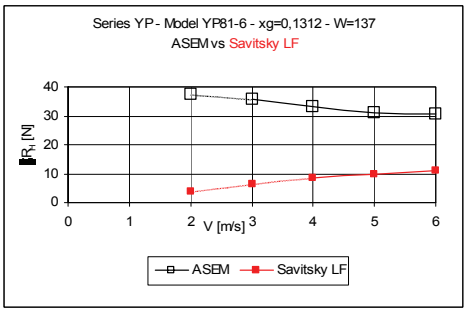

[b]

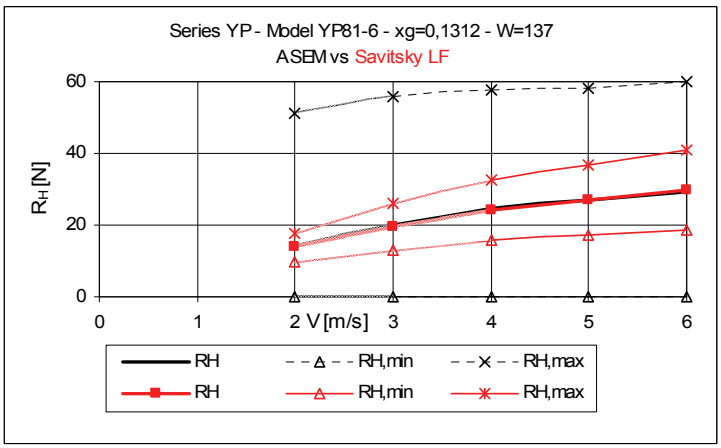

[c]

Figure 14.7-101 Model YP81-6 - xg=0,1312 - W=137

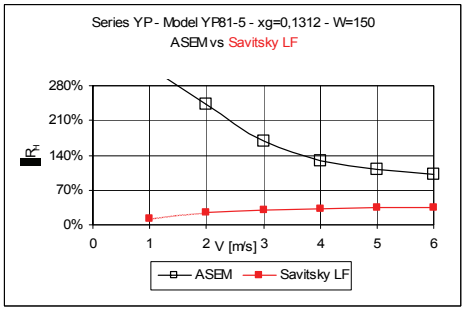

[a]

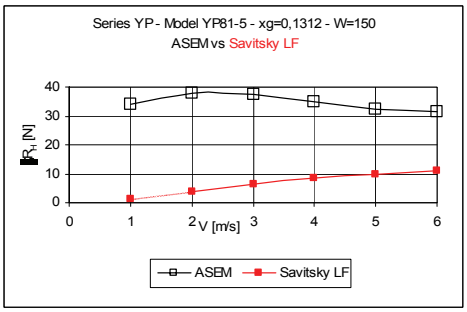

[b]

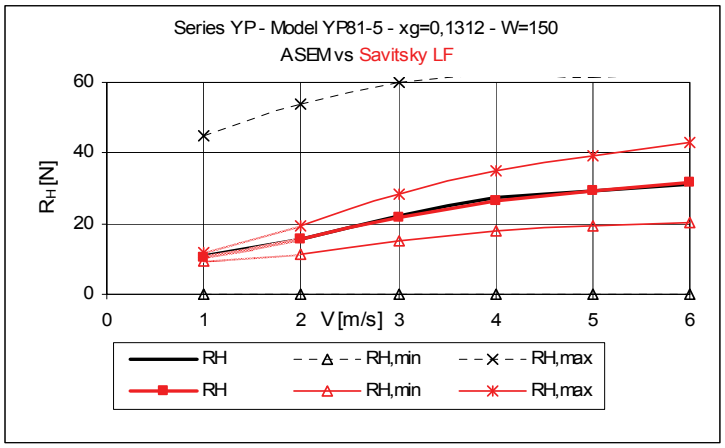

[c]

Figure 14.7-102 Model YP81-6 - xg=0,1312 - W=150

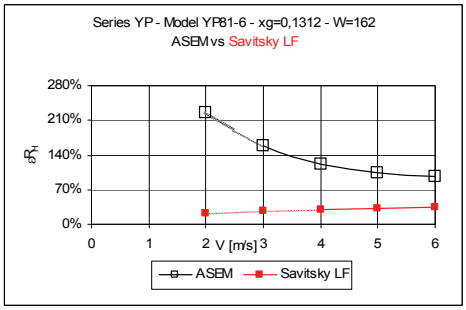

[a]

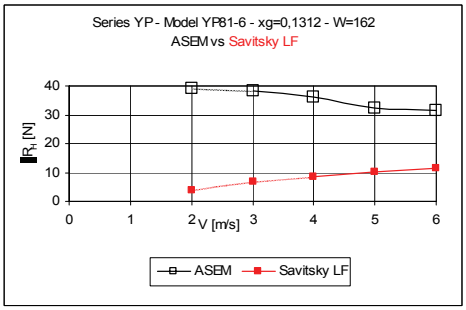

[b]

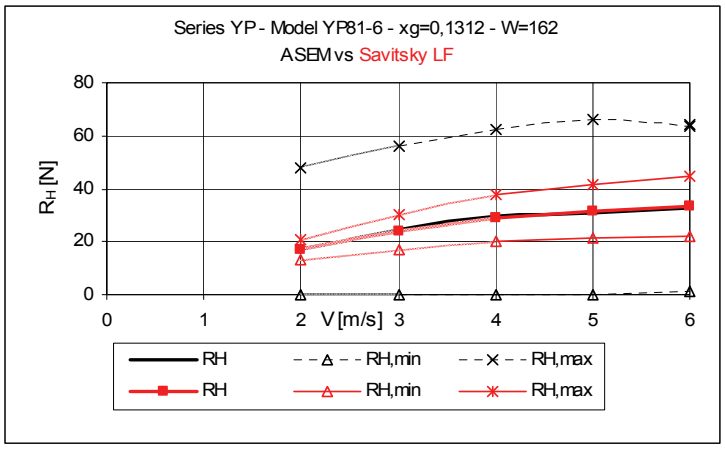

[c]

Figure 14.7-103 Model YP81-6 - xg=0,1312 - W=162

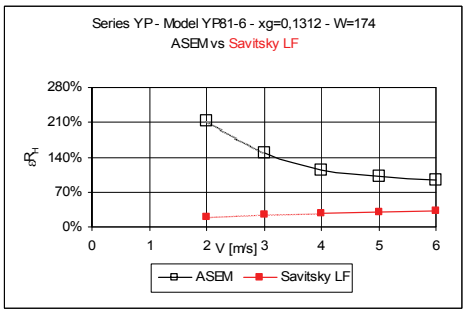

[a]

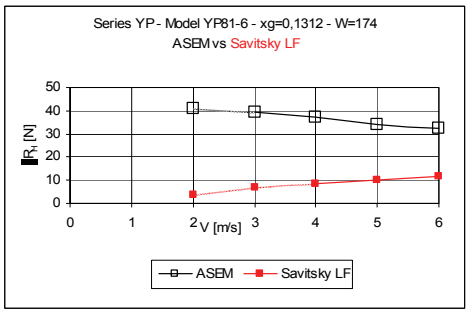

[b]

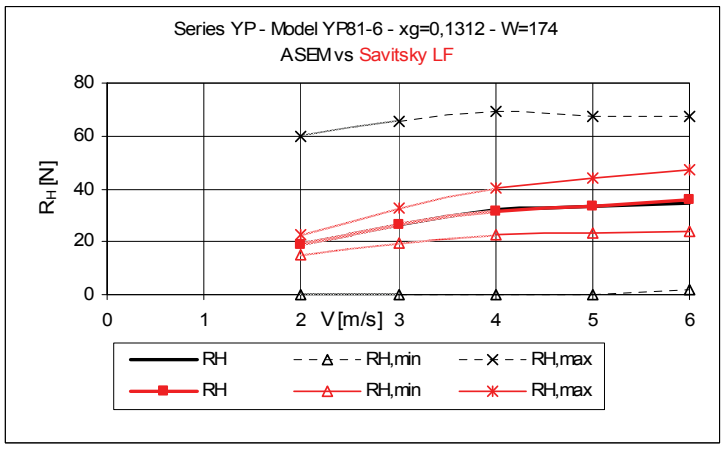

[c]

Figure 14.7-104 Model YP81-6 - xg=0,1312 - W=174

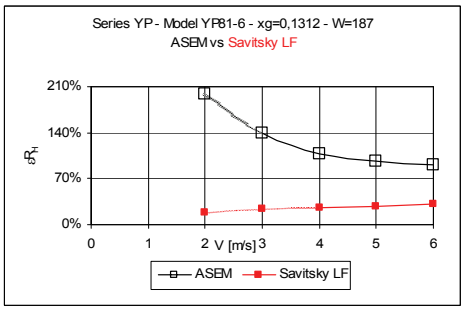

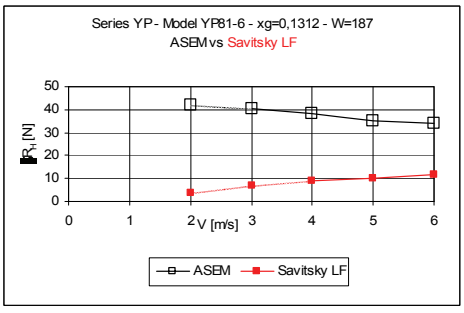

[a]

[b]

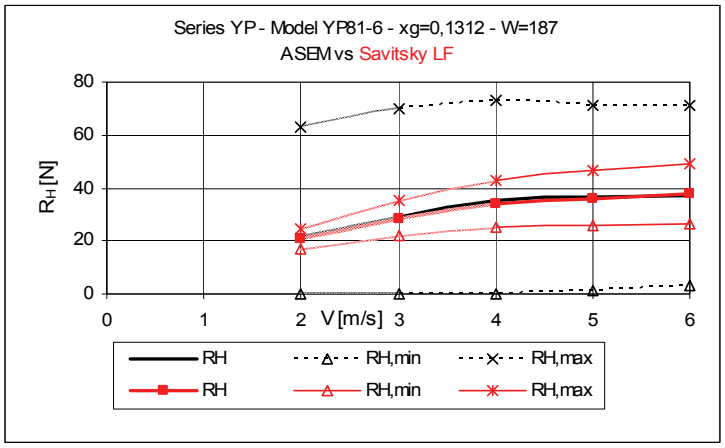

[c]

Figure 14.7-105 Model YP81-6 - xg=0,1312 - W=187

14.8 Conclusion

The error propagation analysis has been applied to ASEM, with the objective of evaluating the sensitivity of this method.

In order to achieve this goal, relative errors (εR_H) as well as uncertainties (∂R_H) have been computed taking in account ASEM results pertinent to different Hull Series.

Further, error propagation analysis has been applied to Savitsky‘s method too, in order to get an overall comparison.

Data comparison has been developed in term of bare hull resistance, uncertainties and relative errors, versus hull speed V .

Errors here computed are “potential” errors: a “real” [144] error will be not higher than its “potential” value.

ASEM and Savitsky’s results without physical meaning has not been taken in account meanwhile results with physical meaning and relate to data out of range have been reported. Further ASEM results has been reported in black as well as Savitsky’s results in red.

In all cases analyzed Savitsky’s relative errors are lower than ASEM ones. This is due to the fact that the number of computational steps in Savitsky’s procedure is lower than ASEM: higher number of calculations higher error magnitude.

In the most of cases ASEM results cover a wider range than Savitsky’s ones and, with the exception of Series 62, they are just a little closer to test results than Savitsky’s ones, but at the same time and for all cases analyzed ASEM results are closer to Savitsky’s ones than test results.

Accordingly to the above remarks, ASEM data are the best in term of results and the worst in term of uncertain of results.

[144] A “real” error is the difference between test result and computed one; this is not true at all, as matter of fact errors related to test results are not available thereby it is not possible to assess their influence on the real error value. Hereinafter all errors (relative as well as uncertainties) considered are “potential”.

14.9 Symbols

B_C	Beam between chines	[m]
C_f	Friction coefficient	
C_F	Corrected Friction coefficient	
$C_{L\beta}$	Lift coefficient for a deadrise surface	
C_{L0}	Lift coefficient of a flat plate equivalent to a V-bottom surface	
${}^iC_{L0}$	Lift coefficient zero deadrise of i^{th} strip	
${}^iC_P$	Wagner's Pressure Coefficient of i^{th} strip	
${}^iC_{P,\max}$	Max Wagner's Pressure Coefficient of i^{th} strip	
${}^iC_P^n$	Normalized Pressure Coefficient of i^{th} strip	
C_V	Froude number related to the beam	
D_F	Friction force	[N]
g	Acceleration of gravity	$9.81 m/s^2$
L_{CP}	Center Pressure position measured from the transom	[m]
L_{WS}	Mean wetted length	[m]
R_H	Bare hull resistance	[N]
R_n	Reynolds number	
V	Hull speed	$[m/s]$
V_m	Mean velocity over bottom of planing surface	$[m/s]$
W	Weight of hull	[N]
∂B_C	Uncertainty of Beam between chines	[m]
∂D_F	Uncertainty of Friction force	[N]
$\partial C_{L\beta}$	Uncertainty of Froude number related to the beam	
∂C_f	Uncertainty of friction coefficient	
∂C_F	Uncertainty of corrected friction coefficient	
∂C_{L0}	Uncertainty of Lift coefficient of a flat plate equivalent to a V-bottom surface	
∂C_V	Uncertainty of Froude number related to the beam	
∂g	Uncertainty of Acceleration of gravity	$[m/s^2]$
∂L_{WS}	Uncertainty of Mean wetted length	[m]

∂R_H , δR_H	Uncertainty of Bare hull resistance	[N]
∂R_n	Uncertainty of Reynolds number	
∂V	Uncertainty of hull speed	$\left[m/s\right]$
∂V_m	Uncertainty of Mean velocity over bottom of planing surface	$\left[m/s\right]$
$\partial\left(V_m/V\right)$	Uncertainty of speed ratio V_m/V	
∂W	Uncertainty of Weight of hull	[N]
$\partial\beta$	Uncertainty of Deadrise angle	[deg]
$\partial\Delta C_F$	Uncertainty of Friction coefficient correction	
$\partial\Delta\lambda$	Uncertainty of Mean wetted length-beam ratio variation	
$\partial\lambda$	Uncertainty of Mean wetted length-beam ratio	
$\partial\lambda_F$	Uncertainty of Corrected Mean wetted length-beam ratio	
$\partial\nu$	Uncertainty of Kinematic viscous coefficient	$\left[\frac{m^2}{s}\right]$
$\partial\tau$	Uncertainty of Trim angle	[deg]
β	Deadrise angle	[deg]
${}^i\beta$	Deadrise angle of i^{th} strip	[deg]
ΔC_F	Friction coefficient correction due to surface roughness of the hull	
$\Delta\lambda$	Mean wetted length-beam ratio variation due to the spray sheet	$\Delta\lambda=\Delta\lambda(\beta,\tau)$
ε_{B_C}	Relative error of Beam between chines	[%]
ε_{D_F}	Relative error of Friction force	[%]
ε_{C_f}	Relative error of friction coefficient	[%]
ε_{C_F}	Relative error of corrected friction coefficient	[%]
$\varepsilon_{C_{L\beta}}$	Relative error of Froude number related to the beam	[%]
$\varepsilon_{C_{L0}}$	Relative error of Lift coefficient of a flat plate equivalent to a V-bottom surface	[%]
${}^i\varepsilon_{C_{L0}}$	Relative error of Lift zero deadrise of i^{th} strip	[%]
${}^i\varepsilon_{C_P}$	Relative error of Wagner's pressure coefficient of i^{th} strip	[%]
${}^i\varepsilon_{C_{P,\max}}$	Relative error of Max Wagner's pressure coefficient of i^{th} strip	[%]
${}^i\varepsilon_{C_P^n}$	Relative error of Normalized pressure coefficient of i^{th} strip	[%]
ε_{C_V}	Relative error of Froude number related to the beam	[%]
ε_g	Relative error of Acceleration of gravity	[%]
$\varepsilon_{\frac{L_{CP}}{L_{WS}}}$	Relative error of Longitudinal Center of Pressure position to mean wetted length ratio	[%]

${}^{i}\varepsilon_{\frac{L_{CP}}{L_{WS}}}$	Relative error of Longitudinal Center of Pressure position to mean wetted length ratio of i^{th} strip	[%]
$\varepsilon_{L_{WS}}$	Relative error of Mean wetted length	[%]
ε_{R_H}	Relative error of Bare hull resistance	[%]
ε_{R_n}	Relative error of Reynolds number	[%]
ε_V	Relative error of hull speed	[%]
ε_{V_m}	Relative error of Mean velocity over bottom of planing surface	[%]
$\varepsilon_{\frac{V_m}{V}}$	Relative error of speed ratio V_m/V	[%]
ε_W	Relative error of Weight of hull	[%]
ε_β	Relative error of Deadrise angle	[%]
${}^{i}\varepsilon_\beta$	Relative error of Deadrise angle of i^{th} strip	[%]
$\varepsilon_{\Delta C_F}$	Relative error of Friction coefficient correction	[%]
$\varepsilon_{\Delta\lambda_F}$	Relative error of Mean wetted length-beam ratio variation due to the spray sheet	[%]
ε_λ	Relative error of Mean wetted length-beam ratio	[%]
${}^{i}\varepsilon_\lambda$	Relative error of Mean wetted length-beam ratio of i^{th} strip	[%]
ε_{λ_F}	Relative error of Corrected Mean wetted length-beam ratio	[%]
ε_ν	Relative error of Kinematic viscous coefficient	[%]
ε_ρ	Relative error of Fluid density	[%]
ε_τ	Relative error of Trim angle	[%]
${}^{i}\varepsilon_\tau$	Relative error of Trim angle of i^{th} strip	[%]
ε_ξ	Relative error of Arbitrary variable in conformal mapping	[%]
λ	Mean wetted length-beam ratio	$\lambda = L_{WS}/B_C$
${}^{i}\lambda$	Mean wetted length-beam ratio of i^{th} strip	
λ_F	Corrected Mean wetted length-beam ratio	$\lambda_F = \lambda + \Delta\lambda$
ν	Kinematic viscous coefficient	$\left[\frac{m^2}{s}\right]$
ρ	Fluid density	$\left[\frac{kg}{m^3}\right]$
τ	Trim angle	[deg]
${}^{i}\tau$	Trim angle of i^{th} strip	[deg]
ξ	Arbitrary variable in conformal mapping	
${}^{i}( )$	Size related to the i^{th} strip	

14.10 References

Bertorello, C. & Oliviero, L. 2007. Hydrodynamic Resistance Assessment of Non-Monohedral Planing Hull Forms based on Savitsky's Method. *Australian Journal of Mechanical Engineering,* Vol. 4 No.2, pp 209-224. Engineers Media, CROWS NEST, Australia. (ACN001311511).

Savitsky, D. 1964. Hydrodynamic Design of Planing Hull. *Marine Technology*, Vol.1, No.1, Jersey City (USA): SNAME

Luciano OLIVIERO

viale CASTELLUCCIO 26F
80059 Torre del Greco (NA) - ITALY

+39 081 882 68 23
+39 347 186 76 21 (mobile)

luciano.oliviero@tin.it
luciano.oliviero@gmail.com